NASA Conference Publication 3178
Part 1

Third NASA Advanced Composites Technology Conference

Volume I

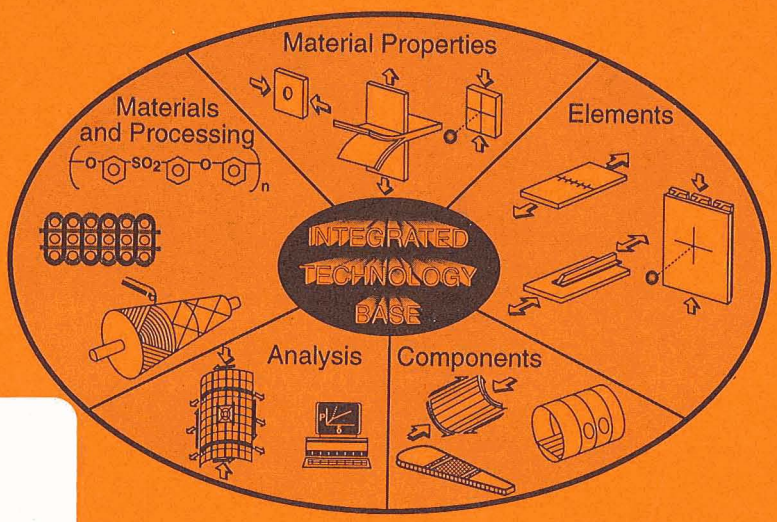

Proceedings of a workshop held in
Long Beach, California
June 8–11, 1992

NASA

NASA Conference Publication 3178
Part 1

Third NASA Advanced Composites Technology Conference

Volume I

Compiled by
John G. Davis, Jr.
Langley Research Center
Hampton, Virginia

Herman L. Bohon
Lockheed Engineering & Sciences Company
Hampton, Virginia

Proceedings of a workshop sponsored by the National Aeronautics and Space Administration, Washington, D.C., and the Department of Defense, Washington, D.C., and held in Long Beach, California
June 8–11, 1992

NASA
National Aeronautics and Space Administration
Office of Management
Scientific and Technical Information Program
1992

PREFACE

This document is a compilation of papers presented at the Third NASA Advanced Composites Technology (ACT) Conference held at Long Beach, California, June 8-11, 1992.

The ACT Program is a major multi-year research initiative to achieve a national goal of technology readiness to introduce composite materials into primary structure of production aircraft before the end of the decade. This initiative is carried out through a cooperative program between industry, universities, and the government conducting research in materials processing, analysis development, innovative designs, and manufacturing methodology. Conference papers recorded results of research in the ACT Program in the specific areas of automated fiber placement, resin transfer molding, textile preforms, and stitching as these processes influence design, performance, and cost of composites in aircraft structures. These papers are published as Volume I in this document.

Conference papers were also presented on the new initiative Design and Manufacturing of Low Cost Composites (DMLCC) sponsored by the Department of Defense. These papers are published in Volume II of this document.

John G. Davis, Jr.
Herman L. Bohon

CONFERENCE ORGANIZATION

Sponsor: Structures Technology Progam Office
Structures Directorate
NASA Langley Research Center
Hampton, Virginia 23665-5225

General Chairman	Technical Chairman	Administrative Assistant
John G. Davis, Jr. NASA Langley Research Center	Herman L. Bohon Lockheed Engineering and Science Company	Stuart E. Pendleton Lockheed Engineering and Science Company

Session Organizers

John G. Davis, Jr.	NASA Langley Research Center
James H. Starnes, Jr.	NASA Langley Research Center
Norman J. Johnston	NASA Langley Research Center
David Beeler	Wright Laboratory

SESSION OUTLINE

THIRD NASA ADVANCED COMPOSITES TECHNOLOGY CONFERENCE

SESSION I (Volume I, Part 1)
Composites in Transport Aircraft
Chairman: John G. Davis, Jr., NASA Langley Research Center

SESSION II (Volume I, Part 1)
Advanced Composites Technology Overview
Chairman: John G. Davis, Jr., NASA Langley Research Center

SESSION III (Volume I, Part 1)
Textile Technology
Chairman: Charles E. Harris, NASA Langley Research Center

SESSION IV (Volume II)
Design and Manufacturing of Low Cost Composites
Chairmen: Paul Pirrung and Richard Holzwarth, Wright Laboratory

SESSION V (Volume I, Part 1)
RTM/Stitched Technology
Chairman: Norman J. Johnston, NASA Langley Research Center

SESSION VI (Volume I, Part 2)
Materials Technology
Chairman: H. Benson Dexter, NASA Langley Research Center

SESSION VII (Volume I, Part 2)
Automated Fiber Placement Technology
Chairman: William T. Freeman, Jr., NASA Langley Research Center

SESSION VIII (Volume I, Part 2)
Design/Analysis Technology
Chairman: James H. Starnes, Jr., NASA Langley Research Center

CONTENTS

†Presented but not included in this publication.

*Appears in Volume II.

Volume I, Part 2*

SESSION VI

MATERIALS TECHNOLOGY
Session Chairman: H. Benson Dexter
NASA Langley Research Center

*These papers are presented in NASA CP-3178, Volume I, Part 2.

SESSION VII

AUTOMATED FIBER PLACEMENT TECHNOLOGY

Session Chairman: William T. Freeman, Jr.
NASA Langley Research Center

SESSION VIII

DESIGN/ANALYSIS TECHNOLOGY

Session Chairman: James H. Starnes, Jr.
NASA Langley Research Center

Session I

COMPOSITES IN TRANSPORT AIRCRAFT

Session Chairman: Charles P. Blankenship
NASA Langley Research Center

IMPACT OF COMPOSITES ON FUTURE TRANSPORT AIRCRAFT

Robert H. Kinder
Douglas Aircraft Company

Direct Operating Cost Objective

In the current environment, new technology must be cost-effective in addition to improving operability. Various approaches have been used to determine the "hurdle" or "breakthrough" return that must be achieved to gain customer commitment for a new product or aircraft, or in this case, a new application of the technology. These approaches include return-on-investment, payback period, and addition to net worth. An easily understood figure-of-merit and one used by our airline customers is improvement in direct operating cost per seat-mile. Any new technology must buy its way onto the aircraft through reduction in direct operating cost (DOC).

Impact Measured by Aircraft Direct Operating Cost

Direct Operating Cost Trends

Advanced technology has played a vital role in the continual productivity improvement of transport aircraft over the past 40 years. Speed, propulsion, aerodynamics, and capacity have contributed to a continual decrease in DOC in each decade. With the introduction of the jet engine, improvement was achieved through increased speed. In the 1970s, wide-body aircraft offered dramatic increases in capacity and fuel efficiency. Over the past two decades, direct operating cost reductions have largely been the result of reduced fuel consumption derived from lower weight, reduced engine SFC, and aircraft drag. But, as the chart shows, it is becoming increasingly difficult to achieve further reductions in DOC.

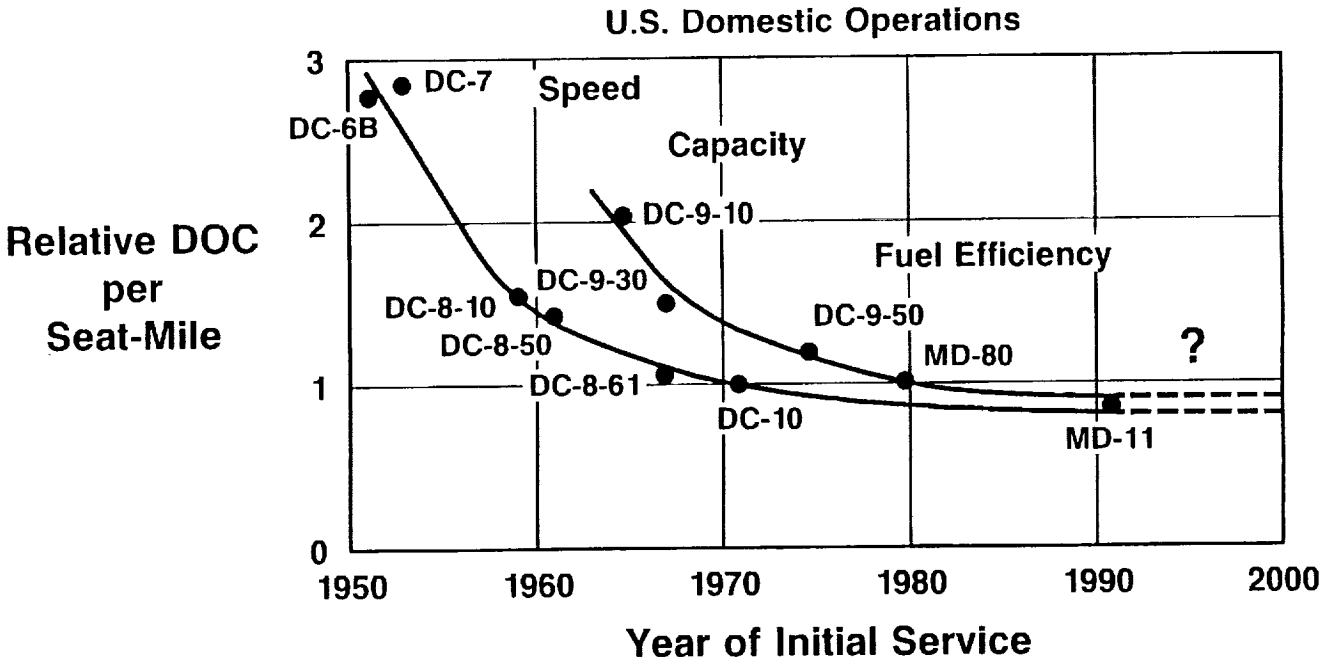

Operating Cost Distribution

The major component influencing direct operating cost is the ownership cost. Future advances in aerodynamics, engine SFC, and structural weight will continue to shrink the fuel contribution to total cost. However, reductions in ownership cost dominate the equation to justify the development of new aircraft.

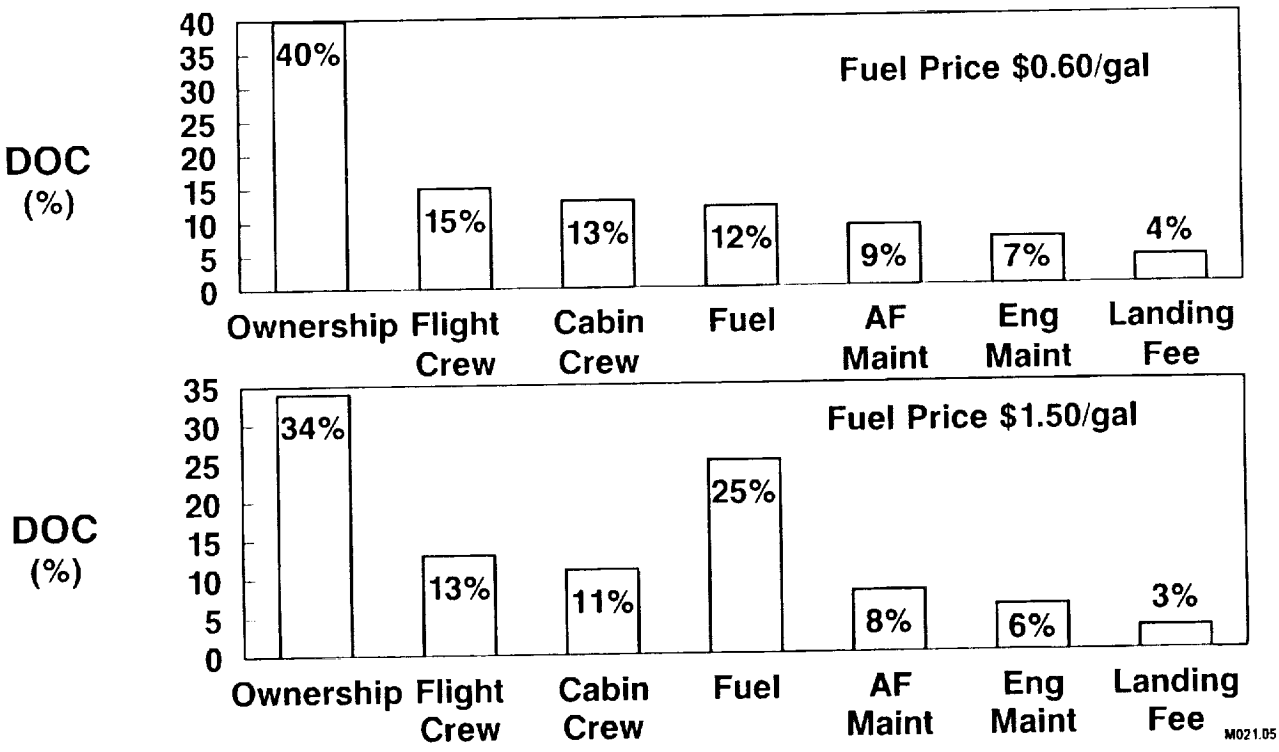

U. S. Jet Kerosene Price

The forecast by McDonnell Douglas is that long-term fuel prices will remain flat in constant dollar terms at about 60 cents per gallon. This is based upon an abundant oil supply remaining (over 40 years supply at present consumption) and the short-term nature of dramatic fluctuations due to political events. Therefore, ownership costs are expected to continue as the largest element in the DOC equation.

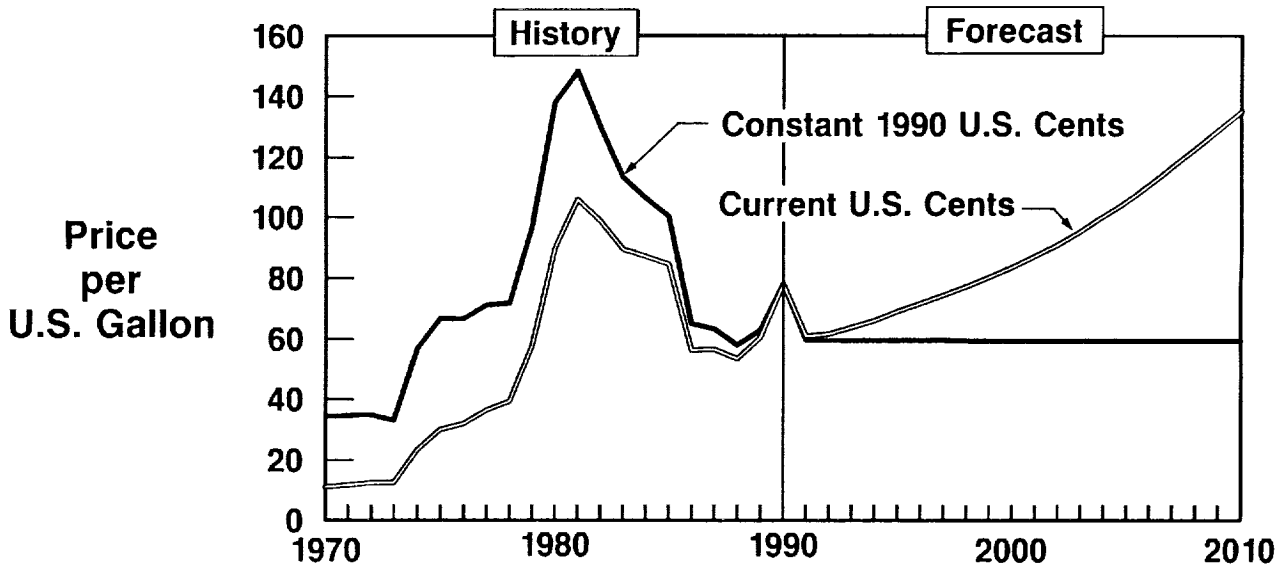

Passenger Aircraft Deliveries

World passenger traffic is expected to grow at a 6.5% annual rate through 2010. During this period, international passenger traffic is projected to grow to 7.8% a year while domestic traffic is predicted to increase 4.9% annually. Pacific/Asia will experience the fastest growth while North American traffic growth will remain essentially constant. To meet the increased traffic demand, the world's jet aircraft fleet is expected to more than double in the next 20 years (17,000 passenger aircraft by 2010 compared to 8,000 today). The requirement for additional capacity combined with aircraft retirements results in a McDonnell Douglas forecast of over 14,000 passenger jet aircraft deliveries during this time period. These aircraft are split almost evenly between narrow-body and wide-body units. In constant 1990 dollars, their value is almost one trillion dollars.

By Domiciled Region, 1991-2010

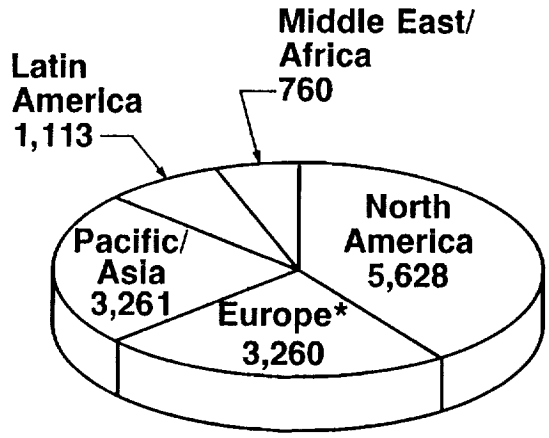

14,022 Units

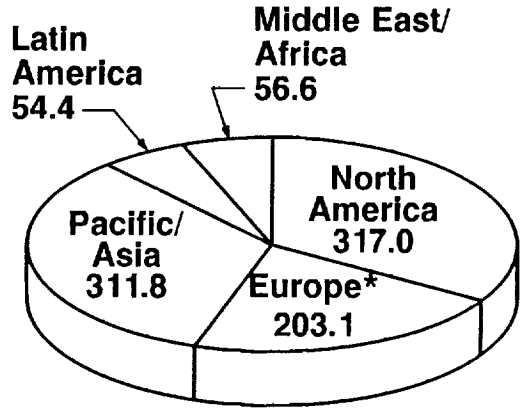

$942.9 Billion
(Constant 1990 Dollars)

*Excludes USSR

The Challenge to Technology

An improvement in any of the DOC parameters is very difficult to achieve. Consider that a ten percent reduction in the cost/price of the aircraft is a very large reduction, but reduces DOC by only four percent. However, a new aircraft should provide roughly a 10% improvement in operating cost to provide the sales potential necessary for production commitment. To contribute to the achievement of that objective, composite primary structure must provide a cost benefit as well as the expected weight savings. This is the goal that must be achieved to realize the use of composite primary structure on a transport (commercial or military) aircraft.

DOC Drivers

A 10-Percent Improvement in Each Parameter Has This Impact on DOC

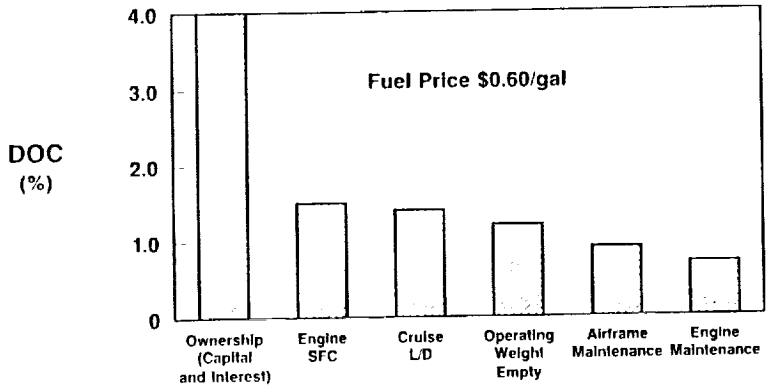

Direct Operating Cost Objective

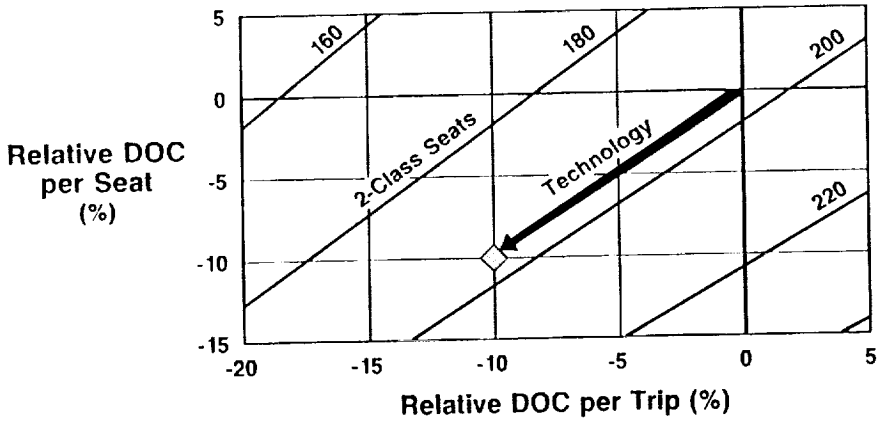

Reductions in operating costs that will justify inclusion in the product

MD-11, C-17, MD-12 Composite Construction

The extent of composites usage has continued to increase with time. Aircraft currently in production utilize composites in numerous secondary structures such as fairings and control surfaces. Composites account for 4 to 6 percent of the empty weight of these aircraft. The MD-12 will utilize composites for the vertical and horizontal stabilizer boxes and floor beams, increasing the composite content to about 9 percent of empty weight.

Composites Application in Douglas Transport Aircraft

MD-11 Composite Construction

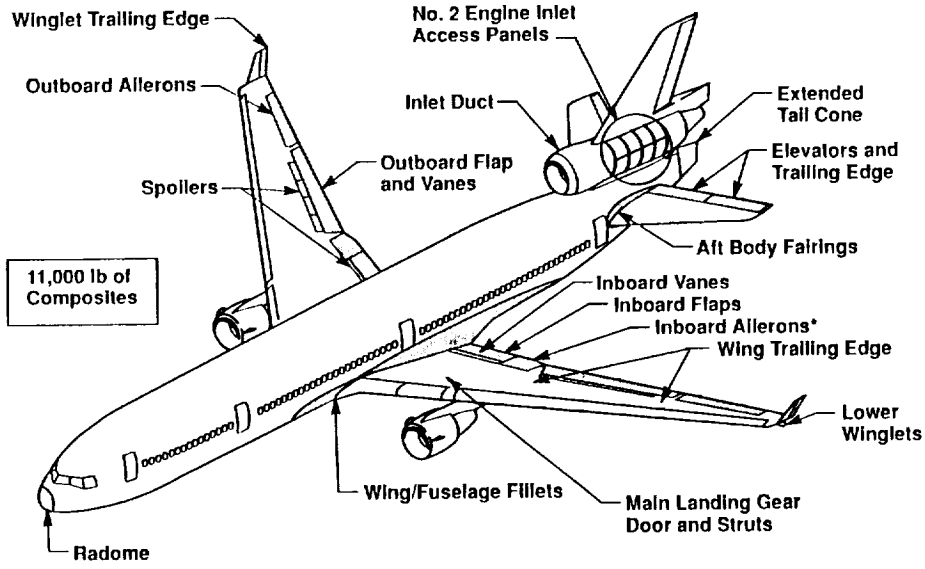

C-17 Composite Applications

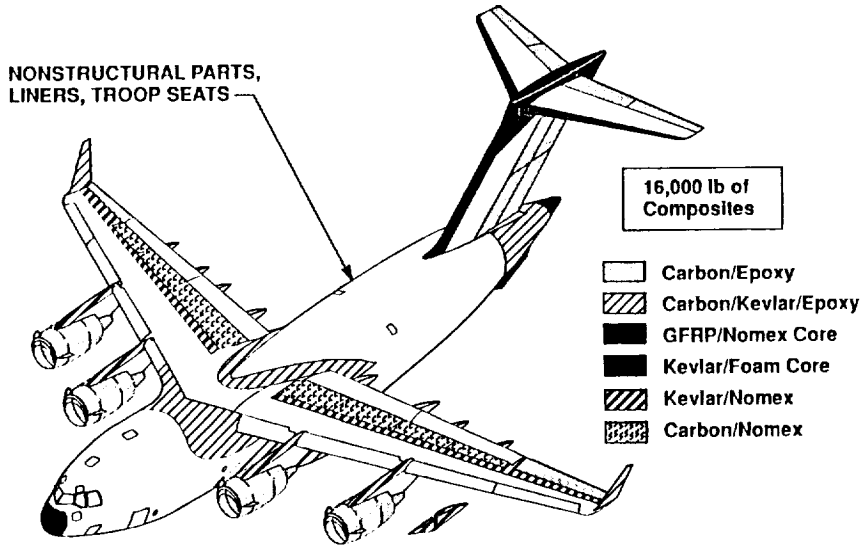

MD-12

Wide-Body Cross Section Comparison

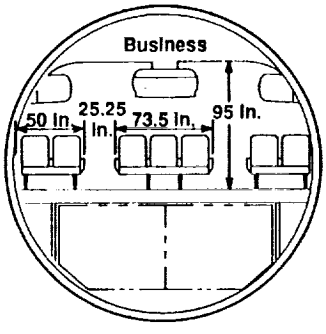

MD-11
237-in. Circular

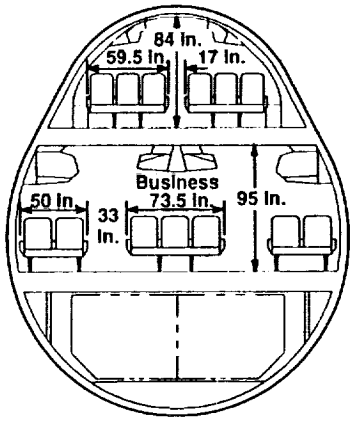

747-400
256 in. Wide
by
309 in. High

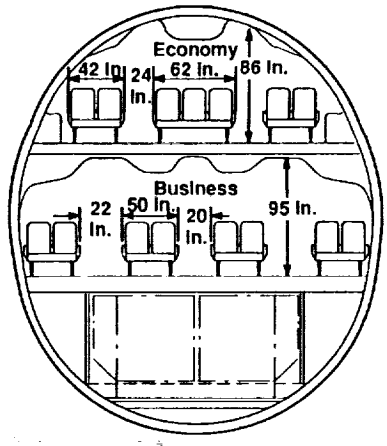

MD-12
291 in. Wide
by
335 in. High

CA3010.02a
GFVC024-7

MD-12 Composite Construction

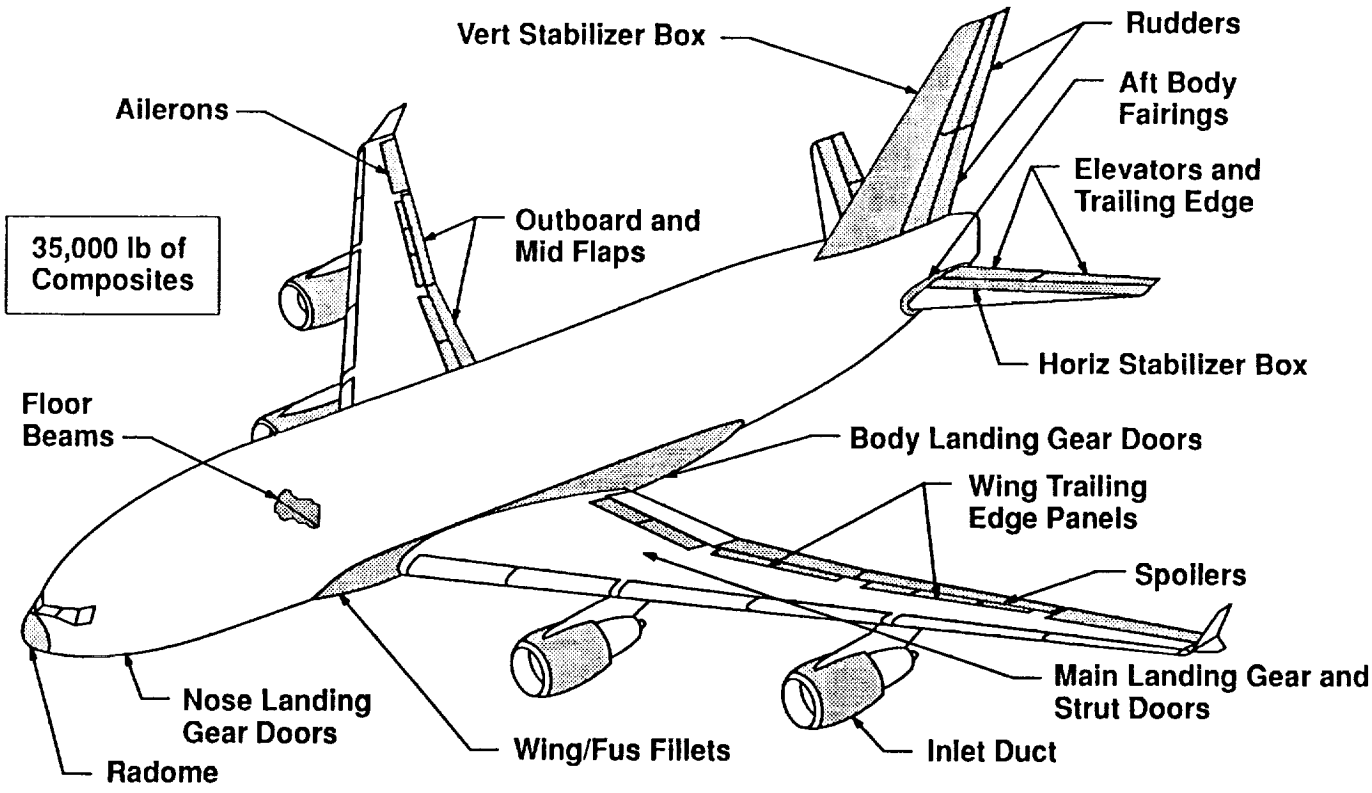

MD-XX Composite Construction

With composite wing and tail, the composite content of the MD-XX will grow to over 20 percent of empty weight. If the MD-XX were to also have a composite fuselage, the percent composite would be over 40% of aircraft empty weight.

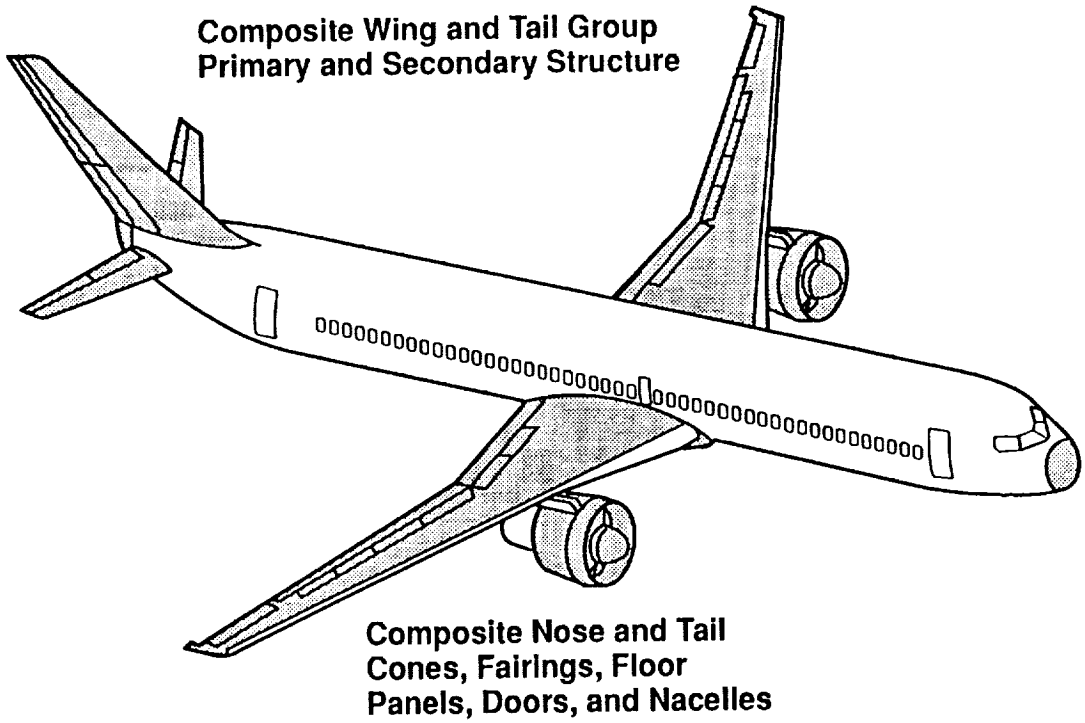

Wing Box Data Projection

Conventional composite construction reduces weight but at increased cost. McDonnell Douglas studies of a wing box unit show a 25 percent weight savings but a 50 percent or greater cost increase for a conventional composite unit. Using the ICAPS methodology, the weight savings will be retained with a goal of achieving better than a 40 percent improvement in cost compared to the conventional composite unit.

Objectives of DAC Composites Program With NASA

Develop Primary Structure Technology

Below the Cost of Metal

Wing Box Cost Data Projection

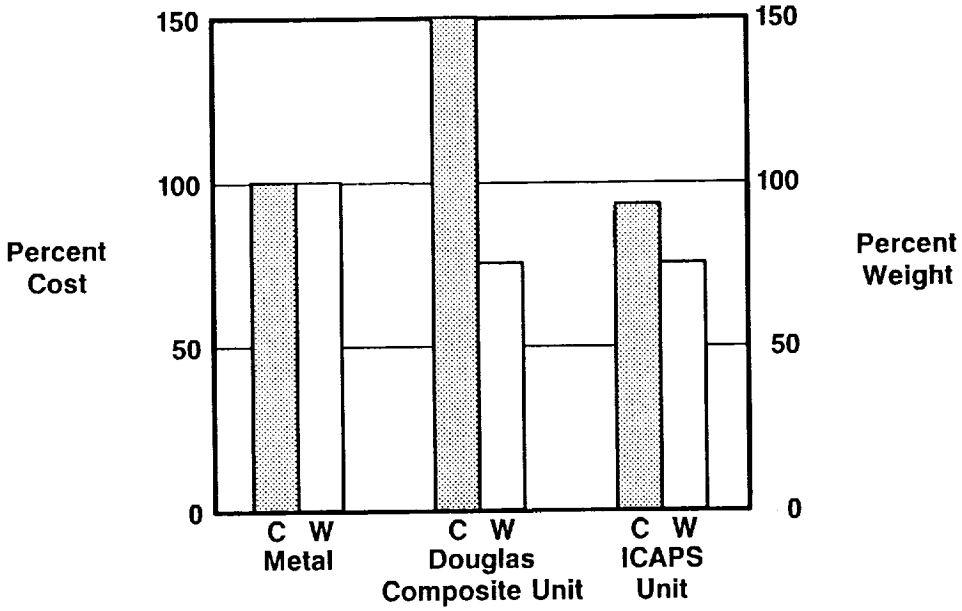

Aircraft Cost Distribution

Ownership costs (to the operator) are directly related to the vehicle price which, in turn, depends on the manufacturer's cost. Structure costs are larger than propulsion, avionics, or equipment costs. The largest components of structure costs are the fuselage and wing. These two components provide the largest potential for a significant impact on ownership cost and total operating cost. McDonnell Douglas has elected to focus its initial effort on the wing. Success with a composite wing will yield two benefits: reduced weight and reduced drag. Reduced drag results from the stiffness characteristics of composite which allows higher aspect ratio without attendant weight penalties.

1990 Technology Aircraft

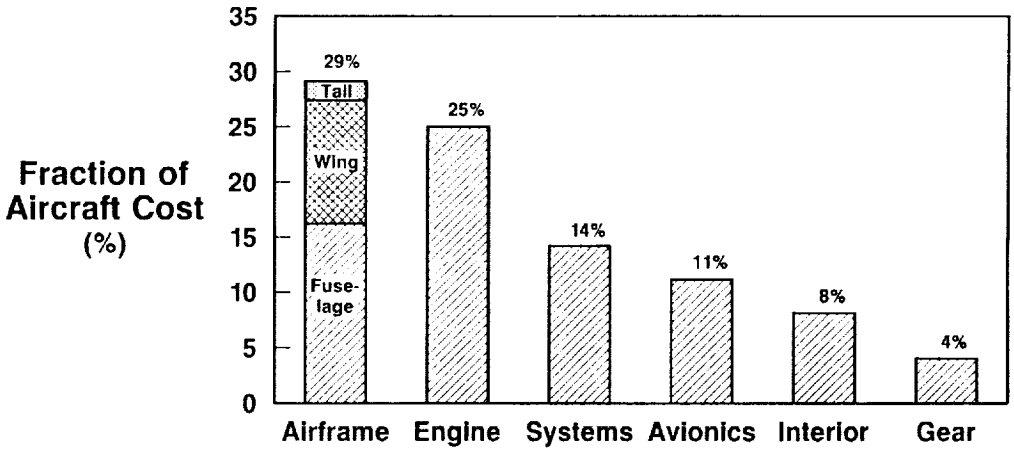

MD-XX Composite Wing Technology

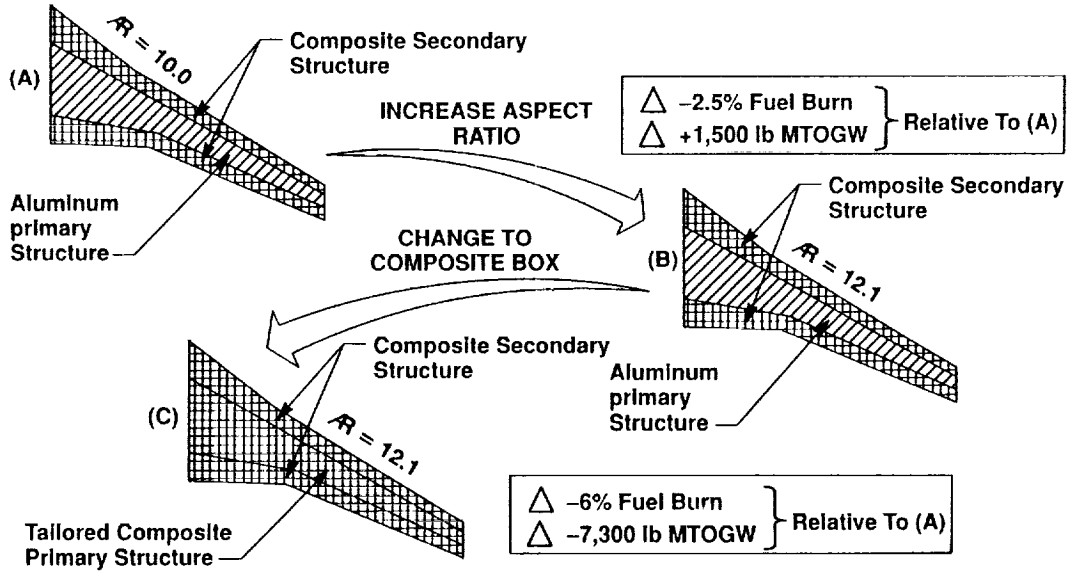

One-Third Reduction in Fuel Burned

It is possible, through incorporation of several new technologies, to achieve a one-third reduction in aircraft fuel consumption. However, a full one-third reduction in fuel burned exclusively is not enough to achieve a ten percent reduction in DOC. An all-new aircraft with a thirty-three percent reduction in fuel burned would provide an economic benefit of only four to eight percent in DOC depending on fuel price.

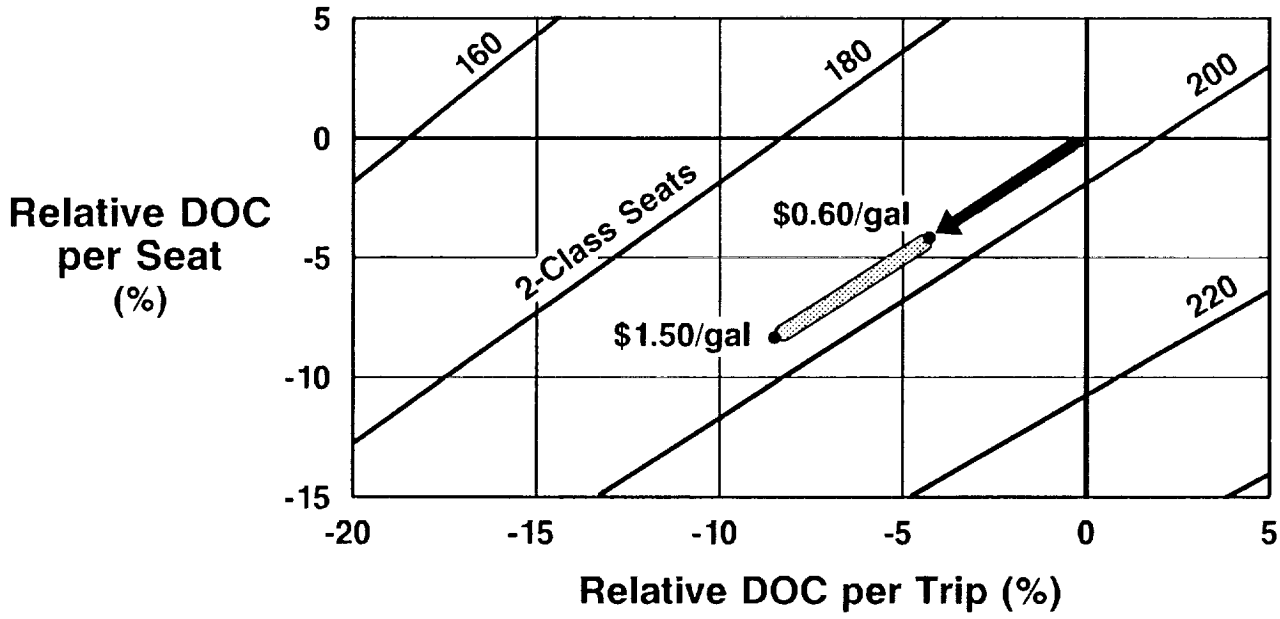

DOC Using Conventional vs. ICAPS Wing Box

The benefit of the ICAPS wing on the total direct operating cost has been calculated for an MD-XX aircraft. Reducing the cost of the wing by just ten percent provides an additional two percent reduction in DOC.

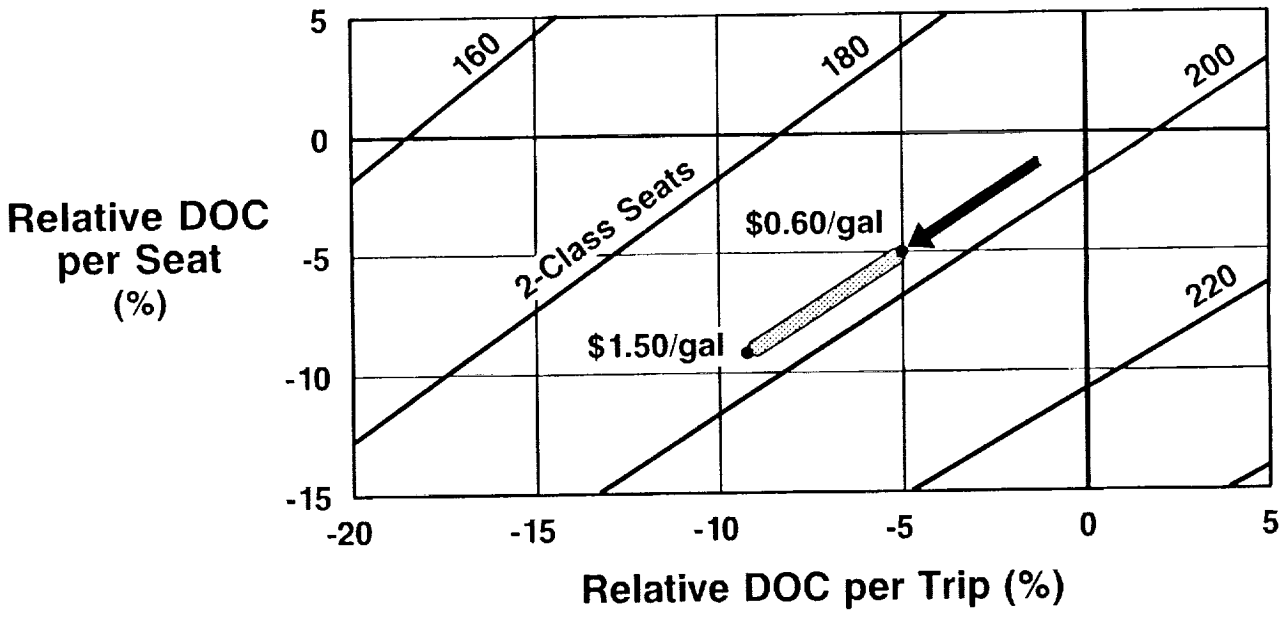

DOC Using ICAPS Wing and Fuselage

Extending the use of the ICAPS methodology (i.e., weight and cost reduction) to include the fuselage improves the total operating cost picture even further.

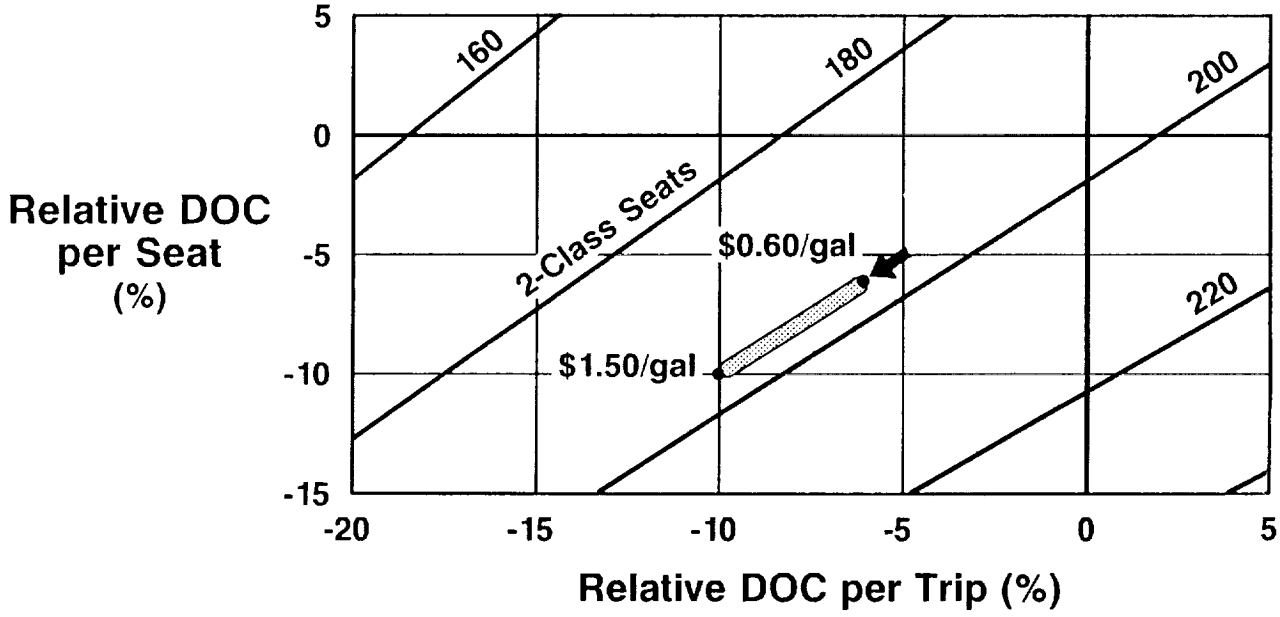

DOC Using Current Composite Construction Costs

Extensive application of composites at today's cost of construction is prohibitive. The resulting increased cost of ownership has offset nearly all the fuel consumption benefits associated with the application of several new technologies.

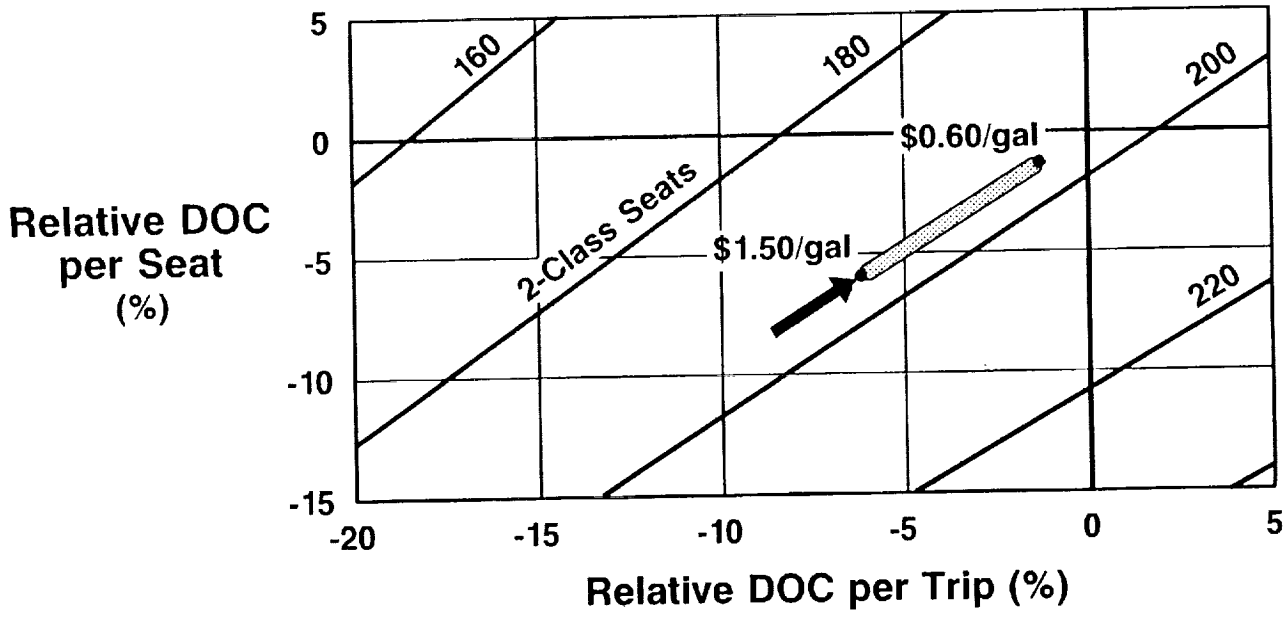

Innovative Composite Aircraft Primary Structure

The following charts depict the schedule and some of the results to date of the Douglas composite primary structure program. The program will conclude with the construction and testing of a full scale (approximately 60 ft.) semi-span. The wing stub box is currently under construction. Single and multi-needle sewing machines are shown making performed parts prior to RTM. These machines will potentially replace expensive drivematic riveting machines used in manufacturing metal wings.

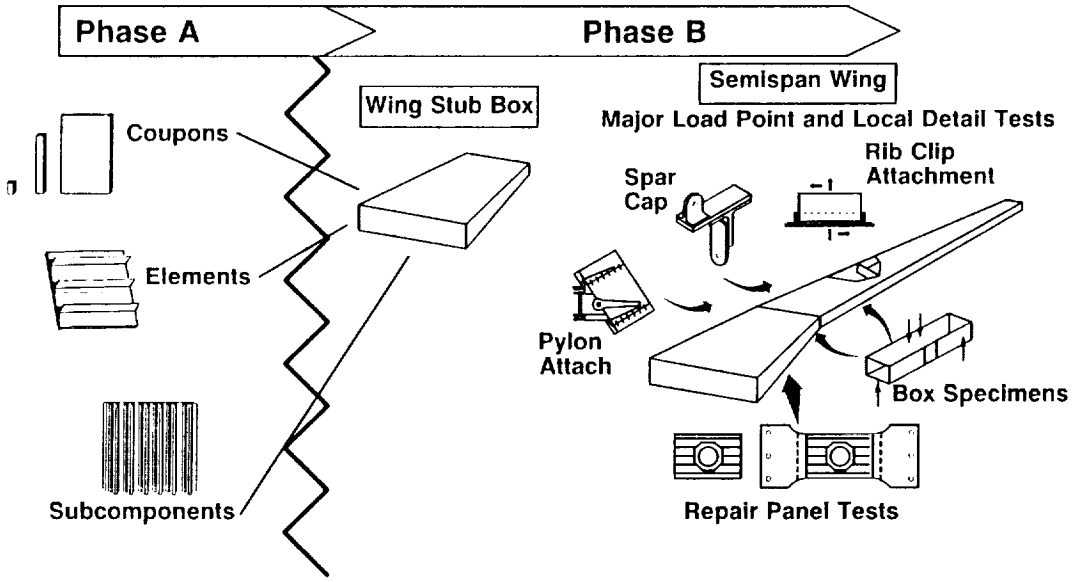

4 by 6 Foot Stitched Preform

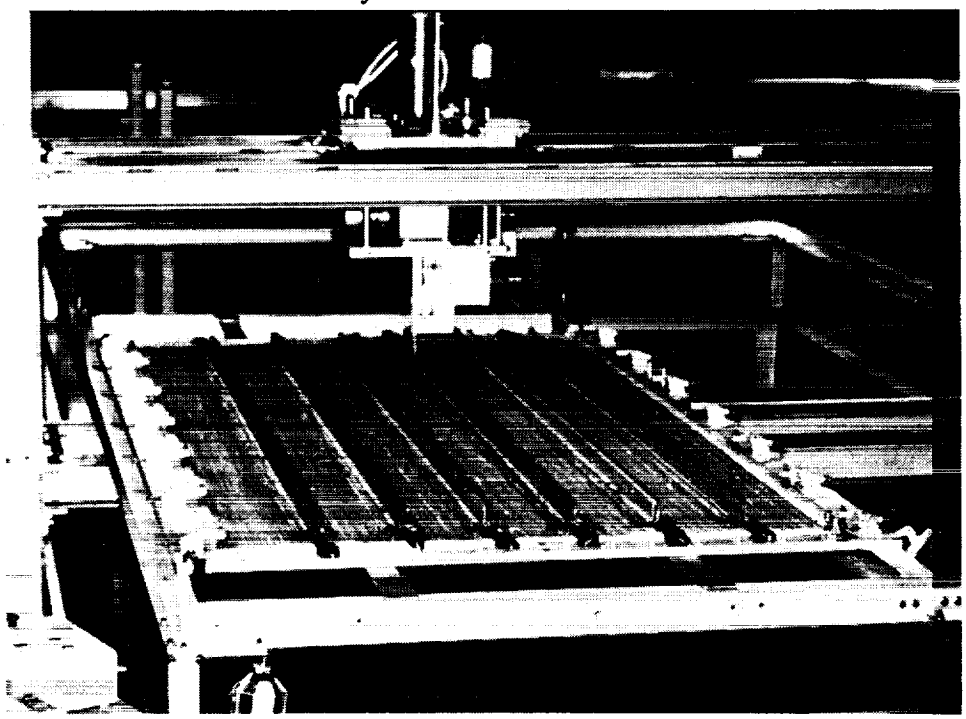

Stitching Machine Operation

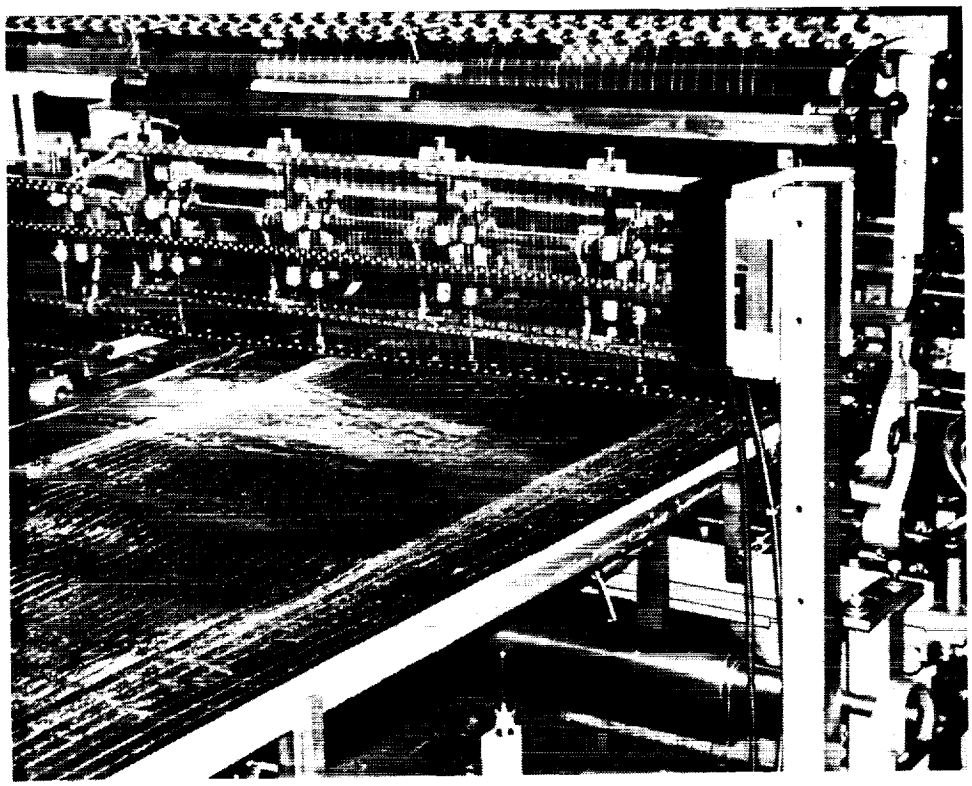

128 Needle Stitching Machine

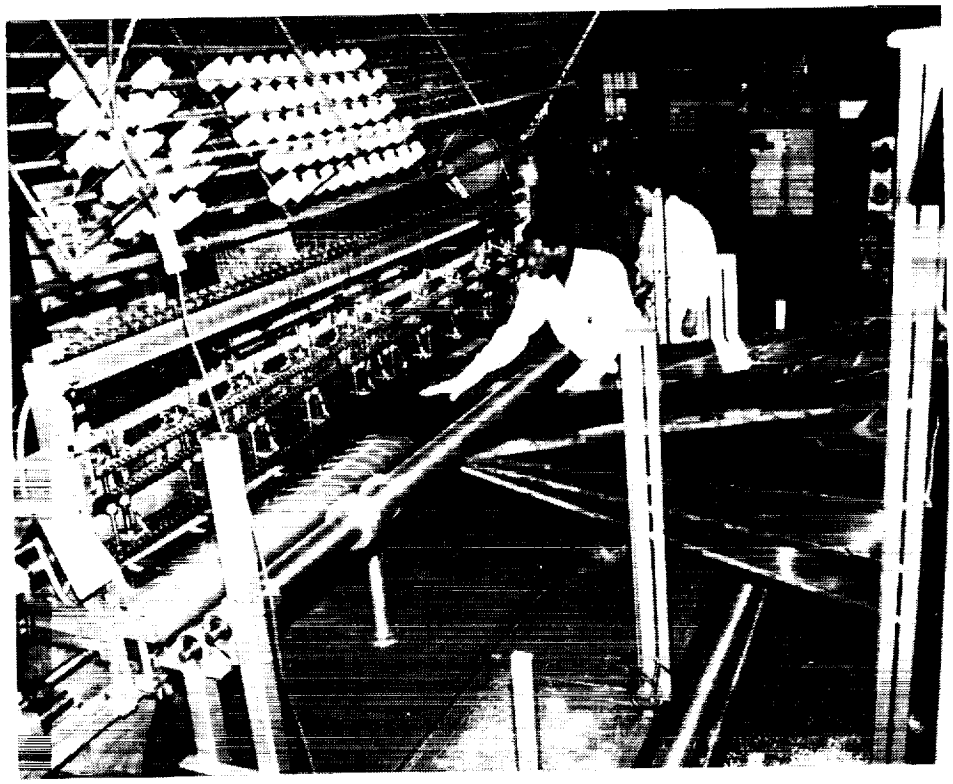

Wing Section In Drivematic

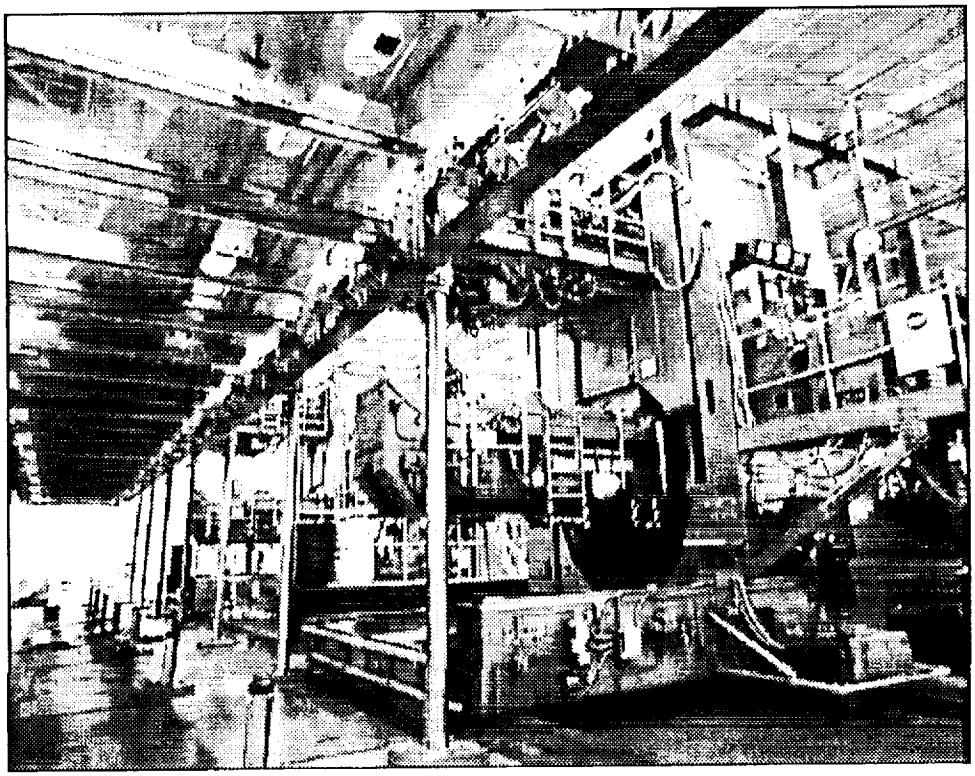

Damage Area Comparison for Blade-Stiffened Panel

While composite laminates have excellent properties in the plane of the layers, they are weak in the through-the-thickness direction. Stitching provides a means for suppressing the types of delamination failures arising from that weakness. One advantage provided by stitching is the reduction in the incidence and size of damage from impacts and the subsequent reduction of maintenance and repair costs. Weight saving is realized because the working allowable stress levels for damaged compression structure is increased.

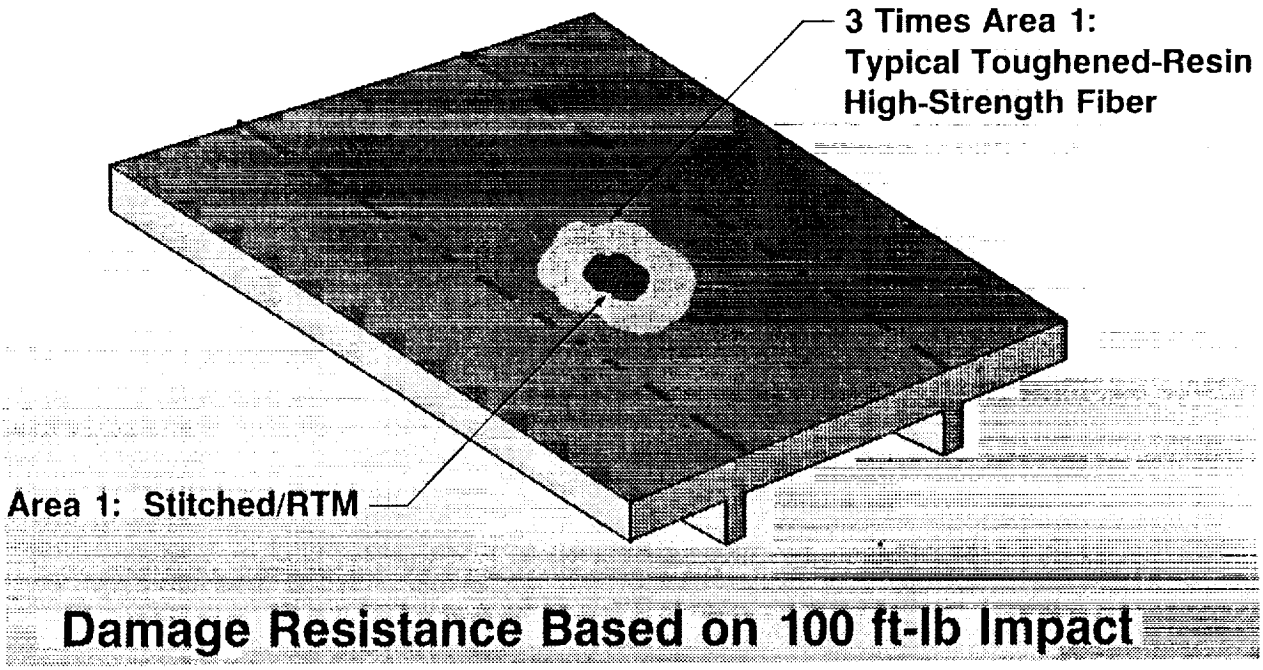

Typical Compression Test

Composite panels loaded in compression typically fail with extensive splitting apart of the laminate layers. This mode of failure can be totally suppressed when high-density stitching is used. Stitched compression panels fail on a 45° shear plane in a manner much more typical of that expected from homogeneous metal panels.

Brooming Failure of Toughened Resin and High Strength Fibers
(Prepreg Panel-Unstitched)

Compression Failure at 45-deg Shear on
Blade Stiffener and Skin (Stitched/RTM–Blade Stiffened)
Wing Compression Test Panel

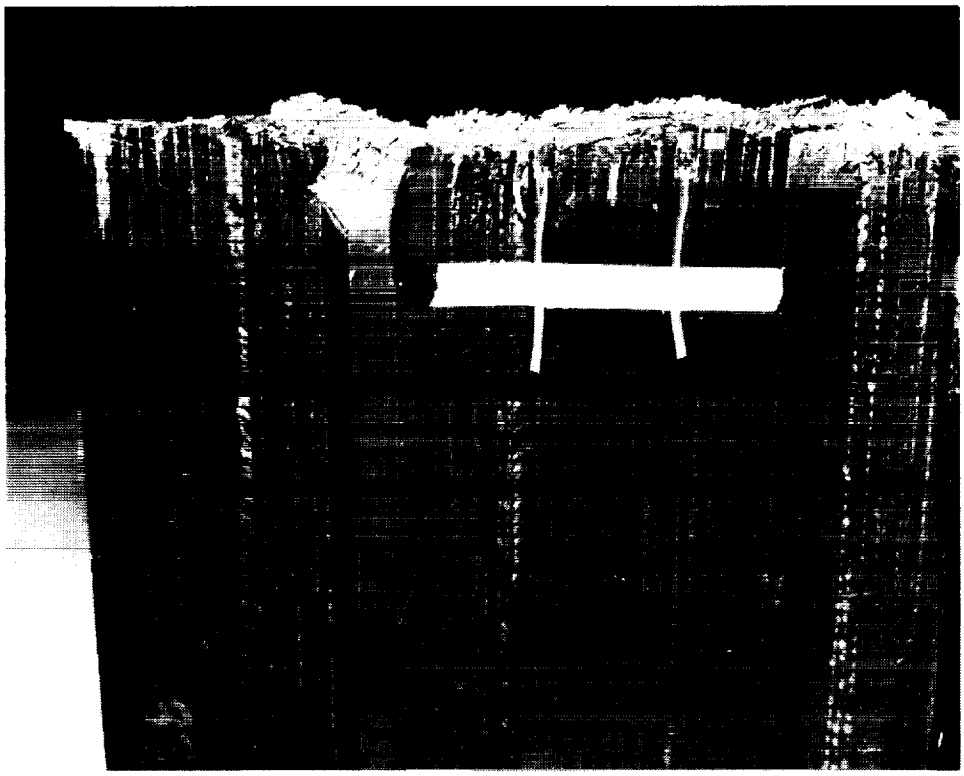

Summary

In summary, there is a requirement for a large number of new conventional aircraft over the next 20 years. Sales of these aircraft will go to the builders who can offer the best operating economics. Ownership costs will continue to dominate the economics equation. To find application on these new transport aircraft, composite primary structure must provide production cost reduction as well as fuel consumption and maintenance benefits.

Conventional subsonic transports will continue to dominate the market.

Ownership cost will continue to increase as a percentage of total operating cost.

Composite primary structure can benefit several elements of the operating cost picture - ownership, fuel, maintenance.

A well-conceived and implemented ICAPS plan will provide major benefit to the next transport aircraft.

[redacted]

CHALLENGES AND PAYOFF OF COMPOSITES IN TRANSPORT AIRCRAFT: 777 EMPENNAGE AND FUTURE APPLICATIONS

JOHN QUINLIVAN

52-24
5/12 85

FIGURE

TITLE PAGE

1. 777 AIRPLANE

The Boeing 777 is the first of a new family of wide body airplanes. The new large twin is sized to accommodate 360 to 390 passengers in typical two-class configurations and planned growth beyond that. The 777 offers airlines three engine options, extremely attractive operating costs, and compatibility with existing airport gates and taxiways. The 777 has a wingspan of nearly 197 feet and is offered with a wing-tip folding mechanism that will reduce the span to 156 feet.

2. COMPOSITES

Extensive use of advanced composites is included in the 777. The applications range from fiberglass fairings to primary structures. Flight control surfaces such as the elevators, rudder and flaps continue the composite design technology established with the 767 and 757. The use of composites is approximately 9% of the structural weight of the 777. This is nearly three times the amount used on previous Boeing transports. Expressed differently, the 777 has nearly 10 times the mass of composites as does the 757.

3. COMPOSITE EMPENNAGE

The 777 empennage includes the vertical fin and a horizontal stabilizer. Each consists of a structural box, an auxiliary or forward torque box, leading edges, tip, fixed trailing edges, elevator or rudder and body gap covers. The structural boxes are manufactured in carbon fiber reinforced plastic (CFRP). The primary structural box configuration is a two-spar, multirib design. The panels are attached to the ribs and spars using mechanical fasteners.

4. TOUGHENED MATERIAL

The material used for the empennage is a new, toughened epoxy material. The material provides outstanding resistance to impact damage. This slide compares the impact damage area of the conventional materials with the toughened material. As measured by damage area, the new material is nearly seven times better than the current production materials.

5. SKIN PANEL

The basic CFRP skin panel incorporates an integral I-section stiffened design. The panels are full span and are joined at the airplane centerline (horizontal stabilizer).

6. RIBS

The majority of the ribs are of a sandwich design using aramid honeycomb core and CFRP face sheets. The slide shows one of the more highly loaded ribs which is fully shear-tied and has mechanically attached chords.

7. SPARS

The CFRP spars are simple channel sections. The rear spar is a single piece with mechanically attached stiffeners, while the front spar is two pieces to allow for manufacturing payoff.

8. VOICE OF THE CUSTOMER

We have spent a great deal of effort on the 777 talking with and listening to our customers. We have worked together to develop the functionality and maintainability they desire. Our airline customers tell us we are doing a great job in meeting our commitments. Our composite service experience has been very good. Questions relating to composites usually came down to two:

How do you inspect it:, and
How do you repair it?

Our plan is use periodic visual inspection for all composite structures, with tools in the existing inventory as referees should a sign of distress occur.

9. REPAIR

The airlines do not give our industry especially high marks for existing composite repair methodologies. We have probed these concerns and have designed the 777 primary laminate structures to accommodate bolted repairs, much like metal structure. The repair is designed to be installed from one side, that is, access to the interior of the box is not required. This slide illustrates the skin side of an instrumented test panel prior to test. The completed repair meets all structural requirements as demonstrated by large panel and full scale structural box testing.

10. 777 EMPENNAGE TEST PLAN

A key milestone in the 777 program was reaching agreement with the certifying agencies as to the empennage certification plan. This milestone was achieved in November 1991. The test plan covers coupons, structural details, structural elements, subcomponents and a developmental test box.

The developmental test box was designed and fabricated using the materials, design concepts and manufacturing approach to be used for the 777. This test article is currently undergoing its planned second life of fatigue testing. This approach will provide the necessary substantiating data in a manner timely to support program schedules.

11. T-TAIL CFRP HORIZONTAL STABILIZER TEST COMPONENT

The success of this approach in providing the necessary test data was developed on the NASA/Boeing 737 horizontal stabilizer program. More recently, a generic T-tail horizontal stabilizer developmental program was patterned after this "building block" approach.

The T-tail horizontal stabilizer test article was subjected to the rigors of testing typical of that required for the certification of composite primary structure. This included a series of limit load tests, a two lifetime fatigue test with major damage, damage tolerance testing, repair and a final destruction test. Final failure occurred as predicted at an easily visible impact damage site after sustaining 166% DLL.

12. DESIGN FOR PRODUCIBILITY

Having the necessary technical data is only part of the equation. A key feature of any composite design is cost. The 777 empennage was designed with automation in mind. We began with a concept of how we wanted to assemble the structure. Final assembly occurs with complete access to the internal structure. The mechanic can stand in any rib bay during final close out.

Having determined the assembly plan, we designed the details to achieve a high penetration of automation. Our goal was to minimize touch labor operations, a large recurring cost driver. It was necessary to simplify the detail design to achieve our goal of automated production.

13. PANEL DESIGN

The panels were designed with automated tape laying equipment in mind. The basic skin plies are relatively simple, doublers inserted as packages. This approach permits all or nearly all of the panel to be laid up by machine.

14. SPARS

The spars are designed as simple constant sections. No padups are required at the spar chord or around the access holes. The front spar is a two piece design to accommodate manufacturing access during closeout.

15. TOOLING

Production tooling uses INVAR to minimize part warpage due to differences in thermal coefficients of expansion and provide the durability of a metal tool. The horizontal stabilizer skin LM is the largest layup tool.

16. SKIN LAYUP

Preproduction verification tests are demonstrating that the manufacturing plan works before production of parts begins. Here plies are being laminated by machine for a preproduction and tool proof 777 Horizontal Stabilizer skin panel.

17. DEMONSTRATION PANEL

The preproduction demonstration panel met all program objectives. First part production began on May 5, 1992 with the fabrication of the first stringer for the 777 horizontal stabilizer.

18. 777 STATUS

The 777 represents a major commitment to composite primary structure. The program is on schedule and is meeting its weight target. The weight reduction projected for the 777 horizontal stabilizer box is in excess of 20% when compared with a modern aluminum design.

19. THE FUTURE OR WHAT'S COMING NEXT!

Dr. Davis requested that I say a few words about the future use of CFRP for commercial aircraft.

We all know that composites are a technology which offers both a performance improvement and a weight reduction. Composite materials will permit subsonic transports to use less fuel operate more efficiently and increase payload/range capability. For supersonic transports, composite materials are crucial to building an aircraft that can withstand the heat of high-speed flight. However, the most significant hurdle facing these potentialities is COST! If we cannot reduce the cost of composites, it may be that none of these developments will occur.

20. WING COST EXAMPLE

Let me share with you an actual example of a composite wing and some of the cost reduction opportunities available. In the example shown, all aspects of design, tooling and manufacturing cost more than the metal wing counterpart.

In the non-recurring area, engineering design costs are higher--primarily due to increased analysis requirements (to say nothing of testing). Tooling costs are higher, even though the total tool count is approximately one-third of that required for a metal wing. Recurring manufacturing costs were higher in all areas-- detail fabrication, minor

assembly and major assembly. As expected, material costs are also higher. Clearly there is ample opportunity to address costs in each of these areas. If we are to reduce costs significantly, it will not be sufficient to focus on just one arena. All aspects of cost must be addressed--Design, Tooling, Manufacturing, Quality and Materials.

21. GROWTH EXAMPLE

A potentially serious constraint for composites occurs when one considers the airplane growth typical for a modern jet transport. Increases in airplane gross weight often require strengthening component parts. Composite tooling concepts and designs must recognize this. Tooling concepts must be flexible enough to handle late design changes, capable of supporting demanding tool design and fabrication schedules and robust enough to handle airplane growth without major investments in retooling. The so-called "single-shot cure" may well be the answer for parts and assemblies not subject to late design load changes or subsequent derivative aircraft development, but such approaches may well be too costly for a large transport in rate production with multiple derivatives on a common production line.

22. SUMMARY

Composites have achieved significant performance benefits:

reduced weight
corrosion free structure
durable structure

Our challenge is to reduce the cost of composite aircraft structures. No program will be successful if it does not deliver the right product at the right time for the right cost. The inescapable connection is that the research we do now will determine our capabilities for the next century.

NASA has gained world renown in the international aviation industry and academia for broadening the frontiers and understanding of aeronautics with the outflow of NASA technology research to all. NASA has been among the leaders in the development of advanced material technologies. But technology is just one of the fronts we must address to remain competitive. Research into what makes a better factory is necessary if we are to bring high quality goods to the market quickly at competitive prices. These advances must be made if advanced composites are to increase their penetration in transport structural applications.

I am pleased that you are addressing these issues now at conferences such as this.

Thank you.

BOEING 777

Figure 1

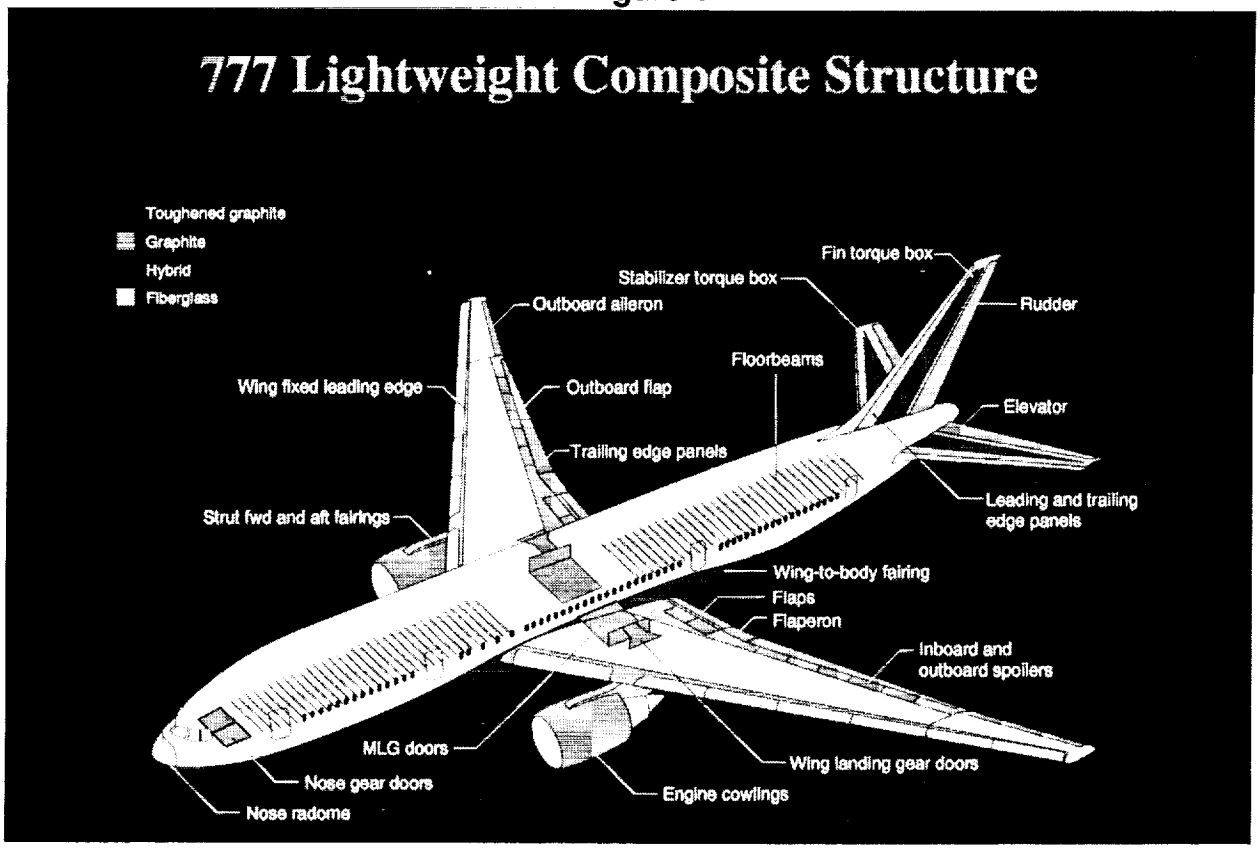

Figure 2

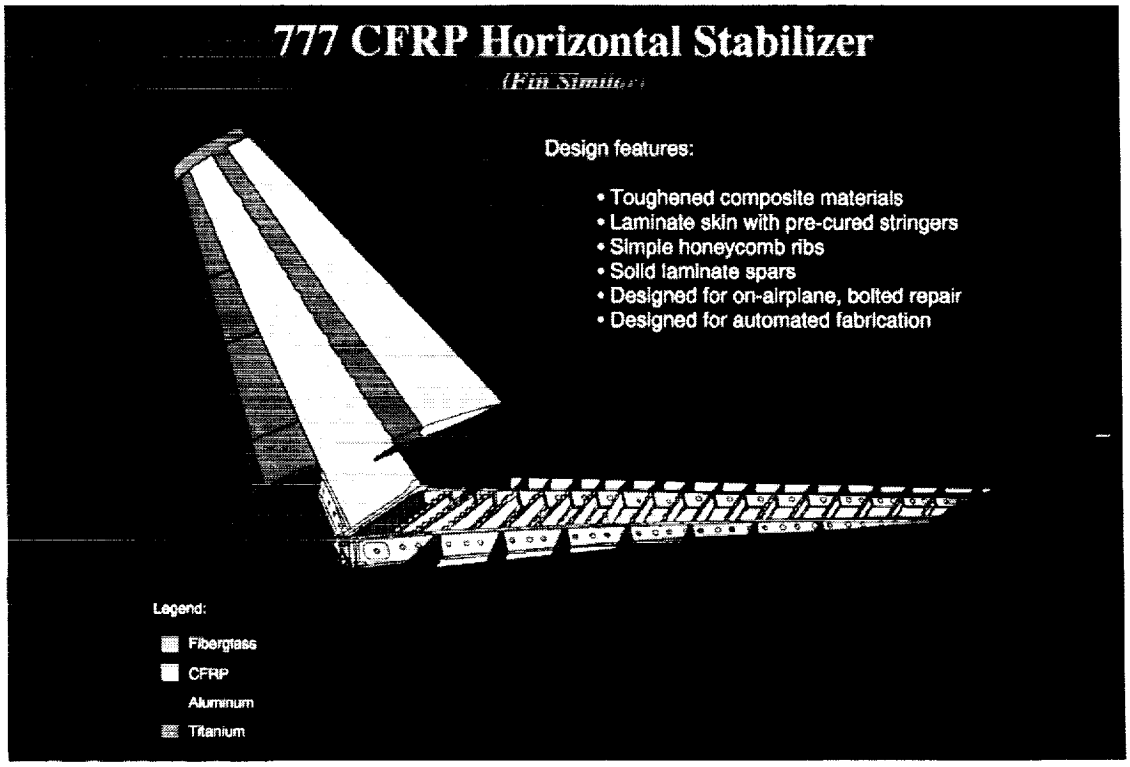

Figure 3

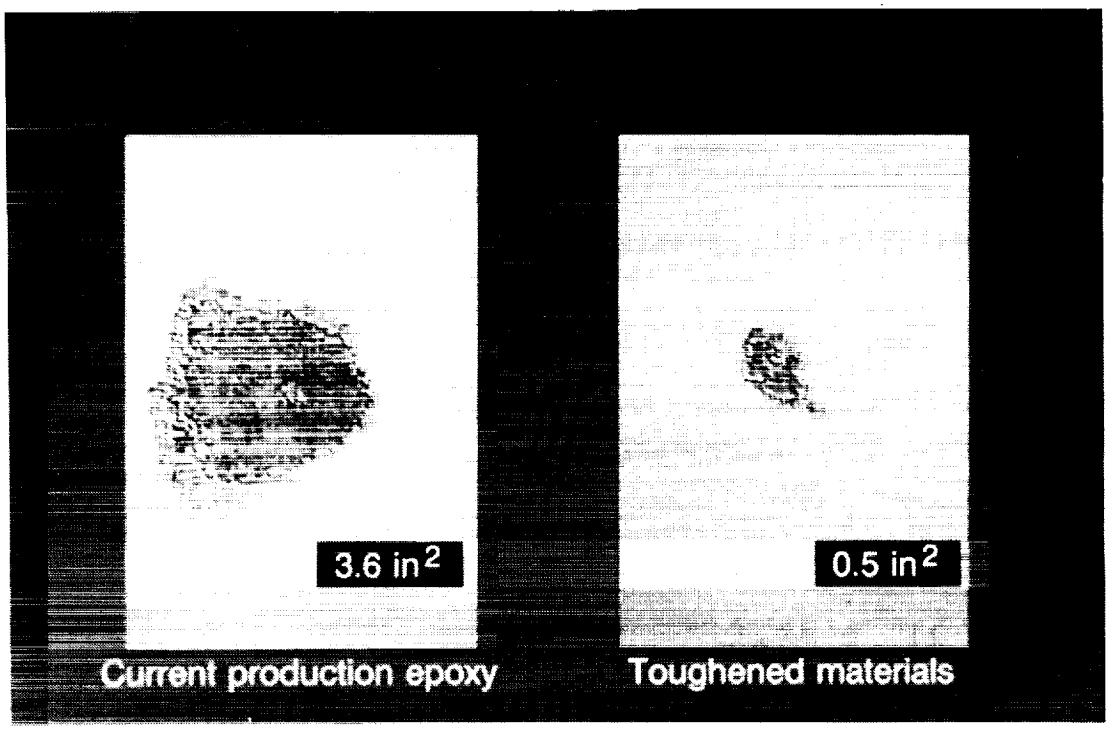

Figure 4

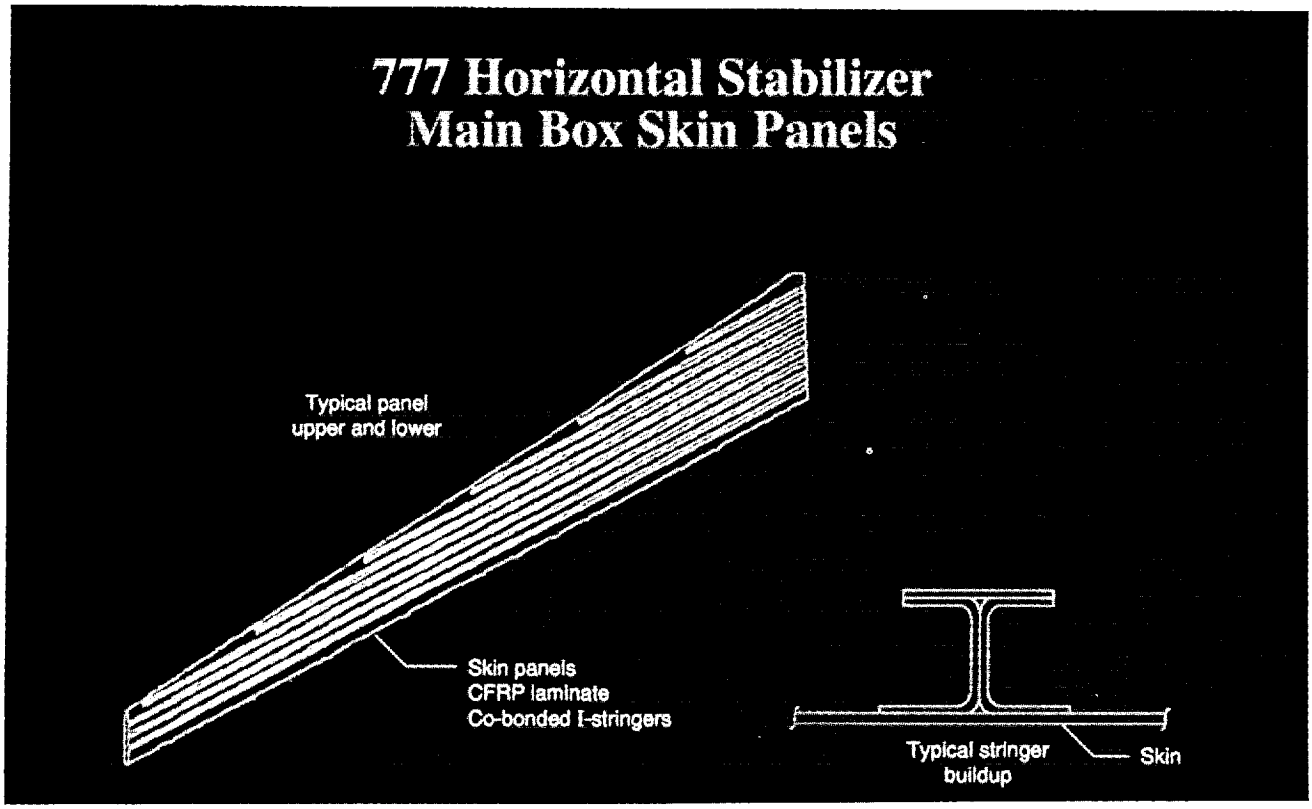

Figure 5

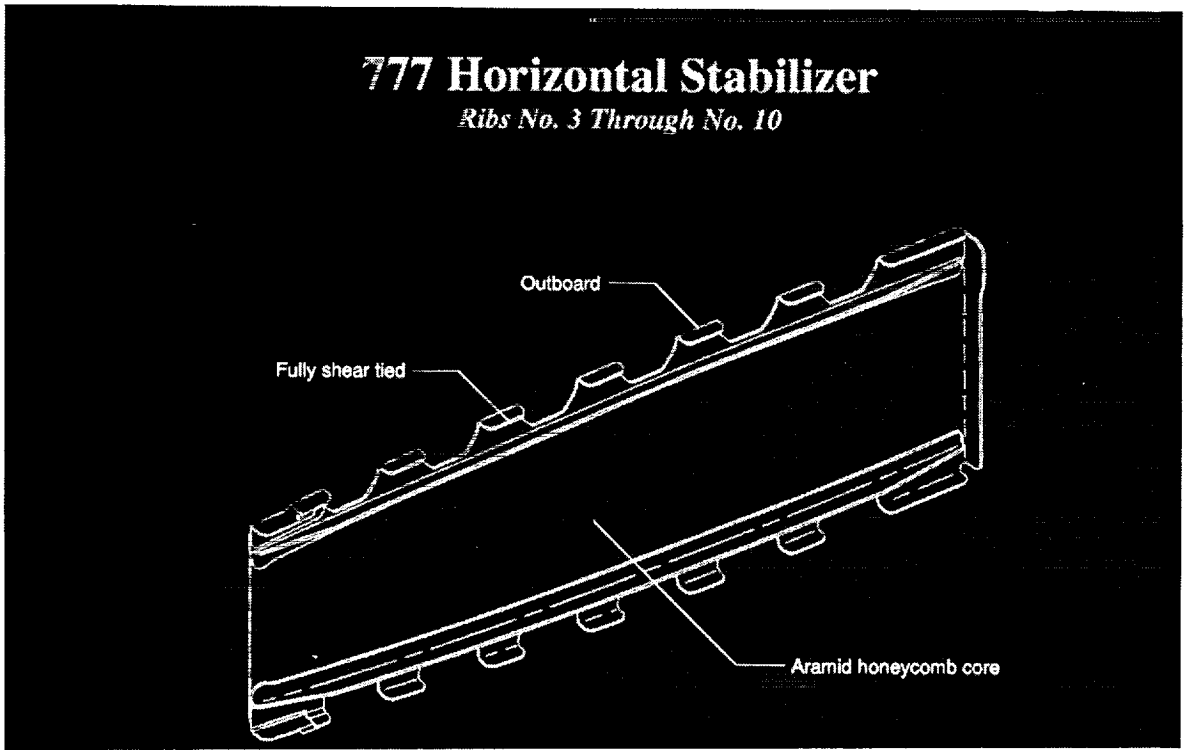

Figure 6

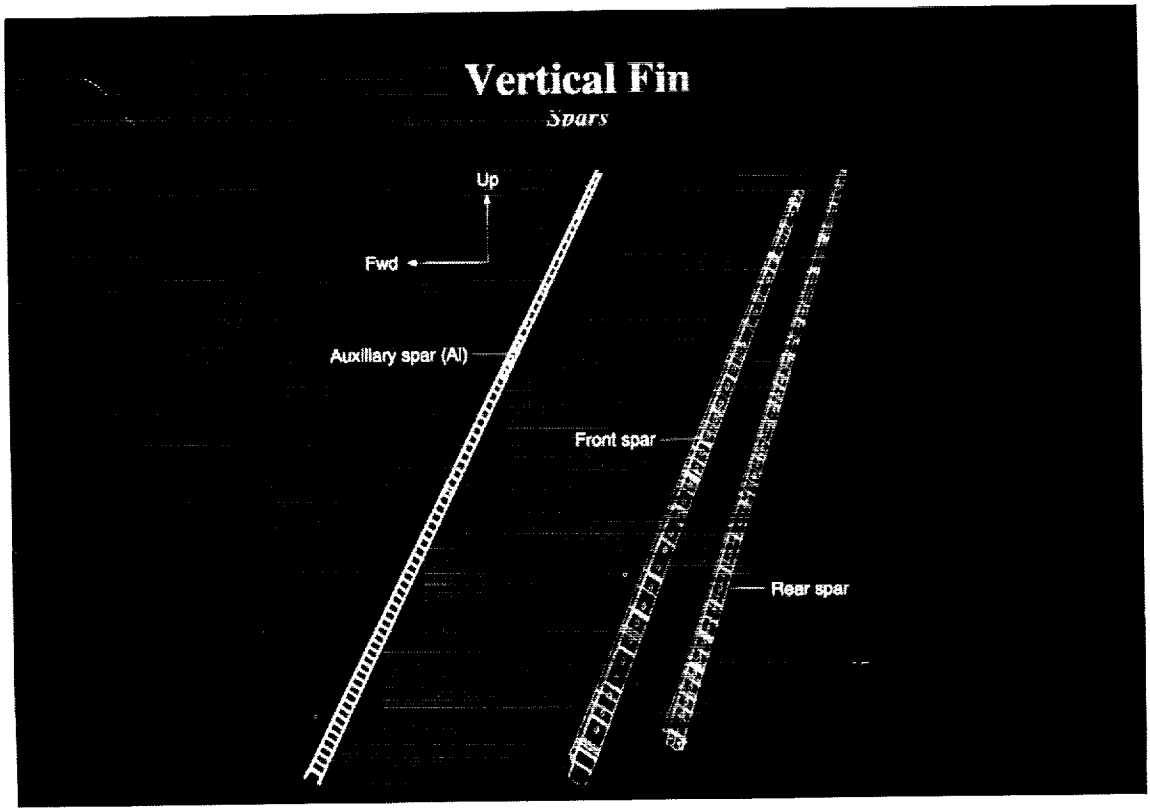

Figure 7

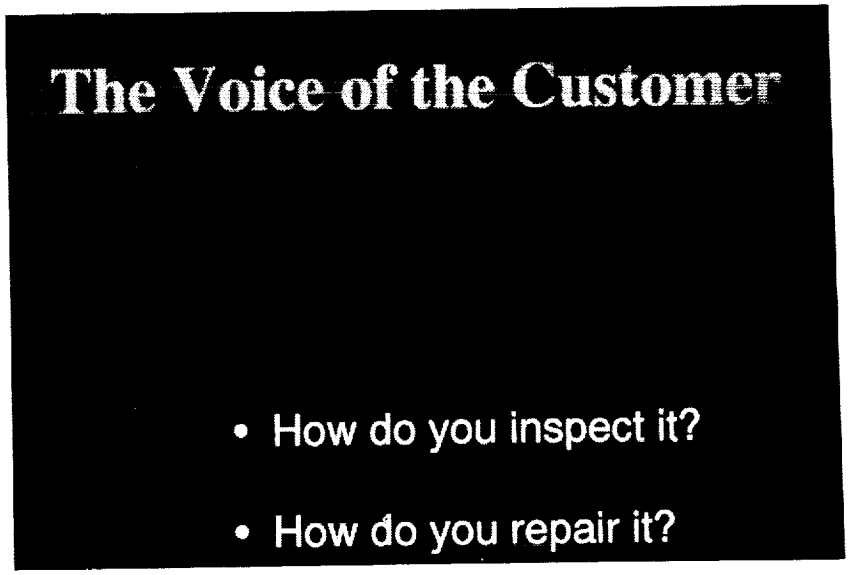

Figure 8

REPAIR

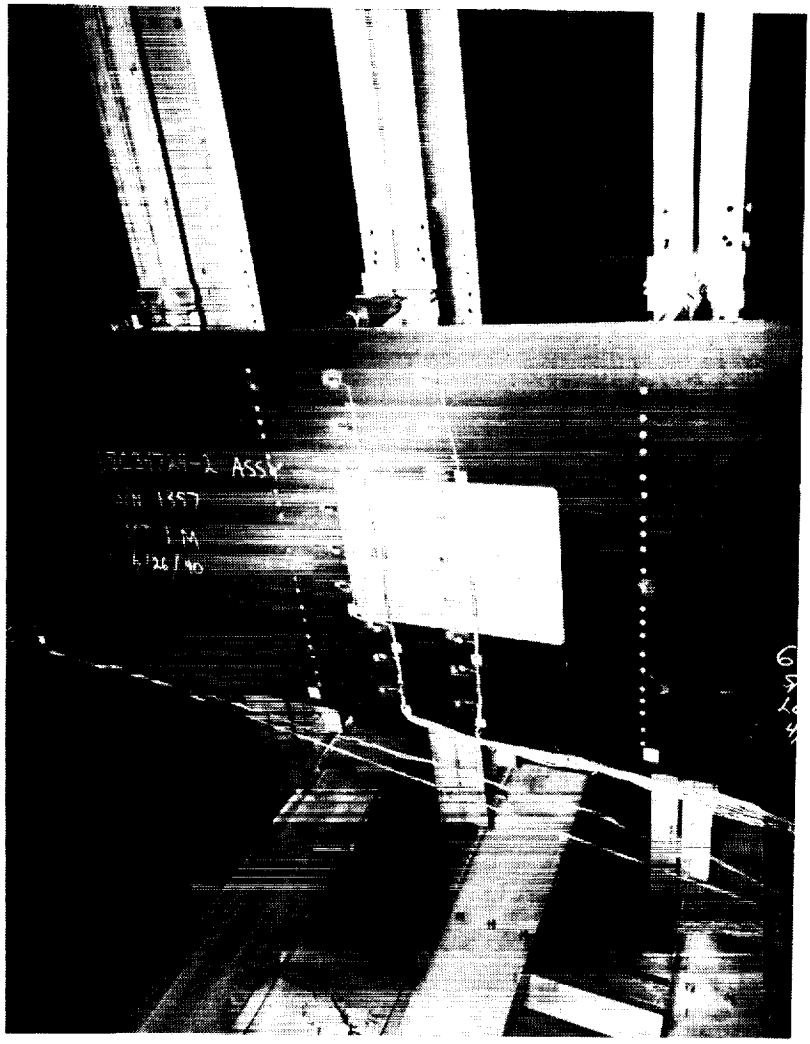

Figure 9

ORIGINAL PAGE
BLACK AND WHITE PHOTOGRAPH

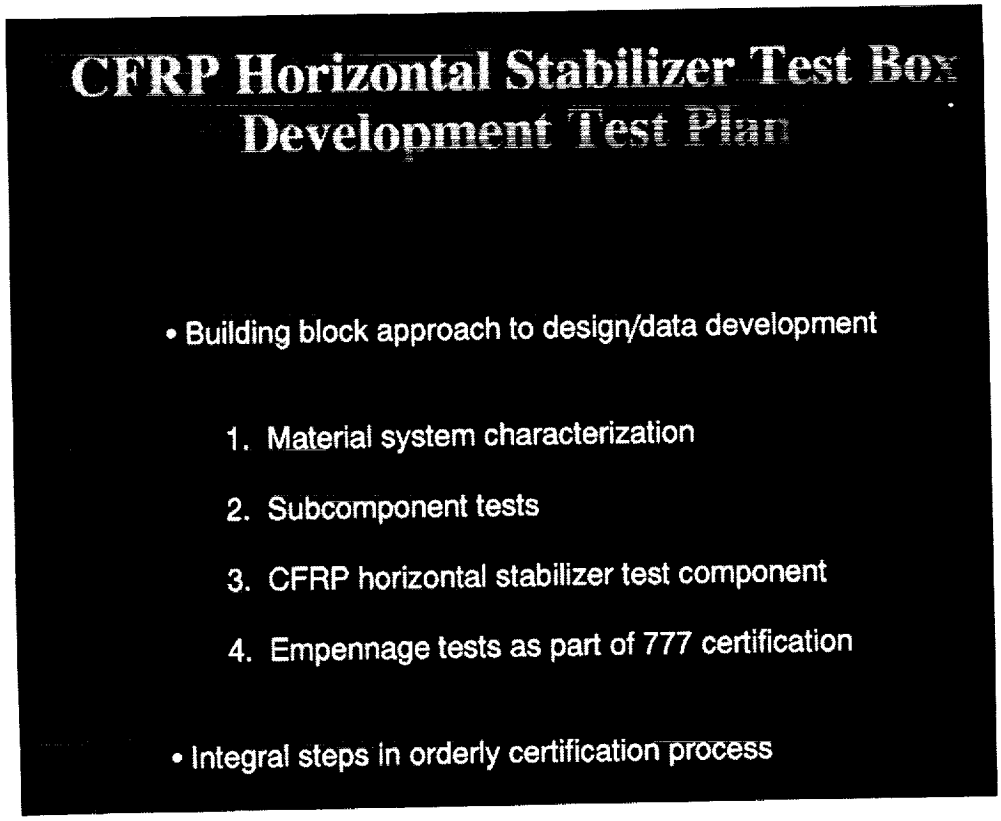
CFRP Horizontal Stabilizer Test Box
Development Test Plan
• Building block approach to design/data development
1. Material system characterization
2. Subcomponent tests
3. CFRP horizontal stabilizer test component
4. Empennage tests as part of 777 certification
• Integral steps in orderly certification process

Figure 10

T-TAIL CFRP HORIZONTAL STABILIZER TEST COMPONENT

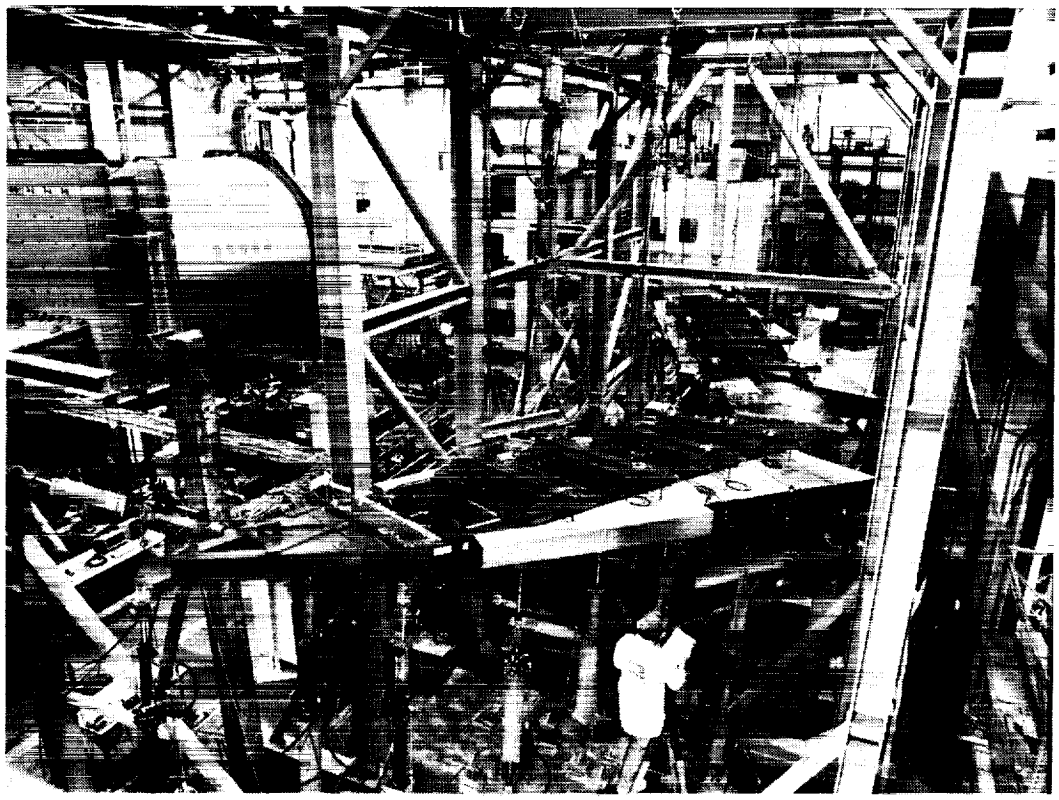

Figure 11

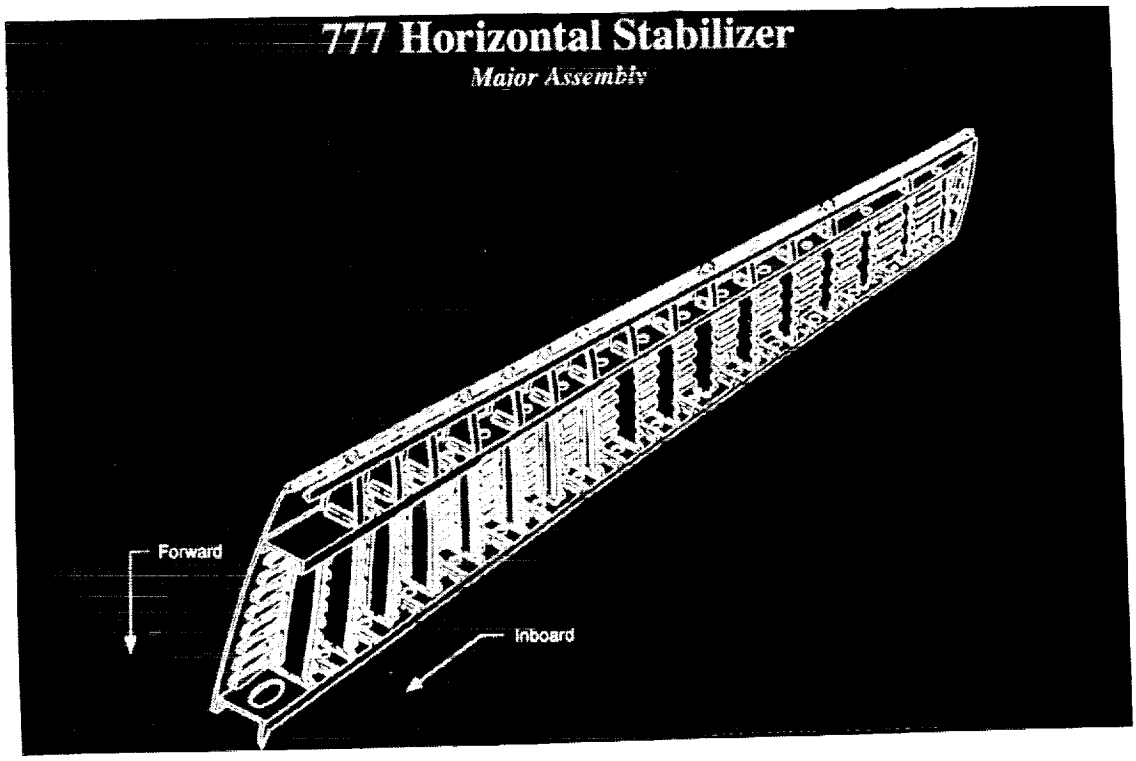

Figure 12

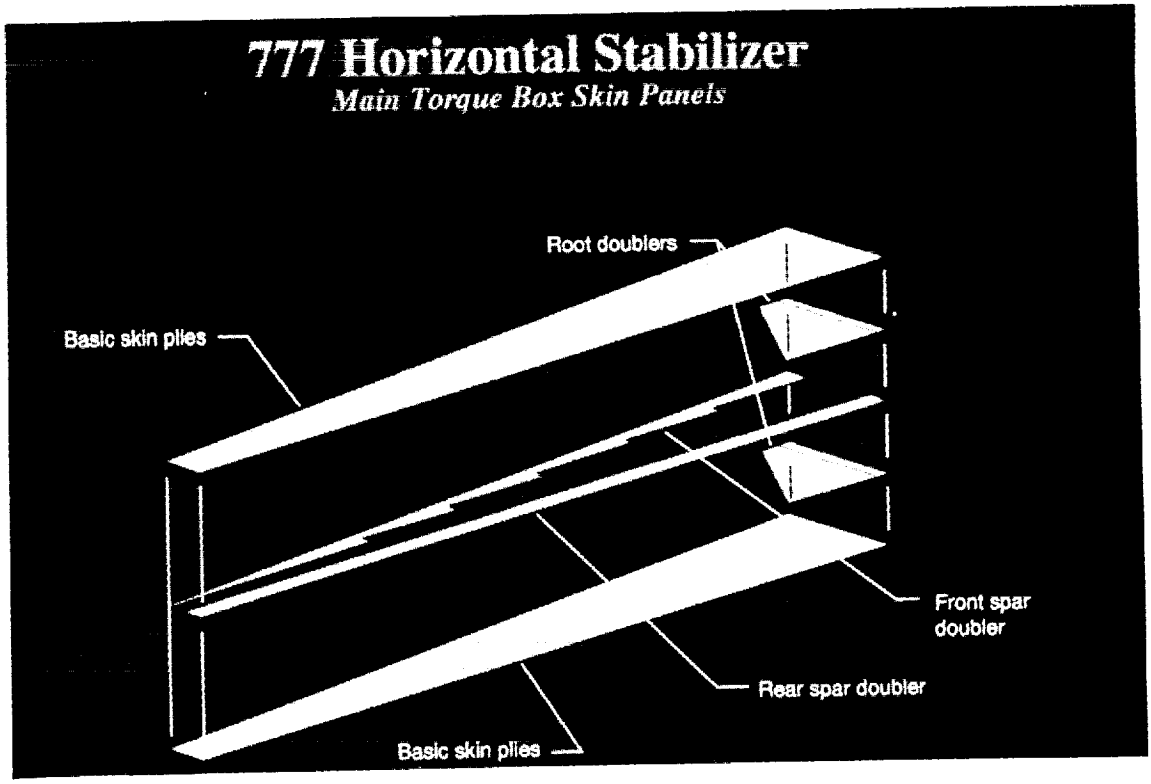

Figure 13

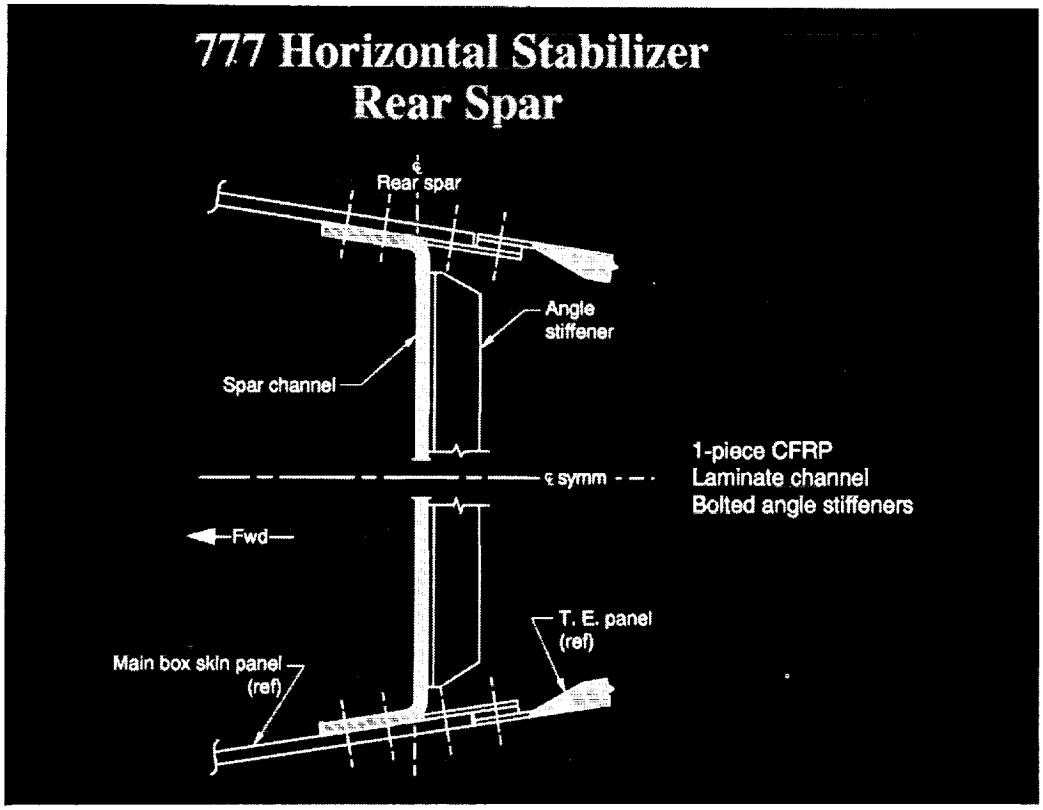
777 Horizontal Stabilizer
Rear Spar
℄ Rear spar
Angle stiffener
Spar channel
℄ symm
1-piece CFRP
Laminate channel
Bolted angle stiffeners
Fwd
T. E. panel (ref)
Main box skin panel (ref)

Figure 14

TOOLING

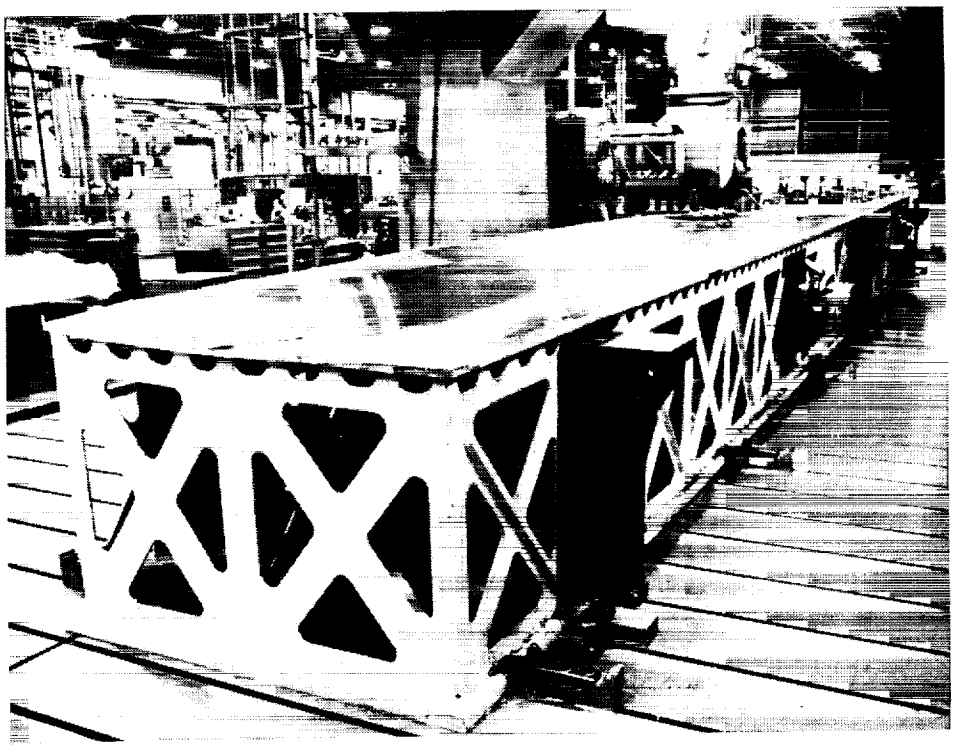

Figure 15

SKIN LAYUP

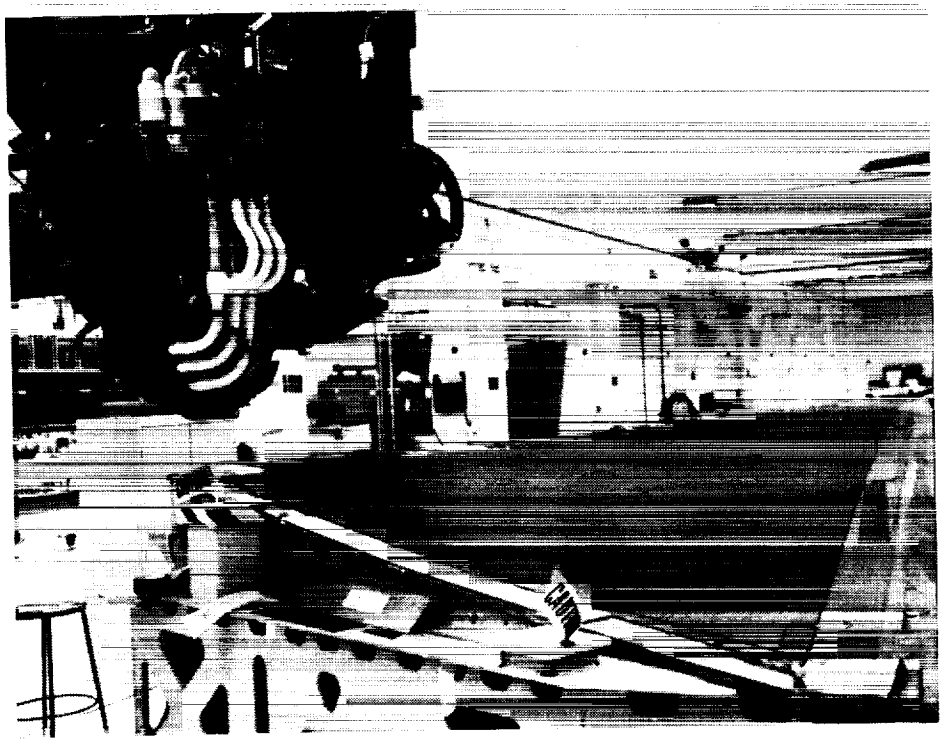

Figure 16

DEMONSTRATION PANEL

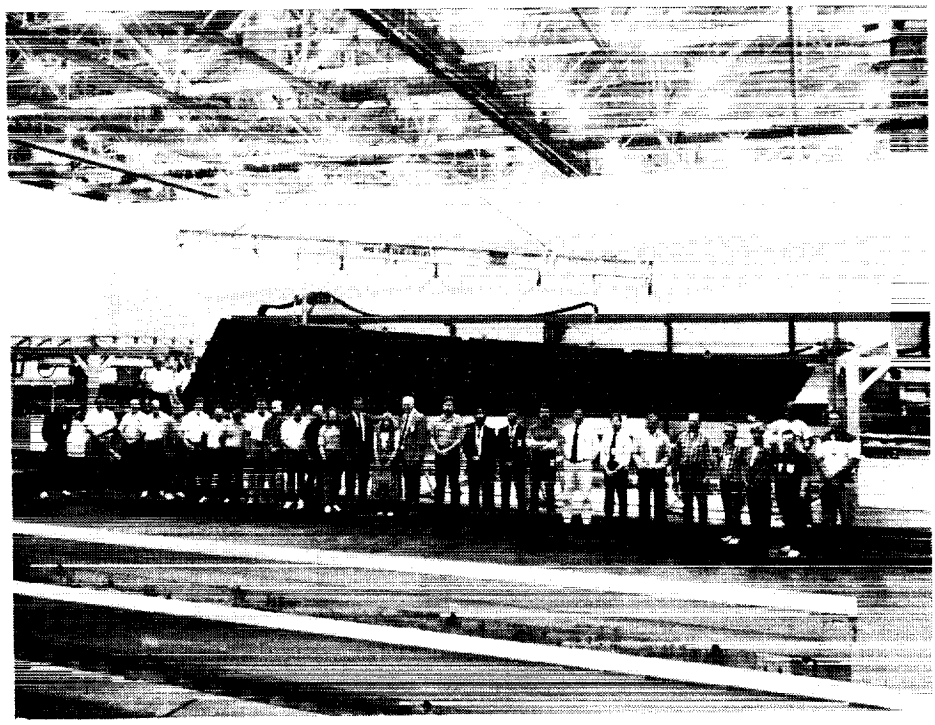

Figure 17

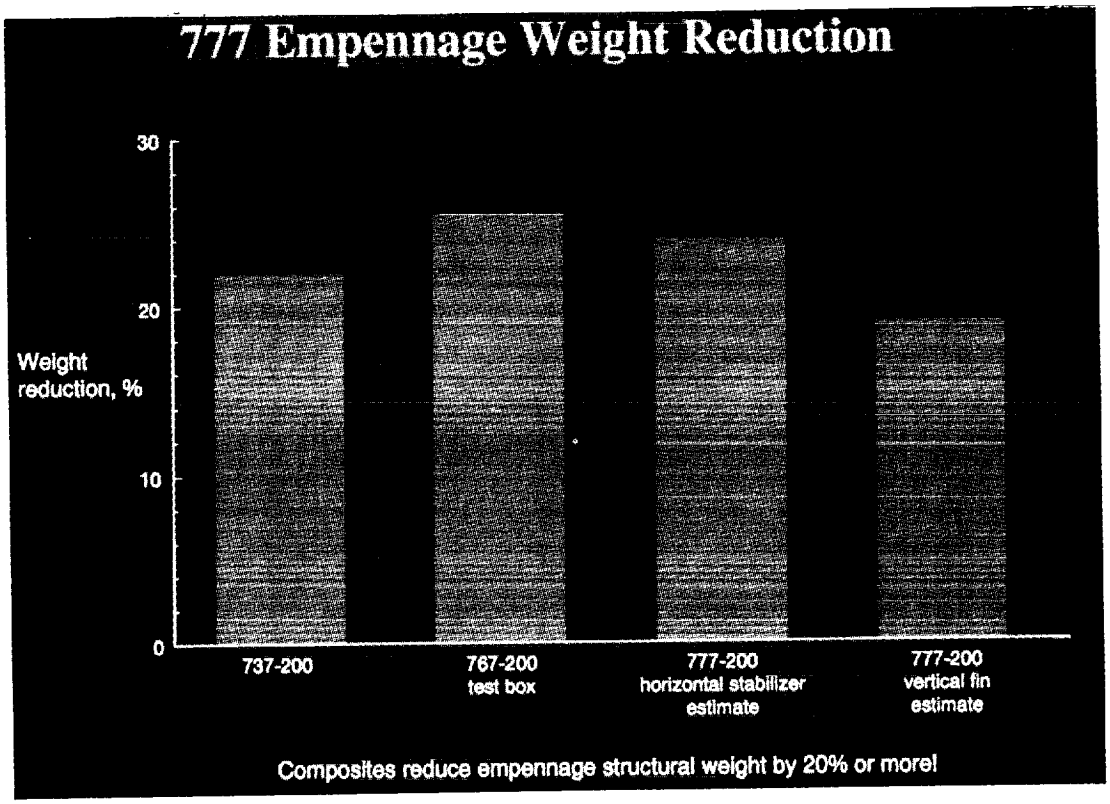

Figure 18

ORIGINAL PAGE
BLACK AND WHITE PHOTOGRAPH

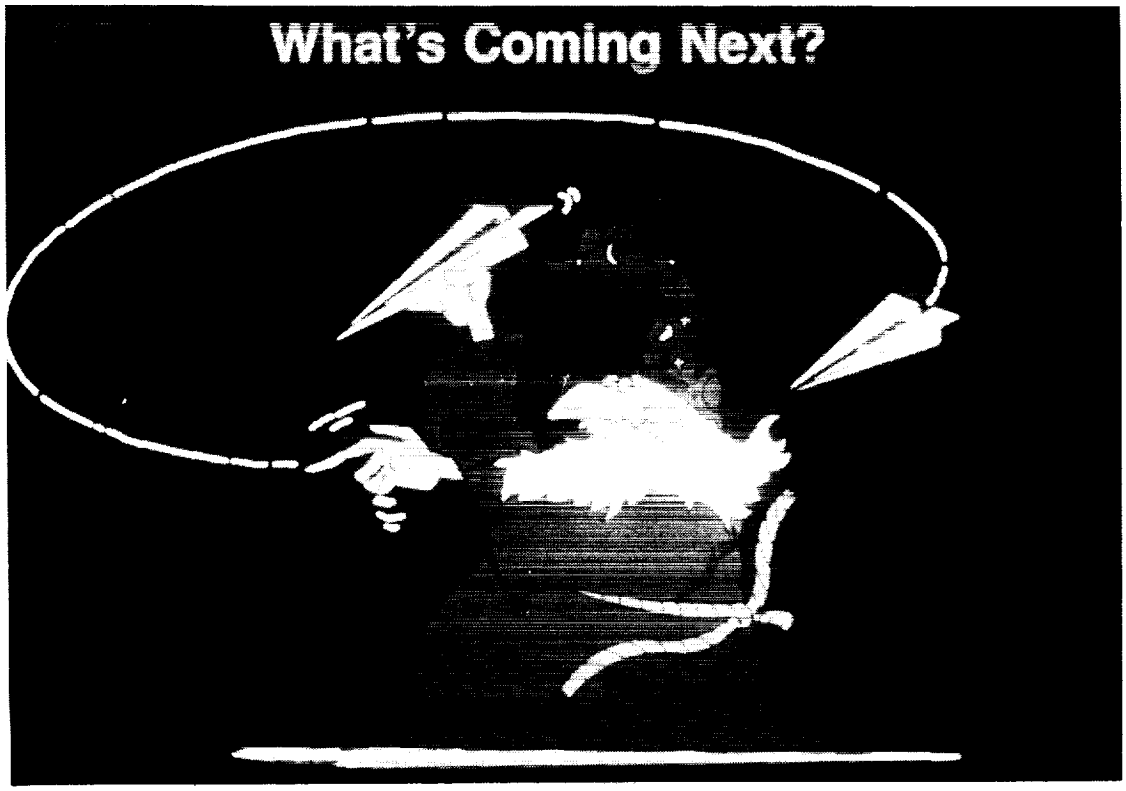

Figure 19

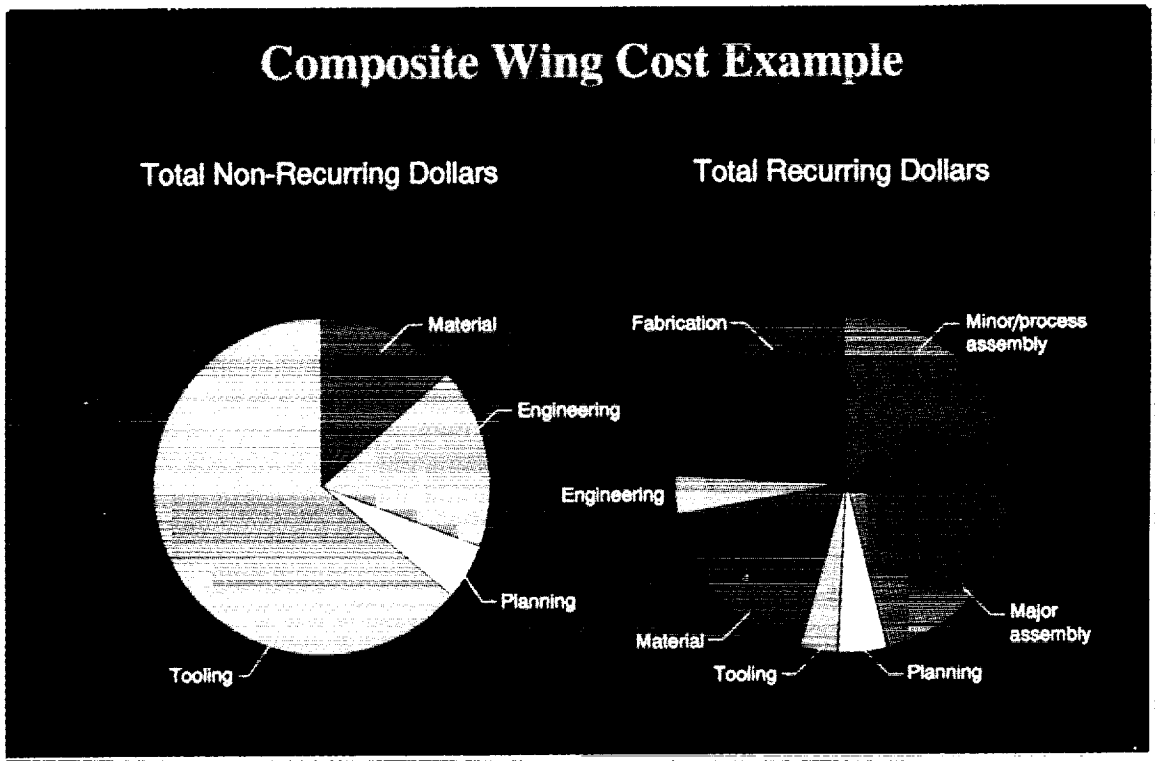

Figure 20

Wing Box Change Versus MTOW Growth Example

Model	MTOW (lb)	Wing Changes				
		Upper Skin	Lower Skin	Insper Ribs	Front Spar	Rear Spar
Basic	Base					
Increase MTOW	+6%					
Extended Range	+11%					
Stretch	+11%		A	A		A
Extended Range Stretch	+21%	A	A	B		B
Extended Range Basic	+23%	A	B	C		B
Extended Range Stretch	+27%	B	C	D	A	C

Figure 21

Summary

Composites have achieved:

- Weight reduction
- Corrosion resistance
- Durability

The remaining challenge:

Figure 22

OMIT

Session II

ADVANCED COMPOSITES TECHNOLOGY OVERVIEW

Session Chairman: John G. Davis, Jr.
NASA Langley Research Center

ADVANCED COMPOSITES TECHNOLOGY PROGRAM

John G. Davis, Jr.
Manager, Structures Technology Program Office
NASA Langley Research Center

INTRODUCTION

This paper provides a brief overview of the NASA Advanced Composites Technology (ACT) Program. Critical technology issues that must be addressed and solved to develop composite primary structures for transport aircraft are delineated. The program schedule and milestones are included. Work completed in the first 3 years of the program indicates the potential for achieving composite structures that weigh less and are cost effective relative to conventional aluminum structure. Selected technical accomplishments are noted. Readers who are seeking more in-depth technical information should study the other papers included in these proceedings.

Outline

- Schedule
- Fuselage Crown
- Fuselage Side
- Fuselage Keel
- Wing
- Summary

FUSELAGE CRITICAL TECHNOLOGY ISSUES

There are numerous technology issues that must be solved to achieve cost-effective primary structure. Most are specifically related to various locations in the fuselage. This attributed to the variation in loads and design requirements for each portion of the fuselage. Biaxial tension appears to be the dominate loading for crown panels, but the other four issues listed are very important. Side panels are subjected to longitudinal bending, hoop tension, and shear, particularly around windows and doors. The keel panel is subjected to a large concentrated load at the forward end that must be redistributed to a uniform load at the aft end.

Splices, frames, and stiffeners are integral parts of each quadrant of the fuselage and directly influence structural efficiency, response to load, fabrication, and assembly cost. The most challenging issue is cost-effective manufacturing. This includes fabrication of components, inspection, and assembly, which must be competitive with metal airframe structure for wide-spread application to be achieved.

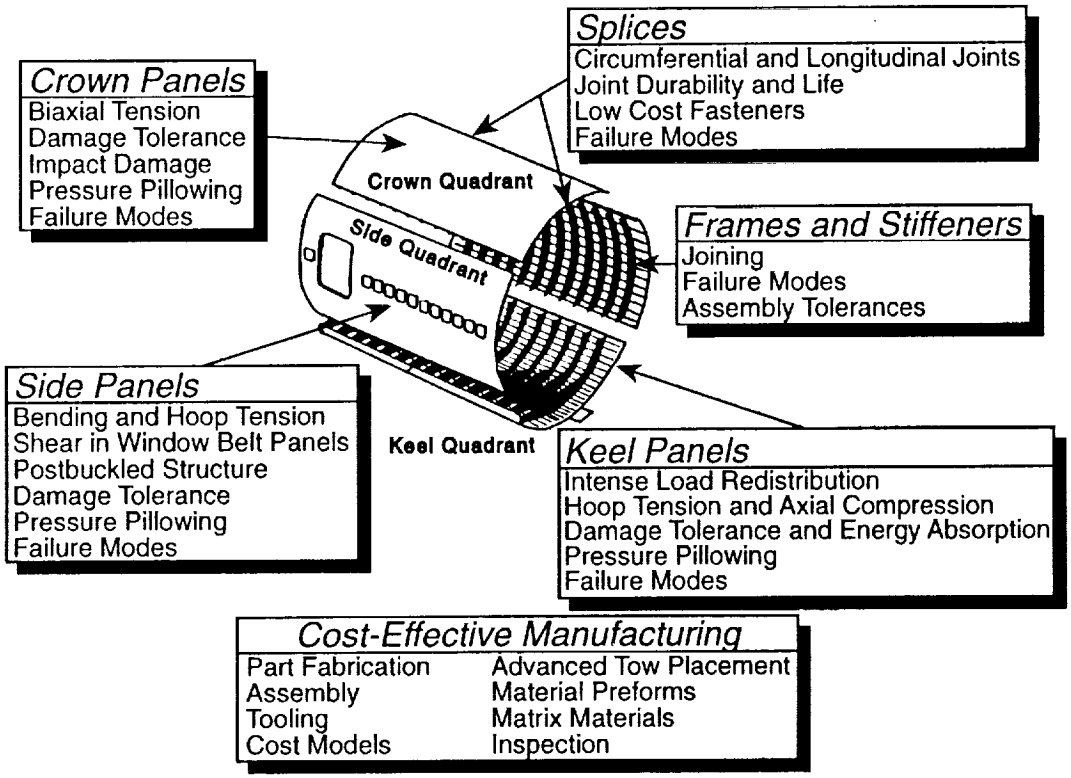

WING-BOX CRITICAL TECHNOLOGY ISSUES

Critical technology issues that must be solved to achieve wide-spread application of composite structures in transport wings are related to the major sub-components. There are nine major issues that influence design of the upper and lower cover panels. Damage tolerance has been a dominate design requirement for conventional two-dimensional reinforced composite panels and was the driving force for developing toughened resin matrix materials. Ribs and spars are integral parts of the wing box and significantly influence structural efficiency, response to load, fabrication, and assembly cost.

Cost-effective manufacturing is also the most challenging goal for composite wing structure. The seven specific technical issues listed are related to the dry fiber stitched resin film infusion approach and are a major focus in the ACT Program.

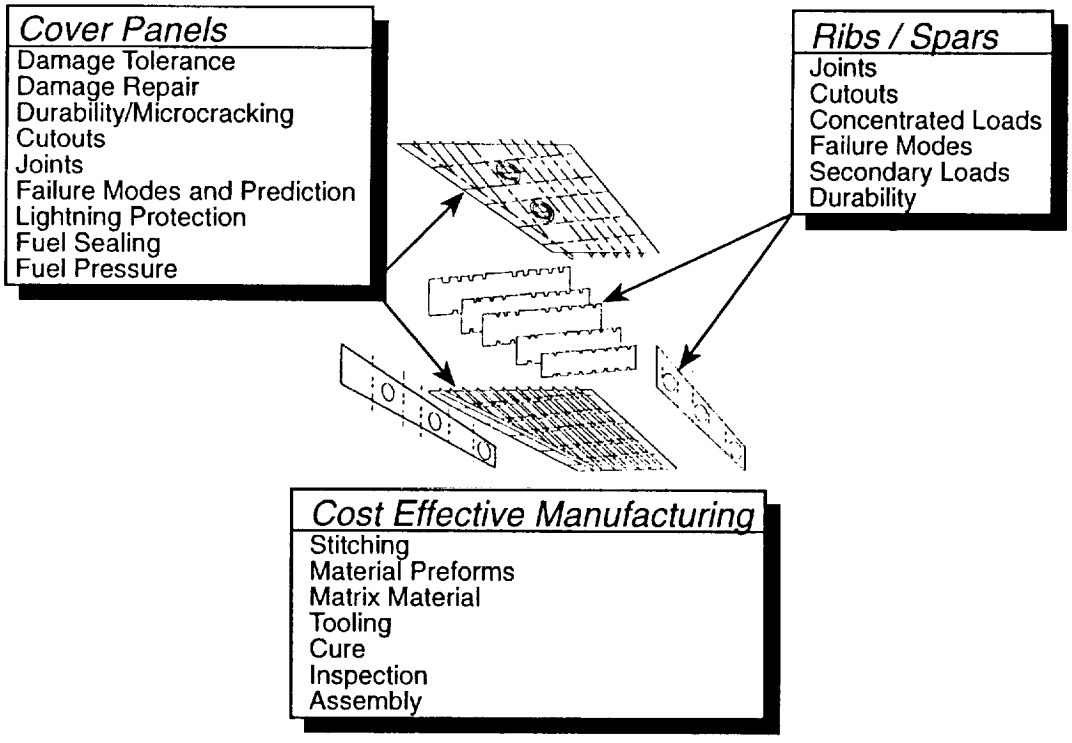

MASTER SCHEDULE

Overall work breakdown structure, major milestones, and schedule for the ACT Program are depicted. During the first 3 years, major progress has been achieved in identifying materials, material forms, fabrication methods, and structural concepts that offer the potential for cost-effective composite primary structures. Exploitation of automated processes, particularly advanced tow placement, textile preforms, and dry fiber through-the-thickness stitched approaches has been emphasized. Major effort has been focused on development of crown quadrant panels and wing cover panels. More results are included in the proceedings for these two program elements than for the remaining elements. Curved panels, 7-feet by 10-feet in size, representative of the crown region, have been fabricated. Small and large panels have been subjected to biaxial tensile loads and a pressure-box test fixture that will be used to assess damage tolerance of skin-stiffened crown panels has been fabricated.

A wing cover panel, 6-feet by 4-feet in size, has been fabricated and tested. Dry fiber stitched resin film infusion with an un-toughened resin was used to fabricate the panel. Prior to resin impregnation, stiffeners and shear clips were attached to the external skin by machine stitching. Test results on small three-stringer and larger six-stringer panels indicate outstanding damage tolerance relative to conventional two-dimensional reinforced composite panels. Delamination was significantly reduced in the stitched panels.

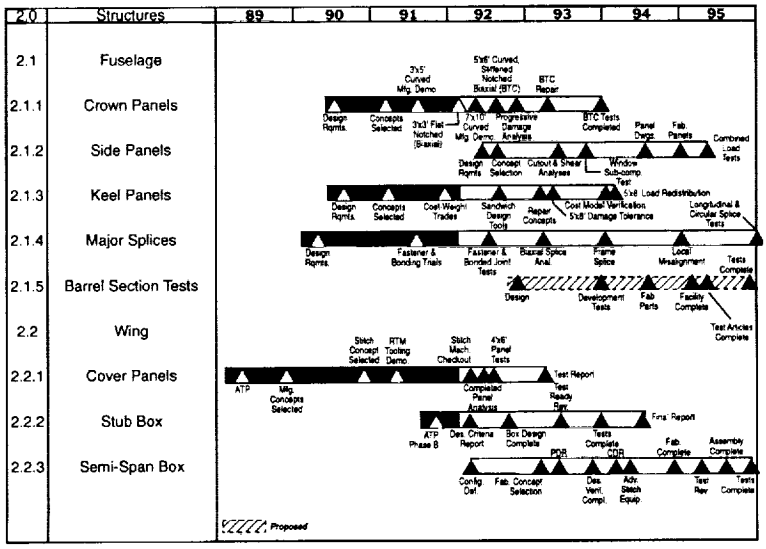

CROWN PANEL

Aluminum and composite crown quadrant panels are depicted. The aluminum design requires three panels to cover the quadrant; contains 24 stiffeners and 12,168 fasteners; and assembly is very labor intensive. The composite design requires only one panel, contains eleven stiffeners and no fasteners for attachment of frames, stiffeners or longitudinal splices within the crown quadrant. Reduction in part count and assembly labor are major contributors to the projected cost savings of 18 percent. In addition, the composite design is estimated to weigh 45 percent less than the aluminum design.

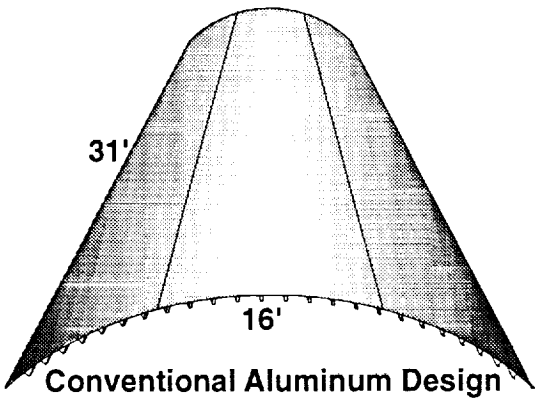

Conventional Aluminum Design

3 Separate Panels
24 Individual Stiffener Attachments
12,168 Fasteners
Labor Intensive Assembly

Boeing

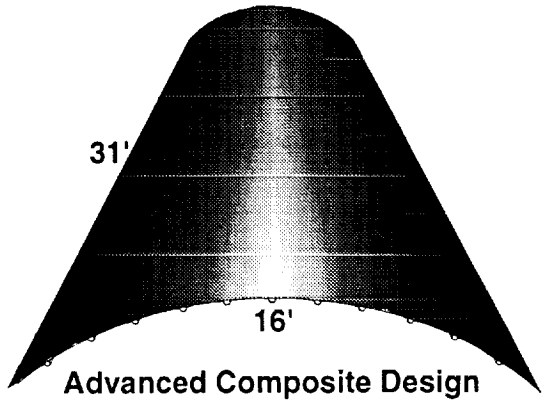

Advanced Composite Design

One Piece Co-cured Panel
11 Co-cured Stiffeners
No Fasteners
45% Weight & 18% Cost Savings

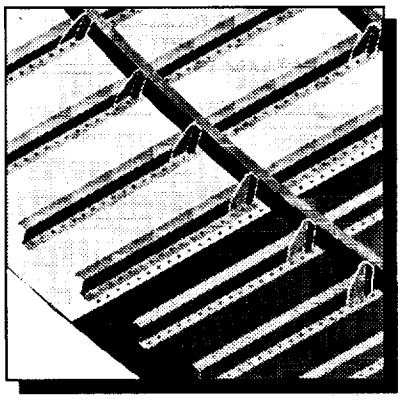

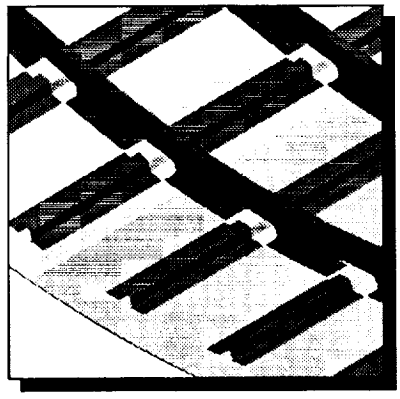

NEW TEST FACILITY APPLIES BIAXIAL STRESS FIELDS TO FLAT UNSTIFFENED NOTCHED COMPOSITE PANELS

A new testing machine shown in this figure was recently assembled at NASA Langley Research Center to apply biaxial stress fields to flat specimens. Specimens are 0.080-inch (11 to 13 plies) thick and 40-inch by 40-inch overall with an 18-inch-diameter test zone. Materials evaluated to date include AS4/938 graphite epoxy and hybrids of AS4/938 with various percentages of S2/938. Specimens were instrumented with 50 strain gages and included penetration-type damage simulated by a 2.5-inch notch at the center of the specimen. These tests are supplying much-needed data on composite skin panels with notches under biaxial stress fields to provide an understanding of composite behavior and damage tolerance.

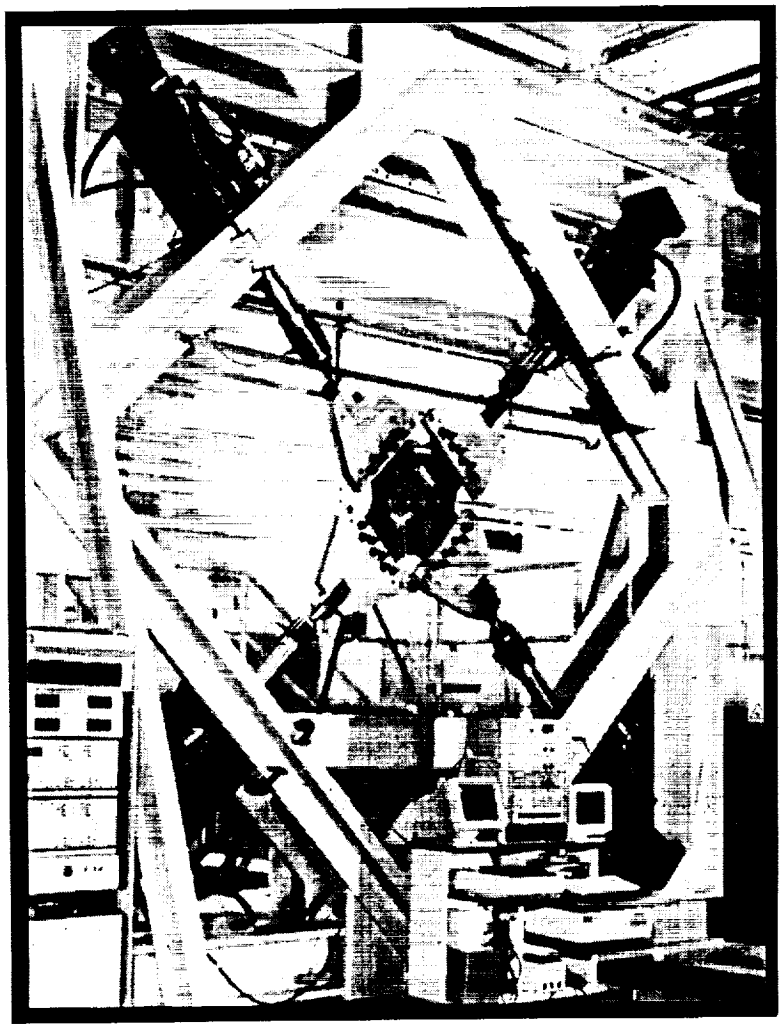

STRENGTHS OF BIAXIALLY LOADED PANELS

The behavior of flat unstiffened panels loaded in biaxial tension is shown on this chart. These panels were tested at NASA Langley Research Center with a 2-1/2-inch slit and two different load conditions. Predicted strengths of the biaxially loaded panels were made using a maximum strain criterion and test data from uniaxially loaded panels. The measured strengths compare fairly well with predicted values.

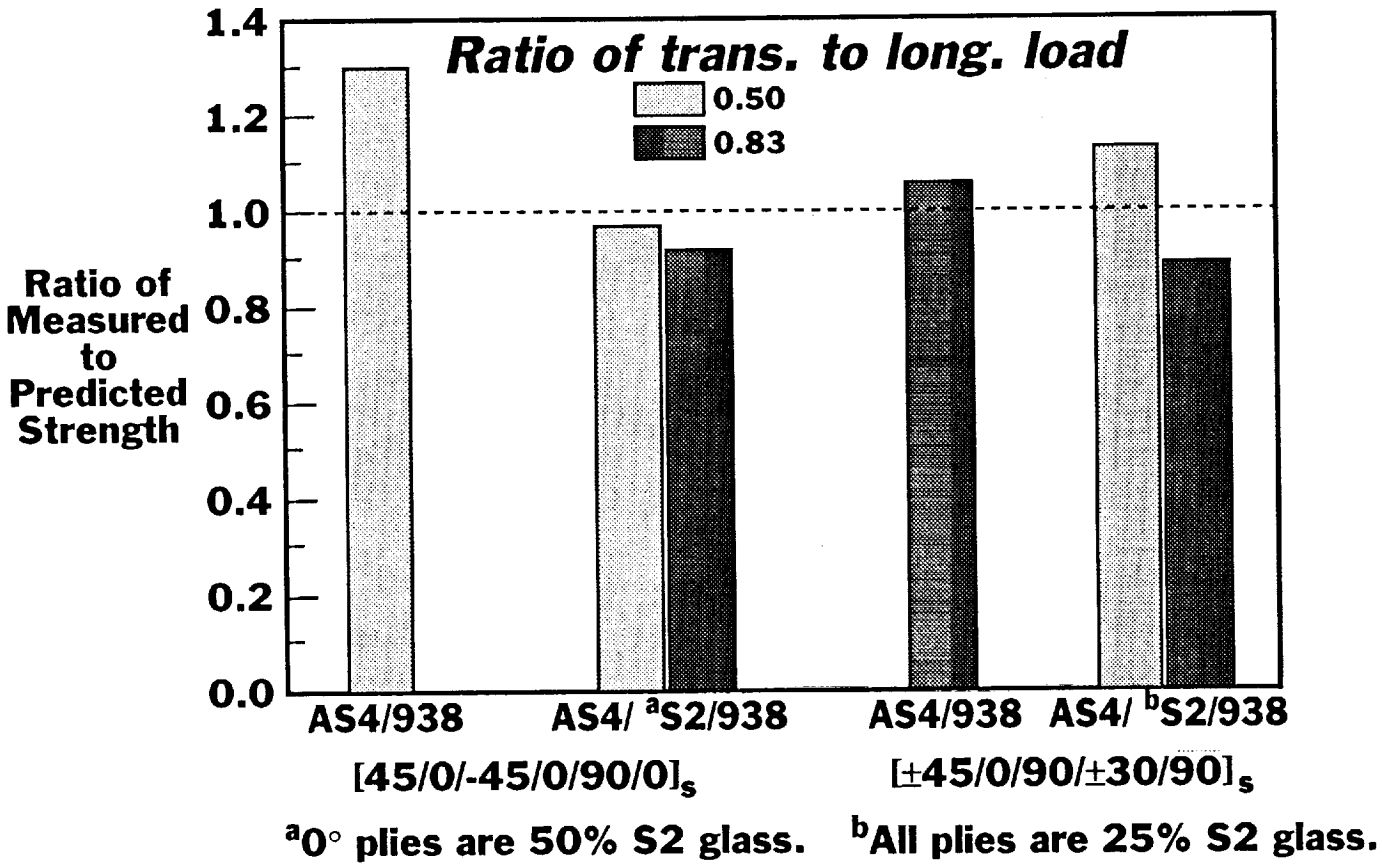

FIRST AXIAL DAMAGE TOLERANCE TEST OF COMPOSITE FUSELAGE CROWN DESIGN

The left-hand photograph shows a five-stringer panel mounted in the testing machine. The overall panel dimensions are: 150 inches in length; 60 inches in width. Prior to testing a 14-inch-long sawcut notch which severed the center stringer and skin was made in the panel to simulate skin penetration and stringer damage. The right-hand photograph shows the notch and strain gage locations near the notch. Failure occurred when the end load reached 284 kips. Average tensile stress and strain at failure were 47 ksi and 0.0051 in./in., respectively. The margin of safety was 23 percent for the axial damage tolerance requirement. Details of these and other tests will be provided in a subsequent paper.

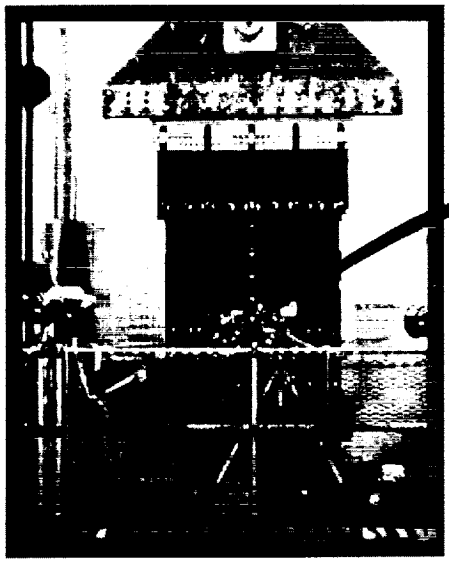

Test article mounted in testing machine

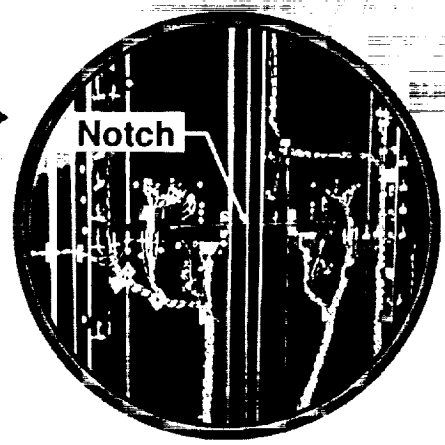

Closeup of test article showing notch and strain gauges

FUSELAGE CROWN PANEL STRUCTURE 7-FEET WIDE BY 10-FEET LONG FABRICATED WITH CO-CURED STIFFENERS

Boeing and Hercules are working jointly to develop fuselage crown structure concepts that incorporate advanced tow place skins, hot-drape formed hat stiffeners, and braided J-frames. The skin is laid on a mandrel with a computer-controlled process in which individual ribbon tows are precisely positioned with proper tension, direction, and contour. Stiffener preforms are hot-drape formed on separate male molds. Frames are braided, resin transfer molded, and cured separately. Assembly consists of placing the uncured tow-placed skin on an outer mold line caul plate, applying uncured stiffener preforms onto the skin, and positioning the cured frames over the skin and stiffeners with adhesive film between the frames and skin. The unitized skin-stiffener-frame combination is cured in a single autoclave cycle that cocures the skin and stiffeners while co-bonding the frames. The photo shows the 7-feet-wide by 10-feet-long sub-component size panel built at Hercules and representative of the section 46 fuselage crown panel for a Boeing wide-body airplane with a radius of curvature of 122 inches. The full-scale panel is 45-percent lighter and 18-percent less expensive to build than an equivalent metal crown panel. The composite crown concept also eliminates 12,200 fasteners compared to the metallic equivalent.

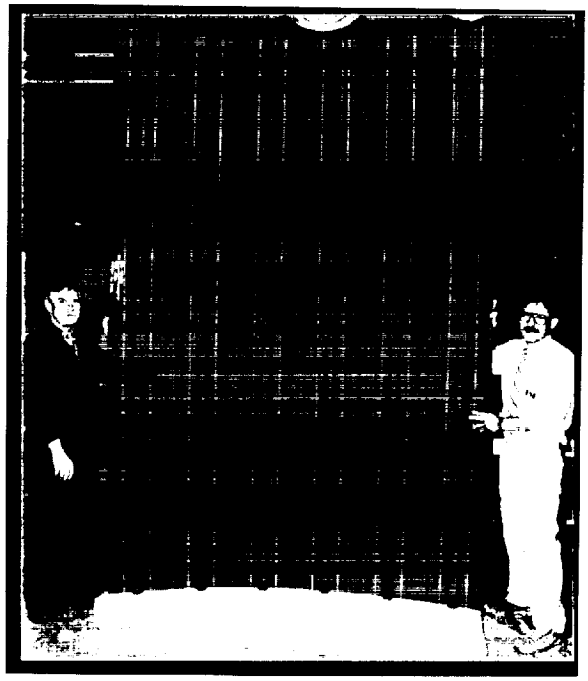

PRESSURE-BOX STRUCTURAL TEST FIXTURE

One of the important tasks in the ACT Program is to develop test fixtures that allow scale-up to large curved structures subjected to combined axial tension, hoop tension, and lateral pressure. The fixture shown in this photograph was designed and constructed at Boeing to test curved fuselage crown panels under combined loads. Maximum panel size is 72-inches long by 63-inches wide. The fixture can apply axial tension loads up to 12,000 lb/in. and a lateral pressure of 40 psi. After a series of initial tests at Boeing, the pressure box will be delivered to NASA Langley Research Center for use in the Benchmark Test Program.

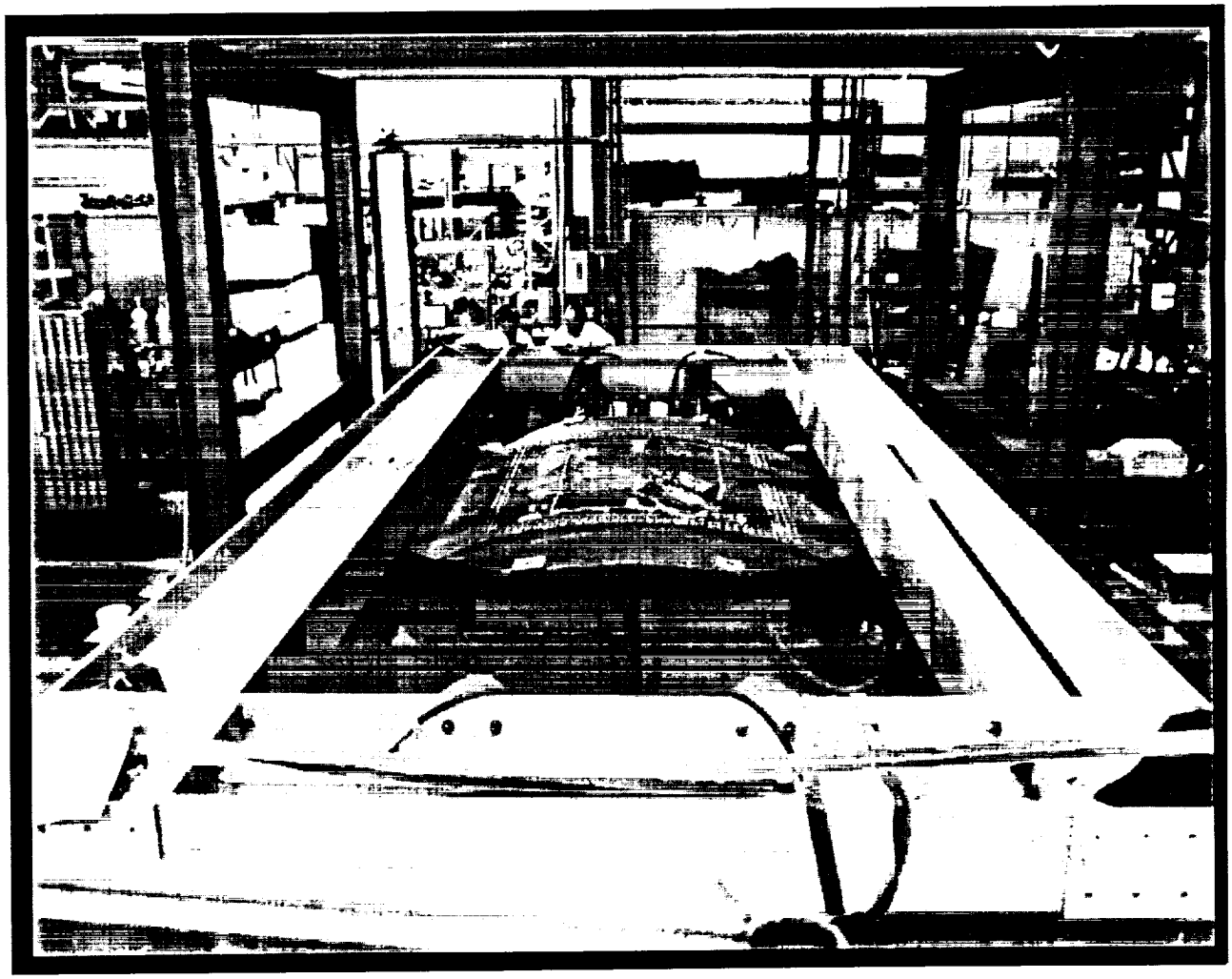

This figure shows the results for one of the cost model evaluations being developed at Boeing. The figure illustrates the strong relationship between cost and frame design details for a typical fuselage frame made by a braiding and resin transfer molding process. Cost for frame manufacture is reduced significantly for frame lengths of up to 100 inches. The figure includes the effect of process operations, amortizing tool set-up and batching of multiple frames per tool. Considerable details are provided on these cost studies in two subsequent papers.

Braid/RTM "J" Fuselage Frames

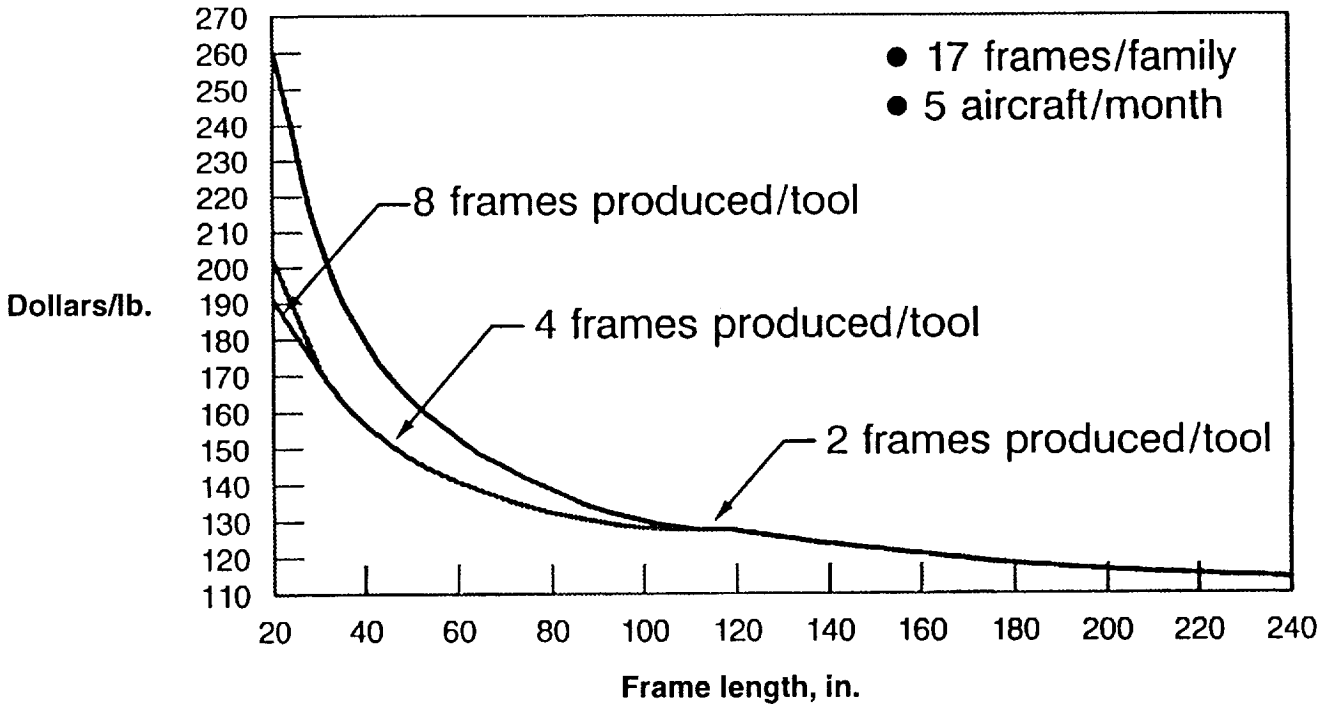

DESIGN/COST MODEL TRADE STUDIES FOR THE FUSELAGE CROWN QUADRANT

This figure illustrates the application of the Boeing COSTADE designers' cost model to local optimization of a composite crown panel. The designers' cost model is based on simplified preliminary analysis design tools for tension damage tolerance, panel warpage, and buckling assessment. For small stiffener spacings the postbuckled design was more cost and weight efficient than the design constrained to resist buckling. The area labeled "transition zone" in the figure illustrates where the critical design constraints are changing. Beyond the transition zone, the design is driven by axial damage tolerance and buckling constraints. For larger stiffener spacings, postbuckling is no longer an effective way to save weight since significant material must be added to satisfy minimum buckling constraints. The incentive for developing the COSTADE model is demonstrated in this chart where the time needed to generate the analysis trends for various load cases, design criteria with cost considerations would be cumbersome if done by hand.

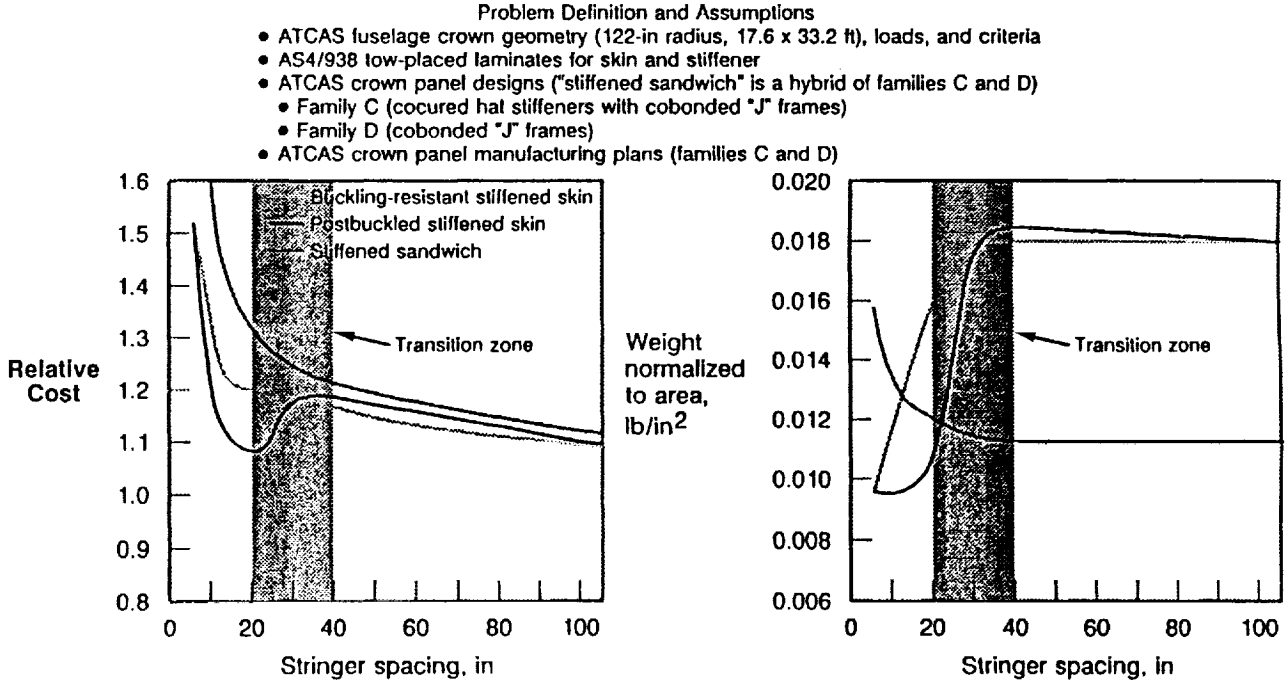

Note that relative trends in the graph are dependent on the body-bending loads.

GLOBAL OPTIMIZED CROWN MANUFACTURING PLANS TO MINIMIZE ASSEMBLY COST

This chart illustrates the manufacturing detail that Boeing is evaluating to obtain cost estimates for composites versus metallic structure. The figure shows fastening approaches for longitudinal and circumferential splices of larger crown panels and frame splice close-out fastening for final assembly. The assembly cost contributors are shown in the bar chart as a percentage of total cost.

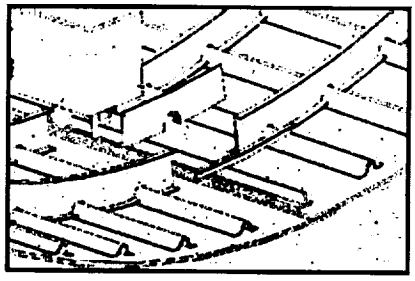

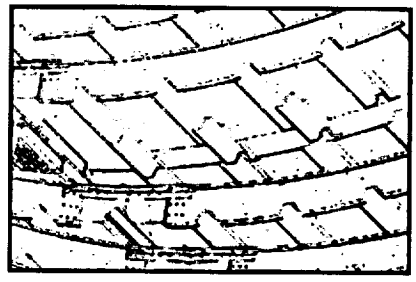

- Globally optimized family C
  - Includes major splices
  - Assumes 300 shipsets

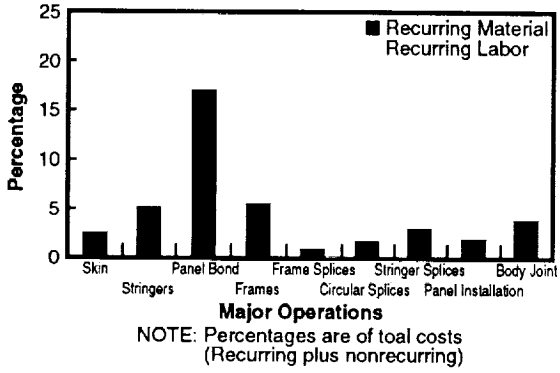

NOTE: Percentages are of toal costs (Recurring plus nonrecurring)

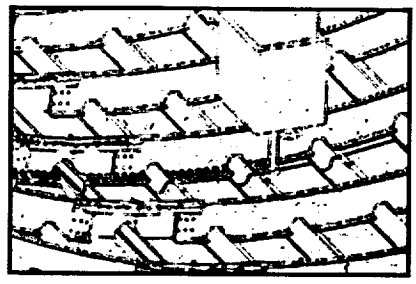

TAPERED KEEL PANEL

The figure shows a manufacturing demonstration panel for one concept Boeing is evaluating for keel structure. The panel has a 42-ply-thick laminate with several ply drop-offs to evaluate the effectiveness of the Hercules tow placement process in dropping plys without stopping the machine. This approach simulates the manufacturing process needed to make a single autoclave cure panel that transitions the high loads from the wing-body carry-through section to the more lightly loaded aft cargo area. Details of the Boeing baseline keel design are discussed in a subsequent paper.

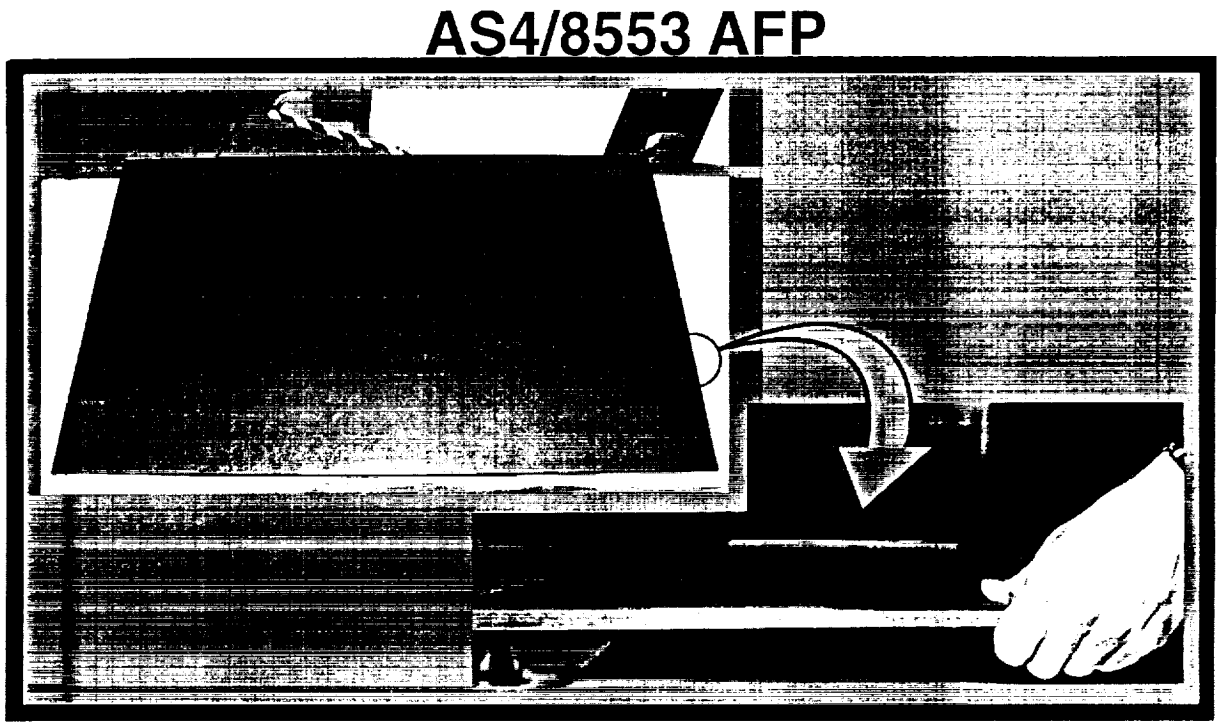

WINDOW-BELT REINFORCEMENT

The window-belt area offers the greatest potential to take advantage of the benefits offered by textile composites. The loading in the window-belt area requires reinforcement around the windows and adequate strength to transfer loads through the skin, the frames, and the stringers. Textile composites offer the best means of providing the needed strength and stiffness in this area. Lockheed is considering several textile composite window-belt concepts in their design trade studies. The concepts include 2D and 3D braiding of window-belt preforms to be attached to ATP skins as shown in the sketch. Their frames and preforms will be cocured or mechanically attached. Final details of these designs, and selection of the preferred concept, are pending the completion of detailed design studies and tests.

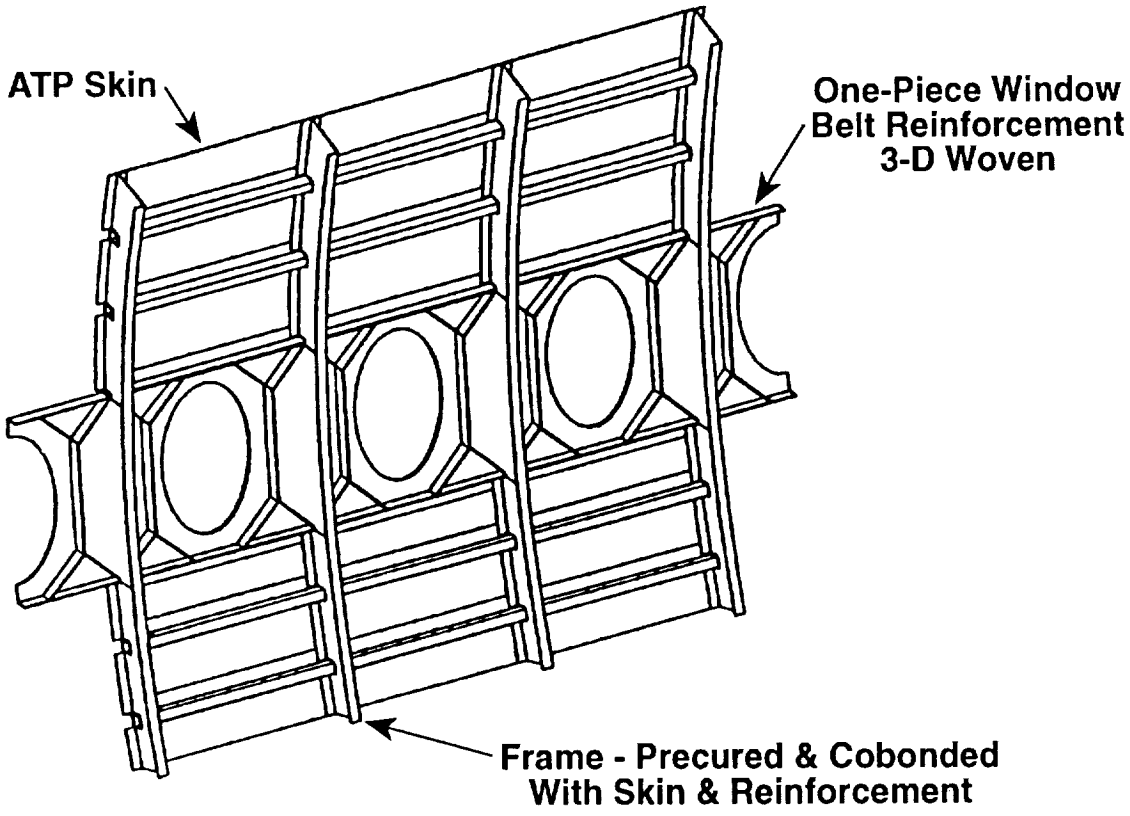

NEW POWDER-COATING TECHNIQUE DEVELOPED AT LANGLEY

New processing techniques that offer potential for producing lower price material are being investigated. One of these processes is dry powder coating of fiber tows, and this sketch shows an approach being worked at Langley. This technique differs from the conventional cloud chamber method in that the powder is dropped directly onto the spread tow by a curtain, or waterfall, feeder. The tow in the chart is shown starting at the supply spool, running through the curtain feeder and the oven, then reversing and running back through another feeder and the oven again. The new system features a simple gravity feed, faster run speeds than the old cloud chamber method, reduced dust (fugitive powder) and improved safety for the operator, better control over resin content, and adaptability to multi-tow production. For multiple tows, the curtain is simply made wider to handle up to 40 or more tows instead of one.

Powder Curtain Towpregging

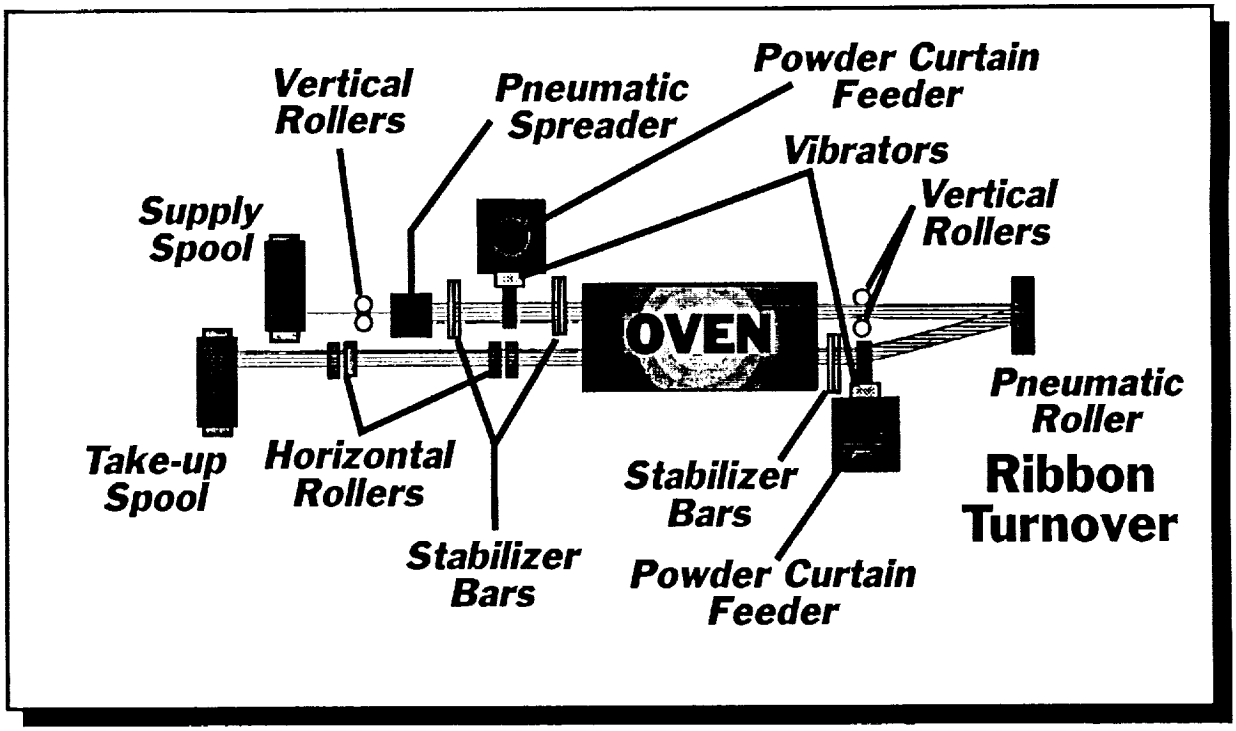

Double-Back Powder Coating Schematic (Top View)

CROSS-STIFFENED MEMBER

One of the advantages offered by textile composites is continuous through-the-thickness fiber reinforcement. For stiffeners that run perpendicular to each other, this could be used to make composite structure with superior strength over conventional laminated or bonded components. The panel preform shown in the figure is a proof-of-concept part woven of IM7 graphite fibers and is to be fabricated using RTM. The fibers in the stiffeners are continuous through the intersection, and the flanges of the stiffeners have continuous through-the-thickness fibers at the flange attachments to the skin. Such a fiber-strengthened arrangement is possible with innovative weaving techniques. Although test articles have been made, there are some obstacles to be addressed in scaling the process up to production sizes and quantities.

Woven Stitched IM7

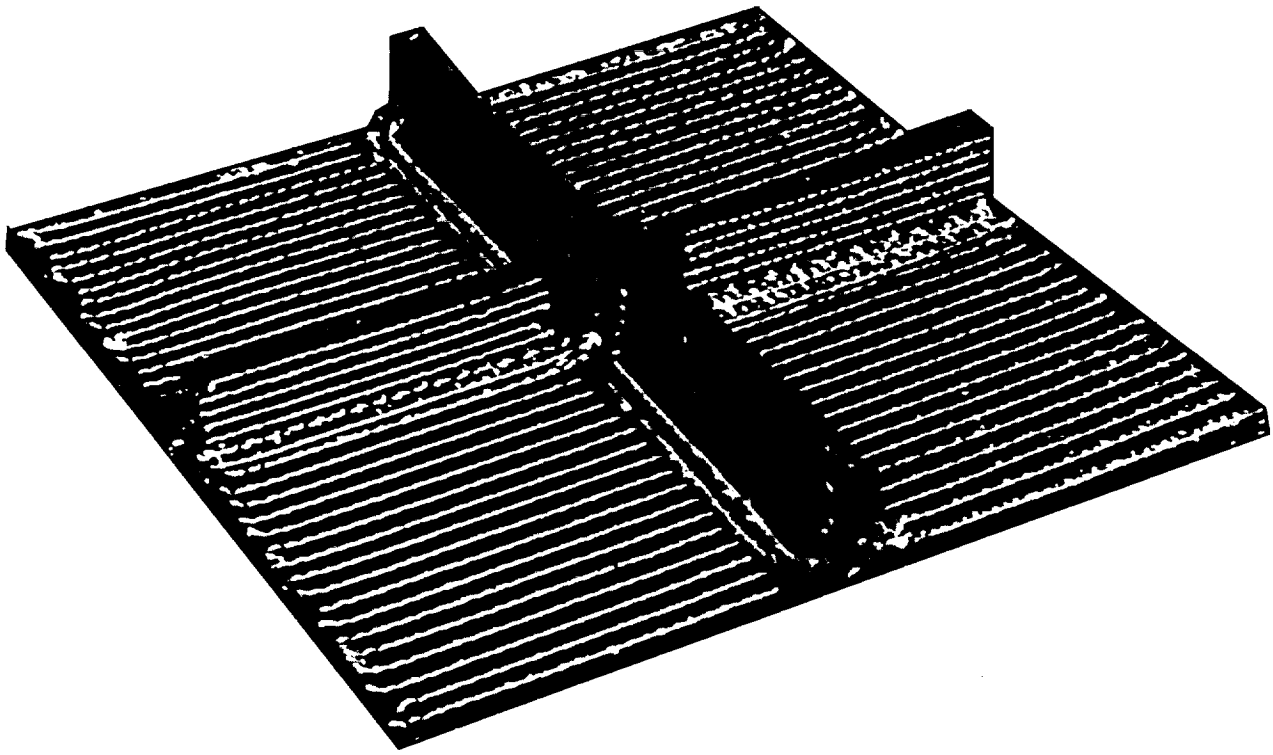

STRENGTH PREDICTIONS FOR BRAIDS USING DIAGONAL BRICK MODEL (TECA)

Part of the effort in textile composites has been developing analysis methods to predict the strengths of various braided preforms. Shown in the figure are measured tension and compression strengths plotted for four braided configurations. The first type of braid has 40-percent axial tows, and the remainder are braided yarns. The second type has all braided yarns. Each of these two types is made using two braiding processes: 2D process with multiple layers of triaxial patterns; and 3D process which yields a single integrated layer. Strength predictions of these four configurations were made using a diagonal brick model or three-dimensional truss model. The predicted strengths were good compared with tests. The braids with axial tows typically show higher strength. The 2D-layered braids typically show higher strengths than the corresponding 3D single-layer braids.

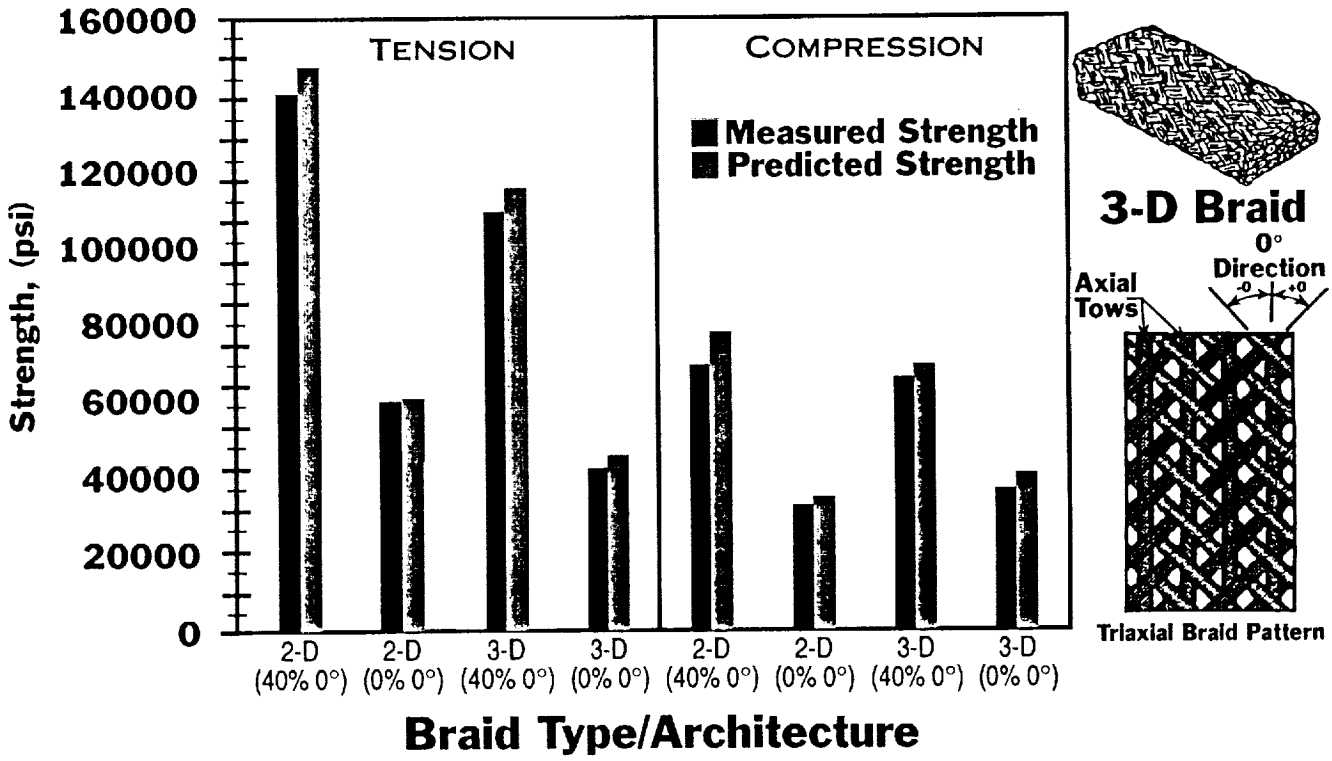

PREDICTIONS OF MODULII FOR 2D BRAIDS

Part of the effort in textile composites has been developing analysis methods to predict the modulus of braided materials. Shown in the figure are measured modulii for tension and compression in various 2D braids. All of the braids tested contained multiple layers of triaxial braid and had essentially straight yarns in the longitudinal direction. All of the braids had equal fiber volume fractions. Some braids used 6K yarn and some 12K yarn, and all of the braids were made over cylindrical mandrels with differing diameters. Both longitudinal and transverse modulii were measured, and the experimental results were essentially the same across the board. The predictions were made with three distinct theories: diagonal brick model (three-dimensional truss); composite lamination theory corrected for undulating braided yarns; and finite-element analysis that discretized yarn and matrix. All of the theories yield approximately the same predicted results. Except for the one transverse case, the predictions were very good compared to experiment.

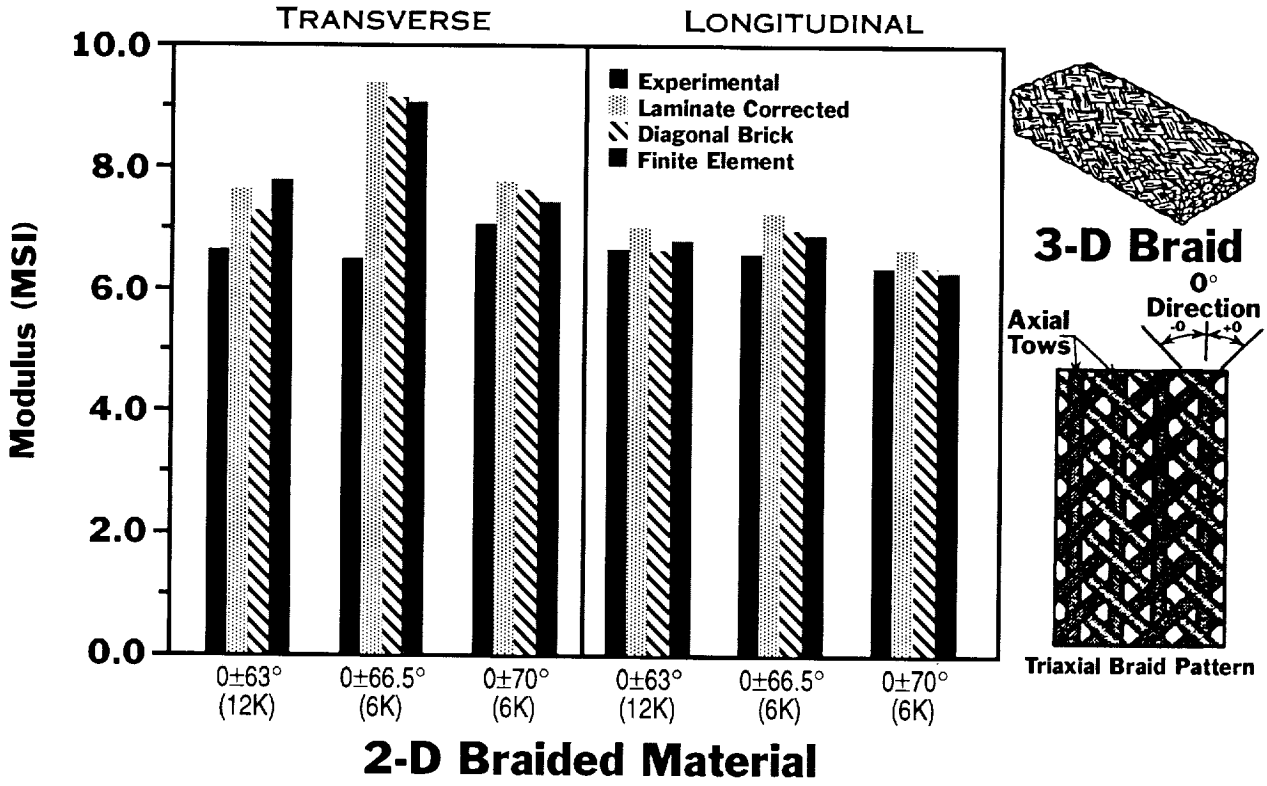

PROCESS CONTROL OF TEXTILE COMPOSITES

A recent workshop was held at NASA Langley Research Center with representatives from the textile industry and airframe manufacturers to assess where we are with quality control and where we need to be. While it is generally concluded that current post-process NDE methods can find most commonly occurring defects, this method is very time consuming and costly. Research is needed to develop effective in-process inspection methods that will preclude costly post-process requirements.

Industry consensus that:

- Current post-process NDE can find any of the commonly occurring defects but is not cost effective
- Post-process NDE must give way to "in-process" inspection/QA control procedures to remove "art" from shop floor
- Research is needed to develop in-process inspection/QA control techniques that will reduce the need for post-process NDE of each part

ADVANCED COMPOSITE STRUCTURAL CONCEPTS AND MATERIAL TECHNOLOGIES

TASK 5--BOX BEAM

Under Task 5 of the ACT contract NAS1-18888 with Lockheed, a wing box was built that represented a half-scale center box for the C-130 to understand the trade-offs between cost and weight of composite wing structure. The center wing-box beam for the C-130 aircraft was selected as the baseline for a typical heavily loaded wing structure. The box is approximately 240-inches long, including load introduction fixtures, and incorporated the best graphite composite fabrication technology available at the time. Design/manufacturing integration has provided an understanding of weight and manufacturing cost trade-offs for composite structures. This type of information will aide in developing the capability to design cost-effective composite structures that offer improved performance over aluminum structure.

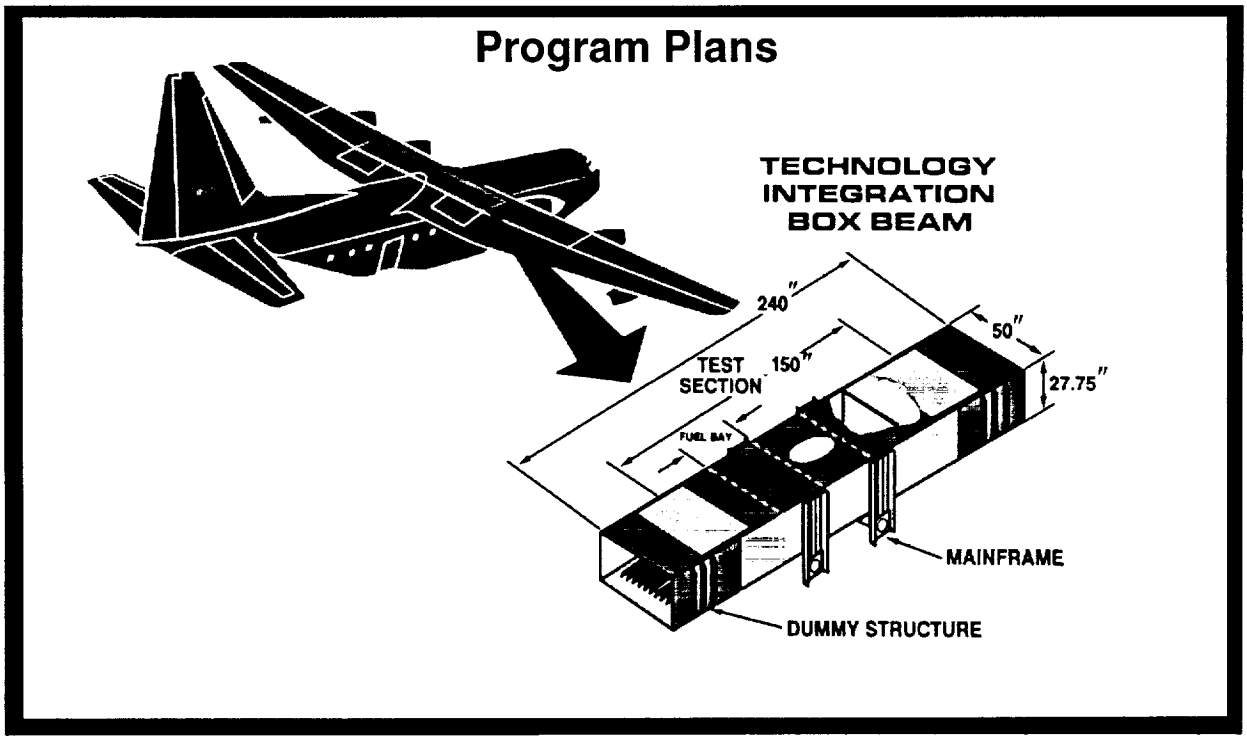

TECHNOLOGY INTEGRATION BOX BEAM TEST DEMONSTRATES IMPORTANCE OF LOAD INTERACTION

The approach was to substantiate the strength of the structure using analysis and sub-component tests. The sketch in the upper left of the figure shows a separate cover assembly that was fabricated and tested prior to building the complete box beam. The cover specimen successfully supported ultimate load in compression. Subsequently, the cover was subjected to impact damage in two critical areas near the elliptical access hole. The damaged cover assembly also survived loading in compression to ultimate load. Fabrication of the box beam was then carried out, and tests were conducted at Lockheed's Kelly Johnson Research Center at Rye Canyon, California. In the final test, the box was loaded in up-bending and torsion. Failure occurred across the right side of the upper cover at 124 percent of design limit load (83 percent of ultimate), causing catastrophic damage to the right side cover and both spars. Since the cover panel alone survived ultimate load, component and load interaction apparently caused a compression failure adjacent to a transverse rib on the upper skin near the end of a truncated hat stiffener. Complete results of an analytical investigation of the TIBB were reported in the presentation entitled "Technology Integration Box Beam Failure Study," by Shuart, Ambur, Davis, Davis, Farley, Lotts, and Wang at the Third NASA ACT Conference, Long Beach, California, June 8-11, 1992.

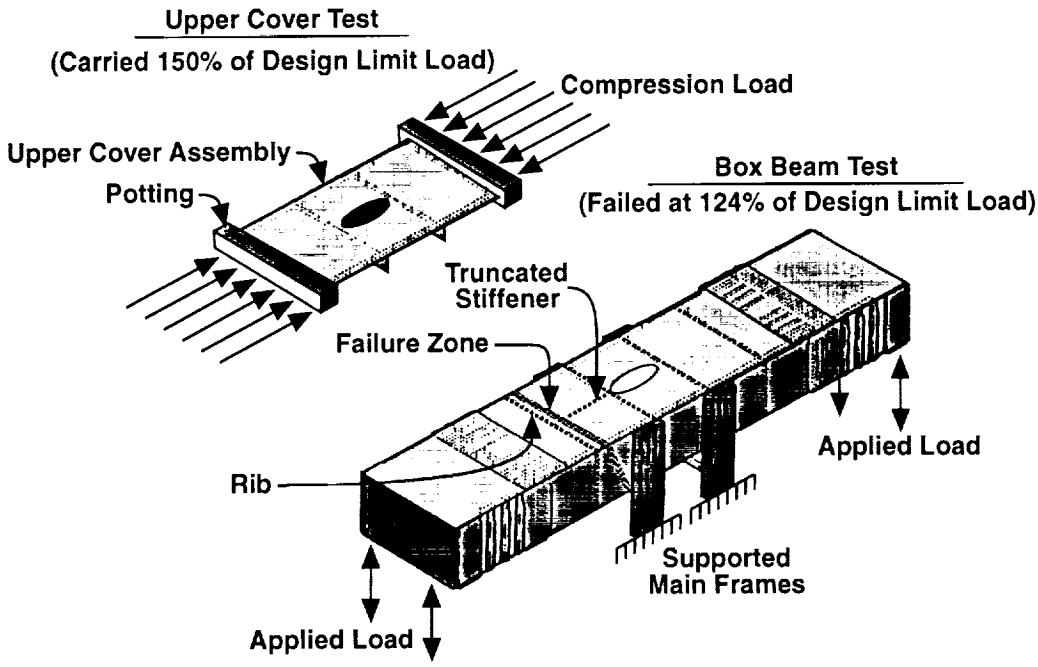

AXIAL DISPLACEMENT OF SRTS

An intense investigation of the failure that occurred in the TIBB was undertaken. The failure occurred in the TIBB upper cover at the point where the central hat-stiffener runs out adjacent to a rib. A Stiffener Run-out Test Specimen (SRTS) was cut from the undamaged side of the TIBB that was representative of the region that failed. The figure shows the axial displacement of the SRTS as it underwent axial compression in a uniaxial test machine. The end shortening analysis correlated well with test, with the analysis being stiffer than test. This was expected because the mesh size and element properties were slightly stiffer than the actual SRTS material they represented. Also, some rib rolling occurred in the SRTS test which was constrained in the analysis. The rib rolling became severe at the predicted failure load causing strain at one of the two ends of the stiffener run-out to intensify and the strain at the other end to lessen. Overall agreement between test and experiment for the SRTS was good, and the results supported the hypothesized mode of failure in the TIBB. Complete results of an analytical investigation of the TIBB was reported in the presentation entitled "Technology Integration Box Beam Failure Study," by Shuart, Ambur, Davis, Davis, Farley, Lotts, and Wang at the Third NASA ACT Conference, Long Beach, California, June 8-11, 1992.

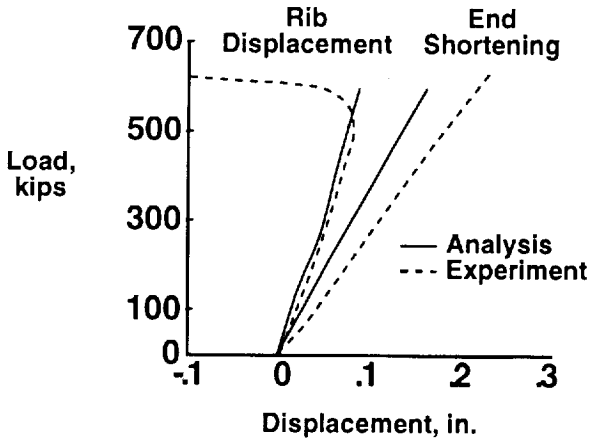

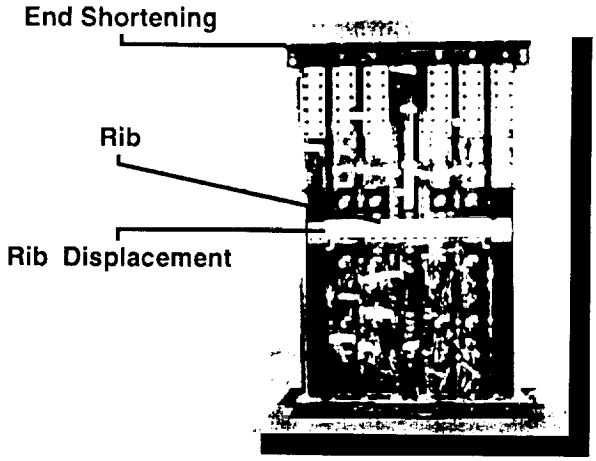

GTU AND ICAPS ACCELERATED WING DEVELOPMENT

Douglas Aircraft Company is the primary contributor to technology for transport wings. This figure shows the components of the ground test article (GTU) which will be manufactured and tested to validate RTM/stitched technology. This test unit, which is 8 feet at the root and has a span of 12 feet, is scheduled for demonstration tests beginning January 1994. Successful completion of these tests will pave the way for scale-up to a full-scale semi-span wing component. Specific details of this program will be provided in subsequent papers.

ICAPS Wing Box Ground Test Unit (GTU) Assembly

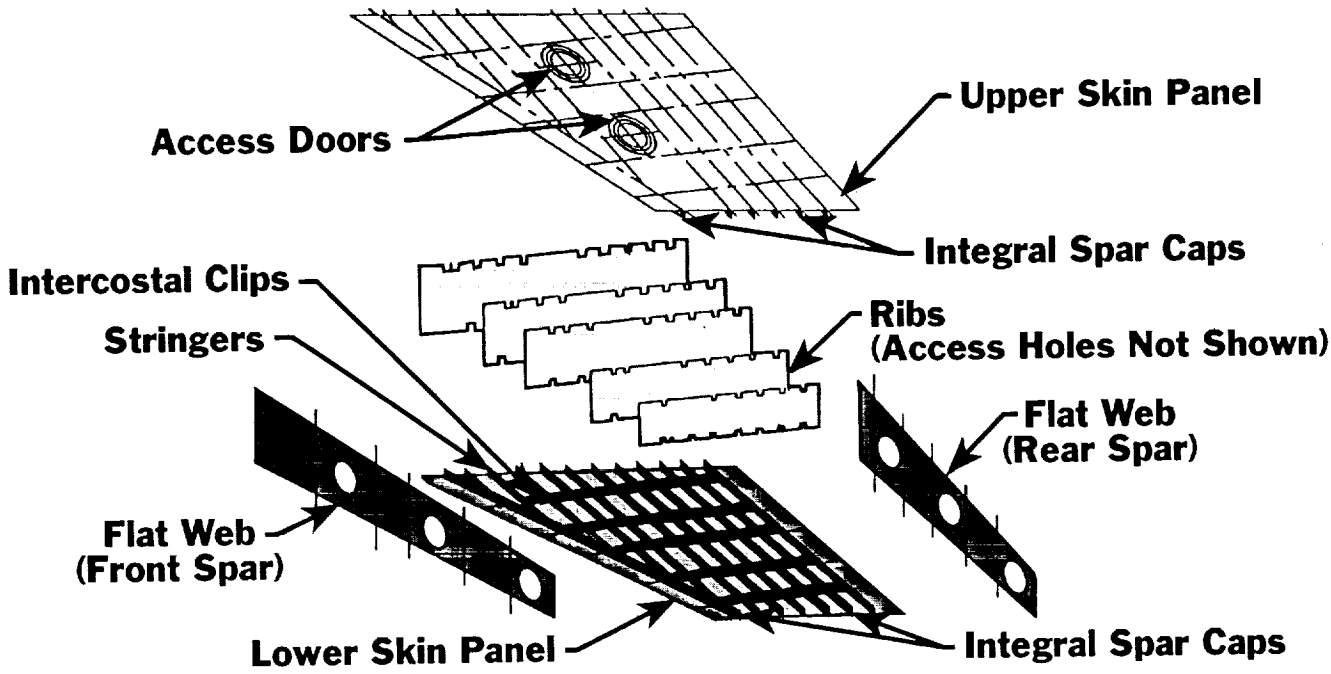

FAILED THREE-STRINGER WING PANEL

One of the major advantages of dry stitching and resin transfer molding is the inherent ability of the structure to resist damage due to impact and, thereby, avoid large strength reduction because of delamination. This figure shows the failure mode of an RTM/stitched panel impacted at 100 ft-lb at mid-bay and tested to failure in compression. The suppression of delaminations results in a well-defined failure mode even for this relatively brittle material system.

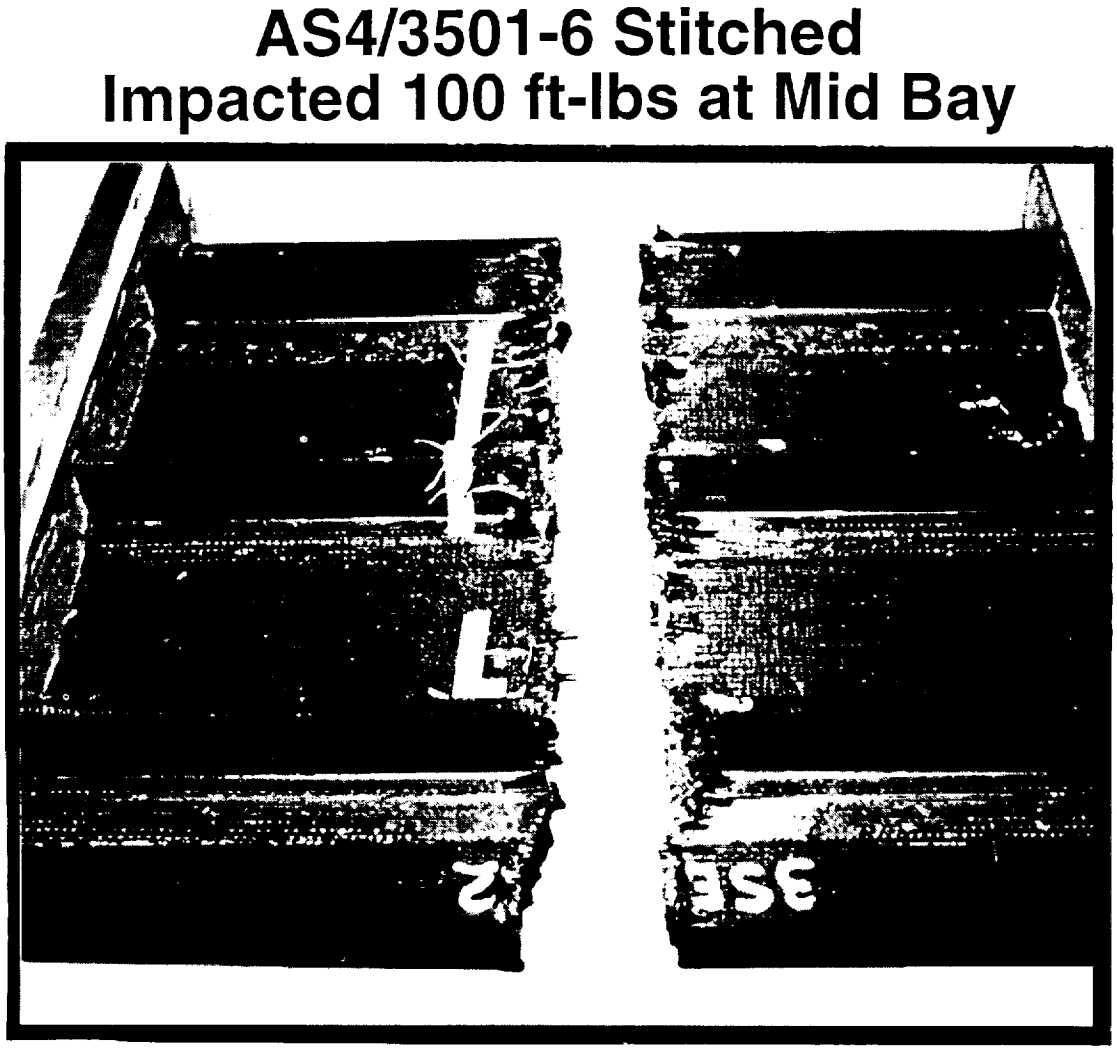

STUDY OF MICROCRACKING IN STITCHED COMPOSITES

Some early standard tests of RTM/stitched components have revealed microcracking believed to be associated with the stitching fibers. Though strength reduction due to microcracking seems to be insignificant and may not be a concern, the influence of microcracking over the long term does need to be evaluated. To better understand the cracking mechanism, a series of tests is being performed on different material systems, as shown on this figure. These tests will include the influence of material processing as well as environmental cycling.

Various Material Combinations

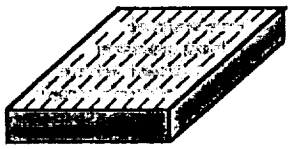

- **48 Ply Laminates**
- **AS4 Fabric**
- **Kevlar Stitching**
- **3501-6**
- **3502**
- **PR 500**
- **CET-3**

Test Types

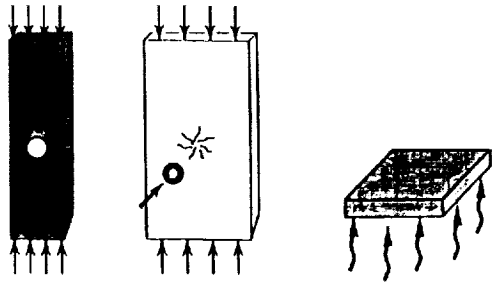

OHC **CAI** **Fuel Seepage**

Environmental Cycling

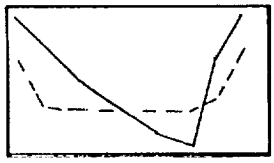

Analysis

Expected Results

- Understanding of cracking mechanism
- Influence of materials and processing on cracking
- Guidelines for reduction or elimination of cracking
- Effects of cycling on residual strength
- Evaluation of materials for surface treatment and fuel sealing

AIRCRAFT FLUIDS AND FUEL EXPOSURE TESTS

The search for new and improved resin systems has resulted in several candidate materials suitable for resin injection. Tests are being conducted to study the influence of exposure of these materials to numerous fluids and aircraft fuel commonly used, as indicated on this figure. Significant details and results of this investigation will be presented in a subsequent paper.

Materials

Carbon Fabric
- 3K AS4 at 145 g/sq m

RTM Resins
- Hercules 3501-6 (Baseline)
- Dow CET-2 Epoxy
- Dow CET-3 Epoxy
- Shell 862 Epoxy
- Shell 1895 Epoxy
- BP E905 L Epoxy
- CG 5292 Bismaleimide

Test Specimen Fabrication

Resin Transfer Molding

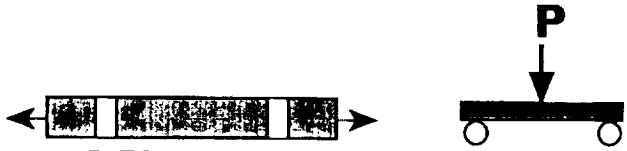

8 Ply Tension

Fluids and Fuel Exposures

- Water at 160°F
- JP-4 Jet Fuel at RT
- Hydraulic Fluid at 160°F
- Turbine Oil at 160°F
- MEK Cleaner at RT
- Paint Stripper at RT
- Deicing Fluid at RT

Results

- Strength Data:
  - Cross plied tension at RT and 180°F
  - 0° shear at RT and 180°F
- Consistent comparative data on the behavior of state-of-the-art resins

ICAPS SEMI-SPAN WING DEVELOPMENT

In reviewing the technical needs of the scale-up from the stub box to the semi-span, there were several required sub-components to design, fabricate, and test. This illustration shows the tension and compression repair panels, similar durability panels, spar cap, and rib clip load transfer areas, the engine pylon attach areas, and two intermediate box specimens representing an inboard and outboard area of the semi-span. The box specimens are approximately 84-inches long and 24-inches wide with typical rib and spar attachments. Tests on these specimens should validate the structural integrity of the stitched/RTM concepts subjected to three-dimensional loadings.

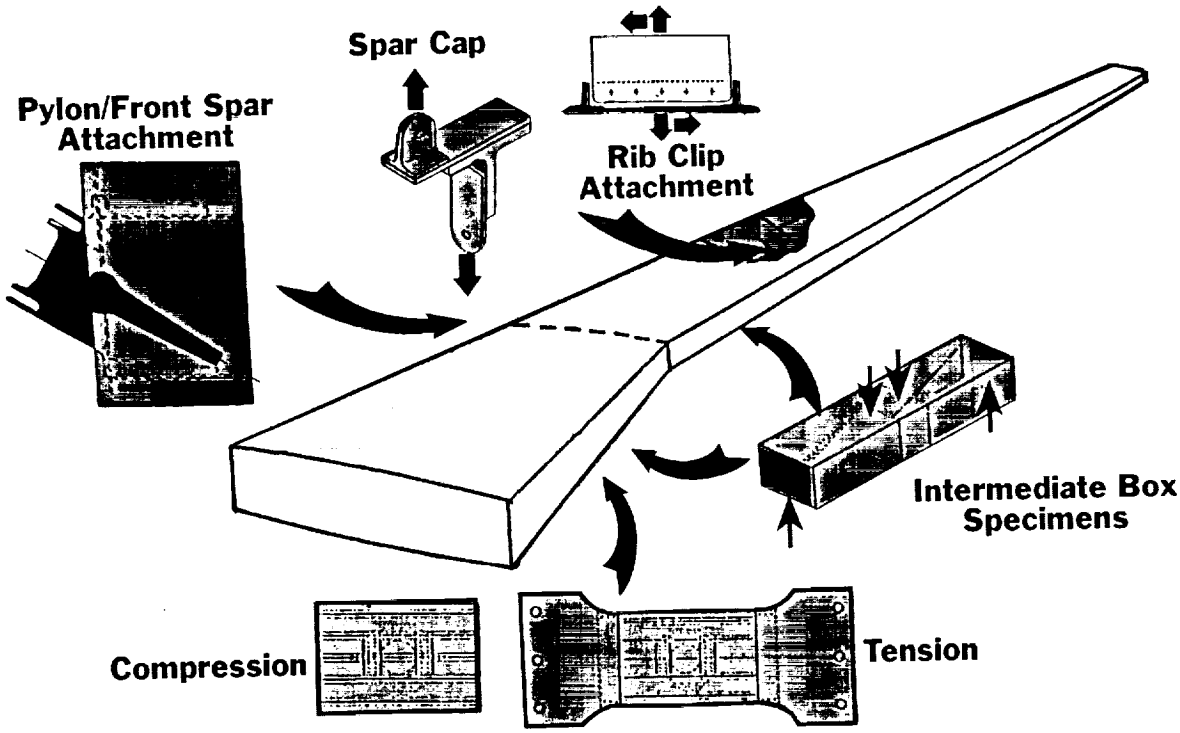

Major Repair Panels

COMPOSITE SEMI-SPAN WING GROUND TEST UNIT

The successful culmination of the composite wing program will rely on the demonstration of technology with ground tests of a semi-span wing component shown on this figure. The wing is about 5.5 feet at the root and over 26 feet in span. Fabrication of this component will demonstrate the scale-up and cost effectiveness of RTM/stitched technology and should provide a wealth of data for analysis verification. This test program is expected to be completed by late 1995.

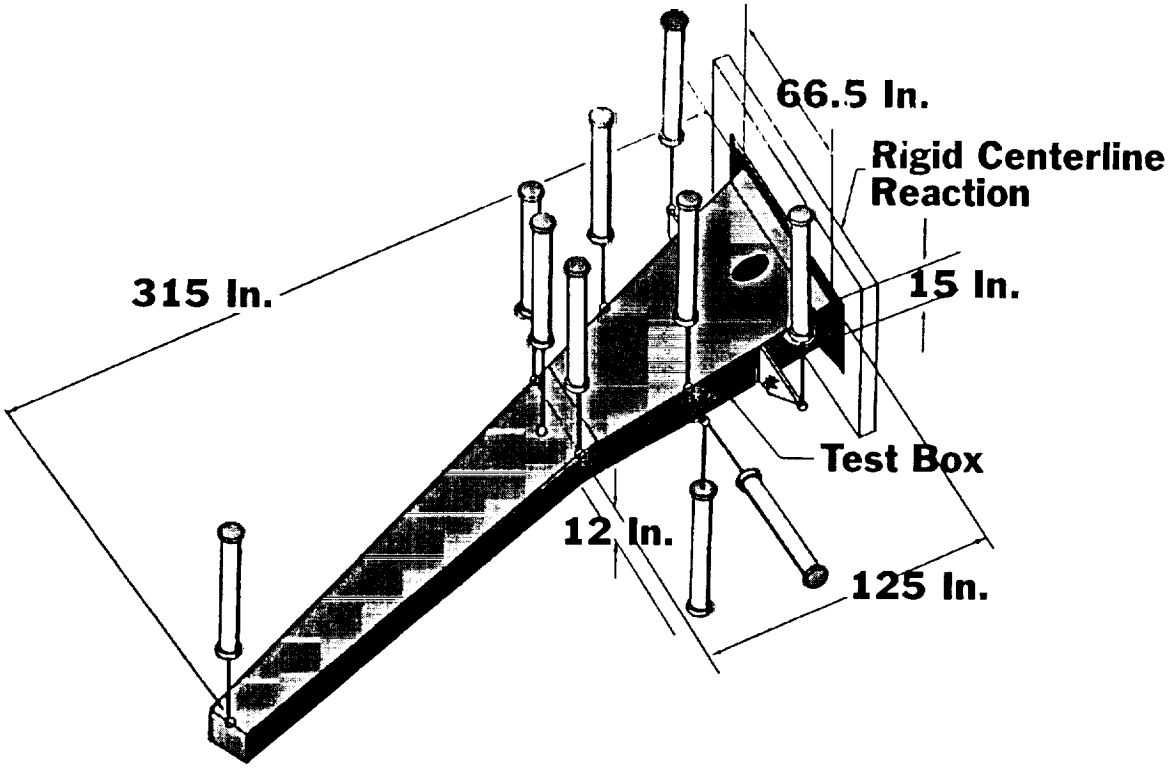

SUMMARY

Progress in the development of cost-effective composite structures over the first 3 years of the ACT Program has been very good. While the program has focused on wing and fuselage primary structure, the application of the three principal technology areas of automated tow placement, RTM/stitched, and textile preforms has provided significant insight into their weight and cost potential. The advantages of these technologies will be clearly delineated over the next 2 years.

Through close coordination with our transport manufacturers, a Phase C plan is evolving. This plan is expected to be approved beginning in 1995 and is designed to provide full-scale verification of an integrated data base grounded on analysis methodology, cost-effective manufacturing, test validation, and certification. The Phase C plan should provide the confidence and experience required for successful application of composites to fuselage and wing components of large transport aircraft. This plan should be well defined before our next conference which will be jointly sponsored by the Air Force and held in June 1993.

- Excellent progress is being made on development of cost-effective primary composite structures
- Development of Phase C Program Plan is underway
- NASA and Air Force will hold a joint Advanced Composite Technology Conference in June, 1993

N95-29033

TEXTILE COMPOSITE FUSELAGE STRUCTURES DEVELOPMENT

Anthony C. Jackson*, Ronald E. Barrie and Robert L. Chu
Lockheed Aeronautical Systems Company
Marietta, Georgia

54-24
51287

INTRODUCTION

Phase II of the NASA ACT Contract (NAS1-18888), Advanced Composite Structural Concepts and Materials Technology for Transport Aircraft Structures, focuses on textile technology, with resin transfer molding or powder coated tows. The use of textiles has the potential for improving damage tolerance, reducing cost and saving weight. This program investigates resin transfer molding(RTM), as a maturing technology for high fiber volume primary structures and powder coated tows as an emerging technology with a high potential for significant cost savings and superior structural properties. Powder coated tow technology has promise for significantly improving the processibility of high temperature resins such as polyimides.

This phase of the contract was initiated in October, 1991 and runs through April, 1995. Figure 1 shows the schedule for Phase II activities.

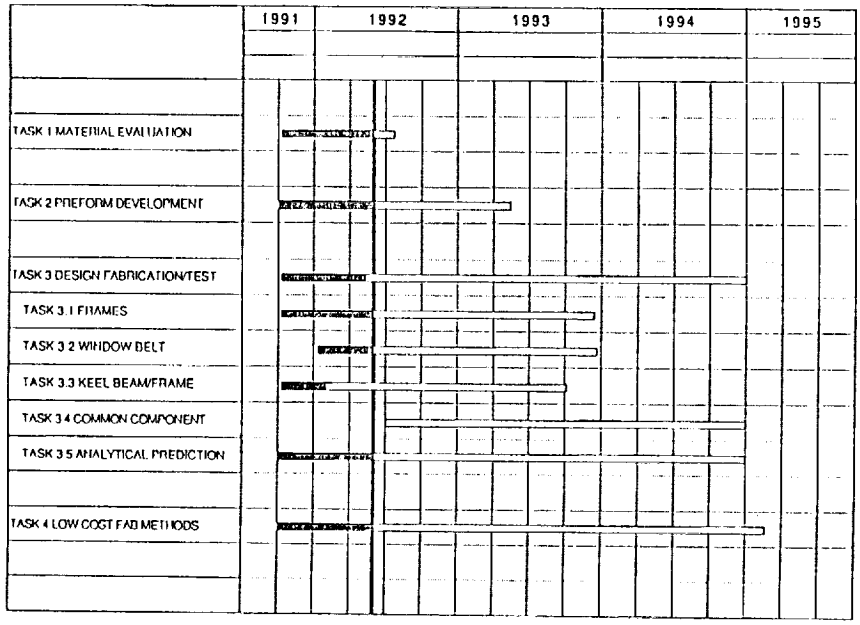

Figure 1, Program Schedule.

PROGRAM DESCRIPTION

This phase consists of four tasks. Task 1 covers material evaluation and involves the screening of three RTM resins and two powder resins for fiber coating. The evaluation approach shown in Figure 2, consists of fabricating panels using 8 harness satin weave fabrics, either dry and then resin transfer molded or woven from powder coated tows. Mechanical and physical tests are being performed on coupons cut from these panels to evaluate each system to aid in the selection of the resins to be used in Task 2.

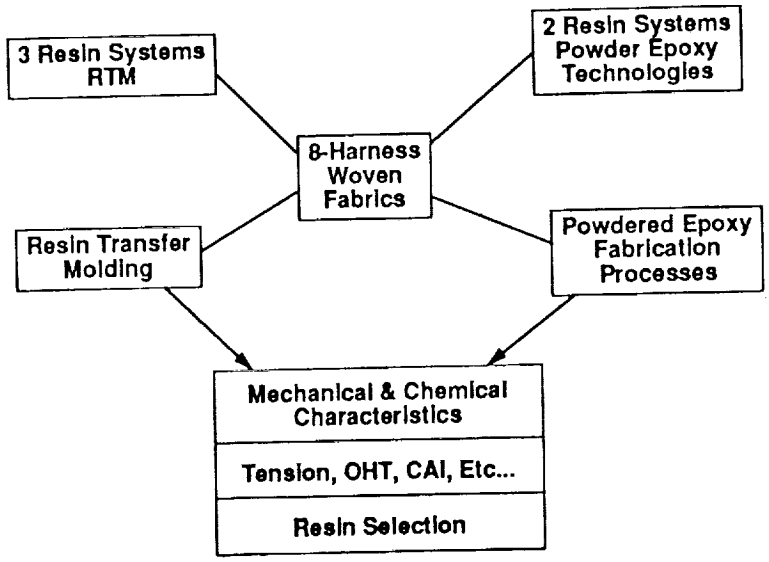

Figure 2, Evaluation Approach, Task 1.

The objective of Task 2 is to develop a data base for the selection of the processes which will lend themselves to the fabrication of net shape preforms for complex structural configurations, such as curved frames and window belt structure. The processes include 2-D braiding, 3-D braiding, 3-D interlock braiding, 2-D weaving, 3-D weaving and fiber placing. The evaluation approach is shown in Figure 3.

Task 3 consists of five subtasks. The first four subtasks involve the design, fabrication and testing of concepts for fuselage frames, window belt structures keel substructure and a common component for NASA testing. The common component was originally a crown panel but has recently been changed to a window belt panel because of the high potential for

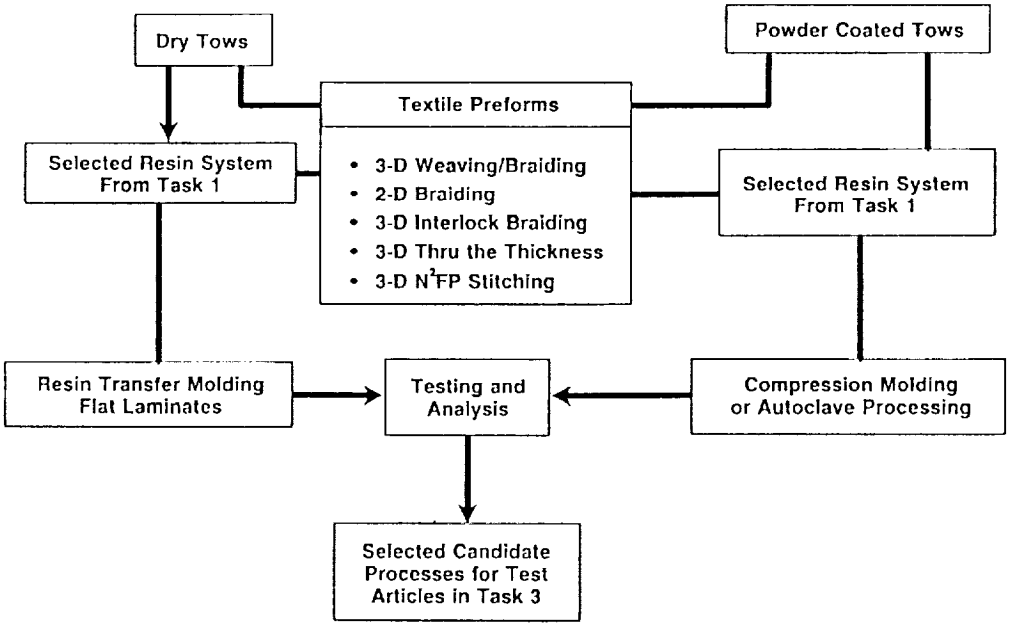

Figure 3, Evaluation Approach, Task 2.

textile preforms to payoff in this location. The fifth subtask covers the development of analytical methods for textile preform structural analysis.

Task 4 covers low cost fabrication development and evaluation for advanced textile preforms. In this task Lockheed has purchased a Venus Gusher RTM machine which is now installed in Marietta. The task also involves the exploration of innovative tooling concepts and establishing advanced machine requirements and automation potential.

RESIN TRANSFER MOLDING

Resin transfer molding has been a commercial process for many years. Until recently however, fiber volumes were generally very low and cured properties poor. In the last few years considerable progress has been made. Parts can now be fabricated with fiber volumes of 60 percent and good cured resin properties, thus making this a viable process for major load carrying structures. The chemical companies have been working to steadily improve both the processibility and the mechanical properties of the resin systems. The resin transfer molding process is illustrated in Figure 4.

Three epoxy resin systems have been evaluated in this program. They are: Shell RSL-1895; 3M PR-500; and BP E905L. This evaluation is discussed in detail in a later paper (Reference 1).

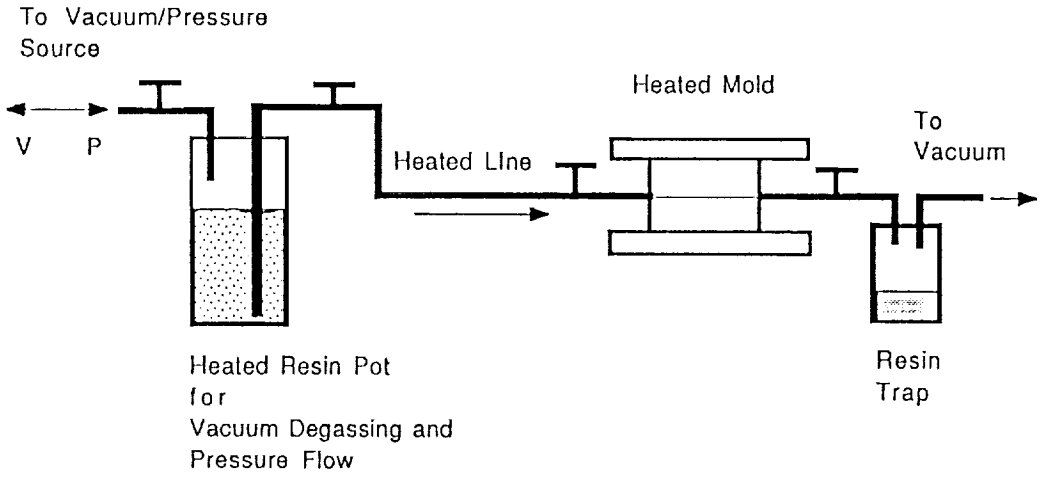

Figure 4, Schematic of RTM Process.

In order for Lockheed Aeronautical Systems Company (LASC) to be able to evaluate the processing of these systems, an RTM machine was purchased from Venus Gusmer and has been installed at LASCs Marietta Georgia facility. A picture of this machine is shown in Figure 5.

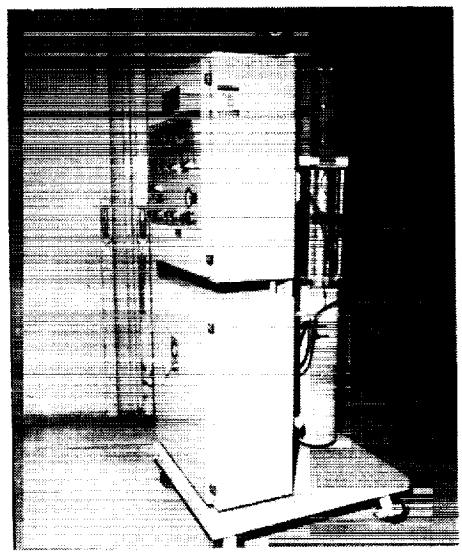

Figure 5, Venus Gusmer RTM Machine.

POWDER COATED TOWS

In the last few years considerable effort has been directed toward the development of techniques for depositing polymer powders on tows and sintering the powder to provide a weavable and braidable tow material. This work has been spearheaded by Norm Johnston at NASA Langley Research Center and by Professor John Muzzy at Georgia Institute of Technology. BASF Materials in Charlotte North Carolina is under NASA contract to scale up a process which they have developed for coating tows. The Georgia Tech process is now being commercialized by Custom Composites Inc of Atlanta, Georgia.

Several other researchers are pursuing new approaches for powder coating , including Professor Larry Drzel at Michigan State University, and Dr. Douglas Hirt at Clemson University.

Currently two resin systems are under evaluation: Shell RSL-1952 coated onto AS4 tows by BASF Materials; and 3M PR500 coated onto AS4 by Custom Composites. These tows were woven into 8 harness satin fabrics by Fabric Development of Quakertown, Pennsylvania and textile Technologies Incorporated of Hatboro, Pennsylvania. LASC used these fabrics to develop the processing and to fabricate panel for mechanical properties. This is also discussed in more detail in reference 1. The powder coating process is shown schematically in Figure 6.

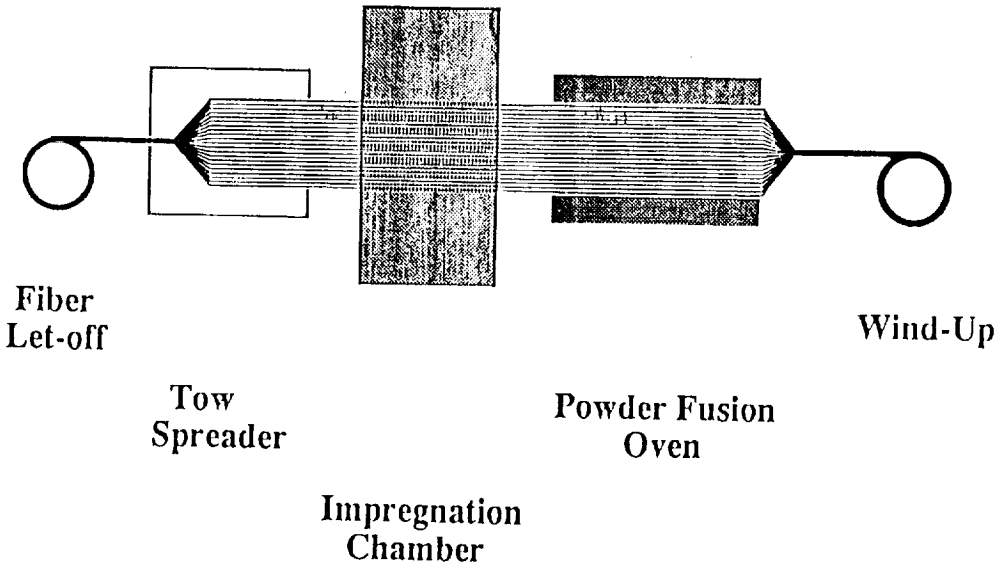

Figure 6, Schematic of Powder Coating Process.

Powder coating of the tows has the advantage that the resin is intimately dispersed through the tows so that flow is not generally a problem. Also, as the powder is sintered on the fibers after deposition, the tows can be stored at room temperature indefinitely. The powder coated tows can be woven , braided, pultruded and processed in other ways without the use of solvents or the emission of hazardous byproducts.

The coating processes fall into two general categories: dry and wet. The dry processes rely on the formation of a cloud of resin powder which is deposited onto the spread tow fibers and adheres by electrostatic means. The powder is then sintered by microwave or other heating process. The wet processes rely on the deposition of a slurry onto the spread fibers with a subsequent drying and sintering process.

Considerable progress has been made in determining the correct amount of resin which needs to be deposited on to the fibers to provide the required cured resin content. The textile processes cause some loss of powder and although this has not proved to be a problem it would be preferable if this could be eliminated or at least minimized.

PREFORM DEVELOPMENT

A survey was made of the weaving and braiding industry and the most promising processes were selected for evaluation. A summary of the vendors and the processes under evaluation is shown in Table 1.

Table 1, Vendors and Processes Evaluated.

VENDOR	PROCESS
Fiber Innovations	2-D Braiding
Albany International	3-D Interlock Braiding
Atlantic Resrarch	3-D Through the Thickness Braiding
Textile Technologies	3-D Weaving
Hexcel Hi-Tech	3-D Multi-Axial Warp Knit
Cooper Composites	Near Net Fiber Placement
Techniweave	3-D Multi-Axial Weave

A large cross section of the weavers and braiders with the capability to do the development work has been included in this program. Under braiding, Fiber Innovations is fabricating the 2-D panels, Albany International the 2-D Interlock panels and Atlantic Research the 3-D Through the Thickness panels. Under weaving, Textile Technologies is fabricating the 3-D panels and Techniweave the Multi-axial panels. Hexcel Hitech is fabricating the Multi-axial Warp Knit panels and Cooper Composites the Near-Net Fiber Placement panels. We are also investigating the Quadrax braiding process which permits continuous braiding of infinitely long panels.

The Atlantic Research braider is shown in Figure 7. A typical loom is shown in Figure 8. Again this task is discussed in more detail in reference 1.

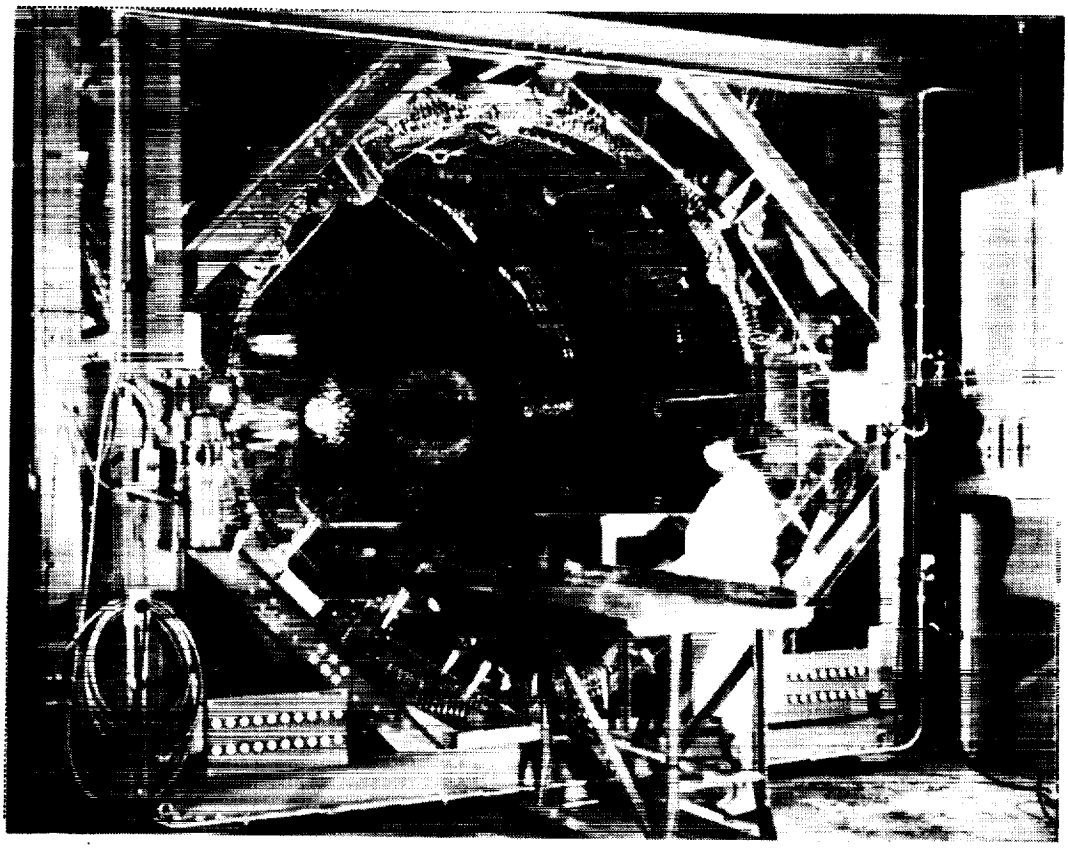

Figure 7, Atlantic Research Braiding Machine.

FUSELAGE BASELINE DESCRIPTION

The baseline airplane for this study is the Boeing 7X7. This is a two engine wide-body passenger transport airplane. A schematic of the fuselage is shown in Figure 9. LASC is

working closely with the Boeing Commercial Airplane Group in the execution of this program and LASC will provide the textile subcomponents for Boeing to incorporate into their tests components. To this end LASC and Boeing have been working in joint Design Build Teams to develop the designs and processes for the frames, the keel and the side panel structure.

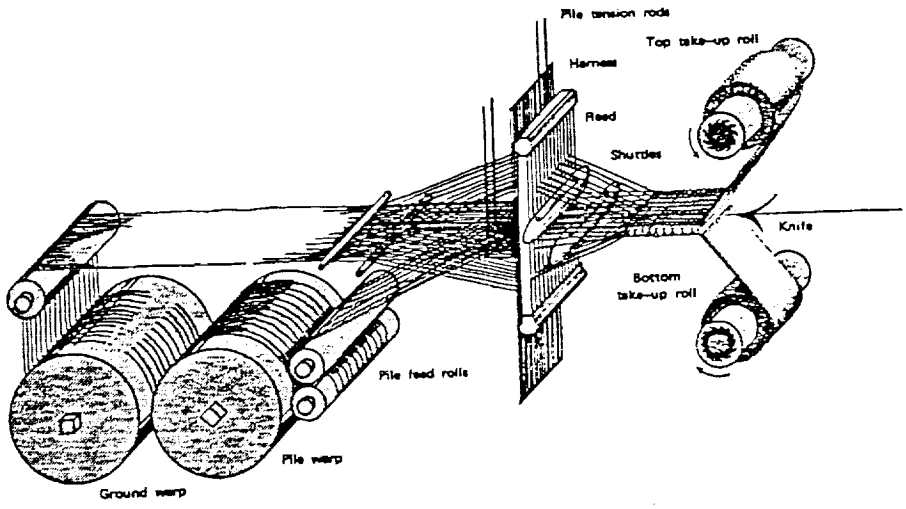

Figure 8, Weaving Loom.

The baseline fuselage is a typical ring and stringer stiffened structure. It is a wide body aircraft designed with up-to-date technologies which are proven low cost. The objective of this program is to develop and demonstrate composite textile technology as a lower cost approach to structures for fuselage frames, window-belt reinforcement, door surrounds and keel frames and intercostals.

FRAMES

The frames are designed primarily by bending loads due to the discontinuity of the floor beams and posts and by the tension due to aircraft pressurization.

Several frame design configurations were initially considered for textile preform

C-2.

application. A simple "J" configuration was determined to be the lowest cost approach. However, when this design was "mouse-holed" to allow the stringers to be continuous the outer frame cap is interrupted and an unsupported edge is introduced in the web area as shown in Figure 10. This unsupported edge is prone to buckling and delamination. In order to eliminate these structural deficiencies, an additional flange is introduced to the frame web immediately inboard of the mouse-hole cut out. The resulting "F" frame configuration is shown in Figure 11. Although this configuration is more complex from the manufacturing standpoint, it is extremely efficient structurally. Consequently the "F" configuration has been selected as the primary concept for the continuing studies.

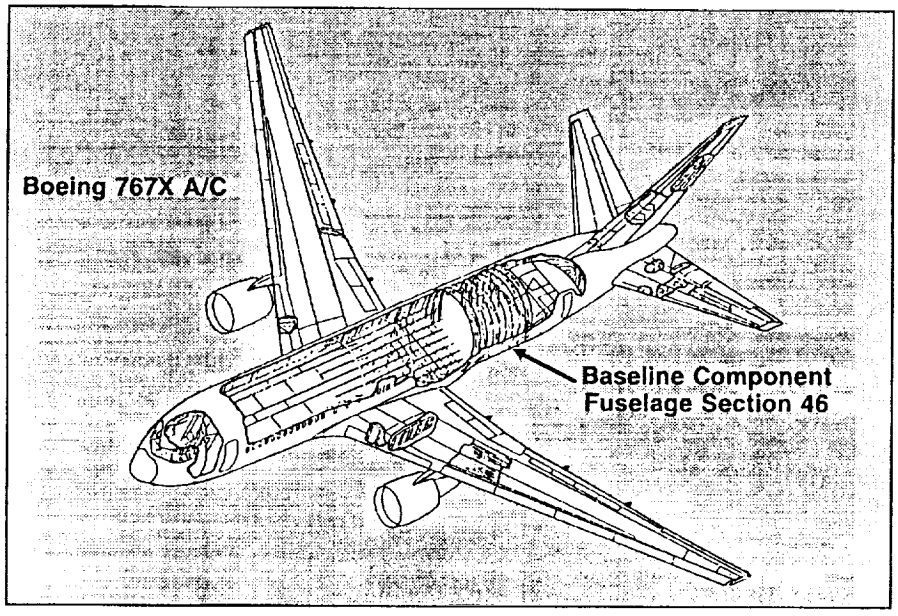

Figure 9, Boeing 7X7 Fuselage Configuration.

Three alternate textile processes are currently being evaluated for the fabrication of the "F" frame preforms: 3-D braiding; 3-D interlock braiding; and 3-D weaving. The 3-D braiding process has been developed by Atlantic Research Corporation, Alexandria, Virginia. The 3-D interlock braiding has been developed by Albany International, Mansfield, Massachusetts. The 3-D weaving process has been developed by Techniweave, Rochester, New Hampshire.

The 2-D braiding process, which is a viable process for the "J" frame configuration,

has been extensively evaluated by Boeing and their results will be compared with the Lockheed results on the various 3-D processes.

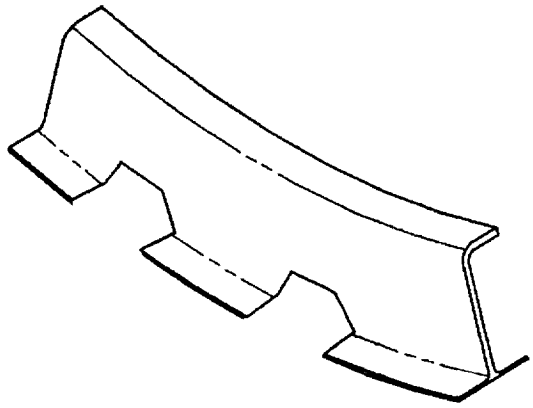

Figure 10, "J" Frame Configuration.

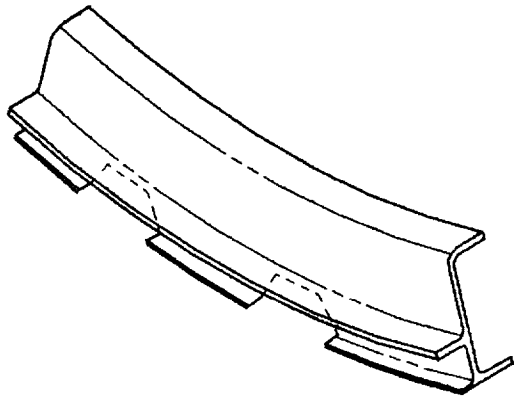

Figure 11, "F" Frame Configuration.

The major advantage of the 3-D braiding process is that one-piece, net-section preforms with full through-the-thickness tow capability can be produced in a totally automated process. One method for achieving this is illustrated in Figure 12, where back-to-back frame segments are produced on a rectangular cross-section mandrel which is curved to match the fuselage mold line. The two flanges shown folded out from the braiding mandrel are achieved by cutting through half of the web thickness in a pocket area where the tows which run through the thickness are in fact terminated at the midplane or other specified level. This feature known as bifurcation can be achieved in both the interlock and the through-the-thickness 3-D process.

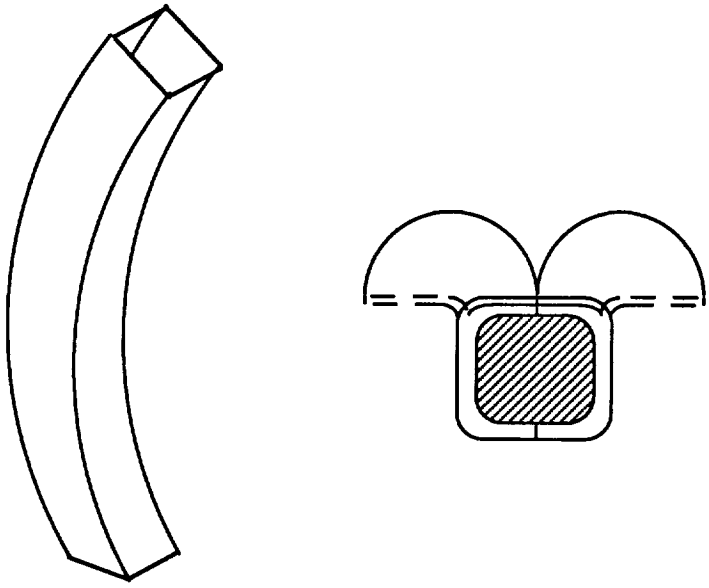

Figure 12, Back-to-Back "J" Frame Braiding.

KEEL AREA SUBSTRUCTURE

The critical studies of the keel area concentrated on the cargo floor support structure, see Figure 13. This structure consists of stiffened web frames, supported by longitudinal intercostals at the more highly loaded regions and floor beams with support posts at the more lightly loaded regions. Figures 14 and 15 show several design concepts incorporating textile preforms which have been evaluated. Before design trade studies of these concepts were completed, Lockheeds efforts were redirected to evaluate only those concepts which

were required for the Boeing test articles, namely the frame caps for attachment to the keel sandwich skin panels. Both "J" and "T" members have been considered for this application, with triaxial solid braiding being the preferred manufacturing process.

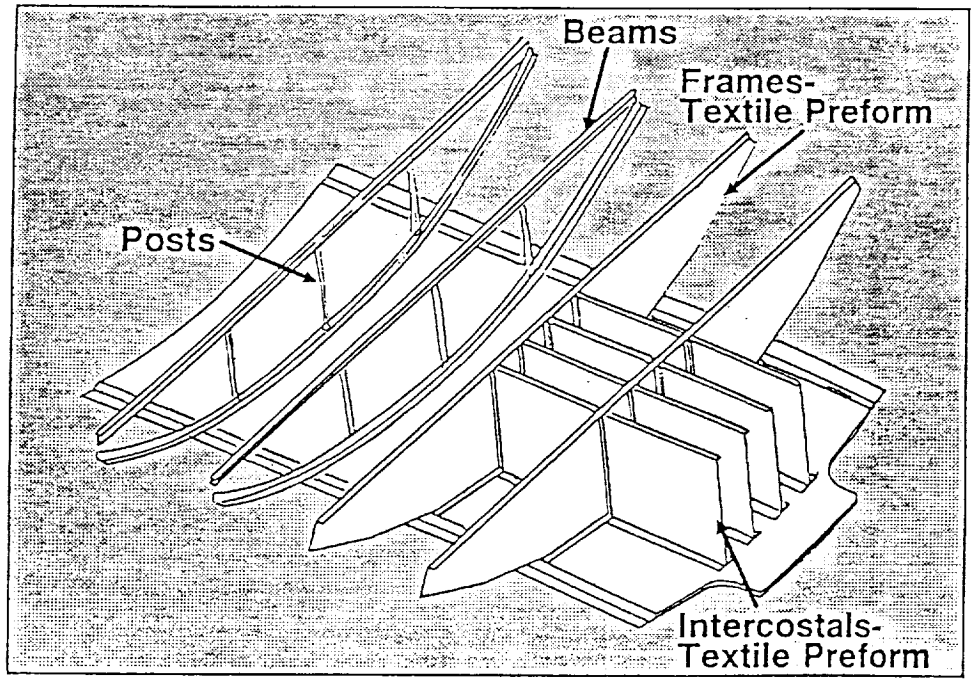

Figure 13, Cargo Bay Subfloor Structure.

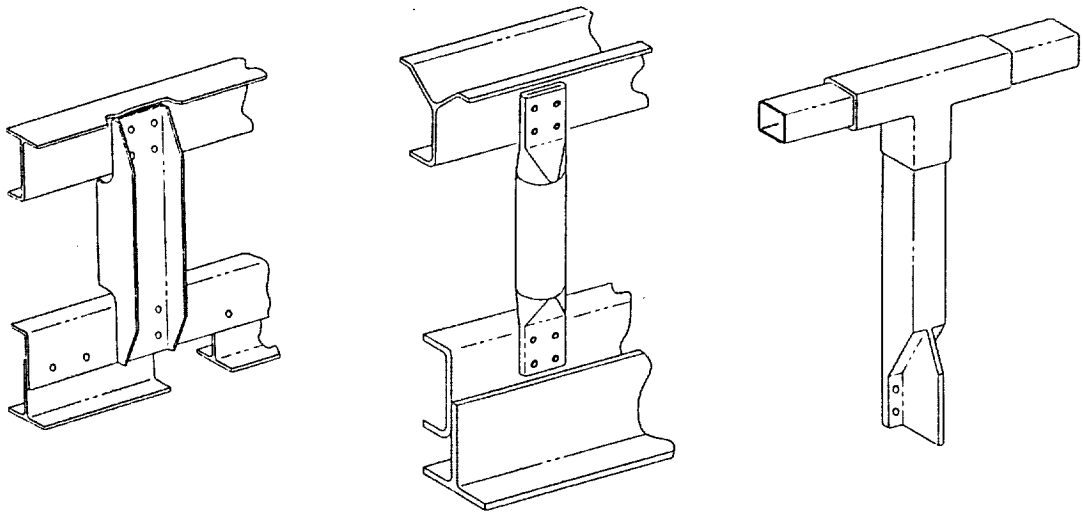

Figure 14, Cargo Floor support Post Concepts.

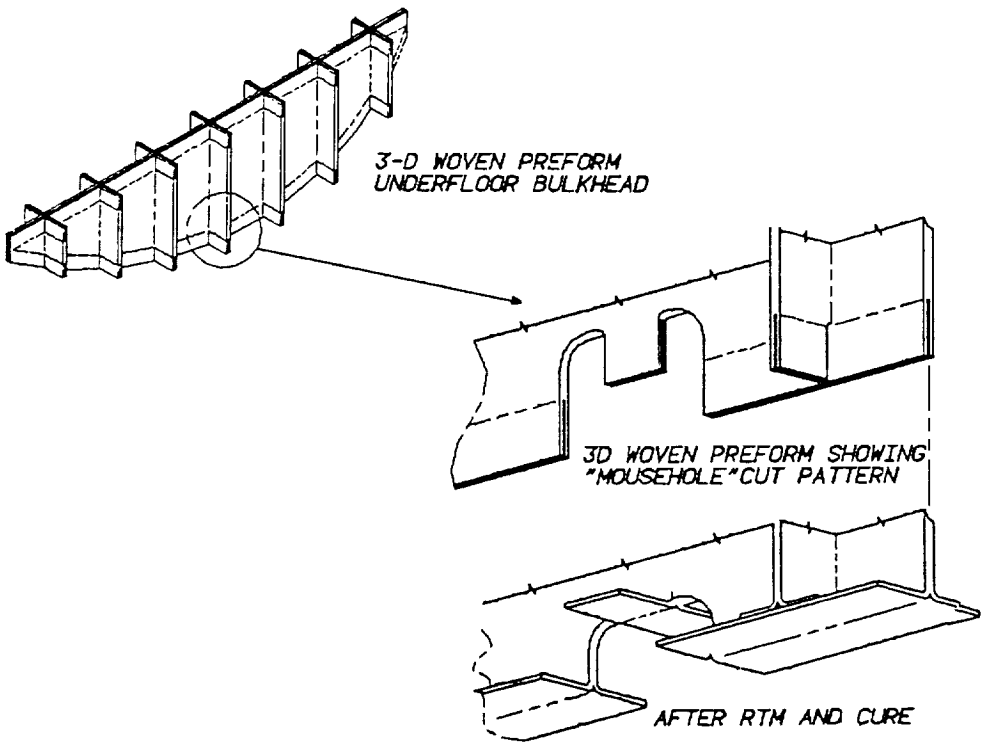

Figure 15, Cargo Floor Support Concepts.

The final design is critical as it is intended to bond or cocure the frame to the sandwich skin. A finite element model of the flange was constructed to facilitate the design effort. The model is shown in figure 16. The analysis showed that the flange must be tapered to minimize the peel stresses.

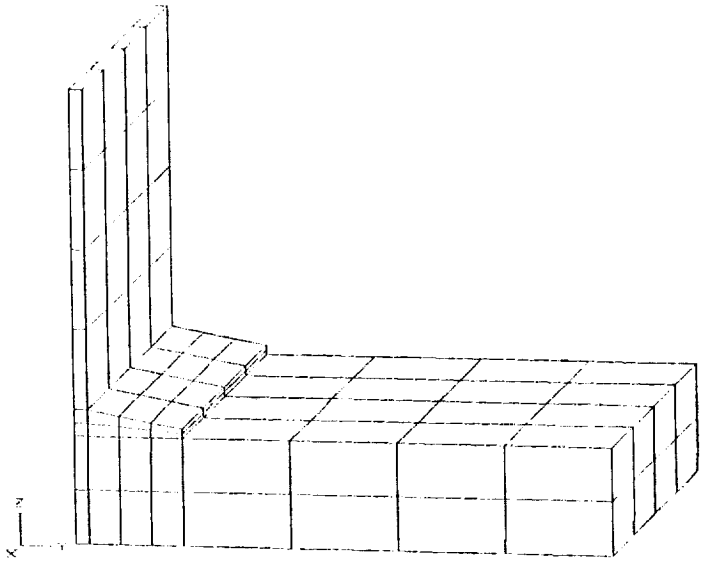

Figure 16, Finite Element Model of "T" Frame.

SIDE PANEL APPLICATIONS

The fuselage side panel is a prime candidate for textiles because of the structural complexity resulting from the window cutouts, window frames, passenger and cargo door cutouts, together with the associated load reinforcement. A typical side panel is shown in Figure 17.

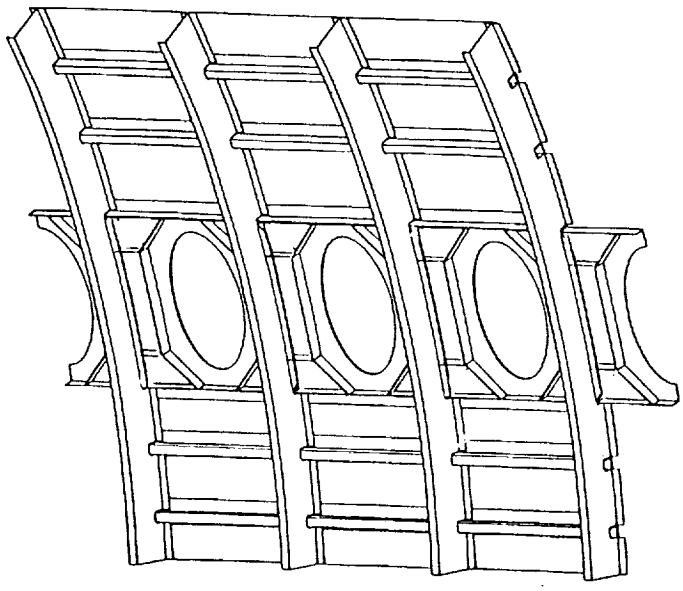

Figure 17, Typical Side Panel.

WINDOW BELT

The side panels in commercial transport airplanes are designed primarily by shear and pressure loads. The structure is complicated by the cutouts required for windows, for passenger doors and for cargo doors. Ideally the frames and longitudinal stiffeners should both be continuous. The window cutout reinforcements can be woven or braided as individual units or integral with other structure. The primary consideration here will be the fail-safe requirements. If the textile preforms do exhibit superior damage tolerance properties, then it may prove possible to meet the requirements without resorting to the traditional multiple element approach.

Two concepts are being evaluated for window belt structure. In the first concept which is

shown in Figure 18, the window belt area is reinforced by the addition of a continuous 3-D woven or braided preform which is approximately 22 inches wide and which incorporates upper and lower longitudinal stiffeners and frame attachment flanges. The window frame is fabricated separately using a 3-D braiding process. These reinforcing members are cocured together with the automatic tow placed skin, by Boeing, in a single autoclave cycle.

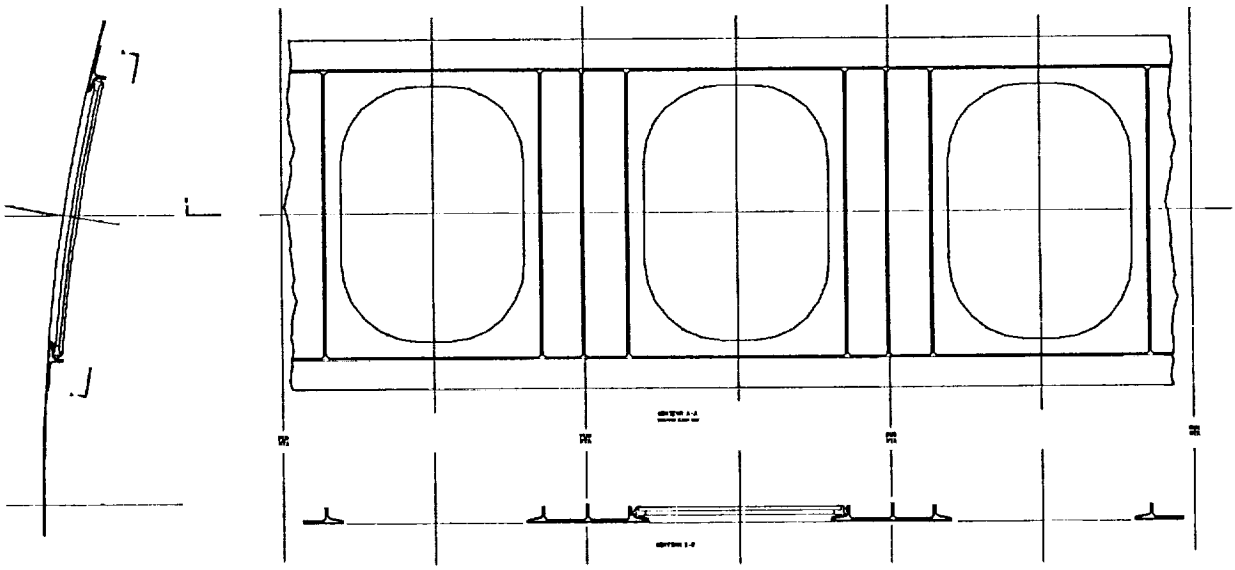

Figure 18, Window reinforcement Concept Number 1.

The second window belt concept, shown in Figure 19, uses a unique 3-D weaving process currently under development by Techniweave of Rochester, New Hampshire. This process allows the window aperture, the window frames, the longitudinal edge stiffeners and the frame attachment members to be produced as a one piece preform. The skin is woven 0°, 90°, and +/-45° tows, while the stiffeners in both directions contain only 0° and 90° oriented tows. The +/-45° at this time has to be added as overwrap fabric.

Door Cutout Reinforcement

The passenger doors remove a large portion of the structure locally in the side of the fuselage. This requires extensive reinforcing of the area around the door to redistribute the axial, the hoop and the shear loads. The door cutout area is also subject to considerable wear and tear and to out-of-plane forces. The z direction reinforcement of textiles makes

them ideal candidates for structures of this type.

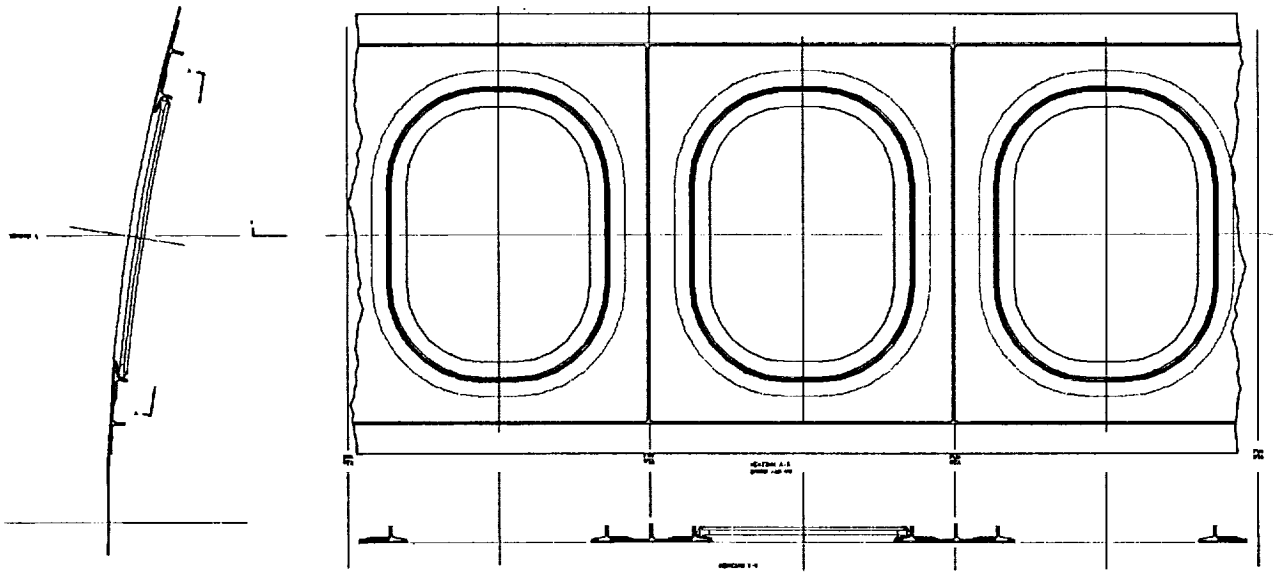

Figure 19, Window reinforcement Concept Number 2.

Side Panel

The side panel as used here refers to the structure outside of the immediate window reinforcement area and generally below the windows. The concept for this structure is similar to that of the crown panels. The frames in this case will be "F" configuration. Figure 20 shows the general approach to the fabrication of this structure.

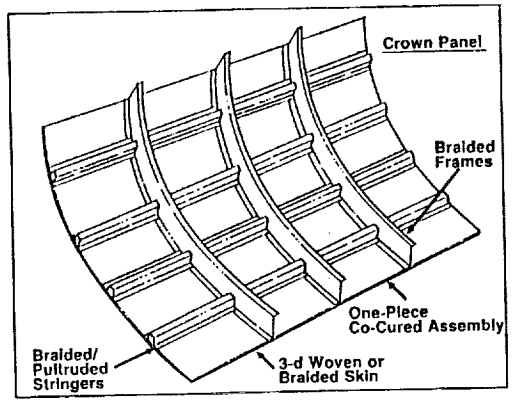

Figure 20, Side Panel Fabrication Approach.

DESIGN/MANUFACTURING DEVELOPMENT

Textile technology for primary structures has been limited to the use of 2-D fabrics and stitching because of the difficulty of impregnation. RTM resins were not available with the high flow and the high structural properties required. The recent development of new resin systems and the advent of powder coated tow technology has opened up a whole new field in manufacturing aircraft structures. Lockheed has purchased an RTM machine from Venus Gusher of Seattle, Washington, under the contract, in order to develop the processing of the RTM preforms and resins. The machine is shown in Figure 5. It is being used to flat panels using the tool shown in Figure 21 and to make frame segments using the tool shown in Figure 22.

The powder coated tow preforms present a challenge in compaction. The coated tows are more bulky than the dry tows and the preforms must be compacted prior to final processing. It is preferable to do this compaction in the final tool if at all possible. This effort is just getting underway. The results will be reported in the Monthly Technical Progress Reports and at the next NASA ACT Conference.

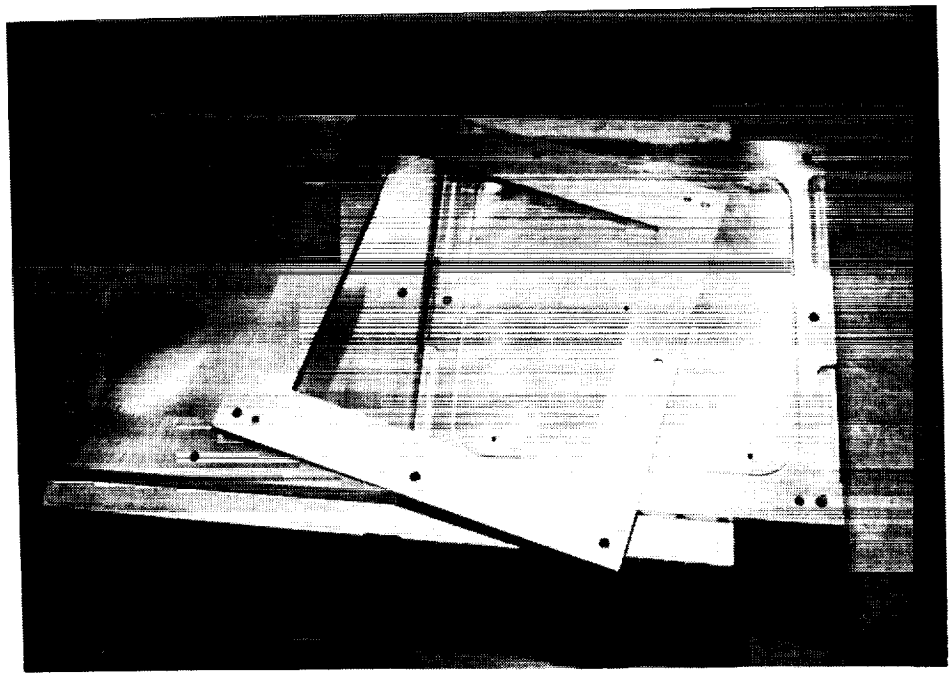

Figure 21, Flat Panel RTM Tool.

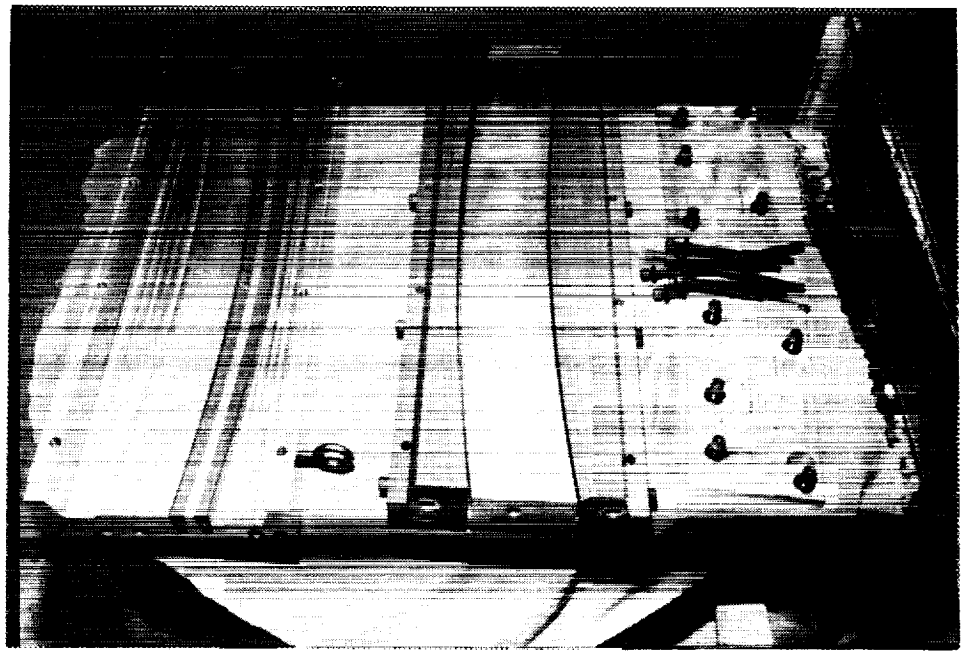

Figure 22, "F" Frame RTM Tool.

SUMMARY AND CONCLUSIONS

A program to evaluate and develop textile technology with RTM and powder coated tows is now well underway. The screening of the resins and the textile processes is progressing well and down select will occur in the next few months. Initial results are promising and show that the technologies are viable. The cost of some of the processes is high at this time. The scale-up and automation potential of these processes is under critical review. Some of the processes show significant potential for meeting the program goals of low cost and structural efficiency.

REFERENCES

1. Shukla, J. G and Bayha T.; Advanced Resin Systems and 3-D textile Preforms for Low Cost Composite Structures, third NASA Advanced Composite Technology Conference, June,1992.

[redacted]

ADVANCED COMPOSITE FUSELAGE TECHNOLOGY[1]

Larry B. Ilcewicz, Peter J. Smith, and Ray E. Horton
Boeing Commercial Airplane Group
Seattle, WA

ABSTRACT

Boeing's ATCAS program has completed its third year and continues to progress towards a goal to demonstrate composite fuselage technology with cost and weight advantages over aluminum. Work on this program is performed by an integrated team that includes several groups within The Boeing Company, industrial and university subcontractors, and technical support from NASA. During the course of the program, the ATCAS team has continued to perform a critical review of composite developments by recognizing advances in metal fuselage technology. Despite recent material, structural design, and manufacturing advancements for metals, polymeric matrix composite designs studied in ATCAS still project significant cost and weight advantages for future applications. A critical path to demonstrating technology readiness for composite transport fuselage structures was created to summarize ATCAS tasks for Phases A, B, and C. This includes a global schedule and list of technical issues which will be addressed throughout the course of studies.

Work performed in ATCAS since the last ACT conference is also summarized. Most activities relate to crown quadrant manufacturing scaleup and performance verification. The former was highlighted by fabricating a curved, 7 ft. by 10 ft. panel, with cocured hat-stiffeners and cobonded J-frames. In building to this scale, process developments were achieved for tow-placed skins, drape formed stiffeners, braided/RTM frames, and panel cure tooling. Over 700 tests and supporting analyses have been performed for crown material and design evaluation, including structural tests that demonstrated limit load requirements for severed stiffener/skin failsafe damage conditions. Analysis of tests for tow-placed hybrid laminates with large damage indicates a tensile fracture toughness that is higher than that observed for advanced aluminum alloys. Additional recent ATCAS achievements include crown supporting technology, keel quadrant design evaluation, and sandwich process development.

INTRODUCTION

The timely development of advanced composite technologies for wing and fuselage structures will ensure that U.S. manufacturers maintain a majority share of the world

---

[1] This work was funded by Contract NAS1-18889, under the direction of J.G. Davis and W.T. Freeman of NASA Langley Research Center.

market for transport aircraft. The US government currently finances such developments under the NASA funded Advanced Composite Technology (ACT) program. Developmental funding such as ACT is crucial to the future of the U.S. aircraft industry and, since a large number of commercial aircraft manufactured in the U.S. are sold abroad, provides long term national benefits. Quoting from the AIAA Bulletin, July 1992, "the U.S. aerospace industry is our country's largest exporter of manufactured goods, generating a $30-billion trade surplus in 1991." In addition to financial support, NASA personnel provide technical direction and support for solving difficult issues associated with the advancement of composite manufacturing, materials, and structures within the ACT program.

Boeing's NASA-funded program entitled Advanced Technology Composite Aircraft Structure (ATCAS) has been active for more than three years. As stated, the objective of this program is to "Develop an **integrated technology** and demonstrate a confidence level that permits the **cost and weight-effective** use of **advanced composite materials in transport fuselage structures for future aircraft**". The three statements highlighted with bold print represent *how, why,* and *what,* with respect to ATCAS activities.

This paper constitutes a technical overview of the ATCAS program and is broken into four main parts. The first section reviews the integrated team approach used in ATCAS and introduces team members supporting the program. The remaining three sections give details on (1) *why* ATCAS believes composite technology will replace aluminum in future fuselage barrel structures; (2) the critical path of *how* ATCAS is pursuing this technology; and (3) *what* ATCAS has achieved since the last ACT conference.

ATCAS TEAM MEMBERS

Early efforts in ATCAS dedicated a significant amount of time to developing a design build team (DBT) approach to concept selection, evaluation, and optimization (see References 1 and 2). This approach provided each member with a sense of ownership in program accomplishments. Initial team developments were not always achieved efficiently and were often the result of long periods of intense discussion which eventually resulted in a compromise between the various engineering and manufacturing disciplines. As time progressed, individual team members became more aware of the overall ATCAS plan and technical issues associated with composite fuselage structures. Less time was spent in DBT meetings because the agendas were clearly defined and team members learned to work closely together without the formalization of a scheduled meeting. As a result, the ATCAS team approach has matured further, yielding timely solutions to the multidiscipline problems which need to be addressed on a critical path to composite fuselage technology development.

The total number of people which have worked ATCAS tasks at Boeing is on the order of 100. The primary ATCAS team members from Boeing Commercial Airplane Group (BCAG) are listed in Figure 1.

Additional team members crucial to the ATCAS program include personnel from other Boeing divisions and industry within the U. S. Figures 2 and 3 list these personnel, their

affiliation, and companies' location in the western and eastern portions of the U.S. Those groups highlighted in bold print have co-authors that directly supported ATCAS papers presented at this conference.

Program Manager:
R. Horton

Technology Manager:
P. Smith

Principal Investigator:
L. Ilcewicz

Business Management:
M. Apeles

Structural Design
M. Morris
K. Griess
M. Schramm
S. Metschan

Weights Engineering:
G. Parkan

Manufacturing R&D:
K. Willden
T. Davies
M. Gessel
K. Goodno
V. Starkey

Material & Processes:
D. Scholz
D. Grande

Operations Technology:
J. Valdez
B. Luck

NDE Development:
B. Lempriere
S. Finn

Structural Mechanics:
T. Walker
E. Dost
G. Swanson
B. Flynn
J. Bodine
G. Mabson

Cost Estimating:
B. Humphrey
K. Venters
D. Tervo
L. Witonsky

Technical Support:
W. Waltari
T. Le

Figure 1. ATCAS team members from Boeing Commercial Airplane Group.

Company	Location	People	Work description
Boeing Defense & Space Group	Kent, WA	W. Avery, K. Nelson, D. Polland	Fabrication analysis and test
Boeing Computer Services	Bellevue, WA	B. Dopker, W. Koch R. Lundquist, D. Murphy	Computational structural mechanics
Hercules Inc.	Salt Lake City, UT	C. Grant, G. Walker, Y. Tokita, T. Brown, D. Cairns, D. Cohen	Advanced tow placement technology
Zetec Inc.	Issaquah, WA	C. Fitch, G. Colvin J. Siegel, P. Spencer	Flexural wave inspection/ damage characterization
ICI Fiberite	Tucson, AZ	R. Hoelthe	Tow and tape materials
Integrated Technology Inc.	Bothell, WA	B. Coxon	• Element and coupon testing • Stiffened panel impact
The Dexter Corporation Hysol Aerospace Products	Seattle, WA	J. Montgomery	Syntactic foam materials
Hexcel	Dublin, CA	F. Lee, Y. Wang	Sandwich core material processes
Hydrosabre Technologies Inc.	Kent, WA	J. Hillman	Water-jet machining
Northrop Corp.	Hawthorne, CA	R. Deo, R. Vastava	Design cost trade studies for fuselage cutout details
TORR Technologies	Auburn, WA	G. Lindstrom	Silicon reusable vacuum-cure bag
Engineering consultant	Bellevue, WA	J. McCarty	Fuselage structures
Aircraft Products	Anaheim, CA	P. Foskett	Silicone extrusions

Figure 2. Other Boeing and industrial groups supporting ATCAS: western United States.

Company	Location	People	Work description
Boeing Helicopters Division	Philadelphia, PA	C. Gunther, P. Grant, M. Fedro, A. Sawicki	• Braided composite mechanics • Bolted and bonded joints
Sundstrand Aerospace	Rockford, IL	H. Saatchi, W. Durako, R. Reynolds	In situ foam process development
Dow UTC	Wallingford, CT	R. Andelman	Design-cost relationships for textile processes
Sikorsky Aircraft	Stratford, CT	C. Kassapoglou	Design and cost contraints for sandwich structure
Fiber Innovations	Norwood, MA	G. Sharpless	Braided preform and RTM process development
Materials Sciences Corp.	Blue Bell, PA	A. Caiazzo, W. Rosen	Keel design stability analysis
3M	St. Paul, MN	W. Schultz, G. Vandesteeg	Powder-epoxy materials
Foster Miller Inc.	Waltham, MA	G. Freitas	Z-reinforcement technology

Figure 3. Other Boeing and industrial groups supporting ATCAS: eastern United States.

To date, the expanded composite expertise that other Boeing divisions and industrial subcontracts bring to the ATCAS team has well justified the additional coordination efforts by BCAG. Detailed monthly reports published for ATCAS serve as an efficient means for continually updating team members on the overall program status and schedules.

Several university subcontracts and co-op students also support ATCAS. Figure 4 shows the universities which were active during the last year and their individual work tasks. Those highlighted in bold print are currently still supporting the program. University subcontracts have been found to require significantly more time to coordinate efforts that directly support the hardware application goals of ATCAS. The additional time required to coordinate university work is primarily due to an education gap that is related to a difference between issues addressed in academia and industry. The Boeing Company recognizes this and has plans to close the gap.

The ATCAS program reflects Boeing's commitment to improving college relations through a close tie with the university subcontracts. Most ATCAS subcontracts which are still active have been focused to specific hardware issues, providing both student and faculty with educational benefits associated with real-world problem solving. Boeing coordination has provided descriptions of fuselage structures and their function, associated problem definitions, test data, and a technical assessment of progress. Technology transferred from university subcontracts to ATCAS team members has been timely, allowing developments to be integrated into design, fabrication, analysis, and testing of major hardware articles. Again, a commitment to detailed monthly reports have been helpful for task coordination and review.

Several lessons learned from the infusion of university subcontracts in ATCAS are worthy of note. First, it is best to select baseline design concepts, define related technical issues, and collect some hardware data before establishing a subcontract. In other words, define problems that relate to the program focus. Second, the solution to many industrial problems requires a multidiscipline approach, again highlighting the need for close

coordination between the DBT and any subcontract. Finally, sufficient manpower and time must be allocated to facilitate education and technology transfer between industry and academia. Schools that encourage student co-op programs and graduate students or faculty that have had industrial experience can help minimize the coordination effort.

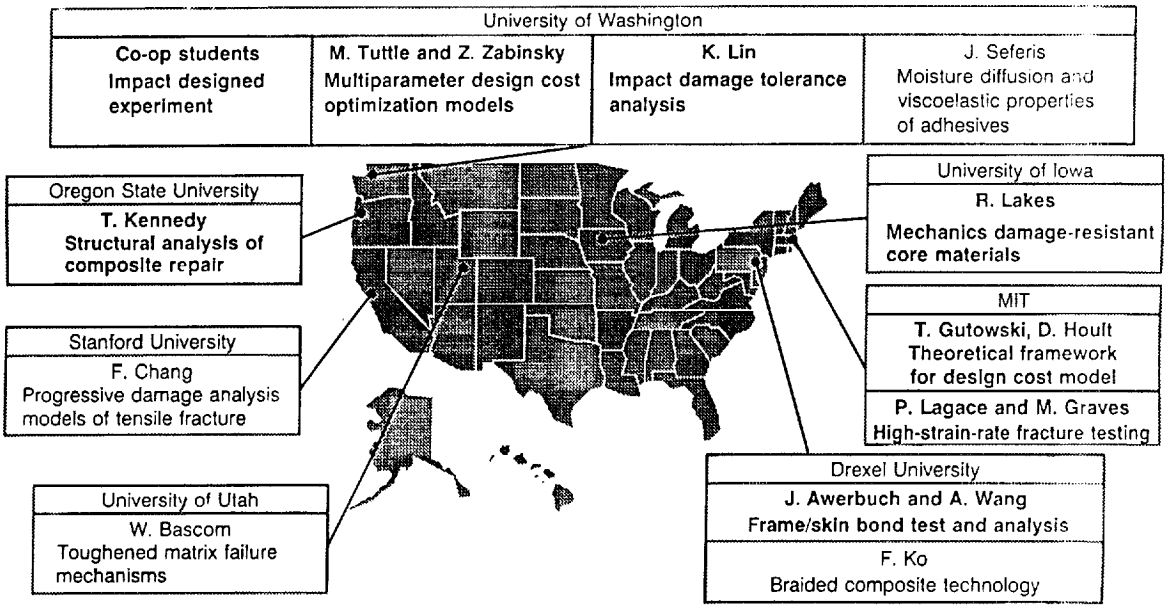

Figure 4. University subcontracts supporting ATCAS.

Several other partners have helped focus and support ATCAS technology development. These include Boeing programs for composite internal research and development, composite 777 empennage, and metal fuselage. Several U.S. airlines (American, United, and Northwest) have reviewed Boeing ATCAS design concepts and associated technology issues (repair and inspection). The Hercules ACT program continues to provide ATCAS with manufacturing and test hardware. The Lockheed ACT program is working to develop and optimize textile technologies for fuselage framing elements. The Lockheed efforts are currently coordinated with the ATCAS DBT for keel and side panels and will eventually yield parts for manufacturing trials and structural tests. As mentioned earlier, personnel from NASA Langley have contributed to ATCAS with analysis, mechanical tests, technical direction, and continuous management review. Although ACT program focussing and the integration of a larger team have not come without growing pains, the overall benefits are evident in ACT achievements.

COMPOSITE VERSUS METALS TECHNOLOGY OVERVIEW

ATCAS Approach and Schedule

An aft fuselage barrel, Section 46 of a wide body aircraft (20 ft. diameter), was selected for Phases A and B studies in ATCAS. As shown in Figure 5, four "quadrant type sections" (crown, keel, and left & right sides) constitute major panel assemblies around

the circumference of the composite study section. The metal counterpart has ten panels that splice to make up a barrel section. As discussed in reference 1, quadrants were selected for ATCAS during baseline trade studies which indicated that automated manufacturing methods for large composite panels are cost competitive with aluminum construction.

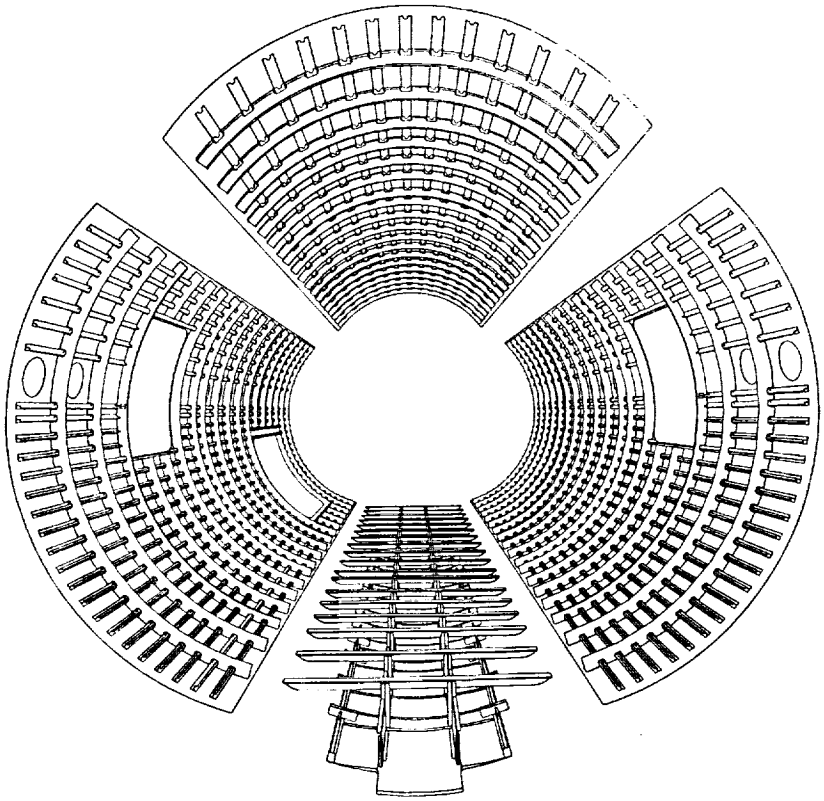

Figure 5. ATCAS quadrants for aft fuselage section.

During the first year of ATCAS, baseline design, manufacturing processes, and materials were selected for the four quadrants shown in Figure 5. Figure 6 shows timelines for work on each quadrant and major panel splices. Work is nearly completed for the crown quadrant. Efforts on the keel quadrant have progressed to local optimization. Keel scaleup and verification will be completed for aft portions of the panel approximately one year before those in the more difficult forward end. Side quadrant cost and weight evaluation is about to start. It will progress in close coordination with the Lockheed ACT program. Local detail studies for splices have just started for the crown and keel quadrants. Note that initial design efforts with major longitudinal and circumferential splices occurred during global evaluation for each of these quadrants.

The primary reason *why* ATCAS is pursuing its objective is to ensure readiness to take advantage of cost and weight savings projected for future composite technology. References 1 and 2 give detailed descriptions of the baseline concepts, associated technical issues, and the global/local DBT approach used to evaluate cost and weight. During global evaluation, initial cost/weight comparisons are made between the ATCAS baseline concept, alternative composite designs, and aluminum technology projected for

1995. This helps to select concepts that: (1) have cost and weight savings potential, justifying more detailed study and (2) have acceptable risk for manufacturing scaleup and test verification within the scheduled timeframe. Attempts to minimize cost and weight focus on the details of a single concept during local optimization. During local studies the DBT gains better understanding of the technical issues, manufacturing cost, material performance, structural design details, and critical interactions. An update on the cost and weight comparison with aluminum fuselage technology is also obtained during this phase of study. Global/local efforts by the DBT continue to justify *why* ATCAS is pursuing composite technology by keeping track of metal fuselage advancements as the composite design matures. At the end of studies for each quadrant, more accurate cost and weight comparisons will be made based on the results of manufacturing trials and major tests.

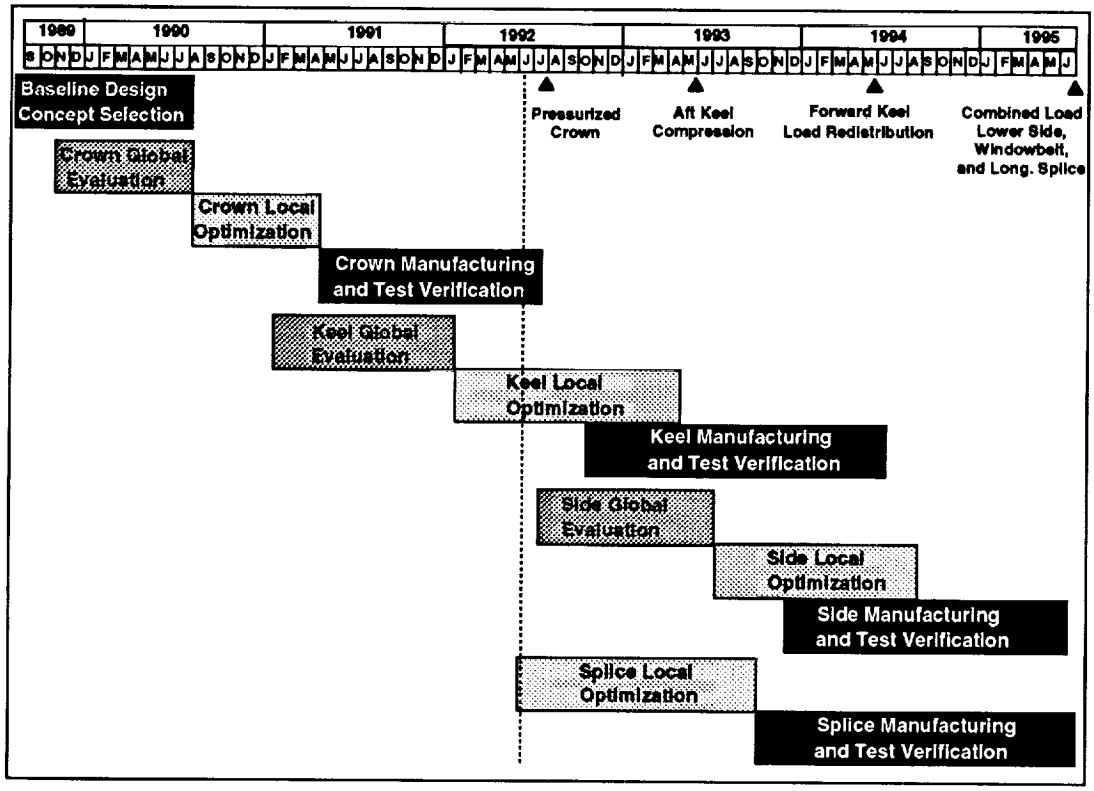

Figure 6. Timelines for crown, keel, side, and splice studies.

Crown Quadrant

Local optimization for the crown was completed in 1991. Since that time, the comparative metal technology has not remained stagnant. Consequently, there was a desire to update trade studies to account for advances in metal technology. In addition, the baseline fuselage configuration changed, affecting loads. Information from crown panel manufacturing trials also lead to a desire to redesign some ATCAS crown structural details. Finally, there was a desire to change ATCAS crown quadrant size from 90^0 to 99^0. All of these issues and the associated ATCAS design changes were addressed at the same time. Technical details of these changes will be discussed in the

final section of this paper. Figure 7 shows the current cost/weight relationship between the updated ATCAS crown concept and advanced aluminum technology. A line is shown to represent the cost/weight trade potential of aluminum structural design concepts, advanced alloys, and manufacturing processes. Note that the composite concept has lost some of its potential weight savings versus that shown in reference 3. This is due to the metal advances, a more detailed investigation of fuselage requirements, and composite design changes.

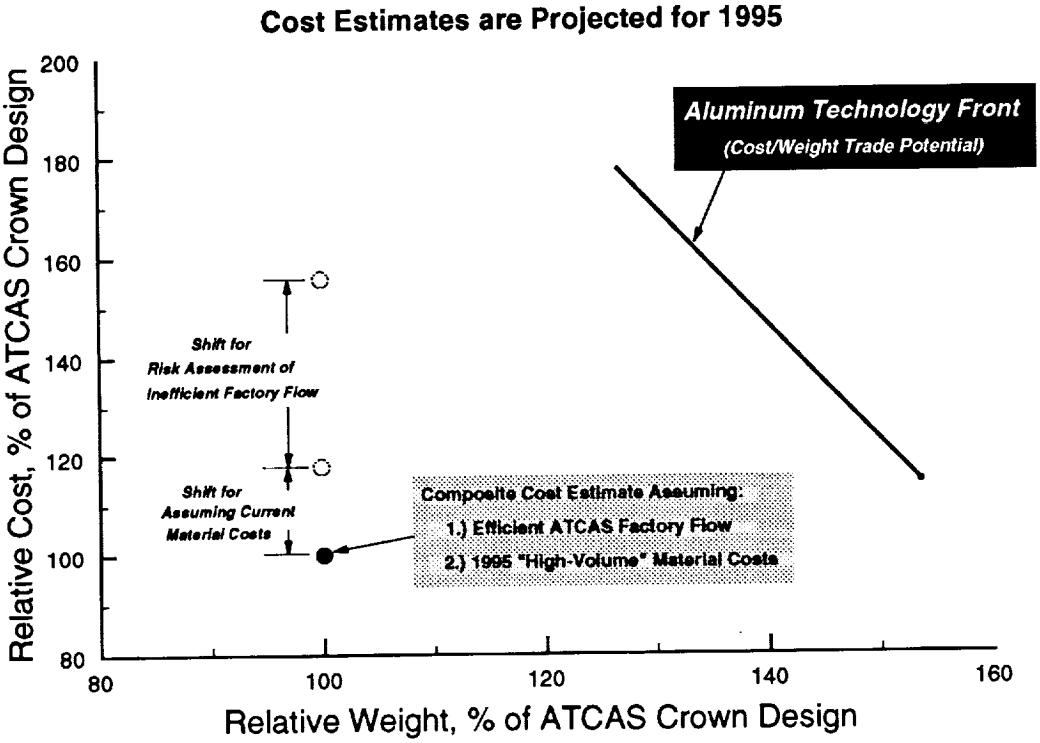

Figure 7. Fuselage crown panel cost/weight comparisons

Trade study results in Figure 7 indicate that the composite concept has potential for significant cost and weight savings as compared to advanced aluminum technology. Assumptions which are critical to these projections include reduced composite material costs and efficient ATCAS factory flow. Current material costs would drive the total cost of the composite crown quadrant up by approximately 20%. An even larger potential cost increase is projected if an efficient factory flow is not achieved. This risk relates to the problem whereby actual design details selected for the structure cause inefficient factory processing (e.g., defect control, machine maintenance, and increased touch labor). Design changes late in a hardware program, which can be forced by factors outside the control of a DBT, could negatively impact nonrecurring tooling costs. Such an effect can be large and is beyond that which is estimated in the risk analysis for Figure 7. A flexible tooling approach is needed to reduce the chance of such problems occurring in a hardware program. Less advancements in the composite manufacturing technology than projected would also increase costs. The study and control of factors affecting the cost of selected processes constitutes efforts being spent on an ACT design cost model. More will be said on this subject later.

Strength Versus Toughness Trades

Several design drivers were important to sizing the ATCAS crown quadrant. These included tension damage tolerance (axial and hoop), panel stability under compression and shear load conditions, minimum skin gage for hail impact, and minimum panel stiffness requirements for overall aircraft stability. In addition to the study section, these design approximately 70% of fuselage area (minimum gage panels). At the start of ATCAS, very little information existed to support the design of composite structures with large damage sizes representative of failsafe conditions. To date, ATCAS crown tasks have included the collection of composite tension fracture data and the application of existing methods for predicting damage tolerance. The latter subject will be covered in the last section of this paper. A review of the fracture data is given here to facilitate a comparison with aluminum alloys used in metal design.

Figure 8 shows tensile residual strength curves generated from small and large notch data for alloys used in aluminum fuselage and for composite laminates studied in ATCAS. A large database supports the metals curves shown in Figure 8, while ATCAS residual strength tests for IM7/8551-7 tape and AS4/938 tow-placed laminates include notch sizes up to 12 in. (refs. 4 and 5). A strength versus toughness trade is apparent in both classes of materials. For example, 7075-T651 and IM7/8551-7 both have high undamaged strengths but lower fracture toughness (i.e., greater notch sensitivity as shown by the rate of decrease in residual strength with increasing notch size) than the other two materials. The lower toughness relates to the small damage zones that occur at a loaded notch tip in 7075-T651 and IM7/8551-7 and the resulting inability to relieve local stress intensity.

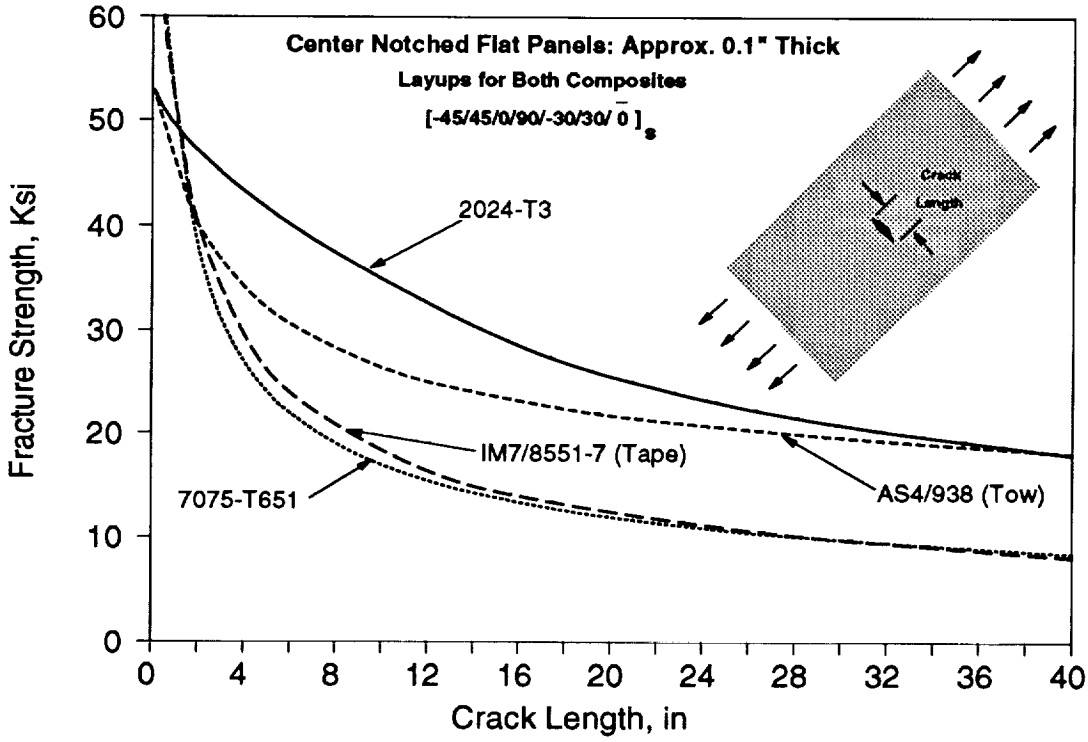

Figure 8. Tension residual strength curves for aluminum and composite materials.

The 2024-T3 aluminum gets its relatively high fracture toughness from crack tip yielding (i.e., plasticity), while AS4/938 gets relief from the notch tip stress intensity through other mechanisms such as matrix cracking and delamination. These same mechanisms lead to relatively low small notch strengths for both 2024-T3 and AS4/938. In metals, the phenomena is referred to as "net section yield". Note that the curve for AS4/938 has a different shape. This is possibly due to a differing relationship with finite panel width, a trait that tends to mask the material's high fracture toughness until larger notch and panel sizes are tested. The lower tensile residual strengths for IM7/8551-7 tape with large damage indicate composite materials that resist some modes of matrix damage (labeled "tough" in past literature) may not be suitable for fuselage skins.

Strength versus toughness trades are well recognized for aluminum alloys used in transport fuselage design (e.g., ref. 6). Skin typically consists of a material with low yield strength and high plane stress fracture toughness (e.g., 2024-T3). This helps to resist skin damage growth under fatigue and also leads to higher stiffened panel residual strength. An advanced aluminum alloy referred to as C-188 has somewhat higher toughness, without reduction in yield strength. This alloy appears attractive for future applications because skin forming processes have been demonstrated with the material at a large scale. Stiffening elements generally make use of alloys with significantly higher yield strength and lower toughness (e.g., 7075-T651). This promotes damage arrestment (failsafe design) and also leads to higher stiffened panel residual strength. The aluminum fuselage is actually a composite optimized for the design requirements; and hence, a better understanding of the years of experience behind such structures can be useful for polymeric composite design. In fibrous polymeric composites, residual strength for accidental damage threats and failsafe design practices become the important issues, while fatigue related skin crack growth similar to that encountered in metals is probably not a problem.

Figure 9 shows the strength versus toughness property trades for several other metals considered in fuselage structures and composite laminates tested thus far in ATCAS. Two sets of X and Y-axes appear in the figure, one for composite laminates and the other for metal alloys. The two X-axes show properties related to strength and "Ultimate" design load requirements (i.e., yield strength for metals and small notch strength for composites). The two Y-axes show properties related to large damage tolerance (i.e., plane stress fracture toughness for metals and an effective fracture toughness parameter representative of large notch data for composites). The location of specific metal alloys on the curve depends on % constituents, grain size, and associated process variables (e.g., heat treatment and stretch forming). In an analogous manner, the position of composites on the figure depends on several material, laminate, and manufacturing process variables. In general, "toughened" matrices, hard layups, and smaller levels of repeatable microstructure lead to high strength and low toughness. Hybridization, "brittle" matrices, soft layups, and larger levels of repeatable microstructure tend to lead to lower strength and high toughness. References 4 and 5 give additional details related to the composite database.

Results given in Figure 9 (plotted as stress parameters) and supporting technical reports represent one of the most significant findings in ATCAS to date. In particular, large

panel tests made possible by ACT funding show that composites considered for advanced fuselage have mechanical properties that are competitive with metal alloys currently used in fuselage. Some composite laminates (e.g., [-45,45,0,90,-30,30,0,30,-30,90,0,45,-45], IM7/8551-7 tape) are shown to have higher strengths than 7075-T6. Other composite laminates (e.g., tow-placed intraply hybrids) have an effective fracture toughness that is significantly higher than 2024-T3. The baseline crown material for ATCAS, tow-placed AS4/938, can trade a wide range of strength and toughness through layup changes. In summary, the advanced technology potential of lower density composite laminates appears very attractive for future applications in minimum gage areas of a fuselage.

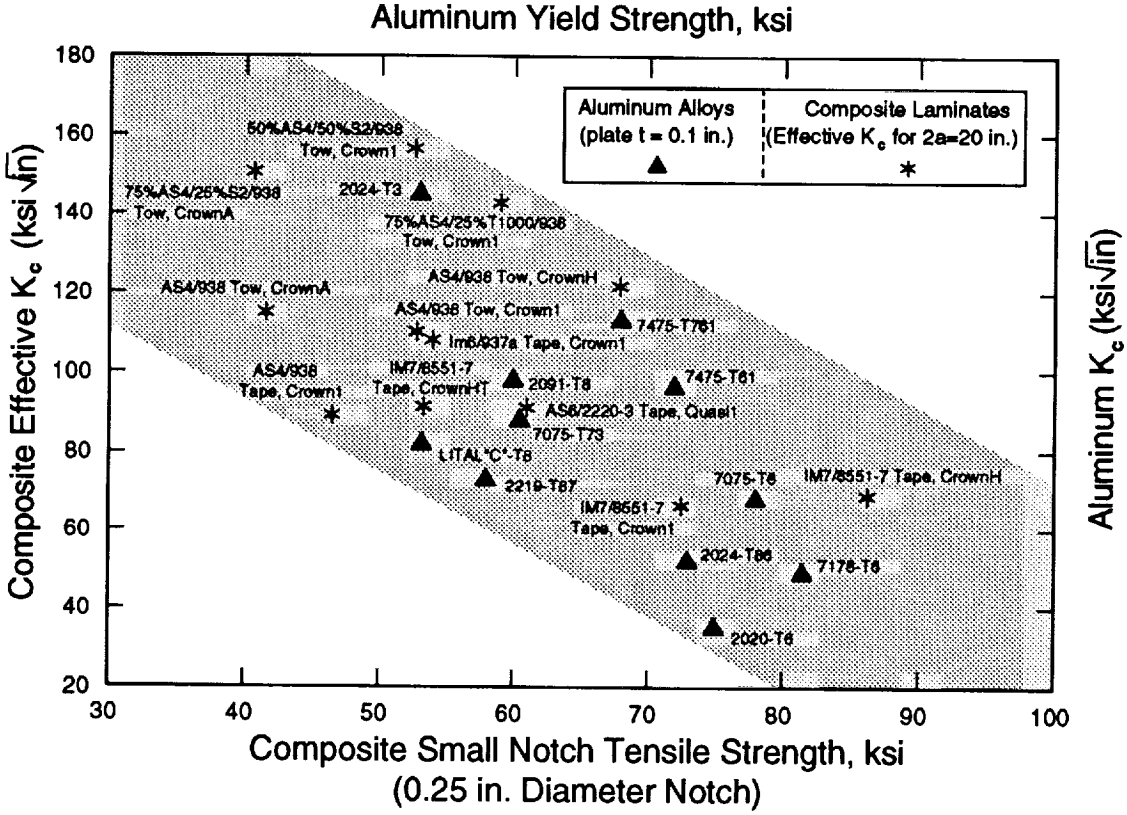

Figure 9. Tension strength versus toughness trades for metals and laminated composites.

Keel Quadrant

Global evaluation of the keel was completed in early 1992, including cost and weight trades between baseline sandwich (Family D) and alternate stiffened panel (Family C) designs. This initial design work for the keel was significantly more difficult than the crown global evaluation due to major load redistribution at the forward end (a result of the large wheel well cutout in the wing/body intersection) and associated design requirements. Composite manufacturing processes suitable for the structural design detail used in aluminum construction would yield high cost and weights. As a result, innovative "panelized keel beam" (i.e., thick laminate) design concepts were pursued to replace discrete keel beam chords at the forward end of the keel quadrant. A panelized

concept was designed for both Families C and D designs. Based on the results of this study, the baseline sandwich design was the desired candidate for more detailed local optimization work. In addition to cost and weight trades, this DBT decision was based on an assessment of technical issues which need to be addressed and the associated risk of demonstrating manufacturing and test verification within the scheduled timeframe. Note that some of the technical issues for a sandwich design have been studied since it was selected as the baseline concept in 1990. Another paper presented at this conference (ref. 7) describes keel global evaluation in detail.

Figure 10 compares the composite Family D keel concept selected for detailed studies and the aluminum technology front. Note that the difference between composite and aluminum weight is significantly less than currently projected for the crown quadrant (see Figure 7). Cost is projected to be competitive with aluminum, as was the case for the best designs and processes from crown global evaluation. A local optimization target zone is shown in Figure 10, representing estimates of additional cost and weight savings possible during more detailed studies. The best scenario projects an additional 20% cost and weight savings. Note how points in Figure 10 shift based on the ability to realize projected material costs and factory efficiency. Discussions given earlier in reference to Figure 7, also pertain to these cost risks.

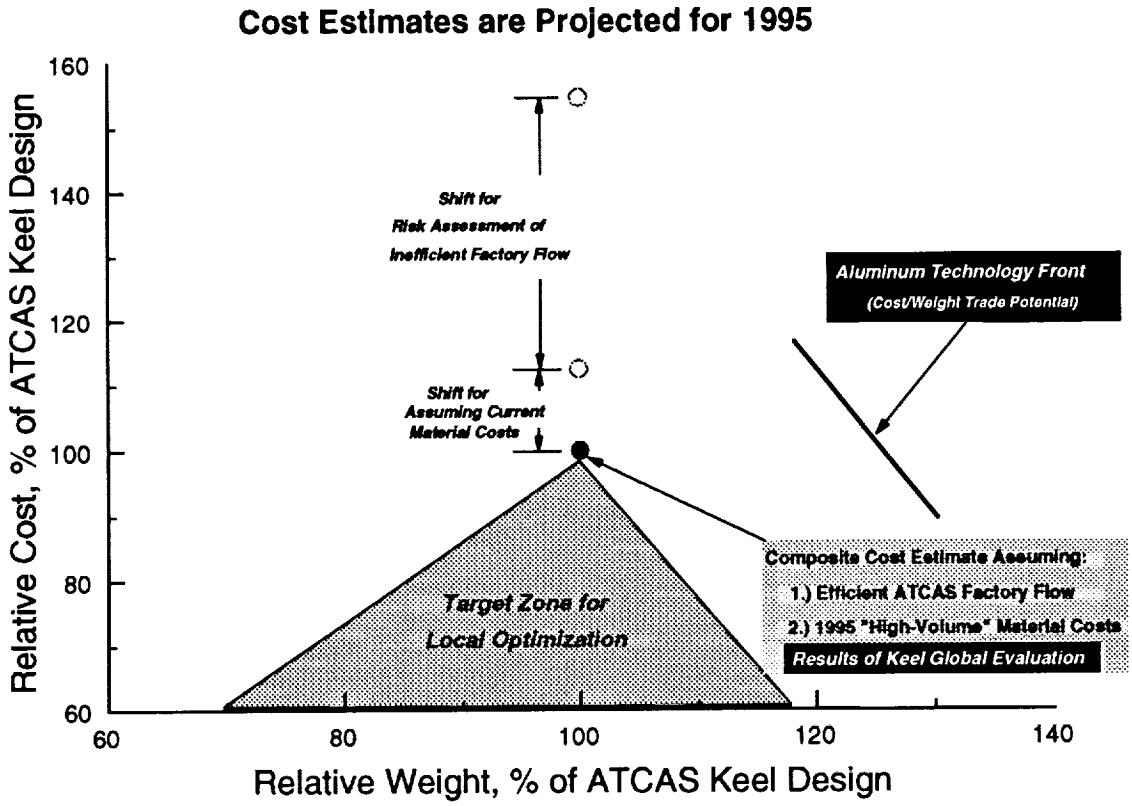

Figure 10. Fuselage keel panel cost/weight comparisons.

CRITICAL PATH TO TRANSPORT FUSELAGE

Phase C Description

As discussed at the start of the last section, an integrated team approach is being used by ATCAS to develop and verify advanced composite technology for transport fuselages. Phases A and B will be completed in 1995, providing a subcomponent database for quadrants and major splices in the full barrel study section. Boeing is currently proposing a Phase C effort to start in 1995. Phase C will concentrate on full-scale manufacturing demonstration and structural verification of the fuselage technology currently being investigated. This section will describe *how* a critical path will be pursued through Phases A, B, and C to be "technology ready" for a composite transport fuselage application.

The combination of manufacturing trials, test database, and supporting analyses from the first two phases will provide fuselage barrel design tools for Phase C. Materials, design concepts, and manufacturing processes are currently selected by DBT cost/weight trades before committing to manufacturing trials and major tests. The DBT also identifies critical issues to solve for selected concepts and then defines appropriate process and test plans. Information collected in fabrication trials (i.e., tooling development and curved panel scaleup) include documentation of process steps, nondestructive inspection data, dimensional tolerance measurements, and cost data. Mechanical tests yield a database to characterize material properties, textile fiber architecture, laminate layup, and structural design details. Building block tests for the latter range from stiffening elements and large unstiffened skin panels to curved subcomponent panels that include stiffeners and frames. An understanding of manufacturing and performance relationships with structural details is critical to the hardware database needed to support Phase C design. As a result, composite parts from process trials are used for mechanical tests. Analyses to support the database include developments in mechanics of materials, structural mechanics, manufacturing science, and design cost modeling.

Phase C will continue to develop and document supporting materials, structures, and manufacturing technologies which facilitate future applications to fuselage sections. Another part of Phase C includes a study to resolve critical issues for the wing/fuselage intersection. This effort will start with DBT cost/weight trades and culminate with detail design, fabrication, analysis, and test of selected structural components (e.g., keel beam). Phase C culminates with a full-scale demonstration of the ability to design and fabricate a fuselage barrel section with predictable performance and manufacturing cost.

Detailed critical path schedules have been developed to guide ATCAS Phase A and B efforts. The scheduled length of bars and associated descriptions shown at the top of Figure 11 (i.e., before the marker indicating an end of ACT Phases A and B) summarize tasks from more detailed schedules. Shaded bars highlight achievements to date. A description and time estimate of major Phase C tasks that complete the critical path to technology readiness are also shown in Figure 11. These tasks span a period from 1995 to 2002. More accurate schedules for these tasks will be created by the end of 1992.

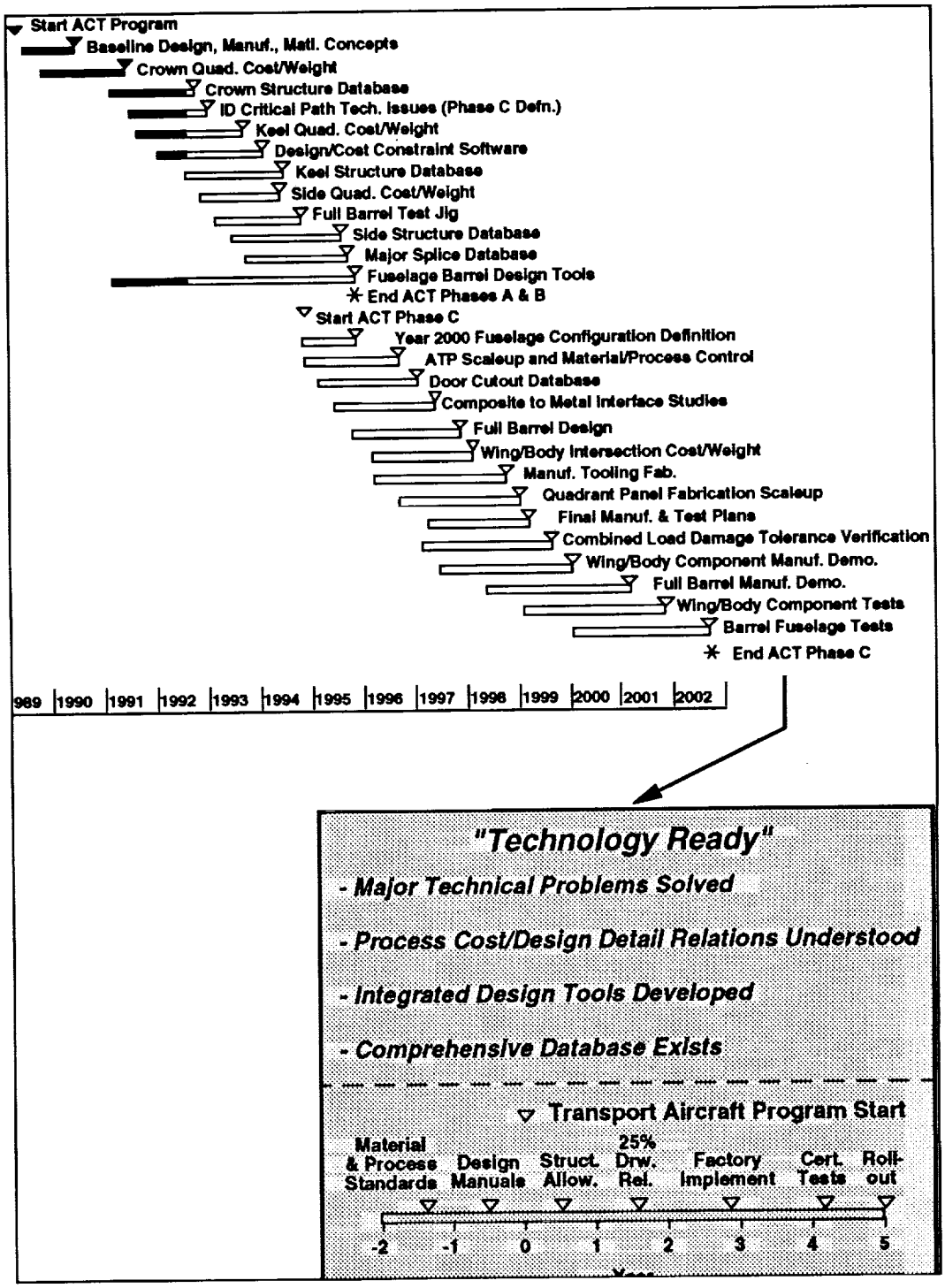

Figure 11. Critical path to composite fuselage.

The bottom of Figure 11 illustrates that the combined results of ATCAS Phases A, B, and C will yield a level of technology readiness which, if combined with Boeing internally funded efforts (e.g., other fuselage sections, material and process standards, design manuals, and structural allowables), would prepare the company for commitment to a composite fuselage application. Major technical problems will be solved during the

course of the program studies. Relationships generated between structural details and total manufacturing costs will provide future hardware designers with insight on how their decisions affect the efficiency of selected processes. These relations will be integrated into design tools that include sizing analyses and comprehensive test results, providing the composite structural database needed to make commitments to a major hardware program. The combination of ATCAS and IR&D results will allow Boeing to generate standards, manuals, and allowables which facilitate hardware design.

List of Ten Technical Issues

The overall ATCAS goal of demonstrating technology readiness will be achieved when major technical issues have been addressed in sufficient detail to provide the necessary confidence for committment of composites to commercial transport fuselage applications. Ten items were identified as representing especially critical issues to be addressed in Phases A, B, and C. These are listed below.

1.) Manufacturing scale-up of configured panels
2.) Damage tolerance of crown, keel, and side panels
3.) Inspection and repair technologies for selected designs
4.) Load redistribution near major fuselage cutouts
5.) Technology developments for low-cost framing elements
6.) Wing-to-body intersection development program
7.) Structural detail/manufacturing cost relationships for selected designs and processes
8.) Integrity of bonded elements in configured fuselage structures
9.) Development of mechanical joints for major panel splices
10.) Metal-to-composite interfaces

A multidiscipline team of manufacturing, structures, materials, and design engineers are currently addressing these issues. All issues but number 6 are currently under study.

Discussion of Technical Issues

Manufacturing scale-up of configured panels. Manufacturing trade studies by the ATCAS DBT has suggested that large composite fuselage panels, referred to as quadrants, have potentially lower costs than aluminum technology. This relates to projected cost benefits of automated tow placement (ATP) and the assumed reduced assembly labor for bonded stiffening elements and less longitudinal splices because of the larger panel sizes (i.e., 4 instead of 10). Key manufacturing demonstrations which are needed to verify such cost savings include: (a) ATP for tailored fuselage skins, (b) panel cure tooling, (c) configured panel process trials, and (d) manufacturing tolerance control. Such technologies will be developed at a subcomponent level during Phases A and B and then scaled to full size in Phase C.

Figure 12 shows the relative size difference between panels manufactured in Phases A and B versus the larger size panels which will be fabricated during Phase C. Initial cure trials are performed at a size less than or equal to the 3 ft. by 5 ft. curved panels shown in the figure. While these small panels yield some useful information on the cure cycle and

tooling details at stiffener and frame intersections, they are not large enough to provide necessary information on manufacturing processes and tolerances. The ATCAS DBT selected 7 ft. by 10 ft., curved panels to more sufficiently evaluate whether the selected design concept and processes lend themselves to the quadrant approach to cost savings. Each panel process step is evaluated versus assumptions used in cost estimating. In addition to demonstrating processes and collecting cost data, ATCAS manufacturing trials provide panels for element and subcomponent tests.

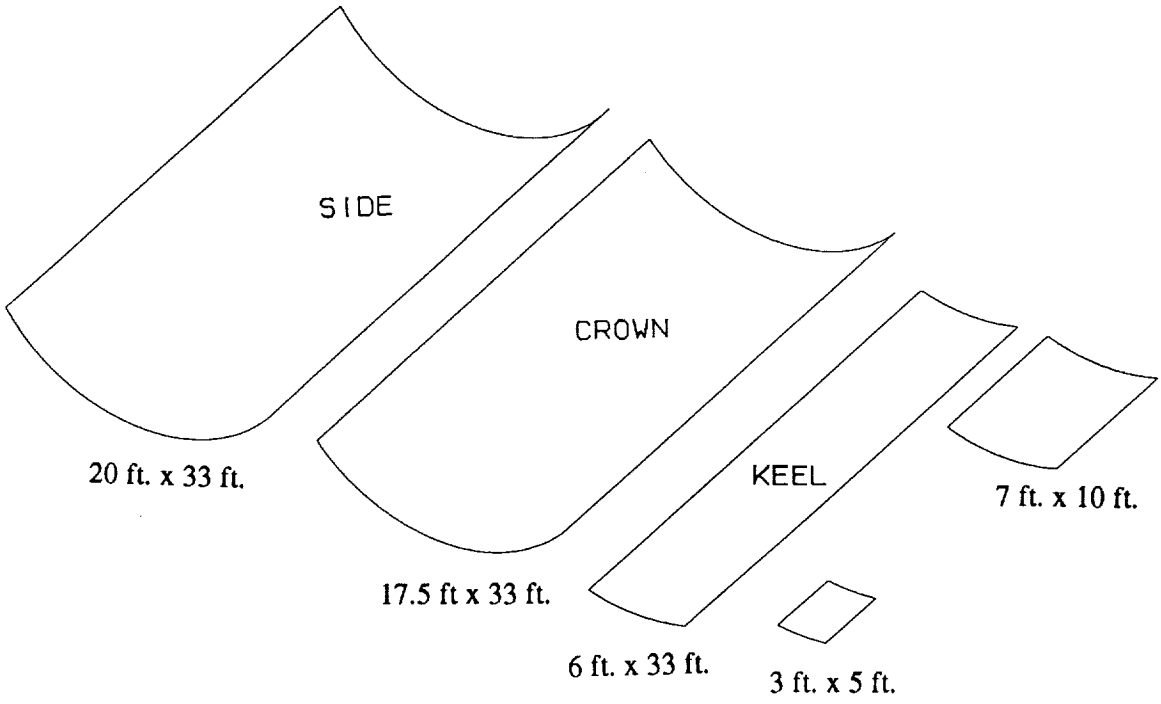

Figure 12. Large panel manufacturing demonstration.

Locational tolerance control and panel dimensional stability must be achieved to reduce the large panel assembly costs. Stiffeners and frames must be processed, machined, and aligned on the skin within tight tolerances to achieve the former, while the latter requires control of overall panel warpage and local distortion of curved design details. Advanced tooling designs are being pursued to ensure that bonded elements are located accurately on the panel. All considered baseline designs (i.e., stiffened panels with bonded stiffeners and frames and sandwich panels with bonded frames) will be sufficiently stiff following cure and; hence, it will not be possible to overcome mismatched tolerances with excessive assembly force. Costly shimming and rework would increase the assumed assembly costs, negating the advantages of large panel fabrication. Measurements taken after cure evaluate the success of each tooling concept considered in ATCAS. The manufacturing issues of overall panel warpage and local distortion (i.e., referred to as spring back) are being addressed by the DBT with the support of test measurements and structural analysis. Test measurements taken for stiffened panels have indicated that the cured panel distortion relates to temperature, local stiffener design detail, and a mismatch between skin and element coefficients of thermal expansion (ref. 8). Analysis developments which have been performed to support these tests will be applied to

constrain detailed design (e.g., element and skin laminate layups, local element geometry) and support tooling design.

Damage tolerance of crown, keel, and side panels. Damage tolerance design criteria consistent with that for current production aircraft has been adopted to ensure structural integrity for damage ranging from nonvisible defects to failed structural units. Design load requirements for the various types of damage are described on the left side of Figure 13. The "Ultimate" design requirements have considerable margin of safety over loads that the aircraft is expected to see during its lifetime. This provides conservatism in designing for a class of damage and defects that are difficult to define, analyze, and test. In practice, this condition is demonstrated for composites with barely visible impact damage or relatively small penetrations (e.g., classified nondetectible). The "Limit" design requirements are governed by larger damage sizes defined as a loss of elements (e.g., stiffener, frame, length of skin) or structural units (e.g., combined loss of stiffener and adjacent skin bay). Since limit loads can occur during the lifetime of an aircraft, requirements to consider large damage sizes promote failsafe design practices in which the damage will likely be found and repaired within inspection intervals. The final part of the damage tolerance design philosophy, continued safe flight, relates to large discrete source damage (e.g., engine failure) which occurs in flight with knowledge of the crew. Lower load conditions are used for this requirement because the crew will knowingly limit aircraft maneuvers. Note that such discrete source damage scenarios that are critical for cabin pressure are designed to limit conditions.

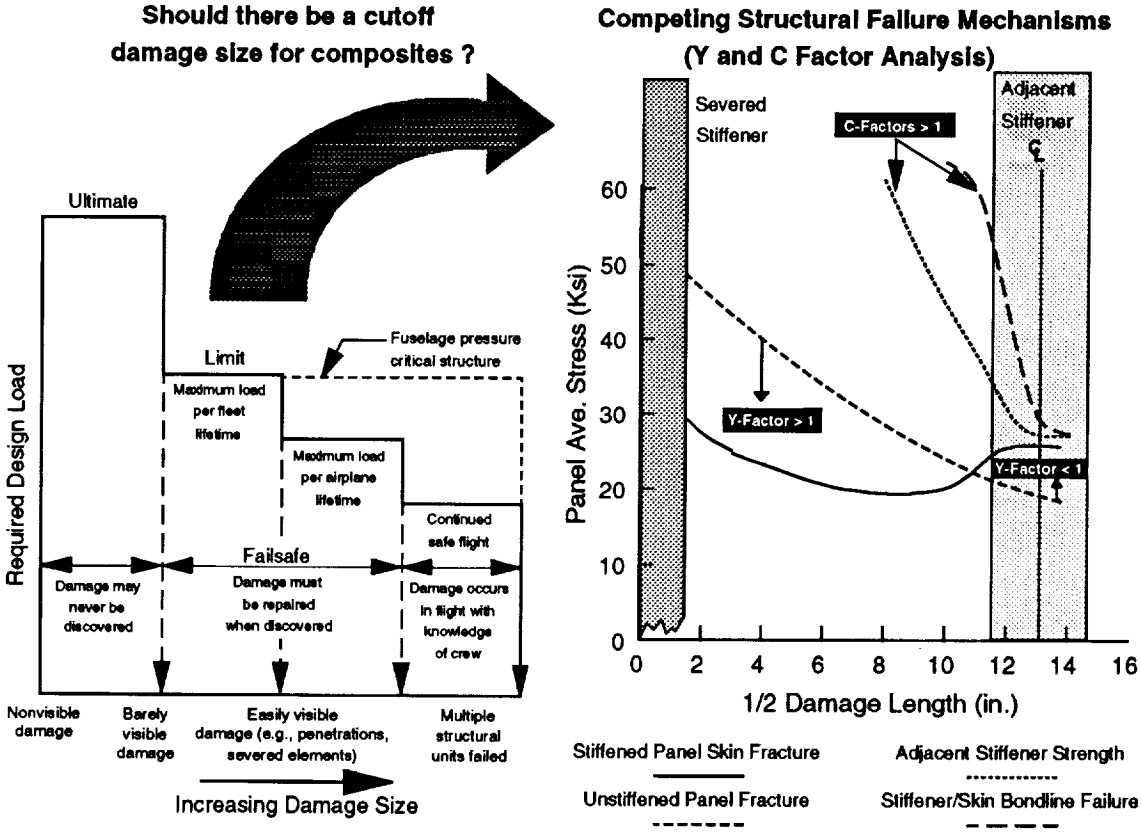

Figure 13. Damage tolerance design philosophy.

Metal fuselage structure has followed failsafe and damage tolerance design practices for some time because fatigue crack growth is a critical issue. The right side of Figure 13 illustrates that redundant structural design practices with multiple stiffening elements promote the arrestment of damage at a sufficiently large size to ensure that it is found and repaired. Note that cracked stiffened structures with severed elements allow small damage growth at lower stress levels than an unstiffened structure (due to loads redistributed to the skin from a severed element). However, larger damage growth is arrested in the former and unstable in the latter. As a result, the redundant stiffened design sacrifices the potential for greater small damage strength for overall improved damage tolerance, assuming that it is easier to find large damage and restore the structure to full capability in a timely manner.

One question often asked for composite structures is "since composites do not have fatigue crack growth problems similar to metals, should there be a cutoff damage size for limit design requirements?" Possible impact or penetration threats for a transport aircraft include (a) large foreign object impacts that occur in service (e.g., runway debris, birds, and ice), (b) maintenance accidents (e.g., tool drop and wind blown scaffolding), (c) collisions with service vehicles, (d) lightning strike, (e) sabotage, and (f) impact events due to the failure of other aircraft parts (e.g., tire burst, systems failures). These events may result in clearly visible damage that may go either unreported or undetected prior to subsequent service. Failsafe design practices for addressing metal fatigue issues have had the additional benefit of ensuring the structure is good for large impact or penetrating damage events. The ATCAS program has adopted damage tolerance design practices which enforce limit load requirements for loss of a structural unit. As discussed in the previous paragraph, the redundancy of a stiffened panel design is such that the structure is failsafe for both small and large damage sizes. This eliminates the need to define a cutoff damage size. The same cannot be said, however, for composite sandwich structures. The question of cutoff damage sizes for composite sandwich designs will be addressed by considering the largest penetrating damage sizes imposed for stiffened structures.

The schematic in Figure 13 shows residual strength analysis for a balanced design in which performance is achieved through a compromise between three competing structural failure mechanisms. The "Y-factors" shown in the figure quantify the effect of structural configuration on the shape of a base residual strength curve (i.e., unstiffened skin fracture). When Y-factors are greater than 1 (e.g., damage sizes in the shadow of the severed stiffener), damage growth will occur at stresses less than those for an unstiffened skin. When Y-factors are less than 1 (e.g., damage sizes approaching the adjacent stiffener), the opposite is true. In the case of Figure 13, structural configuration factors result in damage arrestment. In the analysis of damaged structure, C-factors quantify the effect of load redistribution on panel residual strength. The "C-factors" shown for large damage sizes in Figure 13 are greater than 1, indicating higher stress levels in the adjacent element and skin/stiffener bondline. Load redistribution into adjacent elements results in lower stresses in the damaged skin (i.e., Y-factors less than 1). If either the element or bondline stress exceeds their respective strengths, the Y-factor for skin damage growth will increase, reducing the panel residual strength.

Nonlinear elastic and plastic analyses are needed to calculate accurate configuration and load redistribution factors for metal fuselage structures. In composites, progressive damage aspects of the problem require attention. As in the case of plastic analysis for metal structures (e.g., ref. 9), an efficient method of simulating progressive damage is required to facilitate detailed structural modelling for composites. Strain softening laws which have been used for other structures consisting of heterogeneous materials (e.g., reinforced concrete) appear to have merits for composite structural analysis. Composite structures are also sensitive to impact damage and combined load conditions that include compression and shear. As a result, methods are needed to simulate damage and combined load failure events. ATCAS progress in these areas will be discussed in the last section of this paper. A large structural test database to verify fuselage damage tolerance is planned for Phase C.

Inspection and repair technologies for selected designs. An important part of composite structural design and manufacturing development is the supporting technologies that address the "ilities". These include maintainability, inspectability, and repairability. As more and more composite components are developed and integrated into transport aircraft, airlines are concerned that existing maintenance practices will need to be updated to reflect basic differences in the structure. An airline task group has been studying these issues as related to advanced composite design practices. It is this group's contention that aircraft manufacturers should address the cost of ownership during detailed design. This concern has recently been expressed to the ACT steering committee, including descriptions of design details that have caused problems with existing composite aircraft parts. Similar concerns have been expressed by Boeing sustaining groups for composite secondary structures currently in service (ref. 10).

During the last year, ATCAS detailed design efforts for fuselage structures have been coordinated with the airline task group. When addressing maintenance issues during design and concept development, it is important to realize that the structure can and will get damaged in numerous different ways. Examples of damage occurring to composite structures in service have been brought to the attention of the ATCAS DBT. Members of the airline task group have expressed a concern about specific features of proposed designs including (1) the combination of bonded frame and stiffening elements (i.e., bolted or bonded repair procedures for the bonded frame and stiffener intersection would be difficult), (2) the use of unidirectional lamina for exterior plies (prefer fabric or other form of more robust surface layers for wear resistance and mechanical fastened repairs), and (3) large quadrant panel size (repair procedures for major damage would be forced to occur without panel removal).

The airlines warned that incomplete procedures will result if a too limited number of damage scenarios are considered during inspection and repair technology development. As discussed in the last subsection, a number of different damage conditions are being considered in designing for damage tolerance. The development of suitable repair procedures and nondestructive evaluation (NDE) methods for the selected design details are under study. Examples of NDE technology under development in Phases A and B include ultrasonic procedures for intricately bonded elements, foam core sandwich panels, and an advanced flexural wave method suitable for field inspection. The development and demonstration of mechanically fastened repair procedures for large

penetrating damages that include severed bonded elements is under study for the crown. Non-autoclave bonded repairs with powder prepregs will be pursued for impact damage to keel sandwich panels. Both these efforts will be coordinated with the airlines, with an end goal of having airline maintenance personnel repair representative structural test articles. Expanded efforts in the areas of inspection and repair are planned to be accomplished during Phase C.

Load redistribution near major fuselage cutouts. Load redistribution near fuselage cutouts such as the wheel well and doors (cargo & passenger), complicate the three technical issues discussed thus far. Considerable variations in compression and shear loads exist in the keel and lower side quadrant due to wheel wells and cargo doors. Several developmental tasks for composite design, manufacturing, and performance evaluation are planned to address problems of load redistribution in these areas. Earlier discussions in this paper indicated that some composite materials are damage tolerant due to the ability to redistribute concentrated loads through localized matrix failure mechanisms. While this is a favorable trait for large damage tolerance, localized matrix failure would not be an acceptable mode for transferring flight loads around major cutouts (e.g., possible durability and dimensional stability problems would likely arise due to a lack of local stiffness). The same can be said of metal plastic deformation. As a result, skin thickness tailoring is needed in the neighborhood of major cutouts to ensure that strain levels seen in service remain below that which would cause permanent damage or deformation in the chosen material.

The keel studies have focussed on a thick laminate/sandwich "panelized design concept" in place of the discrete keel beam chords used in aluminum structure to beam loads around the wheel well and aft into the main body of the fuselage shell. Process developments are needed for curing the advanced thick skin/sandwich concept. In addition, ATP manufacturing developments such as laminate thickness tailoring (add/drop on the fly) and lamina fiber angle change are needed in this application to promote composite advantages over metals technology. Personnel from the Hercules ACT program are currently coordinating their efforts with the ATCAS DBT to develop the necessary manufacturing technologies that allow scale-up to 6 ft. by 10 ft. forward keel demonstration panels.

Material and structural details to be addressed for panel areas surrounding major cutouts include (a) the use of toughened matrix materials and higher resin contents to facilitate interlaminar shear load transfer in thickness transition regions, (b) thick laminate response to variable compression/shear load distributions, (c) impact damage resistance, (d) penetration damage tolerance of toughened matrix materials, (e) thick laminate splices, (f) panel dimensional stability, and (g) associated repair and inspection technologies. Building block tests in Phases A and B will address inplane and transverse shear load redistribution. A final curved panel having the same width as the full-scale keel panel and fixturing to simulate compression load redistribution at the forward end of Section 46 will be tested before the start of Phase C.

Global evaluation and detailed design of a passenger door cutout for the side quadrant is currently planned to occur during Phase B. Both the Lockheed ACT program and a Northrop subcontract for the design cost model will support this effort. Due to the level

of effort required, Phase B will not be able to start global/local design studies of the cargo door cutout. Development of door cutout structures including, all remaining design studies, supporting analyses, manufacturing trials, and subcomponent tests are scheduled to occur early in Phase C.

Technology developments for low-cost framing elements. Composite fabrication processes for fuselage framing elements that have relatively complex geometries need to be developed to minimize cost differences with current metal technologies. Elements which require development include circumferential frames, window frame modules, door cutout framing details (e.g., longerons, intercostals), and floor support structures. Early ATCAS trade studies selected advanced textile/resin transfer molding (RTM) processes as having potential for minimizing the cost of frame elements. The dimensional stability of elements processed from textile preforms and the RTM process was also expected to be good. The development of cost-effective fabrication methods and the associated process control is crucial to the acceptance of many textile/RTM material forms. Standard ultrasonic NDI methods used for inspecting tape laminates must be enhanced to separate defects from the higher levels of inhomogeneous textile microstructure.

In addition to process development, mechanics of materials and structural mechanics work is needed for textile materials. For example, constitutive relationships, structural scaling laws, design sizing analyses, and test databases are needed to predict mechanical performance. Since textile failure mechanisms are distinctly different than traditional laminated materials, they must be understood to support this effort. Of particular interest, is the relationship between the large microstructure, failure mechanisms, load redistribution, and structural geometry.

Significant work has been performed in ATCAS to develop braided/RTM fabrication methods for curved crown frame elements. Mechanics of materials analyses have also been developed for braided materials (ref. 11). These efforts will end with crown panel fabrication and testing tasks in 1992. All future efforts in manufacturing will be limited to design build team interactions with the Lockheed ACT program. Lockheed is planning to pursue textile technology developments for side and keel panel elements, yielding optimized framing elements to be included as part of large panel tests. In addition to RTM processes, advanced powder technologies will be evaluated by the Lockheed program.

Wing-to-body intersection development program. A Phase C study is proposed to address critical technical issues for composite structures in the wing to body intersection. Although the issues that need to be addressed are the same as those for other areas of the fuselage, structural details and loads are significantly different. In addition, very little composite work has been performed for this area of a transport aircraft. Phase C design efforts for components of the wing/body intersection will start with a comprehensive cost and weight trade study similar to the global evaluation used in prior phases (i.e., preliminary design, detailed manufacturing plans, and cost estimates for selected concepts). This would be followed by local optimization where detailed design efforts are supported by analysis, fabrication trials, and building block tests. Finally, subcomponents would be manufactured and tested to address critical process and performance issues for selected design concepts. Candidate subcomponent panels and

splice details for this study include: (a) portions of an upper wing panel, (b) sections of a keel beam box concept, (c) elements of the keel beam splice and side of body joint, (d) bulkheads and fittings, (e) portions of the pressure deck, and (f) subcomponents from body side panels.

Advanced technologies for fuselage barrel sections must consider the connection with structures in the wing/body intersection. For example, synergistic relationships exist between a fuselage barrel based on selected design concepts and the ability to develop an advanced keel beam concept in the wing to body intersection. The panelized keel quadrant concept was selected for Section 46 assuming that a keel beam box structure could be manufactured to react large compression loads near the wheel well cutouts. If a different keel beam design configuration is needed due to cost or performance issues (e.g., a design similar to traditional metal structure), the keel quadrant design in the full barrel would require changes due to different internal loads and attachment details. Such changes need to be recognized before committing to a full scale fuselage barrel demonstration. This is one example of the need to do some development work with the wing to body intersection as part of Phase C.

Structural detail/manufacturing cost relationships for selected designs and processes. Manufacturing costs are a major concern in replacing aluminum technology with composites. The ATCAS global/local design build team (DBT) approach was established to study structural detail/manufacturing cost relationships. Manufacturing technologies under development in Phases A and B are projected to have significant cost savings versus advanced aluminum construction. As discussed earlier in reference to Figures 7 and 10, the relationships between manufacturing costs and structural details must be understood prior to the start of a hardware program to constrain design characteristics to a range that ensures efficient factory flow. To achieve this goal, manufacturing studies have been directly tied to detailed design, promoting critical assessment of the capabilities of selected processes. Manufacturing trials are collecting databases to support the development of design cost analysis tools which will help constrain hardware design within a range where process cost savings are achievable.

Design analysis tools are needed to support the hardware program DBT with a timely estimate of the cost of structural details for selected manufacturing processes. Modification 13 to ATCAS will develop and verify a design cost model suitable for transport fuselage structures and composite manufacturing processes (ref. 12). The Phase A and B deliverables for this effort include:

(a) theoretical design detail/cost relationships for fuselage structures and selected composite manufacturing processes

(b) design analysis methods to size fuselage structural details and constrain design decisions affecting manufacturing tolerances

(3) software for predicting design cost, performance, and weight

(4) optimization algorithms to blend design details over variable load conditions and design requirements within cost, weight, and performance constraints

(5) documentation of design tool usage, including results from applications and sensitivity studies.

The model will be packaged as Cost Optimization Software for Transport Aircraft Design Evaluation (COSTADE).

The COSTADE design tool will help the Phase C DBT select design details which are cost effective in fabricating a full barrel with the desired processes and tooling approaches. It will represent the manufacturing and structural databases generated during Phases A and B of the ACT program. A hardware design environment proposed for Phase C (e.g., schedule driven decision gates, long tooling lead times, simulated load changes, and interaction with planning, configuration, and systems groups) will help ATCAS evaluate the utility of COSTADE, flexibility in manufacturing tooling approach, and readiness for composite fuselage design.

Manufacturing scaleup efforts during Phase C will include a critical cost evaluation of the composite processes selected for fuselage barrel fabrication. In particular, ATP, textile/RTM, panel subassembly, curved panel cure, and other selected ATCAS processes will be studied at the detailed step level for recurring labor, machine time, scrap rate, rework, and maintenance issues. Data from these studies will help to judge cost modelling assumptions, update recommendations for future factory equipment needs, and assess the risks of a production program.

Integrity of bonded elements in configured fuselage structures. The designs for crown, keel, and side panels include cobonded frame elements. Crown panels have included cocured hat stiffening elements. Baseline side panels include cobonded window frames and stiffening elements. Manufacturing, analysis, and testing tasks are planned to support the acceptance of such structures by the industry, airlines, and FAA. To date, manufacturing trials have addressed panel subassembly, cure tooling, and autoclave cure issues associated with bonded crown panels. Tests are planned to evaluate the effects of skin postbuckling, pressure pillowing, and various damage scenarios in configured subcomponent panels.

Suitable structural test and analysis methods are needed to evaluate the residual strength and durability of composite panels with bonded elements. The ATCAS program has been performing strength and durability studies with bonded coupons and elements. Structural issues will require a larger scale of investigation. For example, element pull-off tests traditionally used for screening design concepts do not yield sufficient quantitative data to evaluate the debond growth mechanisms between stiffening elements and skin in a configured structure. Analysis and subcomponent tests that include pressure and postbuckling need to be performed to evaluate the effects of design details (e.g., intersecting elements and frame mouseholes) on the driving force for debond growth. The development of test methods which evaluate the durability of partially debonded elements contained within a configured structural arrangement are needed. The associated analysis to ensure proper load introduction into debonded elements contained in pressure boxes and other test fixtures needs to be included in the effort. Other analysis tasks include the development of design configuration (Y) and local load redistribution (C) factors for design details and combined load failure criteria for bonded joints. Sufficient efforts in collecting a database and developing structural analysis procedures will help ensure durable advanced composite designs (i.e., any debond growth is self arresting rather than unstable).

Alternate design concepts having lower risk and less development requirements have been considered. These include mechanical attachment of circumferential frames and elements that frame cutouts to skin panels with cocured stiffeners. Activities to combine bolted and bonded concepts will be pursued as well as studies of structural factors affecting debond growth and arrestment. The favored ATCAS procedure for debonded element repair includes mechanical fastening. Some process studies, analysis, and tests for alternate concepts with mechanically fastened frames will occur in Phase B to ensure the program is able to react to a change in the baseline design for Phase C. Such a change would occur if it is judged that the bonded frame technology has not matured to a level that justifies its risk in the full barrel manufacturing demonstration and test.

Development of mechanical joints for major panel splices. Mechanical attachment methods were selected as baseline for ATCAS longitudinal and circumferential fuselage splices. As discussed for the issue on manufacturing scaleup, dimensional tolerances of large, stiff quadrant panels must be closely controlled to avoid problems in panel splicing and body join. As part of the solution to this problem, innovative splice design concepts and the associated manufacturing methods which allow reasonable misalignment of stiffening elements will be pursued. Quadrant panel blending for longitudinal and circumferential panel splice details will be studied as part of local optimization design tasks for Phase B. Mechanical joint compatibility issues as related to differences between side and keel quadrant design concepts (i.e., stiffened panel and sandwich, respectively) will require special attention at the lower longitudinal splices. This is particularly true in load redistribution shadows near wheel well and cargo door cutouts. Current splice design details for quadrant panels include edge band padups in the skin. These details will be investigated as part of the Phase C manufacturing scaleup (ATP and quadrant panel fabrication).

Phases A and B efforts include the collection of coupon and element mechanical joint test data and supporting analyses for selected advanced material forms such as tow placed laminates and braided frames. The response of configured panel splices to combined load conditions, including pressure will be studied in Phases B and C of the program. Load sharing analysis methods will be developed to include the effects of nonlinear elastic and strain softening laminate behavior. These factors are expected to effect configured panel splice response under combined load conditions. The Phase B fuselage splice efforts culminate with two large longitudinal panel splice and one aft circumferential splice tests in the full-barrel pressurized test jig (Option 1 to Phase B). The Phase C activities will expand this effort, including further addressing damage tolerance and pressure containment issues.

Metal-to-composite interface. Since it is unlikely that all parts of a fuselage will be non-metallic, interface issues between metal and composite parts will need to be addressed. For actual aircraft application, solutions to interface issues may allow the use of composites for some fuselage panels or elements before composite application to an entire full barrel. For example, some fuselage parts in the wing to body intersection have sufficiently complex geometry that current metal processes have clear economic benefits over composites. Advanced hybrid fuselage structures that minimize cost and weight by utilizing the advantages of both metal and polymeric composite components could prove to be better than a structure consisting of one or the other.

As shown in Figure 11, significant time will be spent early in Phase C addressing the issues which relate to attaching composite and metal structures. This effort will include design, fabrication, analysis, and tests. Cost and weight risk analyses will identify fuselage structural components or elements which are best suited for metals. The combined effect of optimizing part cost at the expense of total assembled cost will be addressed while studying metal to composite interface issues. These issues include corrosion, durability, hygrothermal expansion mismatch, mechanical attachments, lightning strike, and electromagnetic force. The DBT will decide the specific composite to metal hardware combinations in which to perform detailed design, fabrication trials, structural analyses, and subcomponent tests.

ATCAS PROGRESS

The last overview paper written for ATCAS was presented at the First ACT Conference and highlighted progress on fuselage baseline concept selection and global evaluation of the crown quadrant (ref. 2). Crown local optimization was presented at the Second ACT Conference (ref. 3). The following discussions highlight crown manufacturing and test verification, keel local optimization progress, and plans for future work in the side quadrant and major splices. Note that the keel global evaluation is detailed in another paper presented at this conference (ref. 7).

Crown

Figure 14 reviews characteristics of the ATCAS crown quadrant. Note that the quadrant has changed from a 90^{o} to a 99^{o} segment. This increase was made based on a desire by the DBT to reduce the size of side quadrants. Any further increase in the crown quadrant size was not admissible due to issues related to the passenger emergency escape doors.

- **Cocured Hat-Stiffeners and Cobonded J-Frames**
- **Tow Placed Skin (AS4/938, 35% RC)**
- **Tow Placed, Drape-Formed Stiffener (AS4/938, 35% RC)**
- **2-D Braided/RTM Frame (AS4/RSL 1895, 37% RC)**

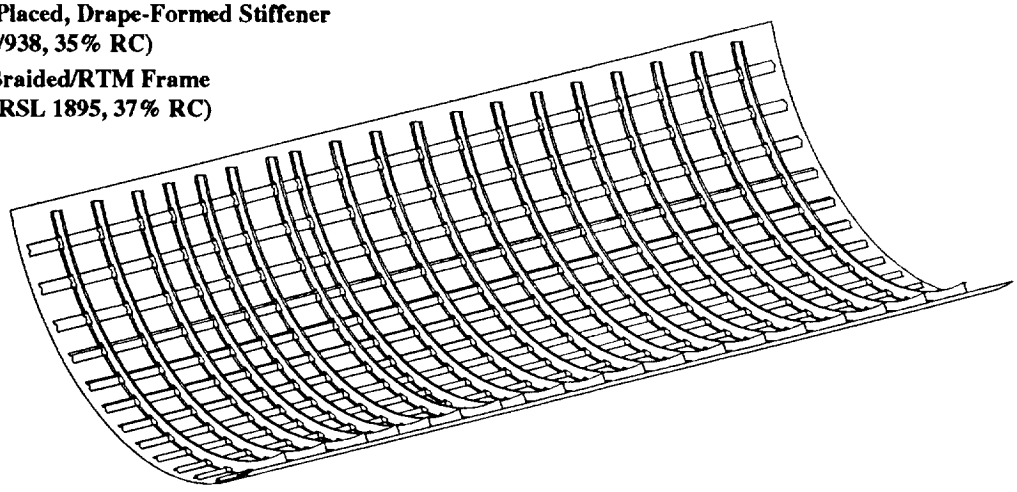

Crown Quadrant: 99^{o} Segment

Figure 14. Baseline crown design, materials, and processes.

Manufacturing Scaleup

Problems in Early Manufacturing Demonstrations. Soft tooling trials for the crown panel design were discussed at the last ACT Conference (ref. 13). These trials ended with two curved 3 ft. by 5 ft. panels that each included three cocured hat-stiffeners and three cobonded J-frames, i.e. braided frames were precured using an RTM process and then adhesively bonded during skin and stiffener cure. When the panels were inspected following the conference, hat-stiffeners were found to have some anomalies and geometric distortion. Skin and stiffener porosity and delamination were found in microscopic inspections. The latter was possibly caused by the laminated aluminum stiffener mandrels being difficult to remove after the panel was cured. Most of these problems were initially thought to be due to the segmented soft tooling approach and loss of the vacuum seal that occurred during the cure cycle.

Proceeding with the investigation, a flat 5.25 ft. by 12.5 ft. five stringer fracture panel without cobonded frames was fabricated at Hercules (ATCAS subcontract) using laminated aluminum stiffener mandrels and traditional bagging procedures instead of soft tooling. The bagging procedure worked well. Microscopy and NDE results indicated that the hat cross-sections were well controlled and the panel was free of anomalies such as porosity. Significant amounts of force and a special procedure for gripping the panel were required to remove the mandrels, causing some delaminations between the skin and stiffeners. Delaminations were repaired using mechanical fasteners and the fracture panel was successfully tested (see discussions later in this section). Past ATCAS hat-stiffened panels were fabricated using traditional bagging, coupled with silicon stiffener mandrels. Silicon mandrels for these trials were easily removed after cure but stiffeners had some fiber volume variation and angle distortion in cross-sections. Since laminated aluminum mandrels have a lower coefficient of thermal expansion (CTE) than silicon, better stiffener cross-sections were expected with the former.

Boeing ATCAS/Hercules ACT Design Build Team for Crown Panel Fabrication. Problems that occurred with curved soft tooling trials and the flat five stringer fracture panel, led to the formation of a special DBT to obtain solutions that would not have a major impact to schedules. The goal was to complete crown manufacturing work by mid 1992 so team members could pursue keel panel developments. Most ATCAS DBT work reported in the past has involved design cost and weight trade studies. The use of small DBTs to address more specific manufacturing and structures issues is common in airplane programs. Reference 14 gives additional details on the crown processing DBT.

Figure 15 shows the DBT members, problem definition, and the recovery schedule developed for the crown panel fabrication tasks. Team members for this effort included Boeing ATCAS and Hercules ACT personnel. A problem definition and several solution paths were obtained during the first month of the DBT work. Six main solution paths were considered based on their estimated chance for success. In order to minimize risk, the two most likely paths were selected. Significant cured panel warpage noted in early crown panel fabrication (overall axial panel warpage and local transverse spring-in at stiffener locations) was included as part of the problem definition in Figure 15. This warpage was thought to relate to thermal expansion mismatches for skin and stiffener layups, stiffener cross sectional geometry, and details of stiffener tooling, e.g. thin

aluminum lamina, thin silicon sheath, and adhesive inserts web/skin flange intersection. Such issues possibly added to problems observed with cure tool removal and cross sectional anomalies (ref. 8). Therefore, some design changes were considered for all solution paths. As part of these redesign efforts, the DBT also desired to increase crown quadrant size and update crown load conditions to facilitate comparisons with advanced aluminum concepts (see discussions in an earlier section). The schedule in Figure 15 shows specific tasks that were performed to obtain a solution to the problems.

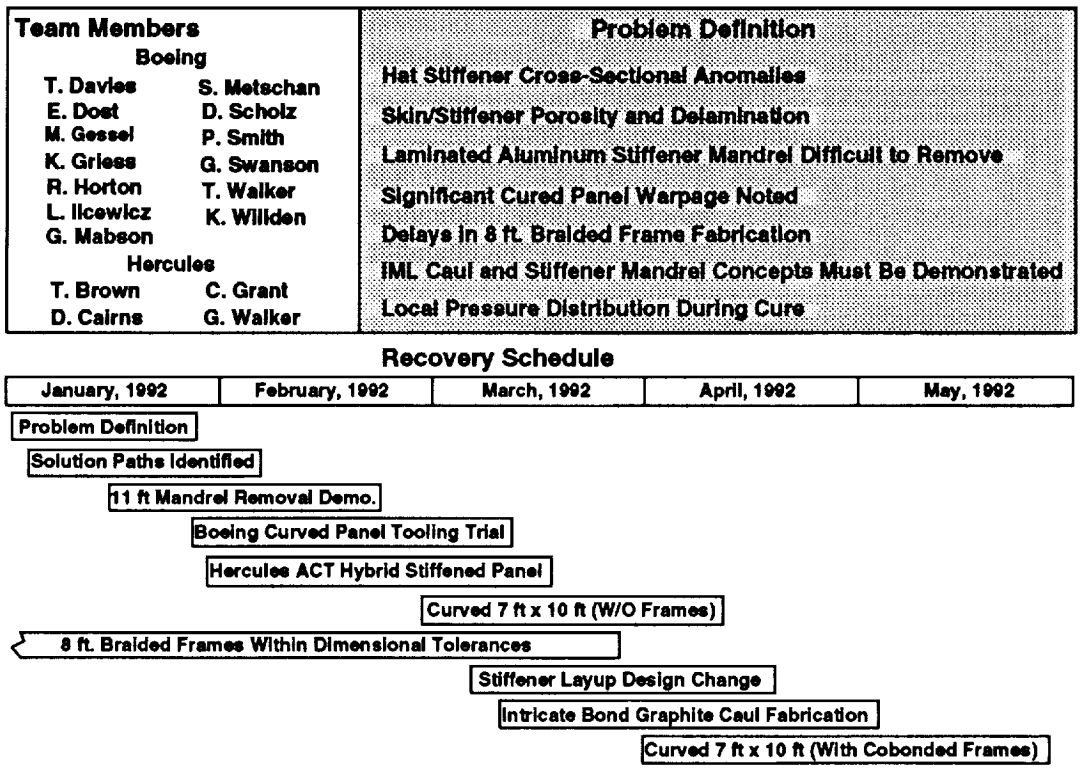

Figure 15. DBT to address crown manufacturing problems.

The solution path favored by the DBT retained the baseline design type, i.e. cocured hat-stiffeners and cobonded J-frames, but considered some changes in cure tooling and detailed redesign. Cure tooling for this option utilized silicon stiffener mandrels and advanced IML cauls. The latter was scheduled to be developed and demonstrated for curved panels over a two month period. The most attractive candidate for the IML caul included a combination of soft tooling at frame locations and segmented graphite cauls, e.g. thin precured fabric, for skin and stiffener areas between frames. Risks for this solution path related to cure tooling development and dimensional tolerance control for braided frames. Curved braided frame manufacturing development was taking considerably longer than expected due to tooling fabrication problems. As a result, braiding and RTM process step scaleup to the 8 ft. size had not yet provided dimensional tolerance data necessary to evaluate whether frames could be cobonded during the panel cure step. As shown in Figure 15, this data was expected by the end of March.

The alternate solution path involved changing to a Family B design concept, i.e. cocured hat-stiffeners and mechanically fastened J-frames, that had significantly less risk. This

concept was developed in parallel with the first solution path and many scheduled tasks supported both. Tooling developments for the Family B concept had significantly less risk for the allotted schedule. The large scale panel fabrication schedule for this concept also had little risk associated with delays in 8 ft. braided frame processes because the frames were not needed until panels were cured. In addition, manufacturing tolerances for a bolted frame concept were thought to be less than those needed for cobonding.

Cure tool developments. The first fabrication task supported both solution paths by demonstrating a skin/stiffener IML tooling approach and the ability to remove silicon mandrels from hat-stiffeners (i.e., "11-ft. mandrel removal demonstration" in Figure 15). The panel used for this task had the baseline skin layup and two stiffeners, one with a layup identical to the skin and the other representative of the original baseline design. Hand laid tape laminates were used for both stiffeners and skin. Three IML cure tooling approaches (two IML caul plate concepts and traditional bagging) were used in three different segments along the length of the panel. The two caul plates were precured graphite fabric (4 plies between stiffeners for flexibility during panel subassembly and 10 plies at the stiffener to help form the hat shape during cure). These cauls were precured on a male metal tool mockup of the panel's IML surface. Following panel cure, no problems were noted in removing the silicon mandrels. Stiffener cross-sections in areas that utilized the graphite cauls were well controlled. Cured panel warpage in the axial direction was distinct on the side with mismatched skin and stiffener layup, and significantly less on the other side. A photograph of the side with greater axial warpage is shown in Figure 16. Upon cutting the panel down the centerline to produce two 10 ft. one-stiffener panels, warpage was seen to increase for the side with mismatched skin and stiffener layup, while the matched side was found to have negligible axial warpage.

Figure 16. Tool development manufacturing trial for a 11 ft. long hat-stiffened panel.

Referring back to Figure 15, the scheduled task entitled "Boeing curved panel tooling trial", directly supported the first solution path. The flexible IML graphite caul concept, which produced good stiffener cross-sections for the flat panel in Figure 16, was modified to allow cobonded frames, characteristic of the baseline design. This tooling

redesign yielded a hybrid consisting of: (a) segmented graphite reinforced cauls for stiffened panel regions between frames, (b) soft tooling at frame intersections, and (c) mouse hole plugs to facilitate stiffener cure at the frame intersection. The modified tooling was successfully demonstrated at Boeing for a 3 ft. by 5 ft., curved, Family C panel with three cocured stiffeners and three cobonded frames. This trial fabrication utilized a 76 in. radius Boeing cure tool, compression molded fabric frames available for this geometry, and tape material for skin and stiffener laminates. With successful completion of this task, the main issue limiting the fabrication of a 7 ft by 10 ft Family C design was delays in the development of braided/RTM frames of acceptable dimensional tolerances for cobonding. A solution to this issue will be discussed later.

Manufacturing demonstration for the second solution path. Major tasks that supported the second solution path included fabrication of two large Family B panels, one flat and the other curved. The flat panel, referred to as the "Hercules ACT hybrid stiffened panel" in the recovery schedule, is shown in Figure 17. This panel was fabricated for the Hercules ACT contract number NAS1-18887 (ref. 15) and tested for axial damage tolerance by ATCAS. Silicon stiffener mandrels were easily removed from the cured panel and stiffener cross sections had no anomalies.

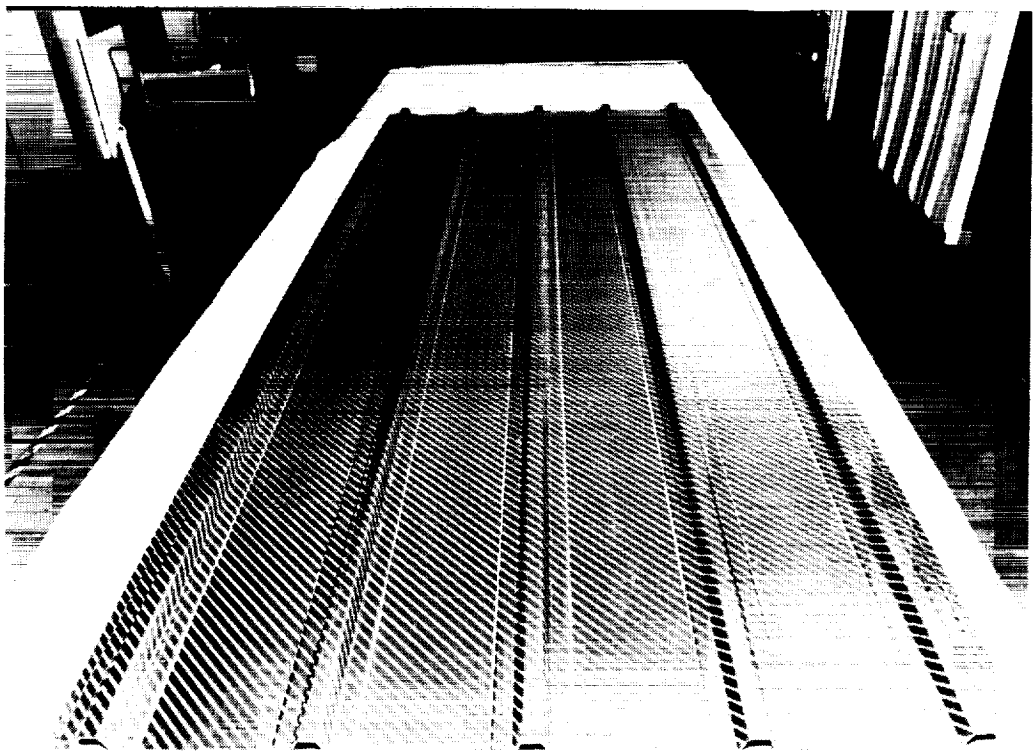

Figure 17. ATP intraply hybrid damage tolerance panel (63 in. by 150 in.) cured using a flexible graphite IML caul.

Figure 18 shows a curved (122 in. radius), 7 ft. by 10 ft. panel, successfully fabricated at Hercules under subcontract to ATCAS. This panel consisted of AS4/938 tow-placed skin and stiffeners. Panels in Figures 17 and 18 both used the same cure tooling, i.e. precured flexible graphite cauls and silicon stiffener mandrels. Since frames were not cobonded,

the IML caul was continuous for each panel. As was the case for the large flat hybrid panel, stiffener mandrels were easily removed and no stiffener cross sectional thickness anomalies were noted. Manufacturing trials that culminated in panels shown in Figures 17 and 18 successfully completed tasks for the second solution path, ensuring ATCAS had a backup position in the event that the cobonded frame concept was unable to scale to the 7 ft. by 10 ft. panel size. Additional manufacturing and test data comparing Family B and C concepts also enhance the DBT database supporting future design decisions (e.g., quadrant panels for Phase C).

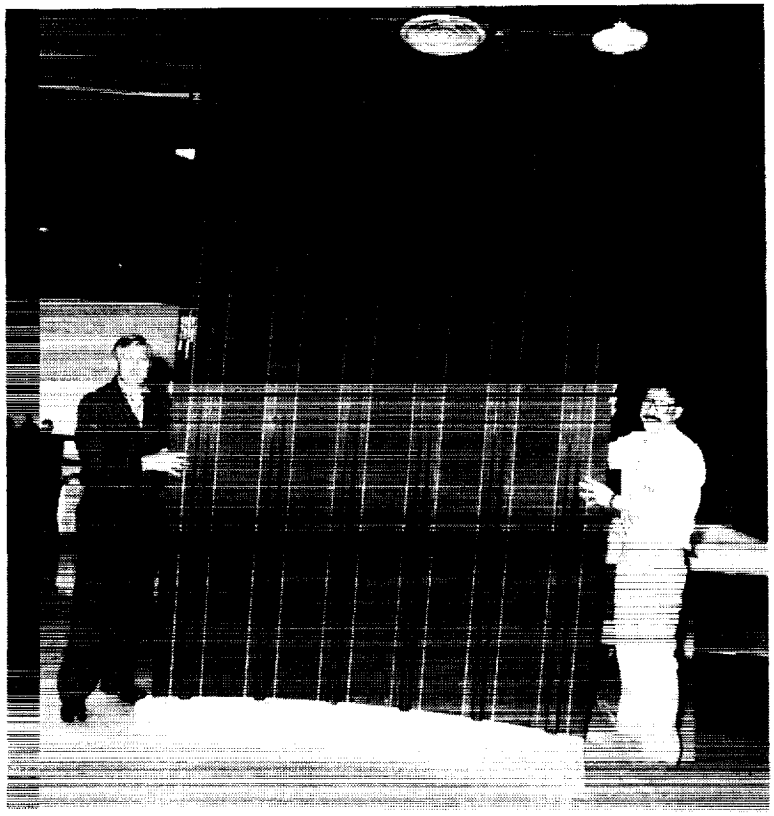

Figure 18. Family B crown quadrant manufacturing demonstration.

Both panels for Family B manufacturing demonstration had skin and stiffener layups from the original locally optimized design (ref. 3). As was the case for other fabrication trials with this design, panels were found to have significant axial warpage and transverse spring-in at each stiffener location. The effect of these manufacturing tolerances on the mechanical attachment of braided frames for the curved panel in Figure 18 will be addressed during the summer of 1992. Assembly issues for major panel splices will also be assessed based on measurements and analysis of panel warpage and local stiffener distortion (see methods described in ref. 8).

Braided/RTM Circumferential Frames. The scaleup of frame manufacturing processes occurred at Fiber Innovations as a collaborative effort with the ATCAS DBT. This task culminated with the fabrication of curved, 8 ft., J-frames for use with the 7 ft. by 10 ft. crown panel manufacturing demonstrations. Braided/RTM batch process developments

are discussed in references 13 and 14. Figure 19 shows one of the processing steps and the finished frames. Although braided frame manufacturing development caused significant schedule delays, the 8 ft. curved frames were of excellent quality. Tolerances measured for the cured frames were within limits that the DBT had set for pursuing the Family C scaleup. Several batches of frames were manufactured, allowing detailed cost studies on the process steps and their relationships with frame design details. Results are presented in another paper for this conference (ref. 16).

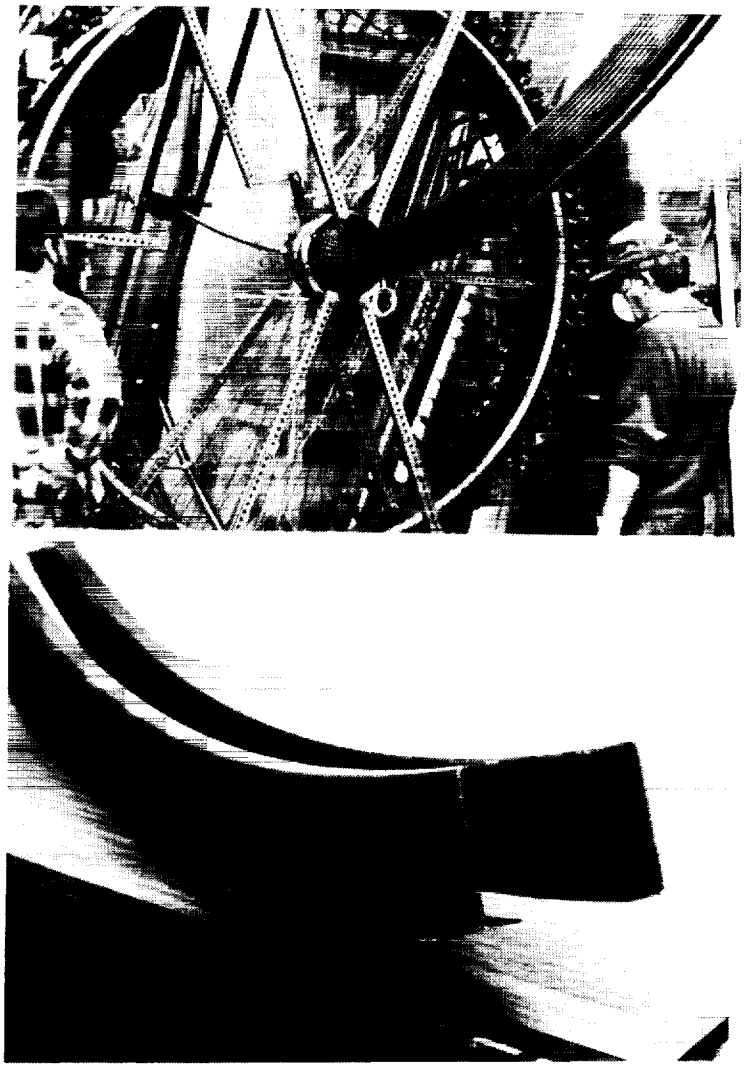

Figure 19. Braided technology scale-up; braiding on RTM cure mandrel (top) and machined 8 ft. frames (bottom).

Crown redesign. Tooling and process developments were successfully completed to solve six of the seven issues defining crown manufacturing problems in Figure 15. The last issue, "significant cured panel warpage", related to the original locally optimized

design. Crown quadrant redesign was performed with the help of the design cost model, COSTADE, over a period of five weeks. The problem description, design constraints, and resulting redesign appears in Figure 20. New constraints for minimizing panel warpage and transverse Poisson ratio mismatch were added to those used for the original design (ref. 3). In addition, aft skin layup and frame geometry were held constant due to commitments to a tension fracture database and process tools, respectively. Utilization of COSTADE to quickly obtain the design cost analyses for problems with imposed constraints is similar to what might be expected of a DBT in hardware applications.

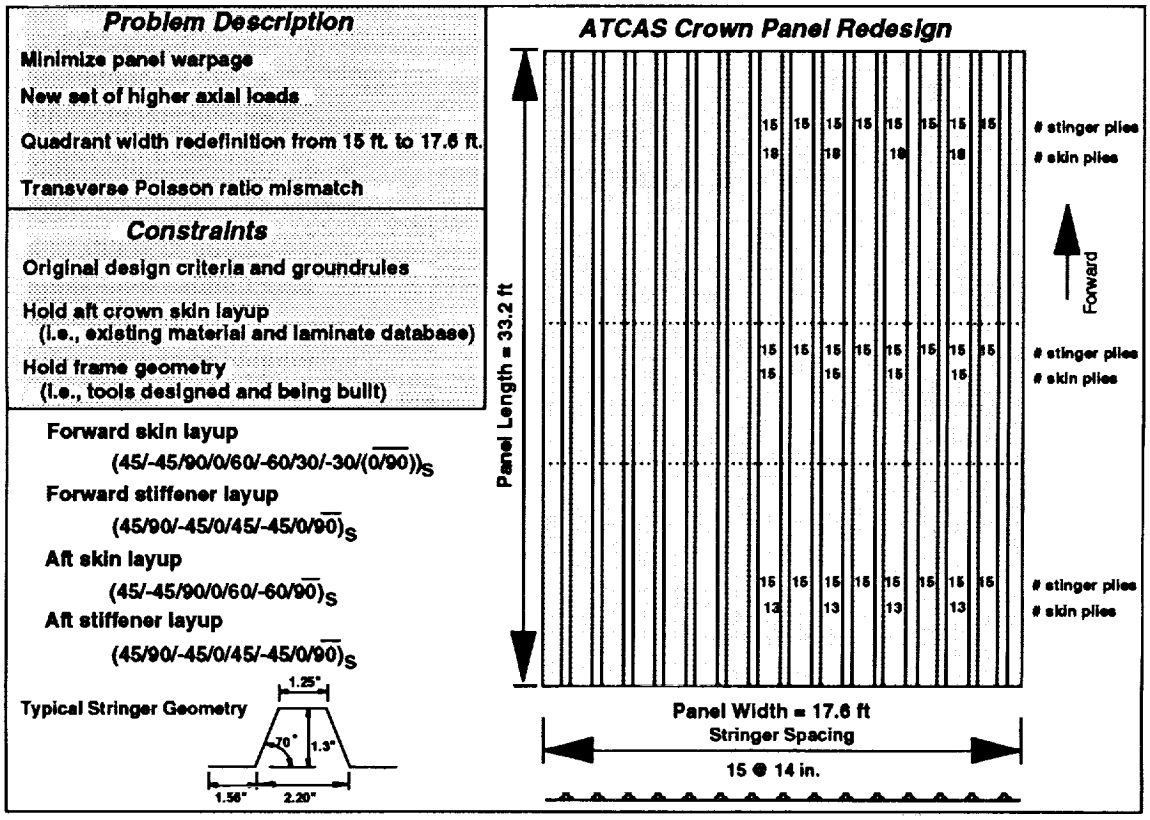

Figure 20. Application of COSTADE for crown redesign.

The COSTADE software was found to be useful in minimizing cost and weight. Several changes from the original locally optimized crown design are evident in Figure 20. Total crown panel cost and weight increased in order to meet higher axial load requirements and larger quadrant size. Some of the weight increase and associated cost related to new constraints which limited skin and stiffener layup mismatch. These increases are directly tied to a desire to reduce assembly risk, e.g. warpage. Changes relative to aluminum technology were discussed earlier. The stringer layup was significantly softer than that of the original composite design in order to meet warpage and transverse Poisson ratio constraints. Stringer spacing was uniformly held at 14 in., rather than the original design layout for increased spacing approaching side quadrants. Skin gage increased in the forward end due to higher axial loads and decreased stiffening ratio. Discussions on the damage tolerance trade between the original and current design will appear at a later date.

Final scaleup of Family C design concept. Figure 21 shows the end product of work performed by the special DBT to obtain timely solutions to manufacturing problems encountered with the baseline crown concept. In summary, several tasks gave the DBT confidence to pursue this curved, 7 ft. by 10 ft., Family C concept with six cocured stiffeners and five cobonded frames. Fabrication trials for a curved, 3 ft. by 5 ft. panel helped develop IML cure tooling that eliminated stiffener cross-sectional anomalies and mandrel removal problems. Successful completion of this task initiated the fabrication of segmented IML caul plates to fabricate the panel in Figure 21. Braided/RTM process scaleup resulted in 8 ft. braided frames with dimensional tolerance control deemed acceptable for cobonding. Five of the frames were cobonded to the panel in Figure 21. Finally, a cost competitive redesign was obtained with the help of COSTADE, eliminating some of the risk associated with assembling large, stiff, Family C concepts. The panel in Figure 21 reflects the updated crown design in an aft location.

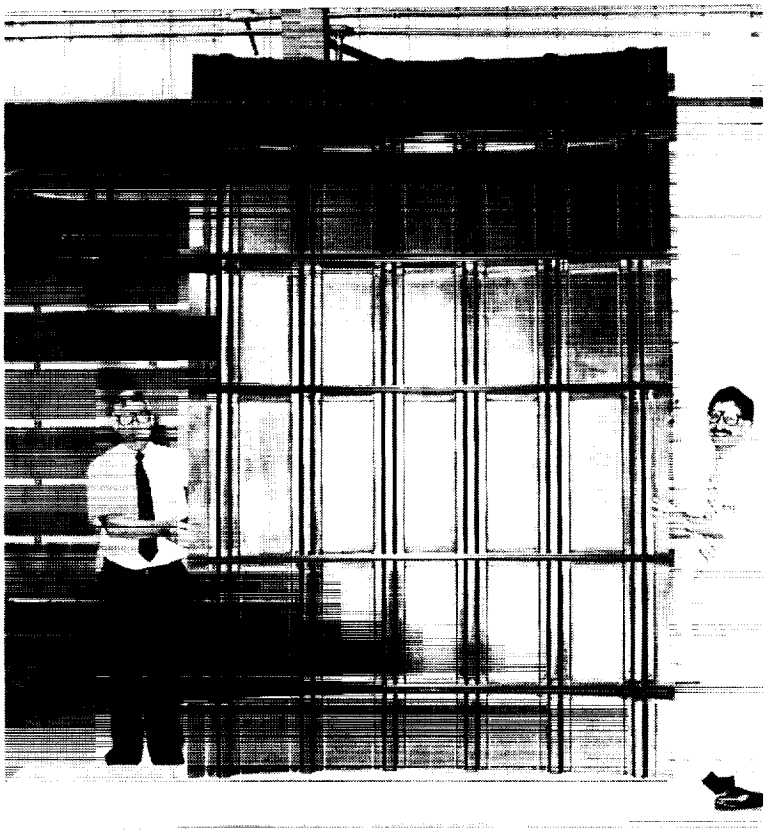

Figure 21. Family C crown quadrant manufacturing demonstration.

Structural Development

Several design drivers for the crown quadrant combine to control minimum skin gage, stiffener spacing, skin and stiffener layups, skin splice padups, and frame attachment details. References 1 and 3 describe technical issues and design sizing exercises for this quadrant. As discussed earlier, axial and hoop tension dominate the loads in the crown. The associated failsafe damage tolerance requirements affect many design details. Some

compression axial loads from reversed body bending and shear loads approaching the side quadrant pose additional requirements for stability and bonded element performance. In ATCAS, tests and analyses efforts are coupled with the manufacturing developments in attempts to understand process induced performance characteristics.

Impact damage to minimum gage fuselage panels. All fuselage quadrants have technical issues related to impact. The minimum skin gage allowed in crown design relates to both failsafe issues (tensile residual strength after massive impact damage that penetrates a structural unit) and hail impact requirements (no visible damage and "Ultimate" load carrying capability). Since 1990, ATCAS has pursued an understanding of the impact damage resistance of composite fuselage structures (ref. 2). The designed experiment described in reference 17 included thirty-two different panels, each with three stiffeners. This experiment was performed to characterize relationships between impact events and fuselage design variables (material, laminate, and structural). Variables for the former included different impactor shapes and impact test events, e.g. low mass/high energy. Critical crown design variables included resin type, resin content, fiber type, stiffener spacing, hat stiffener geometry, and minimum skin gage. Figure 22 shows one example of crown variable combinations from the designed experiment. Hail impact simulation, i.e. 500 in lb impact by 2.5 in. diameter lead ball, was of special interest to the crown.

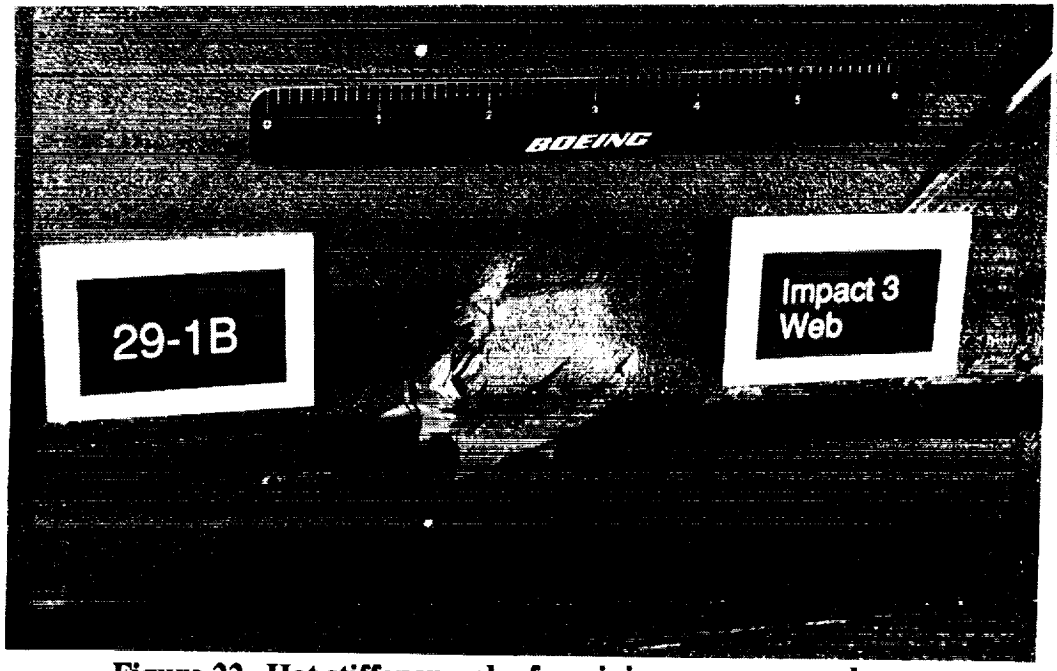

Figure 22. Hat stiffener web of a minimum gage panel consisting of AS4/977-2 (35% RC) ATP material, damaged by high energy impact from a blunt object.

Impact experiments helped to confirm crown baseline design selections. In reference 17, minimum gage hail requirements for tough and brittle matrix materials were found to be similar, i.e. hail impact visibility for thin gage skins appeared to be controlled by fiber failure. Lower resin contents were also found to be better based on similar rationale. As a result, the choice of untoughened matrix and 35% resin content were justified for the crown. The use of high performance fibers appeared to have some effect; however,

crown cost/weight trades resulted in the selection of the lower modulus graphite fiber (ref. 1). After accounting for other design drivers, e.g. failsafe damage tolerance, crown skin gages were sufficiently thick to pass hail requirements. Structural impact tests performed near stiffeners yielded additional insights on design details such as the use of adhesive layers for cocured hat-stiffened panels (see ref. 18, which is part of the current proceedings).

Maintenance personnel desire simple inspection methods capable of determining the extent of impact damage they find and its effect on structural performance. Depending on the variables of an impact event, the ensuing damage to a composite laminate can take numerous forms. Reduction in structural performance relates to damage details which may be difficult to quantify without the help of destructive tests. A combination of tests and analyses reported in the past have successfully quantified structural residual strength as a function of damage occurring from specific impact events (e.g., ref. 19). Such an approach can be used to promote damage tolerant design; however, it has limited use in assessing the need for repair, i.e. there is generally no information on the impact event for damage found in service. A low frequency, ultrasonic, Lamb wave method has been used in ATCAS for quantifying the various damage states created in structural impact experiments. As in the case of pulse-echo ultrasound, the Lamb wave method is useful for single sided access. This method is based on relationships between flexural wave dispersion and laminate bending stiffness (ref. 20). Figure 23 shows typical results of dispersion experiments and calculated values for laminate bending stiffness.

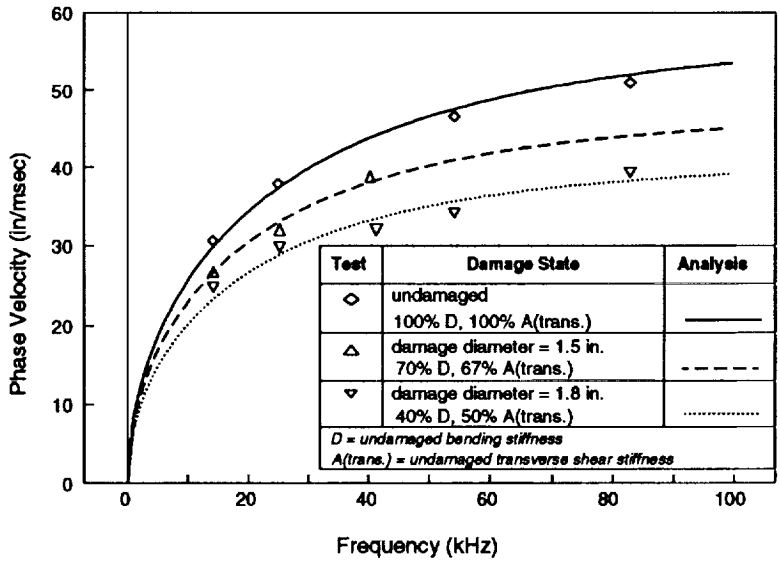

Figure 23. Nondestructive evaluation of impact damage using lamb wave dispersion experiments.

In the case of undamaged laminates (i.e., top curve in Figure 23), theory and test data agree well. Lamb wave inspection data collected over impact damage was used to back-calculate reduced bending stiffnesses for the other two curves. As discussed in reference 18, Lamb wave inspection data was found to have better correlation with a mechanical measurement of the impact damage response than traditional methods, e.g.

ultrasonic c-scan data on damage size or dent depth measurements. Future tests and analysis are scheduled to judge if the Lamb wave method is suitable for quantifying the effects of impact damage on structural response. The method will be used to quantify impact damage prior to residual strength tests. Measured reduced stiffnesses for impact damage will be used to quantify these zones in structural analysis models. Continued work in this area will help to develop tools suitable for aircraft maintenance.

Building block tests and analysis. All major subcomponent tests used to verify the crown concept have supporting tests and analyses that address behavior at the element level. For example, individual stiffening elements and large unstiffened fracture panels are used to quantify local buckling/crippling and skin fracture, respectively. These "building blocks" help to quantify individual laminate and element behavior at a dimensional scale sufficiently large enough to support structural analysis. Such an approach is also conventionally used to support the design of metallic structures due to size effects not evident in small coupons. Numerous competing failure mechanisms at the structural scale require several building block tests and associated analyses.

A large tension fracture database was collected in ATCAS for several laminates of interest in crown studies (refer back to discussions on Figures 8 and 9). The fracture data was used to quantify skin fracture behavior. This database and the need to evaluate tension fracture using large notch tests and panels of sufficient size is discussed further in reference 5. Currently, the most promising analysis for scaling tension fracture data from coupons for use in structural models appear to be strain softening laws (ref. 21).

Several tests that quantify bonded element performance, i.e. cocured hat stiffeners and cobonded J-frames, are under development. A shear lag specimen is being developed to evaluate load transfer between skin and stiffening elements. Results to date indicate long shear lag distances are required for transferring load from the skin into the stiffener cap and suggest a need to include nonlinear material behavior for the adhesive joint. These studies support analysis and test of tension residual strength for configured structure with failsafe damage conditions. Element pulloff tests are also being developed to support compression panel stability studies. Tests have successfully applied buckling mode patterns to the element, yielding data on the skin/stiffener bondline strength.

Frame/skin pulloff tests and analyses are being performed under subcontract at Drexel University. Bonded joint fracture properties have also been collected for various adherend combinations of the braided frame flange and ATP skin laminate. The original frame/skin pulloff test fixture and specimen are being redesigned to account for width and skin curvature effects. Analysis is being performed to quantify pressure pillowing in the current crown design. Results from the analysis will be used to either extrapolate test results or to change the fixture for a more accurate simulation of pressure load reactions. Results from the Drexel work will support configured panel tests in the pressure box.

Plans for compression panel tests. Several compression panel tests will occur later this year to demonstrate crown stability performance. Each test article will be machined from a curved, 7 ft. by 10 ft. crown manufacturing demonstration panel. Building block tests supporting this effort include crippling elements and stability pulloff. Nonlinear finite element analysis will be used to simulate each compression panel test. A total of

three panel crippling tests will be performed using aft crown subcomponents that have three stringers and two frames. Two of the test panels will have bonded frames and the third will have mechanically attached frames. Another compression test will evaluate wide-column buckling for a subcomponent panel having the forward crown design detail. This test article will consist of five stringers and four cobonded frames. Several impact damage scenarios are being considered for compression panel tests based on structural impact resistance results from the designed experiment. The nonlinear analyses will be used to locate impact damage in a critical stress location. Failsafe damage conditions will be considered for one of the load runs with the wide column buckling panel.

Damage Tolerance

Axial damage tolerance tests. Axial damage tolerance was evaluated using flat, five-stringer panels. Failsafe damage conditions for these tension fracture tests included a 14 in. skin penetration that severed a central stringer (simulated by a saw cut). Figure 24 shows a panel mounted in the test machine. Over 100 strain gages were used to help map damage growth and load redistribution. The test was stopped periodically, after incremental load increases, to determine the amount and type of damage growth prior to failure. NDE data collected between load steps included X-ray, pulse-echo ultrasound, and Lamb wave dispersion. Moire' out-of-plane displacement data was collected above and below the severed central stiffener. In addition, video cameras filmed tests during load sequences. This included high speed photography to capture final failure.

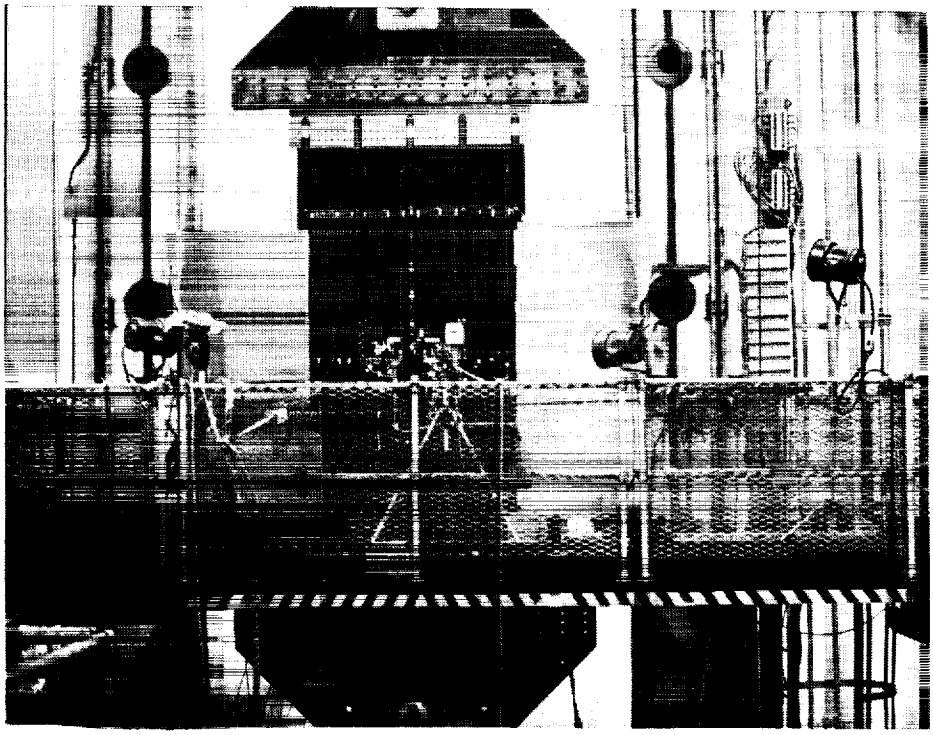

Figure 24. Axial damage tolerance test of initial ATCAS fuselage crown panel design.

Two panels were tested, one consisting of the baseline crown material, i.e. ATP AS4/938 laminates, and the other using an ATP intraply hybrid (75% AS4/25% S2/938). These panels each had the original locally optimized forward crown skin and stiffener layup. Processing of both the panels was discussed in the subsection on "Manufacturing Scaleup" (note that the hybrid is pictured in Figure 17). Hat cure mandrel removal problems occurring with the all graphite/epoxy panel caused localized skin/stiffener delamination. The delaminations were repaired using mechanical fasteners prior to test.

Axial damage tolerance analysis. Residual strength analysis for metallic structures has had to account for competing failure mechanisms and nonlinear material behavior in order to accurately predict panel failures observed in test (ref. 9). Figure 25 shows the analysis and test for a tension panel loaded to failure. The skin half crack length for this static load test started at about seven inches. Elastic and plastic predictions of three competing failure modes are shown in the figure. Note that skin fracture is temporarily arrested, at the expense of higher stresses in the adjacent stiffener and rivets that attach the stiffener to the skin, i.e. panel stresses causing stiffener or rivet failure drop with increasing crack size.

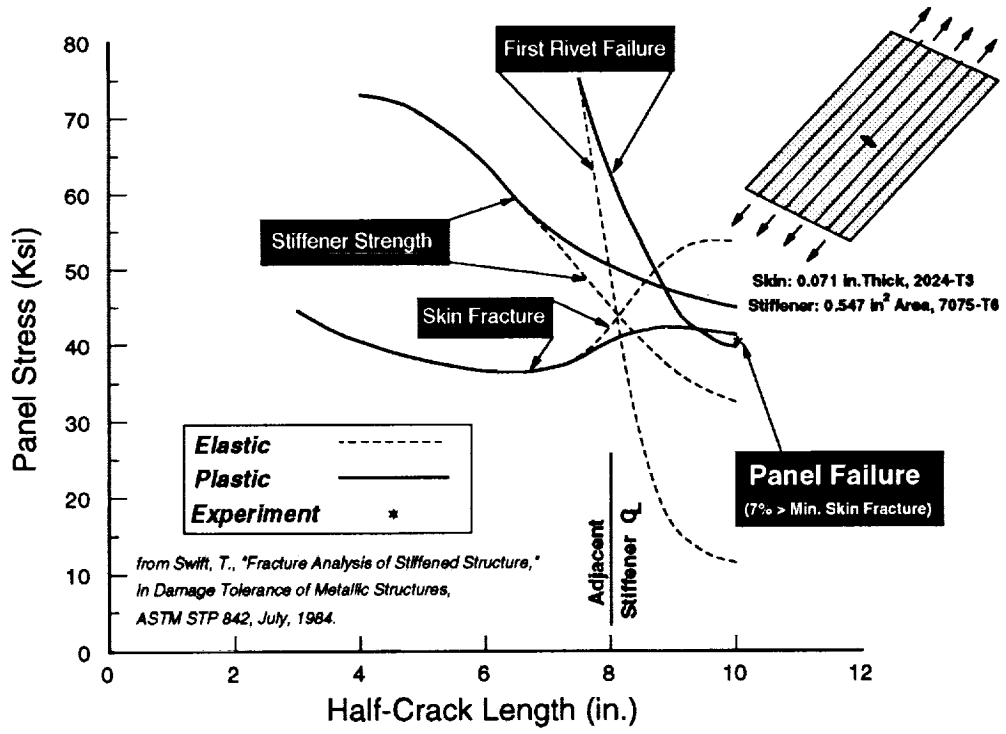

Figure 25. Structural damage tolerance of metallic panel with skin cut and severed stiffener.

Figure 25 shows that as skin damage approaches the adjacent stiffener centerline, elastic and plastic analyses deviate. Plastic analyses are shown to best predict the panel failure observed in the test. The plastic deformation of fasteners is critical to the load transfer between skin and stiffener. As the rivets yield, less load goes to the stiffener, lowering skin fracture strength. The final sequence of failure for the test panel modeled in Figure 25 was triggered by fasteners unzipping along the axis of the panel as predicted by

analyses. Note that the panel failure stress was approximately 7% greater than the lowest part of the skin fracture curve. Plastic behavior effectively compromises the three failure mechanisms, resulting in an optimum strength for the metal panel design in Figure 25.

Figure 26 shows the skin and stiffener layups for the two axial damage tolerance tests. Nearly identical failure mechanisms were observed for both panels, suggesting a relationship with design parameters held constant, e.g. skin laminate stacking sequence. Asymmetrical damage developed at the original notch tips of both panels and grew in a similar manner toward adjacent stiffeners, i.e. damage growth observed from the stiffened side of the panel was above and below the notch for left and right sides, respectively. This asymmetry was also evident in the final failure event, with broken panels skewing to the right. High speed photography taken for each panel indicated that skin damage progressed dynamically from underneath arresting stiffeners and into adjacent skin bays at maximum load. Catastrophic skin damage growth appeared to happen before skin/stiffener separation.

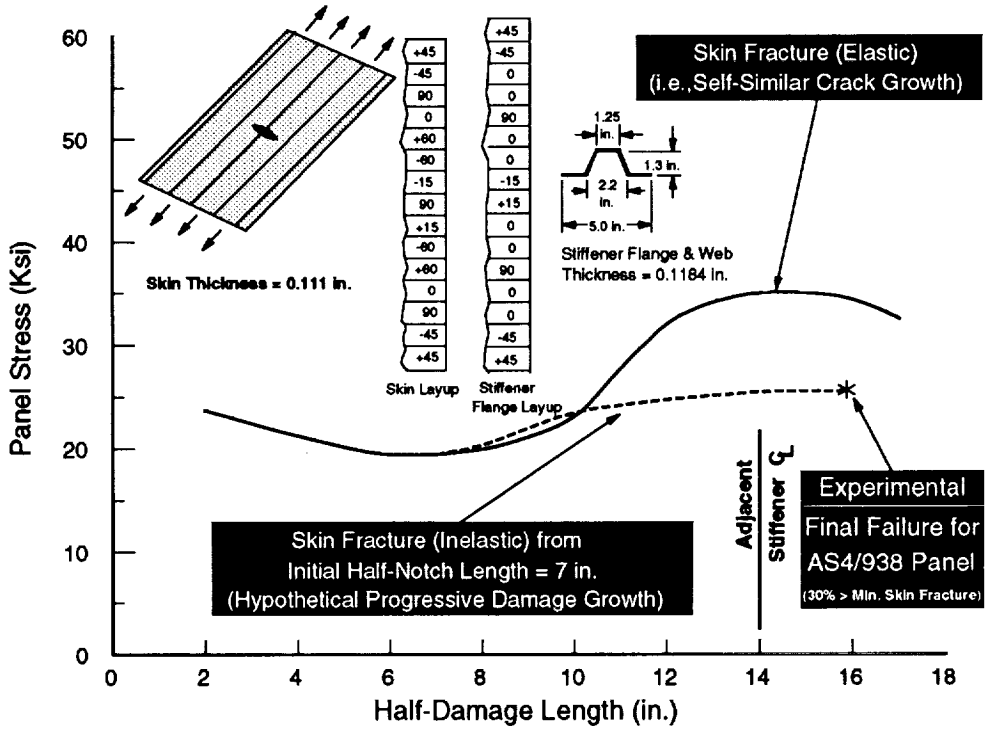

Figure 26. Structural damage tolerance of AS4/938 ATP composite panel with skin cut and severed stiffener.

Several different elastic skin fracture analyses were performed for each panel. These ranged from finite element models of panel design details to existing fracture analysis handbook methods. In each case, skin fracture properties and panel design parameters were used to make predictions of "self-similar" crack growth. A typical elastic prediction for the all graphite/epoxy panel appears in Figure 26. Note that skin fracture is predicted to be stable between half-damage lengths of 7 in. and 14 in. In a manner similar to stiffened metallic structures, the experimental skin damage growth for both composite panels was observed to be stable, arresting at the adjacent stiffeners before

catastrophic fracture. Final failure measured for the all graphite/epoxy panel was 284 kips. As in the case of the stiffened metallic panel in Figure 25, elastic methods overpredicted composite panel failure. The same relative trends appear when plotting analysis and test results for the hybrid fracture panel which failed at 356 kips.

Hypothetical analysis illustrating stable progressive damage growth observed in the all graphite/epoxy panel test is also shown in Figure 26. As discussed earlier, the composite design used for both panels had a large difference in axial skin and stiffener properties. The relatively soft skin and hard stiffener combination resulted in a panel failure stresses that appeared to be 30% greater than the minimum point in the skin fracture curves. This compares to the 7% increase for a metallic structure in Figure 25. However, experimental detection of a minimum point in the composite curve was somewhat arbitrary, i.e. notch tip damage growing to a size larger than observed in unstiffened panels.

In the absence of methods for simulating progressive damage growth in a composite structure, an analysis procedure was inferred based on observations from the first test, i.e. all graphite/epoxy panel. The method assumed panel failure at a far field strain equivalent to that required for skin fracture with a full two bay notch (Y-factor = 1 for a damage length = 2 x stiffener spacing). Important parameters for this residual strength analysis are the skin fracture properties, skin stiffness, stiffener spacing, and stiffening ratio. Figure 27 shows predictions using this method. All designs in the figure used the same stiffener spacing (14 in.) and identical layups for skin and stiffener. These layups are listed in Figure 26. The designs labeled #1 and #2 in Figure 27 correspond to the ATCAS axial damage tolerance panels. The analysis was found to accurately predict the final failure of both panels (to within 2%). The predicted difference between these designs correlates directly with changes in the effective skin fracture toughness for large notches. As discussed earlier, the hybrid skin has approximately 25% higher effective fracture toughness (see "Crown A" points in Figure 9). The additional increase predicted for hybrid design #3 relates to the increased stiffening ratio of using 100% AS4/938 material for stiffeners.

The original loads and axial damage tolerance requirements shown in Figure 27 were easily met by both designs #1 and #2. Hybrid skin designs #2 and #3 also appear to meet the new loads and failsafe constraints without any changes. The increased loads and more stringent failsafe requirements tended to drive non-hybrid designs, particularly at the forward end of the crown quadrant. In addition, redesign of the composite crown panel to help solve manufacturing problems has lead to skin and stiffener layups with more closely matched CTEs (see discussion related to Figure 20). Crown panel weight has tended to increase with the updated loads and constraints. The processability and damage tolerance of different crown designs are currently being studied under other NASA-funded work at Boeing (task contract NAS1-19349). These include the current crown design, hybrid skin designs, and variations on skin/stiffener layup mismatch.

Manufacturing induced performance for advanced material forms. A comparison of designs #1 and #4 in Figure 27 indicates that panel damage tolerance is strongly related to the fabrication process. Predictions in the figure suggest that large cost and weight penalties would be incurred if crown panel skins were tape rather than ATP laminates.

Differences relate to effective skin fracture toughness properties for tow and tape designs. Test measurements from references 4 and 5 showed that the tape material form had lower fracture properties than equivalent constituents and laminates processed using ATP. Several hypotheses currently exist to explain observed differences. Patterns of laps and gaps that occur in a laminate due to ATP processing may lead to a level of repeatable inhomogeneity that is larger than the fiber/matrix scale commonly considered for composites. This microstructure can affect the laminates' mechanical response to stress concentrations in several ways (ref. 22). Additional analysis model developments are needed to quantify unique characteristics of ATP material forms.

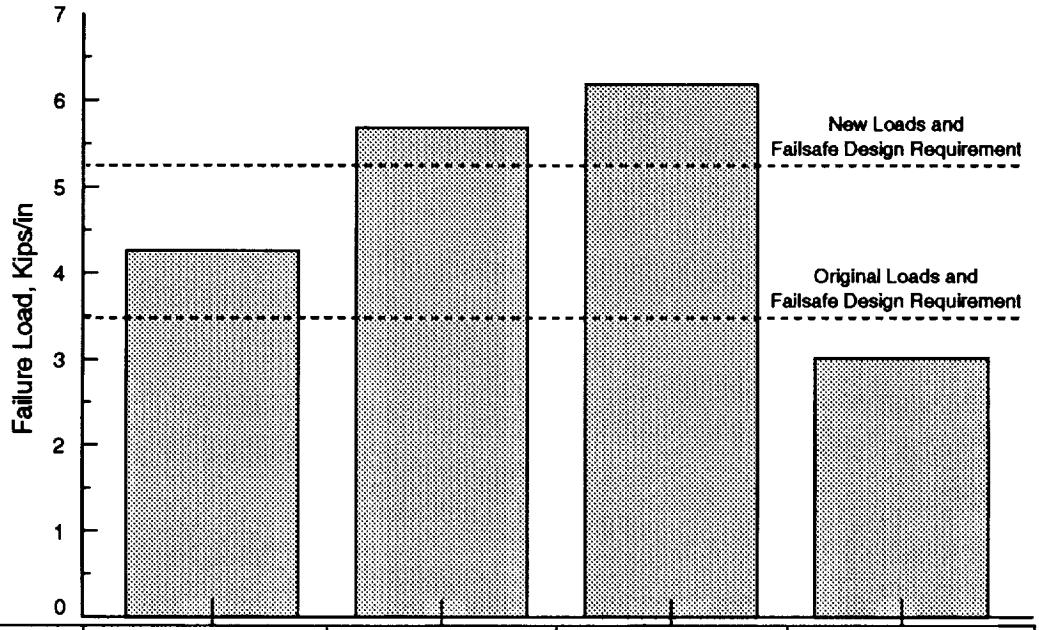

Design	#1	#2	#3	#4
Skin	AS4/938 Tow	75% AS4/25% S2/938 Intraply Hybrid Tow	75% AS4/25% S2/938 Intraply Hybrid Tow	AS4/938 Tape
Stiffener	AS4/938	75% AS4/25% S2/938	AS4/938	AS4/938

Figure 27. Analysis predictions of the effect of material types on tension residual strength for configured panels.

The laps and gaps formed in an ATP process are expected to depend on material type, machine settings, and other process variables. Manufacturing characteristics that affect structural performance must be understood in a way that promotes process and quality control. Performance advantages due to ATP were not fully recognized until the scale of mechanical testing was increased. This was particularly true of intraply hybrid ATP laminates. Nondestructive inspection (NDI) methods are needed to control advanced materials and processes because large scale testing is not economically feasible.

Similar arguments to those used for ATP laminates can be given for braided/RTM parts considered for fuselage framing elements. In each case, microstructural characteristics that affect performance must be controlled in processed structures. The goal is not to eliminate characteristic features of the microstructure, but rather to control the process

such that structural performance is repeatable from part to part. Characteristic microstructure must be distinguished from damage and manufacturing defects.

Several ultrasonic methods may be suitable for monitoring the higher levels of microstructure found with advanced processes and material forms. Ultrasonic NDI using 5 Mhz equipment with enhanced resolution has revealed unique characteristics in the microstructure of ATP panels and braided/RTM frames. Ultrasonic amplitude scans of ATP skin panels were found to have a geodesic pattern that may quantify lap and gap characteristics by detecting point to point variations in laminate density. Unique characteristics of several intraply ATP hybrid microstructures were noted during pulse-echo scans of penetrating impact damage. Differences between impact damage and repeatable microstructure were also evident in the NDI data. Local fiber volume variation in the webs of braided/RTM J-frames was discernible in ultrasonic scans. Lamb wave dispersion experiments taken over varying distances also indicated a possible relationship between flexural wave speed and higher levels of microstructure present in braided plates and intraply hybrid laminate panels.

Pressure test box development. A test box for damage tolerance testing of curved, stiffened fuselage panels loaded in biaxial tension is being developed in coordination with the Structural Mechanics Division of NASA Langley. Figure 28 shows a design pictorial of the test box and control systems. The test box will simulate various combined axial tension and internal pressure load conditions. Subcomponent crown panels that include four stiffeners and three frames fit the test section (63 in. by 72 in.). A total of nine panels will be tested in this fixture to support the ATCAS crown design. To date, the test box has been fabricated and initial loading trials were performed using the first test panel, i.e. a curved, unstiffened skin panel with tear straps.

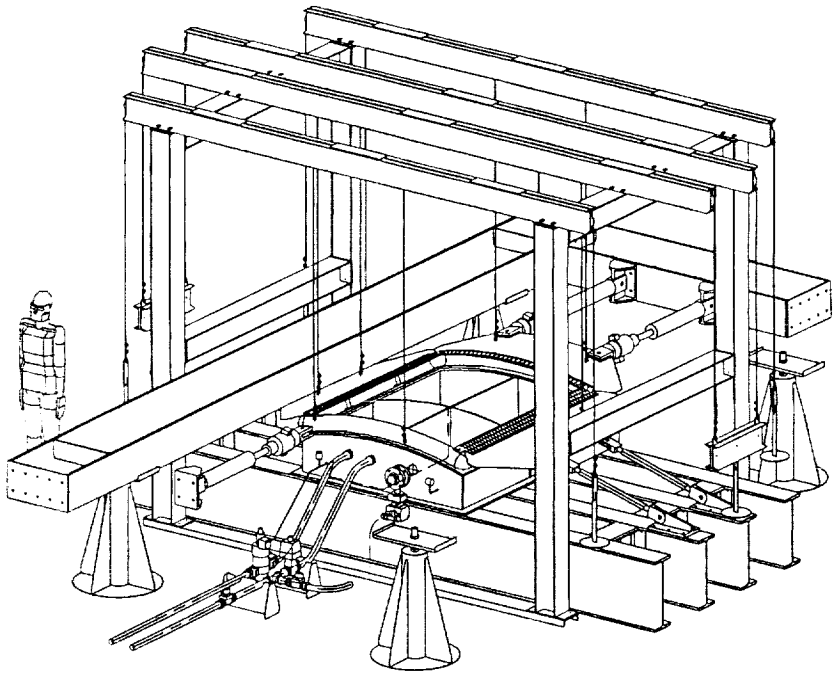

Figure 28. Cutaway view of pressure test box.

Finite element analysis was used to support the pressure test box design. Initial analysis results helped to modify test box design details to minimize interactions between the test fixture and undamaged panel stress states. Major load redistribution associated with large damage in a composite panel will require additional analysis developments to interpret damage tolerance tests performed in the pressure test box. Some issues that need to be addressed analytically relate to competing failure mechanisms similar to those discussed for axial damage tolerance; however, the pressure load component brings additional complexity, i.e. more Y- and C-factors, to stiffened shell problems. Complete documentation of the design, analysis, fabrication, and test performed to date is given in another paper presented at this conference (ref. 23).

Damage tolerance analysis needs. As was the case for metal design, e.g. ref. 9, a physical understanding of competing structural failure mechanisms and nonlinear analyses are needed to optimize the damage tolerance of composite panels. This insight is also needed to scale results from element and subcomponent tests to the full size fuselage. Hypothetically, the damage tolerance of composite designs has a stronger relationship with the scale of structural response than it does for metallic counterparts. This hypothesis is based on work from other engineering structures groups that have used materials which are heterogeneous at a scale larger than metal, e.g. wood and concrete. Fracture analyses for such materials is similar to a stability or collapse analysis in which nonlinear interactions with dimensions of the structural geometry dominate the response.

Damage tolerance analysis must be developed, verified by subscale tests, and then used to scale to a level of structural significance. Current ATCAS funding levels do not allow combined load damage tolerance testing at a scale which would eliminate the size effects predicted by an elastic continuum model. Elastic structural configuration effects (Y-factors) and load redistribution into adjacent stiffening elements (C-factors) for the pressure test box shown in Figure 28 were found to be significantly different than those which occur in the actual fuselage shell. The effects of progressive damage and nonlinear material response further complicates the interpretation of failure data from subscale tests. An estimated threefold increase in panel size would be needed to perform biaxial damage tolerance tests that are independent of the test fixture. Clearly, analysis methods are needed to avoid this expense.

Progressive damage and nonlinear modeling schemes for composites are currently being pursued to accurately predict Y- and C-factors. Damage will be simulated in analysis to represent its average affect on the structural load path as opposed to modeling discrete details. The use of generalized continuum approaches suitable for structural analysis are currently under study. Strain softening methods which have been used for tension fracture analysis, to simulate the reduced load carrying capability of a notch tip damage zone with increasing notch opening displacement, appear to be likely candidates (ref. 21). To date, these models have been developed to simulate reduced inplane stiffness and successfully applied for scaling the performance of concrete structures. Further developments are needed to include reduced bending stiffnesses, important coupling terms, and any out-of-plane plate response needed to simulate damage in problems involving postbuckled skins and pressure pillowing. Nonlinear transverse shear load transfer for both bonded and mechanically attached elements will also be needed for

C-factor analysis. Based on observations that the plastic response of metal joints can enhance damage tolerance, the attachment of elements for composite panels should have some yield to smear load redistribution over a longer shear lag distance.

Lamb wave dispersion measurements taken to characterize impact damage in composites (see Figure 23) directly support a generalized continuum approach to simulating damage. Similar NDE data was also collected for notch tip damage zones at various load levels during the course of stiffened panel fracture testing. The reduced bending stiffness calculated from these measurements tended to decrease approaching the notch tip. These stiffnesses continued to drop at any given location with each increasing load cycle. The zone of degraded stiffness also extended further away from the notch with increasing load application. Current microscopy and deply studies with tension fracture panels are attempting to characterize the details of notch tip damage and add physical meaning to wave dispersion measurements.

Panel Splices and Repair

Bolted joint studies for tow-placed crown laminates. Mechanically fastened longitudinal and circumferential splices are baseline for all ATCAS quadrants. Some bypass and bearing coupon tests for braided/RTM plates and ATP laminates have been performed to support local optimization for crown panel splices. Figure 29 shows plots of bypass and bearing data for the baseline crown skin material (ATP AS4/938) and several ATP hybrids considered for enhanced damage tolerance. Test points labeled "75% AS4/938, 25% S2/938" represent laminates in which each layer is an intraply hybrid. The other hybrid test points correspond to laminates in which only 0^{o} plies are intraply hybrids.

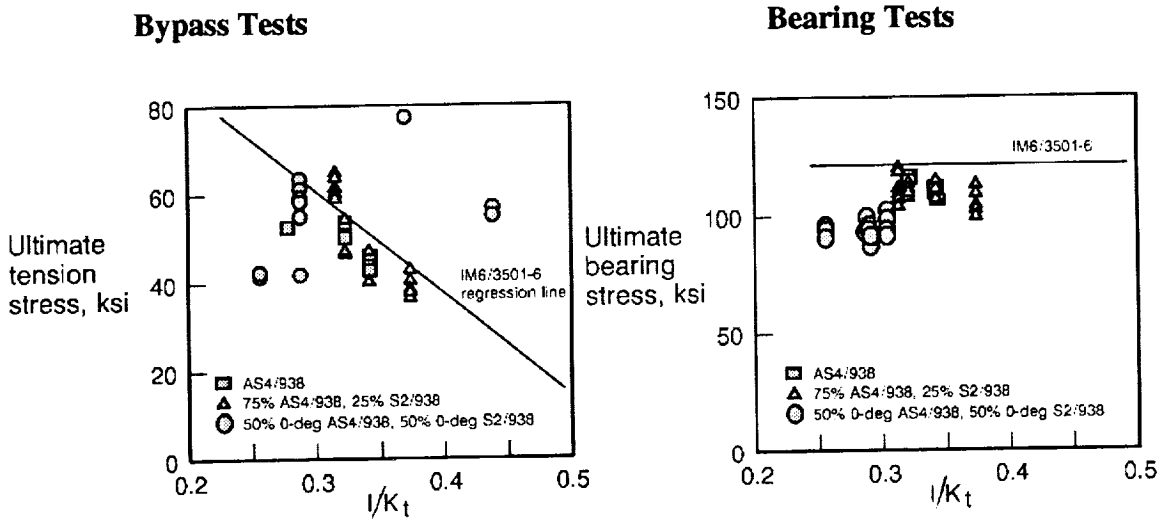

Figure 29. Bypass and Bearing test results for ATP laminates.

Data in Figure 29 is plotted versus the inverse of the orthotropic stress concentration at a hole in a uniaxially loaded plate ($1/K_t$). Regression lines in the two plots shown in the

figure represent average results for a large database of IM6/3501-6 laminates. Bypass data was collected using a filled hole coupon and titanium lockbolts with an effective clamp-up torque of 85 in·lb. High clamp-up torque was used to suppress stress relief mechanisms associated with notched tension failures (e.g., delamination). The bearing data was collected with specimens having low clamp-up torque (35 in·lb). This was done to simulate reductions in bearing strength due to real-time stress relaxation. Bearing and bypass test results are similar for the baseline ATP material and laminates consisting of intraply hybrids in each layer. Bypass data for these laminates tends to follow the regression line, indicating a strong correlation with $1/K_t$ and past IM6/3501-6 results. Bearing data for these two ATP laminates is independent of $1/K_t$ and appears slightly below the IM6/3501-6 trend line. Note that the other ATP hybrid has considerable scatter in the bypass test results. This was found to relate to the location of the hole relative to hybridizing fibers in the 0^0 layer. Bearing results for this hybrid were significantly less than other ATP laminates.

Repair for Large Penetrating Damage. Mechanically attached skin patches and element splice plates are currently being considered in ATCAS for repair of large penetrating skin damage that includes severed elements. One of the panels to be tested in the pressure test box will demonstrate the repair methods developed for failsafe damage. The specific damage case under consideration is an axially oriented, 22 in. long, skin penetration, centered on a severed frame element. A cooperative effort involving airline maintenance personnel will support this task with a critical evaluation of the repair procedure.

Work leading to the subcomponent repair demonstration includes design concept development, finite element analysis, manufacturing trials, and element tests. Several variables for repair design concepts are under consideration including: (a) titanium skin patch thickness, (b) composite patch material and laminate layup, (b) patch geometry, (c) mechanical fastener type, and (d) fastener attachment pattern. Finite element analysis is being performed in a subcontract at Oregon State University to support this effort. Analysis has been able to give some insight on how the repair design variables affect the damage strain concentration and load redistribution near the repair.

Figure 30 shows analysis results relating to the repaired damage strain concentration. Repair concept analyses were performed for the configured fuselage shell subjected to pressure load requirements and a flat stiffened panel having resolved hoop load conditions. A composite laminate patch was used for the analyses in Figure 30. This patch had the same stiffness properties as the undamaged composite skin. Load redistribution associated with the central frame repair was simulated by assuming a continuous element. Analysis results in Figure 30 indicate that the problem involving internal pressure is inherently more difficult. For example, patch geometry and fastening details are found to have a stronger effect for the pressure loaded curved panel. Additional analysis indicated that repair design variables which minimize the damage strain concentration tend to increase bearing/bypass loads for the mechanically fastened repair. The critical "Ultimate" load case for failure to the mechanical fasteners include fuselage body bending. Tension tests for specimens with mechanically fastened patches and nonlinear load transfer analysis of the curved panel will be pursued to avoid conservative predictions of the repair joint capability.

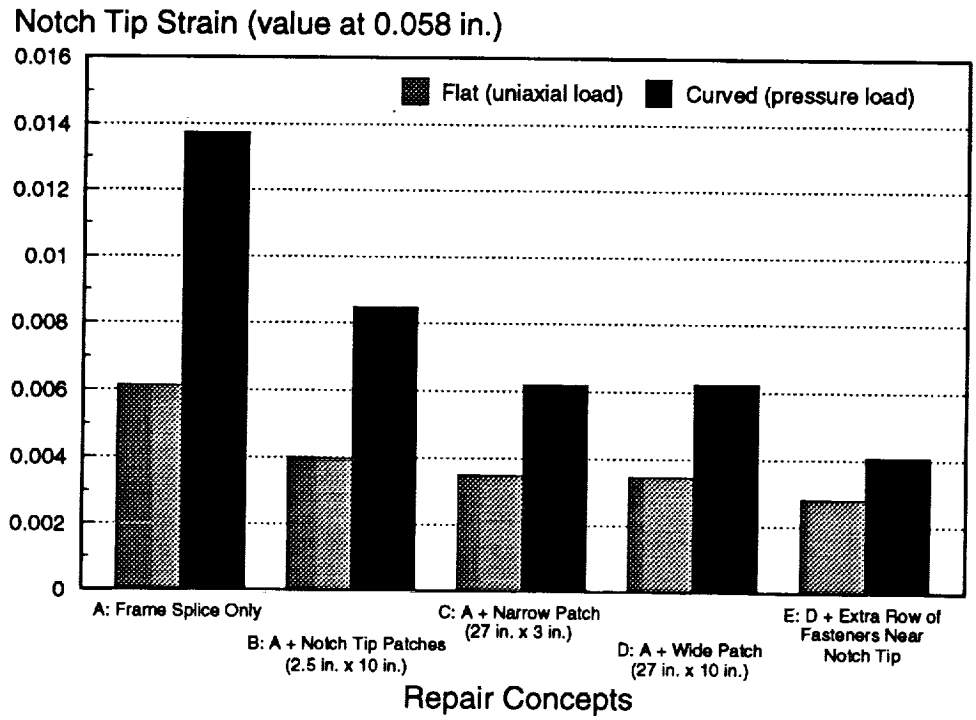

Figure 30. Structural analysis of repairs for large penetrating damage in minimum gage fuselage panels.

Design Cost Model Developments

Most initial efforts with the design cost model have concentrated on the fuselage crown quadrant. Local optimization for the crown was originally performed with the first version of the design cost model, UWCODA, which was developed under subcontract at the University of Washington (ref. 3). As discussed under "Manufacturing Scaleup", an enhanced version of the design cost model, called COSTADE, was used for crown redesign. During crown process development, relationships between manufacturing cost and crown design features were studied in greater detail. Process steps for ATP of skin and stiffener laminates, hat stiffener drape forming, braided/RTM frame fabrication, panel subassembly, and bagging have all been related to fuselage design details.

One example of the approach used for developing design/cost relationships is given in reference 16 for Braided/RTM batch processing of fuselage frame elements. This particular study also describes how fabrication trials for crown frames were used to calibrate the design cost relationships. Subcontract work at Dow/UTC supported this effort with a textile/RTM process database for other hardware design details.

Data was also collected to quantify manufacturing tolerances achieved with process trials. These included the final dimensions of fabricated parts, bonded element locational tolerances, and overall panel warpage. Based on these measurements, additional manufacturing steps will be considered in cost modeling as they relate to element subassembly, panel cure, quadrant assembly, and body join. Sensitivity studies will be used to evaluate the trade between higher tooling costs which help improve

manufacturing tolerances versus the increased costs associated with greater assembly labor for parts having tolerance mismatch. Analysis methods to predict the effect of design details on cured panel imperfections and element cross-sectional distortion were also developed to be included as constraints in COSTADE software (ref. 8).

Advanced crown structures. Although COSTADE software is being developed to support a hardware design engineers needs, it also has applications as a research and development tool. When considering the application of advanced technologies to future fuselage structures, several factors should be addressed by the DBT before committing research and development funds. An assessment of aircraft configuration, cost versus weight goals, and technology risk should be made to support major design decisions, e.g. materials and processes, design family type, and component panel sizes. Data available to the DBT can be combined with the COSTADE tool to perform bounding analyses on the cost and weight of differing configurations, load conditions, and design features. Examples of using COSTADE for such studies on advanced crown structures is presented in another paper given at this conference (ref. 24). The paper explores the effect of loads, fuselage length and diameter, crown panel size, and design type, i.e. stiffened panel versus sandwich.

A designed experiment (DE) module, based on Taguchi principles (ref. 25), was added to COSTADE. This software provides an efficient means of performing sensitivity and risk analyses for input parameters and design variables. The DE can be used to screen the effects of critical input parameters (process cost data, loads, material properties, and design groundrules), helping a DBT to decide what cost or design drivers should receive the most attention during development. For example, a range of estimates on the properties and costs for new materials and processes may exist long before funds have been committed to develop the technology and collect a complete data set. An initial risk analysis can be performed with the estimates to judge if the potential payoff is worth the developments required. The sensitivity of cost or performance to interactions between processes and specific composite design details can also be investigated using a designed experiment. One example of this DE application is the effect of process tolerance control on design detail, e.g. ply layup orientations, and the resulting changes in performance. This would help ensure that the DBT selects design details that are compatible with known process variations.

Blending function development. Advanced optimization schemes are being developed for COSTADE under subcontract to the University of Washington. The goal is to develop methods to facilitate design trade studies that include many design variables and large panels. The global random search algorithm originally developed for UWCODA has been incorporated into COSTADE. A dual cost and weight optimization scheme was added to allow the user to identify an allowable cost increase per unit weight savings.

The "quadrant" fuselage panel approach to cost savings is based on the contention that large composite panels can be effectively designed to meet the requirements of a variable load space. In order to achieve projected cost and weight savings, design details of a large panel must be effectively blended from point to point in a manner that maintains manufacturing efficiency while minimizing weight. Blending design details of a large composite panel is a difficult task for the DBT. This problem relates to current limits in

design sizing methods and a desire to consider the effect of structural details on total costs (element fabrication and assembly) when making design selections. Analysis tools and subcomponent test data used to size panels in hardware programs are based on point load conditions, while the total assembled panel cost will relate to interactions between features of the complete design. As a result, design details that meet load conditions at one spot in the panel must be selected such that they cost effectively blend to match details selected for another part of the panel. Line load diagrams shown in Figure 31 illustrate the difficulty in blending design details for large fuselage panels.

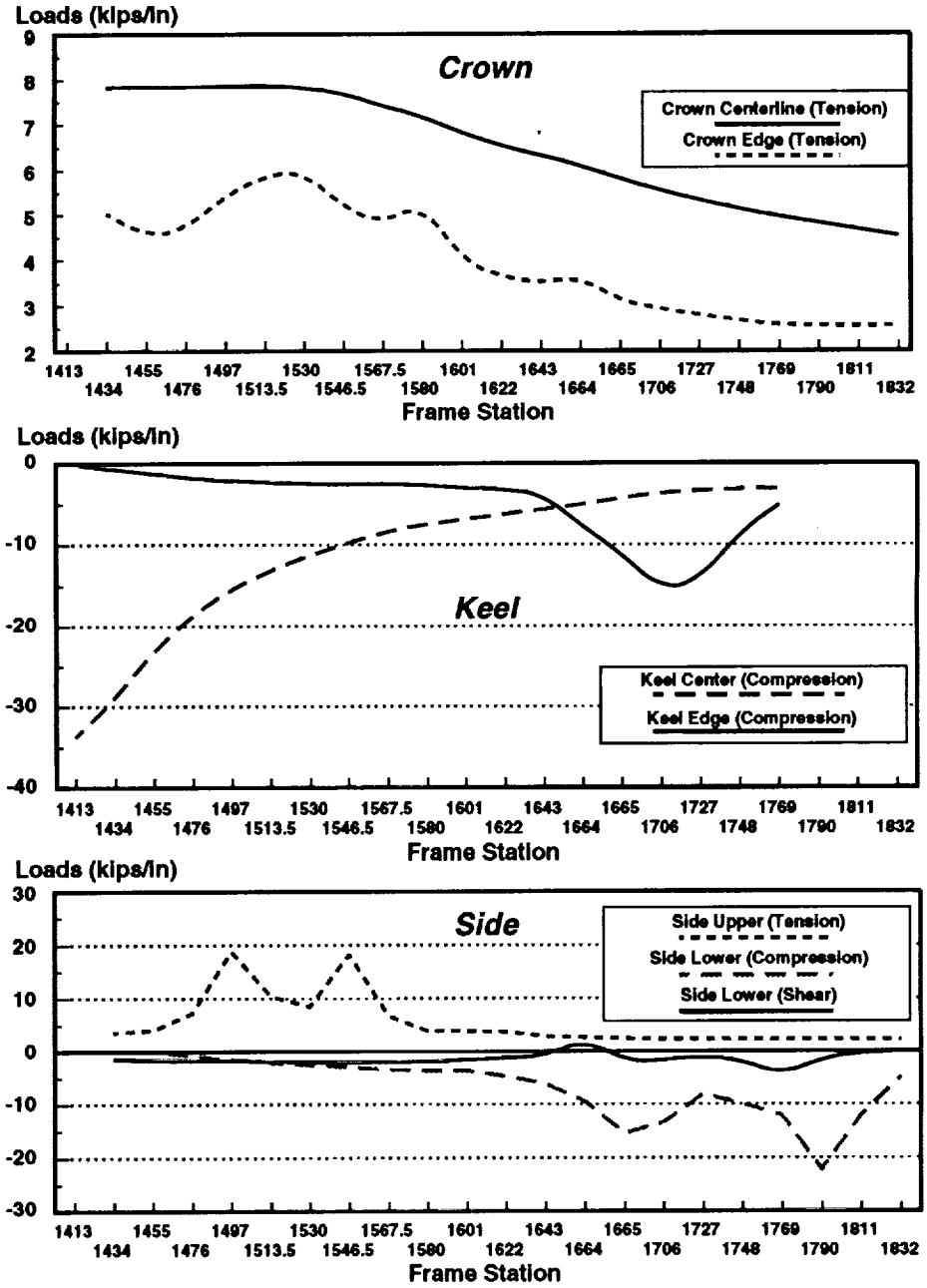

Figure 31. Variations in critical load cases along the length of ATCAS crown, keel, and side quadrants.

The three graphs in Figure 31 plot critical line load variations for portions of each ATCAS quadrant. When attempting to blend design details from point to point in a large panel, the DBT would like to make decisions that minimize total panel cost. This is particularly difficult for side and keel fuselage panels in which major cutouts, such as the wheel wells and cargo doors, cause loads to vary over a wide range. For example, an ATP machine could not be expected to change tow materials when processing from one edge of a side quadrant panel to the other, despite the differing needs in response to 20 kip/in. and -20 kip/in loads near door cutouts in the upper and lower sides, respectively. Similarly, the selection of a constant stiffener spacings that meets load requirements in both the forward and aft ends of a stiffened keel panel design requires blending to minimize cost and weight.

The concept of an automated "blending function" to support design sizing exercises for variable load conditions, while attempting to minimize panel cost and weight, was introduced in reference 12. To date, the University of Washington subcontract has developed crown panel blending software for skin and stiffener layup, ply drops, stiffener geometry, and stiffener spacing. Figure 31 shows that the crown has the least load variation of all quadrants. Difference between maximum and minimum loads for keel and side panels is four times greater than those for the crown. Keel and side panel blending function development is a major task supporting the design cost model.

Keel

Figure 32 shows characteristics of the ATCAS keel quadrant. This quadrant is the smallest of the four that comprise the fuselage barrel section. Several manufacturing and structures technologies for the keel are currently under development. This section will briefly review the work being performed for local optimization, future manufacturing scaleup, and major tests planned in 1993 through 1994.

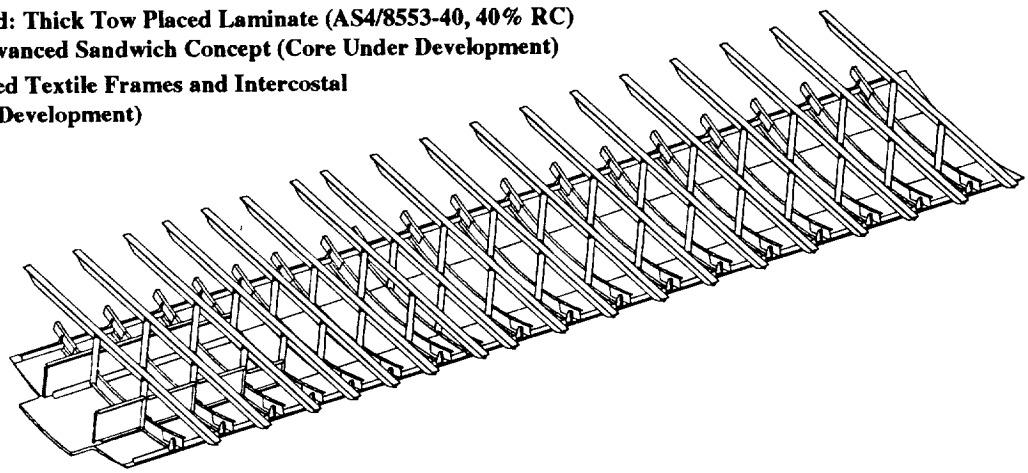

Figure 32. Baseline keel design, materials, and processes.

Some important details of the keel panel design are not evident in Figure 32. A thick laminate is used as a "panelized keel beam" at the forward end of the quadrant to

facilitate major compression load redistribution. This thick laminate transitions into a sandwich panel by dropping plies, while adding core to maintain constant IML and OML diameters along the length of the panel. The aft end of the keel is traditional sandwich with facesheet thicknesses on the order of 0.1 in. Skin material type selected for the keel utilizes a toughened matrix. The DBT selected this matrix based on anticipated benefits from interlaminar toughness and compression damage tolerance. Textile elements selected as baseline for the keel quadrant will be developed and optimized under Lockheed's leadership. Reference 7 gives additional details on the design shown in Figure 32, including projected cost, weight, and technical issues to study.

Local Optimization Tasks

Local optimization for the keel started in the spring of 1992 and is scheduled to be completed early in the summer of 1993. Three main areas of work comprise local optimization. First, manufacturing trials are being performed to help develop processes, quantify cost/design detail relationships, and optimize process steps to minimize labor. Second, a test database and supporting analyses are being generated to quantify skin and core materials. Process development and mechanical characterization of several advanced sandwich core materials is being performed concurrently. A core material will be selected in the fall of 1992, based on results from both activities. The third part of local optimization is the development of design and cost constraints for use in COSTADE. This design cost model tool will make use of results from manufacturing trials and the material database to help the DBT optimize final design details for major keel test hardware.

Process development and mechanical tests for the aft keel design detail will proceed at a faster rate than those for the forward. The final aft and forward keel verification tests will occur in 1993 and 1994, respectively. Additional time is needed for the forward keel due to issues that are inherently more difficult. The aft keel has relatively uniform compression loads that are of a magnitude similar to those at the forward end of the crown; hence, the DBT is better equipped to address aft keel issues in response to the aggressive schedule which has been planned. Crown studies have also indicated that similar cost and weight savings to skin stiffened designs appear possible with sandwich panels (refs. 1 and 24). Aft keel sandwich developments will help supplement the ATCAS crown database in a way that both design families could be considered for quadrants in the Phase C full barrel.

Advanced sandwich concepts. Several core concepts are currently being evaluated for use in the keel panel. The typical range of densities considered for keel requirements range from 7 to 20 lb/ft^3. Some isolated areas near the start of the thick laminate to sandwich core transition and at ramps near splices may reach higher densities. The baseline core material used in global design sizing studies was Rohacell foam. Other candidates under investigation include foams fabricated using the Sundstrand insitu process and an advanced DuPont porous solid. Several glass/phenolic and glass/thermoplastic honeycombs with different cell sizes and density will be screened. The development of foam-filled honeycomb processes will be pursued in coordination with Hexcel. Finally, syntactic foam with significantly higher densities will be considered for use as interlayers between plies in "thick-skin" concepts for stiffened panel design. This design concept is

a mix between skin/stiffened and sandwich designs whereby greater skin bending stiffness helps to satisfy skin buckling and pressure pillowing requirements while allowing wider stiffener spacing and the associated reduced cost (see ref. 24).

Cost savings potential projected for the Sundstrand insitu foams, coupled with a need for significant developments, lead to a desire to begin process trials in support of ATCAS keel technology in early 1991. The Sundstrand process uses a single thermal cycle to create the foam and cure facesheets to form a sandwich panel. This eliminates many of the traditional sandwich manufacturing steps, reducing cost significantly. The ATCAS DBT was interested in developing a thermoset insitu foam technology that was compatible with the baseline keel facesheet material. Following initial trials of foaming the base facesheet resin, a decision was made to use resin in powder forms. The improved mixing obtained with powder resin forms and foaming additives was thought to be critical for process scaleup. Powder resins used for the foaming trials included 3M PR500 and Hercules 8553-40. Several process trials were successfully performed at Sundstrand during the course of their subcontract, yielding samples for mechanical test at Boeing. Figure 33 shows a sample cross-section taken from one of the sandwich panels. The details of thermoset insitu foam process development are given in reference 26.

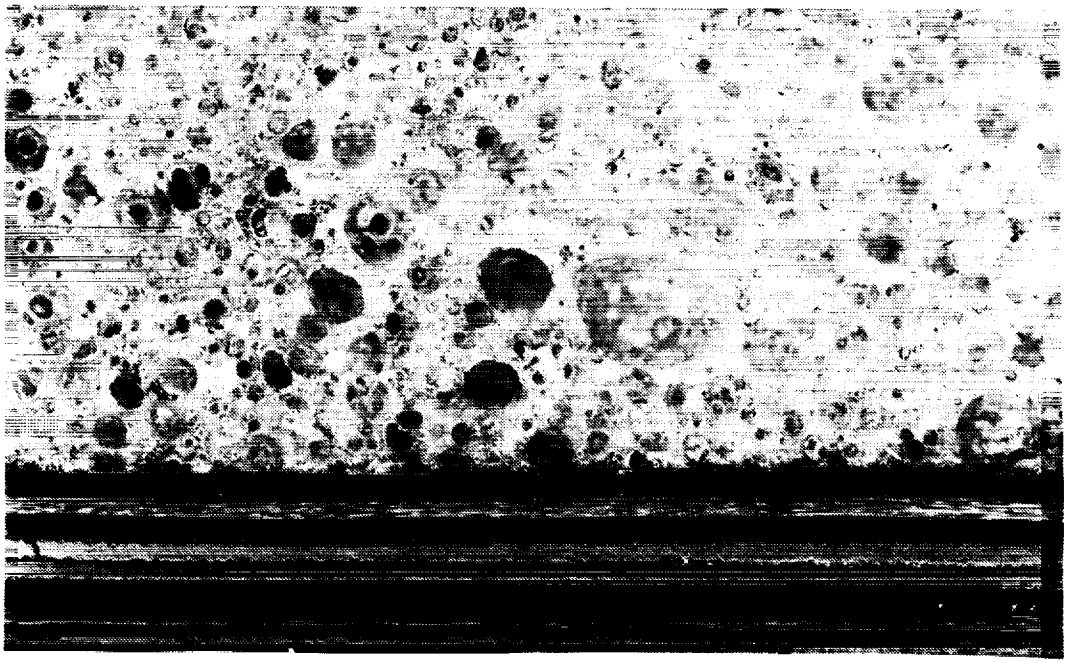

Figure 33. Micrograph taken from an insitu foam process trial.

Mechanical tests performed at Boeing to screen samples of the insitu foamed sandwich included impact resistance, 3- and 4-point flexure, flatwise tension, and flatwise compression. A number of different insitu foams were evaluated, indicating a trade in mechanical properties that depended on process variables. Figure 34 shows a trade between strength and toughness that was observed with 3-point bend tests for two different insitu foam samples. The foam sample which exhibited relatively high strength and low toughness was processed from 3M resin, without fiber additives. The sample

showing higher toughness and a sacrifice in strength had short Amoco P55 fiber additives. Further developments with the insitu foam process are needed to obtain the proper balance in core strength and toughness required for keel applications.

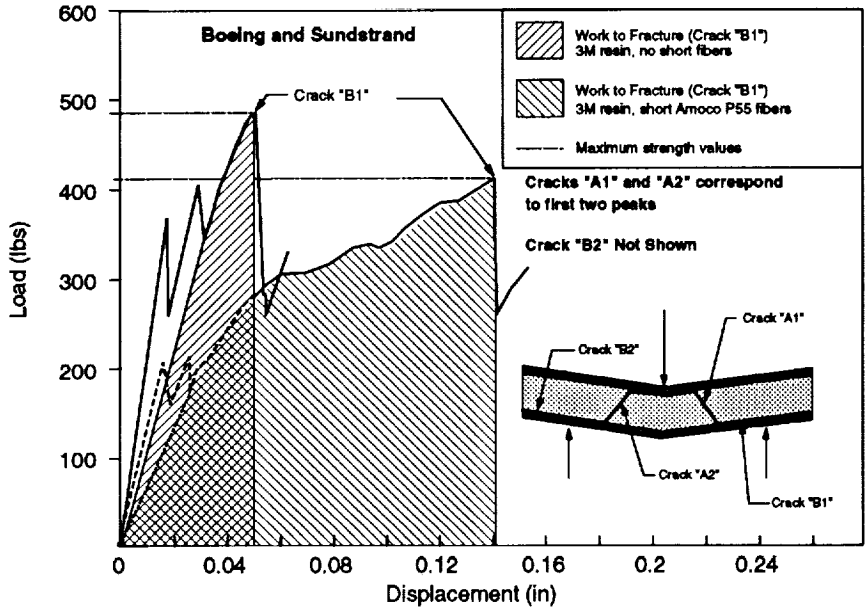

Figure 34. Strength versus toughness trades for insitu foam materials.

Another keel process activity that started early was the development of NDI methods for inspecting foam core samples. A resolution of this technical issue was needed before committing major efforts to foam core process development. Samples of Rohacell foam were used in ultrasonic experiments to judge their wave propagation characteristics. Foam samples effectively filtered the entire signal sent at frequencies typically used for inspecting graphite/epoxy laminates, e.g. 5 Mhz. Experiments performed over a range of frequencies, indicated that foam samples would pass lower frequency ultrasound (between 250 khz and 1 Mhz). Impact damage created in the foam core of sandwich panels was detected using through-transmission-ultrasound at 250 khz. In order to evaluate the extent of impact damage in face sheets over foam core, pulse-echo data was collected at 5 Mhz. These experiments helped to relieve concern on the inspectibility foam cored sandwich panels.

Keel process development needs. Design detail associated with major load redistribution posse a number of challenges in developing composite keel manufacturing technology. One key issue considered during baseline concept selection was a need to maintain IML tolerances as the structure changed from the forward to aft ends of the keel. The advanced sandwich concept selected by the DBT will be developed to maintain tolerances when going from a thick laminate in the forward end to sandwich panel in the aft (i.e., core is added as plies drop). The ATP laminate layup process will need to drop and add plies under tight tolerance control without a major impact on machine speed. This will require advancements in tow placement head technology and machine

programming control. There may also be a need to alter fiber angle within individual plies as a function of distance. This desire will relate to details of composite shear load transfer (both inplane and transverse) near the forward end of the keel. For example, shear load transfer mechanisms may force ply drops over too large an area to achieve economic and weight benefits without fiber angle change.

Other issues to consider in keel process development include a cure cycle for advanced sandwich structure. Time sequences of temperature and pressure for the cure cycle must process toughened matrix material in a thick laminate and sandwich facesheets concurrently. The pressure needed to cure AS4/8553-40 in a thick laminate versus that allowed by the sandwich core may be a critical part of the technology. Alternative facesheet materials will be considered for the keel if AS4/8553-40 is found to be incompatible with keel process requirements.

Building block test and analysis. Plans have been developed to evaluate aft and forward keel design drivers with coupons, elements, and subcomponent panel tests. Tests and supporting analyses will help to design the final curved panel verification tests. Coupons cut from sandwich process trials will be used to obtain core shear properties and impact resistance. These dominate initial aft keel tests and will be used to support core material selection. Aft keel sandwich process trials at a larger scale will yield compression panels for stability, post-impact residual strength, and large notch tests. Curved panels on the order of 3 ft. by 4 ft. will be the largest tested prior to final verification.

Forward keel building block tests will concentrate on issues related to load redistribution and transverse shear properties. Process trials will again provide panels for testing. Forward keel coupon tests will help to characterize the material for thick laminate behavior, ply drop, bearing, and open hole strength. The transverse shear lag response of the composite laminate and its effect on major load redistribution will be a critical issue for these studies. The AS4/8553-40 material has resin-rich interlayers (RIL) that have a lower transverse shear stiffness and high interlaminar fracture toughness. This characteristic is generally good for impact damage resistance, but may affect local load redistribution in areas where plies buildup (i.e., long shear lag distances may limit doubler plies from carrying their full load share).

Unlike results for brittle matrix laminates, uniaxial compression ply drop tests for materials having RIL fail at load levels characteristic of the thin end of the specimen. This suggests RIL laminates have either superior ply drop strength or that the dropped plies did not pick up significant amounts of load for the specimen length. Larger test panels will be designed to evaluate this effect. The tests will include thick laminates having ply drops and major cutouts. The data and supporting analyses will help determine internal load redistribution and required doubler sizes for the forward keel design detail. If the required advances in ATP manufacturing are attained, some tests and analysis will evaluate compression load redistribution for panels with intraply fiber angle changes around cutouts.

Design cost model. Developments for keel cost and design constraints will occur during local optimization. Design/cost relationships will initially be developed based on the global detailed estimates for keel processes. All relationships will be updated based on

data generated during process trials. For example, the cost constraints for ply drop and add will be changed to reflect ATP machine head developments and process trials. Textile relationships will be developed in coordination with Lockheed process studies. Formulation of a blending function algorithm for keel design details will need to account for large load variations discussed earlier in reference to Figure 31. Design sizing tools for sandwich panels will require additions to those currently existing in COSTADE for stiffened crown structures. Design constraints for doubler plies will need to be formulated based on shear lag tests and analysis for the material of interest. Once developed, the COSTADE modules will be applied to optimize a final keel panel design.

Manufacturing Scaleup and Major Tests

Manufacturing scaleup for the aft keel will occur in early 1993. The final panels processed in support of the aft keel will be used for uniaxial compression damage tolerance and repair tests. The panel geometry to be used for aft keel manufacturing and test verification is shown in the top of Figure 35. Due to several difficult manufacturing issues, forward keel scaleup will occur over a longer period of time than the aft panel, culminating with a manufacturing demonstration in early 1994. The forward keel load redistribution test component is illustrated at the bottom of Figure 35.

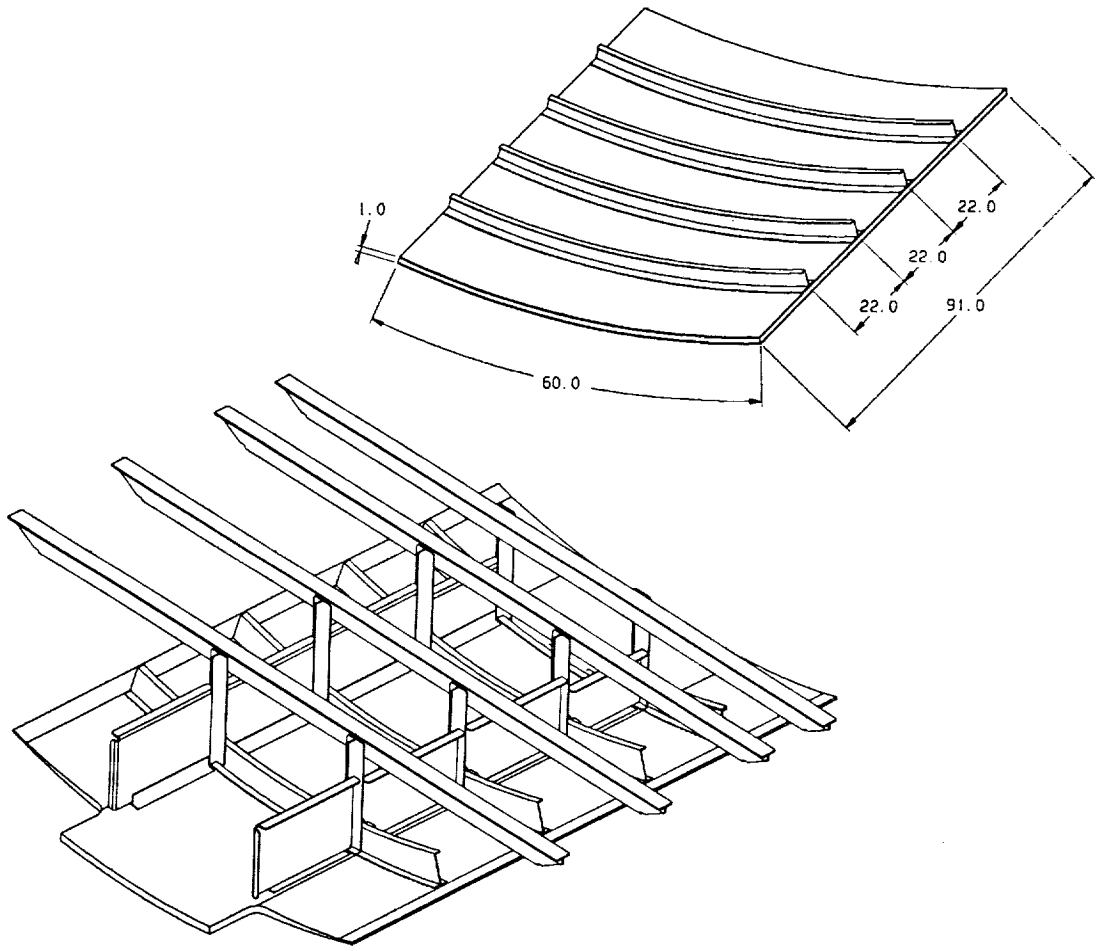

Figure 35. Aft and forward keel verification test panels.

Side

Figure 36 lists initial characteristics of ATCAS side quadrants. These two quadrants are the largest of the four. Only baseline selection is complete for the side. Global evaluation, which will be performed in coordination with Northrop (ATCAS subcontract supporting COSTADE) and Lockheed (ACT contract studying textile technologies), is scheduled to begin shortly. This section will briefly discuss the scope of side quadrant studies.

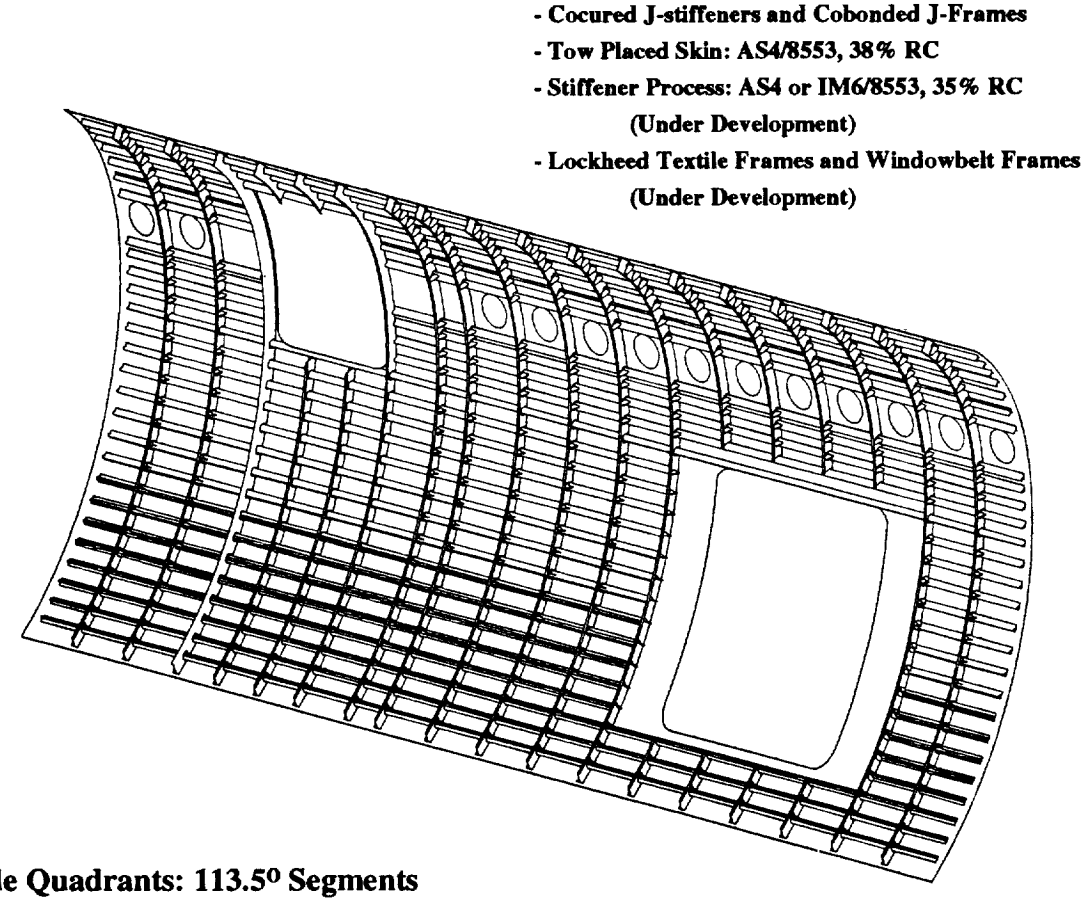

Figure 36. Baseline side design, materials, and processes.

Figure 36 shows the right side quadrant. Global trade studies will begin with the left side which excludes the cargo door. Current ATCAS schedules show that the right side will not be addressed until Phase C. Large side quadrants made selection of the baseline concept difficult. Much of the side panel area is minimum gage and driven by pressure damage tolerance. Some weight penalty will be incurred for using toughened matrix material for these parts of the side; however, compression/shear requirements in the lower side suggest possible advantages in using such material for other issues (e.g., impact). As discussed for the forward keel, it is currently unclear if a toughened matrix material is best suited for ply buildups near cutouts. The use of a Family C design that includes cobonded frames and windowbelt design details will be critically evaluated. Depending on the results of global evaluation, baseline selections may be superseded.

Manufacturing Scaleup and Major Tests

Manufacturing scaleup is planned in four main areas of the side quadrant. A lower side panel will be developed first. The second area includes windowbelt design details. The last two areas to develop are side upper and lower longitudinal splice details with crown and keel panels, respectively. Combined load tests are planned using a fixture that is suitable for compression, shear, and internal pressure loads. It is also desirable to study dynamic pressure release (e.g., simulated blade penetration) and damage containment using the fixture with panels of sufficient size. The supporting analysis will consider coupling fluid flow (dynamic gas release through the penetrated opening) and mechanics (damage containment under combined load conditions) parts of the problem. Figure 37 shows preliminary designs of windowbelt and lower side test panels.Figure 38 shows the upper and lower longitudinal splice concepts.

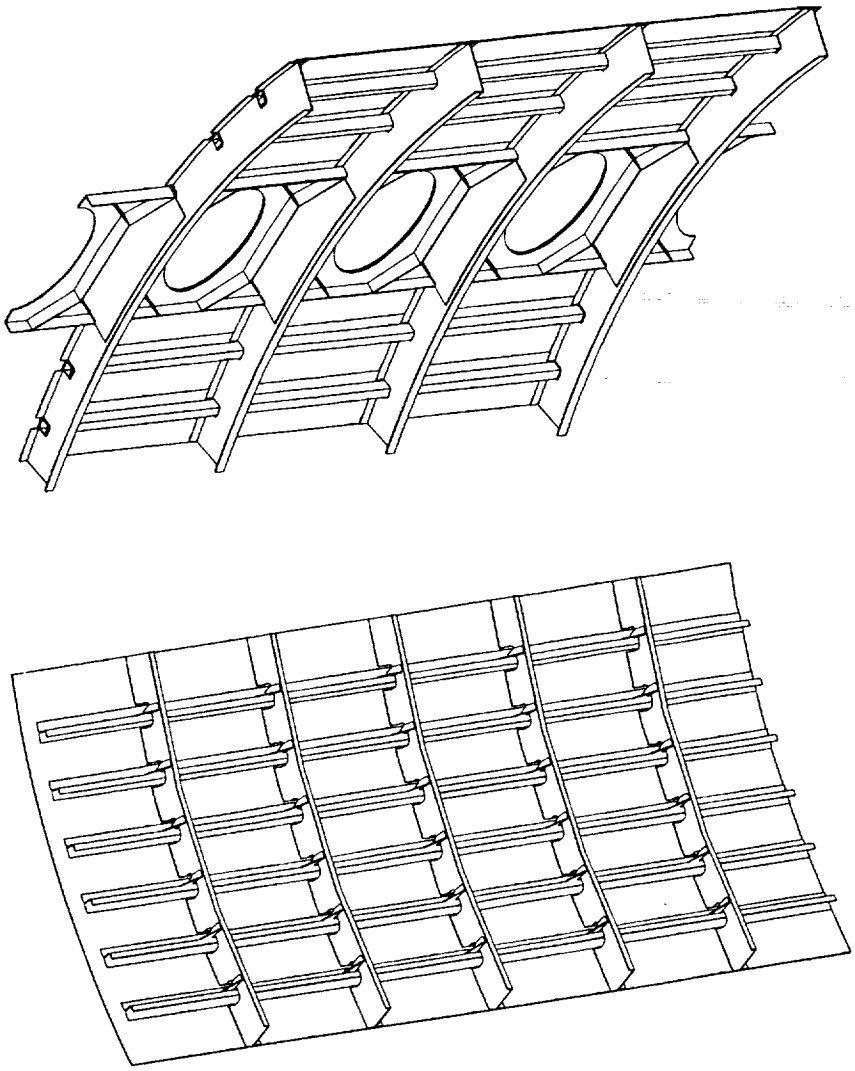

Figure 37. Side quadrant verification test panels.

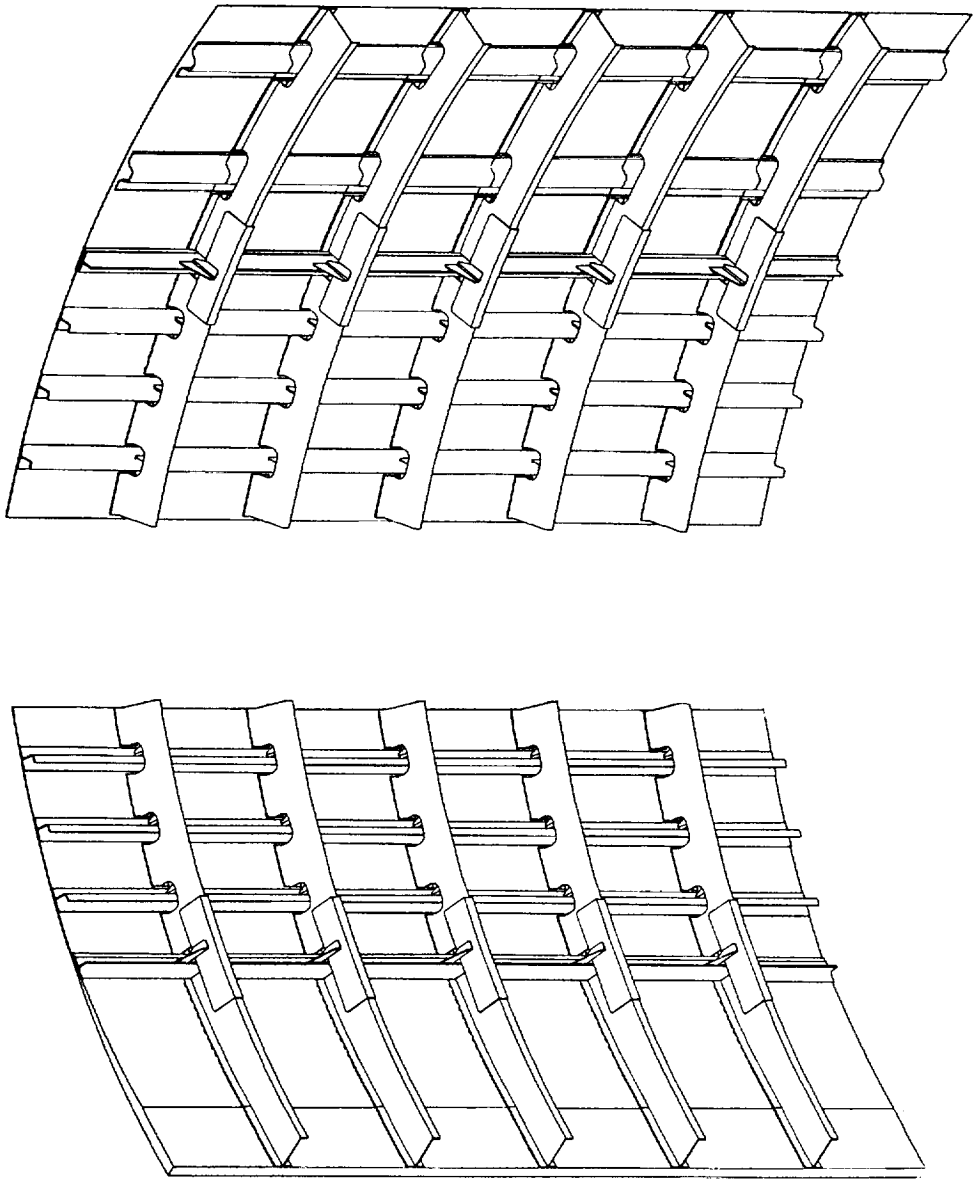

Figure 38. Longitudinal splice verification test panels.

SUMMARY

Boeing's ATCAS program on a composite fuselage barrel section was reviewed. Projections of cost and weight savings versus aluminum transport fuselage highlight *why* ATCAS is pursuing composite technology. Recent metal advancements were found to decrease composite weight savings previously reported for fuselage crown panels from 45% to a range between 20% and 35%. Composite cost savings appear attractive,

assuming material costs can be reduced as projected for the necessary high volumes and efficient factory flow can be achieved with the design details required to meet fuselage performance constraints. In order to ensure the latter, ATCAS is studying manufacturing costs and issues for representative design details. Design cost relationships generated by these studies will be used to form the basis for a model that constrains composite hardware design to promote efficient use of selected processes. The ATCAS program will continue to keep track of metal fuselage advances to ensure a critical assessment of composite technology developments.

A critical technology path describing *how* ATCAS plans to develop transport fuselage technology was summarized. This included an initial Phase C proposal to increase the scale of fuselage barrel manufacturing demonstration and test verification. A task to study structures in the wing to body intersection was also discussed as part of Phase C. Ten technology issues to be addressed during the course of ATCAS Phases A, B, and C were highlighted. The authors would be grateful to receive critical reviews of the plan.

Crown and keel panel tasks dominated *what* has been achieved in ATCAS since the second ACT conference. Important points are summarized below.

1.) A special DBT was established to solve crown design/manufacturing problems, allowing process scaleup to a curved, 7 ft by 10 ft, panel with six cocured stiffeners and five cobonded frames. A number of other large manufacturing demonstrations were performed to develop new processes including braided/RTM frames, automated tow placed skins and stiffeners, and advanced cure tooling.

2.) Design cost model developments for the crown provided timely support to the DBT in obtaining a solution to problems having constraints that are analogous to actual hardware applications. Design and manufacturing relationships for crown processes were studied in detail to update the model. Several advancements in COSTADE software were also achieved for the crown.

3.) Results from a large tension fracture database suggested a composite strength versus toughness trade similar to that observed with aluminum alloys. Automated tow placed laminates were found to have significantly higher large notch strengths (over 30%) than tape materials consisting of the same constituents. Intraply hybrids had toughness properties exceeding those of advanced aluminum.

4.) Axial tension damage tolerance was demonstrated for composite crown designs using 5-stringer panels. A failure strain of 0.004 in/in was measured for a hybrid composite panel having failsafe damage (14 in. skin penetration with severed central stiffener). Similarities in competing structural failure mechanisms for composite and metallic designs were interpreted based on tests and analysis.

5.) Initial design and fabrication of a pressure test box was completed. This test fixture will be used for biaxial tension loading (including pressure) of curved configured fuselage panels.

6.) Global evaluation of an innovative keel panel design was completed, showing cost and weight savings potential versus aluminum structure.

7.) Process and material development for advanced sandwich keel concepts began.

Eleven papers presented at this conference give more details on ATCAS progress.

REFERENCES

1. Ilcewicz, L.B., Walker, T.H., Willden, K.S., Swanson, G.D., Truslove, G., Metschan, S.L., and Pfahl, C.L.: *Application of a Design-Build-Team Approach to Low Cost and Weight Composite Fuselage Structure*, NASA CR 4418, 1991.

2. Ilcewicz, L.B., Smith, P.J., Walker, T.H., and Johnson, R.W.: *Advanced Technology Commercial Fuselage Structure*, First NASA Advanced Composite Technology Conference, NASA CP-3104, Part 1, 1991, pp. 127-155.

3. Swanson, G.D., Ilcewicz, L.B., Walker, T.H., Graesser, D.L., Tuttle, M.E., and Zabinsky, Z.B.: *Local Design Optimization for Composite Transport Fuselage Crown Panels*, Second NASA Advanced Composite Technology Conference, NASA CP-3154, 1991, pp. 243-262.

4.) Walker, T.H., Avery, W.B., Ilcewicz, L.B., Poe, C.C., Jr., and Harris, C.E., *Tension Fracture of Laminates for Transport Fuselage - Part I: Material Screening,* Second NASA Advanced Composite Technology Conference, NASA CP-3154, 1991, pp. 197-238.

5.) Walker, T.H., Ilcewicz, L.B., Polland, D.R., and Poe, C.C., Jr., *Tension Fracture of Laminates for Transport Fuselage - Part II: Large Notches,* Third NASA Advanced Composite Technology Conference, CP-3178

6.) Swift, T., *Damage Tolerance in Pressurized Fuselages,* presented at the 14th Symposium of the International Committee on Aeronautical Fatigue - New Materials and Fatigue Resistant Aircraft Design, 1987.

7.) Flynn, B.F., Morris, M.R., Metschan, S.L., Swanson, G.D., Smith, P.J., Griess, K.H., Schramm, M.R., and Humphrey, R.J., *Global Cost and Weight Evaluation of Fuselage Keel Design Concepts,* Third NASA Advanced Composite Technology Conference, CP-3178, 1992.

8.) Mabson, G., Flynn, B., Swanson, G., Lundquist, R., and Rupp, P., *Dimensional Stability of Curved Panels With Cocured Stiffeners and Cobonded Frames,* Third NASA Advanced Composite Technology Conference, CP-3178

9.) Swift, T., *Fracture Analysis of Stiffened Structure,* in Damage Tolerance of Metallic Structures: Analysis Methods & Appl., ASTM STP 842, 1984, pp. 69-107.

10.) Joynes, D., *Design of Advanced Composite Components for Maintainability Based on Inservice Experience,* presented at the American Institute of Aeronautics and Astronautics Conference, AIAA 92-1085, 1992.

11.) Masters, J.E., and Fedro, M.J., *Observed and Predicted Failure Mechanisms in Triaxially Braided textile Composites,* Third NASA Advanced Composite Technology Conference, CP-3178

12.) Freeman, W., Ilcewicz, L., Swanson, G., and Gutowski, T., *Designer's Unified Cost Model,* Second NASA Advanced Composite Technology Conference, NASA CP-3154, 1991, pp. 27-46.

13.) Willden, K., Metschan, S., Grant, C., and Brown, T., *Composite Fuselage Crown Manufacturing Technology,* Second NASA Advanced Composite Technology Conference, NASA CP-3154, 1991, pp. 263-290.

14.) Willden, K., Gessel, M., Grant, C., and Brown, T., *Manufacturing Scale-up of Composite Fuselage Crown Panels,* Third NASA Advanced Composite Technology Conference, CP-3178

15.) Grant, C.G., Bensom, V.M., *Automated Fiber Placement - Evolution and Current Demonstrations,* Third NASA Advanced Composite Technology Conference, CP-3178

16.) Metschan, S., Willden, K., Andelman, R., and Sharpless, G., *Cost Model Relationships Between Flexible Manufacturing Processes and Design Details for Transport Fuselage Elements,*Third NASA Advanced Composite Technology Conference, CP- 3178.

17.) Dost, E.F., Avery, W.B., Ilcewicz, L.B., Grande, D.H., and Coxon, B.R., *Impact Damage Resistance of Composite Fuselage Structure, Part 1,* Proc. of Ninth DoD/NASA/FAA Conf. on Fibrous Composites in Struct. Design, FAA Publ, 1991.

18.) Dost, E.F., Finn, S.R., Murphy, D.P., and Huisken, A.B., *Impact Damage Resistance of Composite Fuselage Structure, Part 2,*Third NASA Advanced Composite Technology Conference, CP-3178.

19.) Horton, R. et al., *Damage Tolerance of Composites, Final Report,* Vol. 3, AFWAL-TR-87-3030, Air Force Wright Aero. Labs., Dayton, OH, May, 1988.

20.) Tang, B., Henneke, E.G., and Stiffler, R.C., *Low Frequency Flexural Wave Propagation in Laminated Composite Plates,* Proc. of Acousto-Ultrasonics: Theory and Application, 1988.

21.) Mazars, J., and Bazant, Z.P. (eds.), *Cracking and Damage: Strain Localization and Size Effect,* Elsevier Applied Science, 1988.

22.) Cairns, D., Walker, T., and Ilcewicz, L., *Response of Automated Tow Placed Laminates to Stress Concentrations,*Third NASA Advanced Composite Technology Conference, CP-3178

23.) Smith, P.J., Koch, W.J., Bodine, J.B., and Preuss, C.H., *Design, Analysis, and Fabrication of a Pressure Box for Tension Damage Tolerance Testing of Curved Fuselage Panels,* Third NASA Advanced Composite Technology Conference, CP-3178.

24.) Swanson, G.D., Metschan, S.L., Morris, M.R., and Kassapoglou, C., *The Effects of Design Details On the Cost and Weight of Fuselage Structures,* Third NASA Advanced Composite Technology Conference, CP-3178

25.) Wheeler, D.J., *Understanding Industrial Experimentation,* Statistical Process Controls, Inc., Knoxville, Tennessee, 1987.

26.) Saatchi, H., Durako, B., Reynolds, D., Dost, E., and Willden, K., *In-Situ Processing Methods for Composite Fuselage Sandwich Structures,* Third NASA Advanced Composite Technology Conference, CP- 3178

OMIT

Session III

TEXTILE TECHNOLOGY

Session Chairman: Charles E. Harris
NASA Langley Research Center

[redacted]

ADVANCED RESIN SYSTEMS AND 3-D TEXTILE PREFORMS FOR LOW COST COMPOSITE STRUCTURES

J. G. Shukla and T. D. Bayha*
Lockheed Aeronautical Systems Company
Marietta, GA 30063

ABSTRACT

Advanced resin systems and 3-D textile preforms are being evaluated at Lockheed Aeronautical Systems Company (LASC) under NASA's Advanced Composites Technology (ACT) Program. This work is aimed towards the development of low-cost, damage-tolerant composite fuselage structures. Resin systems for resin transfer molding and powder epoxy towpreg materials are being evaluated for processability, performance and cost. Three developmental epoxy resin systems for resin transfer molding (RTM) and three resin systems for powder towpregging are being investigated. Various 3-D textile preform architectures using advanced weaving and braiding processes are also being evaluated. Trials are being conducted with powdered towpreg, in 2-D weaving and 3-D braiding processes for their textile processability and their potential for fabrication in "net shape" fuselage structures The progress in advanced resin screening and textile preform development is reviewed here.

INTRODUCTION

The NASA ACT program underway at LASC is evaluating advanced toughened epoxy resin systems and 3-D textile preforms to develop low-cost and damage tolerant fuselage structures such as frames, window belts, keel beams/frames and skin-stiffened fuselage panels. Phase II, entitled "Development and Verification of Technology", is focused on the evaluation of advanced epoxy resin systems which have been developed both for resin transfer molding (RTM) and pre-impregnation of carbon fiber tow with powdered resin systems in Task 1. Mechanical tests of flat panels using 2-D woven preforms will be performed to make a resin selection for both composite fabrication processes.

The selected resin systems will be used in Task 2 to evaluate the advantages of advanced textile preforms, made by processes such as 2-D braiding, 3-D through-the-thickness braiding, 3-D interlock braiding, 3-D weaving and multi-axial knitting/stitching. Flat preforms using the above processes were made for the Task 2 work, and fabricated into panels by RTM; the powder coated preforms were only fabricated by 2-D braiding and 3-D through-the-thickness braiding for autoclave processing.

TASK 1: ADVANCED RESIN SYSTEMS FOR TEXTILE PREFORMS

Resin Transfer Molding

The resin transfer molding (RTM) manufacturing process offers major cost advantages in the fabrication of "net shape" composite structures from textile preforms. However, high performance resin systems are needed to meet aircraft structural requirements. Three emerging epoxy resin systems (RSL-1895 (Shell), PR-500 (3M) and E-905L (BP)) were evaluated for RTM. Flat panels were fabricated at Brunswick Defense Corporation using AS-4 (6k) carbon fiber tow woven into 8-harness satin fabric; a schematic of the RTM process is shown in Figure 1.

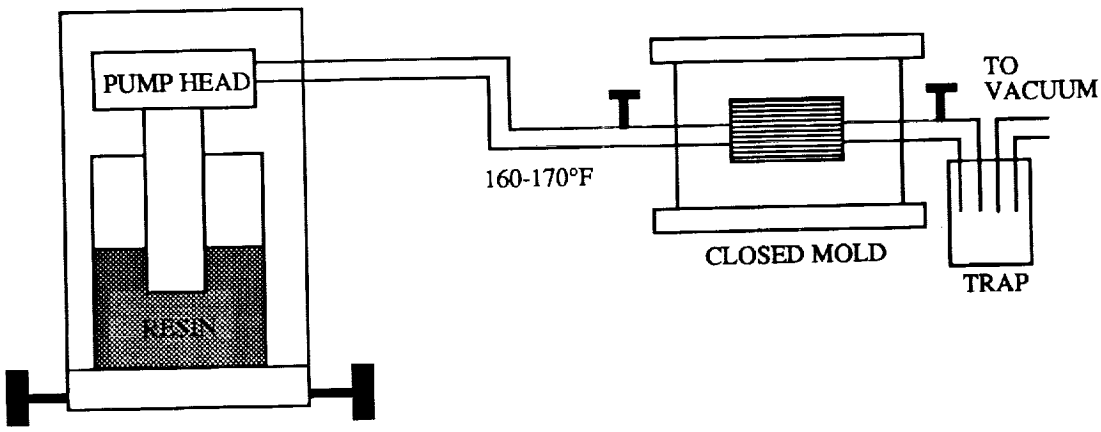

Figure 1. Schematic of the Resin Transfer Molding (RTM) process.

Two part systems such as RSL-1895 and E-905L were mixed and degassed at the required temperature before transfer to the injection cylinder. The process parameters for the resins under study are presented in Table 1. The one-part resin, PR-500, was also heated and degassed before processing. The resin was vented from the center and back of the mold to ensure wet-out of the preform and removal of entrapped air.

The resin systems are being compared using the screening test matrix in Table 2. Of particular interest are the room temperature, hot-wet strengths, notch sensitivity and damage tolerance of the resin systems, since conventional RTM resin systems generally do not have optimal hot-wet and damage tolerance properties.

The Shell resin (RSL-1895) showed the best processability among the three systems evaluated. The shelf life of RSL-1895 is 48 hours at room temperature, and at the injection

Table 1. Processing Parameters for RTM

Resin System	Temperature at Injection, °F		Injection	Cure Temp., Time	Post Cure
	Resin Temp.	Mold Temp.	Pressure, psi	(°F, minutes)	Conditions
RSL-1895	175°	250°	20-80	350°, 30 min.	350°F, 2 hrs.
PR-500	225°	325°	20-80	350°, 60 min.	350°F, 2 hrs.
E905-L	180°	225°	40-80	350°, 30 min.	350°F, 2 hrs.

temperature of 140°F, this system also has a low viscosity (< 100 centipoise at 140°F). The RSL-1895 system is easier to vent and process the part compared to either the 3M PR-500 or BP E-905L resin systems. Temperature control is critical in liquid molding with PR-500; drops in temperature at the injection port, the injection line or in the tool during injection can result in dry spots, voids in the part, and cooling of the resin in the venting lines. E-905L behaves in a similar fashion to RSL-1895 in its flow characteristics, however, temperature control during mixing is required to control viscosity.

Microscopic analysis of the laminates made with all three resin systems indicates good fiber wetout, however, surface pitting was observed in some laminates made with 3M PR-500. Surface pitting was eliminated in subsequent panel fabrication by adequately degassing and controlling temperature. The Shell RSL-1895 laminates showed virtually no porosity, while those panels molded using BP E905-L and PR-500 showed some level of porosity. Photomicrographs of RTM panels are presented in Figure 2. The ultrasonic C-scanning met Lockheed's acceptance criteria.

The bulk cost of the Shell 1895 is $12.00/lb., that of BP E905L is $27/lb., and that of PR-500 is $40.00 per pound.

The testing of RTM panels is being conducted at Delsen Laboratories. Open hole tensile strength (OHT), open hole compression strength (OHC), compression modulus, and Poisson's ratio at room temperature have been completed, and the results are shown in Table 3.

Processing Science for RTM

Resin transfer molding has been used in automotive and other industrial applications where up to 50 volume percent (v/o) fiber is adequate. Aircraft structures require a minimum of 55-60 v/o as well as selected fiber architectures. 2- and 3-D tightly woven or braided preforms being evaluated under this program will require a better understanding of permeability and resin flow through the preform.

Currently, a process model of the RTM process is being developed at the University of Delaware. This modeling effort is to help tool design by providing the location of gates, ports, and vents for optimum mold filling. The flow simulation has been developed based on finite element/control

TABLE 2 : TEST MATRIX

TEST TYPE	LOADING	TEST ENVIRONMENT	INSTRUMENTATION	TEST METHOD (COUPON DWG. NO)
0° Tension	Tension	RTA	T-gage	SACMA SRM4-88 (C1AB)
0° Tension	Tension	-65°F	T-gage	SACMA SRM4-88 (C-1AB)
0° Compression	Compression	RTA	BBTG	SACMA SRM1-88
0° Compression	Compression	180°F, Wet	BBTG	SACMA SRM1-88
Moisture Absorption Travellers	—	—	—	—
± 45° Tension	Tension	RTA	T-Gage	SACMA SRM7-88 (C-3)
Unnotched	Tension	RTA	ASG	SACMA SRM4-88 (C-23)
Open Hole	Tension	RTA	—	SACMA SRM5-88 (C-4NB)
Open Hole	Tension	-65°F	—	SACMA SRM5-88 (C-4NB)
Unnotched	Compression	RTA	B/B	TPS 86-2256 (C-23)
Unnotched	Compression	180°F, Wet	B/B	TPS 86-2256 (C-23)
Moisture Absorption Travellers	—	—	—	—
Open Hole	Compression	RTA	—	SACMA SRM3-88 (C-4NB)
Open Hole	Compression	180°F, Wet	—	SACMA SRM3-88 (C-4NB)
Comp. after Impact	Compression	RTA	B/B	SACMA SRM2-88
Comp. after Impact	Compression	RTA	B/B	NASA 1142 (C-8)

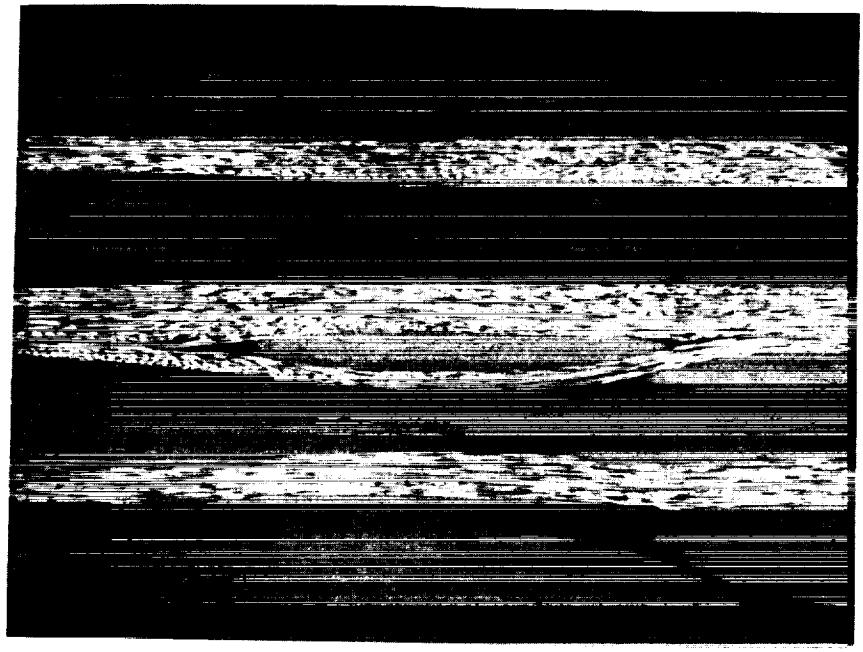

Shell RSL-1895

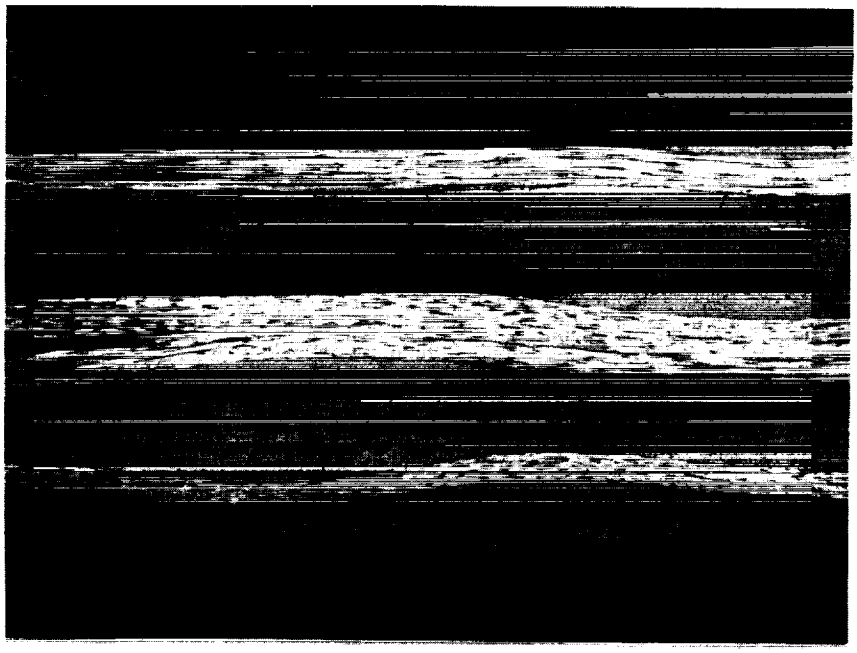

3M PR-500

Figure 2. Photomicrographs of RTM Panels.

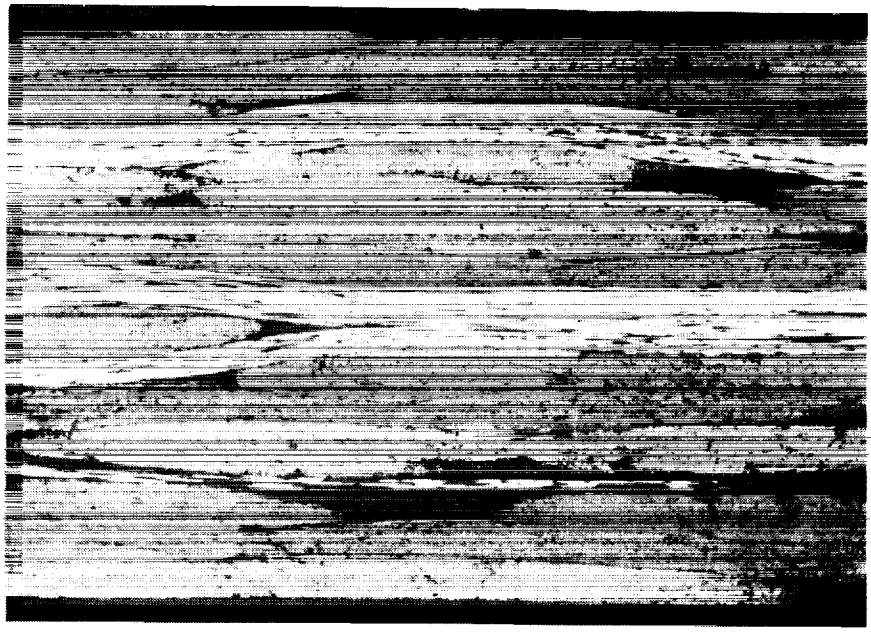

BP E-905L

Figure 2. Photomicrographs of RTM Panels, cont.

Table 3. Test Data* for RTM Laminates (8-Harness Fabric).

Test Type	Condition	3501-6**	Shell-1985	E-905	PR-500
Open Hole Tension Strength, ksi	RT	48.0	54.1	48.1	48.7
	-65°F	47.3	57.0	45.7	47.9
Open Hole Compression Strength, ksi	RT	48.6	43.8	45.7	44.8
Compression Mod, msi		7.5	8.9	8.7	9.3
Poisson's Ratio		0.027	0.024	0.034	0.028

* not normalized
** prepreg

volume method to calculate the flow pattern for mold filling of generalized fluids in anisotropic media. The simulation takes into account the heat transfer between the heated mold, the resin and the fiber perform. Also, resin cure during and after the mold-filling stage is taken into account. The dependence of the resin viscosity on the local temperature and the degree of cure is incorporated in the simulation. Presently, the simulation can model thin planar parts of otherwise arbitrary shape. Since actual resins exhibit a shear-thinning behavior, the simulation takes into account the dependence of the fluid viscosity on the shear-rate. Also along with the flow pattern, the simulation allows one to obtain the progression of the resin cure during the filling stage, and monitor the final cure after the part is filled. Preform permeability studies for 3-D textile architextures and flow simulation for the RTM tool design are underway for the location of gates, vents, and ports for optimum mold filling.

Powder Coating Processes

Two methods of fiber tow impregnation have been studied under the contract: a slurry process developed at BASF Structural Materials, and an electrostatic process devised by Custom Composites. A general schematic for all powder coating processes is given in Figure 3.

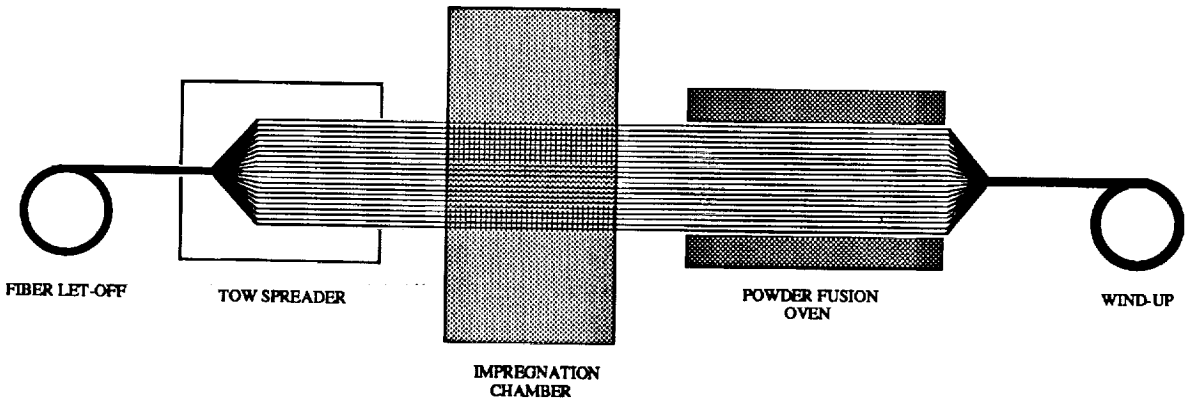

Figure 3. Schematic of Powder Coating Processes.

The BASF process suspends the powder particles in a water-based slurry, and the tow is passed through a bath containing the powder. In line with the slurry bath is an oven to sinter the particles to the carbon fibers before bobbin winding for textile operations. Towpreg was produced with very little variation in resin content by this method.

The electrostatic process uses ionization of the powder particles to induce attraction to the tow. The tow passes through a cloud of powder in the impregnation chamber before sintering in the oven. This process, once stabilized, produces a fairly uniform towpreg; however, some

clumping of powder particles occurs occasionally for some types of powdered resins, especially when a high level of moisture is present.

It is evident from early results that some powder resin variables affect each process differently. For example, in some processes, powder particle size and particle size distribution are critical issues for a consistent, homogeneous coating of powder on the fiber tow. Spreading of the fiber tow is also very important; fibers in the tow need to be individualized in order to guarantee that each interacts with the powder in the impregnation chamber. The degree of fusion of the powder to the fibers is important; the flexibility of the fibers for weaving or braiding into a textile preform is a function of the furnace temperature and speed of the moving tow. The chemical and thermal stability at room temperature to accommodate weaving, braiding and storage are equally important for towpreg materials to be accepted for use in textile preforms.

Advanced Resin Systems for Powder Epoxy Technology

Three emerging epoxy powder systems, RSS-1952 (Shell), Dow CET-3 and PR-500 (3M), are being evaluated. All three resin systems have been screened using a slurry process at BASF. RSS-1952 was chosen to conduct feasibility studies for various textile processes because of its ample supply and processability. Recently, processing criteria for PR-500 and CET-3 have been determined. PR-500 powder was successfully coated by the Georgia Institute of Technology and later by Custom Composites using an electrostatic coating process. Both powder systems were applied to AS4 carbon fiber tow. The processing conditions used to fabricate panels from the two powder systems are listed in Table 4.

Table 4. Processing Parameters for Powder Towpreg Laminates

Powder Resin System	Coating Method	Autoclave Conditions		Curing Conditions	Post Cure Conditions
		Heating Rate	Pressure, psi		
RSS-1952	slurry	5°F/min	85	350°F, 1 hr.	400°F, 4 hrs.
PR-500	electrostatic	5°F/min	85	350°F, 1 hr.	350°F, 2 hrs.

Powder towpreg was woven into 8-harness satin fabric at Fabric Development from towpreg produced at BASF and at Textile Technologies, Inc. (TTI) for the Custom Composites material; the resin content for this fabric construction was 35 ± 2 weight percent (w/o). Flat panels having fiber volume fraction (v/o) of 58%-60% were fabricated and evaluated by Lockheed to compare the two powder coating processes. Photomicrographs indicate good fiber wetout in the Shell RSS-1952 panels and in the 3M PR-500 panels. The photomicrographs of these materials are shown in Figure 4.

Mechanical testing of these panels is currently being performed. The screening test matrix is the same as shown in Table 2 for the panels fabricated by RTM.

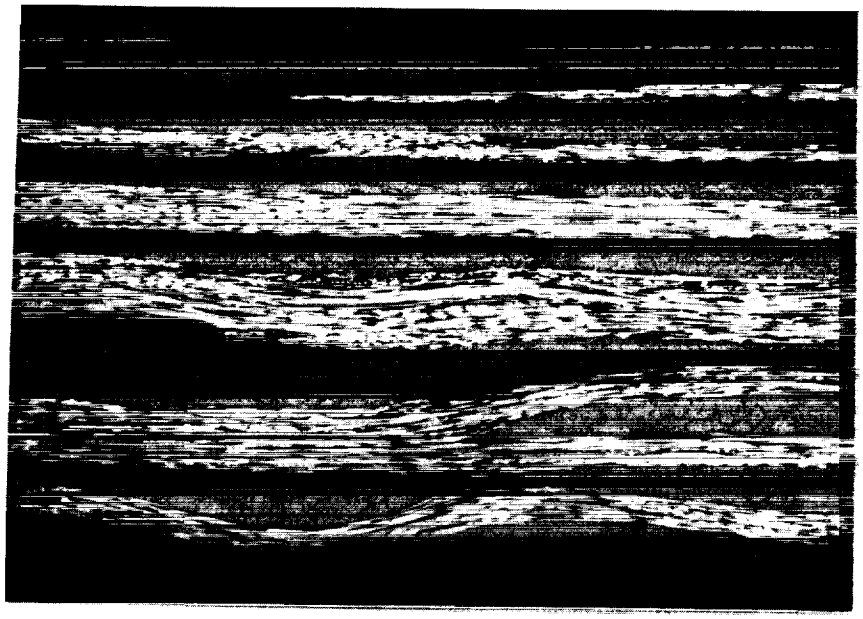

Shell RSS-1952

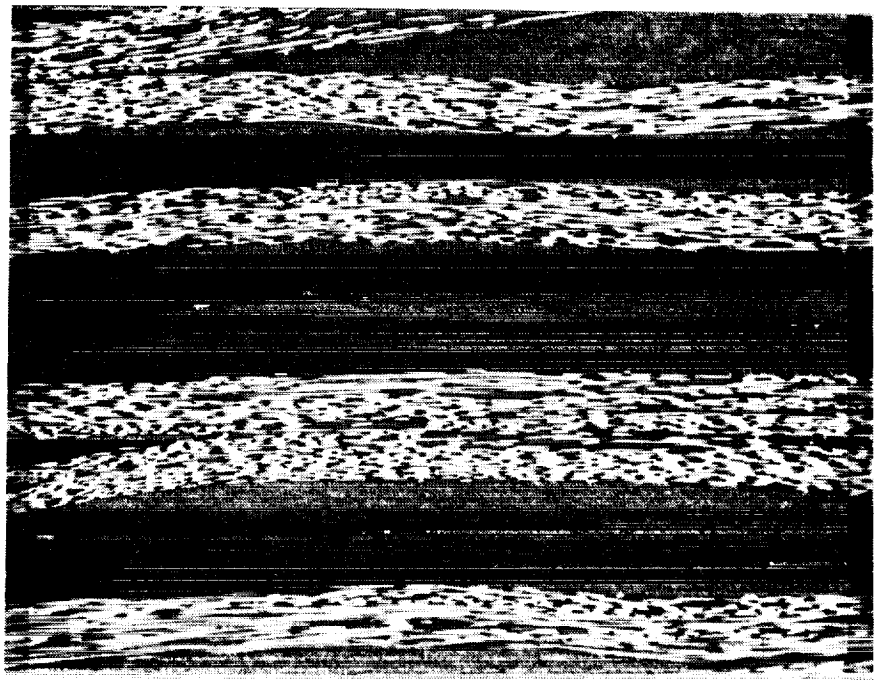

3M PR-500

Figure 4. Photomicrographs of Powdered Epoxy Panels.

TASK 2: PREFORM DEVELOPMENT AND PROCESSING

Task 2 is focused on the evaluation of preforms produced by advanced textile processes. The preform architectures are designed so as to provide improved damage tolerance due to 3-dimensional fiber reinforcement, and have potential cost reductions in the fabrication of composite structures. 3-D textile processes also provide "net" or "near-net" shape preforms, and subsequent fabrication of composites using low cost processes such as resin transfer molding, pultrusion and resin infusion methods reduces part count and therefore assembly steps.

The development of textile processes with fiber continuity between the skin and stiffeners eliminates the problems associated with stiffener separation and significantly improves the structural efficiency of many fuselage structures. Similarly, composite fabrication with textile preforms using low cost powder towpreg offers the same benefits.

The following textile processes are currently being evaluated under Task 2:

- 3-D through-the-thickness weaving with biased yarn;
- 2-D braiding;
- 3-D multi-layer weaving/stitching;
- 3-D interlock braiding;
- 3-D through-the-thickness braiding;
- Multi-axial knitting/stitching; and
- Near-net Fiber Placement (N^2FP) stitching.

Quasi-isotropic flat panel preforms have been produced using most of the above processes with dry Hercules AS-4 carbon fiber tow. These preforms are being fabricated into flat panels using RTM, and will be mechanically tested. The test matrix is identical to the screening test matrix used in Task 1, and presented in Table 2, with the exception that 0° tension and compression, or ±45° tension tests will not be performed. The potential applications, benefits and limitations for preforms made by the respective textile processes are reviewed below. The preform architectures resulting from the above textile processes are shown in Figures 5 and 6.

3-D Weaving

3-D multi-layer [0°/90°] weaving (Figure 5) of preforms was carried out at Textile Technologies, Inc. (TTI). Multi-layer fabrics were stacked to achieve a quasi-isotropic orientation before RTM. This process offers advantages over two dimensional processes due to its relatively low cost, improved damage tolerance and its ability to produce near-net shape preforms. However, the process as it is currently applied has some limitations in introducing biased yarns during weaving, and fiber volume is limited to about 55%.

A 3-D through-the-thickness process has been developed by Techniweave, Inc. The process is capable of weaving multi-axial preforms that include biased plies integral with the skin. The through the thickness yarn is introduced by a chain lock stitch. Window belt panels with window cutouts, stiffened panels and fuselage frame applications all have the potential to be fabricated by this process. Currently, window belt panels with cutouts and stiffeners in both longitudinal and

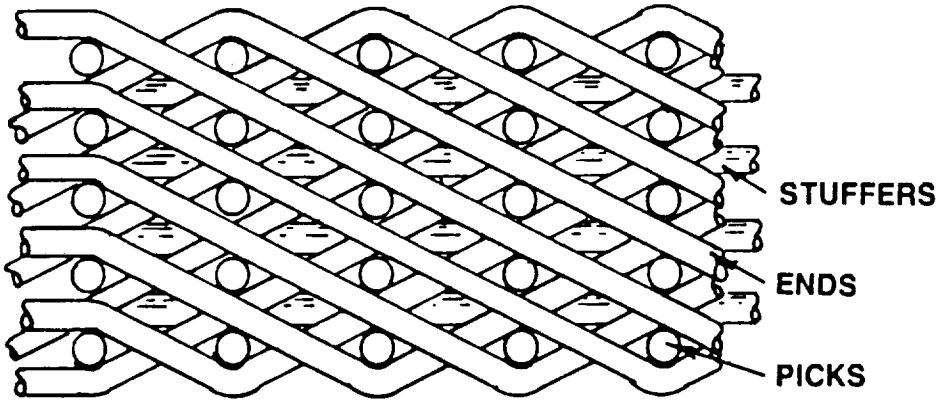

3-D Multi-layer Weaving

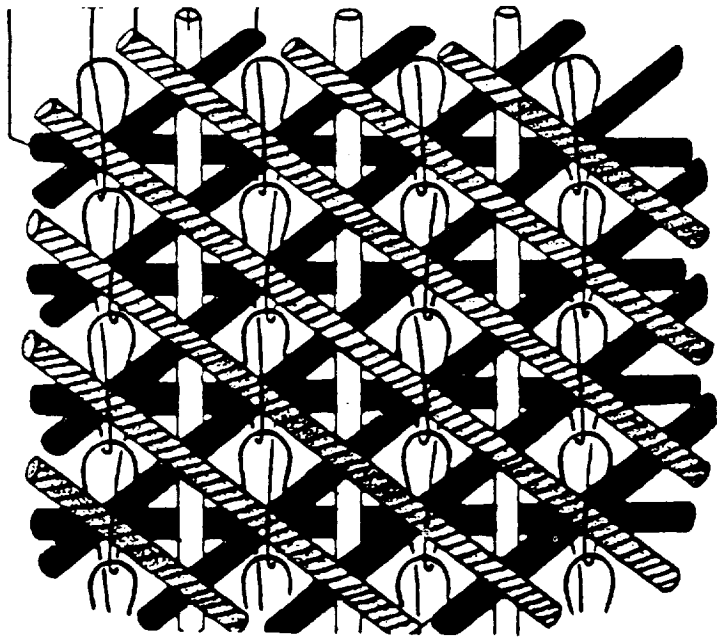

Multi-axial Knitting/Stitching

Figure 5. Textile Architecture for Weaving and Knitting Processes.

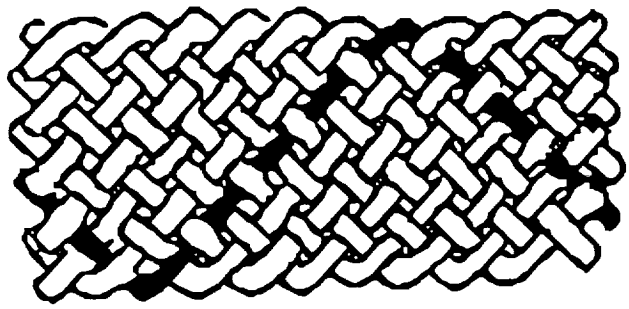

2-D Braiding

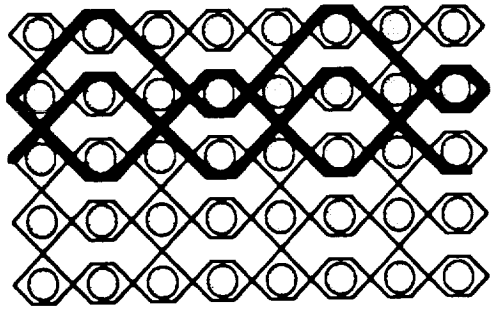

3-D Interlock Braiding

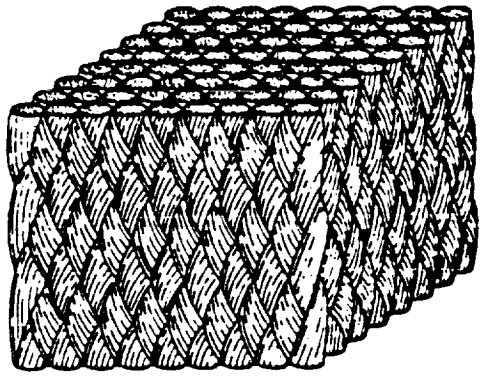

3-D Through the Thickness Braiding

Figure 6. Textile Architecture for Braiding Processes.

transverse directions are being produced, however, the stiffeners will not have biased plies and will have to be stitched. Quasi-isotropic flat preforms are also being produced for testing and evaluation.

2-D and 3-D Braiding

The textile architecture is shown in Figure 6 for various braiding processes. Generally, braiding operations are very versatile, offering reduced cost preforms that can be made in any desired length.

2-D braiding is a low cost textile process to produce preforms to be used in subsequent fabrication of stiffeners and frames by RTM or pultrusion, which offers advantages over conventional autoclave hand layup processes in cost and handling reductions. Low cost, near-net shape preforms can be made by 2-D braiding processes that have improved delamination resistance over hand layups. Preforms manufactured in this manner have only 2-D reinforcement, as well as limitations on the size, thickness and shapes that can be fabricated. Quasi-isotropic ($\pm 60°$, $0°$) flat panels have been made by tri-axial (braid-over-braid) braiding.

An advancement over 2-D braiding is a 3-D interlock braiding process. In this textile process, multi-layer fabric is braided with a layer-to-layer angle interlock. The interlocking fibers provide for z-directional reinforcement, which improves damage tolerance. The cost of these preforms is relatively low, and they can be made in near-net shapes. Potential applications for the 3-D interlock braided preforms include stiffeners and curved frames.

Quasi-isotropic flat panel preforms were made at Albany International on their circular braider. This 3-D braider is currently limited in preform thickness; only five layers can be braided for a given preform with their R & D machine. However, a flat braider is available to make higher thickness braids, as well as braided "net" shapes. Thick panel preforms will be made on this machine in the near future.

Atlantic Research Corporation has an automated 3-D through-the-thickness braiding process that allows production of 72-inch wide preforms. Circular braiding with their bifurcation technique allows integral braiding of stiffened panels and frames in "net" shape. As with the other braiding processes, near-net shapes can be fabricated; however, this process has a greater flexibility in the range of fiber orientations available. At this time, the process is slow and costly, and efforts are underway to increase the speed and reduce preform costs. Quasi-isotropic flat panel preforms have been made by this process at Atlantic Research.

Multi-Axial Knitting/Stitching

Multi-axial stitched panels are currently being fabricated at Hexcel-Hitech. Multi-axial knitting, as shown in Figure 5, provides multi-layer (4-7 layers) fabric with $0°$, $90°$,$45°$,$135°$ fiber orientation, and is probably the least expensive method available to produce multi-layer stitched

preforms for stiffened panels and stiffeners. Multi-layer fabrics will be stacked and stitched for quasi-isotropic laminate and resin transfer mold.

Near-Net Fiber Placement

Quasi-isotropic, multi-layer flat preforms are currently being made at Cooper Composites with their near-net fiber placement technique. The N^2FP process is a fully automated computer-interfaced system which is capable of placing fibers in any predetermined orientation. Volume fractions up to 60% are obtained and near-net shape preforms can be fabricated. While some z-direction reinforcement is available using this method, currently there are limitations in the sizes and thicknesses which can be made. Window frames and window belts are potential applications for composites made from this type of preform.

Powder Coated Advanced Textile Structures

The 2- and 3-D braiding feasibility studies are being conducted with Shell RSS-1952 towpreg produced by BASF. Similarly, feasibility studies are being carried out on 3M PR-500 towpreg. Both materials are braidable, however, both 2- and 3-D braiding processes require an initial resin content on the order of 39±2 w/o resin due to the abrasive nature of the processes. The textile operations reduced the resin/fiber content between 2% and 3% by weight during processing. These preforms are currently being made and tested at Lockheed. BASF/Textile Technologies, Inc. has already woven 3-D multi-layer fabrics from the towpreg and processed them. The 3-D fabrics required higher temperature and pressure to fully consolidate, compared to the 2-D fabrics.

The Custom Composites PR-500 towpreg was woven into 8-harness satin fabric at TTI. The towpreg has been evaluated for its braidability at both Fiber Innovations and Atlantic Research Corp. The initial abrasion tests indicated that the towpreg is braidable. Flat preforms will be braided early in the summer to evaluate any advantages in braiding of the electrostatically towpregged materials over towpreg made by the slurry process.

SUMMARY AND CONCLUSIONS

Resin transfer molding evaluation of all three advanced resin systems was accomplished. The processability of the Shell RSL-1895 resin system was better than the 3M PR-500 and BP E-905L systems. Photomicrographs showed excellent fiber wet-out with all three systems. The current cost of the Shell system is lower than either of the other two.

Mechanical testing of all RTM panels is underway. A selection of an optimal resin system will be made based on processability, cost and performance.

Both powder epoxy resin systems, the Shell RSS-1952 and the 3M PR-500, show promise. Studies of the 2-D and 3-D weaving and braiding feasibility for both powder towpreg systems have been completed, and flat panel evaluation has begun.

The mechanical testing of the autoclave processed panels is expected to be completed by mid-summer of 1992.

WEAVABILITY OF DRY POLYMER POWDER TOWPREG

Maylene K. Hugh and Joseph M. Marchello*
Old Dominion University
Norfolk, Virginia 23508

Janice R. Maiden
Textile Technologies, Inc.
Hatboro, Pennsylvania 19040

Norman J. Johnston
NASA Langley Research Center
Hampton, Virginia 23665-5225

ABSTRACT

Carbon fiber yarns (3k, 6k, 12k) were impregnated with LARC™ thermoplastic polyimide dry powder. Parameters for weaving these yarns were established. Eight-harness satin fabrics were successfully woven from each of the three classes of yarns and consolidated into test specimens to determine mechanical properties. It was observed that for optimum results warp yarns should have flexural rigidities between 10,000 and 100,000 mg-cm. Tow handling minimization, low tensioning, and tow bundle twisting were used to reduce fiber breakage, the separation of filaments, and tow-to-tow abrasion. No apparent effect of tow size or twist was observed on either tension or compression modulus. However, fiber damage and processing costs favor the use of 12k yarn bundles versus 3k or 6k yarn bundles in the weaving of powder-coated towpreg.

INTRODUCTION

In order for composite materials to be utilized as primary structures in subsonic and supersonic aircraft applications, the total production costs of the composite parts must be decreased from their present levels. Developments in the fabrication of composite parts point toward cost reduction through increased automation. In conjunction with the development of automated fabrication techniques, NASA Langley Research Center (LaRC) has developed a method of prepregging carbon fiber with dry thermoplastic and thermosetting polymer powder.

*Work performed under NASA grant NAG-1-1067 with Old Dominion University, Norfolk, VA.

These efforts at NASA LaRC have focused on two established manufacturing technologies - textiles and robotics. In order to be used in these automated applications, powder-coated towpreg must be produced in the form of either a textile quality yarn or an advanced tow placement (ATP) quality ribbon. This study deals with the former, namely, with textile applications such as powder-coated preforms and broad goods.

By coupling powder-coated towpreg with existing, highly automated textile processes, the resulting impregnated fabrics, broad goods and preforms can be easily molded into parts. These combined fabrication processes may be an alternative to resin transfer molding (RTM) of dry preforms in cases where complex mold geometries and tightly fabricated preforms pose wet-out problems. The powder-coated process may offer the only viable method of part fabrication if high melt viscosity polymers are required to obtain improved composite properties, such as thermal stability and/or fracture toughness.

One of the objectives of the present study was to develop the weaving protocol for powder-coated yarns. In earlier studies (1, 2), the process of powder-coating tow and its weaving or braiding into preforms for part fabrication was found generally to be less expensive and inflicted less damage to the fibers when larger tow bundles were used. Offsetting the advantage of using large tow bundles are factors such as potential difficulty in consolidation and possible reduction in composite properties.

In this study, the effects of varying yarn bundle sizes and yarn twist on the weavability of dry polymer powder-coated fibers were studied in detail. The mechanical properties of composites made from resultant woven cloth were determined. G30-500* (BASF) and AS-4* (Hercules) carbon fibers in tow bundles of 3k, 6k, and 12k filaments were used. Each was impregnated with a thermoplastic polyimide, LARC™TPI* 1500 medium flow powder (Mitsui Toatsu Chemicals). Weaving was performed on towpreg yarns that had twist levels of zero twist or 15 twists per meter (tpm). After establishing a weaving protocol, an experimental epoxy (AMD-0029*, produced by 3M) was fabricated into towpreg and woven into eight-harness satin fabric.

POWDER PREPREGGING PROCESS

The dry powder prepregging process involves three steps: tow spreading, polymer deposition, and polymer fusion onto the fibers (3). The carbon fiber tow bundle was first pneumatically spread to approximately 8 centimeters in width, then impregnated with powder by means of a dry, recirculating,

* Use of trade names or manufacturers does not constitute an official endorsement, either expressed or implied, by the National Aeronautics and Space Administration.

fluidized powder chamber. Radiant heating was used to sinter or fuse the polymer powder particles to the tow. The powder line was upgraded to speeds of 10-15 meters/min and over 20,000 meters of towpreg were produced for the current study.

WEAVING CONDITIONS AND PARAMETERS

The primary objective of the weaving study was to learn how to convert powder-coated yarn into quality fabric. The parameters considered in order to establish a weaving protocol for powder-coated towpreg are listed in table I.

Yarn splitting and loose fibers on the yarn surface cause difficulties in weaving. To overcome this, yarn shaping, twisting, serving, wetting, and sizing are common practices. In this investigation, only tow bundle twisting and shaping were used to reduce the separation of filaments, decrease tow-to-tow abrasion, and minimize fiber loss.

Towpreg flexural rigidity was also systematically varied since a previous study indicated that yarn flexural rigidity was an important parameter in successfully weaving towpreg (4). Powder-coated yarn rigidity is a function of percent resin content, oven temperature, and yarn residence time in the oven. These parameters were appropriately altered to furnish the required rigidity variations. Samples were taken from each lot of towpreg yarn, and flexural rigidity was measured by ASTM method D1388-64. Towpreg flexural rigidity values utilized in this study are listed in table II.

OBSERVATIONS AND WEAVING PROTOCOL

Towpreg was woven into eight-harness satin fabric under NASA Contract NAS1-18358 by Textile Technologies, Incorporated (TTI) in Hatboro, PA. The initial work was performed on yarns containing 6k filaments. During this phase, the set-up of the loom and the weaving of the towpreg were examined for ways to minimize damage imparted to the yarn.

The towpreg yarn prepared at LaRC was rewound at TTI onto 40 separate spools in order to produce a balanced 10.2 cm (4") wide fabric with 394 picks per meter (10 picks per inch, ppi). Two rewinding machines were used to determine how best to rewind towpreg. A rewinder that yielded a parallel winding pattern was found to cause less fiber damage than a rewinder that gave a cross winding pattern.

The spools of rewound towpreg were loaded into a rapier-type loom (Iwer 1200), which was used instead of a shuttle-type loom in order to minimize damage on the fill yarn. Initial weaving efforts revealed problems with the surface of the warp towpreg yarns having loose filaments, which accumulated in the heddles and reed. To alleviate this problem, the towpreg was twisted to a carbon fiber manufacturer's standard of 15 twists per meter (tpm). Use of twisted towpreg greatly improved the weaving operation.

Findings from these initial studies can be summarized as follows: the combination of careful rewinding, use of a rapier-type loom, reduction of tension on the warp yarns, and minimizing turns and bends at the loom provided an appropriate protocol for weaving both twisted and untwisted towpreg.

As shown in figure 1, noticeable fiber damage was observed in the woven material. While twisting improves weavability, the action of twisting was found to impart damage to the prepregged yarn. The method of tow twisting at LaRC was performed off-line after the prepregging had been completed, and required additional fiber handling. It is likely that improvements in the twisting equipment and on-line twisting can reduce fiber damage.

An analysis is given in table III of the powder-coated fabric produced for this study from both twisted and untwisted yarn. The weave counts, linear weights and fabric thicknesses are presented for 3k, 6k, and 12k towpreg made with LARC™TPI.

CONSOLIDATION OF WOVEN FABRIC

Several parameters for consolidating woven powder-coated towpreg fabric were investigated. Special consideration in consolidating woven goods, as distinct from consolidating unidirectional tape, had to be given to the elimination of intra- and inter-tow voids within fabric, as well as the elimination of inter-ply voids that are also of concern in conventional tape processing.

The work of Van West et al. (5) on a consolidation model for commingled fiber yarns stitched and woven into drapeable broadgoods and preforms, and the studies of Iyer and Drzal (6) on powder-impregnated thermoplastic composite consolidation as a two-step process provided guidelines for the consolidation studies. The general steps in the consolidation of woven materials established by these studies are illustrated in figure 2. They are intimate contact of the polymer-polymer interface at numerous sites across the composite, followed by deformation and autohesion, or interdiffusion, of polymer chains to cause the interface to disappear. Resin flow, wetting of fibers, and fiber movement are necessary to eliminate voids and fill the intra- and inter-tow spaces.

In order to follow the cycle shown in figure 2, a vacuum press was used to remove air from void spaces in the LARC™TPI/carbon fiber specimens. At maximum temperature, pressure was applied at 0.05 to 0.15 MPa/min to 4.2 MPa in order to allow sufficient time for resin flow, adhesion, and fiber movement. The pressure ramp was followed by a hold period of one hour for final consolidation and stress release at 350°C or 370°C for the unidirectional laminates and 370°C for the woven eight-harness satin prepreg cloth. The part was cooled below Tg at a rate sufficient to stop consolidation before the thickness curve flattened. This avoided resin squeeze-out and resulting dry spots.

MECHANICAL PROPERTIES

A mechanical testing program was developed to determine the effects of tow bundle size and twist on the mechanical properties of unidirectional and eight-harness satin fabric laminates. First, to investigate the effects of tow bundle size, powder-coated towpreg made from LARC™TPI and 3k and 6k G30-500, and 12k AS-4 carbon filaments were frame-wrapped into unidirectional panels to obtain the flexural strength and modulus (by ASTM method D790-84a), the transverse flexural strength (7), and the short beam shear strength (ASTM method D2344-84). The mechanical properties generated from these tests for untwisted tow are compared to the tow bundle size in figures 3-5.

To determine the effects of twisted tow on mechanical properties, tests were conducted on unidirectional composites, specifically, 12k carbon fiber (AS-4) towpreg of LARC™TPI with a twist level of 15 tpm. Flexural strength and modulus (ASTM method D790-84a) values were obtained and compared to untwisted towpreg (table IV). In addition, compression tests were performed by the IITRI method (ASTM method D3410-87, procedure B), where the specimens were 14.0 cm long, 0.64 cm wide, an average of 0.279 cm thick (5.5 in x 0.25 in x 0.110 in), and had a gage length of 1.27 cm (0.50 in). The values for compressive strength, modulus, and Poisson's ratio for twisted tow and untwisted tow are also listed in table IV.

The eight-harness satin fabric, woven from powder-coated towpreg, was consolidated into panels, and then cut into tension and short block compression specimens. The tension specimens were 20.3 cm long, 2.54 cm wide, an average of 0.374 cm thick (8 in x 1 in x 0.147 in), and had a gage length of 10.2 cm (4 in). These specimens were tested untabbed using hydraulic grips. A tensile load was applied only in the warp direction. Insufficient material was available for testing in the fill direction. The short block compression specimens were 4.45 cm long, 3.81 cm wide, an average of 0.635 cm thick (1.75 in x 1.50 in x 0.250 in), and had a gage length of 2.54 cm (1 in). Specimens were tested in

both the warp and fill directions. Tension and compression moduli for eight-harness satin fabric composites are shown as a function of tow bundle size and twist in figures 6 and 7.

DISCUSSION

Learning to use powder-coated tow to make composite materials is an ongoing process. This study has dealt with textile applications, focusing on weaving and consolidation. Some of the operating and design issues in these processes have been resolved while others have been highlighted for further attention.

Weaving powder-coated tow in a conventional rapier loom results in less fiber damage on the fill yarns, since the fill yarn is taken directly from the manufacturer's spool. All weaving operations require that care be taken to minimize fiber damage. There should be as few as possible eyelets, bends and other tow touch points. Tensioning should be kept low. Rewinding and other handling activities should be minimized.

An important observation regarding weaving and tow size selection is the relation between fiber damage and tow size. During both powder prepregging and towpreg weaving, fiber damage is greater for the smaller tow bundles. This is because damage occurs primarily to the fibers that are at the bundle surface. For a given total amount of fiber, the use of small tows results in larger tow surface area and correspondingly higher fiber damage.

A consolidation cycle for woven towpreg, such as that shown in figure 2, must account for the inter-bundle crimp of the weave. Since a higher resin content is needed to fill the interstitial spaces, in general, composites made from woven material will have a lower fiber volume fraction than those made from unidirectional tape. Further studies will be required to establish the optimum fiber volume fraction for powder-coated preforms. Because of the initial bulk associated with woven materials, vacuum should be applied to prevent the formation of air voids. During consolidation, the fibers in woven materials must move and realign, while resin must flow to fill the interstitial spaces. A gradual increase in pressure over time provides for greater ease of fiber movement and resin flow before the fibers align in a tight, compact arrangement. Attention to these factors, together with the general practice of holding for a period of time at maximum pressure and temperature followed by cooling to stop consolidation, yielded composite specimens of woven material that were void-free, as determined by ultrasonic C-scans.

For unidirectional laminates, if the panels are well consolidated and the fiber and matrix are well distributed within each, the tow bundle size should have no effect on mechanical properties. No apparent pattern was found in the mechanical properties of the unidirectional laminates as a result of tow bundle size (figures 3 and 4) with a possible exception in the transverse flexural strength values (figure 5). Unidirectional composites made only with 6k towpreg showed a high flexural strength. This difference may be due to the fact that the 6k material was consolidated at 370°C, whereas the 3k and 12k materials were consolidated at 350°C. The increase in temperature for the consolidation cycle may have resulted in an increase in consolidation due to a decrease in resin viscosity. As the processing cycles for LARC™TPI fiber reinforced composites are improved, more mechanical property data will be generated.

In contrast to the "as expected" unidirectional mechanical properties, the fabric composites were expected to exhibit increased mechanical property values with decreasing tow bundle size due to the contribution of crimp, which increases with increasing tow bundle size. The limited data obtained for composites made with eight-harness satin woven cloth (figures 6 and 7) show no apparent effect of tow size or twist on tension and compression modulus. Because of a lack of material, each data point shown in figures 6 and 7 represented an averaged value taken from testing three to five specimens. A large scatterband was observed for the strength data; consequently, more tests will be required to develop statistically significant strength values.

Mechanical properties of composites made of twisted towpreg displayed little difference from those properties obtained on specimens with untwisted tow (table IV). At 15 tpm the non-alignment effect of fibers in a twisted yarn is negligible (8). This is illustrated in the compression and flexural modulus values. Composites made with twisted towpreg had a 15 percent lower compression strength than those made with untwisted towpreg. Apparently, the additional fiber damage that resulted from the current method of twisting caused the reduction in strength. Twisting the towpreg improved weavability, since it caused the yarn to take on a cross-section that was round and compact. In order to create a suitable yarn for weaving, either the current method of twisting must be improved or the towpreg must be shaped with heated dies or rollers to achieve the same cross-section with less damage.

CONCLUDING REMARKS

The weavability of dry, polymer powder-coated towpreg depends upon a number of material properties and equipment parameters. An optimal weaving protocol requires tow handling minimization, low tensioning, and tow bundle twisting. These textile techniques are important factors for automating the production of quality composite parts from powder-coated towpreg preforms.

Mechanical properties were determined from composite specimens made with carbon fiber tow bundles of 3k, 6k, and 12k that were coated with LARC™TPI 1500 medium flow grade powder. Testing was performed on unidirectional and eight-harness satin fabric composite specimens. No apparent effect of tow size was found in the unidirectional composites. In addition, no effect of twist or tow size was found in the eight-harness satin fabric composites. The lower compression strength that the unidirectional composites made with twisted towpreg displayed was due to apparent fiber damage that occurred during the twisting operation to the tow bundle.

The matter of optimum tow bundle size remains unresolved when comparing the mechanical properties. Fiber damage has been observed to be less when larger tows are used. Weaving equipment capabilities are somewhat independent of tow size. It appears that the choice of tow bundle size is an open one in regard to properties, but that larger tows are favored, especially in regard to powder processing and weaving costs.

ACKNOWLEDGEMENTS

The authors gratefully acknowledge the assistance of Mr. John Snoha for preparing the powder-coated towpreg and the consolidated woven cloth panels, Mr. Ruperto Razon for the unidirectional specimen preparation, and Mr. Benson Dexter for his assistance with the weaving studies and mechanical tests.

REFERENCES

1. Marchello, J. M.; and Baucom, R. M.: LARC™ Dry Powder Towpreg Process. *Science of Advanced Materials and Process Engineering Series*, vol. 36, April 1991, pp. 68-80.

2. Hugh, M. K.; Marchello, J. M.; Baucom, R. M.; and Johnston, N. J.: Composites from Powder-Coated Towpreg: Studies with Variable Tow Sizes. *Science of Advanced Materials and Process Engineering Series*, vol. 37, March 1992, pp. 1040-1051.

3. Baucom, R. M.; and Marchello, J. M.: LARC™ Powder Prepreg System. *SAMPE Q.*, vol. 21, no. 4, July 1990, pp. 14-19.

4. Hirt, D. E.; Marchello, J. M.; and Baucom, R. M.: Study of Flexural Rigidity of Weavable Powder-Coated Towpreg. 22nd International SAMPE Technical Conference, November 1990, pp. 360-369.

5. Van West, B. P.; Pipes, R. B.; Keefe, M.; and Advani, S. G.: The Draping and Consolidation of Commingled Fabrics. *Composites Manufacturing*, vol. 2, no. 1, March 1991, pp. 10-22.

6. Iyer, S. R.; and Drzal, L. T.: Manufacture of Powder-Impregnated Thermoplastic Composites. *J. Thermoplastic Composite Materials*, vol. 3, October 1990, pp. 325-355.

7. Adams, D. F.; King, T. R.; and Blackketter, D. M.: Evaluation of the Transverse Flexure Test Method for Composite Materials. *Composites Science and Technology*, vol. 39, 1990, pp. 341-353.

8. Zweben, C.; Smith, W. S.; and Wardle, M. W.: Test Methods for Fiber Tensile Strength, Composite Flexural Modulus, and Properties of Fabric-Reinforced Laminates. Fifth Conference on Composite Materials: Testing and Design, ASTM STP 674, 1979, pp. 228-262.

Table I. Weaving Parameters

Towpreg Characteristics

- Yarn Shape
- Amount of Twist
- Yarn Flexibility
- Degree of Yarn Damage

Weaving Characteristics

- Passing Yarn Through Eyelets
- Minimizing Turns and Bends
- Proper Tensioning
- Heddles and Reed Action

Final Parts

- Optimal Resin Content
- Bulk Factor

Table II. Flexural Rigidity

Description	Overhang (cm)	Areal Weight (mg/cm^2)	Rigidity (mg cm)
Twisted tow, 6k LARC™TPI	10.16	8.27	1,100
Twisted woven cloth, 6k LARC™TPI	8.26	45.02	3,200
Twisted tow, 6k LARC™TPI	22.86	5.62	8,400
Twisted woven cloth, 6k LARC™TPI	17.78	43.35	30,500
Twisted tow, 12k LARC™TPI	13.97	20.85	7,100
Twisted woven cloth, 12k LARC™TPI	10.16	87.64	11,500
Untwisted tow, 12k LARC™TPI, 34.6% w/w resin	17.15	20.15	12,700
Untwisted tow, 12k 3M epoxy, 32% w/w resin	12.70	19.84	5,100

Table III. Towpreg 8HS Fabric

Towpreg Specification	Weave Count (ppi)	Weave Count (ppm)	Weight (g/m^2)	Thickness (cm)
6k (G30-500) / LARC™TPI, No Twist	10.2 x 9.8	402 x 386	478.4	.170
6k (G30-500) / LARC™TPI, Twisted Tow	10.2 x 9.8	402 x 386	483.7	.180
6k (G30-500) / LARC™TPI, No Twist	10.1 x 10.0	398 x 394	448.2	.196
6k (G30-500) / LARC™TPI, Twisted Tow	10.2 x 9.3	402 x 366	499.4	.262
12k (AS-4) / LARC™TPI, Twisted Tow	8.2 x 8.2	323 x 323	810.5	.320
3k (G30-500) / LARC™TPI, Twisted Tow	20.0 x 19.8	787 x 780	428.1	.147

Table IV. Twisted and Untwisted Towpreg Properties in Unidirectional 12k AS-4 Carbon Fiber / LARC™ Thermoplastic Polyimide (TPI)

Mechanical Properties	Non-twisted towpreg	Twisted towpreg (15 tpm)
Flexural Strength† (MPa)	1760 ± 97	1713 ± 110
Flexural Modulus† (GPa)	107.5 ± 1.7	111.9 ± 2.8
Compression Strength (MPa)	1140 ± 84	968 ± 67
Compression Modulus (GPa)	118.2 ± 5.5	108.4 ± 6.3
Poisson's Ratio††	0.345 ± 0.023	0.382 ± 0.030

† Values have been normalized for 60% fiber volume fraction.

†† Based on IITRI compression data (by ASTM method D3410-87, procedure B).

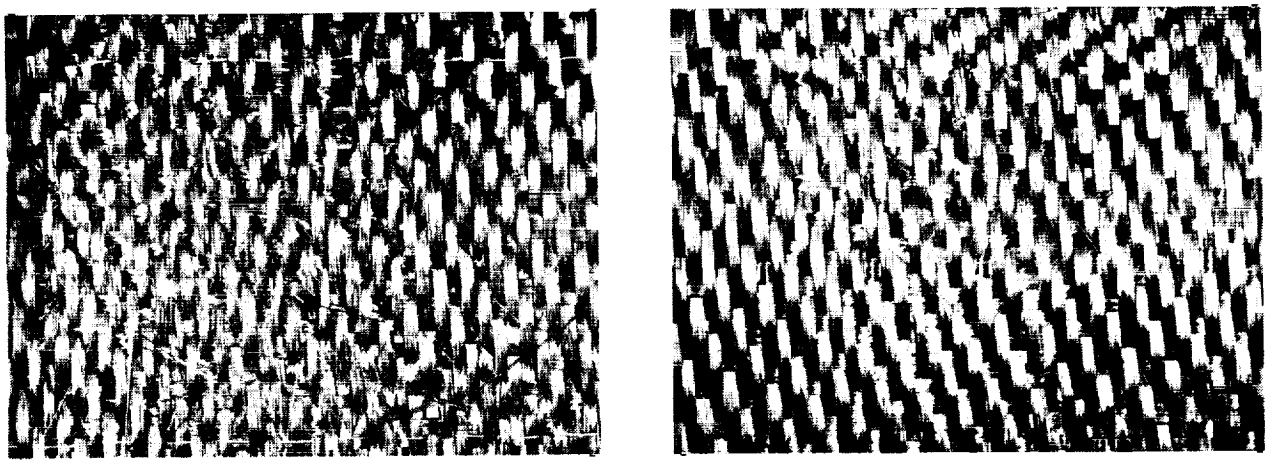

Using twisted towpreg

Using non-twisted towpreg

Figure 1. Photographs of eight-harness satin fabric from 6k carbon fibers and LARC™TPI powder.

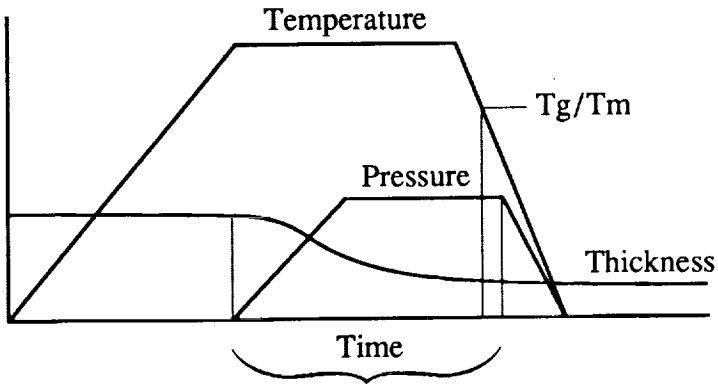

Consolidation and polymer flow

- Vacuum is used to eliminate air voids.
- Pressure ramp allows time for fiber movement into a compact arrangement with minimum fiber crimping and breakage.
- Pressure ramp also provides time for resin flow and adhesion.
- Holding temperature above Tg or Tm anneals the composite and relieves internal stresses.
- Cooling below Tg or Tm stops consolidation before thickness curve flattens and avoids resin squeeze out and resulting dry spots.

Figure 2. Woven towpreg cure cycle.

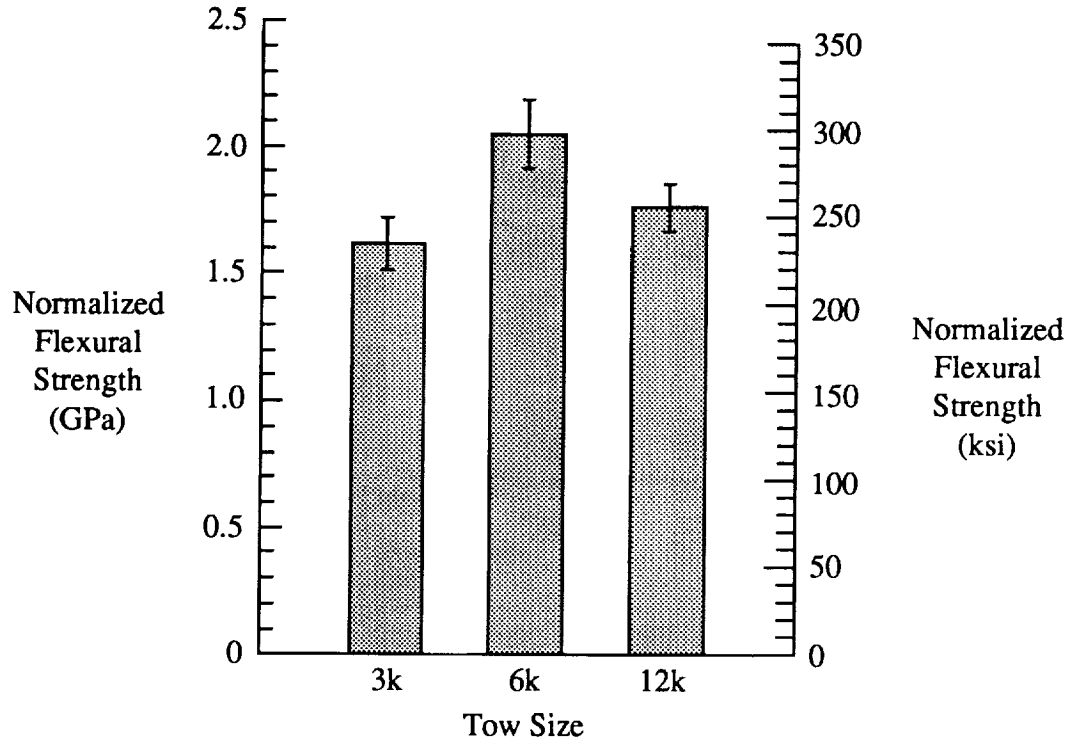

Figure 3a. Normalized flexural strength vs. tow size in untwisted, unidirectional composites of LARC™TPI/AS-4 or G30-500 carbon fibers.

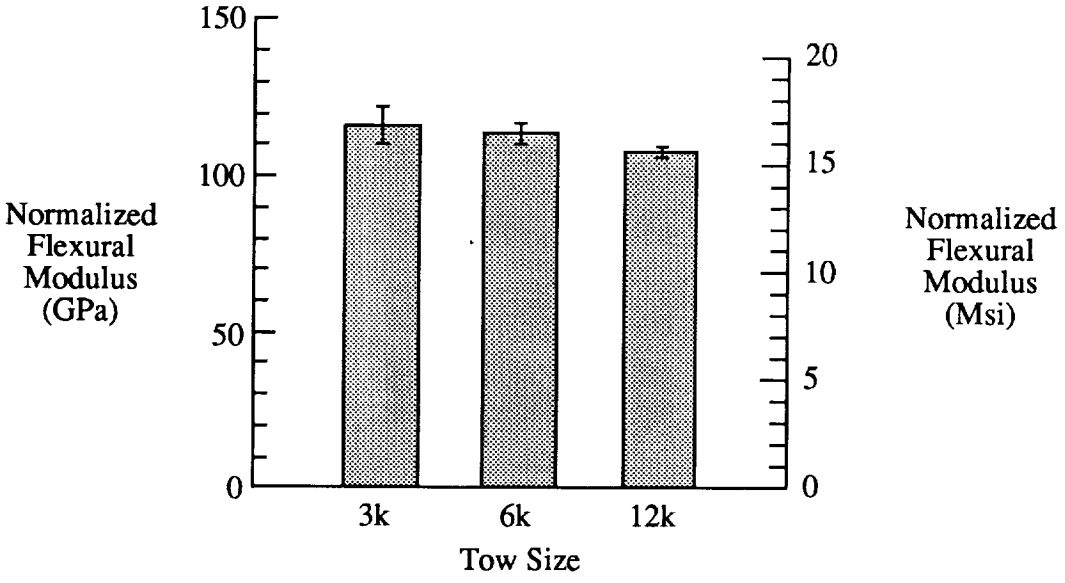

Figure 3b. Normalized flexural modulus vs. tow size in untwisted, unidirectional composites of LARC™TPI/AS-4 or G30-500 carbon fibers.

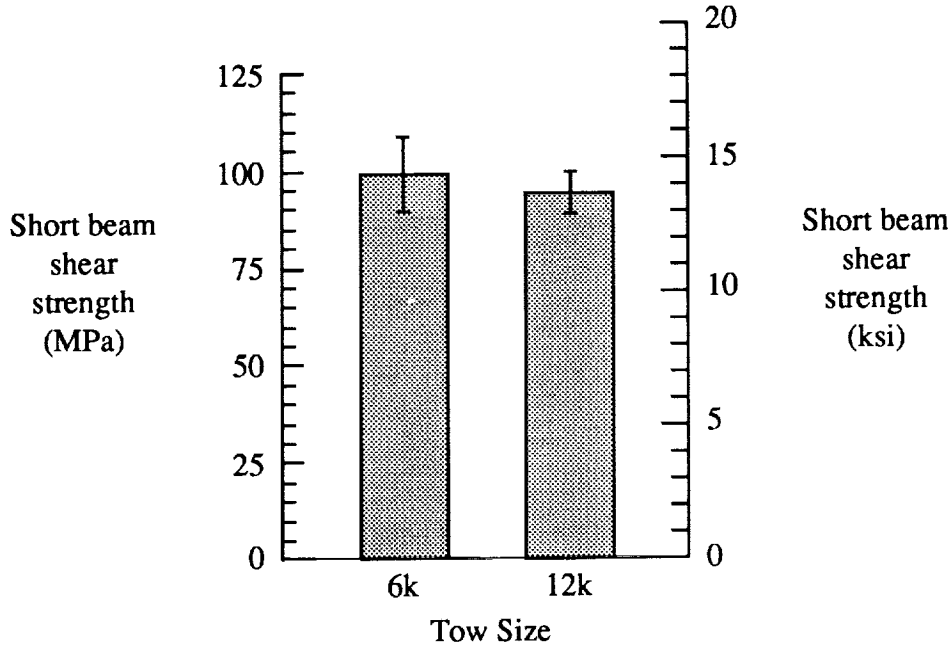

Figure 4. Short beam shear strength vs. tow size in untwisted, unidirectional composites of LARC™TPI/AS-4 or G30-500 carbon fibers.

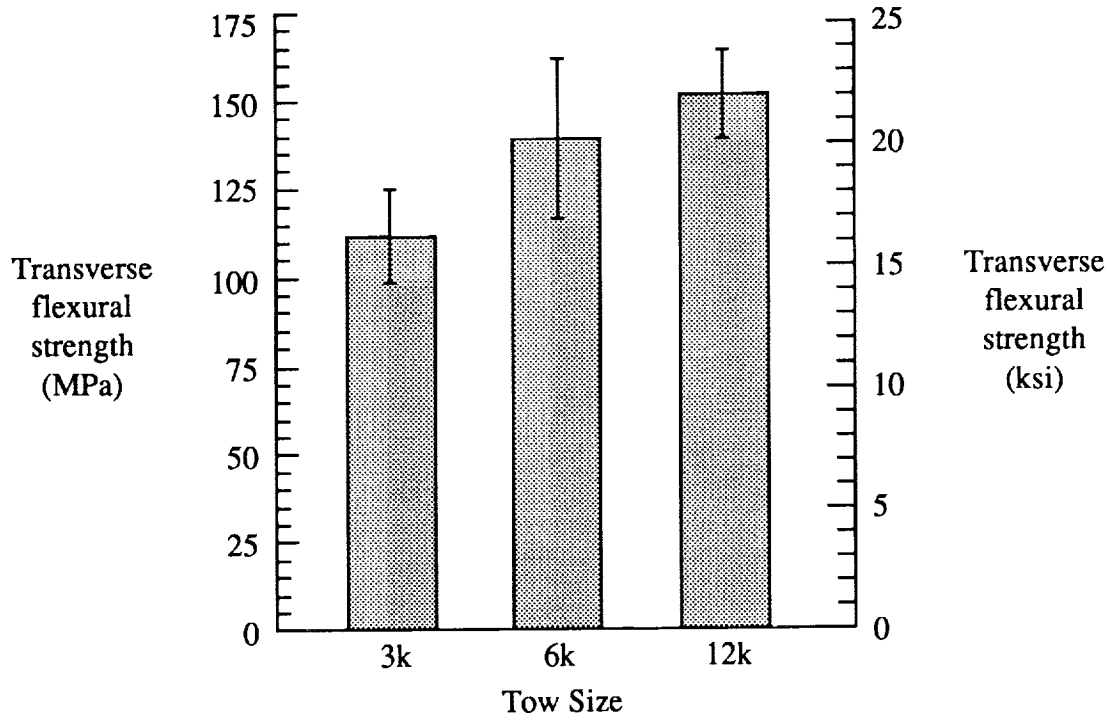

Figure 5. Transverse flexural strength vs. tow size in untwisted, unidirectional composites of LARC™TPI/AS-4 or G30-500 carbon fibers.

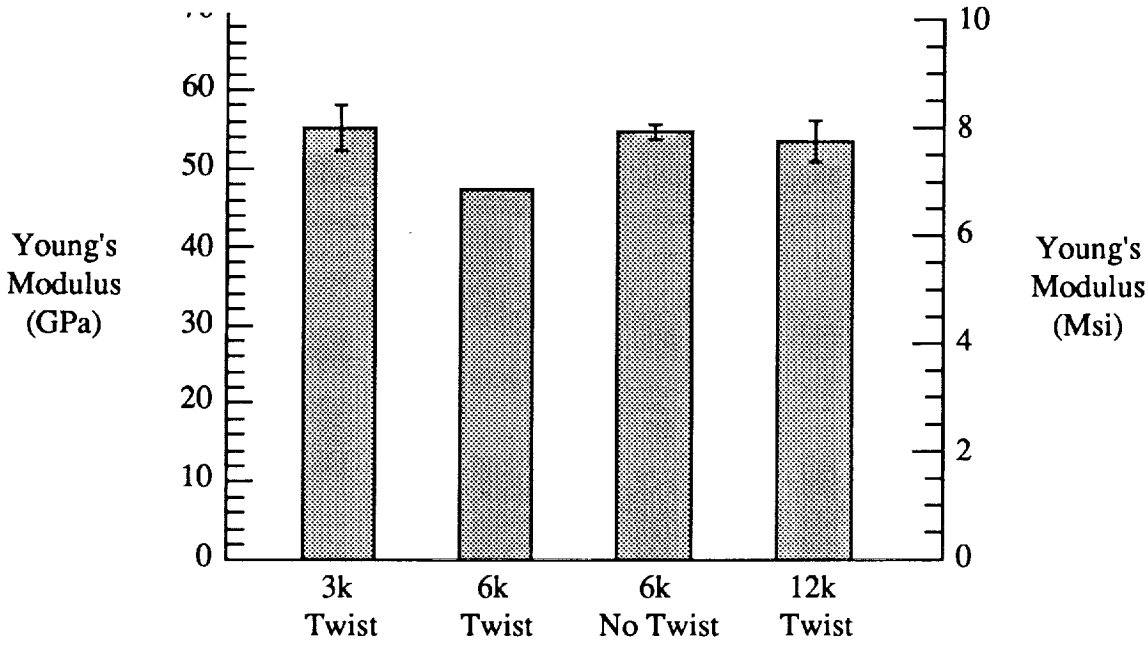

Figure 6. Young's modulus vs. tow size for eight-harness satin woven composites of LARC™TPI/AS-4 or G30-500 carbon fibers. Data collected from tension tests performed in the warp direction.

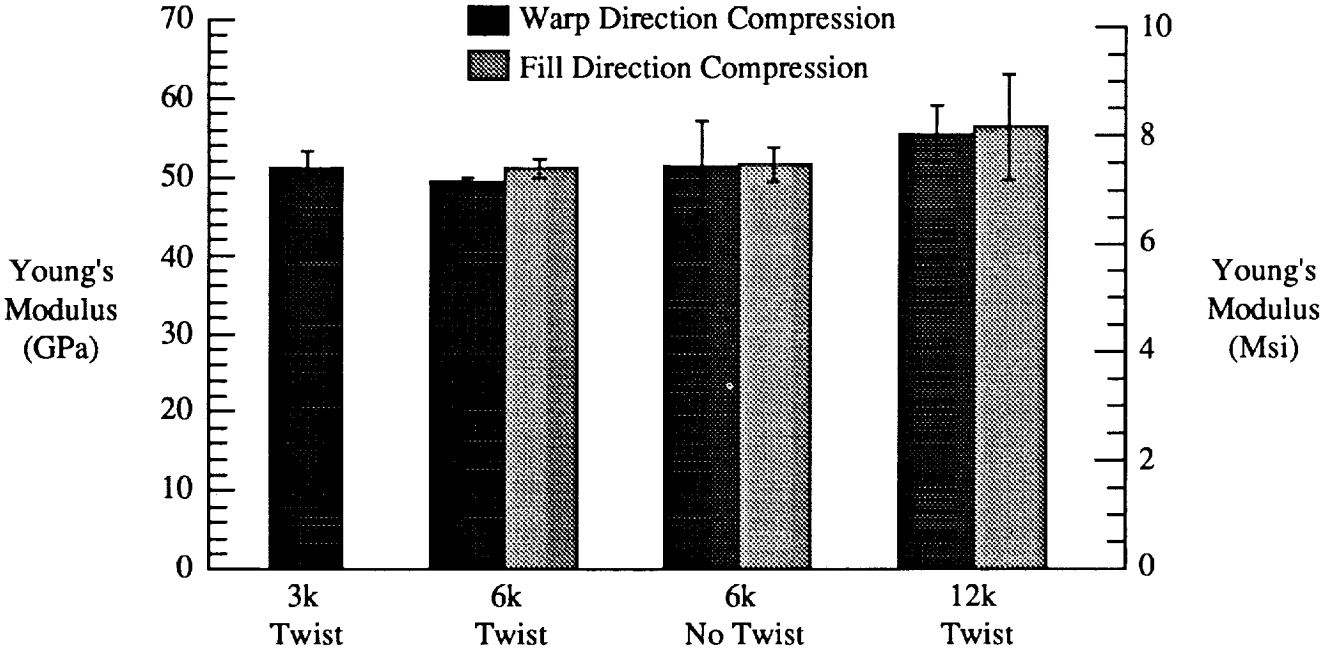

Figure 7. Young's modulus vs. tow size for eight-harness satin woven composites of LARC™TPI/AS-4 or G30-500 carbon fibers. Data collected from short block compression tests performed in the warp and fill directions.

EFFECTS OF TEMPERATURE AND HUMIDITY CYCLING ON THE STRENGTHS OF TEXTILE REINFORCED CARBON/EPOXY COMPOSITE MATERIALS

Roberto J. Cano
NASA Langley Research Center
Hampton, VA 23665

Keith W. Furrow
Virginia Polytechnic Institute and State University
Blacksburg, VA 24061

ABSTRACT

Results are presented from an experimental evaluation of the combined effects of temperature and humidity cycling on AS4/3501-6 composites (unstitched, Kevlar 29 stitched, and S-2 glass stitched uniweave fabric) and AS4/E905L composites (2-D, S-2 glass stitched 2-D, and 3-D braided fabric). The AS4/3501-6 uniweave material had a quasi-isotropic layup, whereas the AS4/E905L materials were braided in a $(\pm 30°/0°)_S$ orientation. Data presented include compression strengths and compression-compression fatigue results for uncycled composites and cycled composites (160, 480, 720, and 1280 cycles from 140°F at 95 percent relative humidity to -67°F). To observe the presence of microcracking within the laminates, photomicrographs were taken of each material type at the end of each cycling period. Microcracks were found to be more prevalent within stitched laminates, predominantly around individual stitches. The glass stitched laminates showed significant microcracking even before cycling. Less microcracking was evident in the Kevlar stitched materials, whereas the unstitched uniweave material developed microcracks only after cycling. The 3-D braid did not develop microcracks. The static compression strengths of the unstitched and Kevlar stitched uniweave materials were degraded by about 10% after 1280 temperature/ humidity cycles, whereas the reduction in compression strength for the glass stitched uniweave was less than 3%. The reduction in compression strength for the glass stitched 2-D braid was less than 8%. The unstitched 2-D and 3-D braids did not lose strength from temperature/ humidity cycling. The compression-compression fatigue properties of all six material types were not affected by temperature/ humidity cycling.

INTRODUCTION

Textile composite materials which incorporate through-the-thickness (TTT) reinforcement (stitching, braiding, or weaving) have demonstrated excellent damage tolerance (references 1, 2, and 3), an important criteria for their use in primary aircraft structures. The development of microcracking in or near stitching threads of textile reinforced composites is an issue of concern. These microcracks are caused by a mismatch in thermal expansion coefficient of the resin and fibers during cool-down from fabrication temperature. The potential for increased microcracking as a result of thermal and moisture cycling during service is an additional concern. The extent to which the presence and growth of these microcracks affects material performance is, therefore, an area of great interest. Thus, a need exists to determine the effects of temperature and humidity cycling on the mechanical properties and fatigue response of textile composites.

This study presents the results of an experimental evaluation of the effects of temperature and humidity cycling on stitched and unstitched AS4/3501-6 uniweave and braided AS4/E905L composite materials. Data presented include compression strength and compression-compression fatigue results for uncycled and cycled (160, 480, 720, and 1280 temperature/ humidity cycles from 140°F at 95% relative humidity to -65°F) quasi-isotropic uniweave and $(\pm 30°/0°)_S$ braided laminates. To observe the presence and development of microcracks within the laminates, photomicrographs were taken of each material type before and at the end of each cycling period.

MATERIALS

Uniweave fabric made from Hercules AS4 carbon fiber was used to make 32 ply quasi-isotropic $(0/45/90/-45)_{4S}$ preforms. These preforms were then stitched (3/16 inch rows by 1/8 inch step along the 0° direction) with Kevlar 29 (1000 denier thread) and with S-2 glass (449-1500 thread). All stitching was performed using a 2-end 200 denier twisted Kevlar 29 needle thread. Unstitched, Kevlar 29 stitched, and S-2 glass stitched composite laminates were then fabricated by McDonnell Douglas Aircraft with Hercules 3501-6 epoxy resin using resin transfer molding (RTM). The unstitched and Kevlar stitched uniweave composite materials were approximately 0.18 inches thick, whereas the glass stitched uniweave laminates were approximately 0.19 inches thick. Unstitched and S-2 glass stitched 2-D fabric, braided by Fiber Innovations, and 3-D fabric, braided by Atlantic Research, were also fabricated into composite panels. Using RTM, Fiber Innovations fabricated the three braided panel types with British Petroleum E905L epoxy resin. All of the braided laminates were around 0.24 inches thick.

TEST PROCEDURES

To simulate the extremes of conditions that a primary structural component on a commercial transport aircraft may be expected to encounter, the test materials were cycled between 140°F, 95% relative humidity and -65°F, no humidity (figure 1) in a programmable temperature/ humidity chamber. The specimens were exposed to 16 cycles per day.

A 120-kip hydraulic testing machine was used to determine the compression properties of the materials studied. All compression values were determined from 1.5-inch wide by 1.75-inch long specimens (3 replicates per test) using the short-block fixture shown in figure 2. Load was applied at a displacement rate of 0.05 in./min. Baseline room temperature (RT) properties were determined from as-fabricated specimens with a moisture content resulting from normal laboratory exposure. Specimens were weighed prior to cycling and upon removal from the chamber to determine the increase in weight due to water absorption. Cycled specimens were strain-gaged immediately upon removal from the temperature/ humidity cycling chamber and tested at room temperature. All compression testing was performed at NASA Langley.

Fatigue properties were determined using the fatigue fixture shown in figure 3. All the fatigue properties were determined using 1-inch wide by 4-inch long test coupons (6 to 8 specimens for each material at each testing condition), a maximum/ minimum stress ratio of 10 and a frequency of 5 hertz. The uniweave fatigue specimens were dried to their RT-equilibrated weight prior to testing. The braided fatigue specimens, however, were tested with their full moisture content from temperature/ humidity cycling (because prior compression testing had shown minimal effect from moisture as well as a lack of material which prevented the planning of a further moisture testing). All fatigue testing was performed at RT at Virginia Polytechnic Institute and State University.

RESULTS AND DISCUSSION

Compression Results

AS4/3501-6 Uniweave

The compression results for the AS4/3501-6 uniweave materials are presented in table 1 and plotted in figures 4 and 5. In figure 4, the RT baseline compression strengths are compared to the compression strengths obtained from cycled specimens. Figure 5 presents the percent retention of baseline strength for the three uniweave materials as a function of temperature/ humidity cycles. All three materials showed a decrease in compression strength compared to the RTD strengths as a result of temperature/ humidity cycling. The unstitched and Kevlar stitched material had initial decreases of 6.4 and 4.8 percent after 160 temperature/ humidity cycles. Although the strength retention continued to decrease with temperature/ humidity cycling, the reductions appear to be leveling off at 1280 temperature/ humidity cycles. The unstitched material and Kevlar stitched uniweave material retained 89.7% and 90.4% of their baseline strengths, respectively, after 1280 cycles. The glass stitched material had an initial reduction in compression strength of 2.5 percent at 160 temperature/ humidity cycles and no further reduction with additional cycling. The glass stitched uniweave material had a lower RTD compression strength, but it retained 97.6% of its compression strength after 1280 cycles. Since the properties of 3501-6 are known to be adversely affected by moisture, the water absorption (table 1) of these materials is most likely the cause of the decrease in compression strength for the unstitched and Kevlar stitched materials. Even though the glass stitched uniweave absorbed similar amounts of water as the Kevlar stitched material, the compression strengths were not degraded. The initiation of failure in the glass stitched material may be dominated by a mechanism which is insensitive to moisture.

The moduli of the uniweave materials (table 1) were not affected by temperature/ humidity cycling which is not surprising since modulus is a fiber-dominated property. All the modulus values for each material are essentially the same within the scatter of the data.

AS4/E905L Braids

The compression results for the AS4/E905L braided materials are presented in table 2 and plotted in figures 6 and 7. In figure 6, the RT baseline compression strengths from reference 4 are compared to the compression strengths obtained from cycled specimens. As shown in figure 6, only the stitched 2-D braided material showed a reduction in compression strength. Although it only retained 91.7% of the RTD compression strength, the scatter in the data (standard deviations of 4 to 6 %) is large enough to suggest that the reduction may not be significant. The unstitched 2-D and 3-D braids were not affected by the temperature/humidity cycling, retaining 99% percent and 100%, respectively, of their RTD compression strength after 1280 cycles. These results are not surprising since the moisture absorption of the AS4/E905L braided material (table 2) was significantly lower than that for the AS4/3501-6 uniweave materials. As for the uniweave materials, the moduli of the braided materials (table 2) were not affected by temperature/ humidity cycling. All the modulus values for each material are essentially the same within the scatter of the data.

Compression-Compression Fatigue

AS4/3501-6 Uniweave

The fatigue data obtained for the three uniweave materials are presented in figures 8-11. The trends of the data are represented by logarithmic regression curves calculated for each material. Although the glass stitched material did have slightly lower fatigue properties compared to the unstitched material (figure 8), on the whole stitching did not significantly affect the fatigue properties of the AS4/3501-6 uniweave. This result agrees with previous fatigue data (references 5 and 6) on stitched uniweave material which also showed no adverse affects from stitching. All three materials showed a reduction in compression strength with cycling (reductions of approximately 50% after 1 million fatigue cycles).

Figures 9 through 11 compare the fatigue properties of the cycled uniweave specimens to the baseline (0 temperature/ humidity cycles) data. As shown in figure 9, temperature/ humidity cycling did not significantly affect the fatigue properties of the unstitched laminates. The glass stitched material, figure 10, similarly appeared unaffected by temperature/ humidity cycling. The Kevlar stitched material, figure 11, also did not appear to be adversely affected by temperature/ humidity cycling. Overall, the compression strengths of all the uniweave materials were reduced to around 50 ksi after 1 million fatigue cycles.

AS4/E905L Braids

The fatigue data obtained for the three braided materials are presented in figures 12 through 15. The baseline (0 temperature/ humidity cycles) fatigue results (figure 12) indicate that the 3-D braid showed better fatigue response in terms of ultimate stress with fatigue cycles than the 2-D and stitched 2-D braids which showed very similar results. As evidenced in figures 13, 14 and 15, temperature/ humidity cycling did not affect the fatigue response of the braided materials. The compression strengths of the braided materials were reduced by 40-45% after 1 million fatigue cycles.

Microcracking

AS4/3501-6 Uniweave

Photomicrographs of each of the three uniweave materials are presented in figures 16-18, respectively. For each material type, a photomicrograph is presented for an uncycled specimen and a specimen after 1280 temperature/ humidity cycles. For the stitched materials, one individual stitch is shown in each photomicrograph. The unstitched material, figure 16, did not show any microcracks in the uncycled specimens. Microcracking between some of the outer plies did develop after temperature/ humidity cycling. It is interesting to note that cracks only developed on one side of the laminate, indicating a possible dependence on the temperature gradients developed within the specimens as they were heated or cooled in the temperature/ humidity environmental simulation chamber.

As shown in figure 17, the glass stitched material had significant microcracking around each individual stitch. These microcracks did not appear to grow with temperature/ humidity cycling as evidenced by the photomicrograph of the glass stitched specimen after 1280 cycles. The microcracks in the specimen with 1280 temperature/ humidity cycles appear to be similar in severity to the uncycled specimen. The severity of these microcracks may dominate the initiation

of failure of these specimens which would explain the lower baseline compression strength compared to other uniweave materials as well as the constant compression strength with increasing moisture content (see figure 4 and table 1). The Kevlar stitched material, figure 18, also showed microcracking around the stitching but not to the degree that the glass stitched material microcracked. Similar to the glass stitched material findings, the microcracks in the Kevlar stitched material did not appear to increase in severity with temperature/ humidity cycling.

AS4/E905L Braids

Photomicrographs for the braided materials are presented in figures 19-21. Similar to the glass stitched uniweave, the glass stitched 2-D braid (figure 19) suffered from significant microcracking around the stitches before and after cycling. The unstitched 2-D material, figure 20, and the 3-D braided material, figure 21, did not appear to develop any microcracking from temperature/ humidity cycling.

Implications

Although the elimination of microcracking is a desirable goal, it appears that their presence in at least these particular textile reinforced composite materials is not detrimental to their potential use in terms of strength. As evidenced by the glass and Kevlar stitched laminates, microcracking did not appear to increase in severity nor did the compression properties of these materials significantly degrade (some effect on compression for the Kevlar stitched materials; no effect on fatigue) after temperature/ humidity cycling. In addition, it does appear possible, by appropriate selection of reinforcement geometry and matrix material, to avoid microcracking altogether (e.g. as was observed to be the case for the 2-D and 3-D AS4/E905L braided composites). The next phase of this work will address the effects of increasing moisture content without temperature cycles as well as the effects of temperature cycling alone on the strengths of textile composites.

CONCLUSIONS

The effects of temperature/ humidity cycling on the mechanical properties, fatigue response, and microcracking of textile reinforced AS4/3501-6 composites (unstitched, Kevlar 29 stitched, and S-2 glass stitched uniweave fabric) and AS4/E905L composites (2-D, S-2 glass stitched 2-D, and 3-D braided fabric) were investigated. Compression strengths and compression-compression fatigue behavior were determined for cycled and uncycled quasi-isotropic uniweave and (±30°/0°) braided laminates. The results obtained in this investigation support the following conclusions:

1. Temperature/ humidity cycling reduced the static compression properties of the unstitched and stitched AS4/3501-6 up to 10 percent.

2. Temperature/ humidity cycling reduced the compression properties of the AS4/E905L 2-D stitched braid by 8 percent but did not affect the compression properties of the unstitched 2-D and 3-D braids.

3. Compression-compression fatigue properties for all the materials were not significantly affected by temperature/ humidity cycling.

4. Microcracks were predominant around individual stitches in both the stitched uniweave and braided materials.

5. Microcracks around glass stitches were more predominant than for Kevlar stitches.

6. The presence of microcracks does not appear to be a significant concern in terms of the compression and compression-compression fatigue properties after temperature/ humidity cycling of the textile composite materials studied.

REFERENCES

1. Dow, M. B.; Smith, D. L.; and Lubowinski, S. J.: *An Evaluation of Stitching Concepts for Damage-Tolerant Composites.* Fiber-Tex 1988 Conference Proceedings, NASA CP-3038, 1989, pp. 53-73.

2. Dow, M. B.; and Smith, D. L.: *Damage-Tolerant Composite Materials Produced by Stitching Carbon Fabrics*, SAMPE Conference Series, Vol. 21, 1989, pp. 595-605.

3. Smith, D. L.; and Dexter, H. B.: *Woven Fabric Composites with Improved Fracture Toughness and Damage Tolerance*, Fiber-Tex 1988, NASA CP-3038, 1989, pp. 75-90.

4. Deaton, J. W.; Kullerd, S. M.; and Portanova, M. A.: *Mechanical Characterization of 2-D, 2-D Stitched, and 3-D Braided/ RTM Materials*, Third Advanced Composites Technology Conference, NASA CP-3178, 1992.

5. Portanova, M. A.; Poe, C. C.; and Whitecomb, J. D.: *Open Hole and Post-Impact Compression Fatigue of Stitched and Unstitched Carbon/Epoxy Composites*, NASA TM-102672, June 1990.

6. Vandermey, N. E.; Morris, D. H.; and Masters, J. E.: *Damage Development Under Compression-Compression Fatigue Loading in a Stitched Uniweave Graphite/Epoxy Composite Material*, Contractor Report CCMS-91-16, July 1991.

Table 1. Averaged Properties for AS4/3501-6 Uniweave.

Material	Number of Cycles	Water Absorption, wt%	Compression Strength, ksi	Modulus, Msi
Unstitched	0	0.000	96.7 ± 2.0*	6.76 ± .67
	160	0.169	90.5 ± 1.5	6.48 ± .09
	480	0.251	95.2 ± 3.1	6.47 ± .08
	720	0.357	88.4 ± 2.1	6.46 ± .02
	1280	0.510	86.8 ± 1.8	6.47 ± .05
Glass Stitched	0	0.000	80.9 ± 0.8	6.28 ± .44
	160	0.300	78.9 ± 0.5	6.13 ± .12
	720	0.617	79.2 ± 1.4	6.03 ± .13
	1280	0.783	79.0 ± 0.8	5.75 ± .12
Kevlar Stitched	0	0.000	92.1 ± 1.0	6.34 ± .28
	160	0.231	87.7 ± 1.8	6.48 ± .07
	720	0.583	84.3 ± 2.0	6.37 ± .16
	1280	0.748	83.3 ± 1.0	6.14 ± .11

* ± indicates standard deviation

Table 2. Averaged Properties for AS4/E905L Braids.

Material	Number of Cycles	Water Absorption, wt%	Compression Strength, ksi	Modulus, Msi
2-D Braid	0	0.000	58.6 ± 1.0*	8.8 ± .5
	160	0.091	56.0 ± 0.7	8.4 ± .5
	480	0.122	58.6 ± 1.2	8.8 ± .7
	1280	0.100	58.0 ± 2.2	8.2 ± .5
2-D Stitched	0	0.000	55.5 ± 2.3	8.3 ± .5
	160	0.158	50.2 ± 1.9	7.8 ± 1.0
	480	0.175	52.1 ± 1.3	8.8 ± .8
	1280	0.143	50.9 ± 2.9	7.4 ± .6
3-D Braid	0	0.000	64.8 ± 1.9	7.3 ± .6
	160	0.097	67.4 ± 5.8	9.9 ± 1.0
	480	0.176	70.1 ± 1.5	8.7 ± .3
	1280	0.206	68.4 ± 1.5	8.7 ± .7

* ± indicates standard deviation

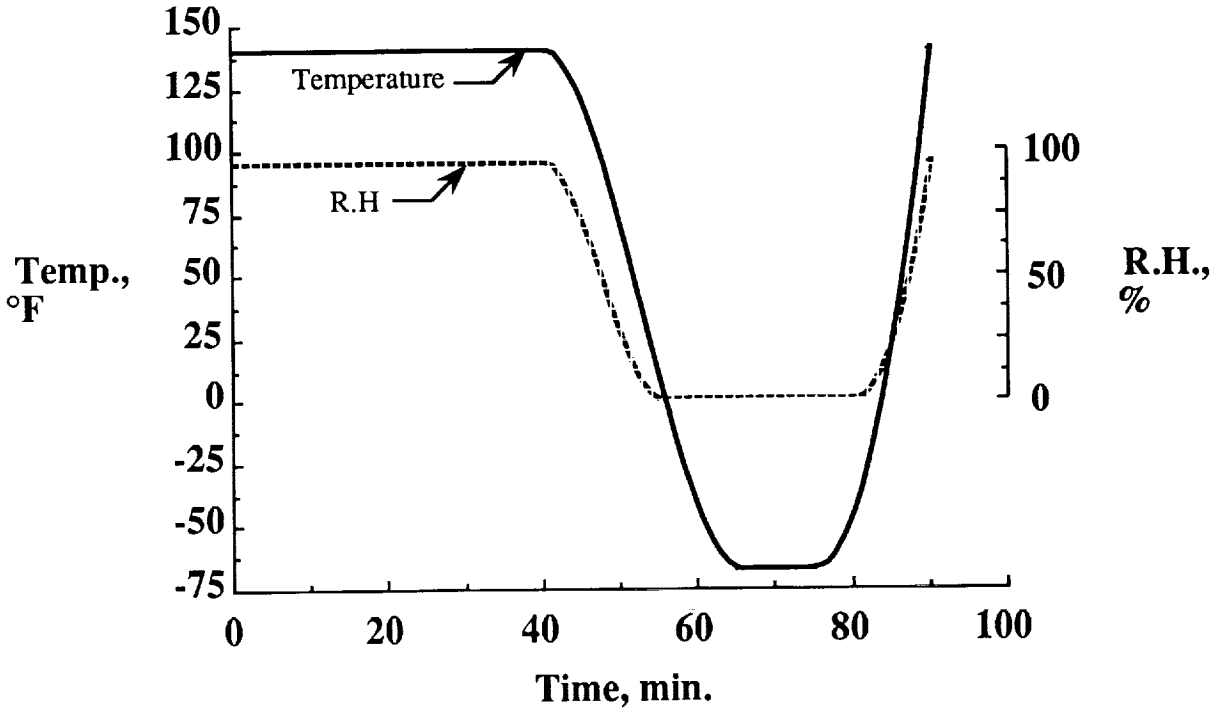

Figure 1. Temperature/ humidity cycle.

Figure 2. Short-block compression fixture.

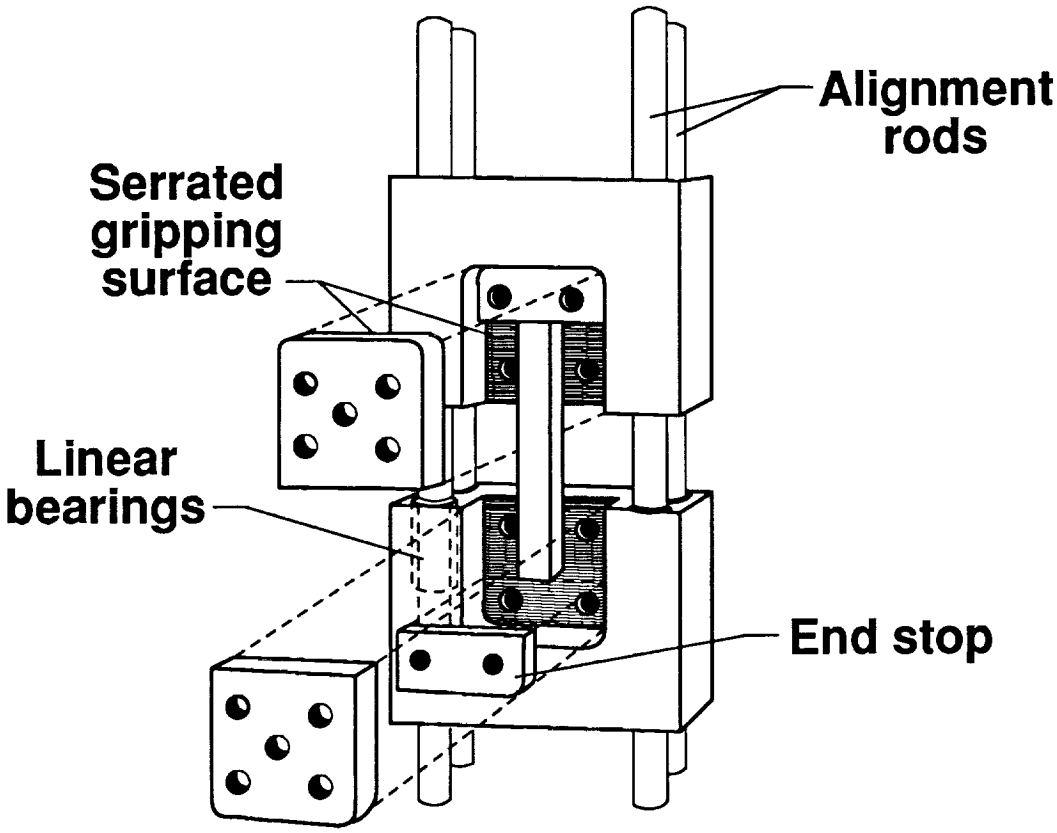

Figure 3. Compression-compression fatigue test fixture.

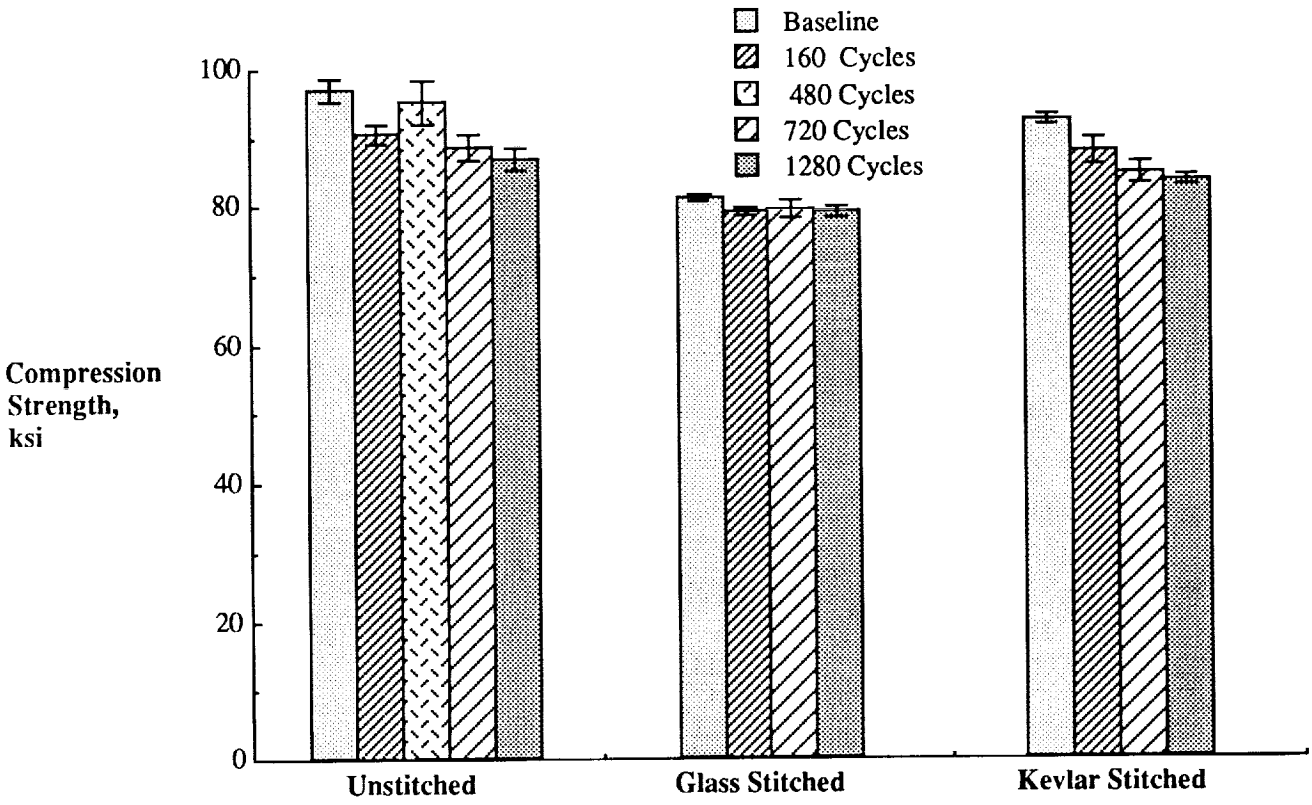

Figure 4. Compression strength for uncycled and cycled AS4/3501-6 uniweave.

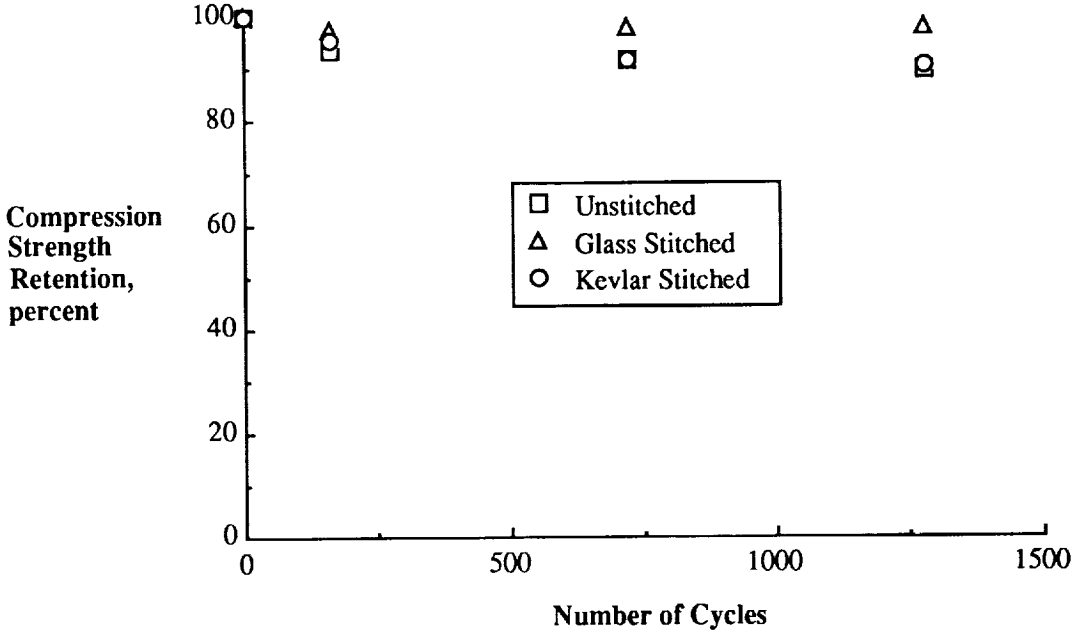

Figure 5. Strength retention of AS4/3501-6 uniweave composites.

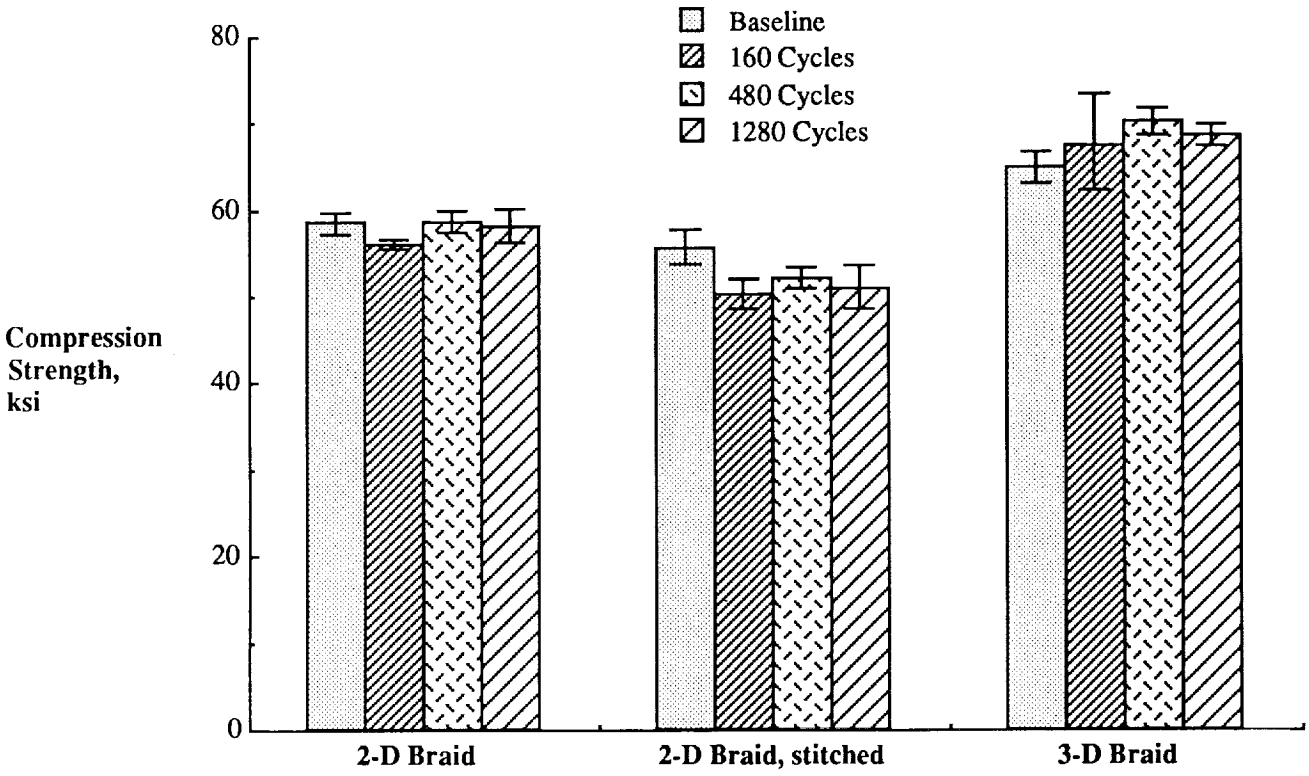

Figure 6. Compression strength for cycled and uncycled AS4/E905L braids.

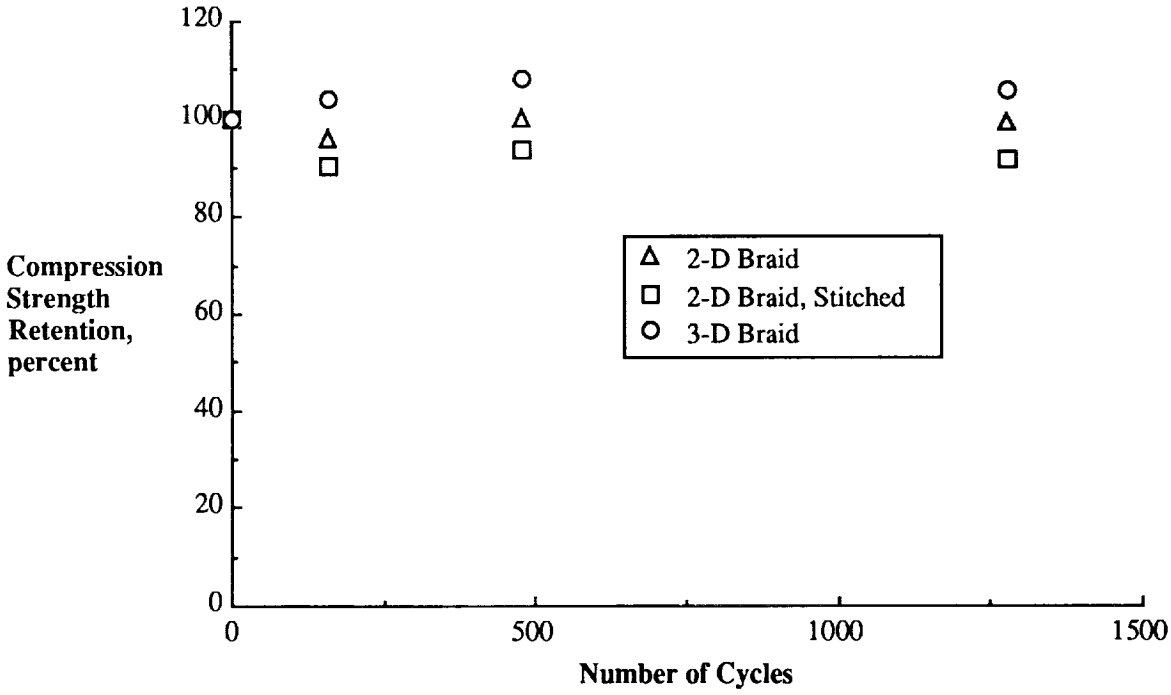

Figure 7. Strength retention of AS4/E905L braided composites.

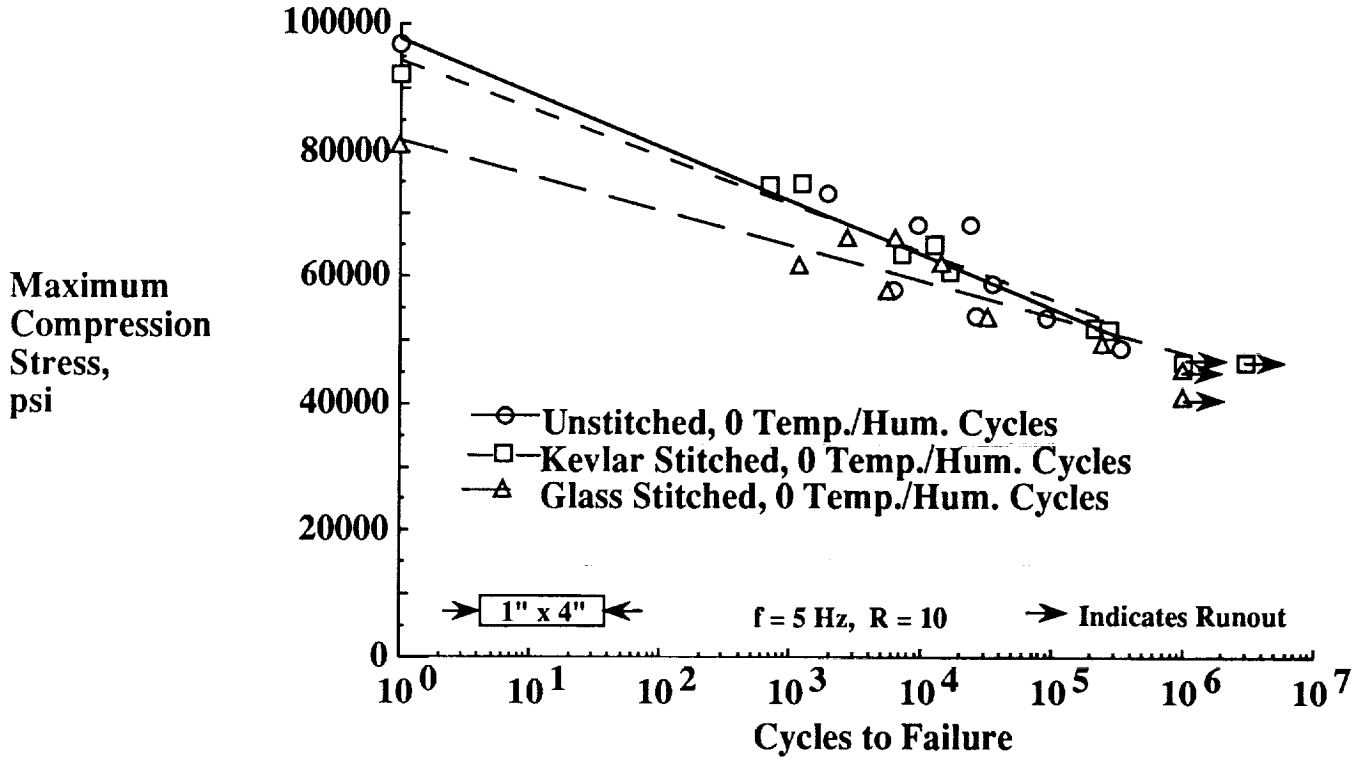

Figure 8. Fatigue data for AS4/3501-6 uniweave laminates without temperature/humidity cycles.

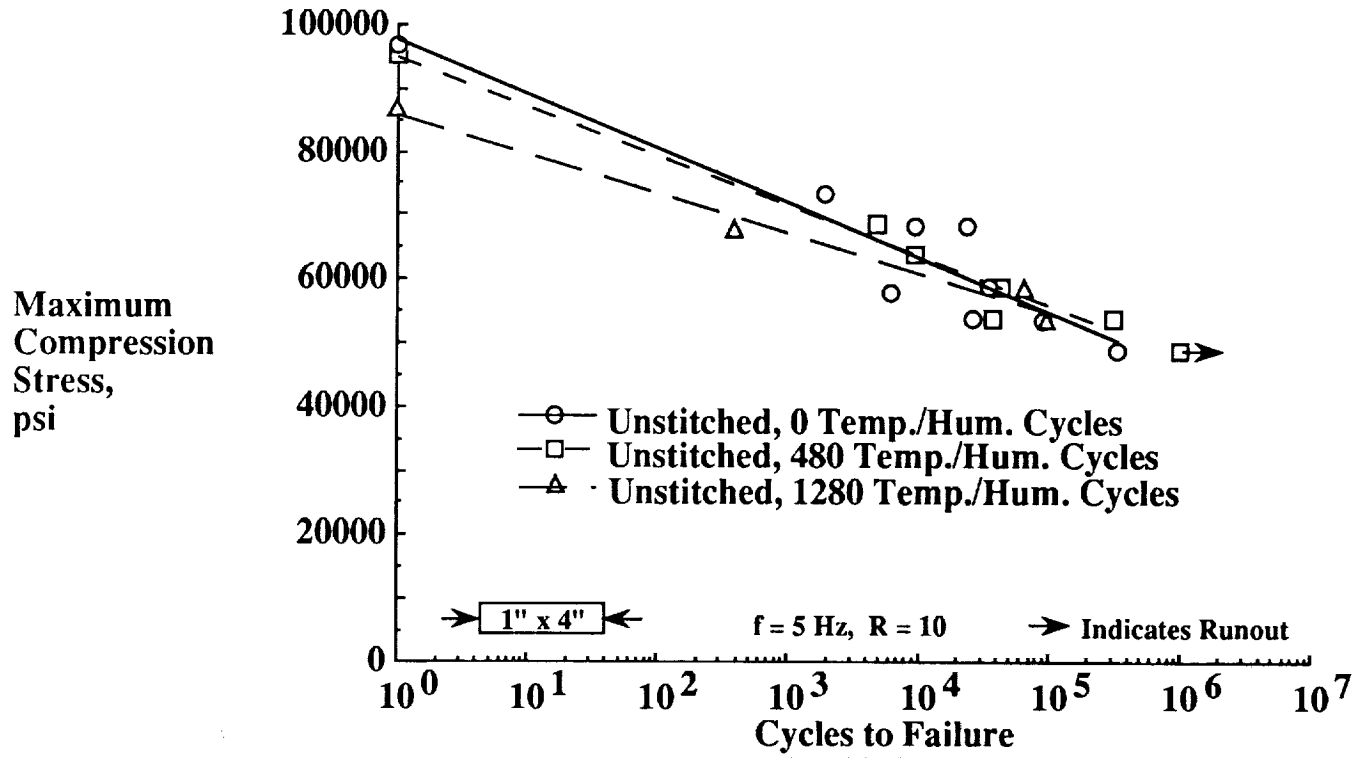

Figure 9. Fatigue data for unstitched AS4/3501-6 uniweave laminates with and without temperature/humidity cycles.

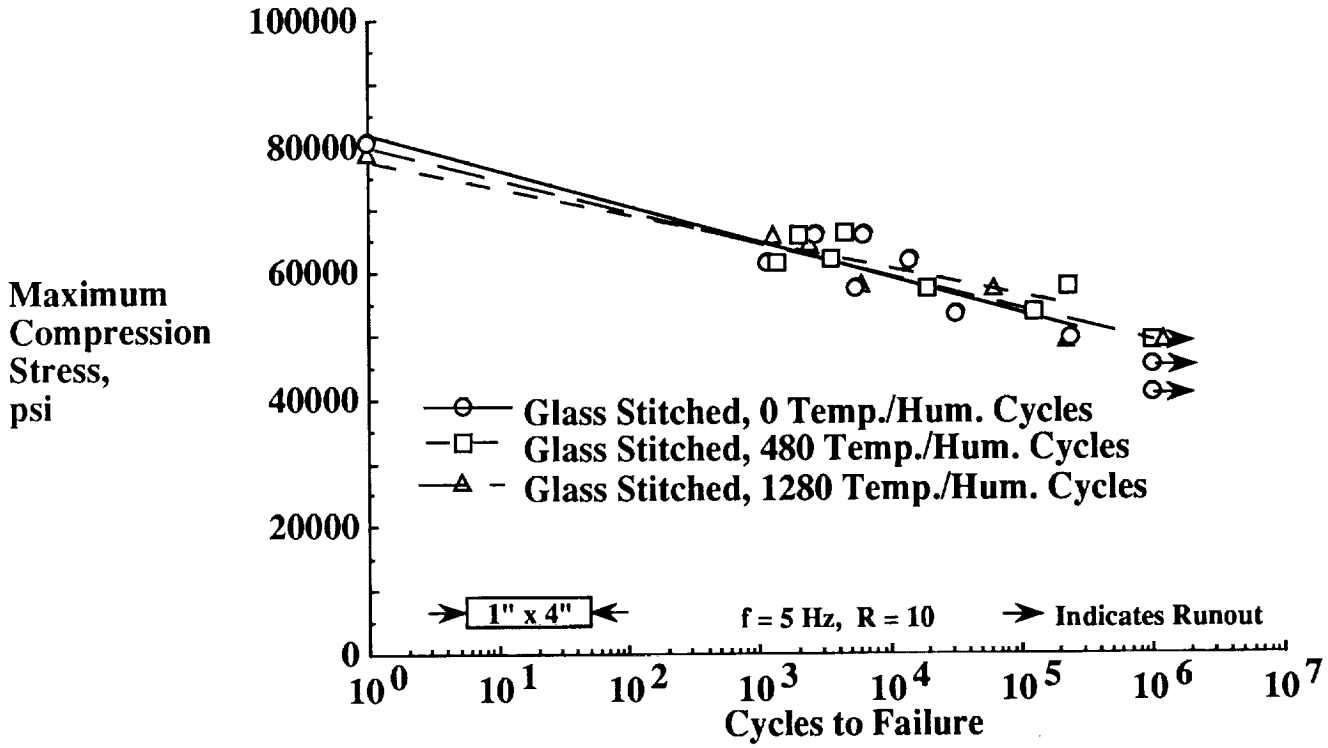

Figure 10. Fatigue data for glass stitched AS4/3501-6 uniweave laminates with and without temperature/humidity cycles.

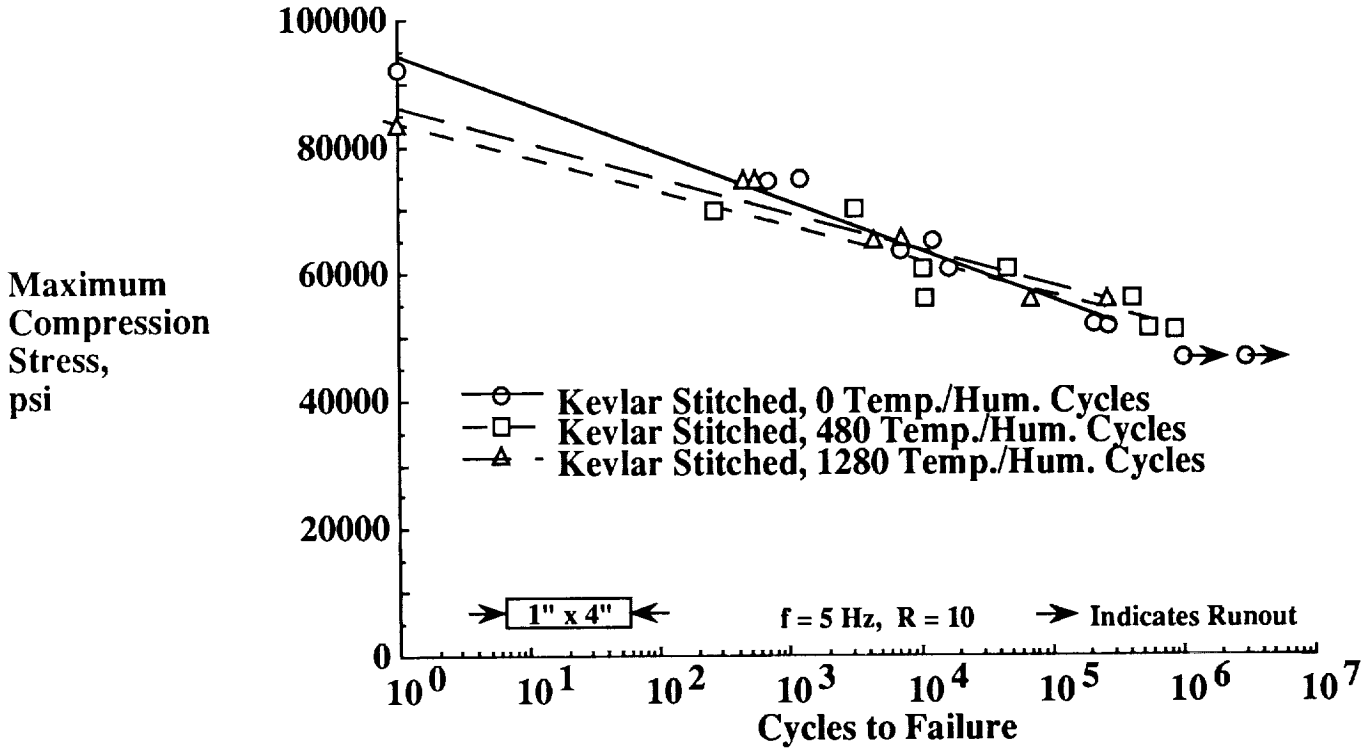

Figure 11. Fatigue data for Kevlar stitched AS4/3501-6 uniweave laminates with and without temperature/humidity cycles.

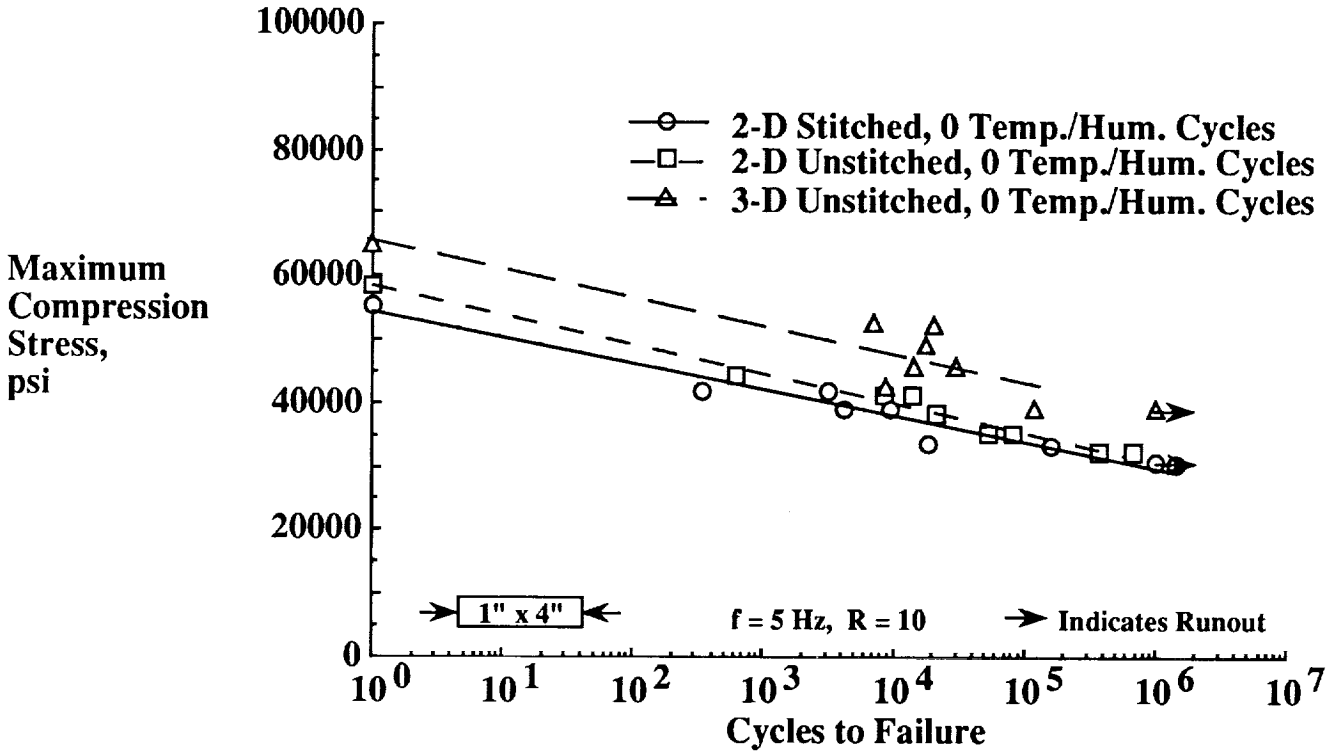

Figure 12. Fatigue data for AS4/E905L braided laminates without temperature/humidity cycles.

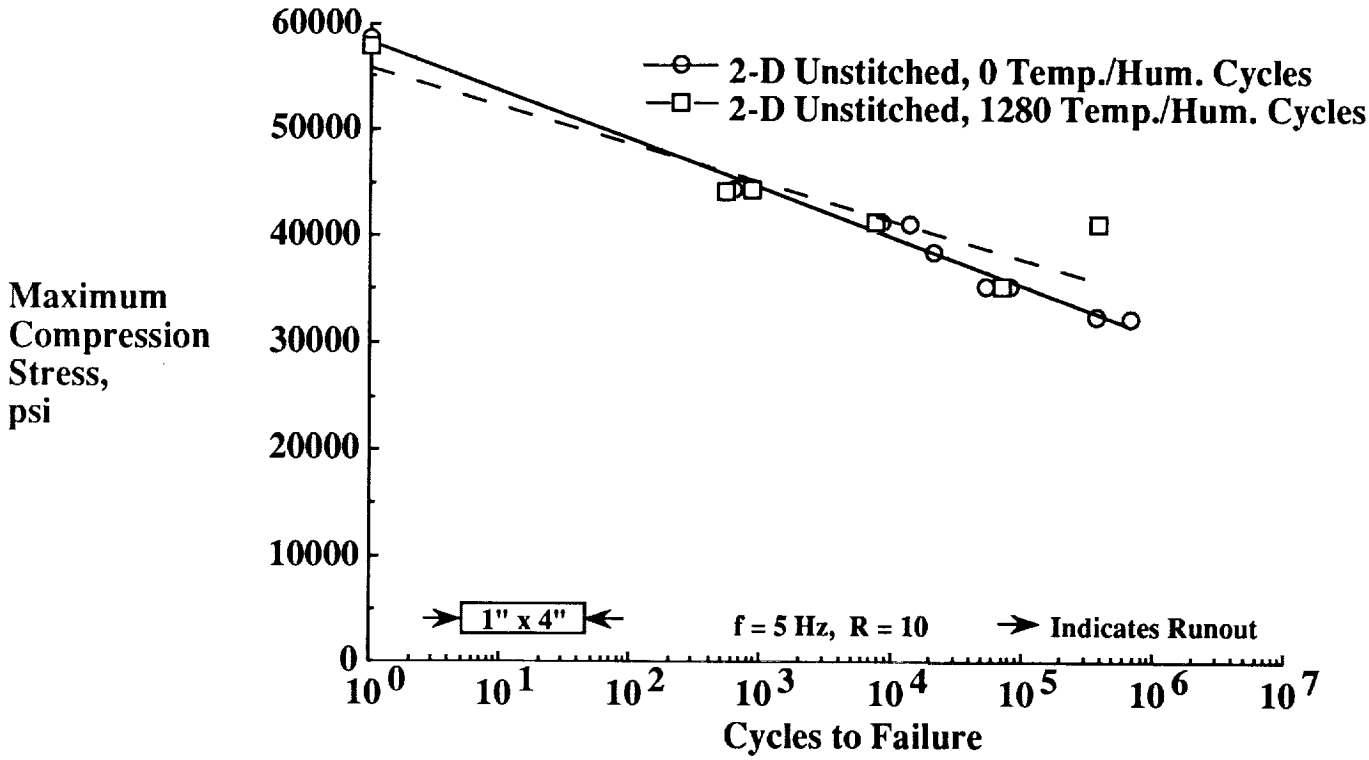

Figure 13. Fatigue data for 2-D unstitched AS4/E905L braided laminates with and without temperature/humidity cycles.

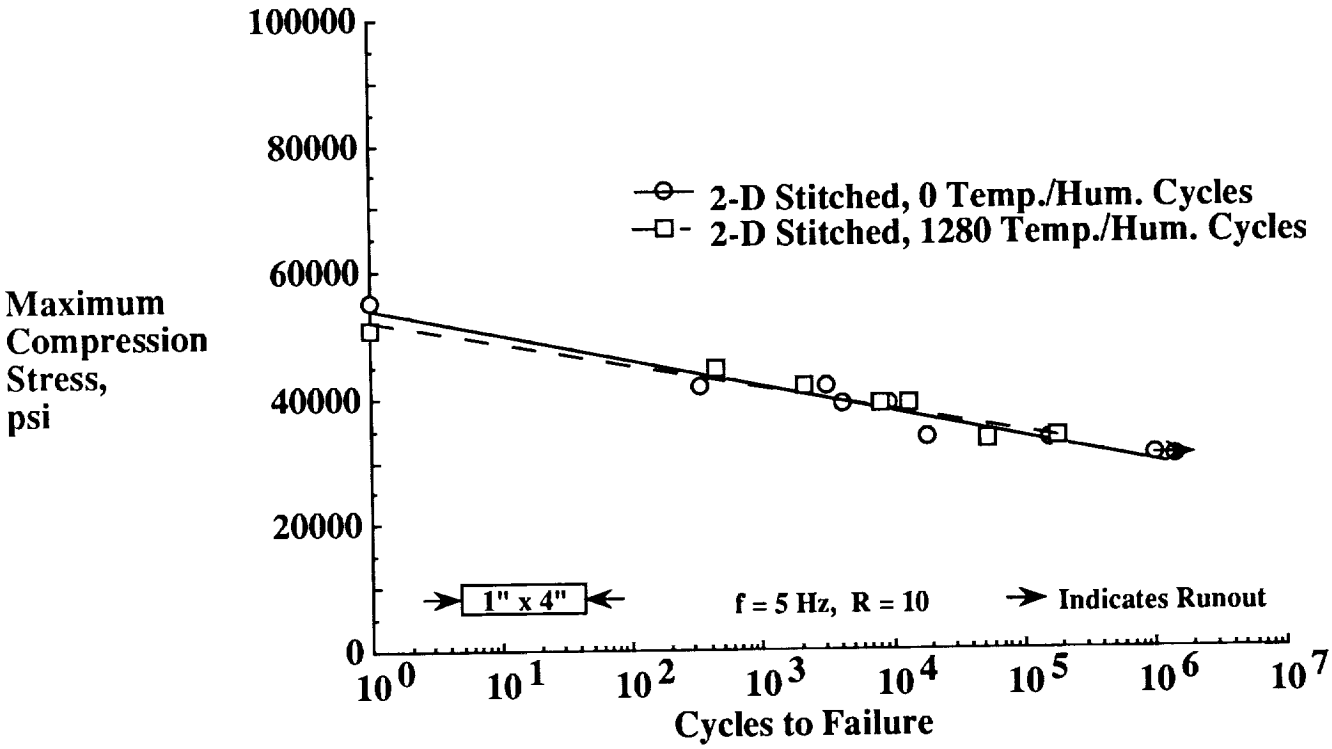

Figure 14. Fatigue data for 2-D stitched AS4/E905L braided laminates with and without temperature/humidity cycles.

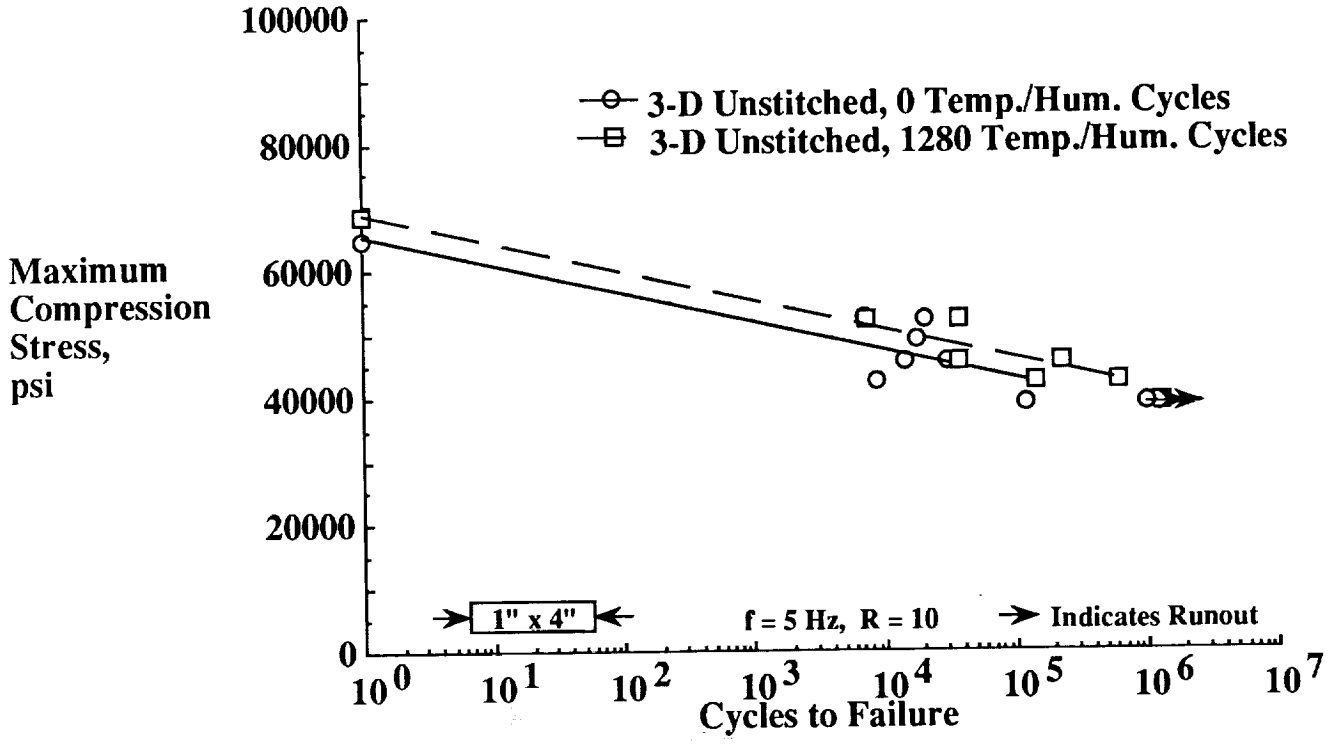

Figure 15. Fatigue data for 3-D unstitched AS4/E905L braided laminates with and without temperature/humidity cycles.

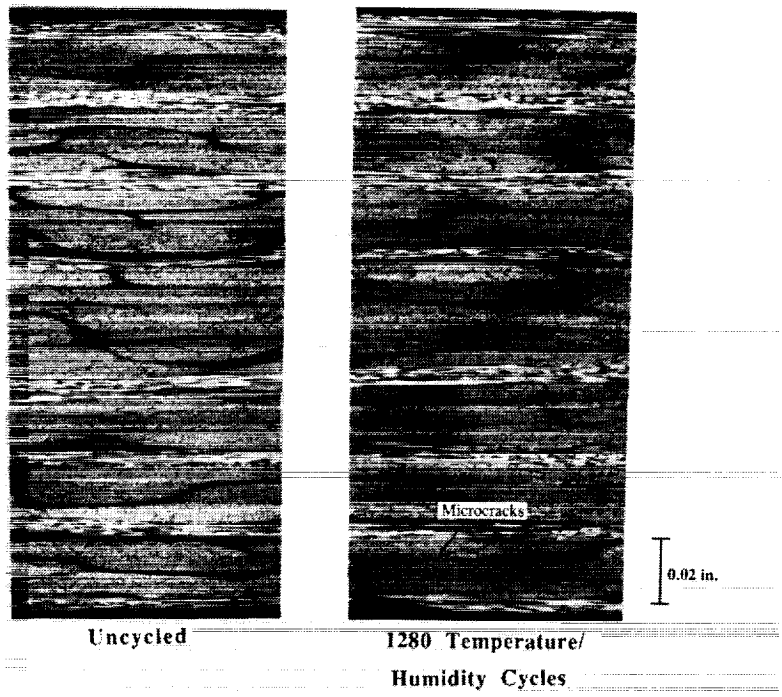

Figure 16. Photomicrographs of unstitched AS4/3501-6 uniweave.

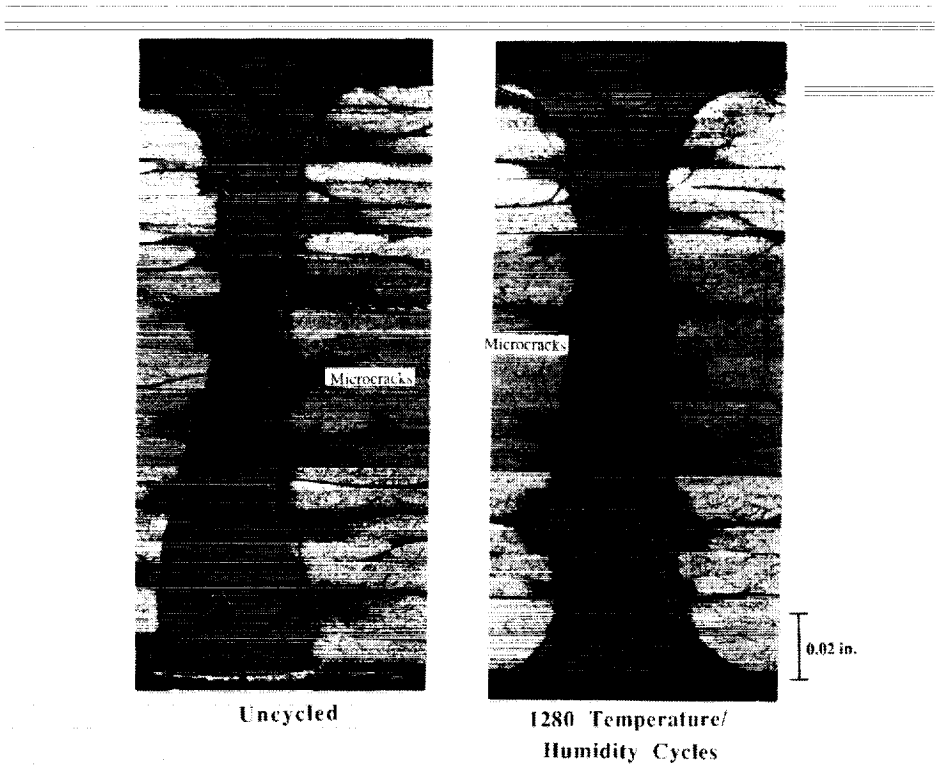

Figure 17. Photomicrographs of S-2 glass stitched AS4/3501-6 uniweave.

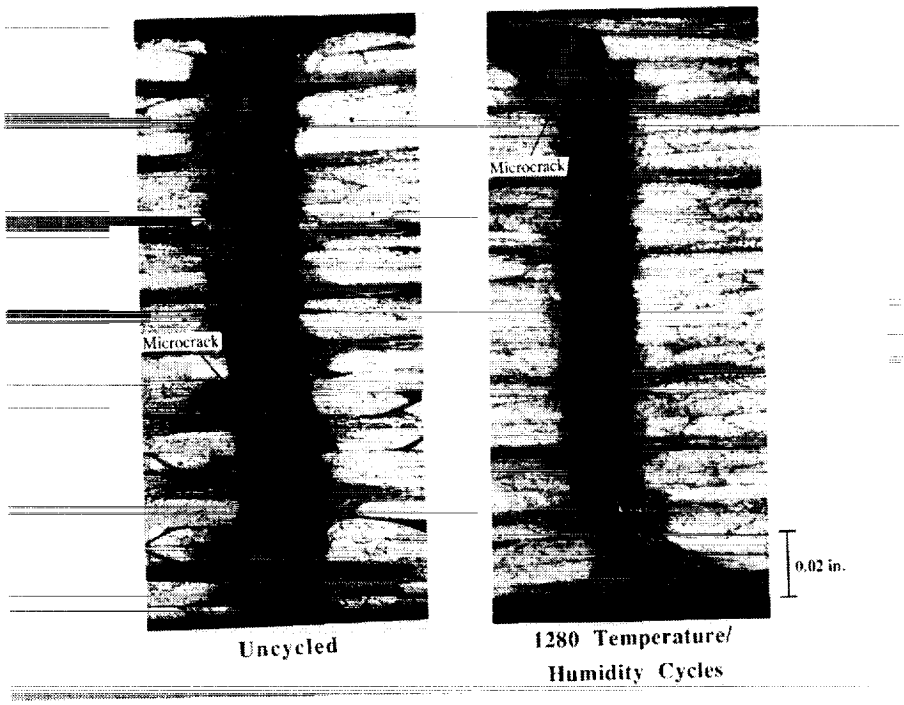

Figure 18. Photomicrographs of Kevlar 29 stitched AS4/3501-6 uniweave.

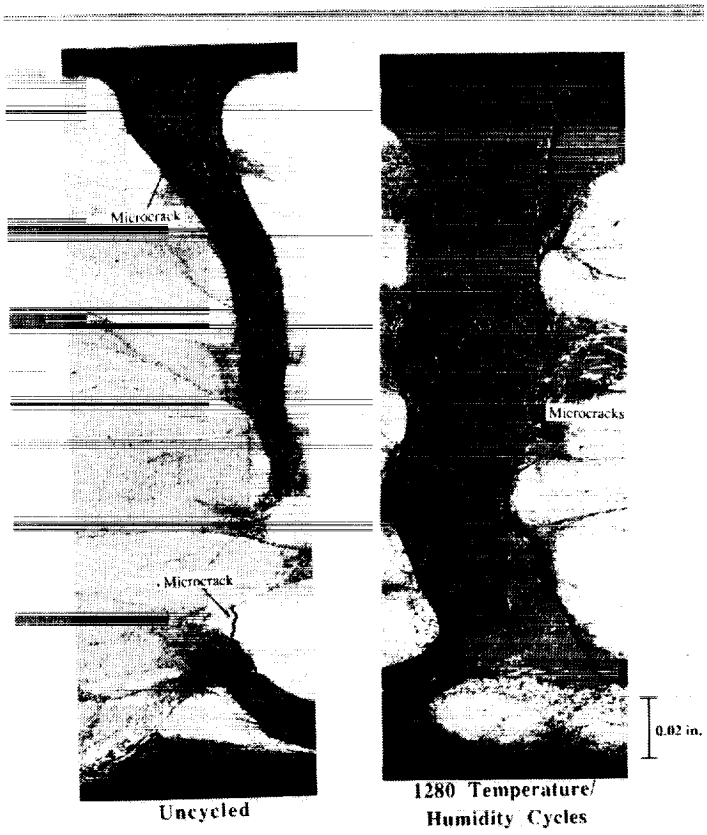

Figure 19. Photomicrographs of S-2 glass stitched AS4/E905L 2-D braid.

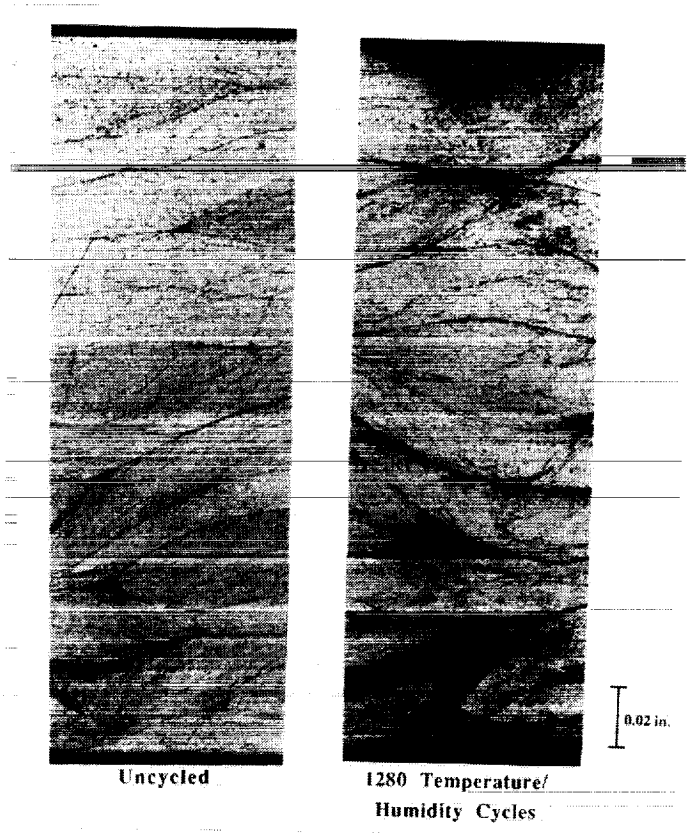

Figure 20. Photomicrographs of unstitched AS4/E905L 2-D braid.

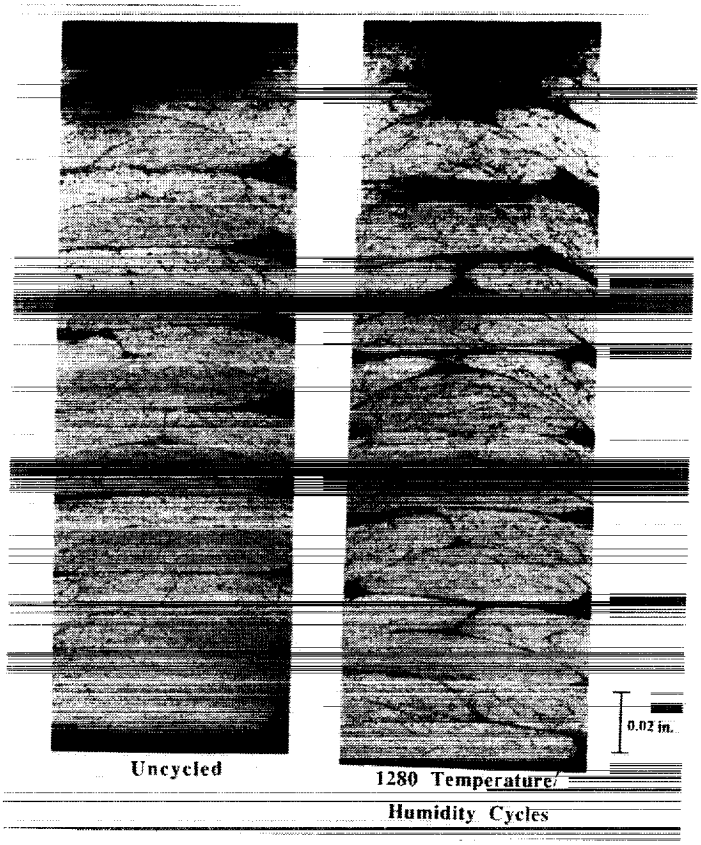

Figure 21. Photomicrographs of Kevlar 29 stitched AS4/E905L 3-D braid.

MECHANICAL CHARACTERIZATION OF 2-D, 2-D STITCHED, AND 3-D BRAIDED/RTM MATERIALS

Jerry W. Deaton
NASA Langley Research Center
Hampton , Virginia

Susan M. Kullerd
and
Marc A. Portanova
Lockheed Engineering and Sciences Company
Hampton, Virginia

INTRODUCTION

Braided composite materials have potential for application in aircraft structures. Fuselage frames, floor beams, wing spars, and stiffeners are examples where braided composites could find application if cost effective processing and damage tolerance requirements are met. Another important consideration for braided composites relates to their mechanical properties and how they compare to the properties of composites produced by other textile composite processes being proposed for these applications. Unfortunately, mechanical property data for braided composites do not appear extensively in the literature. Data are presented in this paper on the mechanical characterization of 2-D triaxial braid, 2-D triaxial braid plus stitching, and 3-D (through-the-thickness) braid composite materials. The braided preforms all had the same graphite tow size and same nominal braid architectures, [±30°/0°], and were resin transfer molded (RTM) using the same mold for each of two different resin systems. Static data are presented for notched and unnotched tension, notched and unnotched compression, and compression after impact strengths at room temperature. In addition, some static results, after environmental conditioning, are included.

Baseline tension and compression fatigue results are also presented, but only for the 3-D braided composite material with one of the resin systems.

Figure 1 outlines the objective and approach utilized in characterizing the braided composites reported herein. An architecture of [±30°/0°] was selected for both 2-D triaxial and 3-D braid preform fabrication and RTM to assess the potential of braided composites for aircraft structures. This architecture was selected since single pass coverage could be accomplished using a 12K graphite tow in the 2-D triaxial braid which would result in a higher volume fraction and be more cost-effective in building up panel thickness by using the larger graphite tow size. The materials selected, panel fabrication, and mechanical property characterization will be discussed in more detail.

OBJECTIVE AND APPROACH

Objective: Assess potential of (±30°/0°) braid architectures for resin transfer molded aircraft structures by mechanical property characterization

- Benefits sought from ±30°/0° configurations:
  - Single pass coverage
  - Higher fiber volume fraction
  - Potential cost saving of 12K tows

Approach: Braided material selection

- Braid architectures
- Fiber
- Resins

Fabrication of panels

Characterization of mechanical properties

- Static
- Fatigue

BRAID ARCHITECTURE

An artist's conception of the two braid architectures evaluated are shown in figure 2. The 2-D triaxial braid preforms were braided by Fiber Innovations, Inc., using two ends of Hercules AS4 graphite 12K tow in the +30° and -30° directions, two ends of Hercules AS4 graphite 12K, and one end of Hercules AS4 graphite 3K tow in the axial, or 0°, direction. The additional 3K tow was necessary for equal amounts of graphite (per inch) in each tow direction. Since stitching has been shown to improve the damage tolerance of other textile composites (ref. 1-3), the 2-D triaxial braid was also evaluated with stitching. Both stitched and unstitched 2-D preforms were resin transfer molded using either British Petroleum E905L resin or Ciba Geigy XUMY722/RD91-103 resin. Hereafter, the British Petroleum and Ciba Geigy resins are referred to as E905L and MY722, respectively. The 3-D braid preforms were braided by Atlantic Research Company using one end of Hercules AS4 graphite 12K tow in each of the +30°, -30°, and 0° directions, resulting in equal amounts of graphite fibers in each direction, as was the case for the 2-D triaxial braids. The 3-D braid preforms were braided in a single pass, then resin transfer molded only with E905L resin. All resin transfer molding was performed by Fiber Innovations, Inc. None of the 3-D braided preforms were stitched. Additional fabrication and processing parameters will be given subsequently.

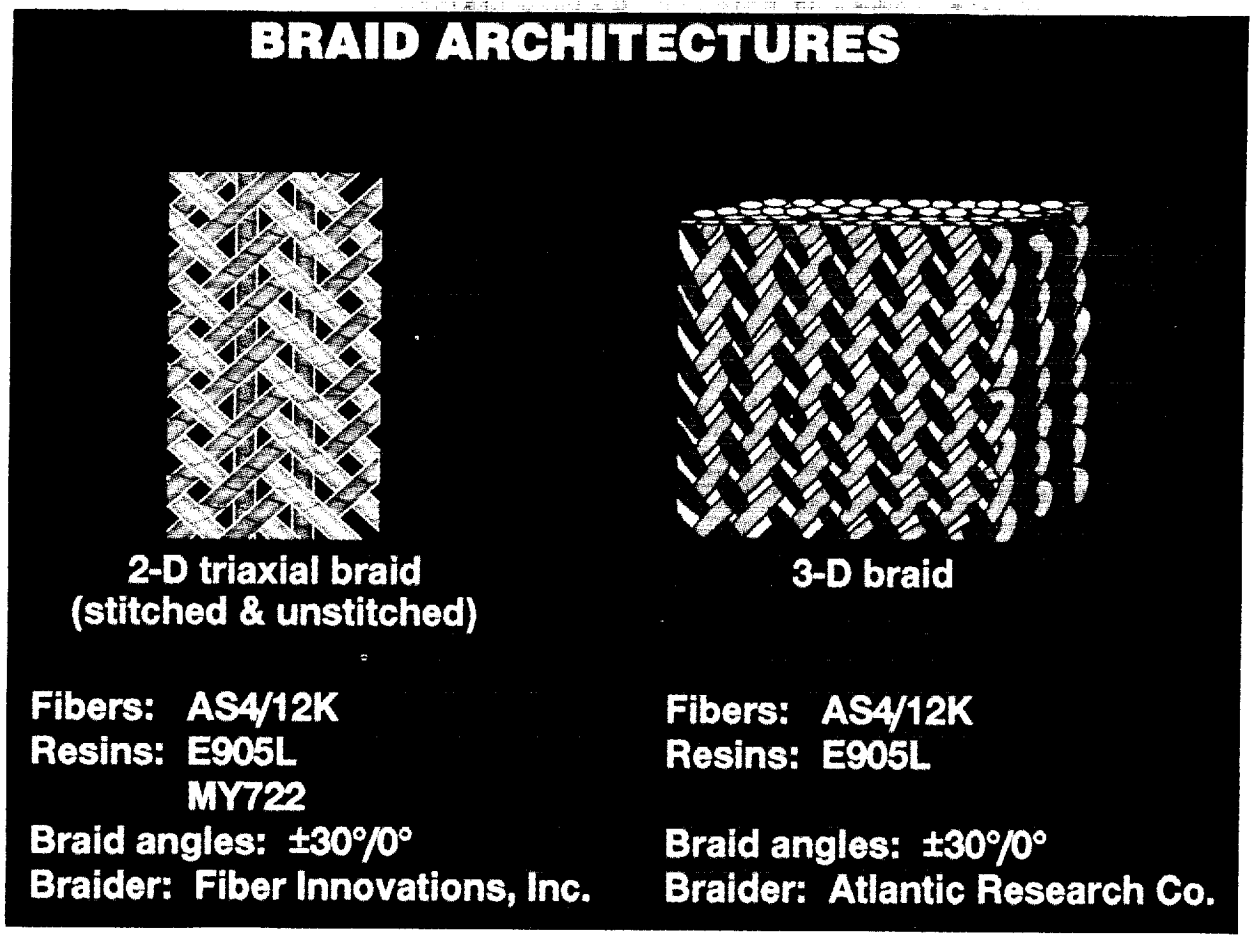

FABRICATION OF PANELS

Figure 3 outlines the fabrication procedure for 2-D and 3-D braided composites. The 2-D triaxial braid preforms were braided as cylinders using multiple passes to obtain either 3 or 6 layers, then slit along the cylinder generator. The cut edges were then stitched to maintain the braid angles. The braided cylinder length and diameter were selected such that the flat preforms would be approximately 7 inches wide and 20 inches long. Half of the 2-D braided laminates were stitched using a lock stitch and S-2 glass needle and bobbin threads. The stitch pitch was eight stitches per inch and stitch row and column spacing was nominally 0.25-inch. The 3-D braid preforms were also braided as a cylinder, but unlike the 2-D braids, the 3-D braids were braided in a single pass for each thickness. All braided preforms were RTM in the same mold for each thickness, resulting in the same nominal fiber volume fraction for each architecture and thickness. All braided laminates were nominally 0.125-inch thick for tension coupons and 0.25-inch thick for compression coupons.

FABRICATION OF PANELS

- Braid as cylinders
  - 2-D triaxial braids of 3 or 6 layers
  - 3-D braid of two thicknesses in single pass
- Slit braided preforms along cylinder generator
  - Stitch cut edges to maintain braid angle
  - Stitch one-half of 2-D triaxial preforms using 1/4 inch rows and columns
- RTM using same mold for all braid architectures
  - 0.125 in. thick for tension
  - 0.250 in. thick for compression

PHOTOMICROGRAPHS OF 2-D AND 3-D BRAIDS

Figures 4a and 4b show photomicrographs of sections indicating 0°, 90°, +30°, and -30° graphite fiber tow orientations for typical 2-D triaxial and 3-D braid architectures, respectively. The 2-D braids had an inplane nominal fiber volume fraction of 59 % and the 3-D braids had an inplane nominal fiber volume fraction of 52 %. The 0° views for the 2-D and 3-D braids appear very similar, however, the 0° graphite fiber tows shown for the 3-D braid are more evenly distributed through the thickness. Comparing the other views, respectively, indicates that the 2-D braid layers nest together with only small resin pockets whereas the 3-D braid has more and larger resin rich areas (which is consistent with the measured fiber volume fractions) with a repeating graphite tow orientation. The +30° view in figure 4b shows the graphite fiber tows traversing through the thickness, giving the composite true through-the-thickness reinforcement.

PHOTOMICROGRAPHS OF 2-D TRIAXIAL BRAID ARCHITECTURE

V_f = 59%

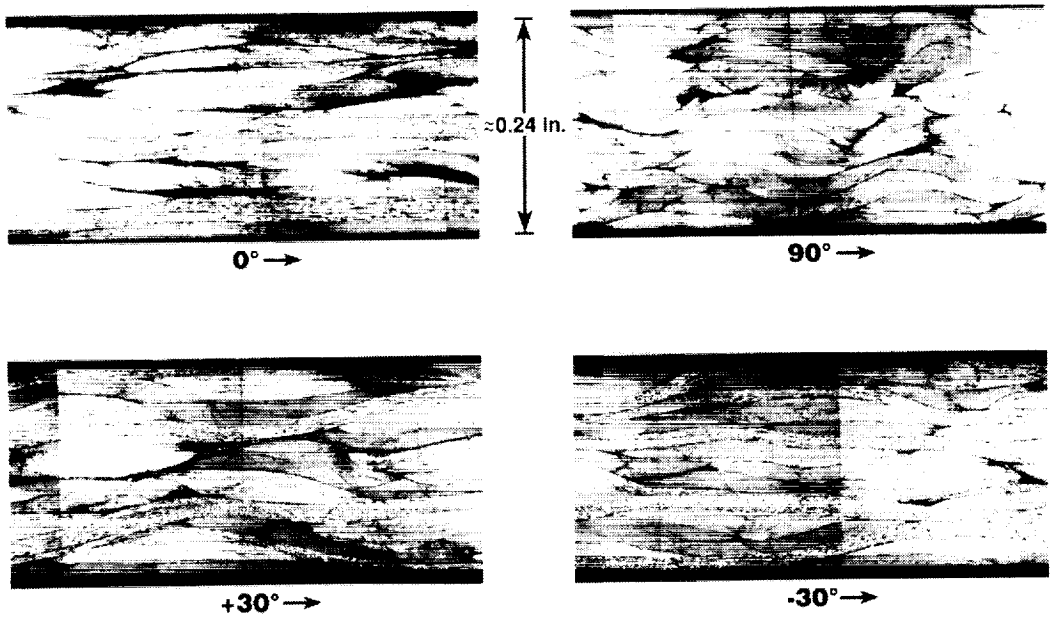

PHOTOMICROGRAPHS OF 3-D BRAID ARCHITECTURE

V_f = 52%

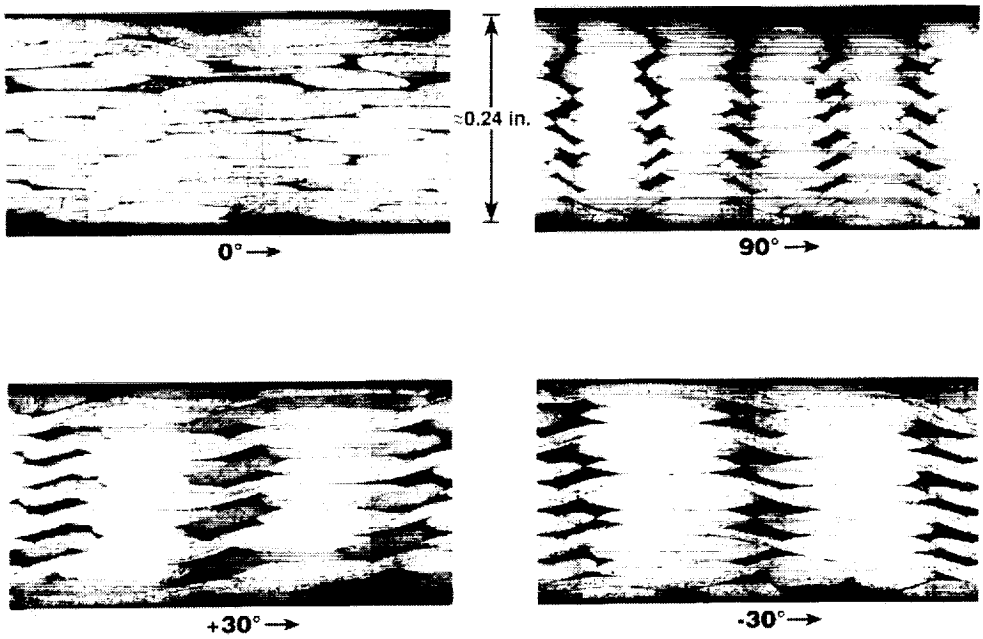

STATIC TEST SPECIMENS

The static test specimen geometries are shown in figure 5. The unnotched tension specimens were nominally 0.125-inch thick. All other specimen thicknesses were nominally 0.25-inch. Specimen lengths and widths are indicated on the figure. The short block compression specimen is a NASA Langley configuration suitable for tests of cross-plied laminates and was instrumented with 0.125-inch long stacked back-to-back strain gages. All other specimen configurations were instrumented with 0.250-inch long back-to-back axial strain gages. In addition, the unnotched tension specimens had 0.250-inch long back-to-back transverse strain gages. The compression after impact specimens were impacted at a nominal impact energy of 30 ft-lbs with the NASA Langley air gun using a 0.50-inch diameter aluminum ball as the impactor. The notched tension specimens had a 0.25-inch diameter hole. There were three notched compression specimen configurations. The 3-inch wide notched compression specimen had either a 0.25-inch or 0.50-inch diameter hole and the 5-inch wide specimen had a 1.00-inch diameter hole.

The short block compression, notched compression, and compression after impact specimens were end-clamped to prevent brooming and were tested to failure at 0.05-inch/minute in a 120-kip capacity hydraulic test machine. The open-hole compression and compression after impact fixtures also had knife-edge side supports. The tension and open-hole tension specimens were end-gripped with hydraulic grips in a 50-kip capacity servo-hydraulic test machine and were also loaded to failure at 0.050-inch/minute. Load, strain, and displacement were recorded continuously for all tests using an IBM PC-based data acquisition system.

STATIC TEST SPECIMEN CONFIGURATIONS

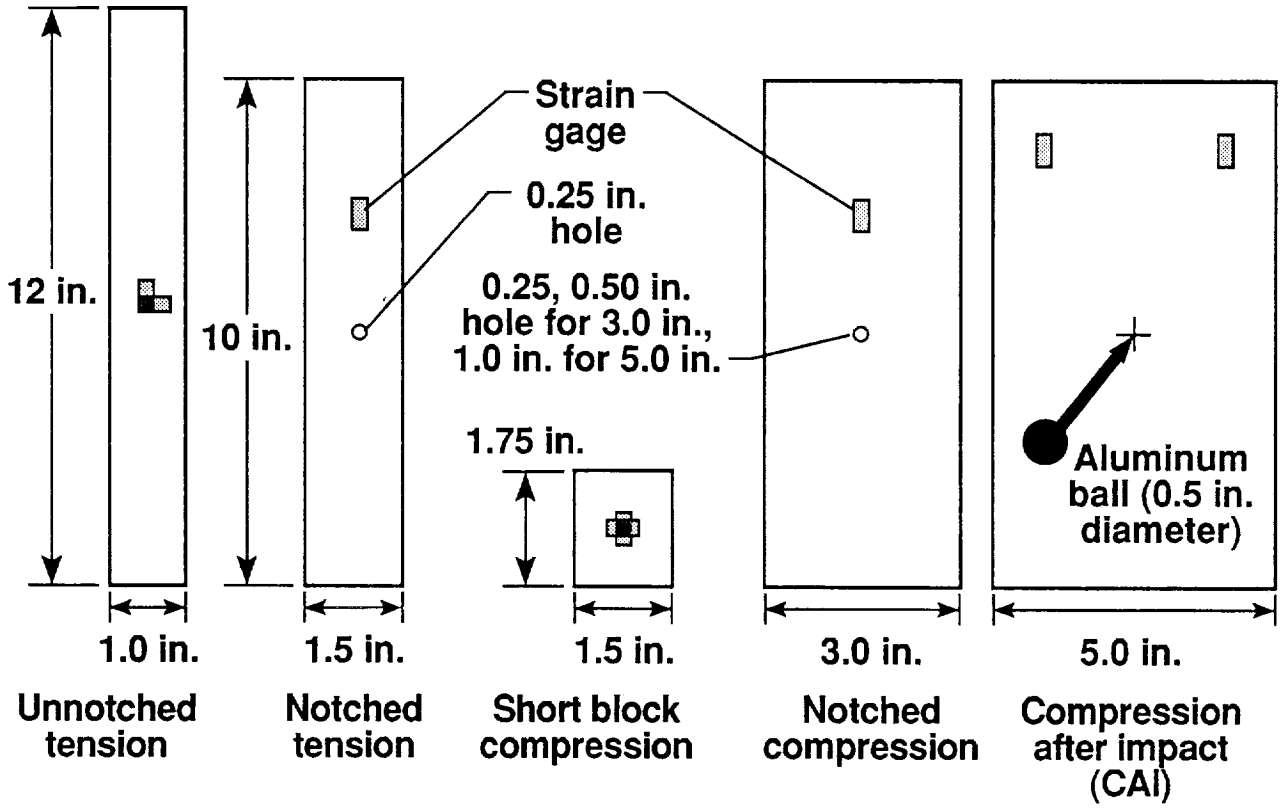

FATIGUE TEST SPECIMEN CONFIGURATIONS

Figure 6 shows the test specimen configurations for the 3-D braid material evaluated in fatigue. All specimen thicknesses were nominally 0.25-inch. Dimensions are given for both tension and compression specimens for each configuration shown in the figure. The tension specimens have longer grip lengths to allow for clamping and load transfer through shear. The compression specimens are all end loaded. Test section gage lengths were chosen to minimize buckling/instability problems in compression. The test section for both tension and compression unnotched specimens were reduced from an overall width of 1.5-in. to 1.0-in. by machining a large radius in the test section which assures that failures occur within the test section. Two notched configurations are being evaluated in fatigue. The 1.5-inch wide notched specimens have a 0.25-inch diameter hole and the 3.0-inch wide specimens have a 0.50-inch diameter hole. The 0.50-inch hole was chosen to provide access to monitor damage initiation and growth inside the hole. The compression or tension after impact specimens are being impacted using a drop-weight impactor at three different energy levels. An impact energy level of 30 ft-lbs will be evaluated first. Subsequent energy levels will depend on the results of these first tests.

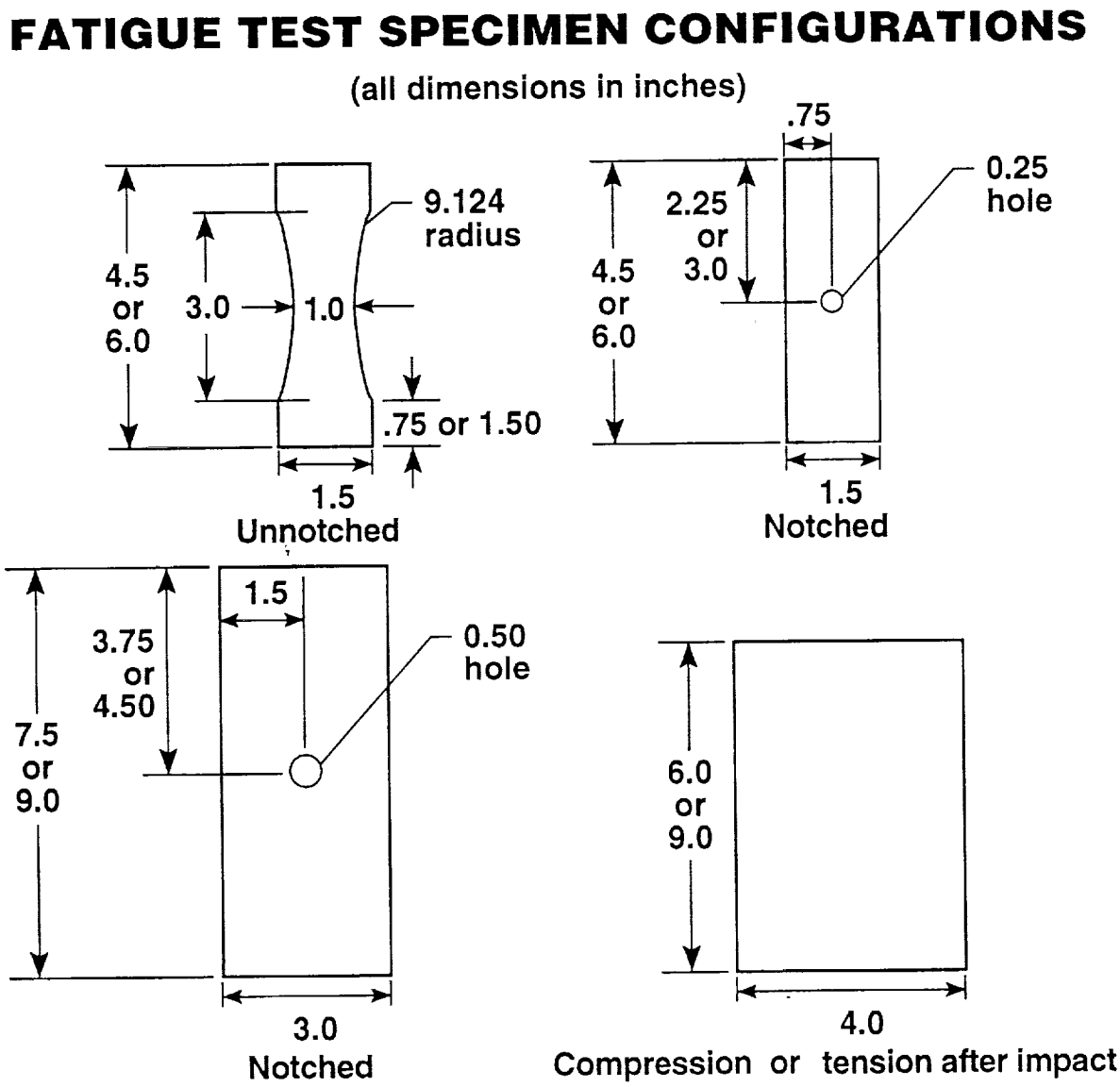

Figure 7 shows the room temperature tensile strengths for each braid architecture and resin system evaluated in this investigation. The unshaded bars represent the average value obtained from the unnotched tests and the shaded bars are the average value obtained from the notched tests. The averages shown have not been normalized to a common fiber volume fraction. The range of values obtained from all tests is also shown on the figure. Six unnotched specimens were tested for each braid architecture and resin combination and either 2 or 3 notched specimens were tested for each combination. The tensile strength of the 3-D braid/E905L is about 6% greater than the tensile strength shown for the 2-D braid/E905L even though it has the lower fiber volume fraction. This could be attributed to the even distribution of 0° fibers through the thickness in the 3-D braid as well as the tensile contribution from the straight segments of the ±30° graphite fiber tows compared to the nested graphite tows for the 2-D braid (see fig. 4). The tensile strength of the 2-D/E905L is approximately 13% greater than that shown for 2-D/MY722. Since tension properties are fiber dominated and each 2-D braid had the same graphite fiber and braiding parameters, this difference is unexplained. Stitching resulted in about a 20% reduction in unnotched tensile strength for the 2-D braid/E905L. The notched tensile strengths exhibited only a slight reduction due to stitching. This may be due to greater stitching damage in the thinner (0.125-in.) unnotched specimens compared to the thicker (0.25-in.) notched specimens.

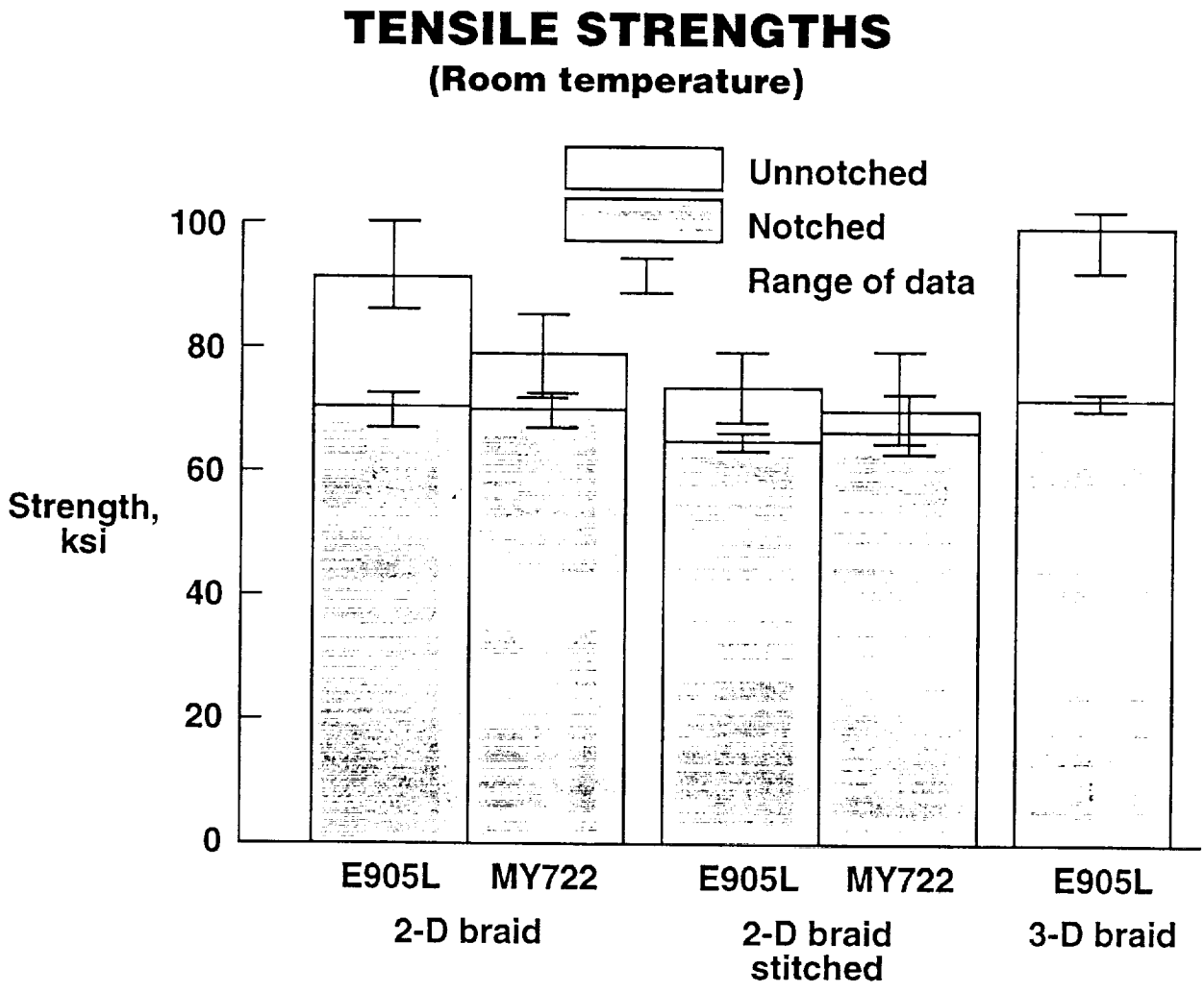

TENSILE MODULI

The average tensile modulus for each braid architecture and resin system is shown in figure 8, along with the range of values obtained. Moduli were calculated by a linear regression over the range of 0.1% to 0.3% strain to eliminate any initial loading artifacts. Also shown on the figure are tension moduli predictions for both the 2-D and 3-D braid architectures. The predicted values were obtained using a 3-D finite element analysis (ref. 4 & 5) approach to analyze a detailed unit cell of each braid architecture. Extensive use is made of photomicrographs, as shown in figure 4, to develop representative unit cell models for the finite element analysis. The measured values for the 2-D and 3-D braids are about the same whereas the 2-D braided composites with stitching are slightly less, possibly due to stitching damage to the fiber tows in the (0.125-in.) thin specimens. The 2-D prediction is shown to be excellent while the 3-D prediction is slightly less than the measured values.

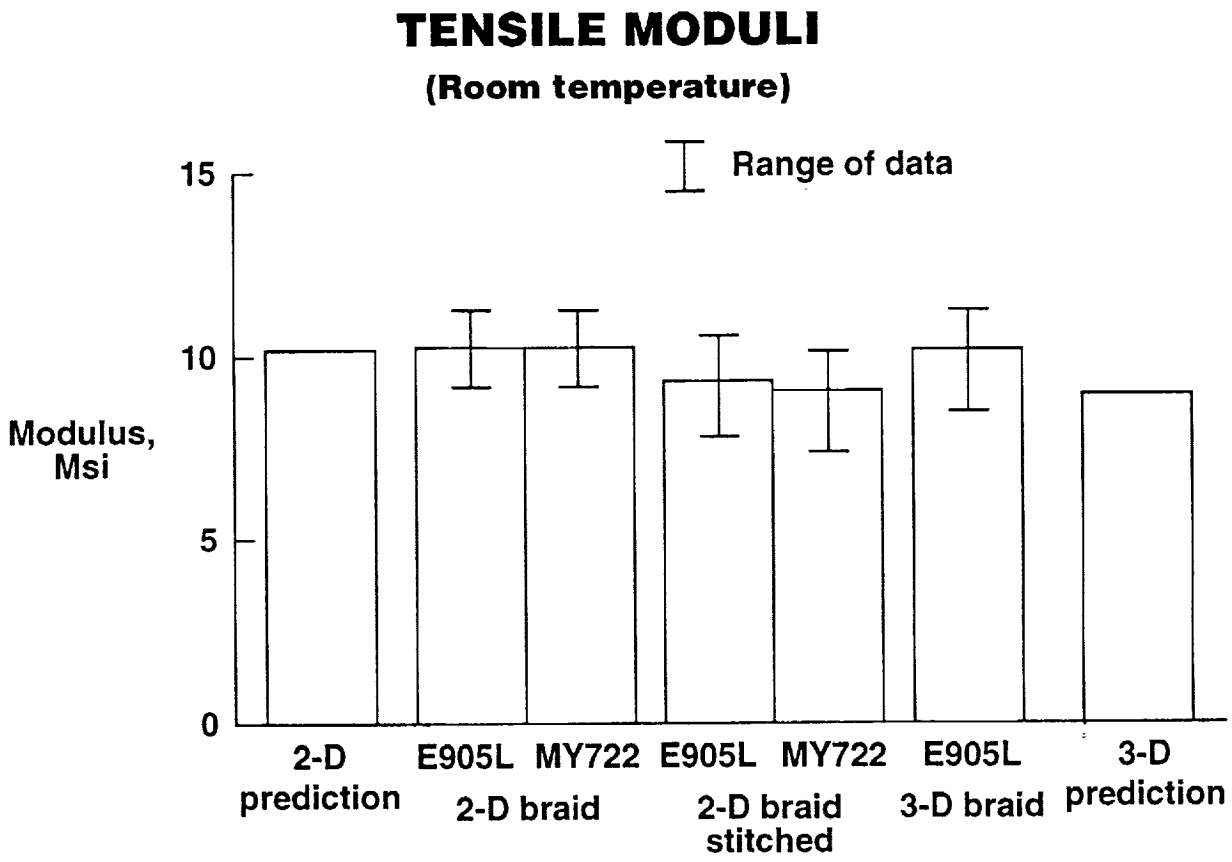

Figure 9 shows the room temperature compressive strengths for each braid and resin evaluated. The average unnotched compressive strengths were obtained from the short block compression specimens and are given by the unshaded bars. The shaded bars represent the average value obtained from the notched compression tests. Four unnotched and two notched specimens were tested for each braid architecture and resin system shown. The range of data values are also shown for each case. The 3-D braid/E905L is shown to have 10% and 15% higher unnotched compression strength than the 2-D braid/E905L and stitched 2-D braid/E905L composites, respectively. The 3-D/E905L also has the highest notched compressive strength, 15% greater than the 2-D/E905L, and 20% greater than the stitched 2-D/E905L composites. The unnotched strengths for the two stitched 2-D braid composites are the same whereas the unnotched compression strength of the 2-D braid/MY722 is considerably less than that for the 2-D braid/E905L. This is similar to the differences noted for the tensile strengths discussed in figure 7 and is also unexplained. However, one would not expect the inplane unnotched strength to increase with stitching as is indicated for the stitched 2-D braid/MY722.

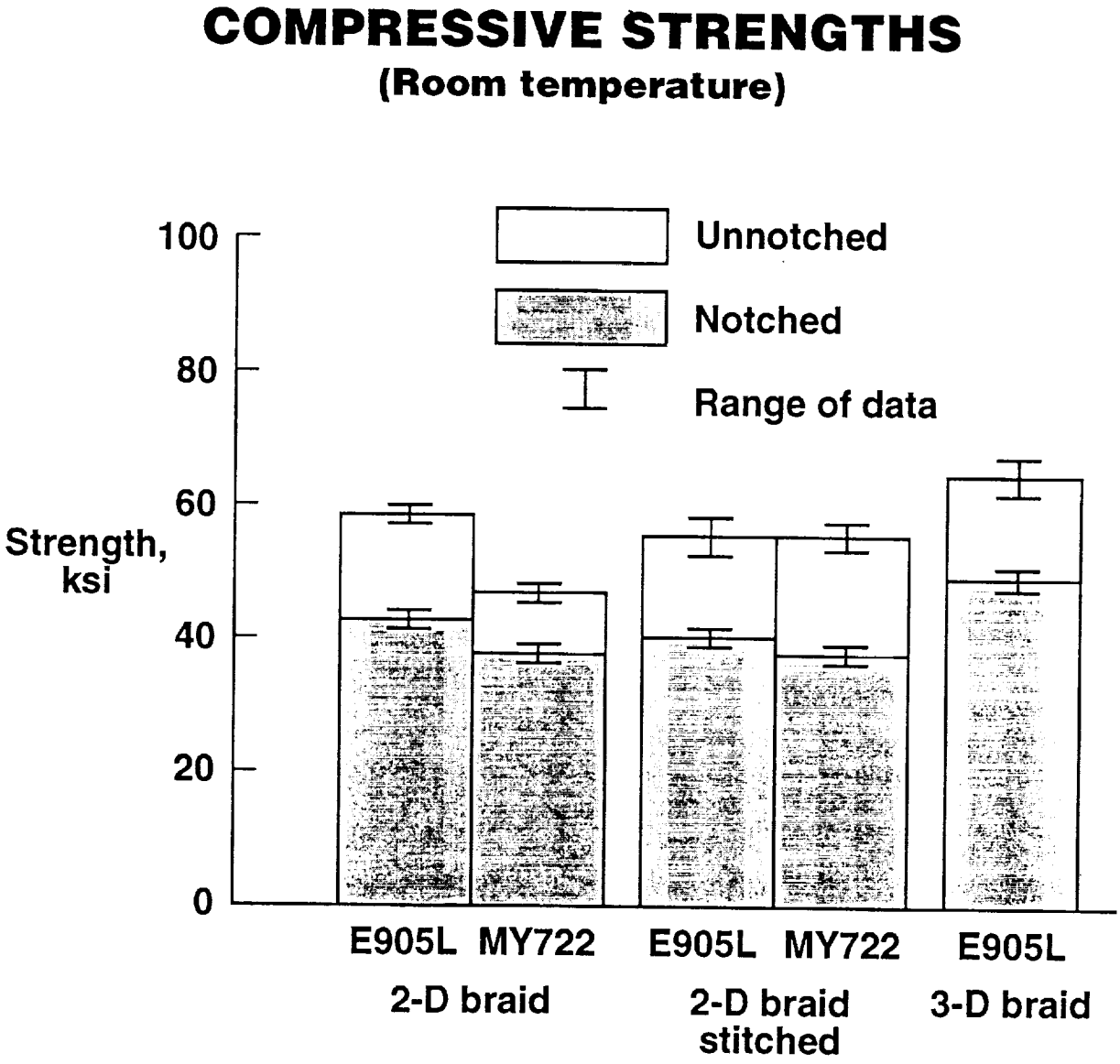

The average compressive modulus for each braid architecture and resin system is shown in figure 10. Compressive moduli were also calculated by a linear regression over the range of 0.1% to 0.3% strain to eliminate any initial loading artifacts. Also shown on the figure are compressive moduli predictions for the 2-D and 3-D braid architectures. The predictions were based on the 3-D finite element analysis discussed previously. The measured value for the 3-D braid is slightly less than that of the 2-D braid composites. The 2-D and 3-D predictions are shown to be slightly more than the average measured values but are within the range of measured values obtained for both braids.

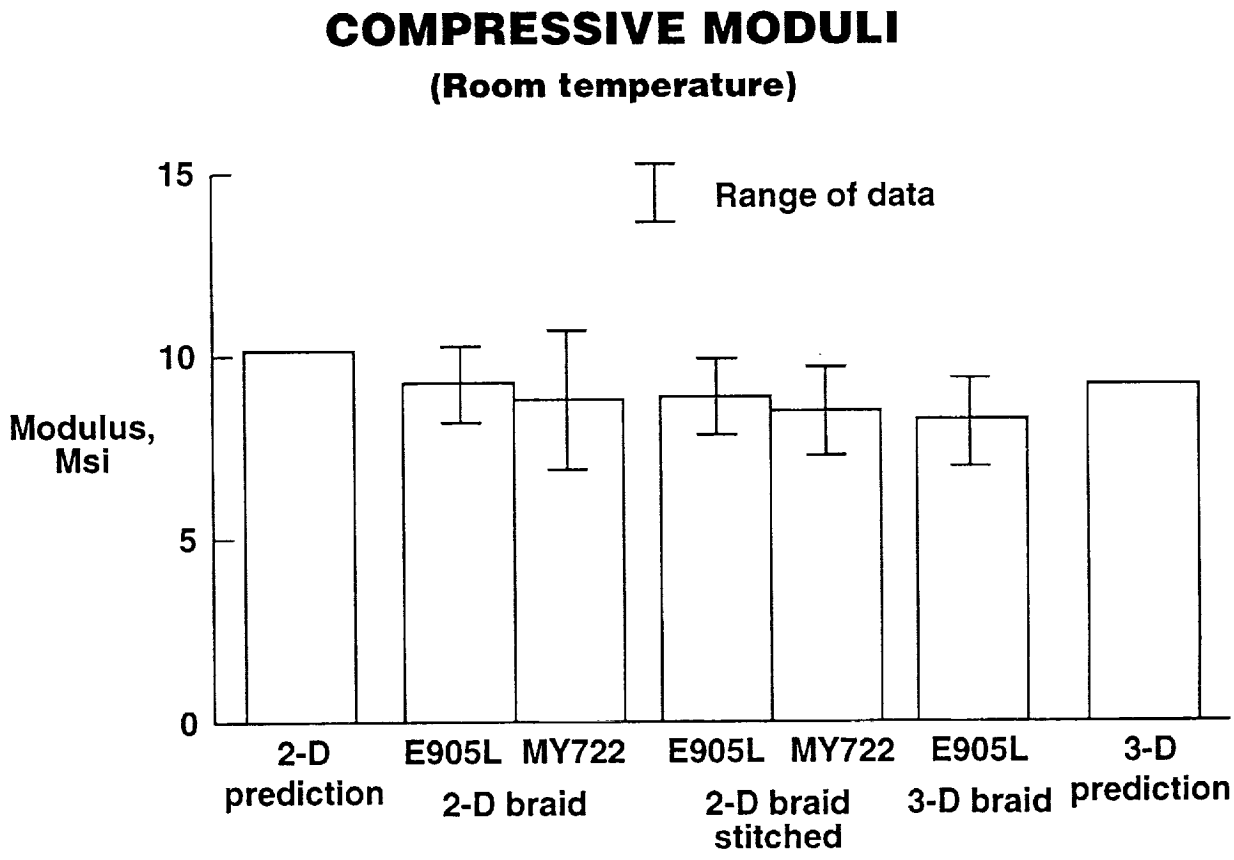

Figure 11 shows the compressive strengths for each braid architecture and resin system tested at 180° F after being soaked in 160° F water for 45 days. The average hot/wet unnotched compressive strengths were obtained from short block compression specimens and are represented on the figure by the unshaded bars. The hot/wet notched strengths are indicated by the shaded bars. Four unnotched specimens and two notched specimens were tested for each braided composite evaluated except for the notched MY722 composites where only one specimen was tested. Comparison of the hot/wet unnotched compression strengths (fig. 11) with the room temperature unnotched compression strengths (fig. 9) indicates that the 2-D/E905L and 3-D/E905L strengths are only reduced about 5% whereas the stitched 2-D/E905L strength is reduced about 17% due to the environmental conditioning and elevated temperature testing. The same trend is also noted for the notched strength comparisons (figs. 9 & 11) of the 2-D/E905L and 3-D/E905L where a reduction of about 7% was obtained for the hot/wet condition and the stitched 2-D/E905L experienced a larger reduction of about 11%. The best compression performance observed for the 3-D braids at room temperature (fig. 9) also occurs in the hot/wet test (fig. 11).

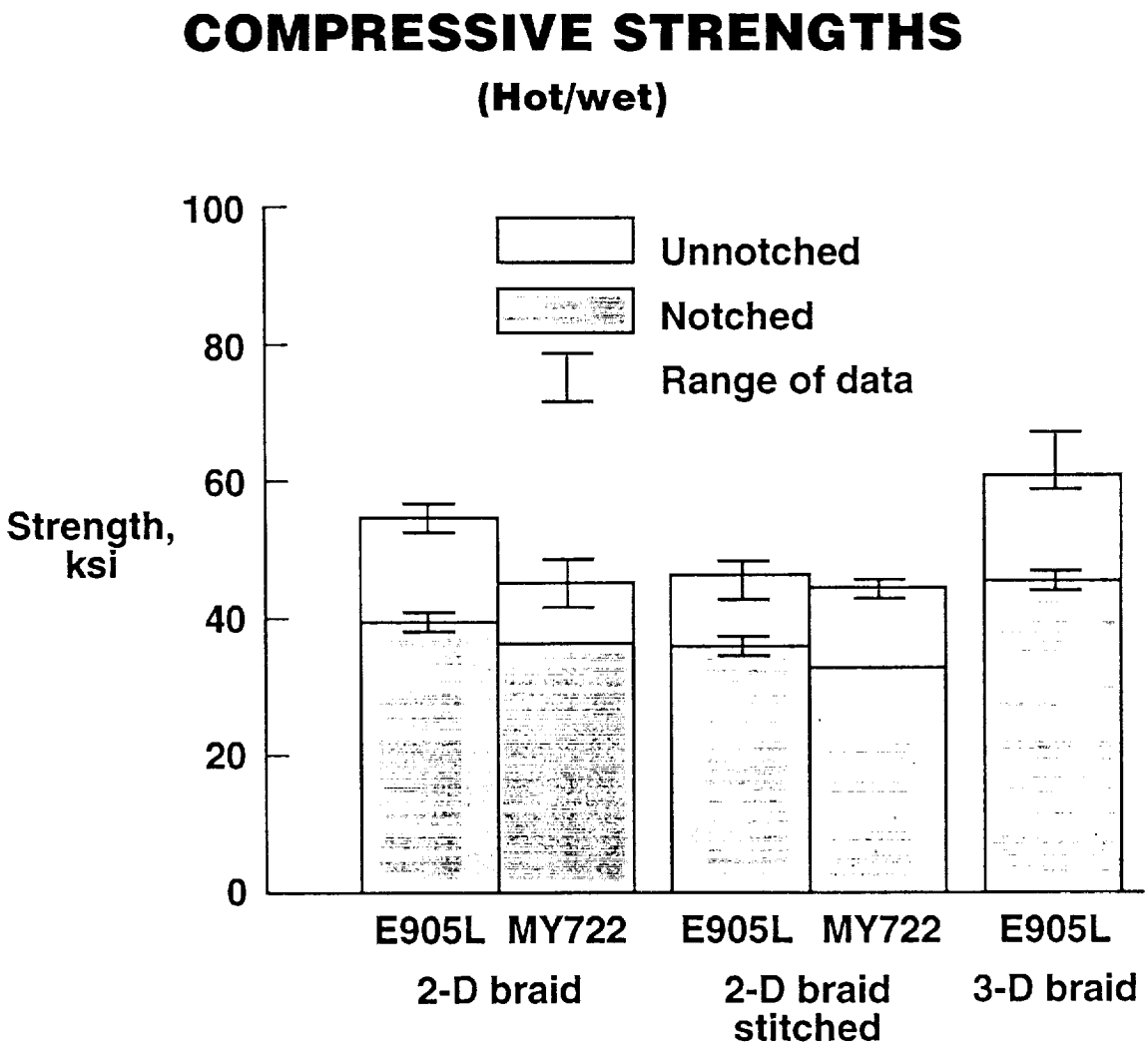

POISSON'S RATIO

Average values of Poisson's ratio obtained from both the unnotched tension and compression test for each braided composite are shown in figure 12. Also shown on the figure are the predicted values obtained from the 3-D finite element analysis discussed previously. Note that the analysis for this particular 2-D braid architecture, [±30°/0°], predicts values of Poisson's ratio greater than 1.0, which is within the range of measured values for the 2-D/E905L and 2-D/MY722 composites. The average value measured for the 3-D/E905L is almost identical to the predicted value whereas the average values measured for the 2-D/E905L and 2-D/MY722 are slightly less than the predicted value. This difference could be due to small variations in the ±30° braid angles for the 2-D braid architectures (see fig. 11 of ref. 5).

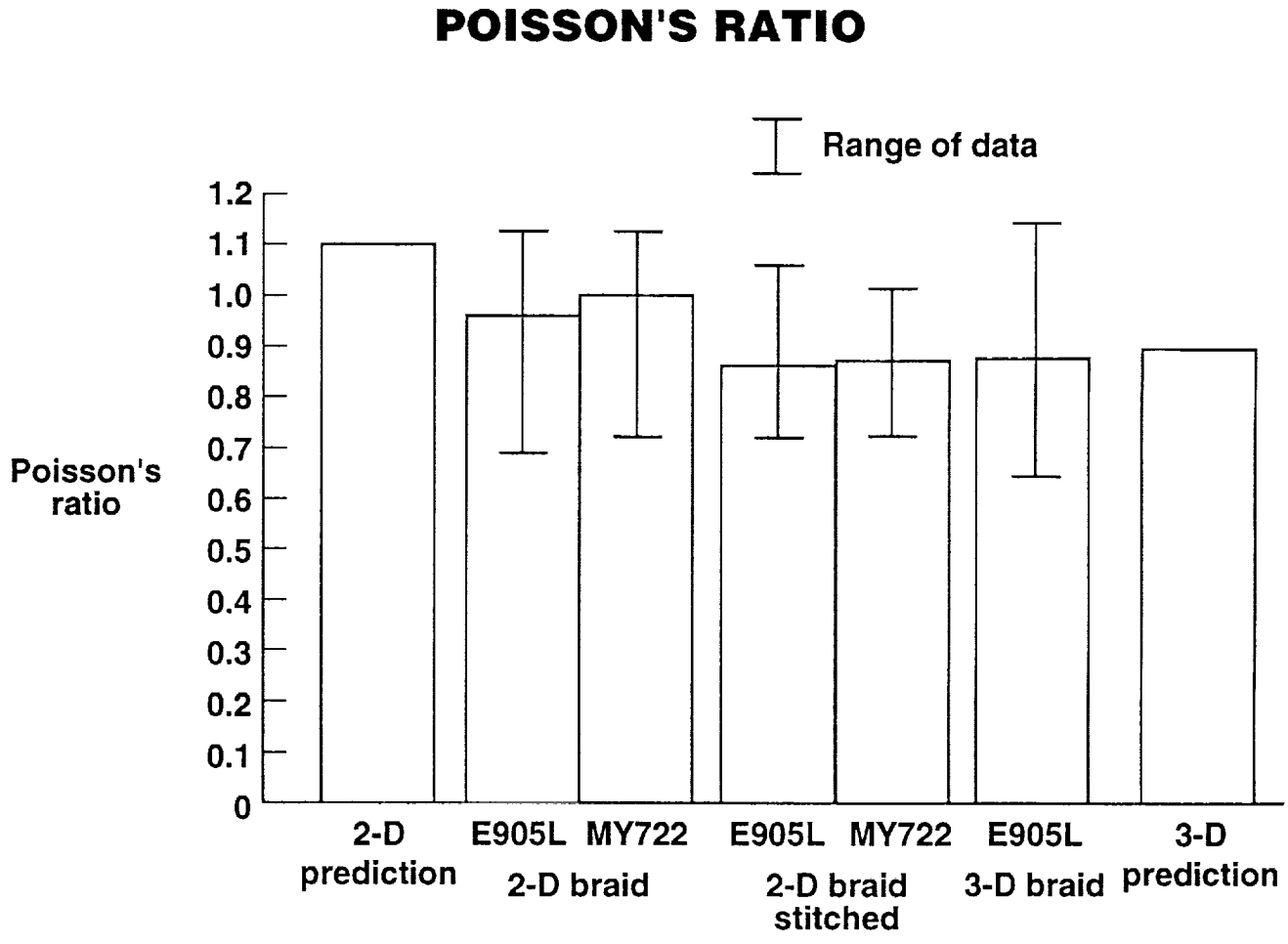

ROOM TEMPERATURE COMPRESSION AND COMPRESSION AFTER IMPACT STRENGTHS

Figure 13 shows the compression and compression after impact (CAI) strength properties measured for each braided composite under evaluation. The unshaded bars are the room temperature unnotched compression strengths from figure 9 and the shaded bars are the average room temperature CAI strengths. Three specimens were impacted for each braid and resin system (two specimens for room temperature testing and one for hot/wet testing) and the range of room temperature CAI strength values is indicated on the figure. The numbers shown in parenthesis at the top of the shaded bars represent the average damage area (2 room temperature and 1 hot/wet specimen) as determined from C-scans obtained after impact. The CAI strength of the stitched 2-D/E905L is the only braided composite which exceeded 40 ksi and is approximately 12% greater than the CAI strength of both the stitched 2-D/MY722 and 3-D/E905L composites. Comparison of the stitched 2-D braids with the unstitched 2-D braids indicates a 20% to 25% greater CAI strength increase due to stitching. This improved CAI performance is also consistent with the smaller damage areas for the respective stitched configurations. However, it should be noted that the 3-D/E905L braided composite had the smallest average damage area.

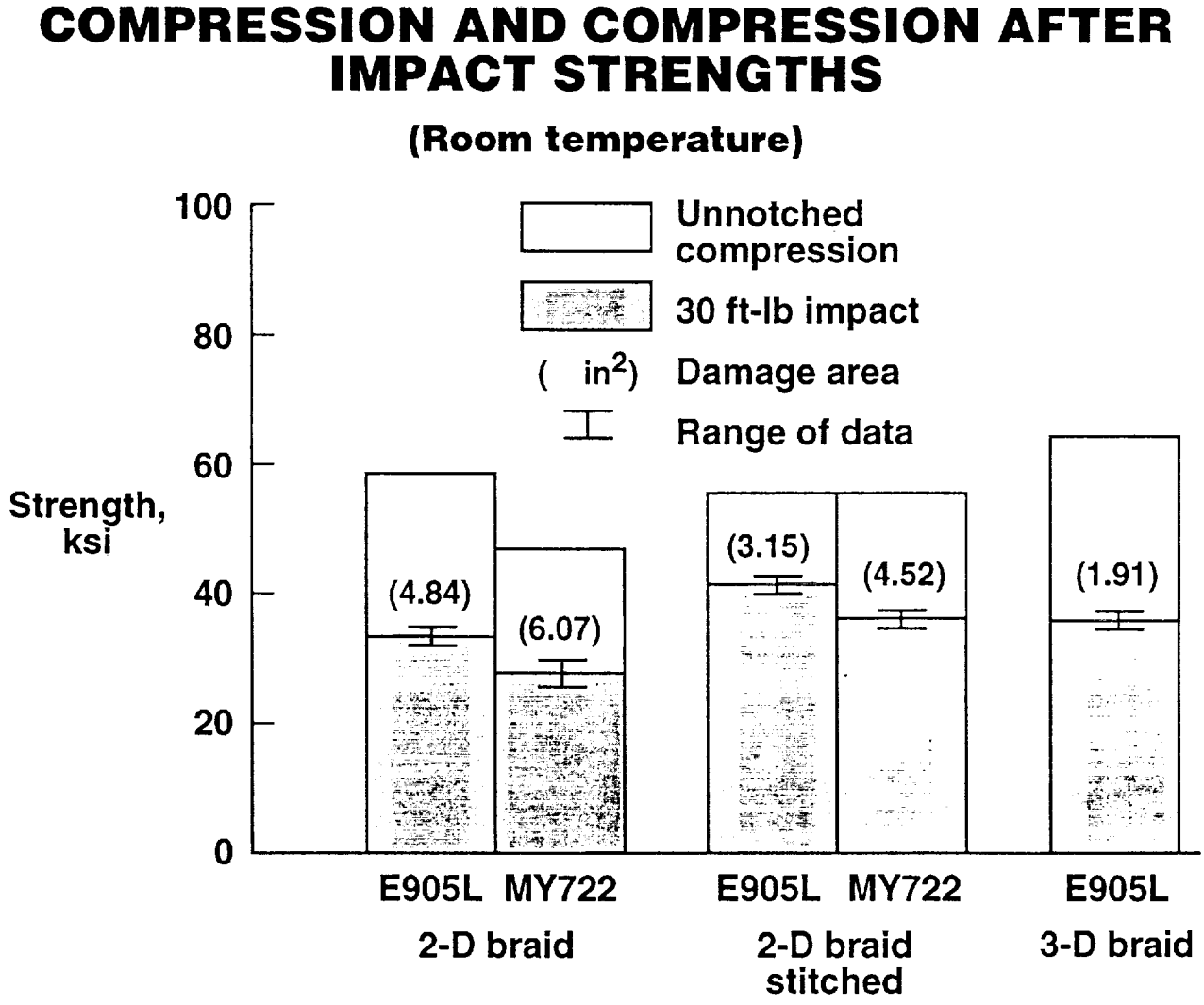

HOT/WET COMPRESSION AND COMPRESSION AFTER IMPACT STRENGTHS

The hot/wet CAI strengths of each braided composite are shown in figure 14. The unshaded bars are the hot/wet unnotched compression strengths from figure 11 and the shaded bars are the average hot/wet CAI strengths obtained from the impact specimens which were soaked in 160° F water for 45 days and then tested at 180° F, after the impact event. Only the 3-D/E905L composite had a repeat test under these conditions and the range is indicated on the figure. The stitched 2-D/E905L braid which exceeded 40 ksi CAI strength at room temperature (fig. 11) is shown to suffer the largest decrease in hot/wet CAI strength where a 25% decrease in the room temperature value is observed. The two stitched 2-D braids and the 3-D braid have about the same hot/wet CAI strengths, which are about 16% greater than the unstitched 2-D braided composites. Although only one hot/wet CAI test is reported for each 2-D and 2-D stitched braid composite, it is felt that these results are representative since small ranges in measured property values were obtained in the other hot/wet and notched compression test data previously discussed.

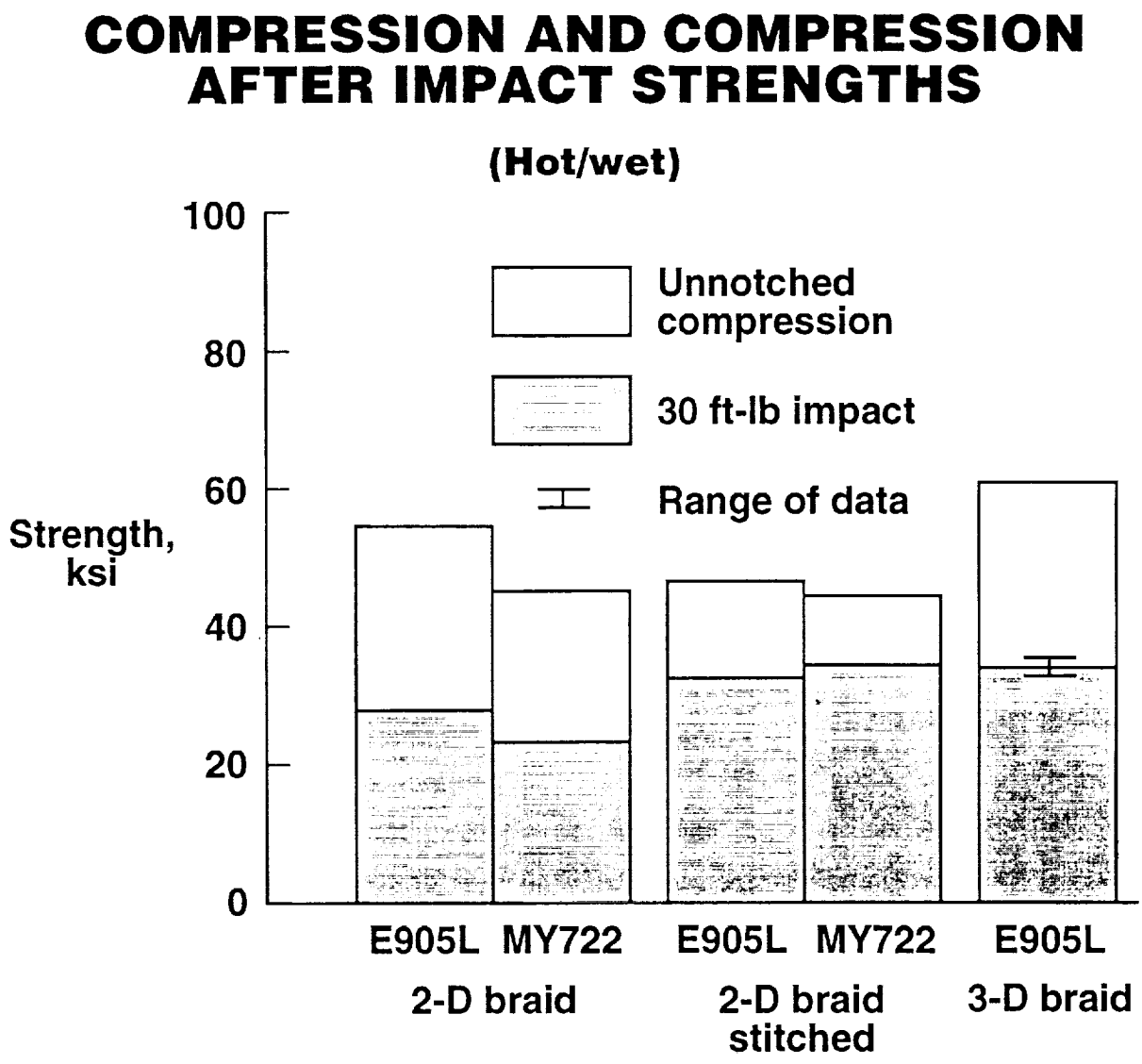

EFFECT OF HOLE SIZE ON COMPRESSIVE STRENGTHS

Figure 15 shows the effect of various hole diameters and specimen widths on the compressive strengths of the 3-D/E905L braid. The unnotched strengths were obtained from the 1.5-inch wide short block specimen data previously shown in figure 9. The data shown for the 0.25-in. diameter hole are also repeated from figure 9. In addition, two specimens having a 0.50-in. diameter hole and a specimen width of 3.0-inch, and two specimens having a 1.0-in. diameter hole and a specimen width of 5.0-inch were tested and the data is presented in the figure. Also shown on the figure is the CAI strength for this material (average damage area of 1.91-in.^{2} from figure 13). The data indicate a decrease in compression strength, compared to the unnotched strength, with increasing hole size.

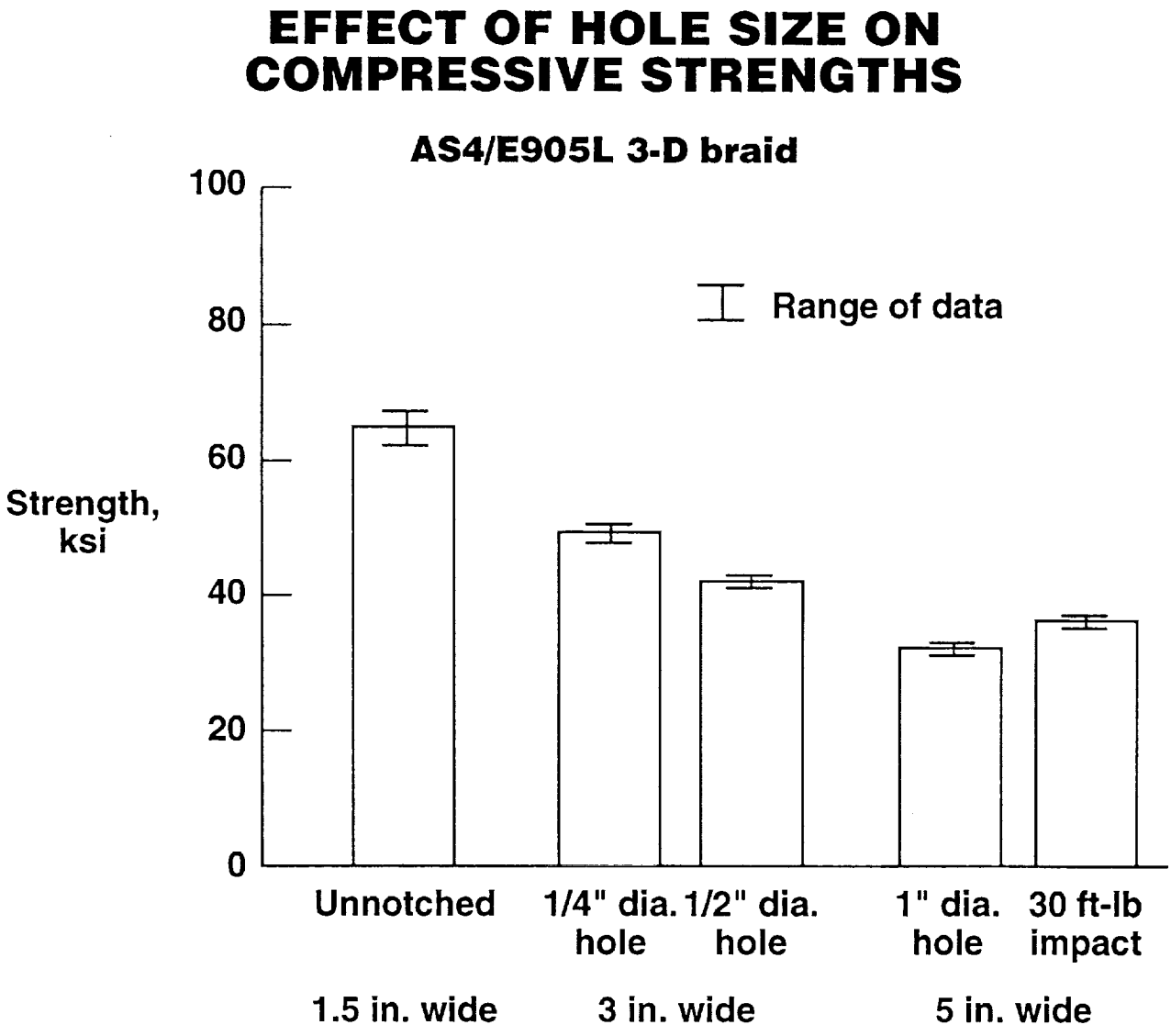

Figure 16 shows the 3-D fatigue test matrix and the number of specimens allotted for each of the test configurations previously described in figure 6. The baseline unnotched compression-compression and tension-tension fatigue tests have been completed and the results are discussed in subsequent figures. Drop weight impact at the first (30 ft-lb) of three energy levels has been performed and damage areas are being determined from C-scans prior to fatigue testing. All remaining fatigue test data will be reported at a future conference.

3-D BRAID FATIGUE TEST MATRIX

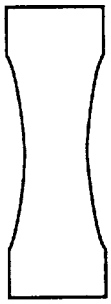

Unnotched tests:

10 specimens loaded in compression-compression fatigue

12 specimens loaded in tension-tension fatigue

Impact tests:

7 specimens at three impact levels loaded in compression

4 specimens at two impact levels loaded in tension

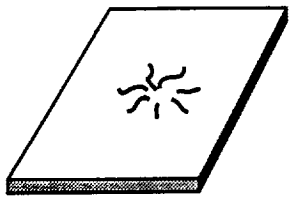

1/4 inch Open hole tests:

2 specimens static loaded in compression

16 specimens loaded in compression-compression fatigue

2 specimens static loaded in tension

10 specimens loaded in tension-compression fatigue

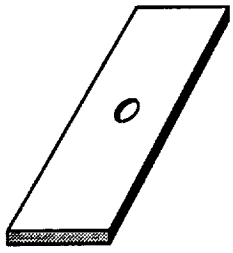

1/2 inch Open hole tests:

2 specimens static loaded in compression

4 specimens loaded in compression-compression fatigue

2 specimens static loaded in tension

4 specimens loaded in tension-compression fatigue

Maximum compressive stress is plotted against cycles to failure in figure 17. The value plotted at one cycle is the static failure stress from the room temperature short block compression test plotted in figure 9. A linear least squares regression fit to the data is also plotted. The linear regression fit to this data is the same as obtained in reference 6 for the same material tested with a constant cross-section area test section. The data shown in figure 17 indicates that the 3-D braids experienced a reduction in compression strength of about 44 % at 10^6 cycles. The 3-D braid material exhibits a wide range of fatigue lives for a fairly narrow range of cyclic stresses. This response is typical of that obtained in tape materials of similar constituents.

Airframe manufacturers typically design aircraft for a fatigue life of two lifetimes, where one cycle is equivalent to one takeoff and landing, and one lifetime is approximately 20 years or 60,000 hours of flight (see ref. 7). A design ultimate strain allowable of 0.004 has been suggested for tape laminates on the basis of damage tolerance. To evaluate the fatigue performance of the 3-D braided material, a region covering 1 to 2 lifetimes has been shaded and a dashed line placed at "limit condition" (2/3 times 0.004 strain level), based on the 3-D braided materials initial modulus given in figure 10. For wing bending on a typical transport aircraft, the strains will reach limit condition only a few times in a lifetime.

The compression fatigue response shows that the 3-D braid material, in the unnotched form, has more than adequate fatigue capability. The static strength of the notched 3-D braid was approximately 24 % less than the unnotched strength (fig. 9). Assuming that the slope of the S-N curve will be similar, the notched 3-D braid material may have marginal fatigue capability. The open-hole fatigue tests will help establish whether or not the 3-D braided material has adequate fatigue capability in compression.

COMPRESSION FATIGUE OF 3-D BRAIDS

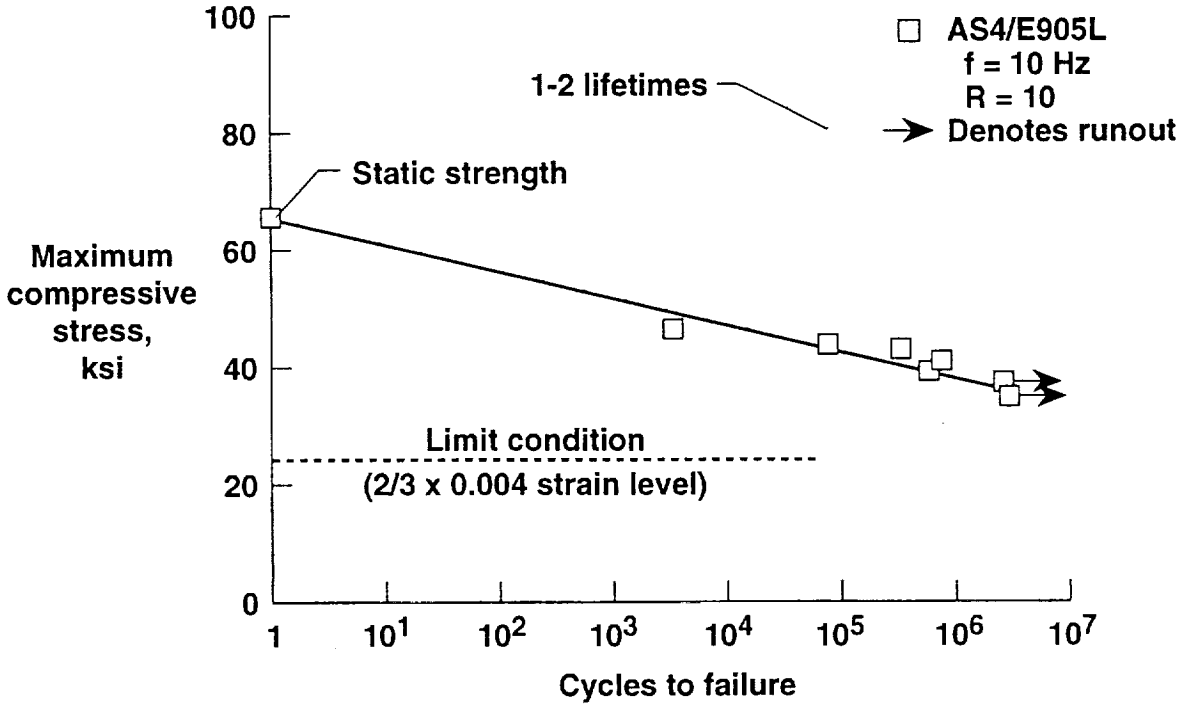

Figure 18 shows the maximum tensile stress plotted against cycles to failure for the 3-D braided material. The value shown for one cycle is the static failure stress from the room temperature tension test plotted in figure 7. A polynomial curve was fit to the data. The data shown in figure 18 indicates that the 3-D braids experienced a reduction in tensile strength with constant amplitude tension fatigue cycles of about 22 % at 10^6 cycles which is about one-half the loss experienced in compression fatigue at 10^6 cycles. For less than 10^5 cycles, the strength reduction was much less than that for compression fatigue data. Tensile strength is largely dependent upon the percentage of 0° fibers. The tension fatigue response of the 3-D braid material suggests that, although the off axis fibers may fail early in the life, the strength retains most of its initial unnotched strength.

Again, a region representing 1 to 2 lifetimes has been shaded and the design limit condition (2/3 times 0.004) is indicated on the figure by the dashed line. The unnotched tension fatigue response of the 3-D braid material is more than adequate. The notched static tension strength (fig. 7) is approximately 28 % less than the unnotched strength. Assuming the S-N responses to be similar, the notched fatigue response should also be more than adequate.

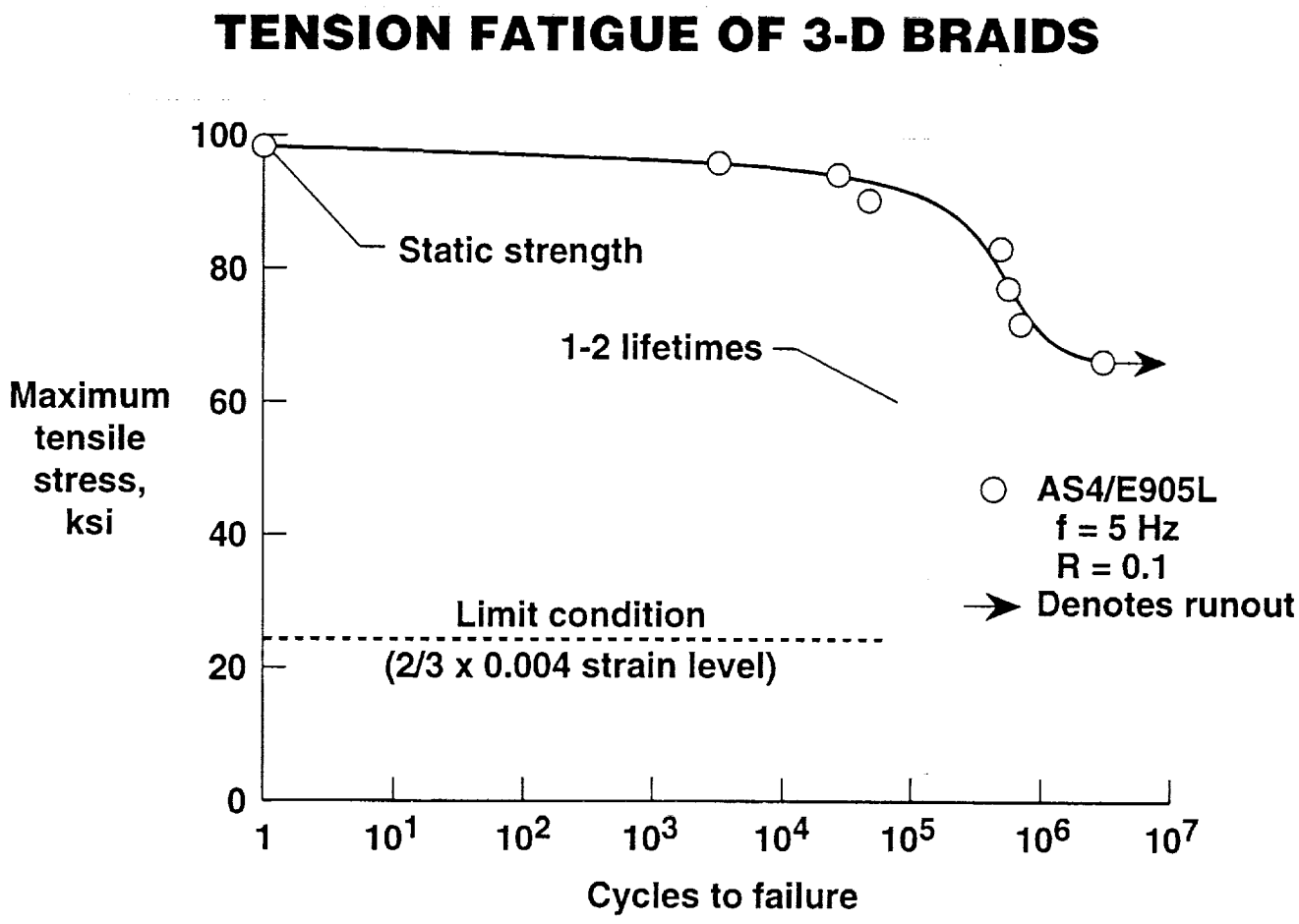

CONCLUDING REMARKS

Three different braided preform configurations, resin transfer molded with two different resin systems, have been evaluated to access their potential for applications to aircraft structures. The preforms evaluated include 2-D triaxial braid, 2-D triaxial braid with rows and columns of glass stitching, and 3-D through-the-thickness braid, all of which utilized AS4 12K graphite tows and the same [±30°/0°] braid architecture. The resin systems evaluated were British Petroleum E905L and Ciba Geigy MY722. Static mechanical tests were performed and include notched and unnotched tension, notched and unnotched compression, and compression after impact at room temperature and at 180° F after a 45 day water soak at 160° F. In addition to the static test performed, the baseline fatigue properties of the 3-D/E905L braided composite have been determined at room temperature. The results of this investigation support the following observations.

Static mechanical properties of the three braid architectures:

1. Unnotched tensile and compressive strengths varied among braided composites.

2. All notched tensile strengths were about equal.

3. Only the stitched 2-D/E905L composite exceeded a CAI strength of 40 ksi.

4. The 3-D braid has the best hot/wet notched compression and hot/wet CAI properties.

5. The 3-D braid appears to be showing the best overall combination of properties.

Fatigue results for 3-D/E905L braid:

1. Both unnotched tension and compression fatigue response are within current target values for fatigue life and strain levels for transport aircraft.

Future work will complete braided preform assessment.

REFERENCES

1. Palmer, Raymond J., Dow, Marvin B., and Smith, Donald L.: Development of Stitching Reinforcement for Transport Wing Panels, First NASA Advanced Composites Technology Conference, Seattle, WA, Oct. 29-Nov. 1, 1990. NASA CP-1304, Part 2, pp.621-646.

2. Dow, M.B., Smith, D.L., and Lubowinski, S.J.: An Evaluation of Stitching Concepts for Damage Tolerant Composites, Presented at Fiber-Tex 1988 Conference held in Greenville, South Carolina, September 13-15, 1988. NASA CP-3088, June 1989.

3. Dow, M. and Smith, D.: Damage-Tolerant Composite Materials Produced by Stitching Carbon Fabrics, International SAMPE Technical Conference Series, Volume 21, pp. 595-605.

4. Foye, R.L.: Finite Element Analysis of the Stiffness of Fabric Reinforced Composites, NASA CR 189597, February, 1992.

5. Masters, John E., Foye, Raymond L., Pastore, Christopher M., and Gowayed, Yasser A.: Mechanical Properties of Triaxially Braided Composites: Experimental and Analytical Results, NASA CR 189572, January, 1992.

6. Cano, Roberto J. and Furrow, Keith W.: Effects of Temperature and Humidity Cycling on the Strength of Textile Reinforced Carbon/Epoxy Composite Materials, Third Advanced Composites Technology Conference, NASA CP-3178.

7. Goranson, Ulf G. and Miller, Matthew: Aging Jet Transport Structural Evaluation Programs. Presented at the 15th Symposium of the International Committee on Aeronautical Fatigue (ICAF), Jerusalem, Israel, June 21-23, 1989.

PERFORMANCE OF RESIN TRANSFER MOLDED MULTIAXIAL WARP KNIT COMPOSITES

H. Benson Dexter
NASA Langley Research Center
Hampton,Virginia

Gregory H. Hasko
Lockheed Engineering and Sciences Co.
Hampton, Virginia

INTRODUCTION

Composite materials that are subjected to complex loads have traditionally been fabricated with multidirectionally oriented prepreg tape materials. Some of the problems associated with this type of construction include low delamination resistance, poor out-of-plane strength, and labor intensive fabrication processes. Textile reinforced composites with through-the-thickness reinforcement have the potential to solve some of these problems. Recently, a relatively new class of noncrimp fabrics designated as multiaxial warp knits have been developed to minimize some of the high cost and damage tolerance concerns. Multiple stacks of warp knit fabrics can be knitted or stitched together to reduce layup labor cost. The through-the-thickness reinforcement can provide significant improvements in damage tolerance and out-of-plane strength. Multilayer knitted/stitched preforms, in conjunction with resin transfer molding (RTM), offer potential for significant cost savings in fabrication of primary aircraft structures.

The objectives of this investigation were to conduct RTM processing studies and to characterize the mechanical behavior of composites reinforced with three multiaxial warp knit fabrics. The three fabrics investigated were produced by Hexcel and Milliken in the United States, and Saerbeck in Germany. Two resin systems, British Petroleum E905L and 3M PR 500, were characterized for RTM processing. The performance of Hexcel and Milliken quasi-isotropic knitted fabrics are compared to conventional prepreg tape laminates. The performance of the Saerbeck fabric is compared to uniweave wing skin layups being investigated by Douglas Aircraft Company in the NASA Advanced Composites Technology (ACT) program. Tests conducted include tension, open hole tension, compression, open hole compression, and compression after impact. The effects of fabric defects, such as misaligned fibers and gaps between tows, on material performance are also discussed. Estimated material and labor cost savings are projected for the Saerbeck fabric as compared to uniweave fabric currently being used by Douglas in the NASA ACT wing development program.

MULTIAXIAL WARP KNIT FABRIC

A schematic of a (0, 90, +45, -45) multiaxial warp knitted fabric is shown in figure 1. The knitting yarns are in the warp (0-degree) direction. The sketch indicates a chain knit to tie the four layers of carbon fabric together. Other types of knit, such as a tricot, can be used to tie the layers together. A tricot knit is normally used if 0-degree tows are on the surface of the fabric.

The potential benefits of multiaxial warp knitted fabrics are indicated in the figure. Significant cost savings are possible since layup time will be reduced compared to conventional unidirectional tape and biaxial broadgoods. Compared to woven broadgoods, the knitted fabric will have less crimp since the individual tows are not interlaced. Another benefit of multiaxial knitted fabric is reinforcement tailorability. In general, the off-axis ply orientations can range between 30 and 60 degrees. In addition, the tow size can be different for each ply of the fabric. Damage tolerance of the fabric can be controlled by the type and volume fraction of the knitting yarn. Polyester knitting yarn is generally used to hold 4-ply stacks together. However, Kevlar knitting yarn can be used to provide further improvements in damage tolerance.

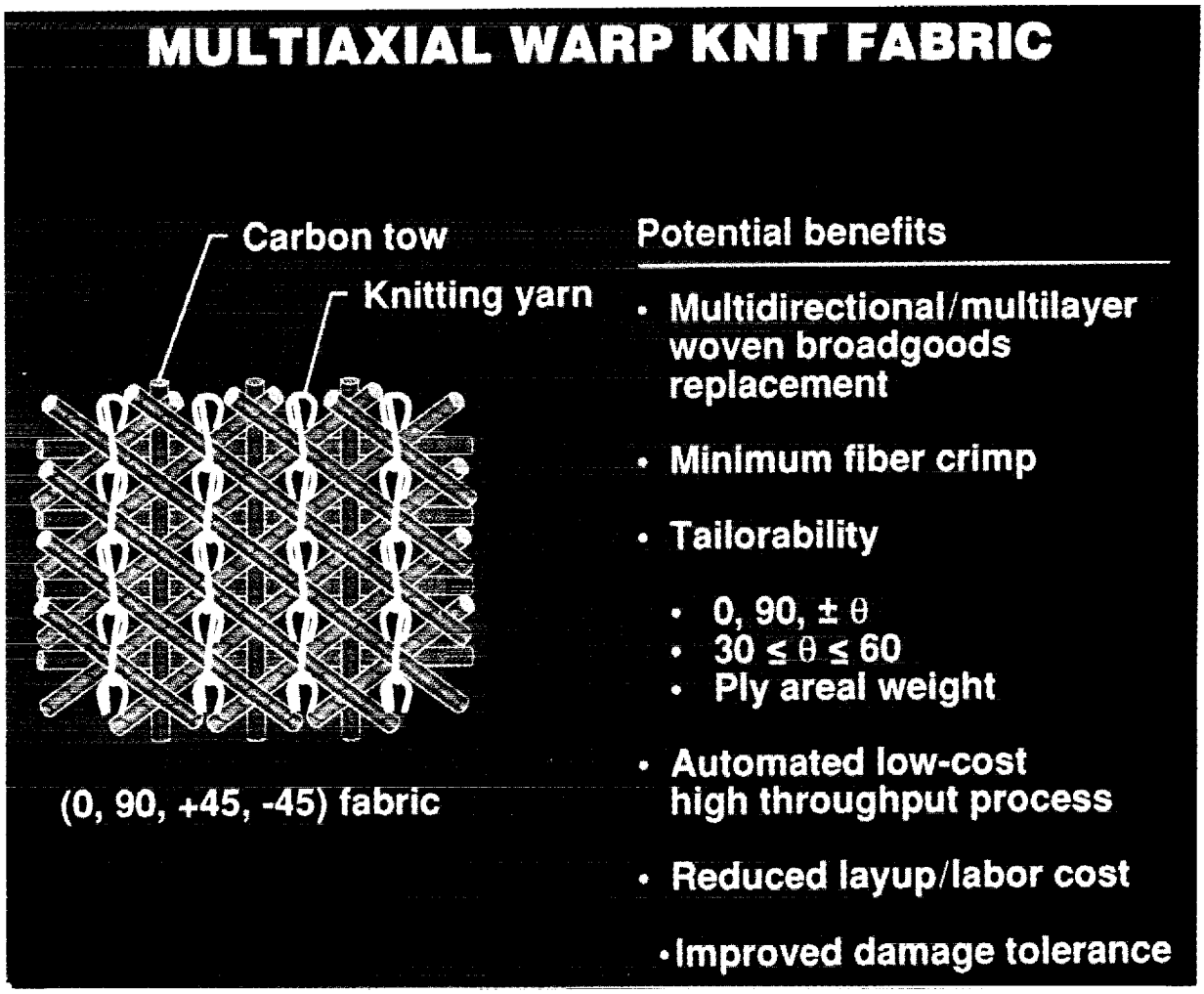

MULTIAXIAL KNITTED FABRICS EVALUATED

The multiaxial warp knitted fabrics evaluated in this investigation are described in figure 2. Fabrics were supplied by Hexcel, Saerbeck and Milliken. Seven fabrics from Hexcel with different tow sizes were evaluated. The results from the first Hexcel fabric listed in figure 2 with AS4-6K carbon fibers and polyester chain knit were reported on in reference 1 and will not be discussed here. The Hexcel fabrics with AS4 -3, -6, and -12K tows and a Kevlar chain knit were tested to evaluate the effects of tow size on mechanical properties and damage tolerance. The 3K, 6K, and 12K Hexcel fabrics had areal weights of 850, 1140, and 1695 g/m^2, respectively. The Hexcel fabric that had a mixture of 3 , 6, and 12K T300 fibers was evaluated in a cooperative effort with Boeing. This fabric had 0-degree fibers on the surface and a polyester tricot knit, as previously mentioned, was used to tie the four layers of fabric together. This fabric had an areal weight of 760 g/m^2.

The German made Saerbeck fabric was evaluated in a cooperative effort with Douglas Aircraft Company. The Saerbeck fabric was knitted together with a polyester alternating tricot/chain knit. The Saerbeck fabric had a tailored areal weight to achieve a fabric with 44 percent of the fibers in the 0-degree direction, 44 percent of the fibers in the ±45-degree directions and 12 percent of the fibers in the 90-degree direction. This layup was selected to meet design requirements for the wing panels being developed by Douglas under the NASA Advanced Composites Technology (ACT) Program. The Saerbeck fabric had an areal weight of 1305 g/m^2.

The Milliken fabric consisted of 9K AS4 fibers in the ±45-degree directions and 12K fibers in the 0-degree and 90-degree directions and had an areal weight of 1730 g/m^2. This architecture was based on the Milliken machine set-up and was required to achieve a balanced weight quasi-isotropic layup.

MULTIAXIAL KNITTED FABRICS EVALUATED

Material Supplier	Fiber	Orientation / Tow size (K)	Knit Material (knit type)
Hexcel	AS4	(+45, 0, -45, 90) (← 6 →)	Polyester (chain)
Hexcel	AS4	(+45, 0, -45, 90) (← 3 →) (← 6 →) (← 12 →)	Kevlar 29 (chain)
Hexcel	AS4	(+45, 0, -45, 90) (← 3 →) (← 12 →)	Kevlar 29 (chain)
Hexcel (w/Boeing)	T300	(0, -45, 90, +45) (12 3 6 3)	Polyester (tricot)
Saerbeck* (w/Douglas)	AS4	(0, +45, 90, -45) (12 6 3 6)	Polyester (alternating tricot/chain)
Milliken	AS4	(-45, +45, 0, 90) (9 9 12 12)	Polyester (chain)

* Douglas ACT wing layup: 44% 0°, 44% ±45°, 12% 90°

KNITTING CONCEPTS FOR MILLIKEN AND HEXCEL FABRICS

The knitting concepts for the Milliken and Hexcel fabrics are indicated in figure 3. The Milliken fabric is knitted on a Mayer multiaxial warp knitting machine that spaces the carbon fiber tows leaving gaps that allow the knitting needles to pass through the fabric without damaging the carbon tows. As indicated in the figure, a chain knit is used.

Hexcel fabrics were knitted with both chain and tricot knit styles, as shown in the figure. As indicated previously, the tricot knit is required to hold 0-degree tows on the surface of the fabric. The Hexcel fabric is knitted on a Liba multiaxial warp knitting machine that does not provide gaps for the knitting needles to pass through the fabric. As a result, the knitting needles impale and damage the carbon fiber tows as they pass through the fabric. Fiber misalignment is caused by the needle penetration and lack of tension on the carbon tows. The tradeoff in the two knitting methods is between fiber damage and misalignment and fiber volume fraction. The Mayer machine produces a fabric with less fiber damage but has a lower as-fabricated fiber volume fraction. Fiber volume fractions of over 60 percent have been achieved with the Milliken fabric but a consolidation pressure of well over 100 psi is required to spread the fibers and close the gaps between the carbon tows.

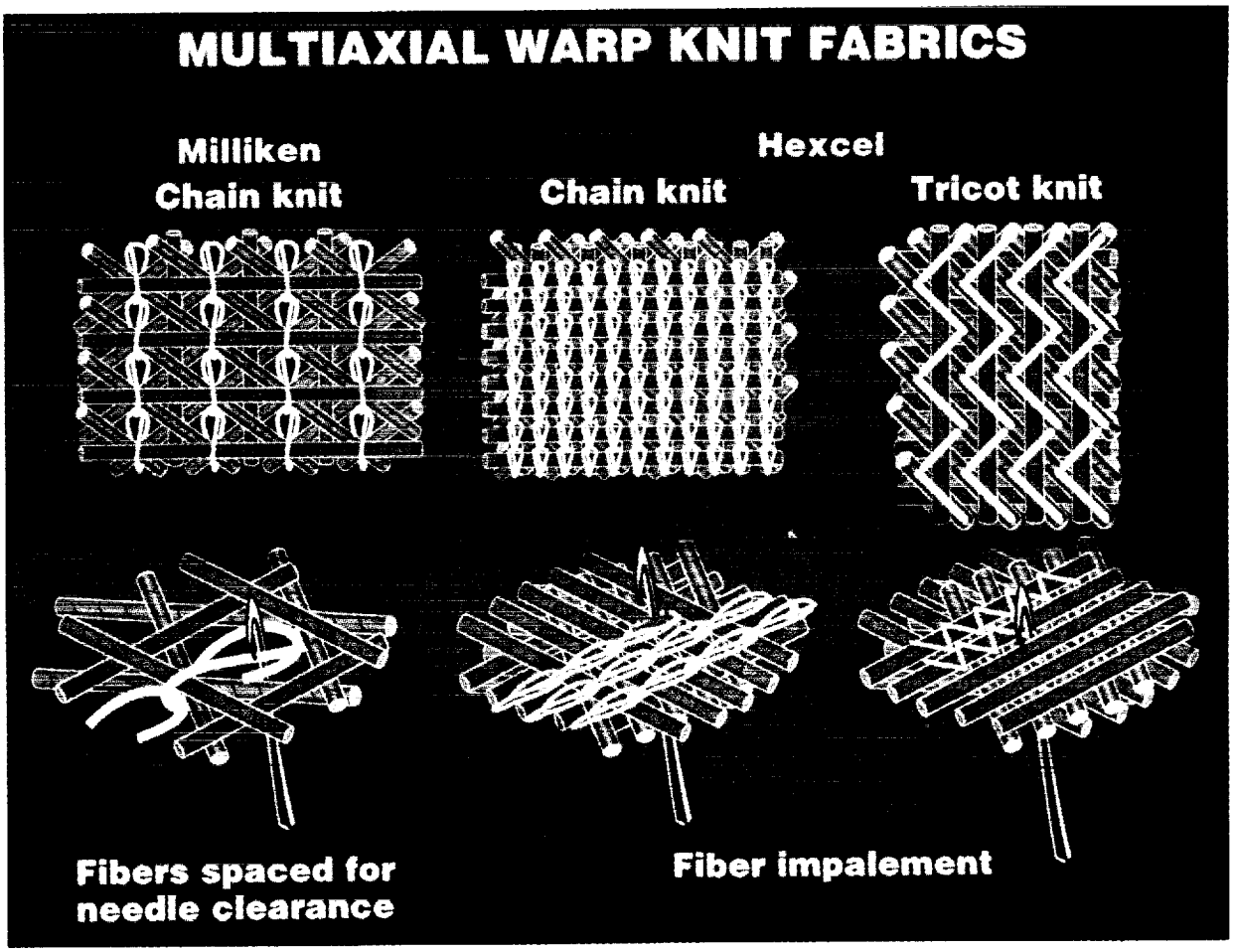

PHOTOGRAPHS OF KNITTED FABRICS

Photographs of the Hexcel, Milliken, and Saerbeck knitted fabrics are shown in figure 4. The Hexcel (+45, 0, -45, 90) chain knitted fabric shown in the upper left of the figure indicates significant gaps and fiber misalignment in the surface tows. Also, some fiber damage can be seen where the knitting yarns penetrate through the fabric. The Milliken (-45, +45, 0, 90) chain knitted fabric shown in the upper right of the figure indicates uniform gaps and minimal misalignment.

The Hexcel (0, -45, 90, +45) tricot knitted fabric has significant gaps between the 0-degree surface tows, whereas the Saerbeck (0, +45, 90, -45) fabric photograph indicates only small gaps between the 0-degree surface tows. However, some slight fiber waviness is evident in the Saerbeck fabric. The gaps in all the fabrics are potential sites for resin pockets to form during the resin transfer molding process. These resin pockets can contribute to the formation of microcracks in the cured composite.

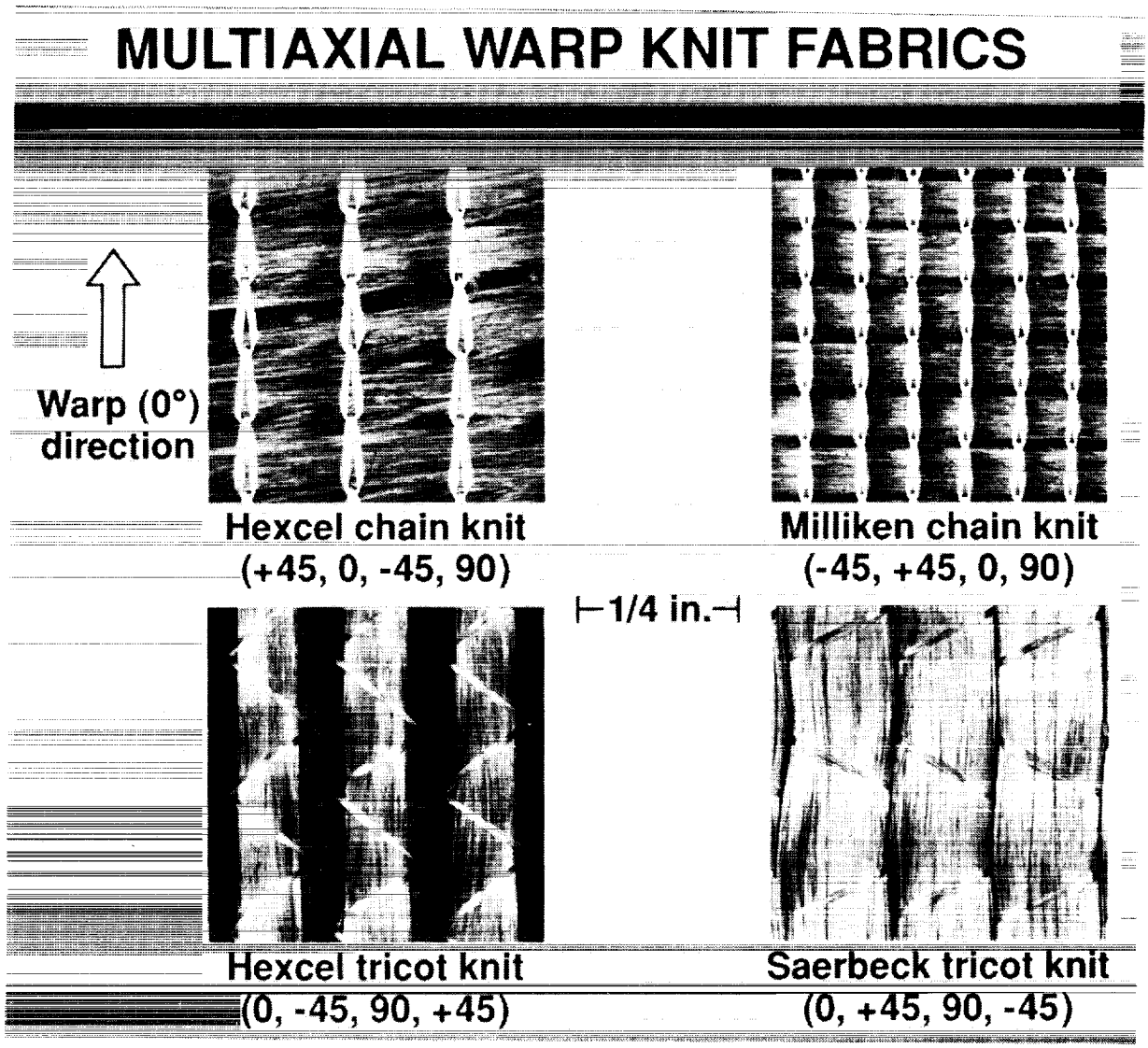

HEXCEL MULTIAXIAL WARP KNITTING MACHINE

The multiaxial warp knit fabrics obtained from Hexcel and Saerbeck were fabricated on machines that were developed by Liba, a German-owned company. The Hexcel machine shown in figure 5 can produce up to an 8-ply fabric with ply orientations of (0, 90, $\pm\theta$), with θ ranging from 30 to 90 degrees. The machine can produce fabric up to 100-inches wide at a rate of 50 lineal yards/hour. Yarn carriers with multiple tows traverse the fabric width and place the tows around pins that are attached to a moving belt. The tow size and the number of tows per inch determine the fabric areal weight. Different tow sizes can be used in each direction if desired. The sketch in figure 5 shows that the 90- and ±45-degree tows are laid down by the yarn carriers moving along fixed guides. The 0-degree tows are laid down off a beam just prior to the 4-ply stack being knitted together. Either a chain or a tricot stitch can be used to knit the fabric plies together.

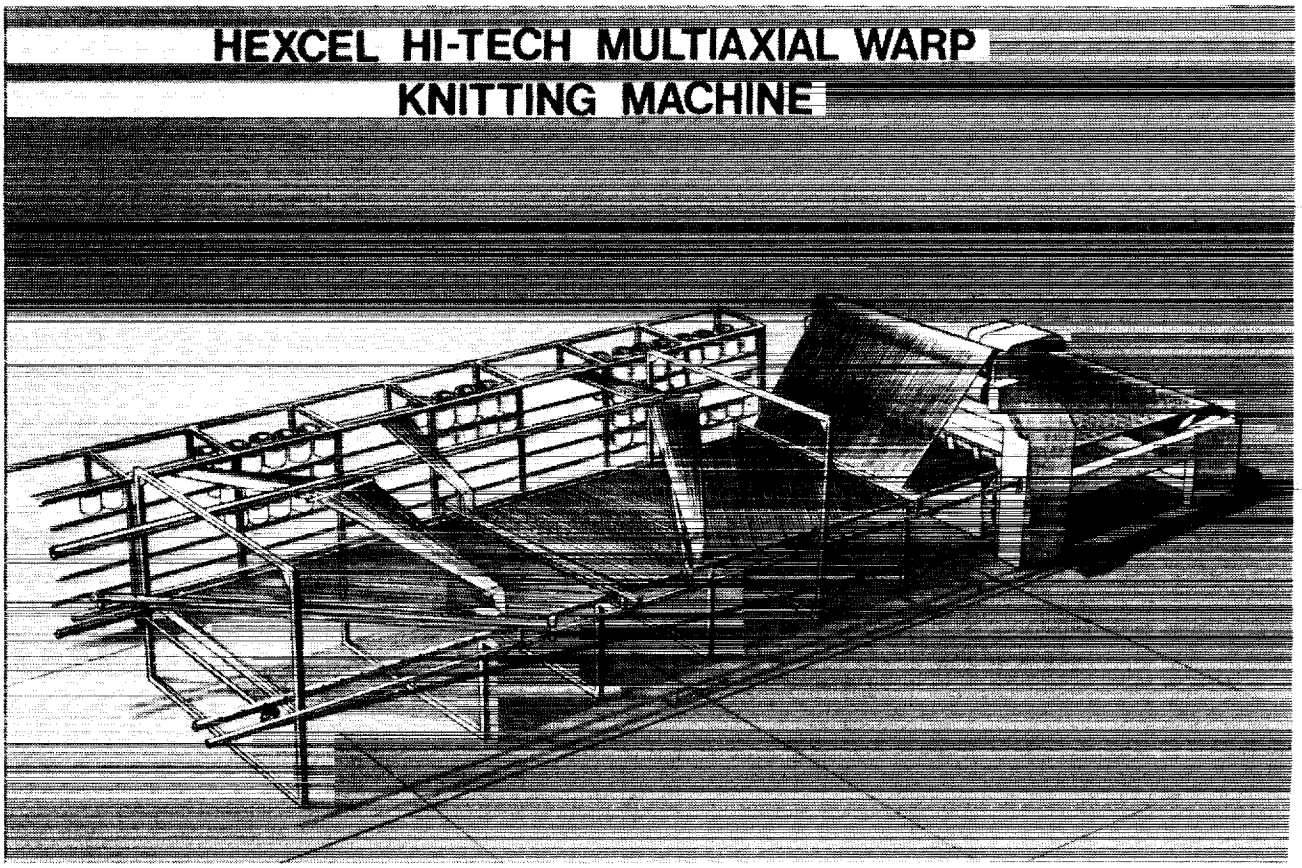

MILLIKEN MULTIAXIAL WARP KNITTING MACHINE

The multiaxial warp knit fabric obtained from Milliken was fabricated on a machine manufactured by the Mayer Textile Machine Corporation in Germany, figure 6. This machine can produce a 4-ply fabric with ply orientations of (0, 90, ±θ), with θ ranging from 30 to 60 degrees. Fabrics with (0, 90), (90, ±θ), and (±θ) fiber orientations can also be produced. The Milliken machine can produce fabrics up to 62 inches wide at a rate of 50 lineal yards/hour. For the fibers used in this investigation, the machine was operated at a speed of approximately 30 yards/hour to minimize damage to the carbon tows. The tow count for this fabric was 12 tows/inch in the warp direction and 17 tows/inch in the ±45-degree directions. A chain knit was used to knit the (-45, +45, 0, 90) plies together.

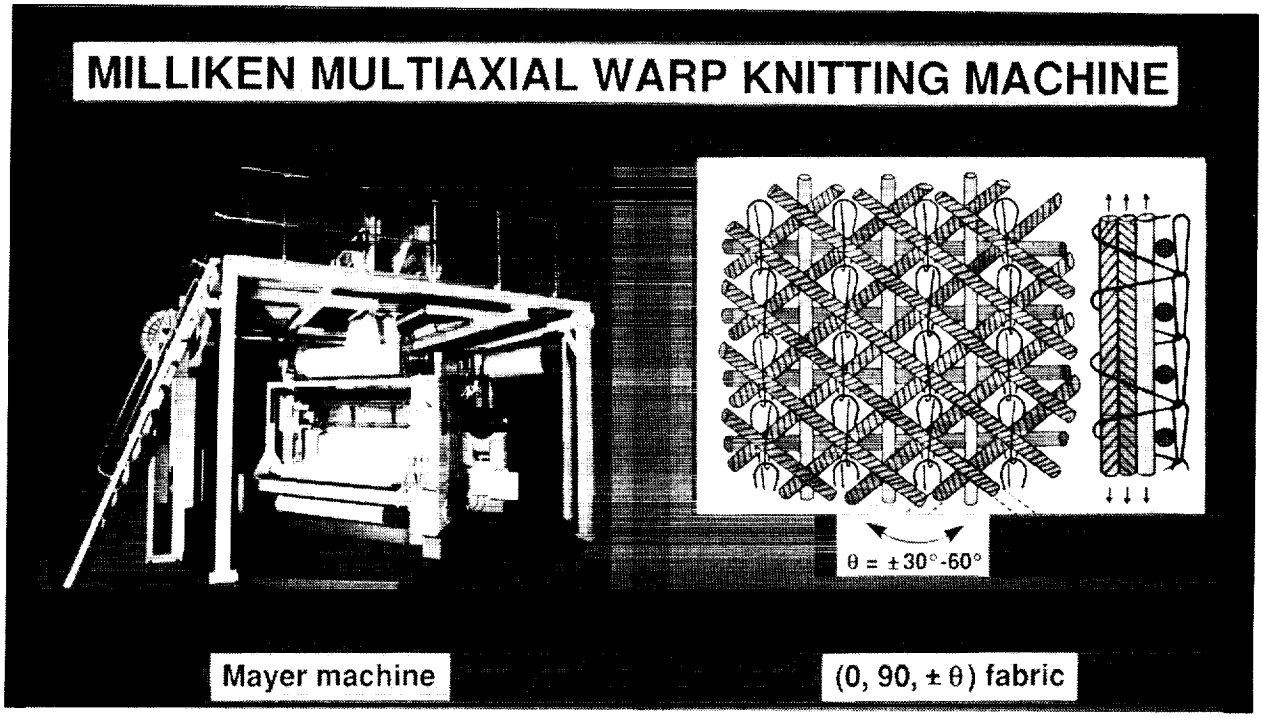

RTM RESINS EVALUATED

The five different resins evaluated for resin transfer molding the knitted fabrics are indicated in figure 7. The three one component epoxy resins, Hercules 3501-6, 3M PR 500, and Dow CET-3 were characterized for use in a vacuum infusion process, with a primary goal of establishing a suitable processing window for each of the resins. The 3501-6 resin melts during a ramp up to 245°F at which time a minimum viscosity of approximately 500 cps is achieved. The 3M PR 500 resin has a minimum viscosity of approximately 30 cps at 320°F. The Dow CET-3 epoxy-thermoplastic resin has a minimum viscosity of approximately 60 cps at 350°F.

The two component resins shown in figure 7 and evaluated in this study included British Petroleum E905L and Shell 1895. These resins were used in a pressure injection process. The E905L resin is heated to 200°F to achieve a minimum viscosity of approximately 100 cps. The Shell 1895 resin is heated to 250°F to achieve a minimum viscosity of approximately 10 cps. In this process the resin is pumped into the mold, the air is evacuated, the vent ports are closed, and the mold is closed to predetermined stops to set the final thickness of the panel.

RTM RESINS EVALUATED

- **Hercules 3501-6** - one component semi-solid epoxy at room temperature (vacuum infusion)
- **3M PR 500** - one component paste epoxy at room temperature (vacuum infusion)
- **Dow CET-3** - one component semi-solid crosslinkable epoxy thermoplastic at room temperature (vacuum infusion)
- **British Petroleum E905L** - two component liquid epoxy at room temperature (pressure injection)
- **Shell 1895** - two component liquid epoxy at room temperature (pressure injection)

EFFECTS OF MOISTURE AND TEMPERATURE ON RTM COMPOSITES

As part of the resin characterization study, the effects of moisture and temperature were investigated. To minimize data scatter, a well characterized state-of-the-art IM7 eight harness satin woven fabric was selected. Quasi-isotropic compression specimens were soaked in 160°F water for 45 days and tested at 180°F. The five resins discussed in figure 7 were tested in the as-fabricated condition and after the 45-day hot-wet exposure. The test results shown in figure 8 indicate that the composite with Shell 1895 resin had the best strength retention, about 90 percent, however, it had the lowest as-fabricated strength, about 65 ksi. The composite with BP E905L resin had a strength retention of about 82 percent and an as-fabricated strength of about 80 ksi, the highest of the systems tested. The composites with 3M PR 500 and the Hercules 3501-6 resins performed similarly to the BP E905L resin with the 3M PR 500 resin having a slightly lower strength retention of about 77 percent. The composite with Dow CET-3 resin had the lowest strength retention, about 75 percent, compared to the other four resins. Based on these results, availability of resins, and state of resin characterization, the BP E905L and the 3M PR500 resins were selected for the knitted fabrics evaluation. The BP E905L knitted fabric panels were processed at Boeing and the 3M PR500 knitted fabric panels were fabricated at NASA Langley.

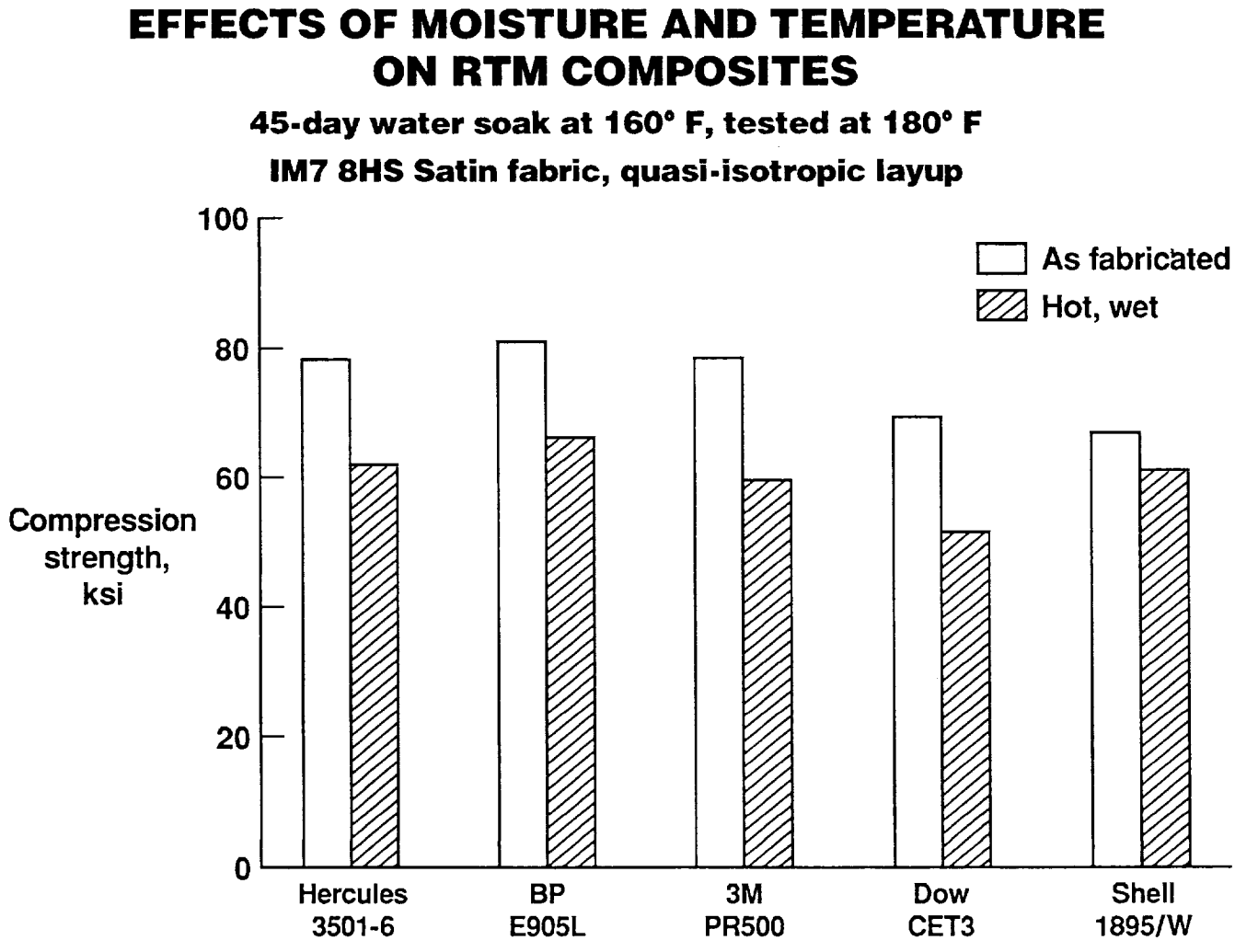

RESIN TRANSFER MOLDING METHODS

Two resin transfer molding methods were used to fabricate composite test panels for this investigation. The vacuum infusion method shown in figure 9 is similar to the process developed by Douglas Aircraft Company for fabrication of wing panels. The 3M PR 500 knitted panels were fabricated with the vacuum infusion method at NASA Langley in a vacuum press. The first step involves degassing the resin in a vacuum to remove any entrapped air. The second step consists of pouring the resin in the bottom of the picture frame tool in a predetermined amount to achieve the desired volume fraction. The knitted fabric is carefully trimmed to fit the 12-inch by 12-inch mold cavity and placed in the mold so that all edges have a tight press fit. This insures that there are no gaps for resin to escape around the fabric. A breather layer of porous Teflon-coated fiberglass is placed over the fabric to allow air to escape and to prevent excessive resin bleed. The upper caul plate is placed on top of the preform and the assembly is placed in a hydraulic press for resin infusion and curing. The required pressure is based upon compaction measurements conducted to establish volume fraction as a function of applied load on dry knitted fabric preforms. For the panels fabricated in this investigation, the fiber volume fractions were nominally 58 percent.

The pressure injection molding process shown in figure 9 was developed by Boeing Aerospace under contract to NASA Langley, and was used to mold the BP E905L knitted panels. This process involves resin flow in the plane of the fabric. As indicated in the figure, an O-ring is used to seal the mold to prevent resin leakage and air entrainment. The mold assembly is placed between two platens in a hydraulic press to close the mold and apply sufficient pressure to debulk the fabric and seat the O-ring. The mold cavity depth is sized to achieve a prescribed fabric thickness and fiber volume fraction. Resin enters the mold from a pressure pot and fills a channel around the perimeter of the fabric. Resin flows radially inward through the fabric to an exit port located in the center of the mold. A vacuum pump is attached to the exit port to remove excess air. Once the fabric preform is fully saturated and all the air is evacuated, the exit valve is closed and the prescribed cure cycle is followed. For the panels fabricated in this investigation, the fiber volume fractions were nominally 62 percent.

RESIN TRANSFER MOLDING METHODS

Vacuum Infusion

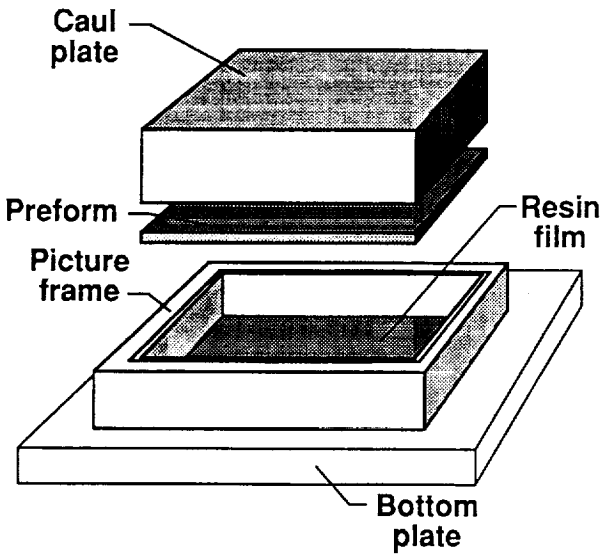

Pressure Injection

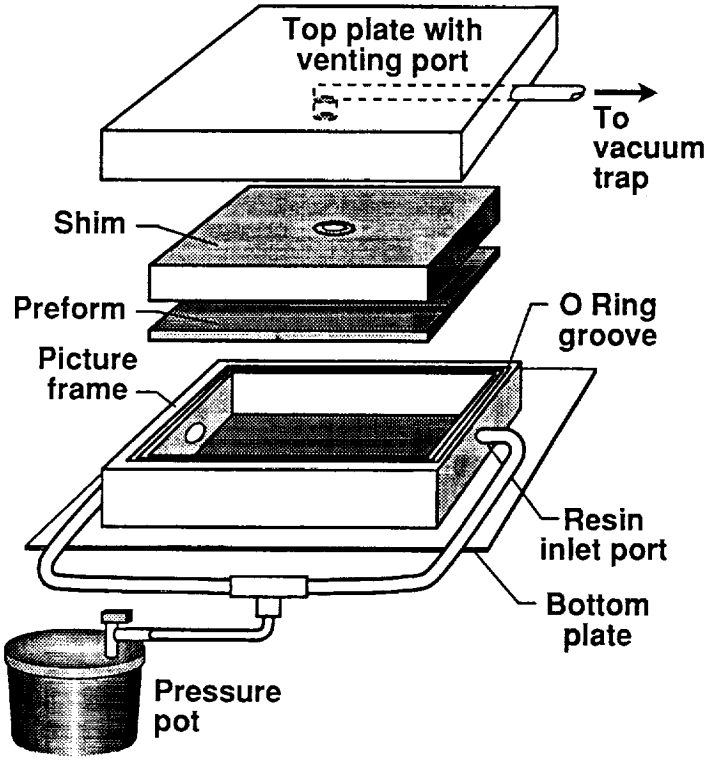

COMPACTION AND PERMEABILITY BEHAVIOR OF HEXCEL MULTIAXIAL WARP KNIT FABRIC

Compaction and permeability characteristics of the knitted fabrics were used as aids in developing infiltration and cure cycles. Compaction experiments were conducted to establish relationships between fiber volume fraction and compaction pressure. Test results for the 12K Hexcel knitted fabric are shown in figure 10. The results indicate that a pressure of approximately 50 psi is required to achieve a fiber volume fraction of 60 percent.

Also shown in figure 10 is the effect of fiber volume fraction on permeability. Permeability is a function of fabric architecture, compaction, porosity, and direction of resin flow. Test results are again presented for the 12K Hexcel knitted fabric. Note that for a given fiber volume fraction, the permeability for in-plane flow is much higher than for out-of-plane flow. These results indicate that flow along the in-plane fibers is much easier than flow through-the-thickness of the preform or across the fiber bundles. Results of other experiments indicate that through-the-thickness stitching can enhance out-of-plane flow, however, stitching may also inhibit resin flow in the plane of the fabric.

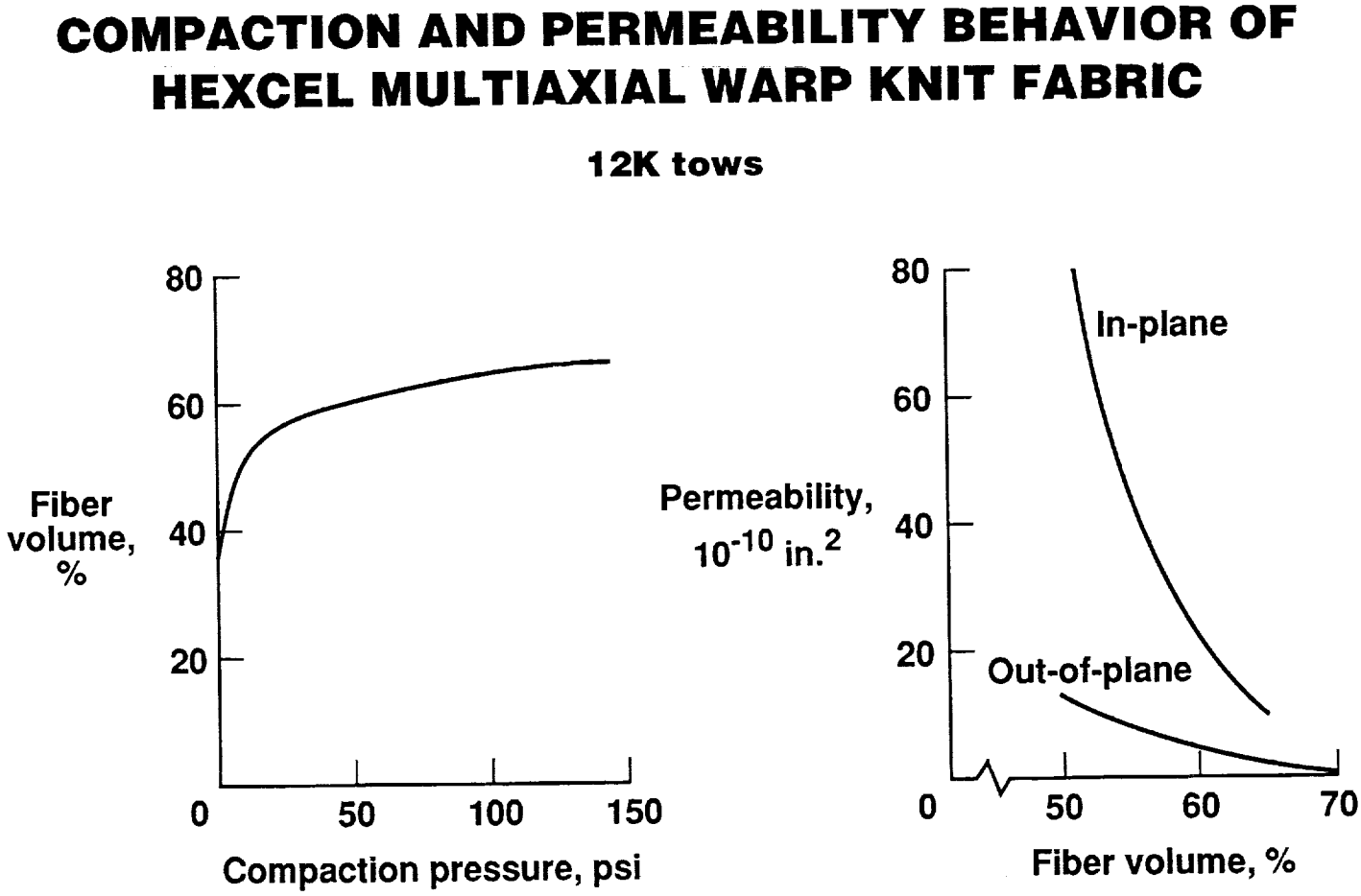

PHOTOMICROGRAPHS OF QUASI-ISOTROPIC LAMINATES

Cross-section photomicrographs of the Hexcel and Milliken knitted fabric composite laminates are shown in figure 11. For comparison purposes, a photomicrograph of a prepreg tape laminate is also shown. The Hexcel chain knitted laminate exhibited more out-of plane fiber crimp than would be expected for knitted fabrics. This can be explained by examining the photographs of the dry fabrics shown in figure 4, where significant gaps between tows of the Hexcel fabric was seen. Close examination of the Hexcel composite laminates indicated that the gaps in the fabric allowed adjacent tows to displace out-of-plane and fill the gaps during panel consolidation. As noted in figure 4, large gaps between the 0-degree surface tows were also evident for the Hexcel tricot knitted fabric. These gaps allow significant undulation in carbon fiber tows in adjacent plies, as shown in the figure.

As previously indicated in figure 4, the Milliken fabric had uniform gaps between all the tows to allow the knitting needles to pass through the fabric without damaging the carbon fibers. These gaps lead to numerous resin pockets in the composite laminate as shown in figure 11. However, these gaps do not appear to contribute to significant fiber undulations as were seen in the Hexcel laminates. Compared to the prepreg tape laminates, all the knitted fabrics have larger resin pockets and more fiber distortion.

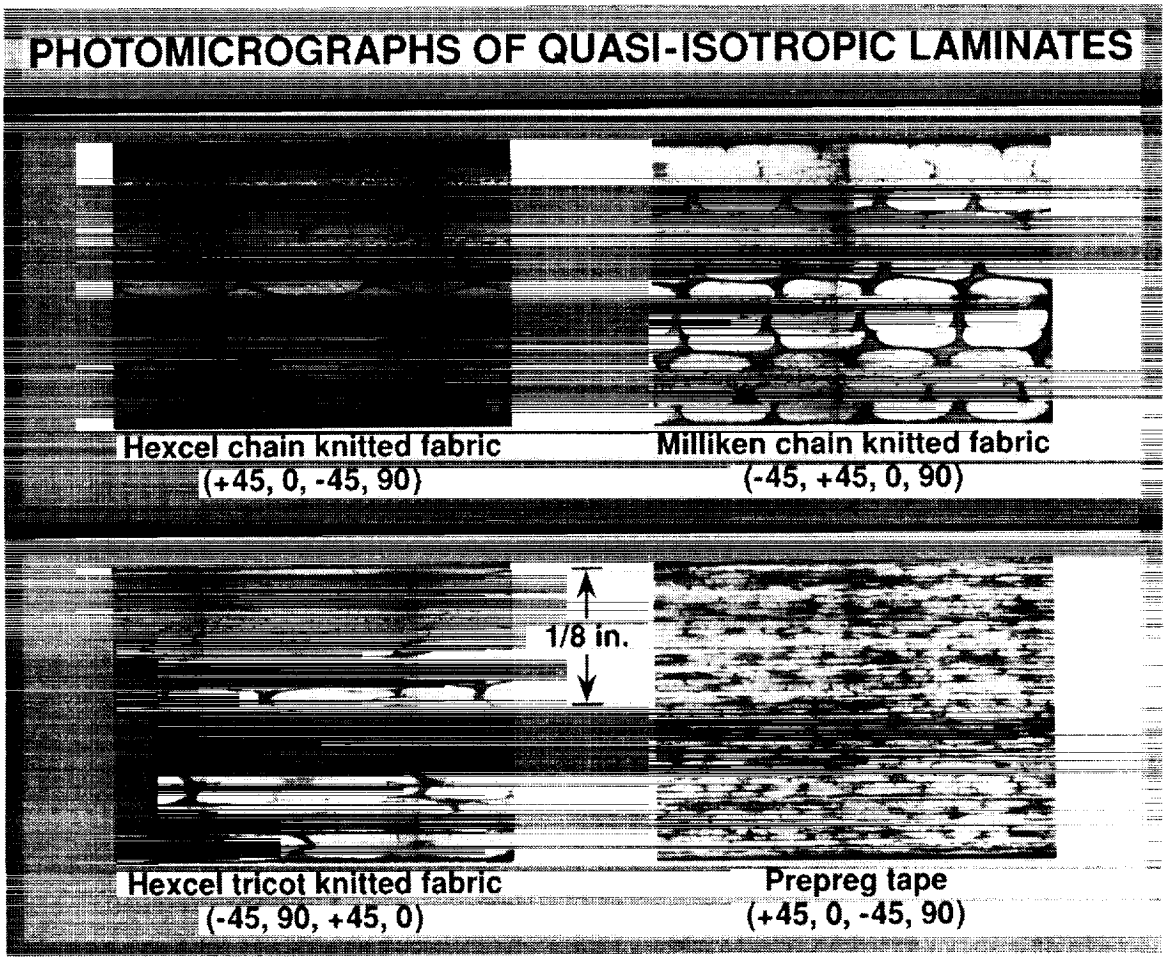

PHOTOMICROGRAPHS OF DOUGLAS WING SKIN LAYUP

Cross-section photomicrographs of uniweave, Saerbeck knitted, and Saerbeck knitted/stitched composite laminates are shown in figure 12. The uniweave fabric is the baseline fabric selected for the Douglas wing skin layup. The wing skin has a layup that consists of 44 percent 0-degree fibers, 44 percent ±45-degree fibers and 12 percent 90-degree fibers. The Saerbeck fabric is a potential alternate to the uniweave fabric. The Saerbeck fabric was knitted in a 4-ply stack to have the same areal weight (1305 g/m^2) as a 9-ply stack of the uniweave fabric. Fifty-four plies of uniweave fabric are required to fabricate the wing skin layup, whereas only six 4-ply stacks are required with the Saerbeck knitted fabric. To achieve the desired damage tolerance for the wing skin, through-the-thickness stitching with 1500 denier Kevlar thread is being investigated.

The photomicrographs shown in figure 12 indicate good fiber compaction. Some resin pockets are evident in the Saerbeck fabric laminate, however, the in-plane fibers have less undulation compared to the Hexcel fabric discussed in figure 11. The Saerbeck stitched fabric laminate shown in the lower part of figure 12 was infused with 3M PR 500 resin and no microcracks are evident around the Kevlar stitches. This resin has also been shown to be microcrack resistant in other stitched fabrics.

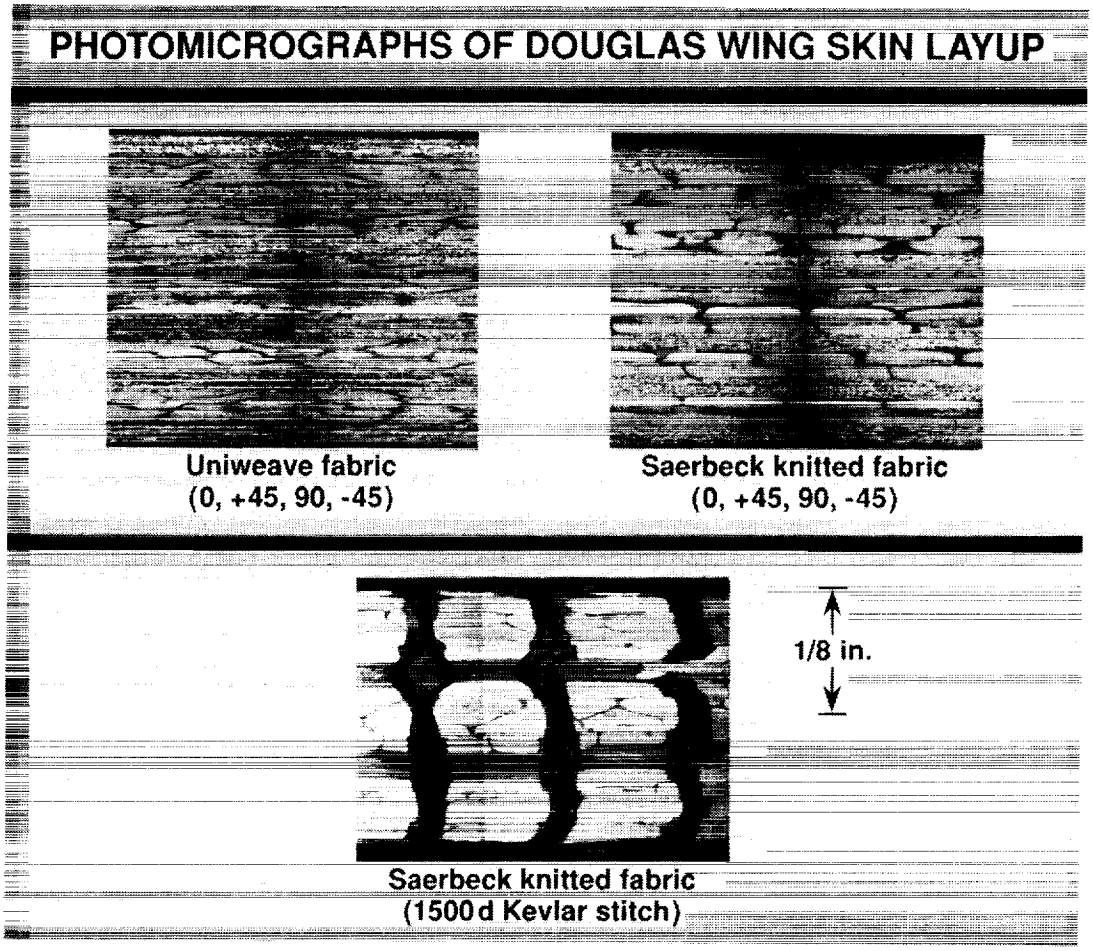

TEST SPECIMENS

The test specimens used in the NASA Langley in-house test program are shown in figure 13. The Hexcel and Milliken knitted fabric specimens have a nominal thickness of 0.25-inch whereas the Saerbeck knitted specimens have a nominal thickness of 0.30-inch. Specimen lengths and widths are indicated in the figure. The compression and tension specimens were instrumented with 0.125-inch long stacked strain gages, and the compression after impact, open hole tension, and open hole compression specimens were instrumented with 0.250-inch long axial strain gages. The compression after impact specimens were impacted at a nominal impact energy of 30 ft-lbs with the NASA Langley air gun using a 0.500-inch diameter aluminum sphere as the impactor. A 0.250-inch diameter hole was drilled in the center of the open hole tension and open hole compression specimens. Most of the tension specimens were tested without loading tabs, however, fiberglass tabs were required for the specimens fabricated with the Douglas wing lay-up. The test apparatus and loading rates described in reference 1 were also used in this investigation.

TEST SPECIMENS

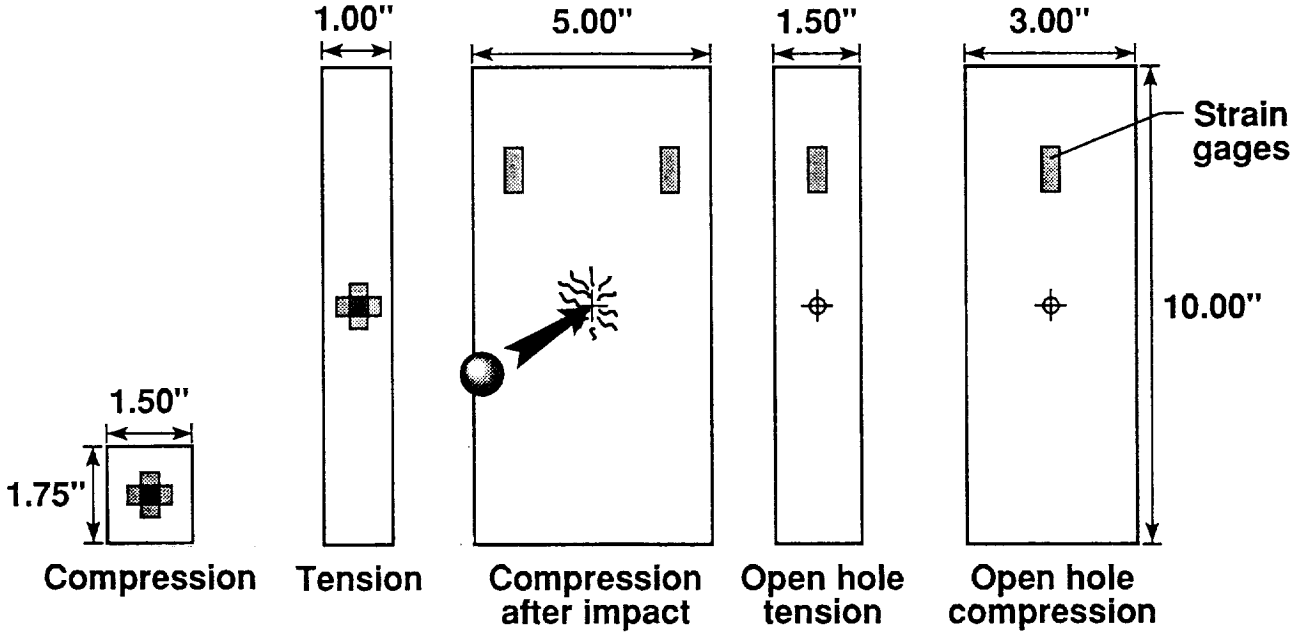

COMPRESSION STRENGTH VARIABILITY FOR MULTIAXIAL WARP KNIT COMPOSITES

Excessive data scatter was evident for the Hexcel knitted fabric laminates early in the mechanical property test program. Fabrication and testing continued and additional fabric was ordered with the expectation that a higher quality fabric could be produced. Compression strength results for 135 tests from 17 panels fabricated with both E905L and PR 500 resin systems are plotted in figure 14 for Hexcel, Milliken, and Saerbeck knitted fabrics. The results indicate excessive strength scatter in the Hexcel fabric panels, especially in the 3K panels. Compression strengths ranging from 48 ksi to 85 ksi were achieved. The Milliken laminates, in particular the panel with 8 replicates, also indicated excessive strength scatter. Although only two Saerbeck knitted fabric panels were tested, the strength scatter is much less. It should be noted that the Saerbeck fabric has the highest strength because it has a higher percentage of 0-degree fibers compared to the Hexcel and Milliken fabrics.

These results indicate that additional process controls must be instituted to achieve higher quality knitted fabrics. The Saerbeck machine, which was also produced by Liba in Germany, is a third generation machine compared to the Hexcel machine, and improved tension control mechanisms could possibly account for the reduced compression strength scatter for the Saerbeck fabric.

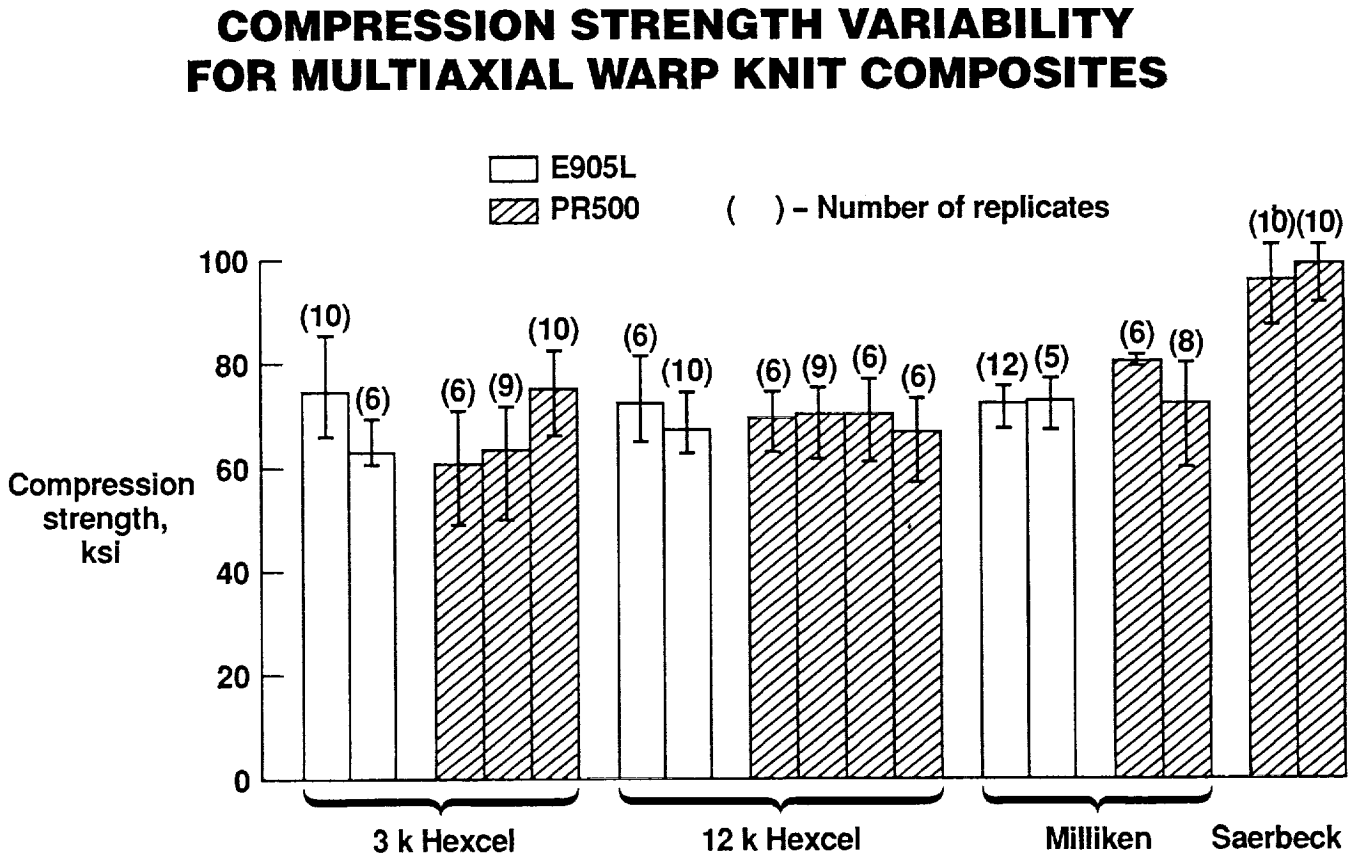

TENSION STRENGTH OF KNITTED FABRIC COMPOSITES

Average tension strengths for the Hexcel and Milliken fabric laminates are shown in figure 15. Test results are shown for E905L and PR 500 resin systems for the various fiber orientations and tow sizes indicated in the figure, and are compared to results of prepreg tape laminates fabricated with Hercules 3501-6 resin. The average tension strength of the Hexcel knitted fabrics is about 15 percent lower than the strength of the prepreg tape laminates. There is no appreciable difference in strength between the Hexcel knitted laminates fabricated with 3, 6, or 12K tows. These results are important because significant labor savings can be achieved through reduced machine running time and laminate layup time. For example, a 1/4-inch thick laminate requires eight 4-ply stacks of 3K tow fabric, whereas only four 4-ply stacks are required with 12K tows.

Average tension strengths for the Milliken fabric laminate specimens are about 30 percent lower than the strength of the prepreg tape laminate. Part of this additional strength decrease compared to the Hexcel fabric can be attributed to the gaps between the tows and the lower fiber volume fraction of the Milliken fabric. Additional Milliken laminates will be fabricated and tested to achieve a larger data base for comparison with the Hexcel knitted fabric laminates.

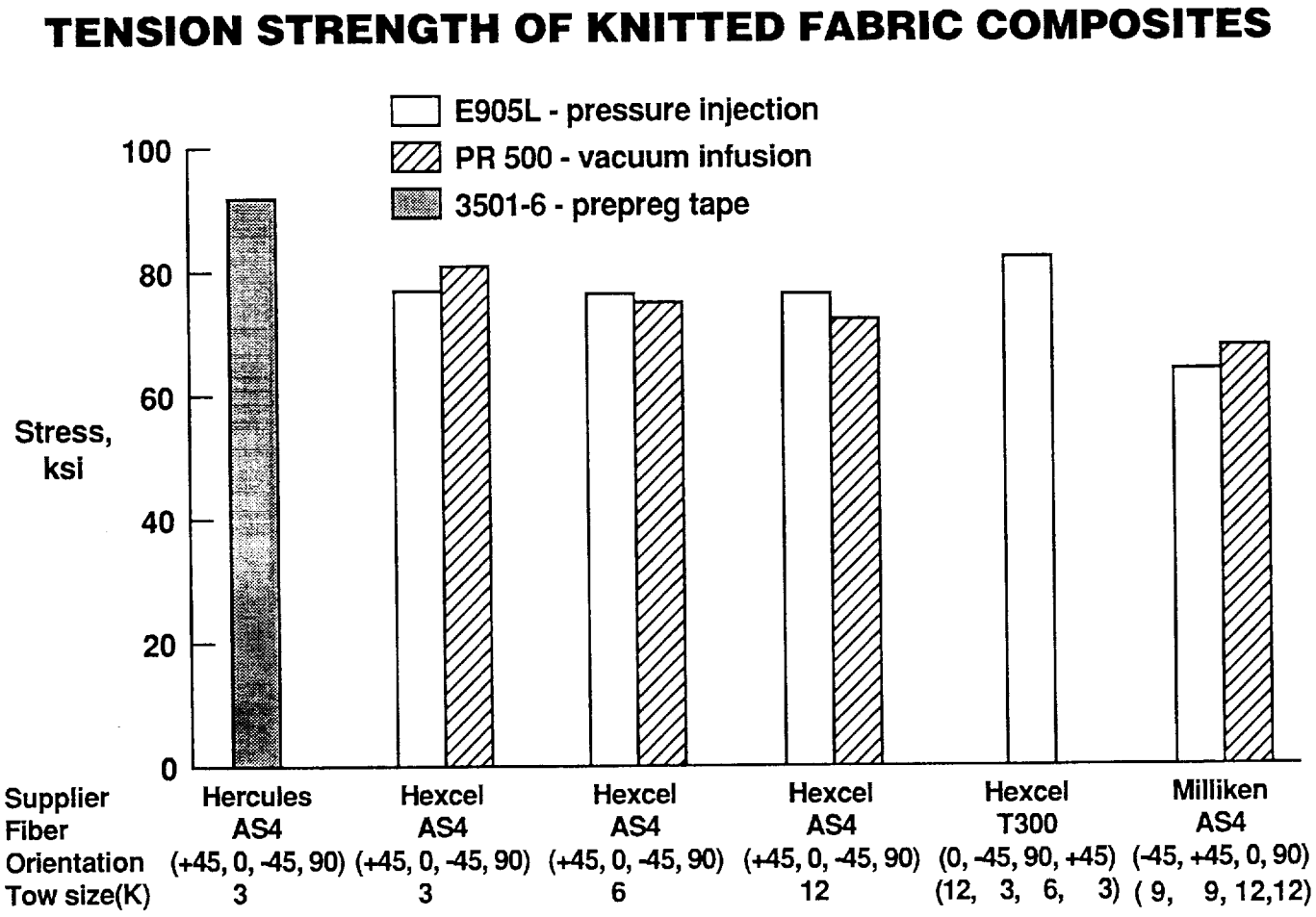

TENSION MODULUS OF KNITTED FABRIC COMPOSITES

Average tension moduli for the Hexcel and Milliken fabric laminates are shown in figure 16. Test results are compared for E905L and PR 500 resin systems for the various fiber orientations and tow sizes indicated in the figure, and again are compared to prepreg tape laminates fabricated with Hercules 3501-6 resin. The tension moduli for all the E905L laminates are slightly higher than the modulus for the prepreg tape laminates, whereas the tension moduli for the PR 500 laminates are slightly lower. These variations are attributed to fiber volume fraction variations. Nominal fiber volume fractions for the three materials are as follows: E905L knitted fabric - 62 percent, PR 500 knitted fabric - 58 percent, and 3501-6 prepreg tape - 60 percent. As was noted in the tension strength results, no significant differences in moduli were observed between 3, 6, or 12K tows of the Hexcel knitted fabric laminates.

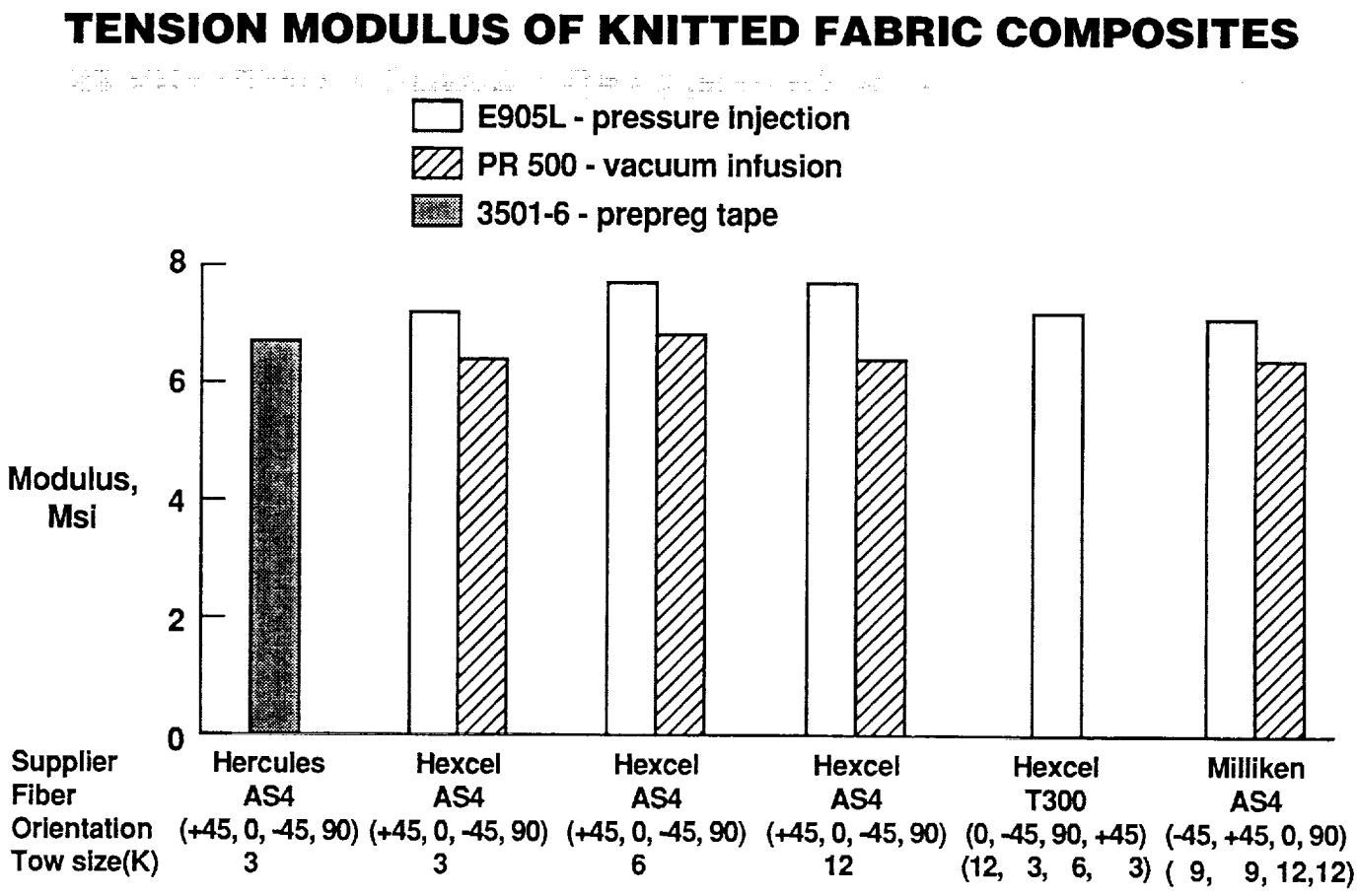

OPEN HOLE TENSION STRENGTH OF KNITTED FABRIC COMPOSITES

The effects of a 1/4-inch diameter hole on the tension strength of the Hexcel and Milliken knitted fabric laminates are shown in figure 17. The average strength for all the knitted fabric laminates is approximately 50 ksi. The open hole tension strength for the prepreg tape material is slightly below 50 ksi, although similar data reported in Hercules product literature indicates that the open hole tension strength of 3501-6 prepreg tape is 50 ksi. Hence, based on these results, knitted fabric laminates and prepreg laminates have similar open hole tension strengths and they meet the Boeing Material Specification BMS 8-276 target value of 50 ksi.

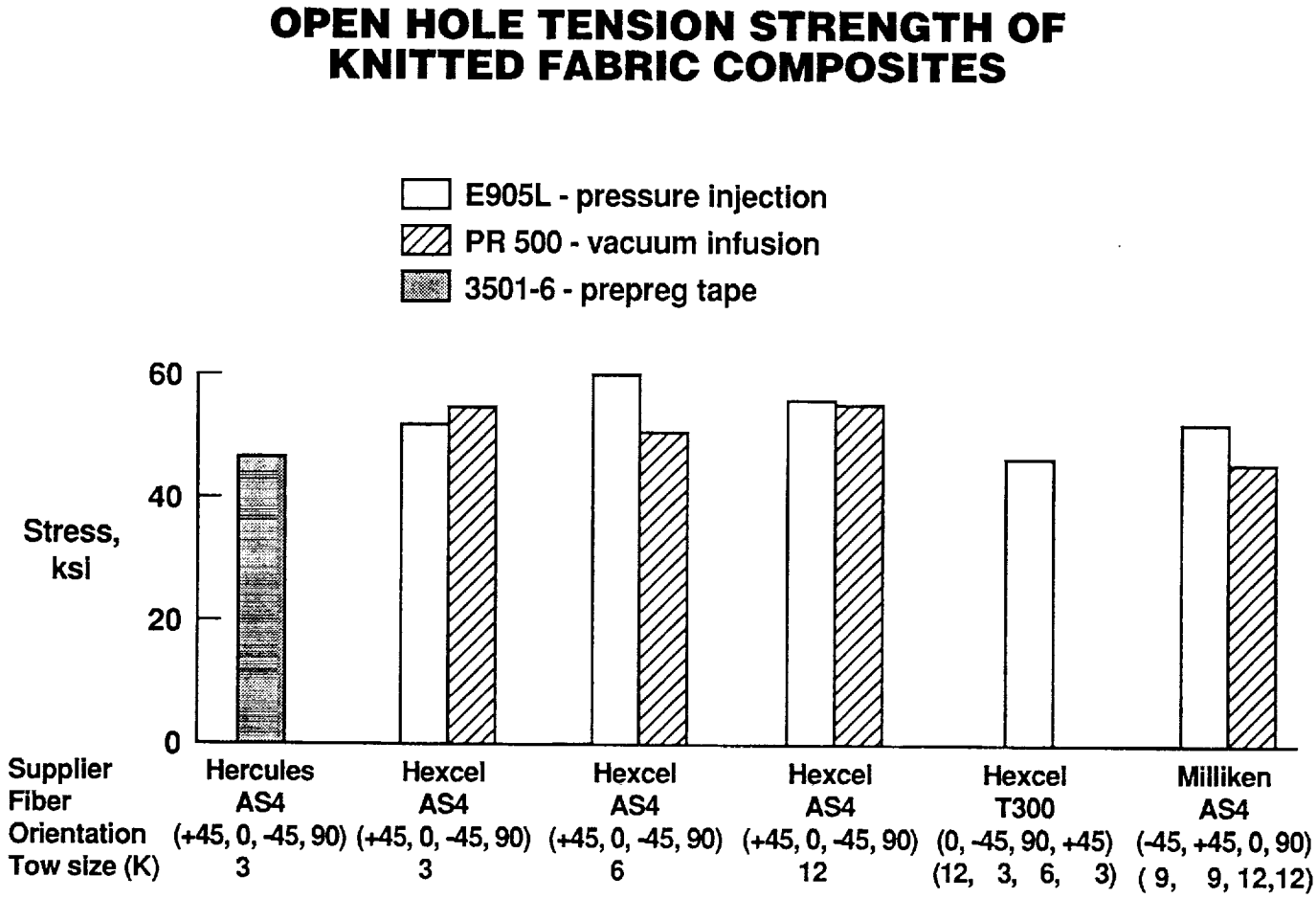

COMPRESSION STRENGTH OF KNITTED FABRIC COMPOSITES

The compression strengths of the Hexcel and Milliken knitted fabric laminates are compared with the strength of prepreg tape laminates in figure 18. Results indicate that the average compression strength for the Hexcel knitted fabric laminates is about 25 percent lower than the strength for the prepreg tape laminates. The Milliken knitted fabric laminates indicate a 20 percent reduction in compression strength compared to the prepeg tape laminates. These reductions in strength are partially attributed to fiber waviness caused by gaps in the knitted fabrics. Photomicrographic studies, shown earlier in figure 11, indicated that the carbon fiber tows tend to deflect out-of-plane to fill gaps in adjacent layers. As with the tension results, no significant differences in compression strength were indicated between 3, 6, or 12K tows for the Hexcel knitted fabric laminates, or between the two resin systems used in either knitted laminate.

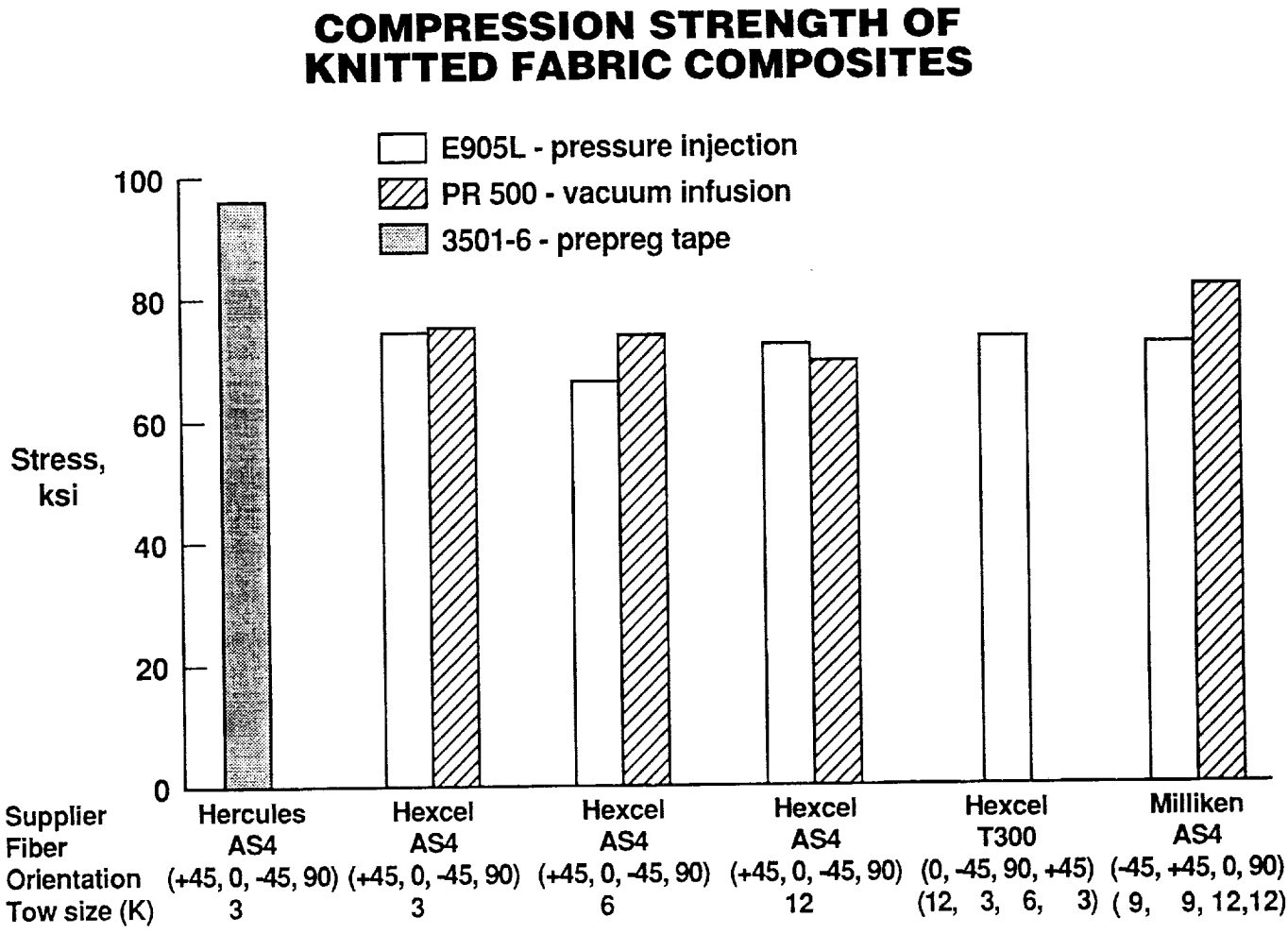

COMPRESSION MODULUS OF KNITTED FABRIC COMPOSITES

Average compression moduli for the Hexcel and Milliken fabric laminates are compared with the modulus of prepreg tape laminates in figure 19. The average compression moduli for the knitted fabric laminates with E905L resin are similar to the modulus achieved for the 3501-6 prepreg tape. The moduli for the knitted fabric laminates with PR 500 resin are about 15 percent lower than these values. As mentioned previously, the knitted fabric laminates with PR 500 resin had a lower fiber volume fraction compared to the knitted fabric laminates with E905L resin. However, this difference in fiber volume fraction would not account for a 15 percent reduction in modulus.

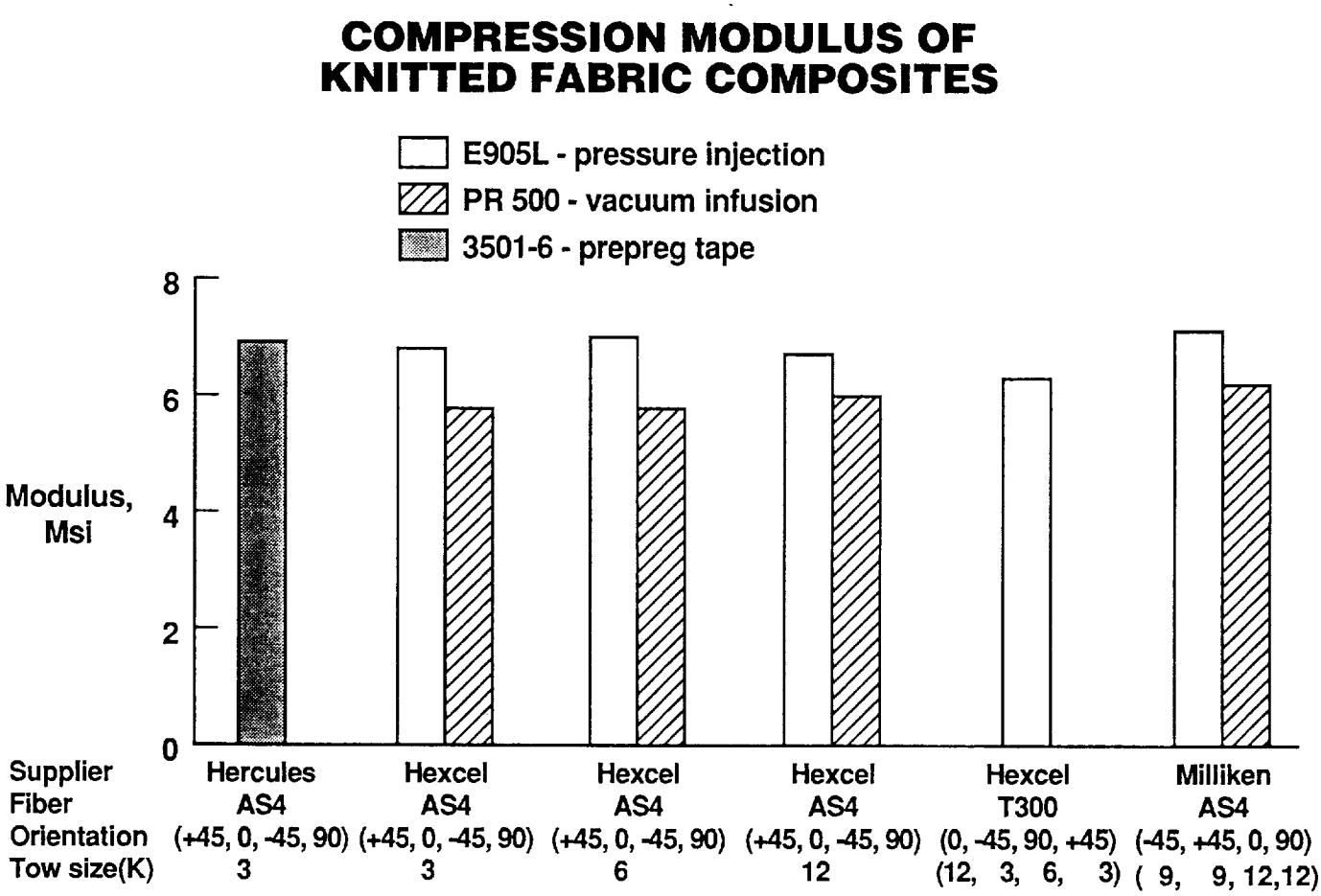

OPEN HOLE COMPRESSION STRENGTH OF KNITTED FABRIC COMPOSITES

The effects of a 1/4-inch diameter hole on the compression strength of the Hexcel and Milliken knitted fabric laminates are shown in figure 20. The results indicate similar performance for the knitted fabric laminates and the prepreg tape laminates. In addition, these results compare favorably with the Hercules product literature value of 45 ksi and the Boeing Material Specification BMS 8-276 target value of 42.5 ksi.

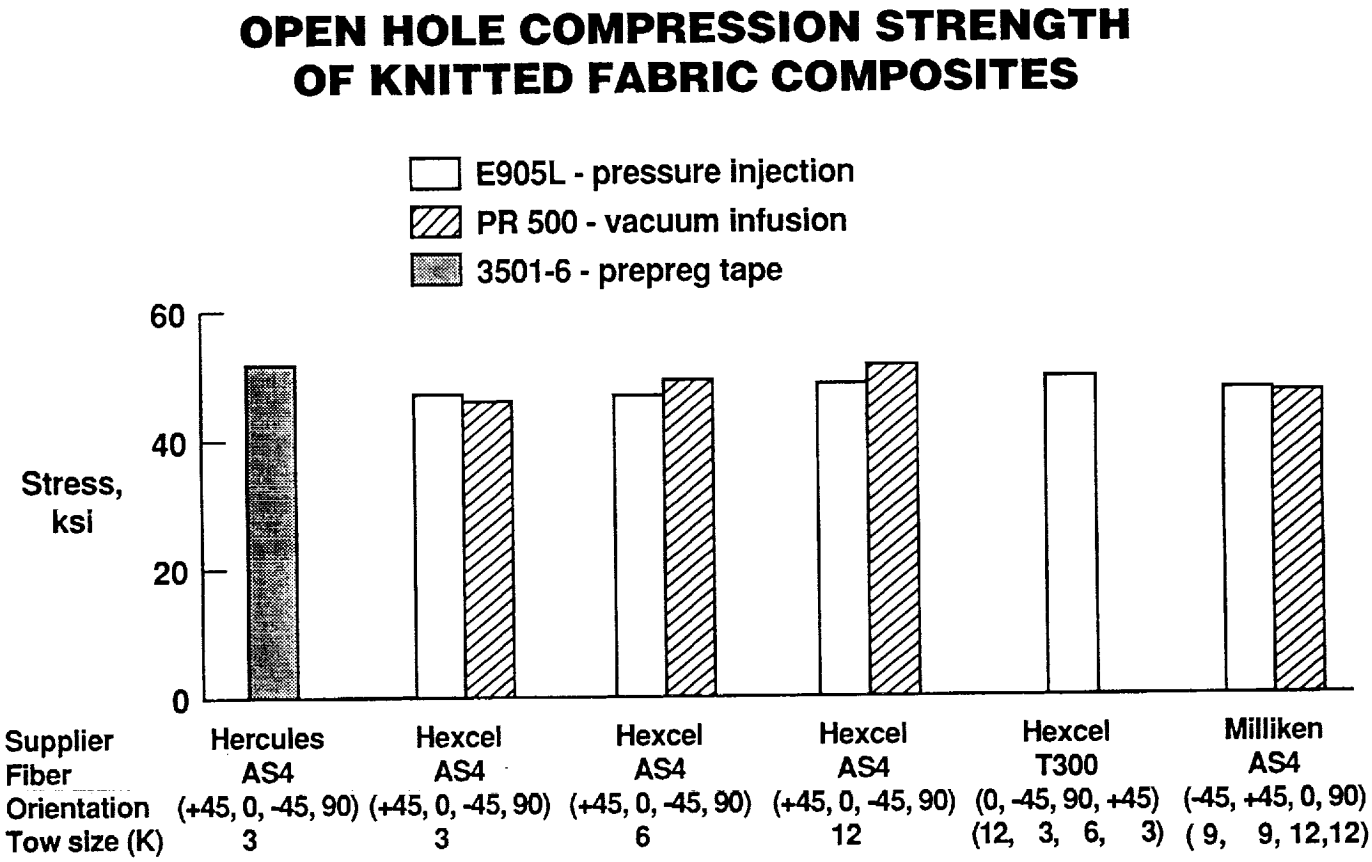

COMPRESSION AFTER IMPACT STRENGTH OF KNITTED FABRIC COMPOSITES

Compression after impact (CAI) strength tests were conducted to compare the damage tolerance of knitted fabric laminates with conventional prepreg tape laminates. The 1/4-inch thick laminates were impacted with 1/2-inch diameter aluminum spheres at an impact energy of 30 ft-lbs with the NASA Langley air gun. The test results shown in figure 21 indicate that the knitted fabric laminates that were resin transfer molded with the toughened PR 500 resin had CAI strengths up to 50 percent higher than the brittle 3501-6 prepreg tape laminates. The knitted fabric laminates with E905L resin had CAI strengths that were up to 30 percent higher than the prepreg tape laminates. These results indicate significant improvements in damage tolerance for the knitted fabric laminates. However, they still fall well below the target of 40 ksi. Additional through-the-thickness reinforcement such as heavy density stitching is required to achieve the target value.

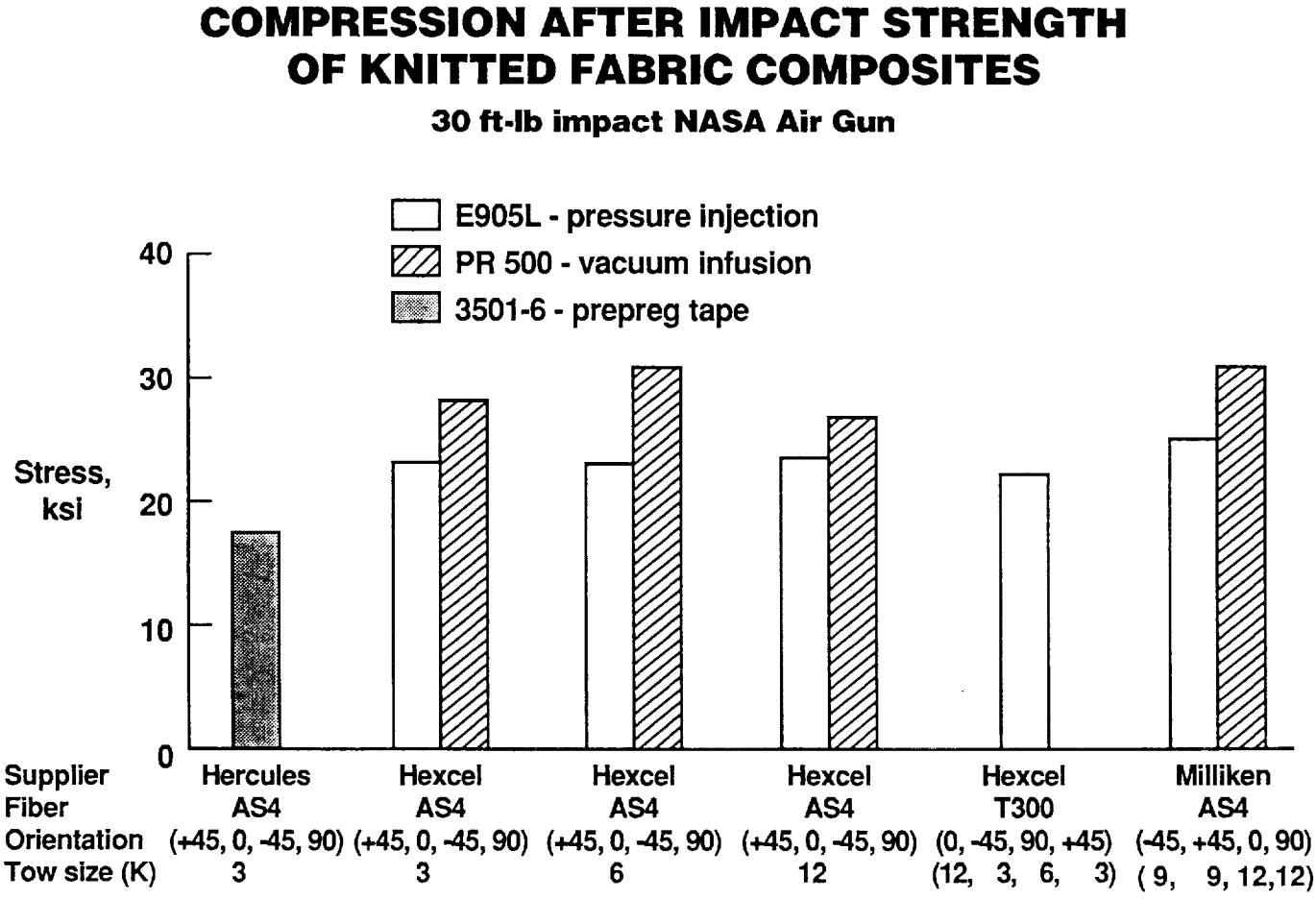

COMPRESSION AFTER IMPACT STRENGTH OF KNITTED/STITCHED FABRIC COMPOSITES

Compression after impact strength tests were also conducted to determine the effect of stitching on the strength of knitted fabric laminates, figure 22. The Hexcel preforms that were knitted with 3K and 12K tows were stitched by Ketema with a modified lock stitch. The preforms were stitched in the 0-degree direction in columns 0.33-inch apart with a stitch pitch of 1/8-inch. The Milliken preforms were stitched by Puritan Industries with a chain stitch. The panels were chain stitched in the 0-degree and 90-degree directions with rows and columns 1/4-inch apart with a stitch pitch of 1/8-inch. All the preforms were stitched with a 1500 denier Kevlar thread.

The panels were impacted at an energy level of 30 ft-lbs with the same procedure described earlier. The Milliken knitted/stitched fabric laminates with the PR 500 resin system achieved the target of 40 ksi CAI strength. The Hexcel knitted/stitched laminates fell below the target. The toughened PR 500 resin system exhibited consistently higher CAI strengths than the E905L, as was noted in the unstitched results. Results of a previous stitching study, reference 2, indicated strengths over 45 ksi with stitched uniweave fabric laminates when a stitch spacing of 3/16-inch was used. Based on those findings, it is expected that the Hexcel fabric laminates would achieve the target value if the stitch spacing were reduced to no more than 3/16-inch.

COMPRESSION AFTER IMPACT STRENGTH OF KNITTED/STITCHED FABRIC COMPOSITES

30 ft-lb impact NASA Air Gun

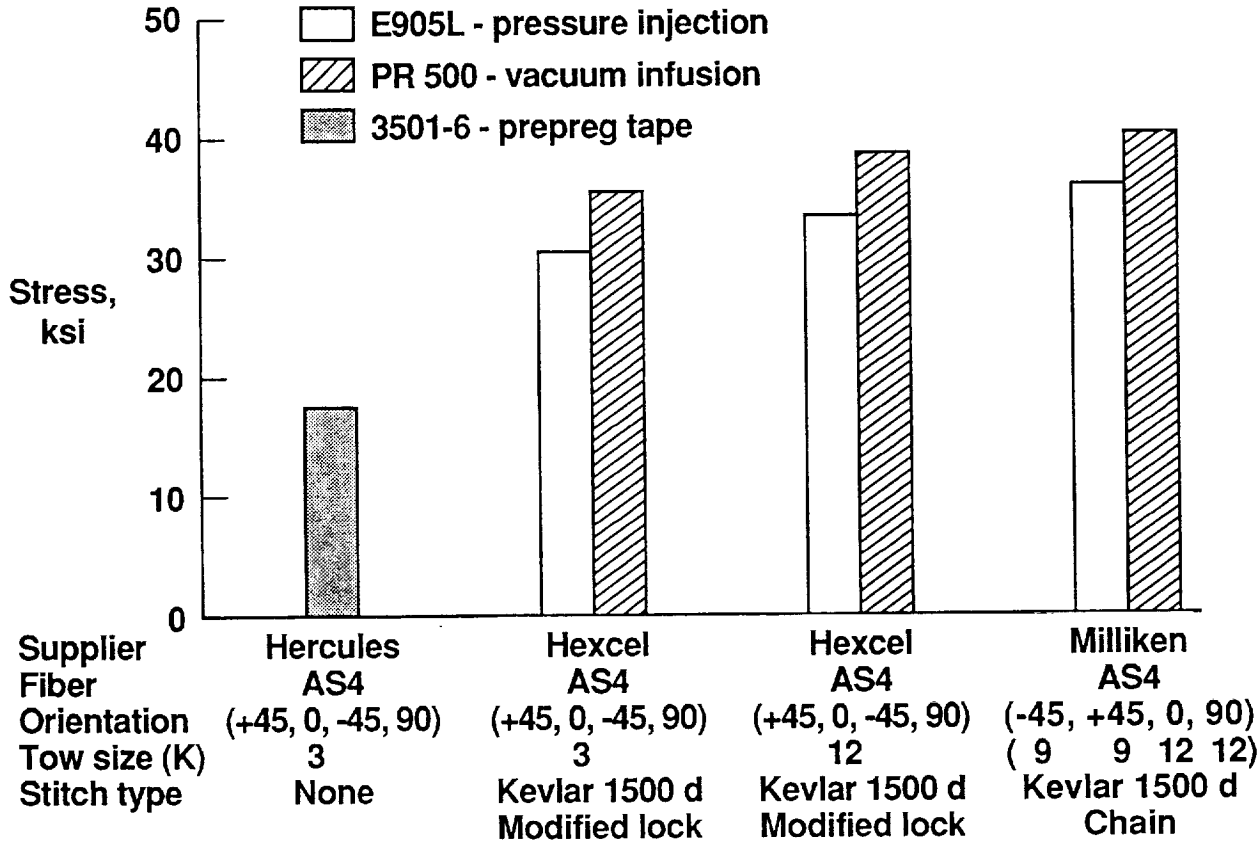

Supplier	Hercules	Hexcel	Hexcel	Milliken
Fiber	AS4	AS4	AS4	AS4
Orientation	(+45, 0, -45, 90)	(+45, 0, -45, 90)	(+45, 0, -45, 90)	(-45, +45, 0, 90)
Tow size (K)	3	3	12	(9 9 12 12)
Stitch type	None	Kevlar 1500 d Modified lock	Kevlar 1500 d Modified lock	Kevlar 1500 d Chain

PERFORMANCE COMPARISON OF AS4/PR 500 SAERBECK KNITTED AND UNIWEAVE FABRIC COMPOSITES

Douglas Aircraft Company and NASA Langley have been developing a data base on uniweave fabrics for application to wing structural components. The Douglas design for the wing skin material consists of 54 plies of uniweave fabric with 44 percent of the fibers in the 0-degree direction, 44 percent of the fibers in the ±45-degree directions, and 12 percent of the fibers in the 90-degree direction. Concerns for stability and handleability of the uniweave fabric led Douglas to investigate other fabric options. A knitted fabric produced by Saerbeck in Germany was selected. A description of the fabric was presented in figure 2. The test results presented in figure 23 were developed at NASA Langley in a cooperative effort with Douglas. It should be noted that the test results are preliminary and additional tests are planned to expand the data base.

Tension, compression, open hole tension, open hole compression, and CAI tests were conducted to compare the performance of the knitted and uniweave fabric laminates. All of the fabrics were resin transfer molded with the 3M PR 500 resin except the stitched uniweave CAI panel which was fabricated with Hercules 3501-6 resin. Also, the uniweave panel was stitched with S-2 glass whereas the Saerbeck panel was stitched with Kevlar. The stitched uniweave panel was impacted at an energy level of 40 ft-lbs with a drop weight apparatus. The other panels were impacted at an energy level of 30 ft-lbs with the air gun previously described. Test results shown in figure 23 indicate comparable performance between the two fabrics. Both fabrics meet the design requirements for the Douglas wing skin. It should be noted that the Saerbeck knitted fabric consisted of six 4-ply stacks whereas the uniweave fabric consisted of 54 plies to build up the required thickness of 0.30-inch. This difference has important cost implications and will be discussed in a subsequent figure.

PERFORMANCE COMPARISON OF AS4/PR 500 SAERBECK KNITTED AND UNIWEAVE FABRIC COMPOSITES

Douglas ACT wing layup (0, +45, 90, -45)
[44% 0°, 44% ±45°, 12% 90°]

Tension strength/modulus

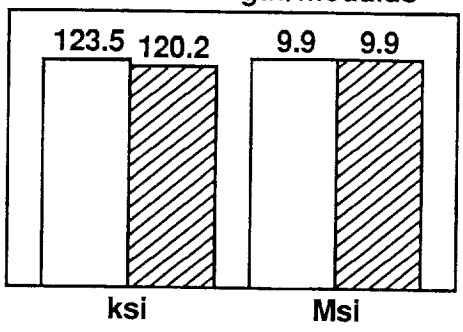

Open hole ten./open hole comp. strength

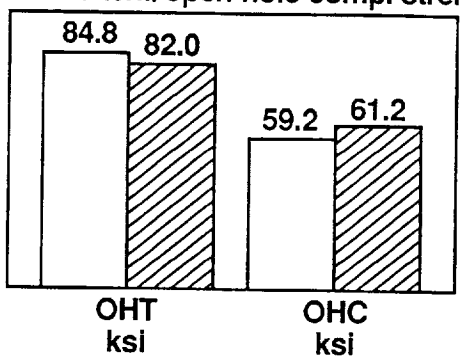

Uniweave (3k)

Saerbeck knitted (12k – 0°, 6k – ±45°, 3k – 90°)

Compression strength/modulus

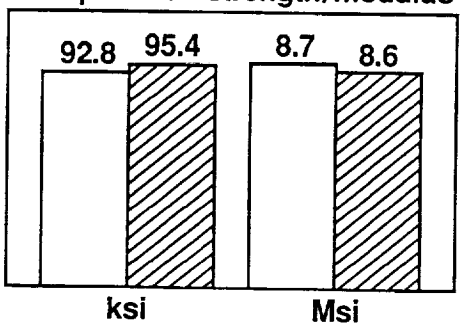

Compression after impact strength
30 ft-lbs impact

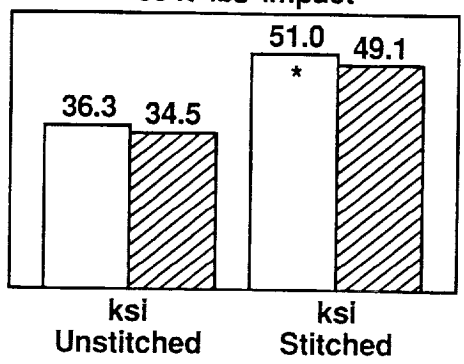

* - RTM with 3501-6 resin
- Stitched with S-2 glass
- Impact 40 ft-lbs drop wt.

ESTIMATED LABOR/MATERIAL COST FOR STITCHED CARBON FIBER PREFORMS

Estimated labor and material costs were projected by Douglas Aircraft Company for two different carbon fiber preforms with the same wing skin layup. The preform was assumed to be 8-feet wide by 60-feet long by 0.30-inch thick with a layup consisting of 44 percent fibers in the 0-degree direction, 44 percent of the fibers in the ±45-degree directions, and 12 percent of the fibers in the 90-degree direction. The baseline used for these estimates is the 3K uniweave fabric that is currently being used by Douglas in their wing skin development. Fifty-four plies of the uniweave fabric are required to produce the 0.30-inch thick preform. The preform is produced by lightly stitching 9-ply stacks of fabric with a multineedle machine and subsequently stitching six of the 9-ply stacks together with a heavy-duty single needle machine.

An alternate approach consisted of using the Saerbeck knitted fabric. This fabric consisted of a 4-ply stack that was equivalent in properties and areal weight to the 9-ply stack of uniweave fabric. Six stacks of the Saerbeck fabric were required to produce the 0.30-inch thick preform. The six stacks of Saerbeck fabric were stitched together with the single needle machine. The uniweave and Saerbeck fabrics are currently available in 50-inch widths. The cost analysis results presented in figure 24 are based on weaving and knitting machine developments required to produce 100-inch wide fabrics.

The cost analysis indicates that the Saerbeck knitted preform material cost will be 35 percent lower than the uniweave cost and the labor cost for the Saerbeck knitted preform will be 40 percent less. The material cost savings is due to the high speed, multilayer knitting processes compared to the slower single layer weaving processes. The labor cost savings are attributed to elimination of the stacking required for the 9-ply uniweave elements plus the elimination of the multineedle stitching operation. These results, along with the performance results shown in figure 23, indicate that knitted fabrics are excellent candidates for the Douglas wing skin material. A scale-up in equipment and on-line process controls are required to meet the long term needs for airframe production.

ESTIMATED LABOR/MATERIAL COST FOR STITCHED CARBON FIBER PREFORMS

8 ft wide x 60 ft long x 0.30-in. thick
[44% 0°, 44% ±45°, 12% 90°]

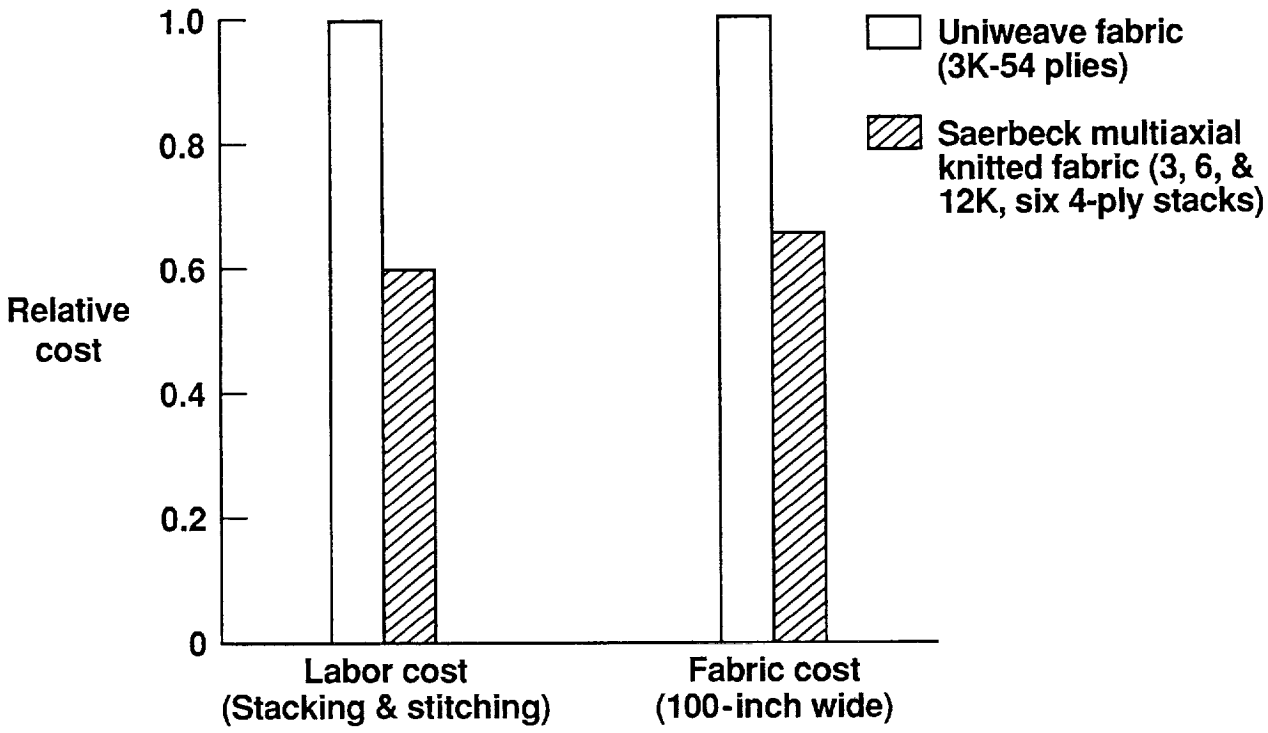

CONCLUDING REMARKS

Three relatively new multiaxial warp knitting processes were evaluated to establish their potential to produce aerospace quality fabrics for composite structural applications. Quasi-isotropic knitted fabrics were produced by Hexcel and Milliken and a knitted fabric with the Douglas Aircraft Company wing skin layup was produced by Saerbeck in Germany. All of the fabrics were fabricated into composite test panels using the resin transfer molding process. Two new resin systems, British Petroleum E905L and 3M PR 500, were selected for the processing studies. Compaction and permeability studies were conducted on the dry fabric preforms to aid in development of infiltration and cure cycles. Viscosity profiles and cure cycles for both resin systems were developed to insure high quality composite test laminates. Low void content laminates were produced with the PR 500 resin in a vacuum infusion process and with the E905L resin in a pressure injection process. Prepreg tape laminates with AS4/3501-6 graphite/epoxy were used as a baseline to compare the performance of the knitted laminates.

Tension, compression, open hole tension, open hole compression, and CAI tests were conducted to compare material performance. In addition, some dry preforms were stitched with 1500 denier Kevlar thread to evaluate the effects of stitching on damage tolerance. The mechanical performance of the Hexcel and Milliken fabric laminates was compared to quasi-isotropic prepreg tape laminates and the performance of the Saerbeck fabric laminates was compared to uniweave laminates with the Douglas wing skin layup. Compared to prepreg tape laminates, the Hexcel and Milliken knitted fabric laminates had tension and compression strengths that were up to 30 percent lower. The open hole tension and compression strengths were similar to the prepreg tape laminates. However, the CAI strengths of the knitted fabric laminates were up to 50 percent higher than the CAI strength of the prepreg tape laminates. The addition of stitching increased the CAI strength of the knitted fabric laminates near the target value of 40 ksi. A limited data base was generated for the Saerbeck knitted fabric and the performance was comparable with the performance of uniweave fabric in all the tests conducted.

Excessive data scatter was evident for the Hexcel and Milliken fabric laminates. Contributing factors to the scatter include misaligned fibers and large gaps between tows. To achieve aerospace quality fabrics, the Hexcel and Milliken knitting processes must incorporate stringent on-line process controls that will control fiber tension, alignment, and gaps between tows. The overall quality of the Saerbeck fabric was superior to the Hexcel fabric, mostly in the areas of fiber alignment and reduced gaps.

Preliminary cost analyses conducted by Douglas Aircraft Company indicate that the Saerbeck knitted fabric can save 35 to 40 percent in material and labor costs for fabrication of wing skin preforms. The results of this investigation indicate that multiaxial warp knit fabrics can be used to produce high quality resin transfer molded composites for aircraft structural applications. Significant cost savings are possible compared to conventional unidirectional and bidirectional woven fabrics.

REFERENCES

1. Dexter, H. Benson, Hasko, Gregory H., and Cano, Roberto J: Characterization of Multiaxial Warp Knit Composites, First NASA Advanced Composites Technology Conference, Seattle, Washington, October 29-November 1, 1990, NASA Conference Publication 3104, Part 2, pp. 589-619.

2. Palmer, Raymond J., Dow, Marvin B., and Smith, Donald J: Development of Stitching Reinforcement for Transport Wing Panels, First NASA Advanced Composites Technology Conference, Seattle, Washington, October 29-November 1, 1990, NASA Conference Publication 3104, Part 2, pp 621-646.

Experimental and Analytical Characterization of Triaxially Braided Textile Composites

John E. Masters
Lockheed Engineering and Science

Mark J. Fedro
Boeing Defense and Space Group

Peter G. Ifju
Virginia Polytechnic Institute

OUTLINE:

- DEFINITION OF MATERIAL
- EXPERIMENTAL RESULTS
- ANALYTICAL RESULTS
- SUMMARY

There were two components, experimental and analytical, to this investigation of triaxially braided textile composite materials. The experimental portion of the study centered on measuring the materials' longitudinal and transverse tensile moduli, Poisson's ratio, and strengths. The identification of the damage mechanisms exhibited by these materials was also a prime objective of the experimental investigation. The analytical portion of the investigation utilized the Textile Composites Analysis (TECA) model to predict modulus and strength. The analytical and experimental results were compared to assess the effectiveness of the analysis.

The figures contained in this paper reflect the presentation made at the conference. They may be divided into four sections, as the outline listed above illustrates. A definition of the material system tested is contained in the next two figures. This is followed by a series of figures summarizing the experimental results. These figures contain results of a Moire interferometry study of the strain distribution in the material, examples and descriptions of the types of damage encountered in these materials, and a summary of the measured properties. A description of the TECA model follows the experimental results. This includes a series of predicted results and a comparison with measured values. Finally, a brief summary completes the paper.

TRIAXIAL BRAID PATTERN

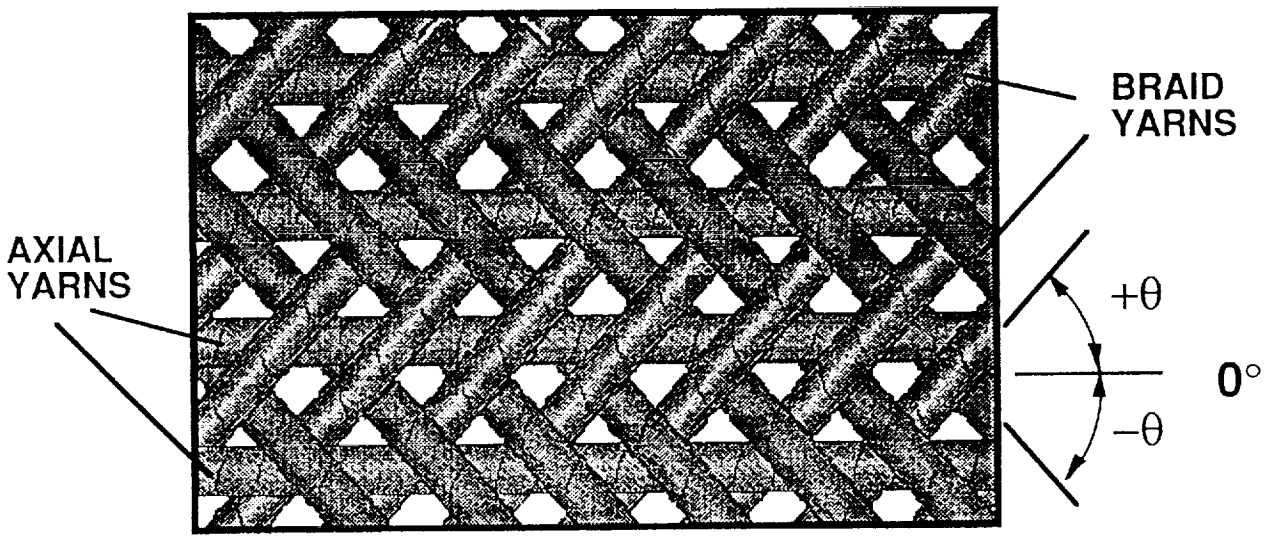

The specimens studied in this investigation featured 2-D triaxially braided AS4 graphite fiber preform impregnated with Shell 1895 epoxy resin. In a triaxially braided preform three yarns are intertwined to form a single layer of 0/±Θ material. In this case, the braided yarns are intertwined in a 2X2 pattern. Each +Θ yarn crosses alternately over and under two -Θ yarns and vice versa. The 0° yarns were inserted between the braided yarns. This yields a two dimensional material; there are no through-the-thickness fibers.

The yarns were braided over a cylindrical mandrel to a nominal thickness of .125 in. The desired preform thickness was achieved by overbraiding layers. After braiding, the preforms were removed from the mandrel, slit along the 0° fiber direction, flattened and border stitched to minimize fiber shifting. The resin was introduced via a resin transfer molding process.

TRIAXIAL BRAID CONFIGURATIONS

MATERIAL	BRAID PATTERN	BRAIDER YARN SIZE (K)	0° YARN SIZE (K)	PERCENT 0° YARNS (%)	0° YARN SPACING (YARN/IN.)	BRAID YARN SPACING (YARN/IN.)
A1	0/± 63°	12K	24K	31.5	4.17	9.16
B1	0/±66.5°	6K	18K	37.6	4.77	11.98
B2	0/±70°	6K	18K	34.0	4.37	12.74

Three preform parameters, braid angle, yarn size, and 0° yarn content, were varied in this study. The last parameter listed is typically expressed as a percentage of 0° yarns. It is the volumetric proportion of longitudinal yarns to total yarn content and is a function of braid angle and yarn size. Yarn size is expressed in terms of the number of filaments per yarn. The AS4 yarns used in these materials have a nominal diameter of 7 microns. The longitudinal yarns were larger than the braided yarns in all cases. The B1 and B2 architectures had the same yarn sizes; they differed in braid angle and 0° yarn content. The preform parameters are listed in the table.

The fabrics were formed with a 144 carrier New England Butt triaxial braider, incorporating 72 longitudinal yarns. The mandrel diameters varied for each architecture. Since the number of carriers was constant, this had the effect of changing the yarn spacing. These parameters are also listed in the table.

The increased 0° yarn content, increased 0° yarn spacing, and decreased braid angle of the B1 architecture compared to the B2 architecture are of note. These factors, cumulatively, may aid in interpreting the experimental results.

MOIRE INTERFEROMETRY
2-D Triaxial Braid - 1200 Microstrain

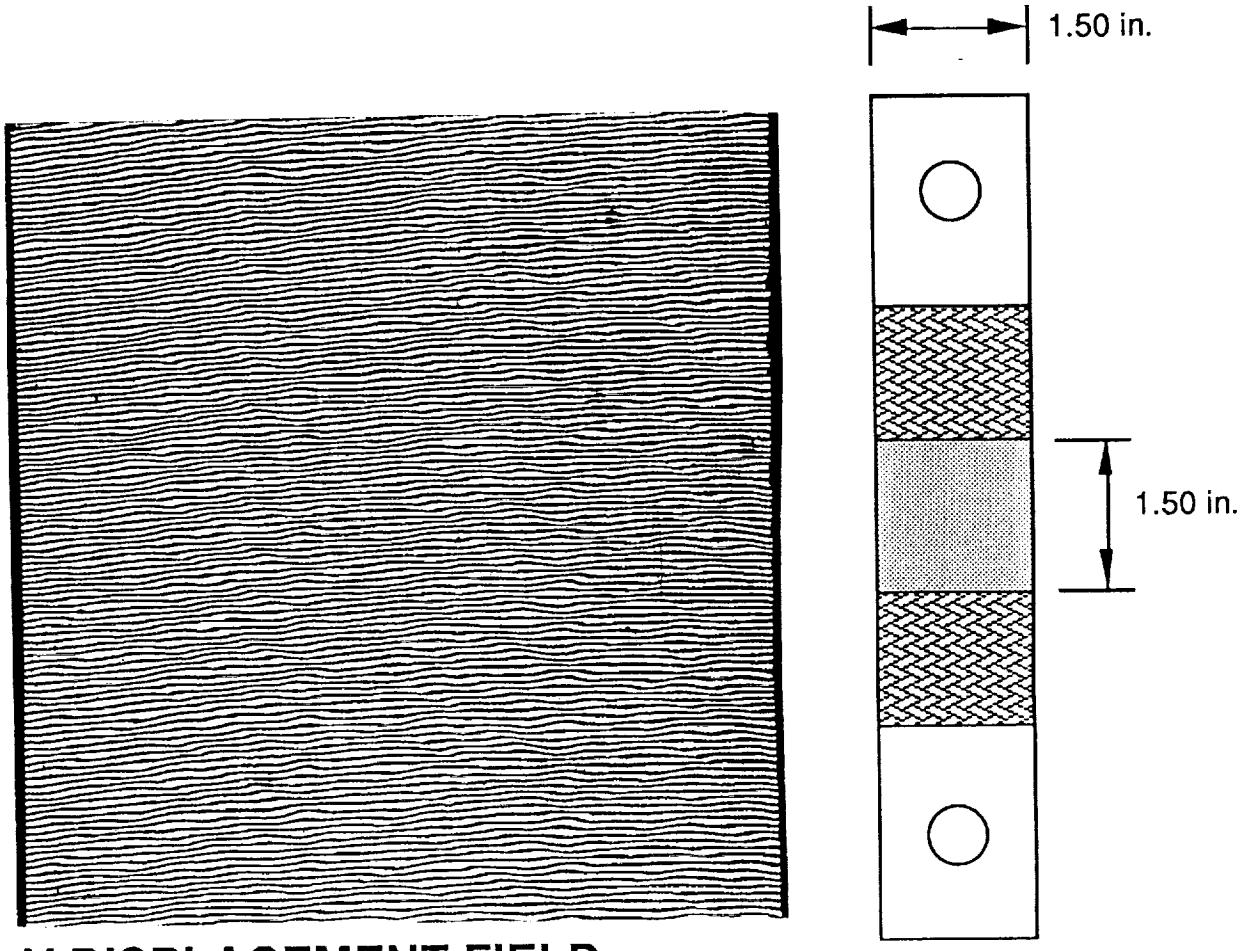

V DISPLACEMENT FIELD

As indicated earlier, Moire interferometry was used to define the full field strain distribution in these braided specimens. The technique defines deformation patterns in both the vertical and horizontal directions. These results are shown in this and the following figure.

The vertical displacement fields (V fields) consist of basically horizontal fringes; this indicates specimen extension where points along one fringe have been displaced vertically with respect to points along a neighboring fringe. For a uniform extension the fringes should be evenly spaced and straight. The fringes for the specimens tested, however, are wavy and the spacing between them varies. The variation is cyclic and coincides with the repeated unit of the textile architecture.

MOIRE INTERFEROMETRY
2-D Triaxial Braid - 2400 Microstrain

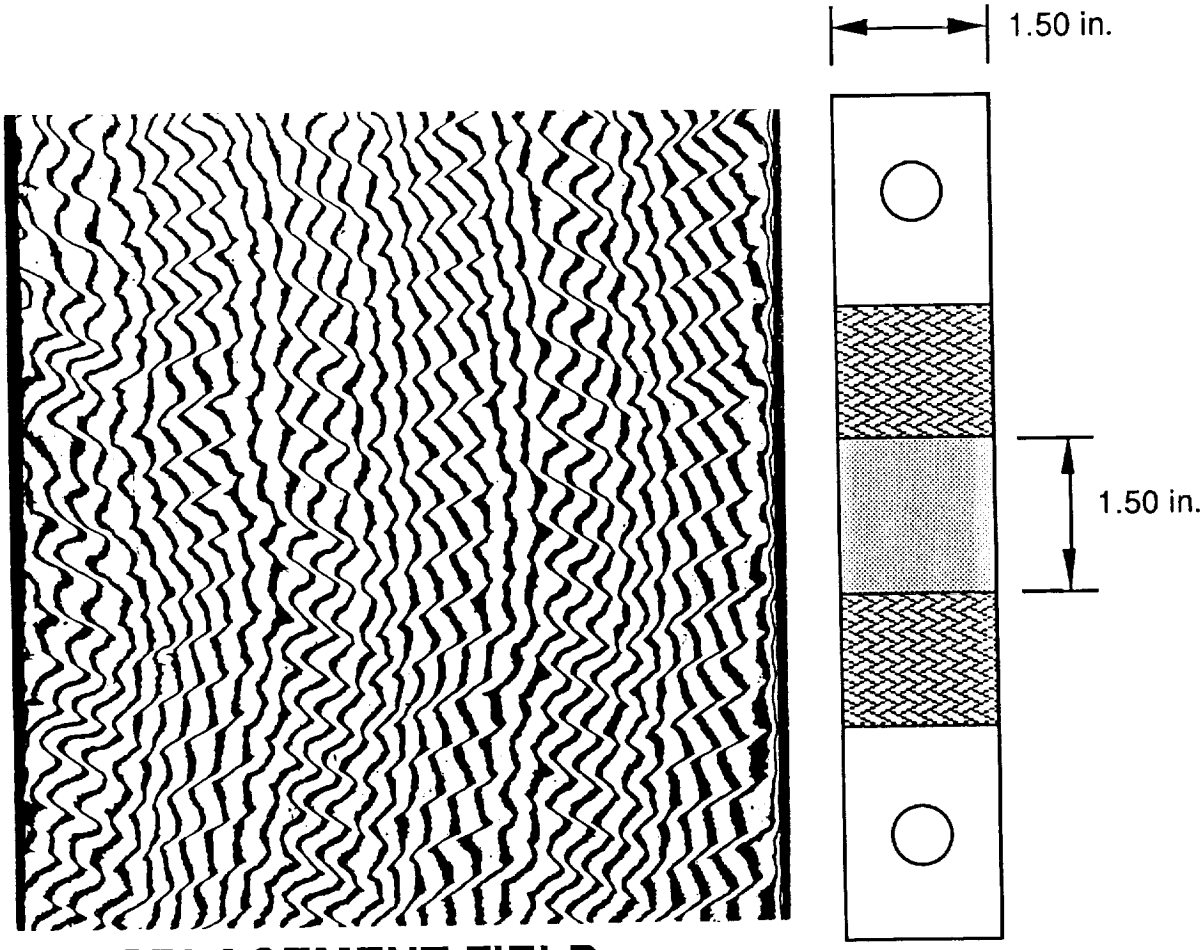

U DISPLACEMENT FIELD

The horizontal displacement patterns (U fields) consist of zigzag vertical fringes that display the Poisson's effect. For uniform contraction the fringes should be straight and the spacing constant. The fringes, however, display a variation which is cyclic, and matches that of the weave geometry. The sharp kinks in the U field fringes reveal the presence of shear strains between the fiber bundles.

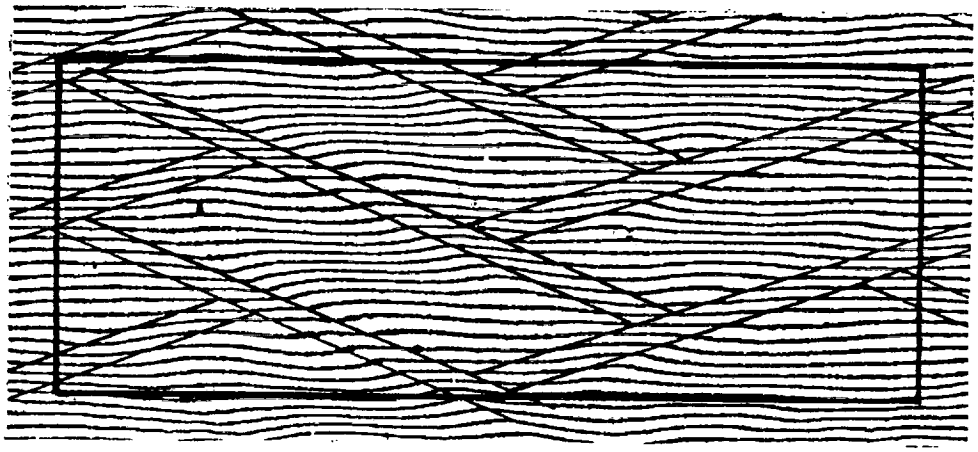

ENLARGED VIEW OF TWO UNIT CELLS - V FIELD

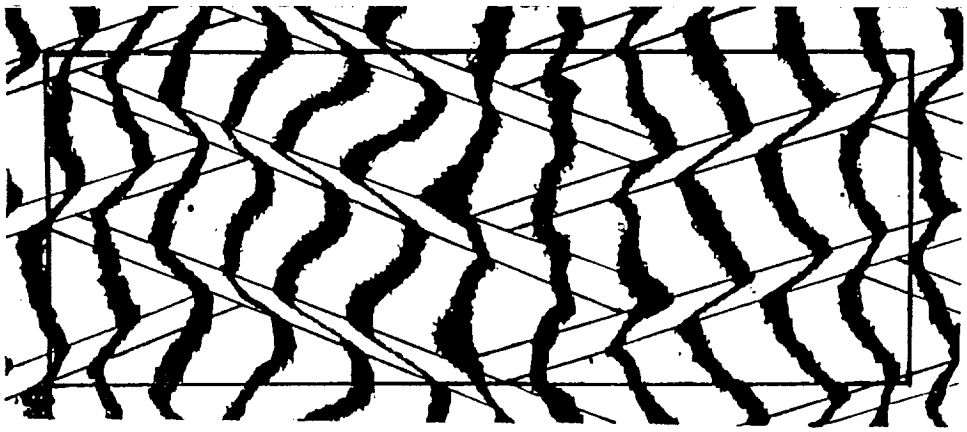

ENLARGED VIEW OF TWO UNIT CELLS - U FIELD

The figure shows the V and U fields of a highly magnified region of specimen that consists of two unit cells. The boundaries between adjacent fiber bundles and the outline of the cells are marked. It was revealed that the shear deformation at interfaces between the fiber bundles occurred over a finite width. This width is illustrated in the patterns as the distance between the closely spaced lines. This is consistent with the presence of the resin rich areas between the fiber bundles, which was on the order of one fifth of the width of the fiber bundle itself. The U field shows that the shear strain γ_{xy} in the resin rich zones was on the order of 0.5 times that of the average applied normal strain ε_y. Additionally, the U field shows that the Poisson effect was nearly constant across the unit cell. The V displacement pattern clearly shows that the strain ε_y varies significantly within each unit cell as can be seen by the nonuniform fringe spacing. The ratio of maximum strain ε_y to minimum strain was about 2.1. The normal strain varies on top of the fiber bundles and is nearly constant throughout all of the resin rich zones.

DAMAGE DEVELOPMENT 2-D TRIAXIAL BRAID (3000 Microstrain)

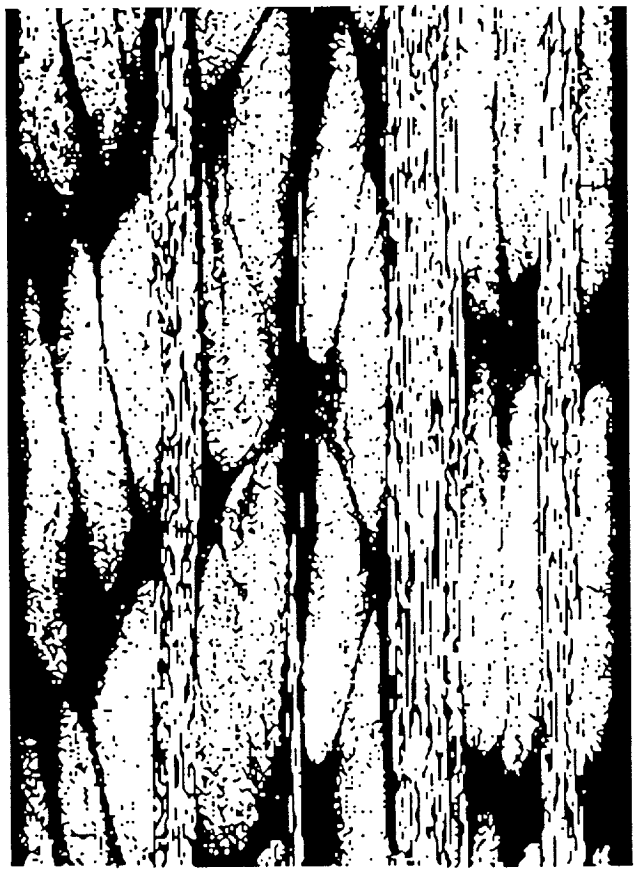

TRANSVERSE CRACKS
- within the braided yarn bundles

A series of tests were conducted to identify the types and locations of damage that developed in the specimens. The test procedure in these tests was to load the specimens in displacement control while monitoring load and strain. Loading was halted at set strain levels, the specimen was unloaded to a nominal strain level, and inspected. Two nondestructive test techniques, enhanced X-ray radiography and edge replication, were employed. After inspection, the specimen was reloaded to an increased strain level and reinspected. The test continued in this manner until the specimen failed.

Examples of these results are contained in the following figures. They illustrates the damage that developed in B1 specimens under tensile loading in the longitudinal direction.

Damage, in the form of transverse cracks within the braided yarn bundles, was first evident at 3000 - 3500 microstrain. There were very few cracks found at this strain level. They occurred at scattered locations along the specimen length and were evident at the specimen surface only. The crack locations roughly correspond to the regions of high strain identified in the Moire interferometric study.

DAMAGE DEVELOPMENT 2-D TRIAXIAL BRAID (6000 Microstrain)

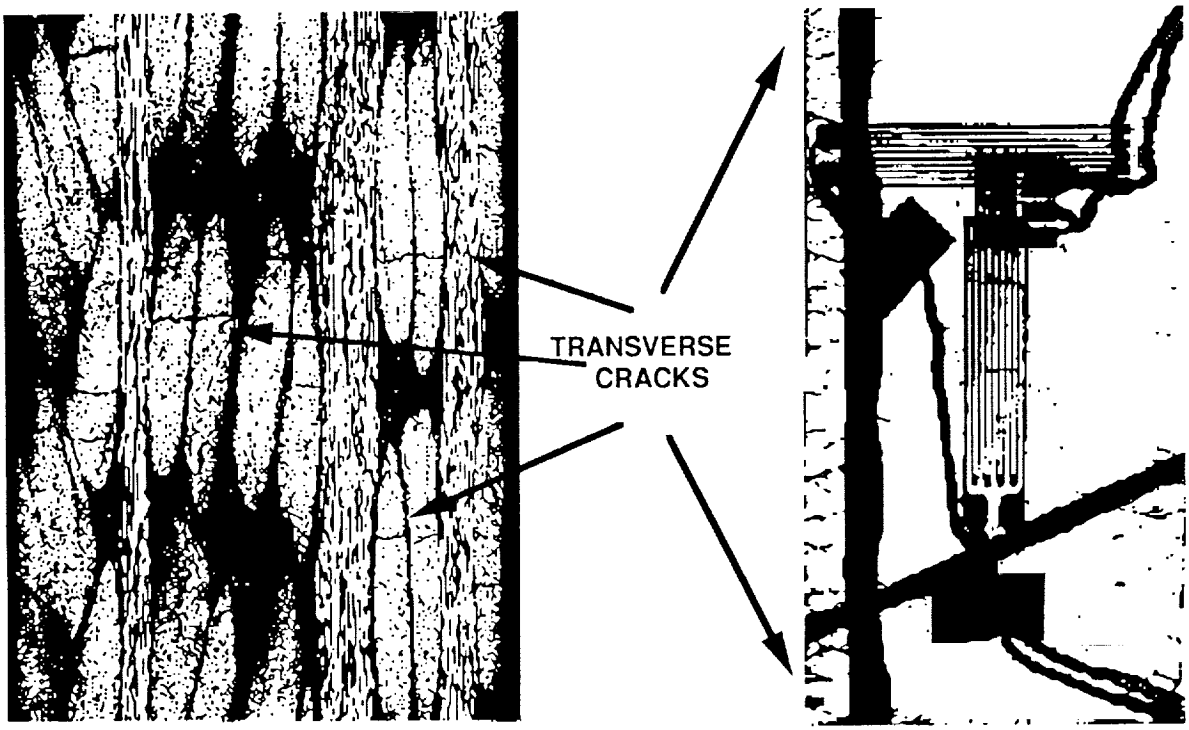

PHOTOMICROGRAPH OF SPECIMEN EDGE

ENHANCED X-RAY OF SPECIMEN FACE

At 6000 microstrain, transverse cracking was evident all along the length of the specimen. This is evident in the enhanced X-ray radiograph shown in this figure. The dark vertical and slanted lines in the radiograph are nickel coated yarn bundles incorporated into the braid to verify yarn orientation. The 1.0 in. long strain gages used on this specimen are also evident in the radiograph. In contrast to the previous figure, the photomicrograph of the specimen edge shown here indicates that damage is evident in the interior of the specimen. Transverse cracks are found in the inner yarn bundles.

DAMAGE DEVELOPMENT 2-D TRIAXIAL BRAID (9500 Microstrain)

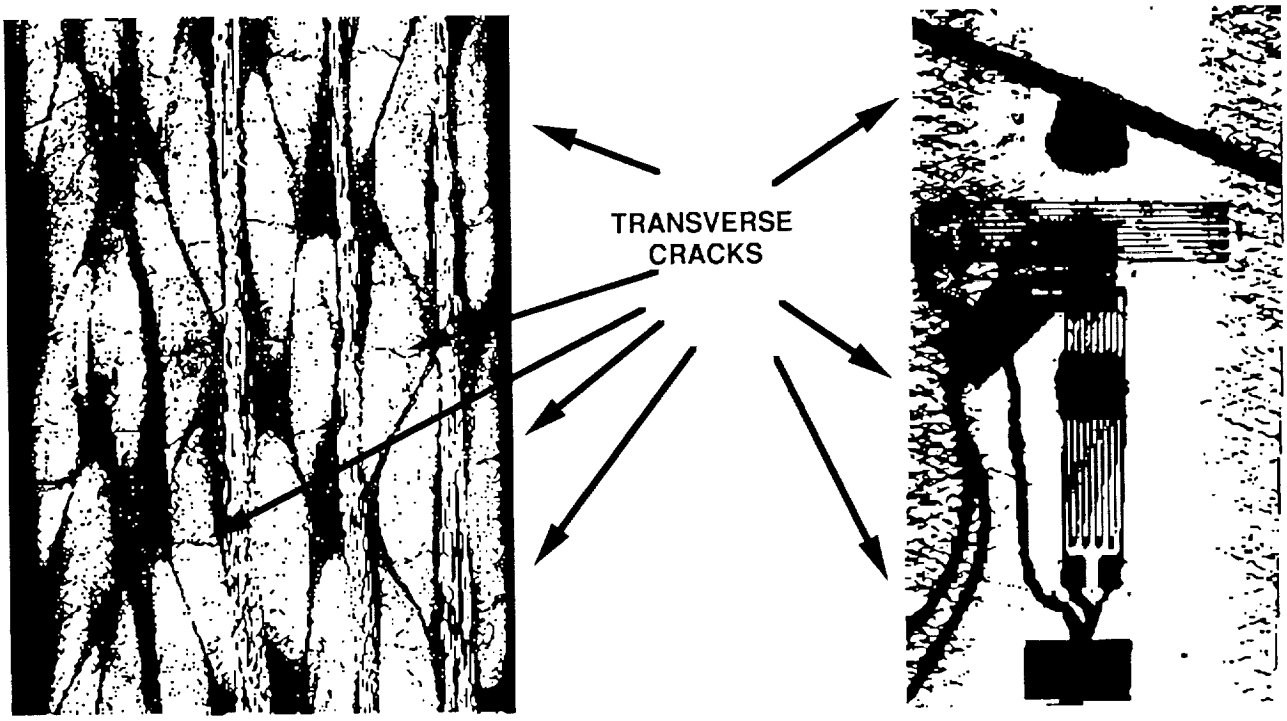

PHOTOMICROGRAPH OF SPECIMEN EDGE

ENHANCED X-RAY OF SPECIMEN FACE

Photomicrographs of the edges of the specimen indicate that transverse cracking has increased significantly at 9500 microstrain. Many yarn bundles have sustained multiple transverse cracks. The enhanced X-Ray radiography demonstrates the increased density of the cracks. Even at this advanced load, delamination was rarely evident (none is shown in the figure). When it did occur it developed at the interface of a cracked yarn bundle and the surrounding matrix. These delaminations were limited to a small local regions.

MODULUS AND POISSON'S RATIO TEST RESULTS

MATERIAL	THICKNESS (in.)	FIBER VOLUME (%)	LONGITUDINAL MODULUS (MSI)	LONGITUDINAL POISSON'S RATIO	TRANSVERSE MODULUS (MSI)	TRANSVERSE POISSON'S RATIO
A 1	.136	54.0	6.62 ± .22	.300 ± .031	5.64	.264
B 1	.136	48.2	6.55 ± .25	.268 ± .026	-	-
	.127	52.3	7.22 ± .24	.227 ± .007	6.34 ± .09	.214 ± .013
B 2	.138	48.9	6.59	.155	7.12 ± .42	.191 ± .010

The results of the modulus and Poisson's ratio measurements are contained in the table. Strain measurements were made using either 0.500 in. or 1.0 in. long strain gages. The moduli and Poisson's ratios were computed over the 0 to 3000 microstrain region of the stress-strain curves. The slopes of the curves were established through linear regression to the data.

The data in the table indicates that the A1, B1, and B2 architectures had comparable longitudinal moduli. They showed greater sensitivity to architecture when loaded in the transverse direction. As a general observation, the use of strain gages with increased gage length in this study (.500 in. and 1.0 in. vs .062 in., .125 in., and .187 in. used in the previous investigation) reduced the scatter in the data. This was particularly evident in the transverse modulus measurements.

TENSILE STRENGTH TEST RESULTS

MATERIAL	THICKNESS (in.)	FIBER VOLUME (%)	LONGITUDINAL STRENGTH (KSI)	LONGITUDINAL ULTIMATE STRAIN (%)	TRANSVERSE STRENGTH (KSI)	TRANSVERSE ULTIMATE STRAIN (%)
A 1	.136	54.0	62.7 ± 3.0	1.06 ± .22	36.1 ± 2.0	0.65 ± .11
B 1	.136	48.2	80.7 ± 1.4	1.36 ± .07	-	-
	.127	52.3	87.3 ± 9.1	1.26 ± .12	41.9 ± 2.5	.70 ± .10
B 2	.138	48.9	57.1 ± 1.6	.95 ± .12	45.0 ± 5.0	.67 ± .12

The tensile strength and ultimate strain measurements are summarized in the table. The data reported show little variation from results reported in a previous evaluation of these materials (NASA Contractor Report 189572, Jan. 1992). Longitudinal strengths and strains were greater than transverse strengths and strains for all three materials. Similarly, the transverse strengths were again comparable for all three materials.

The superior longitudinal strength of the B1 architecture compared to the A1 and B2 materials is again demonstrated in the data. The specimens evaluated in this series of tests had an average fiber volume content of 52.3% and an average tensile strength of 87.3 KSI compared to 48.2% and 80.7 KSI, respectively, in the previous tests. These results confirm observations made in the previous study and again raise the issue of which, if any, braid or material parameter accounts for this dramatic increase in strength over the B2 materials. The two architectures use the same size yarns for both the 0° and braid yarns. However, when laminates of equal fiber volume are compared, the B1 material has a 40% greater longitudinal strength. It may be that the combined effects of the increased 0° yarn content (37.6% vs 34%), the increased 0° yarn spacing (4.77 yarn/in vs 4.37 yarn/in), and the decreased braid angle (66.5° vs 70°) cumulatively account for this discrepancy. This remains a subject of investigation.

5 Modules of Analytical Model

I. FIBER ARCHITECTURE

II. STIFFNESS COMPONENTS OF TEXTILE COMPOSITES

III. SHEAR DEFORMABLE PLATE THEORY

IV. FAILURE MECHANISMS

V. FAILURE PREDICTION

The Textile Composites Analysis (TECA) Model was developed to support Boeing's Advanced Technology Composite Aircraft Structures (ATCAS) Program. In general, TECA predicts the stiffnesses and strengths of textile composites under a variety of loading conditions. The capabilities of TECA have been utilized in a variety of ways during the ATCAS Program. These roles are fiber architecture optimization, parametric studies, material cards for finite element modelling, efficient material characterization, failure mechanism prediction, and insight to potential problem areas. The five modules of TECA are listed below.

Module I: Fiber Architecture Geometry

OBJECTIVE: DETAILED PHYSICAL REPRESENTATION OF THE BRAID GEOMETRY

ARCHITECTURE TYPES: 2-D BRAID
2-D TRIAXIAL BRAID
3-D BRAID
WOVEN FABRICS

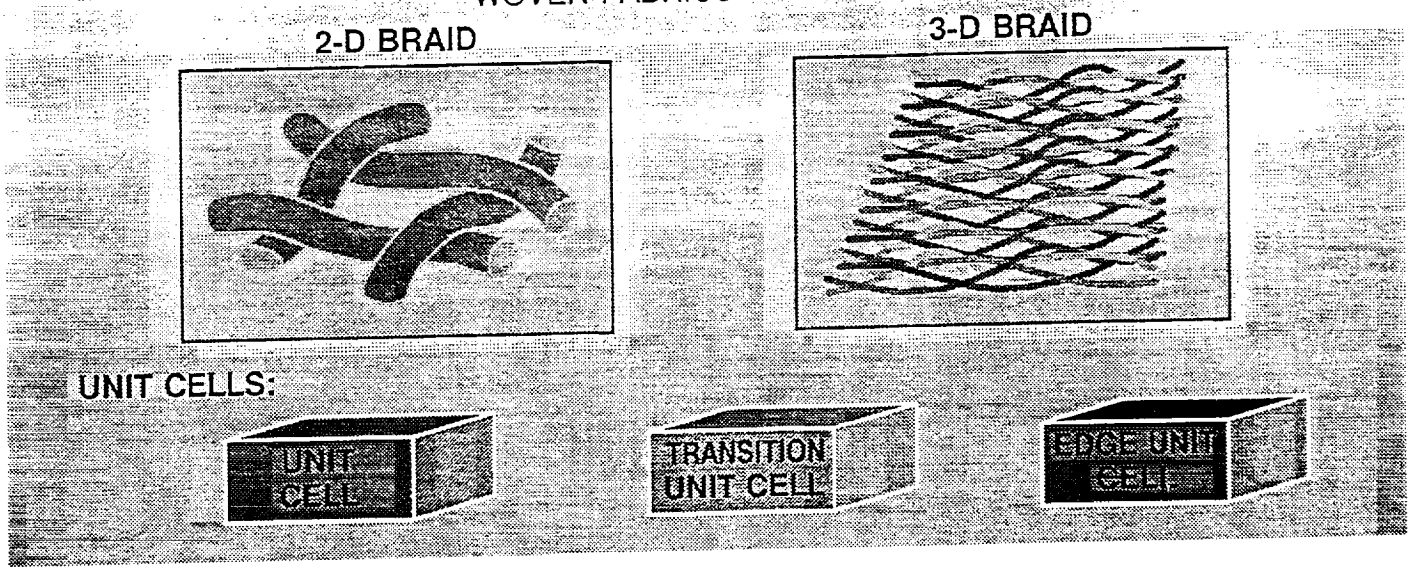

The analysis of textile composite structures requires the knowledge of the internal fiber architecture of the structures. The overall purpose of the Fiber Architecture Geometry Module is to produce a detailed physical representation of the fiber architecture in a braided composite structure. The types of architectures that can be represented by this module include 2-D braids, 2-D triaxial braids, 3-D braids, and woven fabrics.

Module I: Fiber Architecture

3-D UNIT CELL

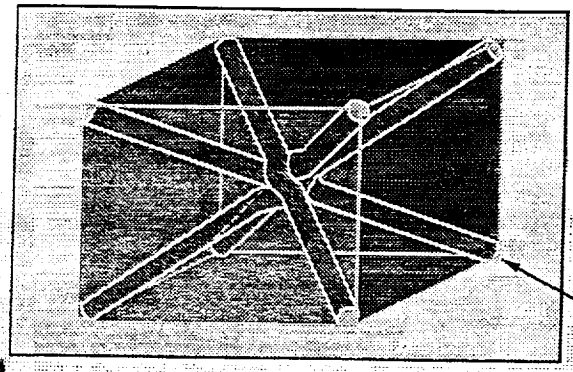

MODEL INPUT:

- TOW SIZE
- BRAIDING RATIO
- LOOM CONFIGURATION

MODEL OUTPUT:

- DIMENSIONS OF UNIT CELLS
- INTERIOR FIBER ANGLES OF UNIT CELLS
- NUMBER OF UNIT CELLS IN A STRUCTURE

The main assumption contained in the Fiber Architecture Geometry Module is that one can assume that the internal fiber architecture of a braided structure can be represented by a series of repeating building blocks called unit cells. A unit cell is comprised of elemental component tows (an extracted 3-D unit cell from a 3-D braided architecture is shown below). The physical properties of the unit cell are dependent on the manufacturing set-up and the tow characteristics.

Module II: Global Stiffness of Textile Composites

OBJECTIVE: PREDICT THE EFFECTIVE ELASTIC CONSTANTS OR INELASTIC CONSTITUTIVE RELATIONSHIPS OF TEXTILE PREFORMS FOR STRUCTURAL ANALYSIS

APPROACH:

- CALCULATE THE STIFFNESS MATRIX FOR EACH ELEMENTAL COMPONENT TOW
- TRANSFORM THE ELEMENTAL COMPONENT TOW LOCAL STIFFNESS MATRIX IN SPACE TO FIT THE COMPOSITE AXES
- APPLY A VOLUME AVERAGING APPROACH TO DETERMINE GLOBAL STIFFNESS

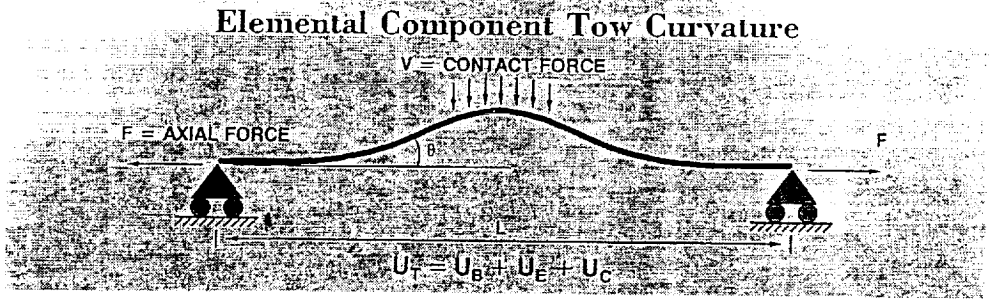

The overall objective of the Global Stiffness Module is to predict the effective elastic constants or nonlinear constitutive relationships of textile preforms for structural analysis. Non-linear response mechanisms such as shear deformation of the preform, matrix properties, and the effect of matrix cracking are taken into consideration when determining the nonlinear constitutive relationships.

The global stiffness matrix of a braided structure is calculated through the following steps: 1) the stiffness matrix for each elemental component tow is calculated through micromechanics relationships, 2) the local stiffness matrices of the elemental component tows are transformed in space to fit the composite axes, and 3) a volume averaging approach is applied to determine the global stiffnesses.

Stiffness modifications were introduced into the model to account for fiber bending because a tow experiences waviness around areas of interlacing and turn-around points as it traverses through a preform. The stiffnesses were modified by an elastic strain energy approach which uses beam elements to represent the bending behavior of a braided tow. The total strain energy includes the strain energy due to bending and extension of the beam elements, and compression in the region of contact in tow cross-over areas.

ORIGINAL PAGE IS
OF POOR QUALITY

Module III: Stress Analysis

OBJECTIVE: PROVIDE PROPERTIES FOR TRADITIONAL PLATE/SHELL ANALYSIS

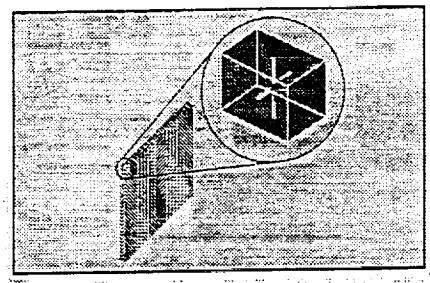

APPROACH:

1. $$\begin{bmatrix} C_{11} & C_{12} & C_{13} & C_{14} & C_{15} & C_{16} \\ & C_{22} & C_{23} & C_{24} & C_{25} & C_{26} \\ & & C_{33} & C_{34} & C_{35} & C_{36} \\ & & & C_{44} & C_{45} & C_{46} \\ & & & & C_{55} & C_{56} \\ & & & & & C_{66} \end{bmatrix}$$

2. APPLY CONDITION $\sigma_z = 0$

3. INTEGRATE TO OBTAIN EXTENSIONAL AND BENDING STIFFNESS MATRICES

4. ANALYSIS
   - PLATE ANALYSIS
   - SHELL ANALYSIS
   - STRESS CONCENTRATION FACTORS

Since most engineering problems are set-up for plate or shell analysis, properties are required in a form compatible with this type of analysis. The third module of TECA performs the necessary analysis utilizing the 3-D stiffness matrix determined in the previous module. First, a plane stress condition is applied (via static condensation) to the 3-D stiffness matrix. Next, integration is performed to obtain the extensional and bending stiffness matrices. Following this step, the stress field in the composite can be calculated using shear-deformable plate analysis or shell analysis.

Module IV: Failure Mechanisms

OBJECTIVE: PREDICT HISTORY OF DAMAGE INITIATION AND FAILURE FOR DIFFERENT TYPES OF LOADING CONDITIONS

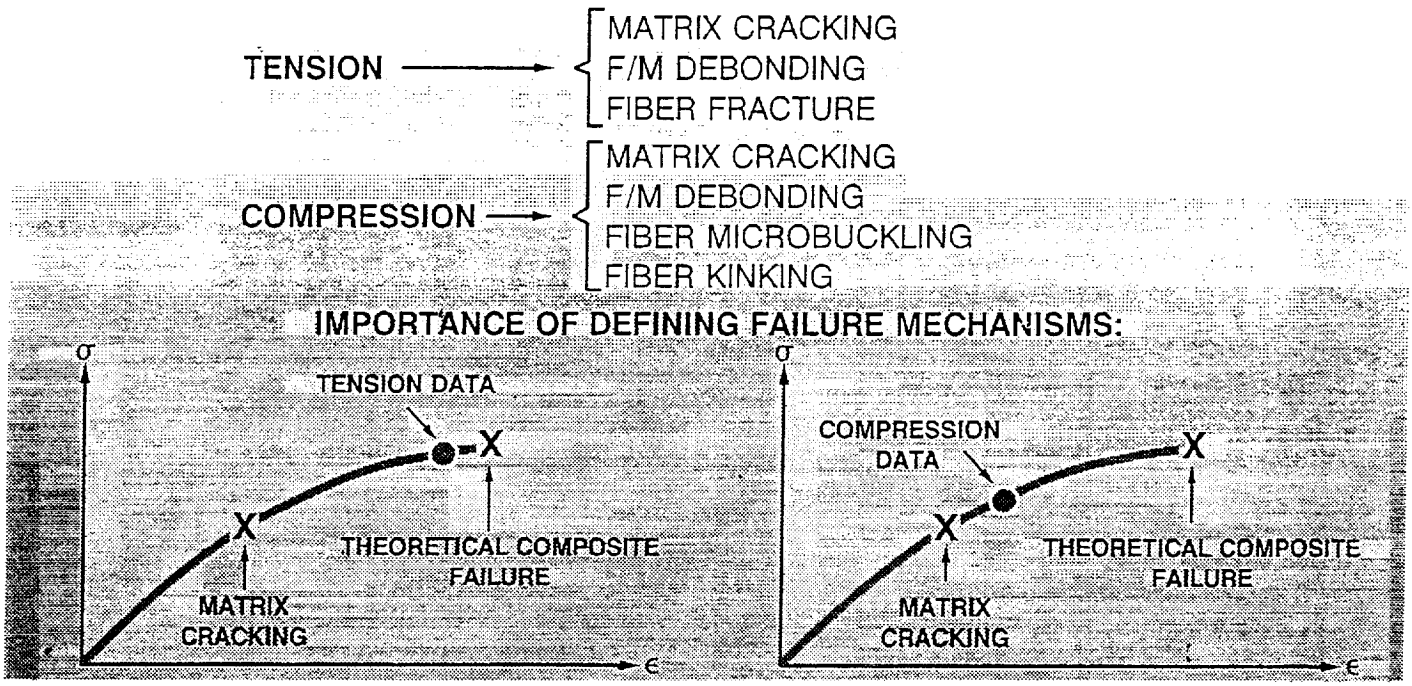

In conjunction with the Failure Prediction Module (see next page), the Failure Mechanisms Module identifies the history of failure of textile composites. Specifically, the Failure Mechanisms Module predicts the history of damage initiation and growth to failure for many different types of loading conditions.

Flow Chart of Failure Prediction

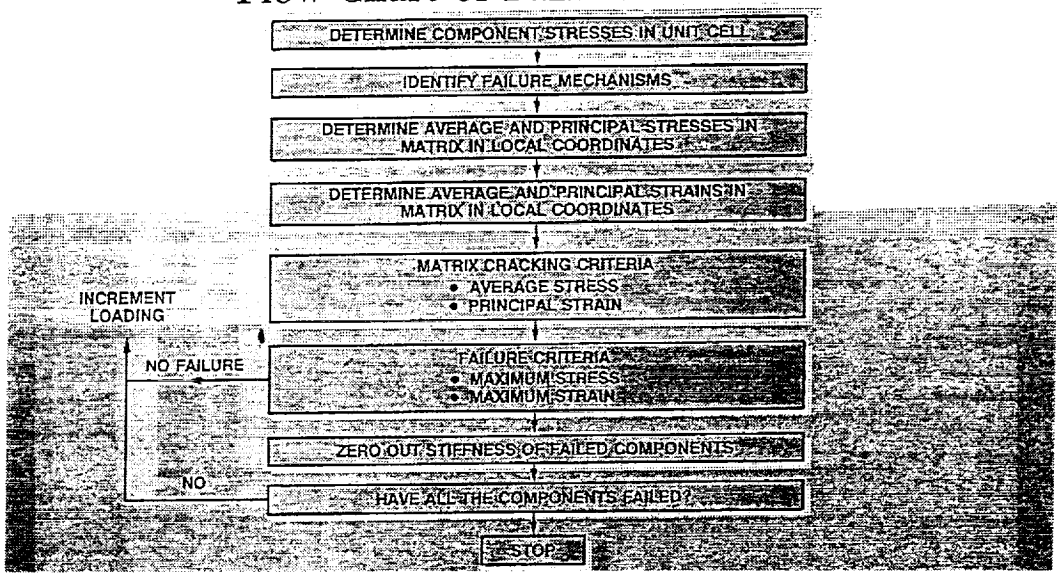

The overall objective of the Failure Prediction Module is to predict the history of failure of a textile composite from average stresses obtained from global structural analysis.

The Strength Module is set-up for a progressive failure analysis using the following sequence of steps: 1) the failure mechanism for the loading condition is identified, 2) the average and principal stresses and strains in the matrix are determined on a local level, 3) the matrix cracking criterion is applied via either an average stress or principal strain criterion (if matrix cracking is detected, the necessary adjustments are made to the local stress field and component stiffnesses), and 4) the failure criteria is applied via either a maximum stress or maximum strain criteria.

Analysis of Braided Composite Mechanical Behavior

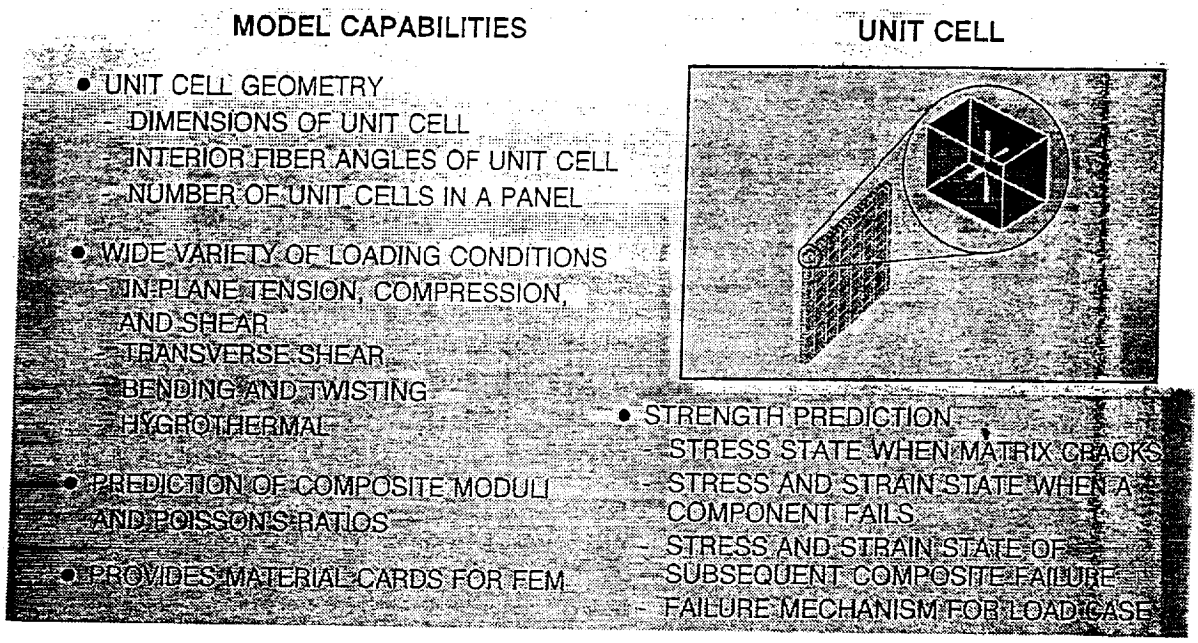

The figure above summarizes the capabilities of the five modules contained in TECA. TECA produces a detailed description of the unit cell geometry for braided composites. The model is capable of performing analysis for a wide variety of loading conditions including in-plane tension, in-plane compression, in-plane and transverse shear, bending, twisting, and hygrothermal loading. The model can predict the composite moduli, composite Poisson's ratios, and composite coefficients of thermal expansion. TECA is also capable of producing material cards for finite element models in which complex shapes can be represented. And finally, the failure criterion contained in TECA can predict the history of failure in a braided composite.

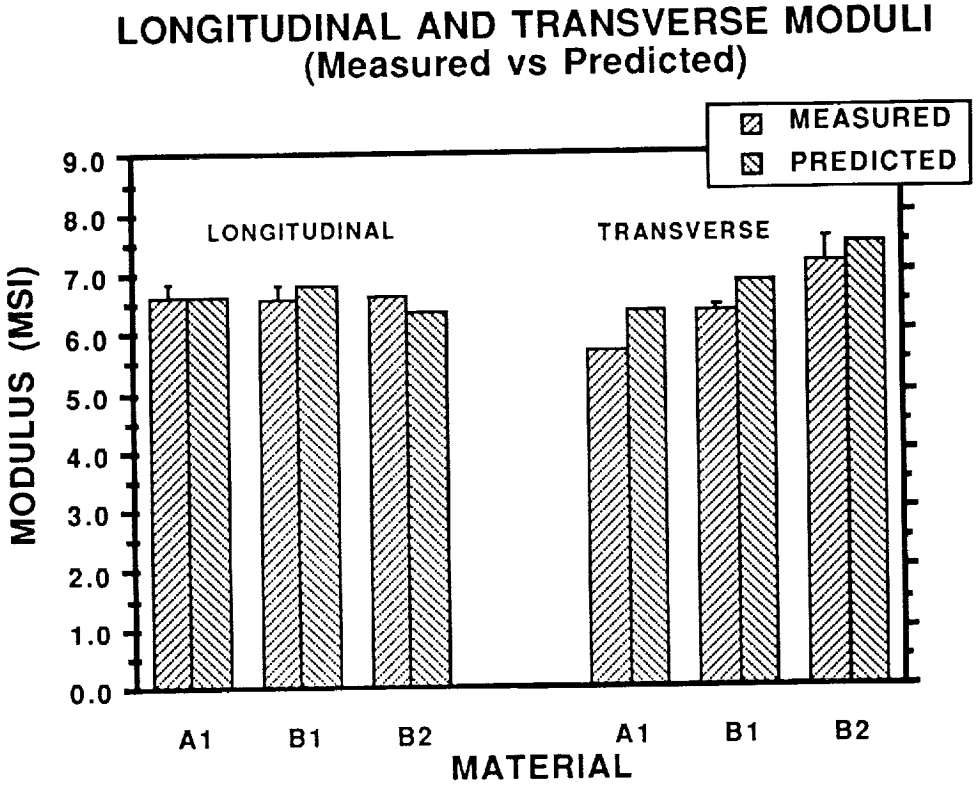

A comparison of the measured and predicted longitudinal and transverse moduli for the three architectures tested is shown in the figure. The data indicate that the values predicted by the TECA model are in close agreement with the experimentally determined values. Previous modelling efforts (NASA Contractor Report 189572) accurately predicted the longitudinal moduli but not the transverse values.

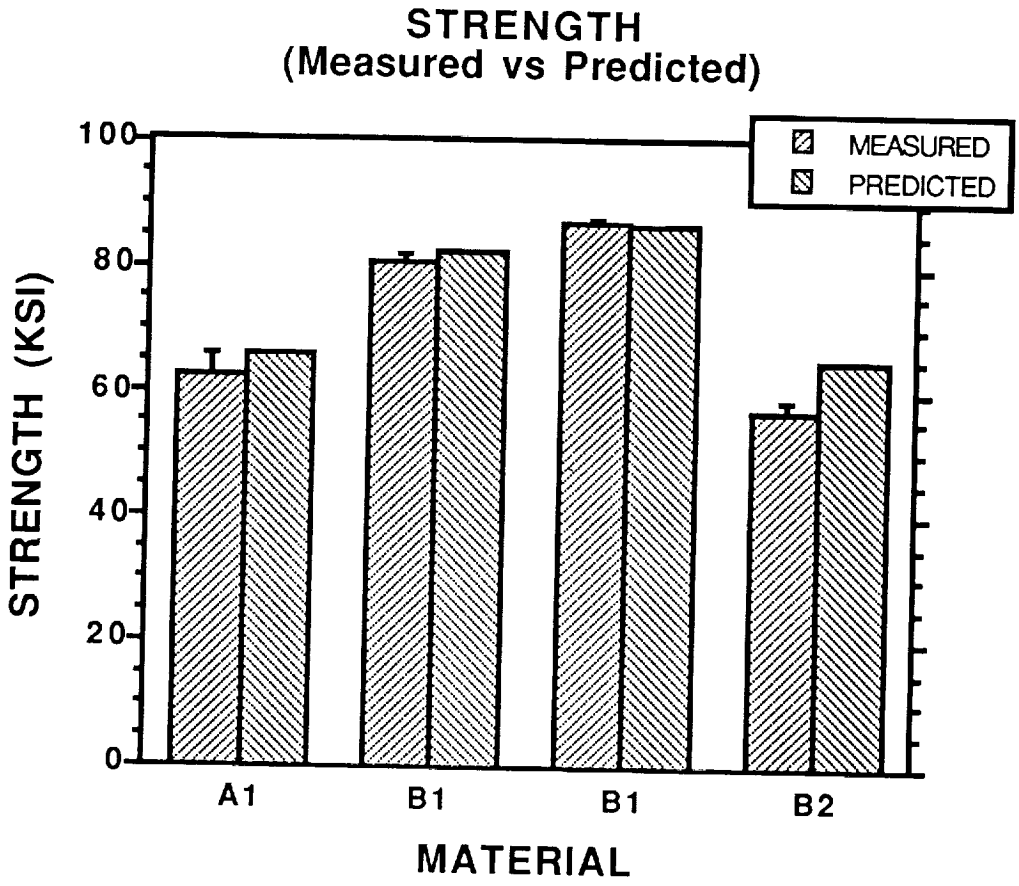

As indicated earlier, an iterative scheme has been incorporated into the TECA model to predict strength and ultimate strain of the braided laminates. The strengths predicted by the model are compared with the experimentally measured values listed previously in this paper. Two strengths are given for the B1 material due to the variation in resin content of the two panels tested.

Although predicted strengths of the A1 and B2 materials were higher than the measured values, the agreement between experimental and analytical values is quite good.

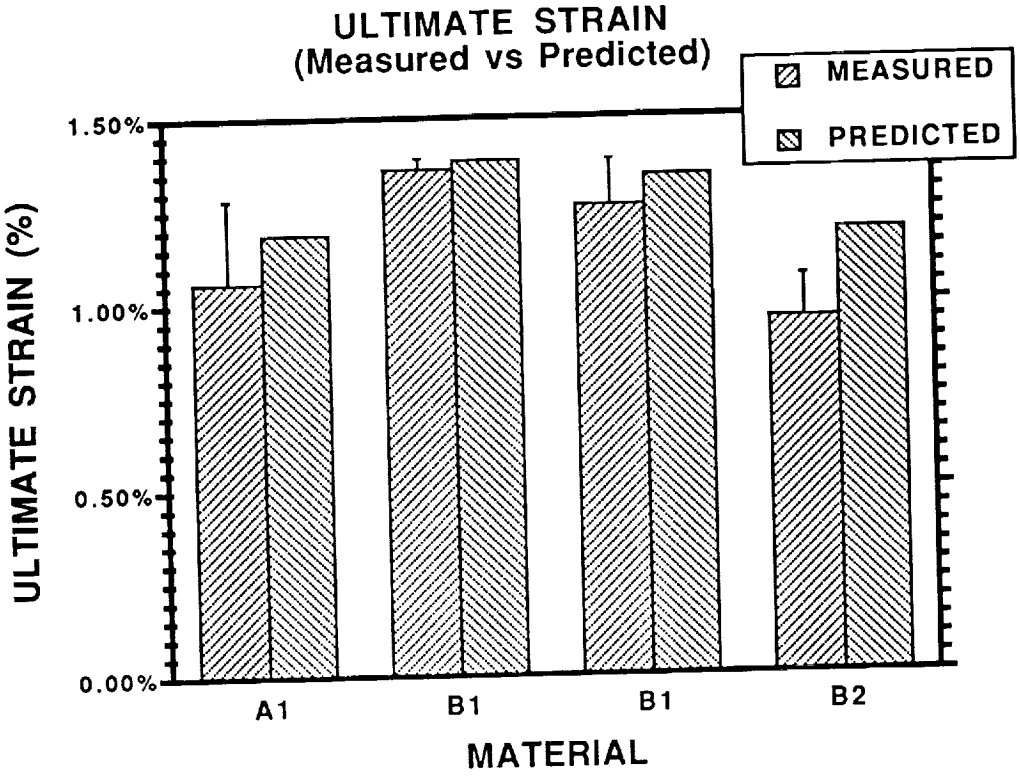

The comparison between measured and predicted ultimate strains for the three architectures is contained in this figure. In general, the model predicted higher strains at failure than were experimentally observed. The predicted values are, however, within the scatter in the data in most cases.

SUMMARY:

- **MEASURED MATERIAL RESPONSE**
- **DEFINED FAILURE MECHANISMS**
- **MOIRE DEFINED DEFORMATION FIELD**
- **MODEL ACCURATELY PREDICTED MECHANICAL RESPONSE**

In summary, the investigation was able to mechanically characterize the mechanical response of the three triaxially braided architectures under tensile loading in both the longitudinal and transverse directions. The materials' moduli and Poisson's ratios were measured along with their strengths. Modulus measurements were improved through the use of .500 in. and 1.0 in. long strain gages but much work is required to develop instrumentation practices for textiles.

The Moire interferometry technique proved to be an effective tool. The definition of the full field strain distribution will be useful both in establishing instrumentation requirements as described in the previous paragraph and in interpreting failure events.

Through the combined use of enhanced X-ray radiography and edge replication, the types and locations of damage were defined. Under this type of loading, damage consists primarily of matrix cracking in the braided yarns. This is first evident at 3000 to 3500 microstrain and continues to develop until failure occurs. Only minor delamination was observed at high strain levels.

The TECA model was effective in modelling both the moduli and strengths of the three architectures. The agreement between measured and predicted longitudinal and transverse moduli were improved compared to previous efforts. The strength predictions also closely agreed with the experimental values.

CROSS-STIFFENED CONTINUOUS FIBER STRUCTURES

JOHN R. EWEN
GRUMMAN AIRCRAFT SYSTEMS
BETHPAGE, NEW YORK

JIM A. SUAREZ
GRUMMAN AIRCRAFT SYSTEMS
BETHPAGE, NEW YORK

SUMMARY

Under NASA's Novel Composites for Wing and Fuselage Applications (NCWFA) program, Contract NAS1-18784, Grumman is evaluating the structural efficiency of graphite/epoxy cross-stiffened panel elements fabricated using innovative textile preforms and cost effective Resin Transfer Molding (RTM) and Resin Film Infusion (RFI) processes. Two three-dimensional woven preform assembly concepts have been defined for application to a representative window belt design typically found in a commercial transport airframe. The 3D woven architecture for each of these concepts is different; one is vertically woven in the plane of the window belt geometry and the other is loom woven in a compressed state similar to an unfolded eggcrate. The feasibility of both designs has been demonstrated in the fabrication of small test element assemblies. These elements and the final window belt assemblies will be structurally tested, and results compared.

INTRODUCTION

Several attempts have been made to provide structural continuity through the intersection of cross-stiffened graphite composite structure. Initial attempts included bonding metal cruciforms to the graphite stiffeners at the intersection and alternately placing unidirectional tows across the intersection. Adaptations of tow placement have been successfully tried using syntactic foam to accommodate the cross intersection lay buildup. These methods and others have met with varying degrees of success. The primary focus of all of these innovative concepts was to improve the composite structure load-carrying capability through the cross-stiffened intersection.

It was recognized that an effective solution was necessary to further advance the utilization of advanced composites in airframe structures. Successful application of cross-stiffening would permit designs that could, until this time, only be effectively achieved with metallic designs. Efficient, supportable, and affordable graphite solutions would permit more effective composite applications for airframe components such as bulkheads, doors, window belts, and skin panels. Essentially, any cross-ribbed structure is a potential candidate.

The resulting benefits for developing such a capability are reduced weight, improved material utilization, reduced number of parts, and a potential for reduced costs.

With the technology development and introduction of three-dimensional textile weaving and braiding processes, new opportunities became available to present solutions to this problem. Weaving technology has progressed significantly for use in structural composite applications. More importantly, these processes offer the potential to achieve continuous through-the-intersection fiber integrity with high-strength graphite fibers.

These textile processes permitted new composite material fabrication methods to be developed. Dry unimpregnated assemblies were produced by combining/stitching various textile products, such as 2D woven broadgoods, 3D woven assemblies, and braided items, to form complex shapes. These resulting textile assemblies provide preforms for subsequent processing.

In addition, processing methods have been developed that are compatible with textile preform assemblies. Resin Transfer Molding (RTM) and Resin Film Infusion (RFI) are two such methods presently being applied to the fabrication of airframe parts.

Grumman is currently under contract with NASA to develop innovative, cost-effective, damage-tolerant design concepts for airframe structure. A major task of this program is to design and demonstrate the effectiveness of a textile cross-stiffened continuous fiber structure. This demonstration will utilize advanced textile preform architectures and processing technologies to fabricate a commercial transport demonstration subcomponent. For this demonstration, the airframe part selected is a window belt typical of that found in a commercial transport. The specific reasons for this selection are: the design is generic to cross-stiffened biaxial loaded structure; it is highly loaded, carrying both fuselage bending and cabin pressure loads; it presents a fair degree of complexity; and it is a repetitive assembly along the length of an aircraft. Figure 1 depicts the area of interest, a detail of an existing metallic assembly, and an isometric of the textile subcomponent.

The remainder of this paper will discuss the technical data related to this task. This includes the requirements, component definition, materials, selection of textile process, textile preform assembly methodologies, test plan, tooling, and lesson learned.

REQUIREMENTS/CRITERIA

The design loads used to size the window belt subcomponent were obtained from Boeing Commercial Aircraft and are representative of a typical wide-body fuselage window belt region. Figure 2 displays the direction and magnitude of the ultimate design axial loads and shears for two maximum load conditions.

The fail-safe design allowable strain (80% limit) was selected to be 2400 μin./in. for this application. This is commensurate with Boeing's fail-safe allowable strain of 2000-3000 μin./in. The resulting design ultimate strain is 4500 μin./in.

The geometrical definition was also obtained from Boeing and was used as a guide to define the subcomponent. The actual fuselage side panel containing the window belt has a radius of 122 in. The subcomponent was configurated flat to reduce test costs. The window spacing is 22.00 in. and the longitudinal stiffener spacing, which frames the windows, is 19.00 in.

COMPONENT DEFINITION

The textile preform window belt subcomponent design, drawing D19B1865, is shown in Figure 3. The drawing presentation defining the composite layup is significantly different from one applied to a unidirectional or broadgoods composite design. For typical 2D composite applications, fiber orientation, number of plies, and stacking sequence can be defined exactly on the engineering drawing and, in turn, fabricated as specified. Three-dimensional woven preform assemblies, on the other hand, cannot be as simply defined because of the diversity of weaving/stitching processes, complexity of fiber orientations, yarn tow size and variation of fiber architecture.

To enable preform fabricators to exercise creative solutions, promote freedom in design, and avoid imposing adverse restrictions to a design, drawing D19B1865 stipulates target values for fiber volume and percentage of 0, 90±45 directional yarns and stitching yarns. This notation provides the freedom to develop a complex fiber architecture and preform assembly using the techniques and equipment familiar to each potential supplier. However, this method, if not concurrently engineered, can compromise the structural capability of the resulting assembly.

The geometrical definition, particularly the thickness dimensions, are called out as are net final cure dimensions. It is desirable that the preform be within 10% of this dimension to enable tooling to be effectively designed. Preforms with bulk factors as high as 200% will impose restrictions on tooling designs, with the potential to increase complexity and related costs.

The window belt subcomponent, as shown in Figure 3, is 38 in. x 62 in. and consists of two primary longitudinal members, 0.48 in. thick, six transverse stiffeners, 0.17 in. thick, and a 0./17 inc. in-plane skin. The intersections of these transverse and longitudinal stiffener members have continuous fibers through the intersection to provide structural continuity at each joint. These intersecting members are attached to the skin panel with flanges to provide a load path to transfer the panel shears to the stiffeners. The entire assembly is stitched to provide stability to the dry preform and to enhance the damage tolerance of the final article. The stitching density is to be a maximum of 6% to prevent strength degradation. Two elliptical cutouts, with a major diameter of 17.25 in., replicate the windows. The provision of through-the-intersection fiber continuity is the main focus of attention .

ANALYSIS

The subcomponent was sized using composite laminate analysis methods with adjustments for through-the-thickness reinforcement, assuming a 60% fiber volume, 4500 μin./in. allowable ultimate strain, and IM7 graphite properties. AS4 was considered as an alternate material for the subject application.

A three-dimensional NASTRAN finite-element model of a repeating section of the window belt subcomponent was constructed and is shown in Figure 4. The section consists of a single window section with three ring stiffeners and two associated longitudinal stiffeners with the adjoining skin. A complete model of the subcomponent to be tested will be comprised of two such repetitive models and a boundary region component model. The latter will also be derived from a generic boundary model.

The general window component model is represented by 1066 node points (GRID) interconnected by 1004 quadrilatral bending elements (CQUAD4). This model depicts the stiffeners as a combination of bending elements which provides for the geometric distribution of the structure and is also capable of representing the structural response of the extended stiffeners. The FEA will be used to predict strains in critical areas for the subsequent component structural tests.

MATERIALS AND PROCESSES

The principal graphite fiber material selected for this woven and stitched preform assembly is IM7. AS4 graphite was considered as an alternate material because of its lower cost, availability and widespread use. Stitching is to be performed using high-strength Toray graphite thread or Kevlar thread as an alternate. The size of the tows and yarns was left to the suppliers and was dependent on the individual weaving process.

The composite processing will be achieved using either RTM or RFI. Both processes are compatible with the preform assembly. Grumman has successfully demonstrated both the RFI and RTM methodology in the Novel Composites for Wing and Fuselage Applications program in the manufacture of "Y" spars.

The epoxy resin materials that are being considered for RTM of the window belt article include Shell 1895, British Petroleum E905L two-part systems, and 3M PR500 one-part system. The resin film material being considered for RFI of the window belt is 3501-6 epoxy.

EVALUATION CRITERIA

Evaluation criteria were established to compare the preform assemblies and textile processes that were proposed by suppliers. These criteria were based on parameters that would be necessary for a cross-stiffened design. The primary comparative evaluators were ability to provide true through-the-intersection fiber continuity, ability to provide and control the percentage and direction of yarn orientations, ability to vary the thickness of the skin panel and provide different stiffener thicknesses, and use of a process that has application for large scale-up production. Other considerations included viability of the process, cost of the final preform, and delivery schedule.

Five textile fabricators submitted proposals which described eight concepts to develop solutions for the window belt design. The designs varied and consisted of braided details, 3D woven details, stitching, and assemblies of these and 2D components. Of the five evaluated two were selected to produce the preform and related test elements. These two supplies are Techniweave, Inc., Rochester, New Hampshire and ICI Fiberite, Greenville, Texas.

The two processes are significantly different. The ICI Fiberite approach employs a conventional weaving loom with a Jacquard head to fabricate the cross-stiffeners and then attaches them to 2D woven broadgoods. The Techniweave process utilizes an integral weaving technique whereby the structural preform is achieved by interlacing graphite yarns around closely spaced pins. The primary distinguishing differences is that Techniweave can weave the stiffeners integral with the skin in the plan form of the subcomponent, whereas ICI Fiberite unfolds a loom-woven 3D cross-stiffened rib structure and assembles it to the 2D woven skin panels by using a uncatalyzed epoxy resin and stitching.

PROCESS DESCRIPTION

Techniweave Process

The Techniweave fabricated preform is an assembly consisting of a large 3D integrally woven detail and several 2D woven broadgood ply details. Figure 5 is a schematic representation of this final product. The 3D detail as shown is the predominant feature which integrates the panel skin and stiffeners, and provides the continuity of fibers through the intersection. The 2D bias broadgood plies are stitched to the stiffeners and skin panel to complete the assembly.

This 3D weaving process employed to fabricate the core detail is unique. It is a method which has been demonstrated in various thick preform assemblies made by Techniweave and others. More recently, Techniweave has developed fabrication technology for application to thin wall sections such as defined for the window belt design. Currently, it is a manual process where the weaving is done in layers following predescribed paths. Registration of successive layers is assured with the use of tooling to define through-the-thickness yarn sites. Figures 6, 7, and 8 show vertical yarn stitch sites for a 7-in. by 7-in. test element and two skin surface weave layer definitions, 0° and 45°.

Initiation of the weaving starts from the surface panel and continues vertically to build up the skin thickness and stiffener heights. The yarns are interwoven through the predescribed paths as shown in the layer diagrams, in the required orientations 0, ±45, 90. Since this is a planar process, the bias weave is easily accommodated in the skin panel but is unable to be incorporated in the stiffeners. The applied stiffener yarns consist of the 0-degree orientations that are continuous through the intersection and "Z" weaving yarns that are woven through the thickness, as shown in Figure 9.

Upon completion of this initial weaving phase, the vertical yarn sites are consecutively stitched. These yarns provide the 90-degree orientation in the stiffeners and the stitching in the skin panel area. The preform is completed, as shown in Figure 5, by stitching the bias 2D details to the main core piece.

The completed preform will have a 120-180% bulk, or 1.2 to 1.8 times the drawing net final thickness. Debulking will be done to compress the preform using a combination of stitching and a low-temperature melting point uncatalyzed epoxy resin binder.

Techniweave is currently in the process of installing a machine to automate the 3D weaving process and is scheduled to be on-line in the summer of 1992. The Grumman Window Belt subcomponent will be one of the initial products.

The translation of the original design into a preform required some compromise in fiber volume, stacking and percentage of fiber orientations. Table 1 shows the initial target fiber orientation percentages from the engineering drawing and the resulting preform compromise from Techniweave. Techniweave will use AS4 - 3K yarn for the stiffener 0-degree orientations and panel 0, 90, ± 45-degree orientations. The "Z" direction weaver yarns will be T300-1K. The stiffener 90-degree orientation and all stitching will be achieved using Toray T900 high-strength graphite yarn. The 2D material will be AS4-5H. The basic design concept for the stiffeners is shown in Figures 10, 11 and 12.

There are several unique aspects of this process that are beneficial to fabricating preforms. Among these are the ability to weave the preform in the draining orientation without requiring an unfolding op-

eration, the ability to weave the skin and intersecting stiffeners as one core detail, the potential for automation and scale-up, and the ability of weaving in-plane holes into the preform.

ICI Fiberite Process

The ICI Fiberite approach to the window belt design is conceptually shown in the schematic of the test element in Figure 13. It consists of a 3D woven core and several 2D woven details that are assembled and debulked to form the preform. The core is produced on an ICI built loom capable of weaving thicknesses up to 3.5 in. and outfitted with a Staubli electronic Jacquard head.

The 3D core is the principal feature of the design and provides the through-the-intersection fiber continuity. Figure 14 shows the woven preform prior to being expanded and erected vertically. Essentially, it resembles a collapsed egg crate. The preform exits the loom in the longitudinal direction parallel to the 0-degree fiber orientation direction.

A schematic representation of the 3D fiber architecture is shown in Figure 15. The preform consists of three principal fiber orientations: 0-degree, which are depicted by the solid horizontal lines; "Z" direction, which are represented by the angular translational lines; and the 90 degree fill yarns shown by the circles. The through-the-intersection fiber continuity is shown and is achieved by rotating the 0.17 in. thick stiffener legs 90 degrees.

Producing this preform is a compromise of the initial target drawing fiber volumes and percentages, as shown in Table 1. For this process, "Z" yarns are introduced and are required to interlock the longitudinal and fill yarns together, thus giving a structural rigidity to the preform. These "Z" yarns replace some of the longitudinal 0-degree, as they do in the Techniweave process. The angular paths are expected to reduce the stiffener axial load capability. This will be verified during the testing phase. Also, the angular path of the "Z" yarns is related to the thickness of the assembly. The longitudinal stiffener (0.24 in. thick) angle is 44 degrees and the vertical stiffener (0.17 in. thick) angle is 20 degrees. The severity of the angle is expected to be directly related to the stiffness and axial load capability.

The 2D broadgood material that makes up the remainder of the preform definition is assembled to the 3D core to form the skin panel, stiffener buildups, and flanges. For this application these plies take the form of strips, sheets, and pans. Figures 16 and 17 show the completed preform cross-sectional assembly of the longitudinal and vertical stiffeners. Figure 18 shows the plan view of the assembled stiffener intersection.

ICI debulks the complete preform to as close to net shape as possible using a tackifier or binder resin. An uncatalyzed epoxy resin, 8% volume, is sprayed on the woven details prior to the preform assembly to provide a tackiness to hold the net dimensional compressed shape and to add rigidity to the preform. This tackifier is a Shell product, a combination of Epon 836 and 1001F, and has a low melting point of 130 deg F. This compressed preform is stitched using a Kevlar thread at a 1/4 in. stitch pitch in 3/8 in. spaced rows. The stitching provides additional rigidity to the preform and aids in holding the net dimensional shape. Stitching is a requirement to enhance the damage tolerances of the assembled 2D material. For this application the stitching volume percent is less than 2.

A 14 in. x 14 in. cross-stiffened preform test element fabricated by ICI is shown in Figure 19. This cross-stiffened element represents a stiffener intersection of the window belt and was used to demonstrate the preform fabrication methodology. Similar test elements will be used during subsequent tests

to demonstrate RTM and RFI processibility and structural performance.

This preform will utilize IM7 graphite for the preform yarn and 2D woven broadgoods as the basic construction material. The 3D core woven detail will be fabricated using 12K yarn for the 0°, 90°, and "Z" angular directions.

TOOL DESIGN

The tooling concept employed for the RTM process will be a bolted multi-piece steel mold that provides a compression/wedge action. An assembly of the subcomponent tool is shown in Figure 20. Although a press is preferred for tool closure, a bolted strong back design was selected due to the size limitations of the current prototype RTM lab facility press, 30 in. x 30 in. The wedge action provides the side pressure on the preform as the mating tool is closed to complete the debulking to the final part dimensions and to attain the required fiber volume. Inserts within the tool are free and permitted to float.

Other tooling concepts considered include aluminum mandrels/steel base plate, an aluminum-filled epoxy casting system, and rubber intensifiers. These concepts were discarded in favor of the steel wedge design based on positive past experience.

The injection design will be multi-port, one at each center support post, with four vent exits. Also included in the design is a resin reservoir on the two long sides which provides resin reserve to back-fill the preform during cooling.

Resin flow will be initially determined by using a broadgoods replica preform in the tooling proveout phase. The tool will be evacuated and the resin introduced at 50 psi and 180°F. Upon resin introduction, the exit ports will be opened and flow regulated to ensure complete filling. Sequencing and utilization of the exit ports will be determined. This trial method will provide confidence in the process prior to curing the graphite preform.

TESTING

The cured 30-in. x 62-in. window belt subcomponent and 7-in. x 7-in. element preform assemblies will be tested as shown in the test matrix, Figure 21. These tests will evaluate the tension, compression, shear and normal tension, and related elastic properties of the two textile preform supplier's test articles. The small elements are representative of the cross-stiffened intersections. Results from the finite-element analysis will be used to predict failure and the high-strain areas to locate the strain gages.

All testing will be accomplished at the Grumman Elements and Material Test facility. An MTS servo-hydraulic 'mega' machine, 1,000,000 lb calibrated capacity, will be used to test the subcomponent and a MTS servo-hydraulic, 90,000 lb, machine will be applied to the smaller test elements.

DESIGN CONCERNS

Designers who employ textile preform technology for airframe structures need a significant insight into the processing methodology to adequately define the part, design the tooling, and be confident in the end product performance. Based on the two preform methods presented in this paper, there is a significant difference in approach and final end product. The difference in material, tow and yarn sizes, weaving architecture, utilization of binders (tackifiers), stitching, and bulk will interact and is expected to result in different end product performance. There is much that must be developed further, and standardized, or at least controlled, to ensure repeatability and structural integrity from one textile supplier to another.

The engineering drawing presentation utilizing percentages of fiber orientations provided freedom to define the preform but resulted in diverse approaches that will have an impact on the end product performance. Drawing improvements and standards must be defined that will more capably control the end result. There is much to be learned in providing engineering definition to woven preform assemblies. As it stands now, this type of design freedom would not be permitted for production hardware since geometry and structural integrity are essential for product performance.

The test base for recurring weaving architectural patterns must be expanded in order to assess the impact on structural properties. The knockdowns associated with the 'Z' weaver locking yarns and stitching must be determined.

The analytical methodologies must be further developed to be able to predict structural capability considering the variation of architecture, varying yarn size, fiber volume, and defects.

The application of the uncatalyzed epoxy binders and tackifiers which are used to enable debulking of the preform must be thoroughly evaluated to assure that there is no deleterious effect on the processed article. These assessments should consider the effects of percentage of resin content, effects of nonuniform mixture with the structural resin, necessity to purge, and compatibility with both RFI and RTM processing methods.

The preform net final dimensions must be closely controlled to enable effective tooling to be designed. Bulk factors of 100 - 200% are unacceptable for pocketed cross-stiffened preforms. It would be desirable to provide debulked preforms to 10% of net.

CONCLUSIONS

The final assessment is that through-the-intersection continuous fiber cross-stiffened woven preform assemblies that offer a scale-up potential are feasible. This potential offers unique composite material solutions to all cross-stiffened applications such as bulkheads, frames, keels, beams, skin panels, and doors. The focus should be expanded to develop a solid data base and preform definition.

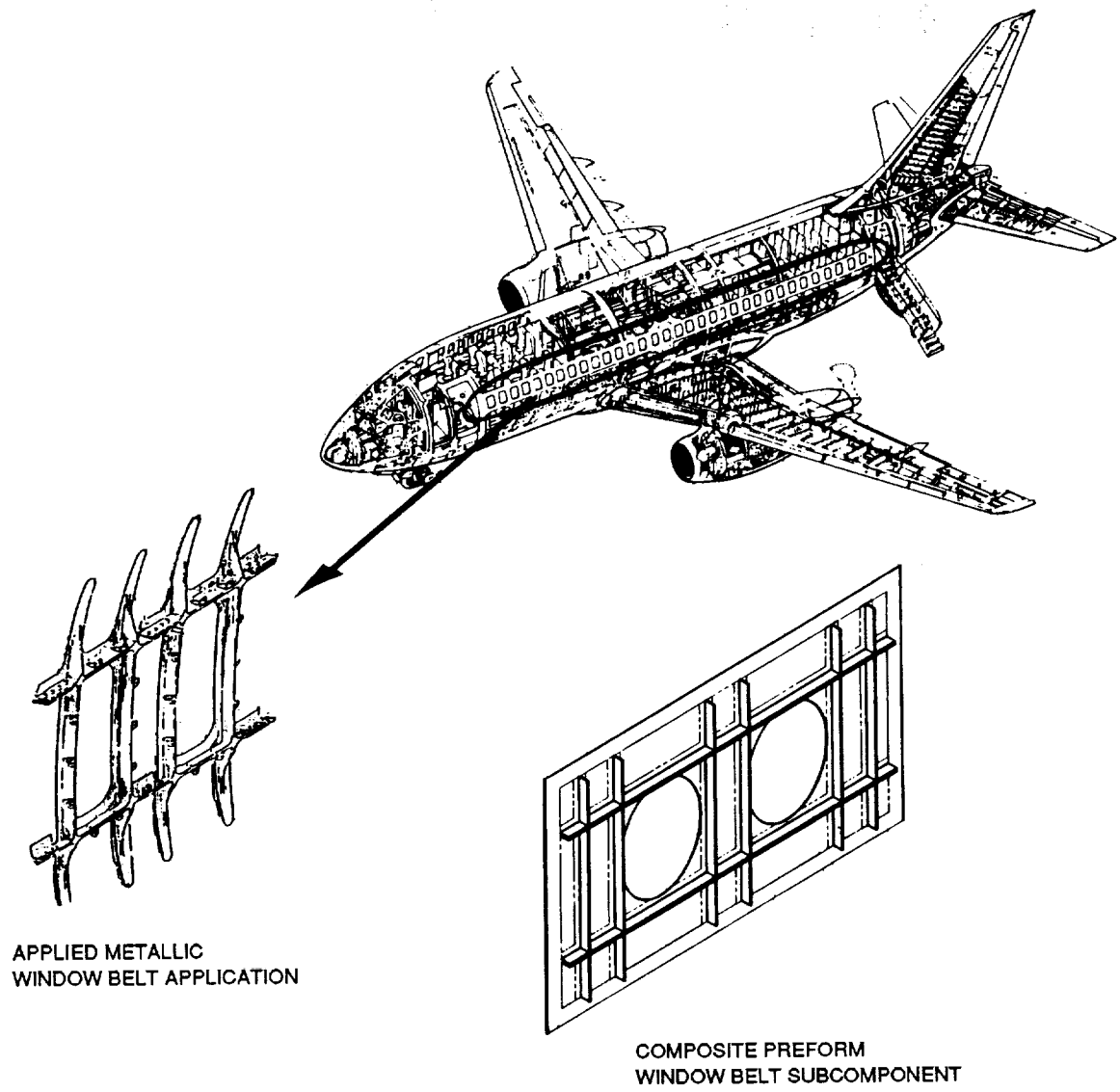

R92-0343-001

Figure 1. Cross stiffened structure airframe application.

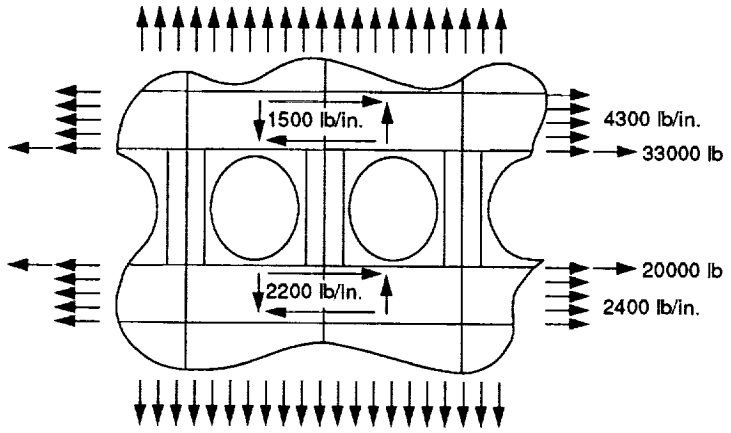

2200 lb/in. (ACTING ALONE)
1600 lb/in. (COMBINED)

A. MAXIMUM TENSION AND SHEAR STA 1424

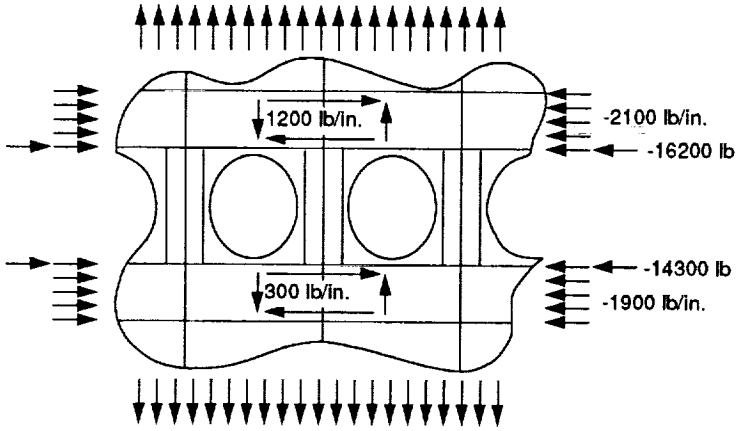

2200 lb/in. (ACTING ALONE)
1600 lb/in. (COMBINED)

B. MAXIMUM COMPRESSION AND SHEAR STA 1424

MR92-0343-002

Figure 2. Window belt maximum load conditions.

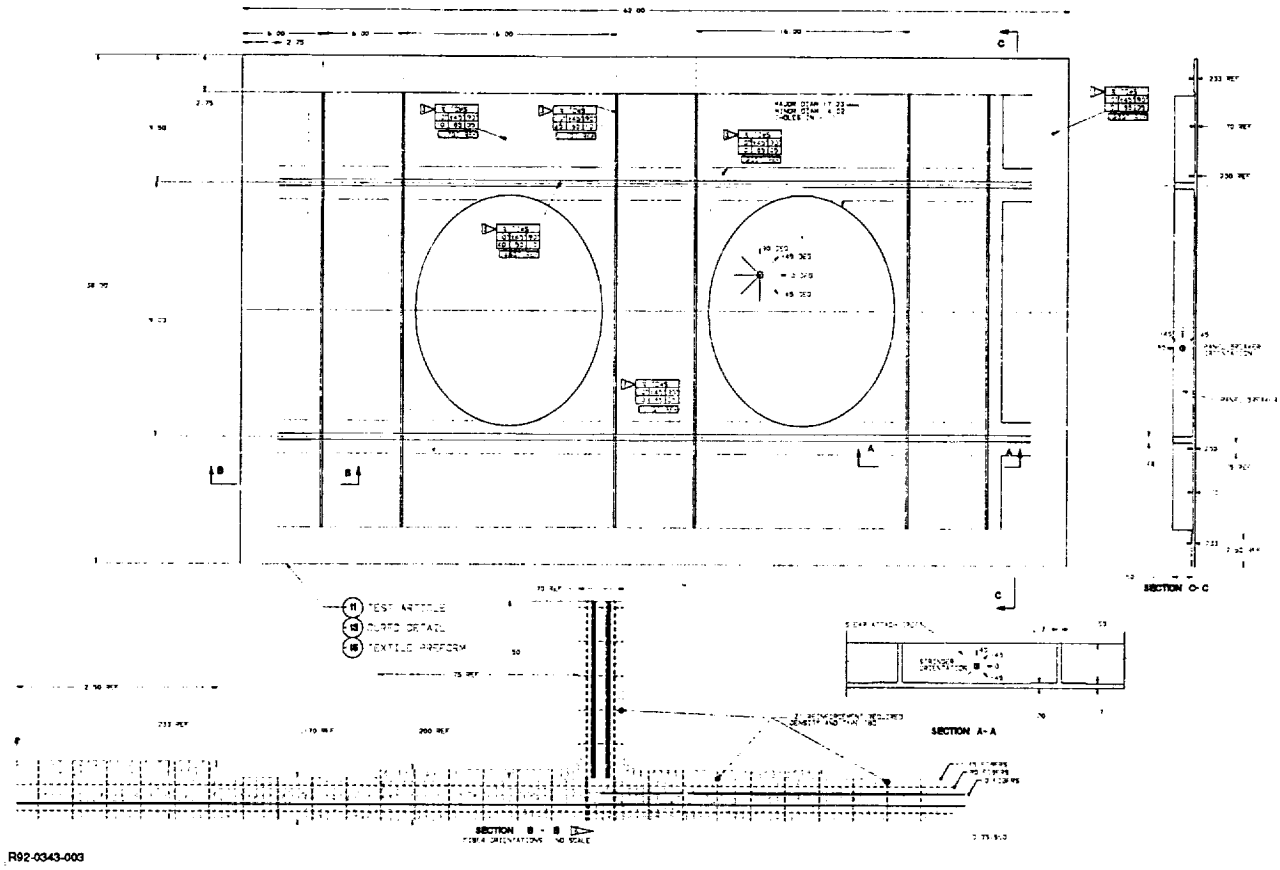

Figure 3. Cross-stiffened 3D woven window belt design, Dwg D19B1865.

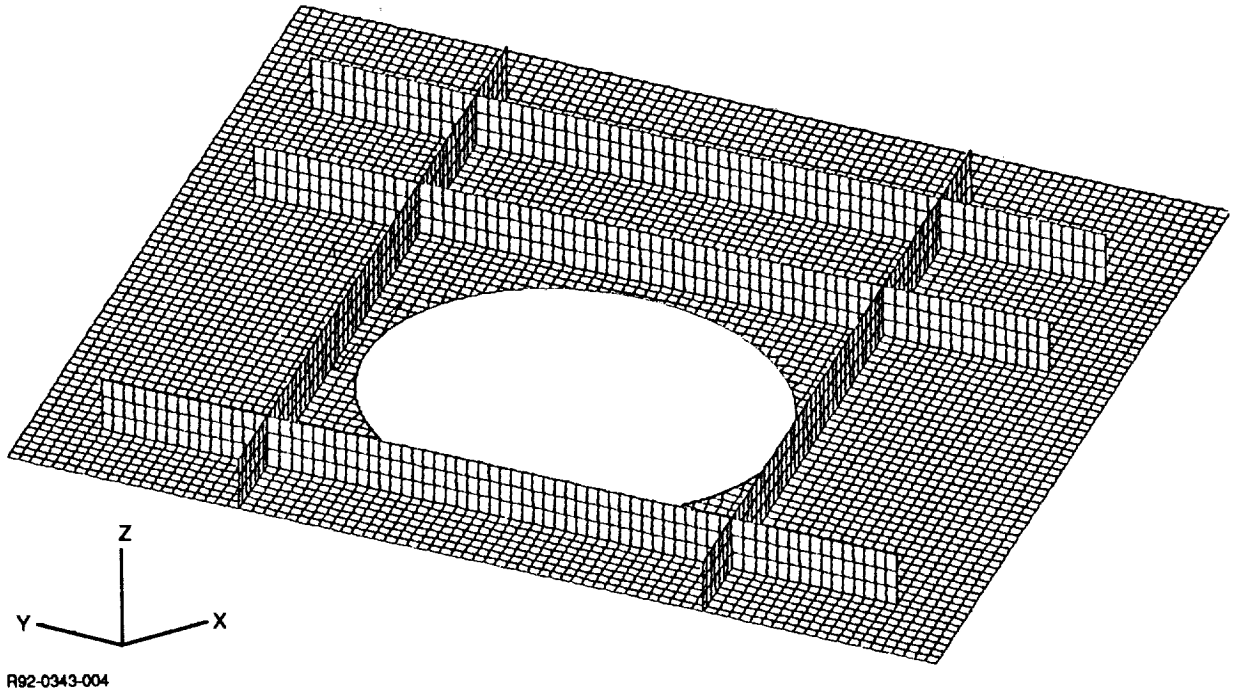

Figure 4. Finite element model, repeating section of window belt.

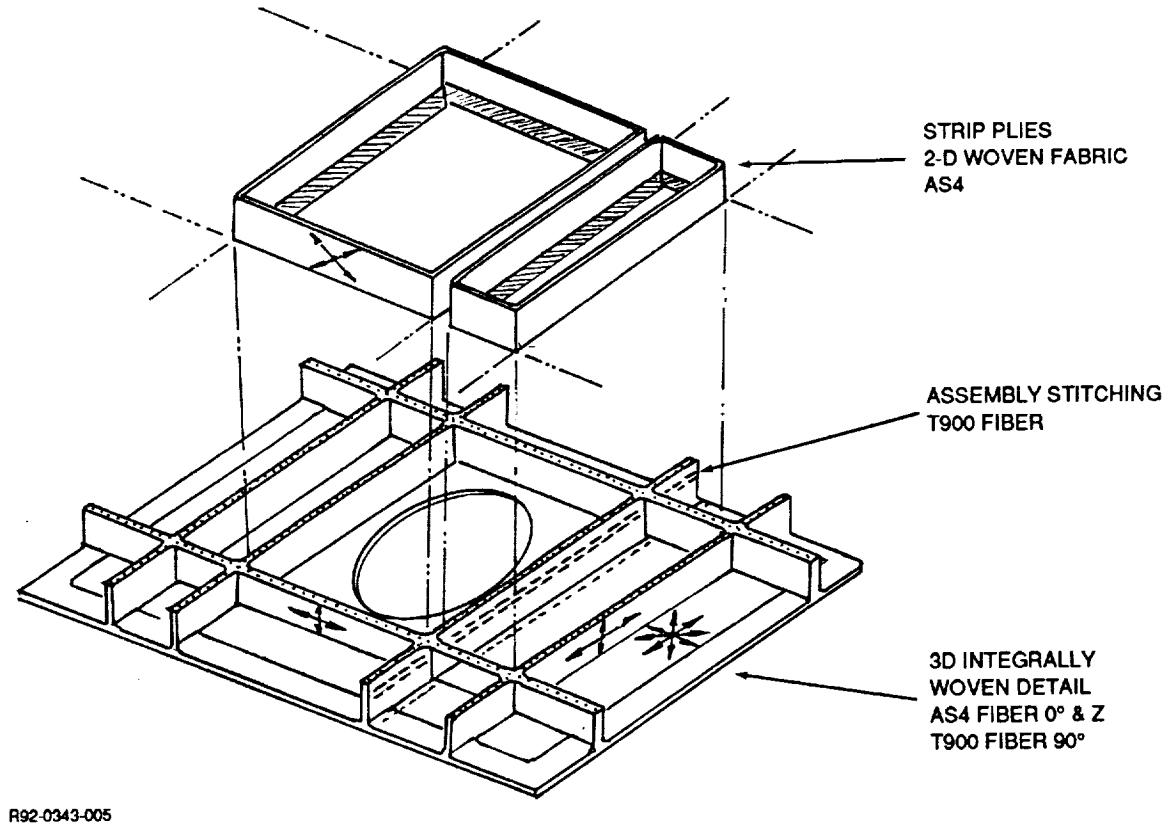

Figure 5. Preform assembly Techniweave, Inc. method.

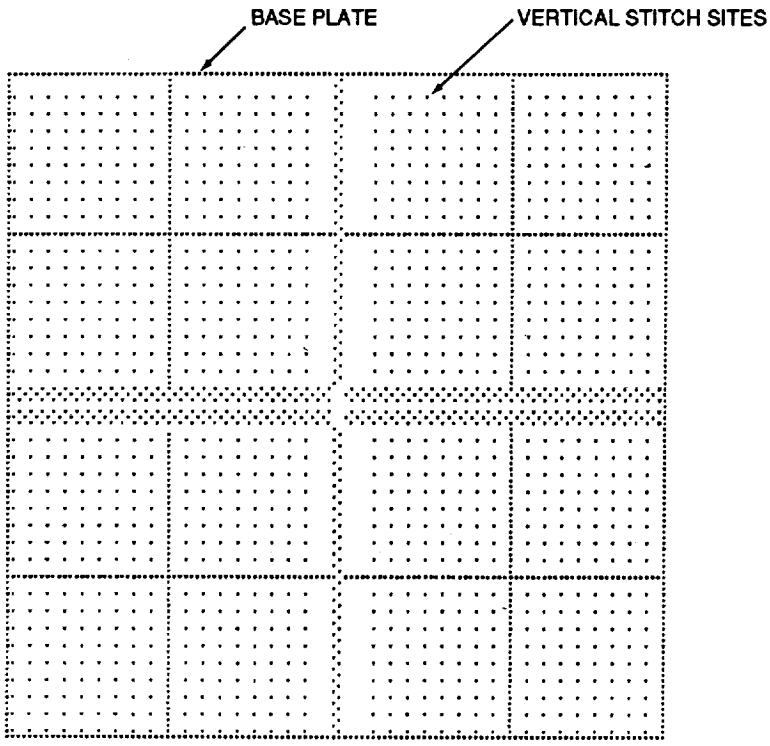

R92-0343-006

Figure 6. 7 x 7 test element pin pattern.

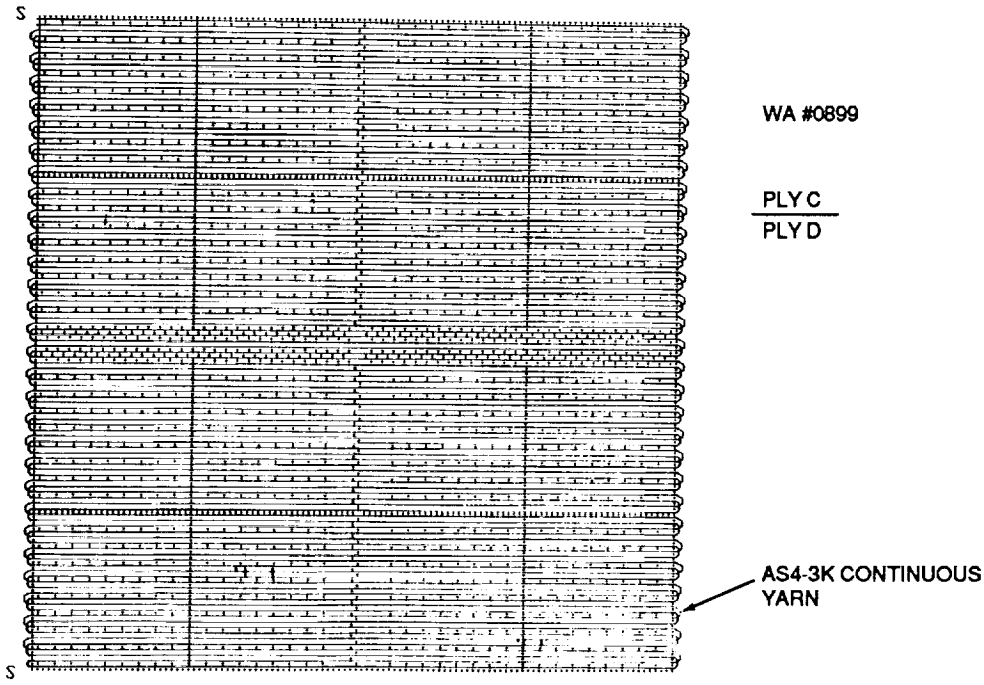

R92-0343-007

Figure 7. 7 x 7 test element skin panel, 0° layers.

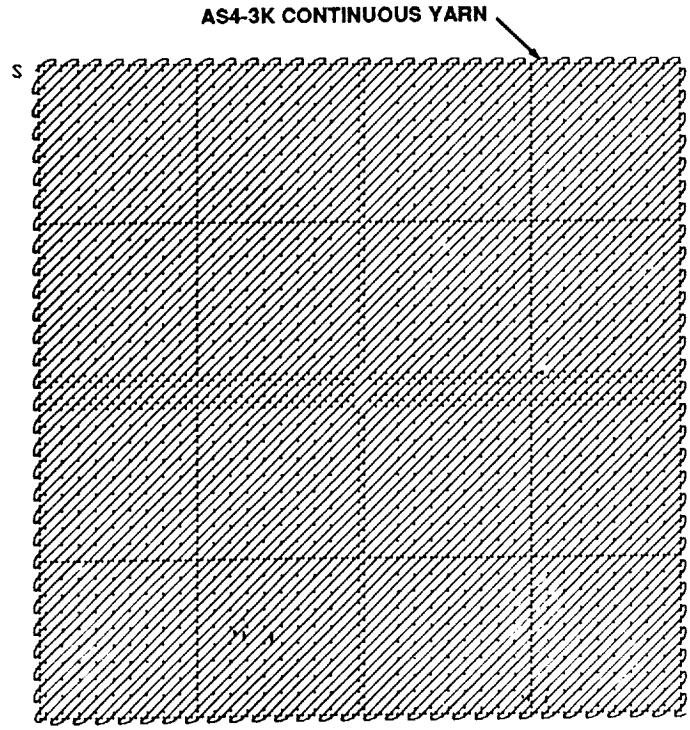

R92-0343-009

Figure 8. 7 x 7 test element skin panel, 45° bias layers.

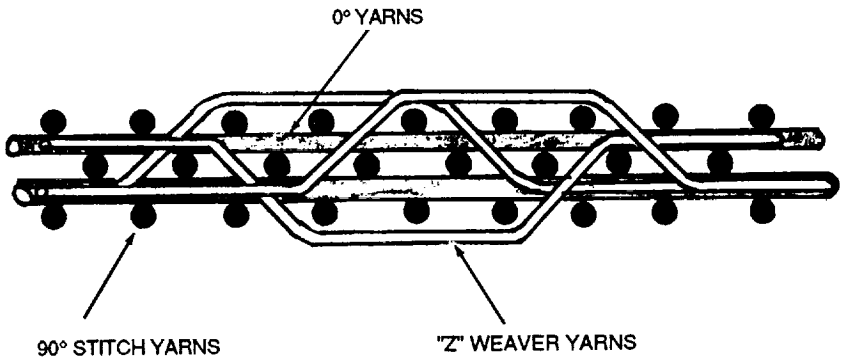

R92-0343-008

Figure 9. Weaving pattern - Technlweave.

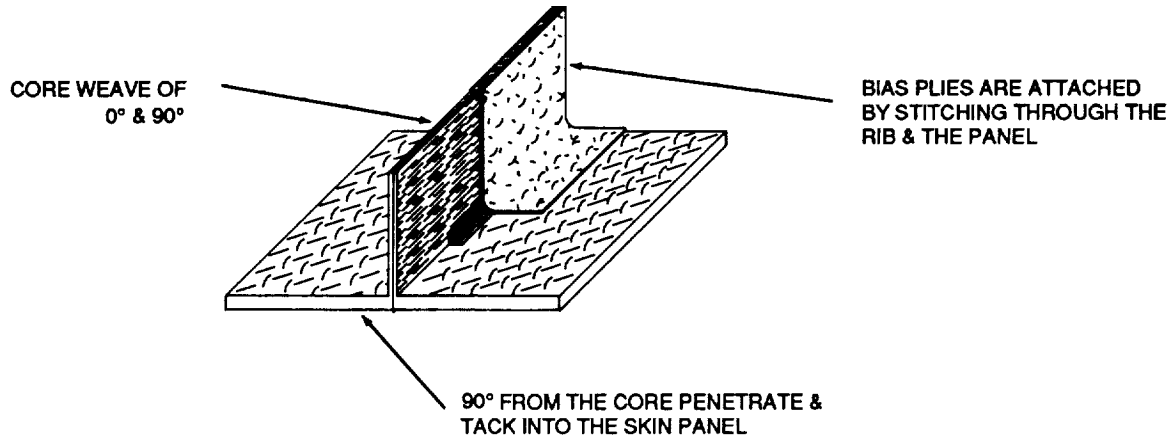

R92-0343-011

Figure 10. 0.17 stiffener construction.

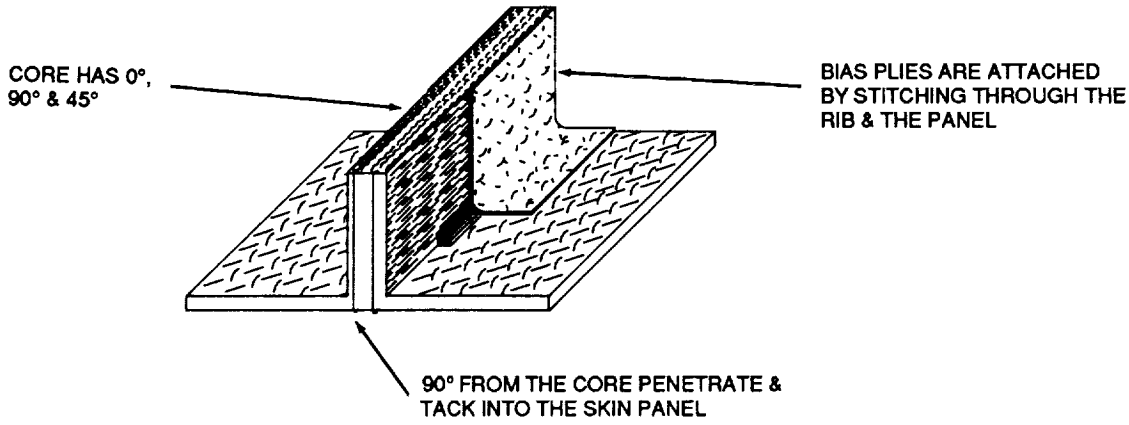

R92-0343-012

Figure 11. 0.48 stiffener construction.

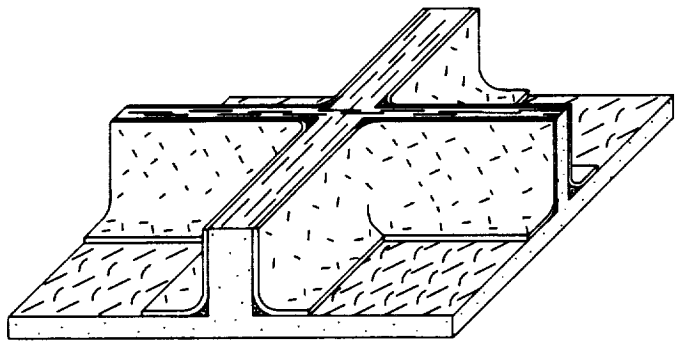

ALL OF THE 0° DIRECTION REINFORCEMENTS IN THE RIBS ARE
CONTINUOUS THROUGH THE INTERSECTIONS

R92-0343-013

Figure 12. Typical rib intersection.

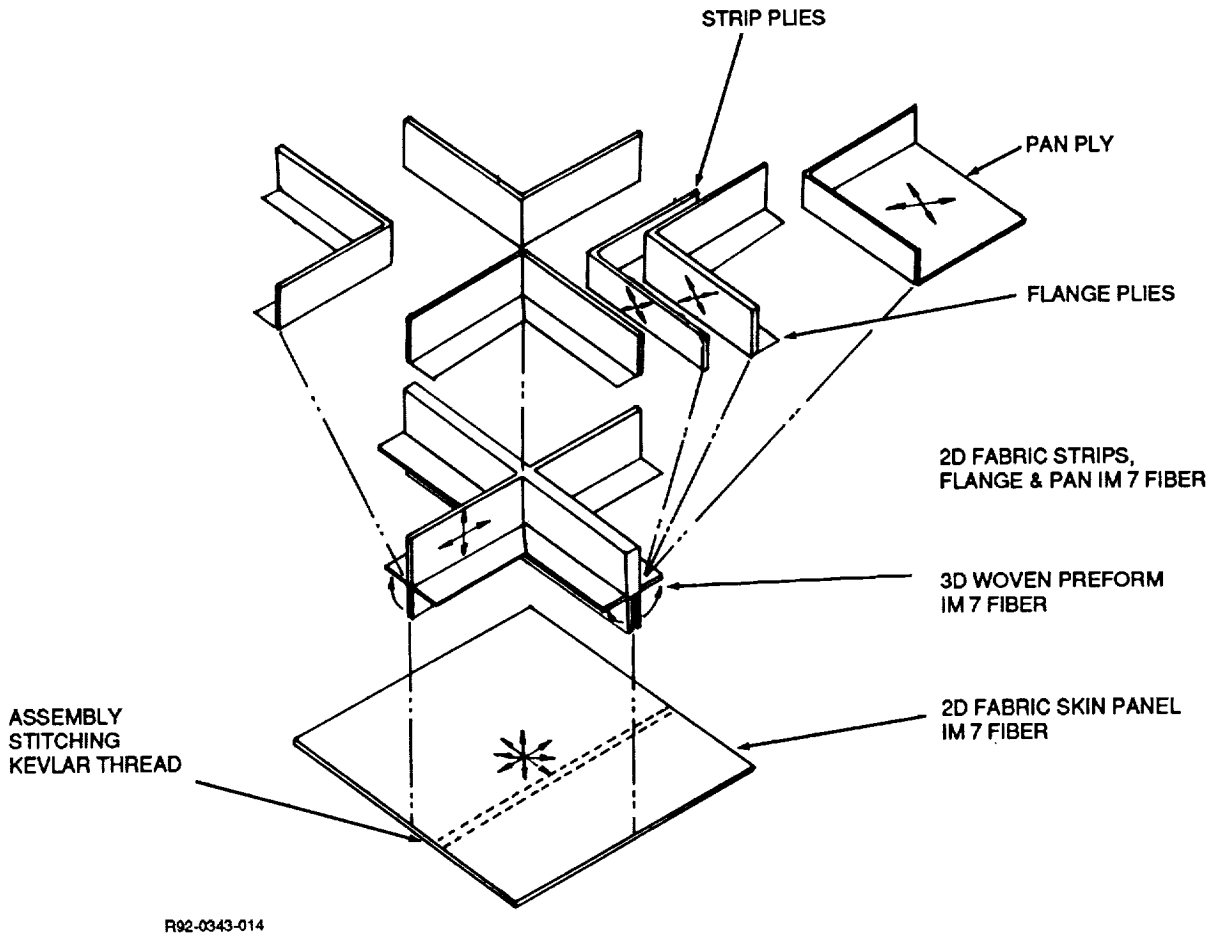

Figure 13. Test element preform assembly, ICI method.

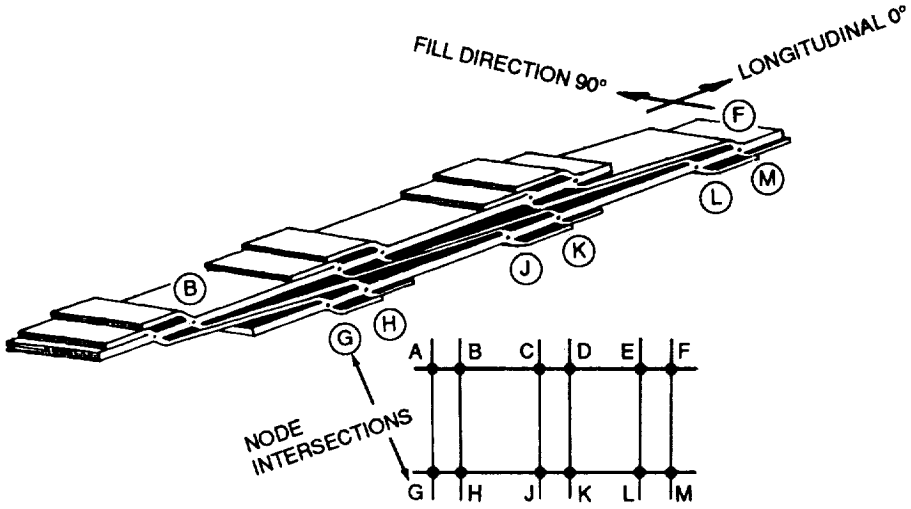

R92-0343-015

Figure 14. Unexpanded as-woven, core detail by ICI Fiberite.

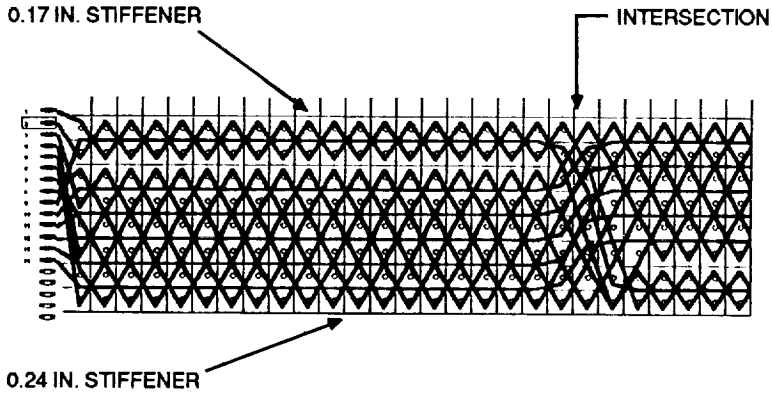

R92-0343-016

Figure 15. Fiber architecture 3D woven core perform, ICI method.

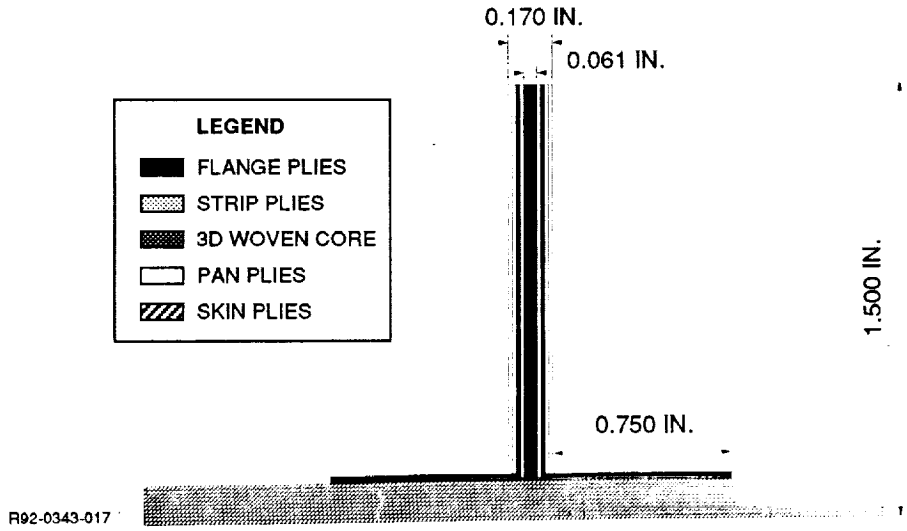

Figure 16. 0.17 in. thick stiffener – ply layup, ICI.

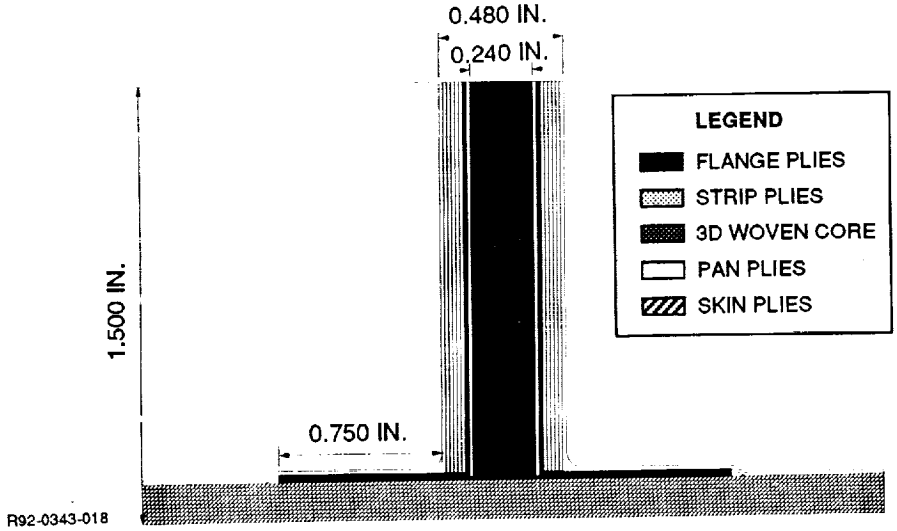

Figure 17. 0.48 in. thick stiffener – ply layup, ICI.

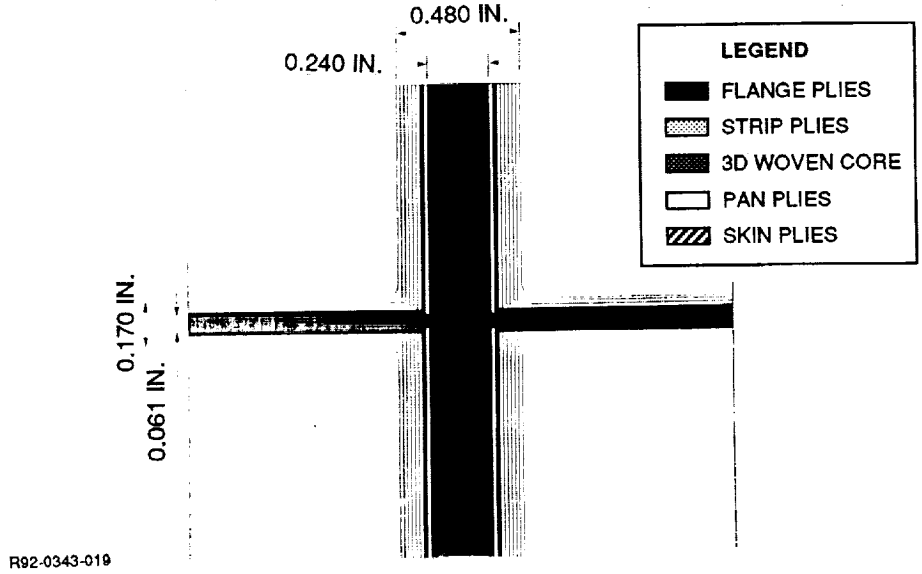

Figure 18. Intersection — ply layup, ICI.

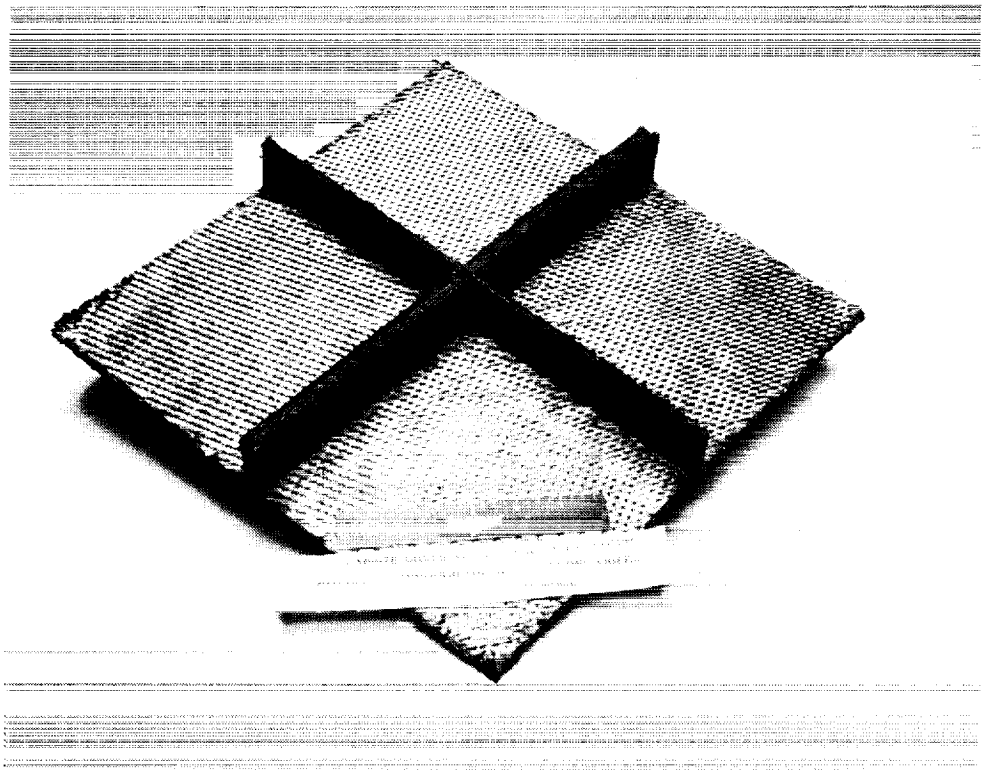

R92-0343-020

Figure 19. 14 In. x 14 In. woven cross-stiffened test element, ICI Fiberite .

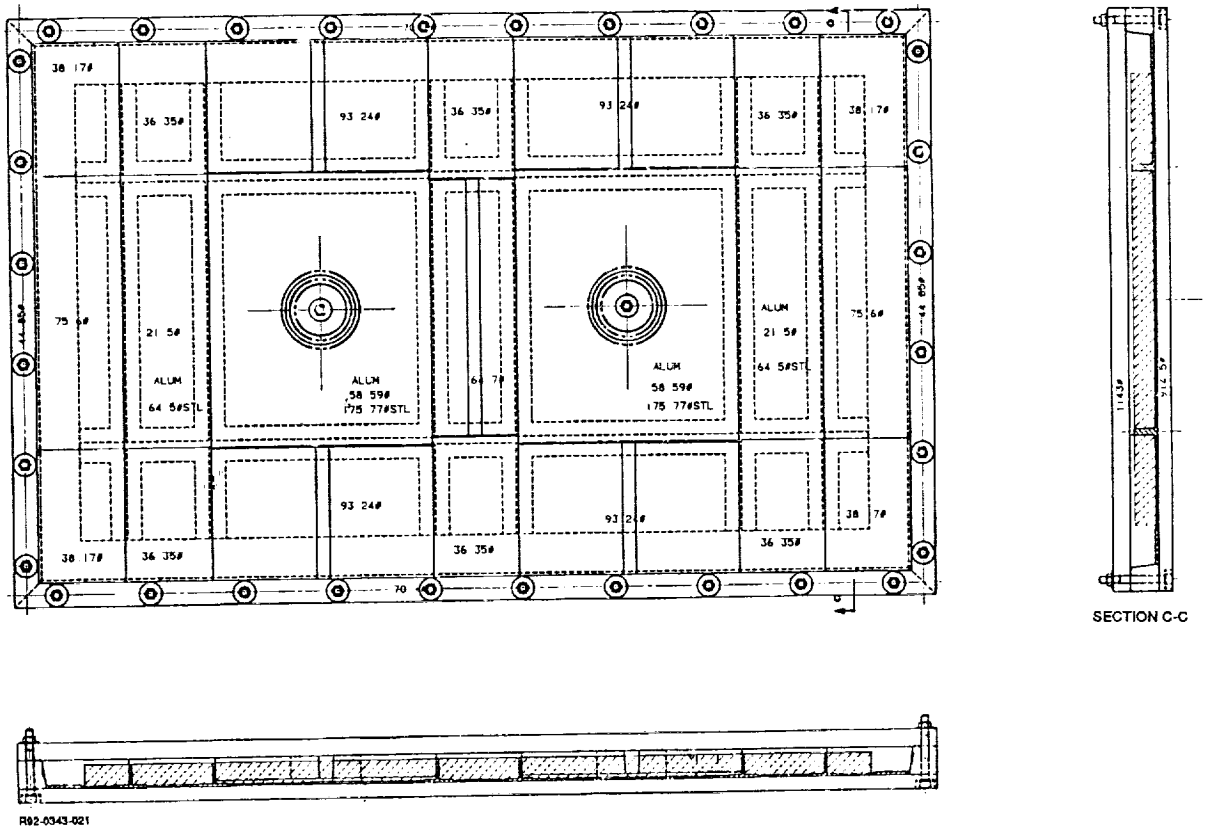

Figure 20. Tooling design concept, window belt subcomponent drawing D19B1865-11BOF .

SPECIMEN	TEST	DESCRIPTION
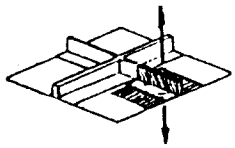	ELEMENT NORMAL TENSION AMBIENT COND	1.5 x 1.5 3 ARTICLES, TECHNIWEAVE 3 ARTICLES, ICI FIBERITE
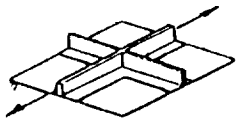	ELEMENT AXIAL TENSION LONGITUDINAL AMBIENT COND	7.0 x 7.0 2 ARTICLES, TECHNIWEAVE 2 ARTICLES, ICI FIBERITE
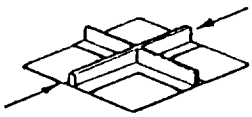	ELEMENT AXIAL COMPRESSION LONGITUDINAL AMBIENT COND	7.0 x 7.0 1 ARTICLES, TECHNIWEAVE 1 ARTICLES, ICI FIBERITE
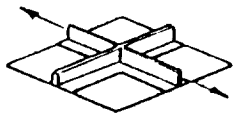	ELEMENT AXIAL TENSION CIRCUMFERENTIAL AMBIENT	7.0 x 7.0 1 ARTICLES, TECHNIWEAVE 1 ARTICLES, ICI FIBERITE
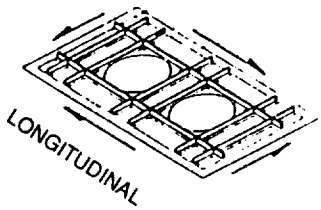	SUBCOMPONENT SHEAR AMBIENT COND	38.0 x 62.0 1 ARTICLES, TECHNIWEAVE 1 ARTICLES, ICI FIBERITE

R92-0343-022

Figure 21. Test matrix, cross-stiffened structure.

Table 1. Preform Fiber Orientation Percentages, Fiber Volume and Material.

APPLICATION & ORIENTATION	GRUMMAN D19B1865 TARGET VALUES	TECHNIWEAVE METHOD	ICI FIBERITE METHOD
PANEL			
0 DEG	10%	12% AS4-3K	9%
±45 DEG	85%	82% AS4-3K	82%
90 DEG	5%	6% AS4-3K	9%
Z	NA	N/A	NA
FIBER VOLUME	58%	57%	58%
HORIZONTAL STIFFENER			
0 DEG	40%	38% AS4-3K	28% IM7-12K
Z	NA	3% T300-1K	8% IM7-12K
±45 DEG	50%	46% AS4-5H	54% IM7-5H
90 DEG	10%	10% T900-3K	10% IM7-12K
FIBER VOLUME	58%	57%	52%
VERTICAL STIFFENER			
0 DEG	25%	28% AS4-3K	15% IM7-12K
Z	NA	6% T300-1K	5% IM7-12K
±45 DEG	65%	56% AS4-54	72% IM7-5H
90 DEG	10%	9% T900-3K	8% IM7-12K
FIBER VOLUME	58%	54%	56%
ASSEMBLY			
STITCHING	LESS THAN 6%	2% T900-3K	2% KEVLAR

R92-0343-010

[redacted]

An Engineering Model of Woven Composites Based on Micromechanics

W.C. Carter, B.N. Cox, M.S. Dadkhah, W.L. Morris

Rockwell International Science Center
1049 Camino Dos Rios
Thousand Oaks, CA

INTRODUCTION

Composites with three-dimensional woven architectures exhibit large strains to failure when compared to composites made up of the same materials but not with three-dimensional interlocking tows. The fracture mechanics of such three-dimensional architectures is a subject requiring substantial investigation and experimental testing.

Classical fracture mechanics concepts (for instance, an isolated defect in a homogeneous body) will not be applicable to the woven fracture test specimen. The use of an isolated singularity to characterize an entire specimen is inadequate when the density of defects is considerable and the material is heterogeneous. Modelling of such a complex system requires a great deal of insight and consideration as well as prudent choices of model sizes to make numerical schemes feasible.

The purpose of this manuscript is to review our recently acquired knowledge of damage accumulation in woven composites and to describe a practicable model of the macroscopic behavior in these and other complex composite architectures based on such knowledge. In this manuscript, discussion will be limited to uniaxial compressive loading; considerations of general loading (monotonic and cyclic) will appear in a subsequent manuscript.

Our modelling efforts may be briefly described as follows: the composite is subdivided into microstructural elements (*microelements*) in which the micromechanical modelling is either understood rigorously or can be represented adequately by statistical parameters. There can be microstructural elements for many different types of composite components, such as the various types of warp and weft and matrix for three-dimensional woven composites. The physical dimensions of microelements are made as large as possible while the response within the element can still be represented by a single micromechanical calculation. The various elements are linked together (sometimes by associating distinct corners and edges, sometimes by superposition) in a pattern which resembles a particular weave architecture (Fig. 1). The model can then be loaded in any manner and the linear and nonlinear elastic responses of representative weaves can be calculated. After the elastic regime, the fracture response is determined by monitoring the damage accumulation.

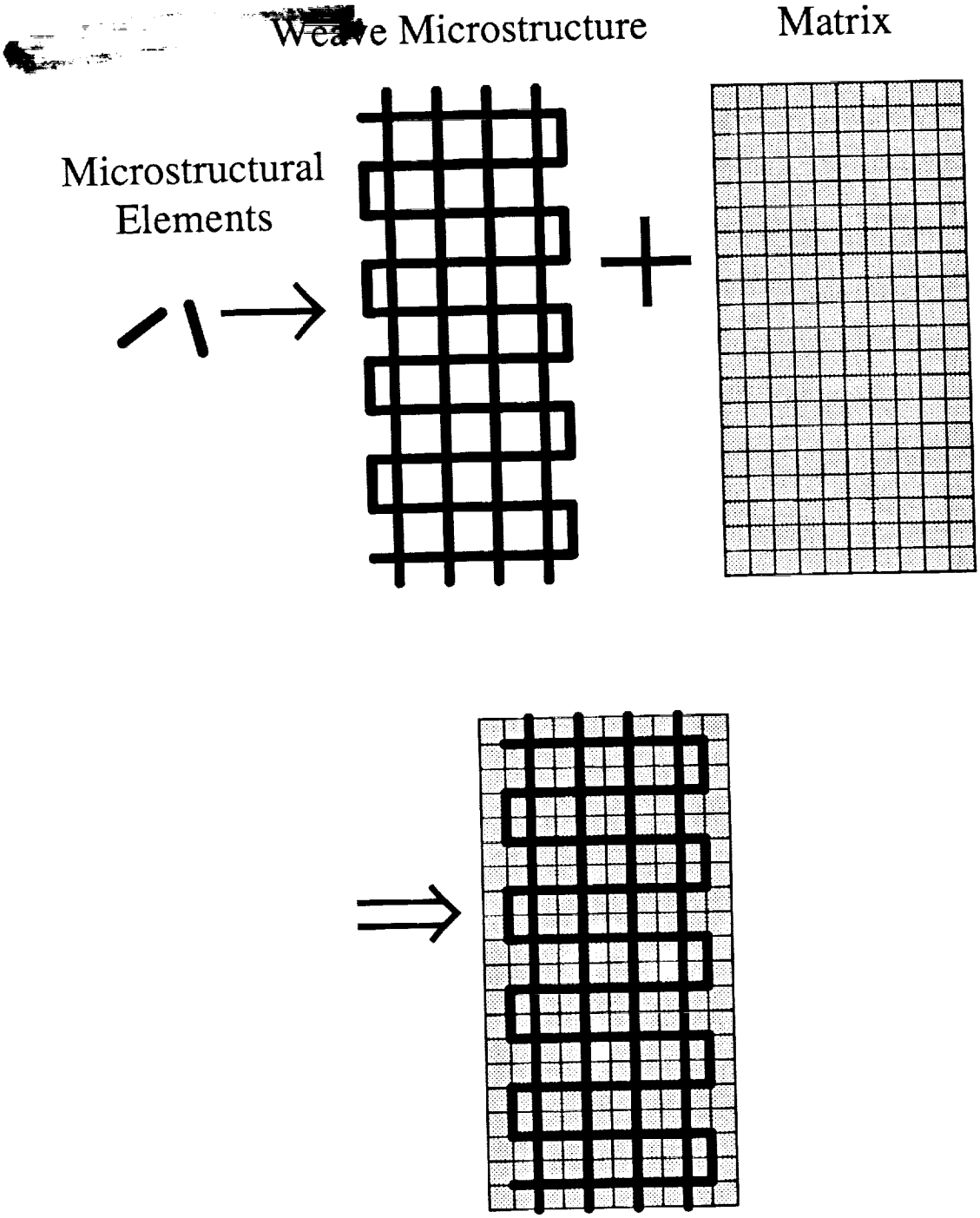

Figure 1: Illustration of Micro-element Model

Microstructural elements are designed to mimic derived micromechanical results; in the case shown, the microelements duplicate the derived response of kinking (on compression) or rupturing (tension) tows which are embedded in an elastic matrix. The microelements are assembled into an architecture which mimics that of a particular composite, in this case an ideal (two-dimensional) through-thickness orthogonal interlock weave. The architecture is then embedded into a matrix which has micromechanical behavior of its own and the model is loaded. Initial fracture can be predicted and damage accumulation can be monitored.

BACKGROUND

The nature of the *local* failures in the three-dimensional woven composites is similar to those observed in other fibrous composites. For the case of uniaxial compressive loading, possible local failure mechanisms are listed below; not all of these mechanisms have been experimentally observed.

1 *Buckling* The entire specimen may fail macroscopically by classical Euler buckling; this is determined by component geometry and design and does not fall under the subject micromechanics since it is a material failure. Localized buckling of tows does occur either with or without matrix-fiber delamination discussed below.

2 *Matrix Failure* The matrix may fail along plains of maximum shear. Intact tows will act as bridging mechanisms for mode-II matrix cracks which will typically lie along planes oriented at 45° to the loading axis.

3 *Fiber Crushing* If the compressive strength is exceeded in the tows whilst being supported by an intact matrix, the fibers may fail with no out-of-plane displacement. The crushing strength of the tows is expected to follow weak-link statistics.

4 *Fiber Kinking* In kinking, a segment of a tow rotates away from the loading axis as a rigid body and the tow is ruptured along parallel planes (Fig. 2). The tow loses its load bearing capacity at the kink; but, if the matrix is still intact, stresses will build back up in the tow as stress is transferred back to the fiber over a characteristic distance called the shear transfer length. The micromechanical conditions for kinking are known [1, 2, 3]. The critical axial stress, σ_c, for kinking is:

$$\sigma_c = \frac{k^* - \tau^\infty}{\phi_{total}} \tag{1}$$

where k^* is related to the matrix yield stress, τ^∞ is the remote shear loading, and ϕ_{total} is the total tow misalignment away from the load axis. Significantly lower critical kinking stresses occur in segments of tows which are misaligned. The effect of fiber misalignment in two-dimensional woven composites has been observed [4].

Interactions between tows can also lead to the formation of kink bands. Such a case is illustrated in Fig. 3 where a warp weaver pushes a filler (weft) against a stuffer (straight warp). The additional contact load has the effect of increasing the magnitude of the shear at the tow and knocks down the critical kinking stress as in Eq. 1.

5 *Delamination* Delamination of the tow-matrix interface is a possible, but not a necessary, precursor to kinking. If delamination occurs over a sufficient length of a tow, then the loss of constraint will allow the tow to rotate freely into greater misalignment—thus knocking down the kinking critical stress. Delamination may also occur as a result of a fiber kinking in a previously un-delaminated region.

Fiber kinking has been observed in many composite systems: carbon-carbon composites [5], glass fiber-epoxy matrix [6], aligned carbon fiber-polymer composites [7], [4], carbon, and glass fiber-epoxy matrix [8]. The micromechanical models leading to Eq. 1 [2] are applicable in each case.

SC53780
SC53600

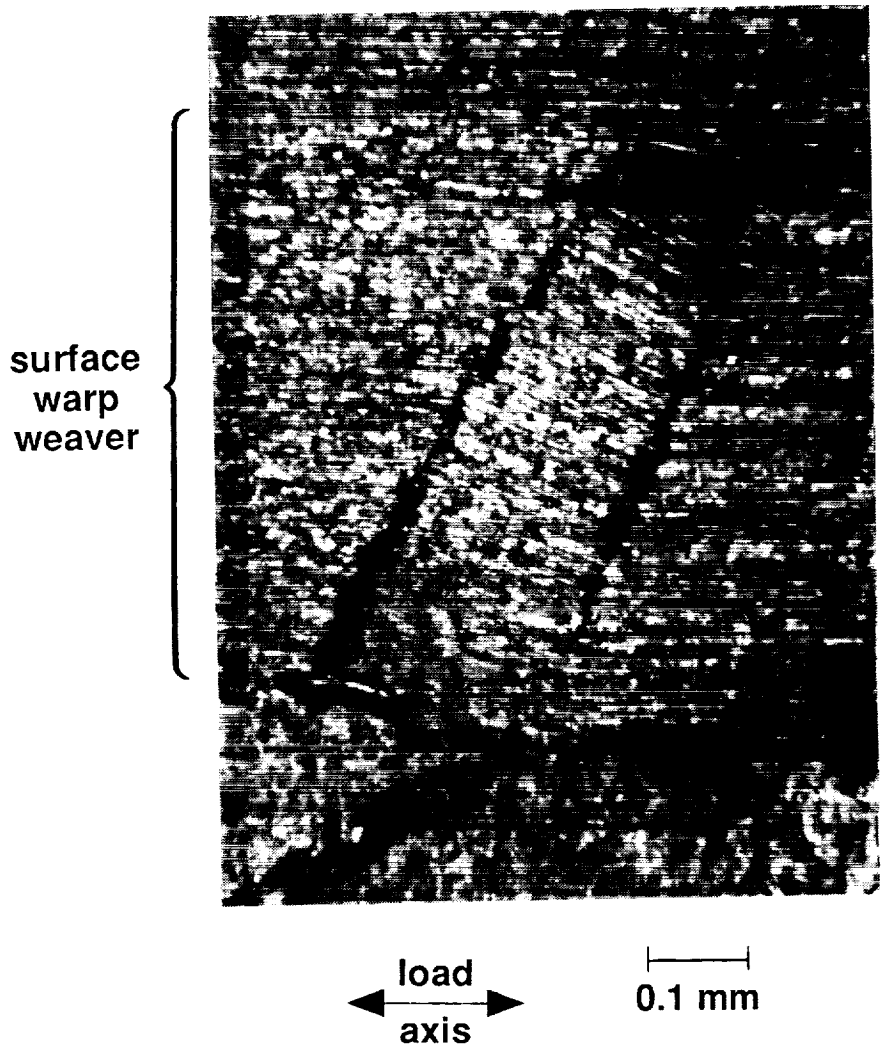

Figure 2: Kink Band Failure in Compression

Layer-to-layer angle interlock – AS4/Tactix 138-H41

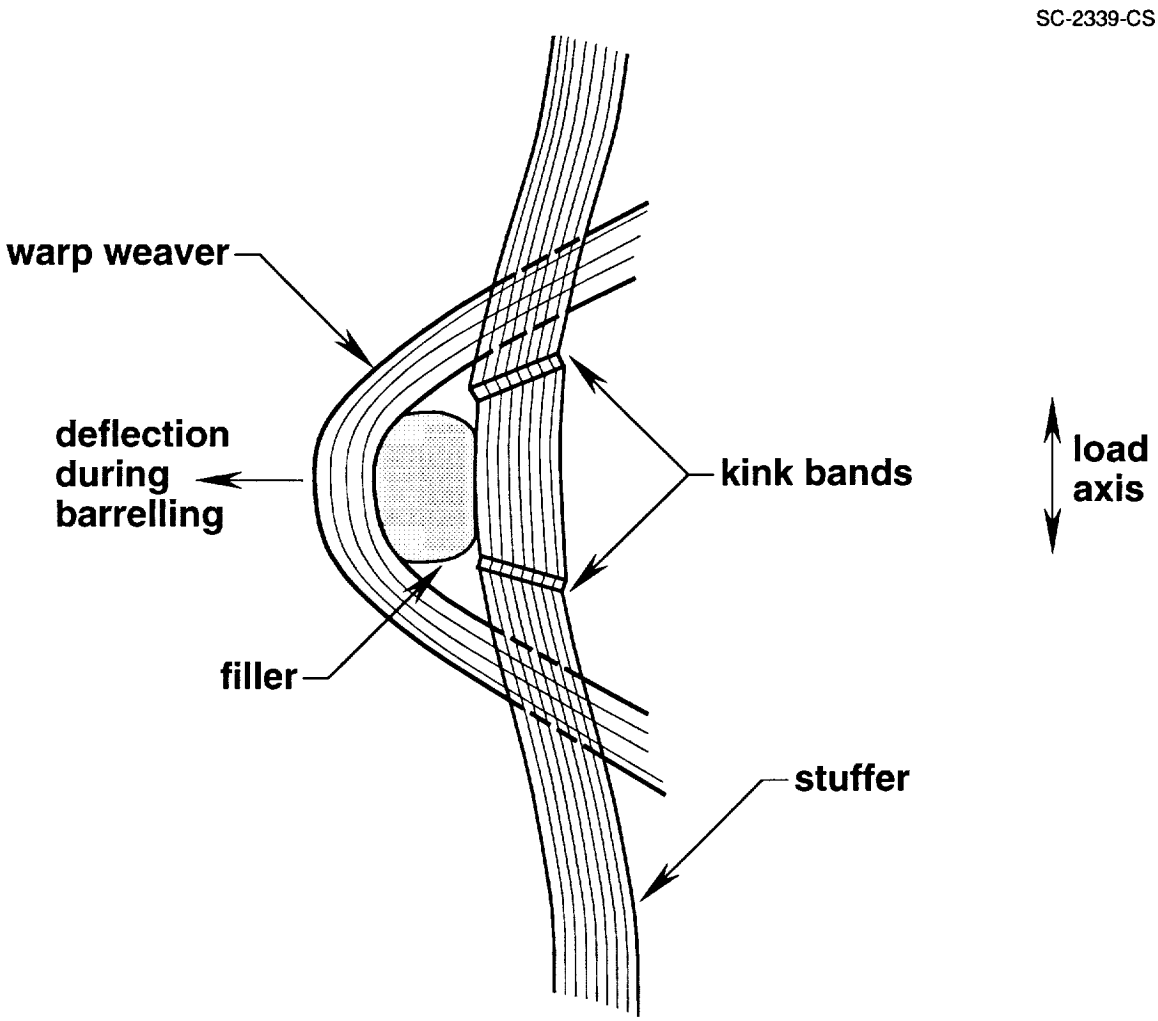

Figure 3: Illustration of Contact Between Tows

Modelling must incorporate interactions between various parts of the structure. This illustrates a kink band which has formed when a warp weaver pushed a filler against a stuffer.

EXPERIMENTAL OBSERVATIONS IN 3D WOVEN COMPOSITES

Results of several monotonic compression tests are illustrated in Fig. 4. Experimental techniques and specimen preparation may be found in a previous publication [8]. All of the weave architectures show considerable ductility after the initial load drop. Yield strengths are typically 150-200 MPa with yield strains of 0.5%. Typical strains to failure are 5-12%.

At the initial yield, damage appears at the specimen surface as tows which have buckled and kinked out of the interface where the constraint is lowest. Sectioning of a just-yielded specimen did not show any fiber failures or delaminations in the specimen interior: all initial failures are correlated with the lack of tow constraint at the specimen surfaces.

Sectioning of specimens which have undergone some plastic loading (here, plasticity refers to the load-displacement diagram, not to the physical process of deformation) revealed kinks adjacent to small delamination cracks. In the interior of the specimen, the locations of the kinks appear to be spatially uncorrelated. Kinks observed near the specimen surface are either uncorrelated with any previous damage or they appear where a delamination crack veers from the surface into the matrix and terminate at a kink site.

At later stages of plasticity, kink failures become spatially correlated and link up via delamination cracks which veer into the matrix and intersect one another. Several such growing defects begin to link together along a shear band at 2-4% strain. Subsequently, deformation becomes localized to the shear band with intact tows providing mode-II bridging tractions. Final failure occurs when the tows can no longer provide sufficient bridging.

MACROSCOPIC MODEL BASED ON MICROSTRUCTURAL ELEMENTS

The composite architecture is subdivided into regions, each of which is to be represented by a particular micromechanical model or by an appropriate statistical model. Such regions become *microelements* which will implicitly represent an averaged mechanical behavior. The microelement need not have the same measure as the region to which it is applied; in the woven materials for instance, a one dimensional object (i.e., a geometric length, L_s) with six degrees of freedom (displacements and rotations) at each of its two nodes represents the volume in a tow segment of length L_s. With the understanding that the model need not be elastic or even plastic in the conventional sense, such a one-dimensional element can be called a beam. The beams can be assembled together and superimposed into a three-dimensional network of brick elements which represent the micromechanical behavior of the matrix. Because the elements are linked together at nodes, only the *average* behavior of the representative region is probed. This provides a practical way of realistically modelling fracture and damage in a complicated composite architecture; such averaged behavior is reasonable when applied to a micromechanical model. It may not feasible to model the continuum mechanical behavior in a heterogeneous, geometrically disordered composite architecture. To summarize, the microelement model consists of three parts: 1) the micromechanical models, 2) the various types of representative elements, and 3) the geometry of the element connectivity.

Working models for fracture and damage accumulation in woven composites follow from the results of idealized micromechanical calculations. For instance, a segment of tow (over which the

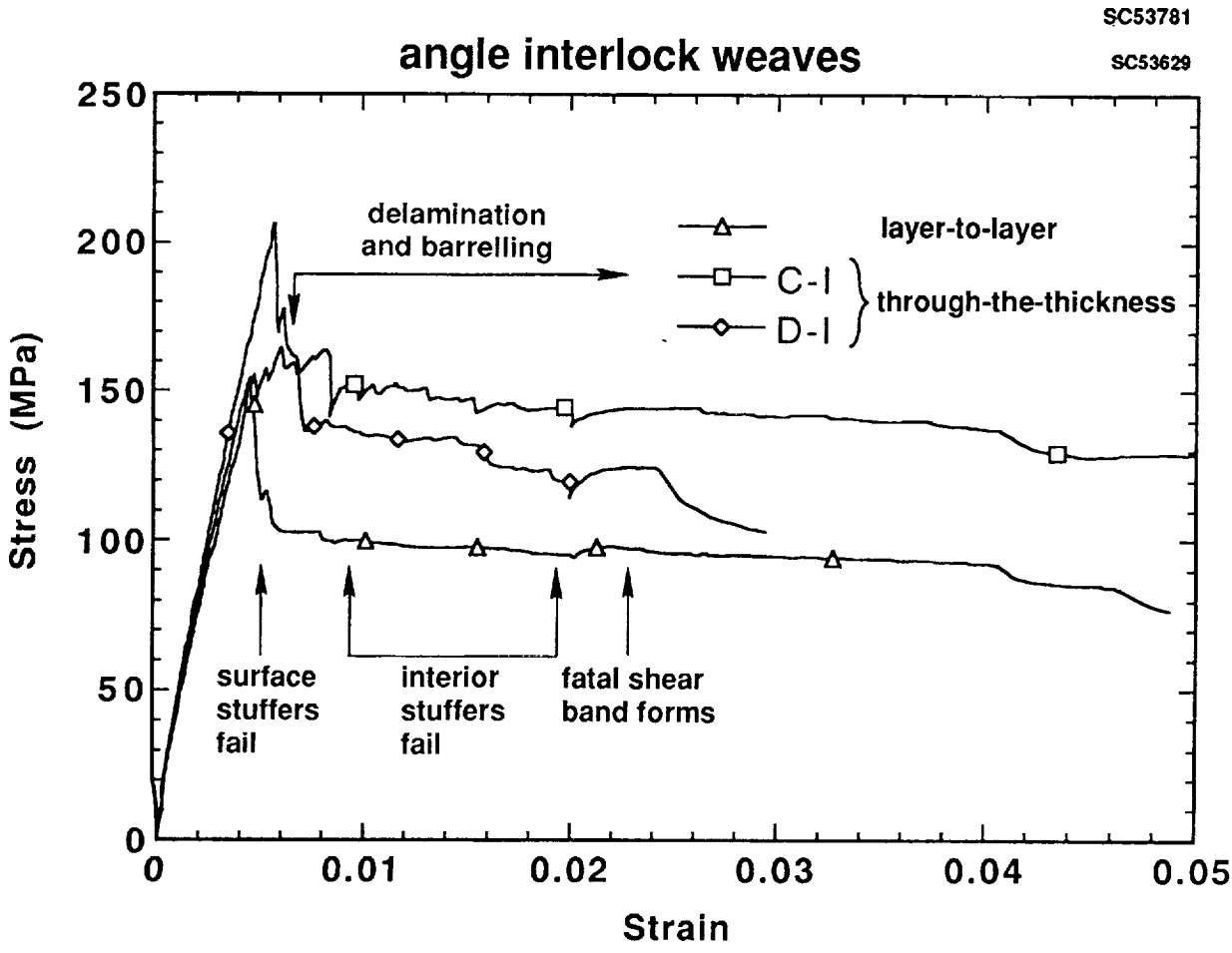

Figure 4: Monotonic Compression Dog-Bone Specimens

matrix stress transfer is changing slowly) may be considered an elastic flexural member until the condition for fracture (Eq. 1) is satisfied whereupon the tow's load bearing capacity drops significantly and the load is shed to the matrix. The matrix can be considered an effective anisotropic medium which can delaminate or fail depending on its immediate environment and stress. Every element is positioned in a manner which reflects the geometry of the composite (Fig. 1) and then the system is numerically loaded as desired.

Stochastic effects can be modelled in two distinct ways: 1) by picking critical microstuctural flaw sizes (or, fracture strengths) according to some distribution, or 2) perturbing the coordinates of the element nodes about some idealized position (Fig. 5); in this way effects of tow waviness can be simulated. Monte Carlo simulations can be performed and design parameters such as the lower limit and variability of strength, or the distribution of the work of fracture can be assessed in terms of inherent material variability.

One major function of the model is to evaluate the failure mechanisms and damage accumulation as a function of composite architecture. The size scale of the element is picked to be the largest value over which the micromechanical models apply, or the scale over which large gradients in stress decay. A reasonable value of the element length scale for the woven composites is the shear transfer length, l_s:

$$\frac{l_s}{R_f} = \frac{\sigma_c}{2V_f \tau_y} \tag{2}$$

where σ_c is the interface delamination stress, V_f and R_f are the tow volume fraction and radius, and τ_y is the matrix yield stress. The ratio l_s/R_f is approximately 10 for the woven composites illustrated in Fig. 4. Element length scales smaller than l_s should not affect the quality of the damage simulation, but larger element sizes will introduce an artificial scaling. In practice, scales are picked to be less than l_s, but large enough to result in a relatively small number of elements. It should be reiterated that the purpose of the simulation technique is not to calculate approximations to the continuum stress and strain values; stresses and strains are calculated, but on a mesh which is typically more coarse than used in other finite element methods.

The results of the simulation which we will show below were obtained through the use of a commercial solver (ABAQUS) but the method could be used—in principle—with any finite element code routine. The method is a hybrid finite element technique and the idea of superimposing elements has been utilized before in studies of the elastomechanics of reinforcement structures (e.g., strut and frame structures on a fuselage). The idea of using microstructural fracture mechanics for elements to model the accumulation of damage has been suggested previously [9]. Methods of arranging the microelements to mimic the composite architecture continue to be investigated carefully.

MODELLING RESULTS

Modelling is still in progress in two and three dimensions for a variety of different microstructural elements. Some of the initial results appear below; even more promising results are being obtained at the writing of this manuscript.

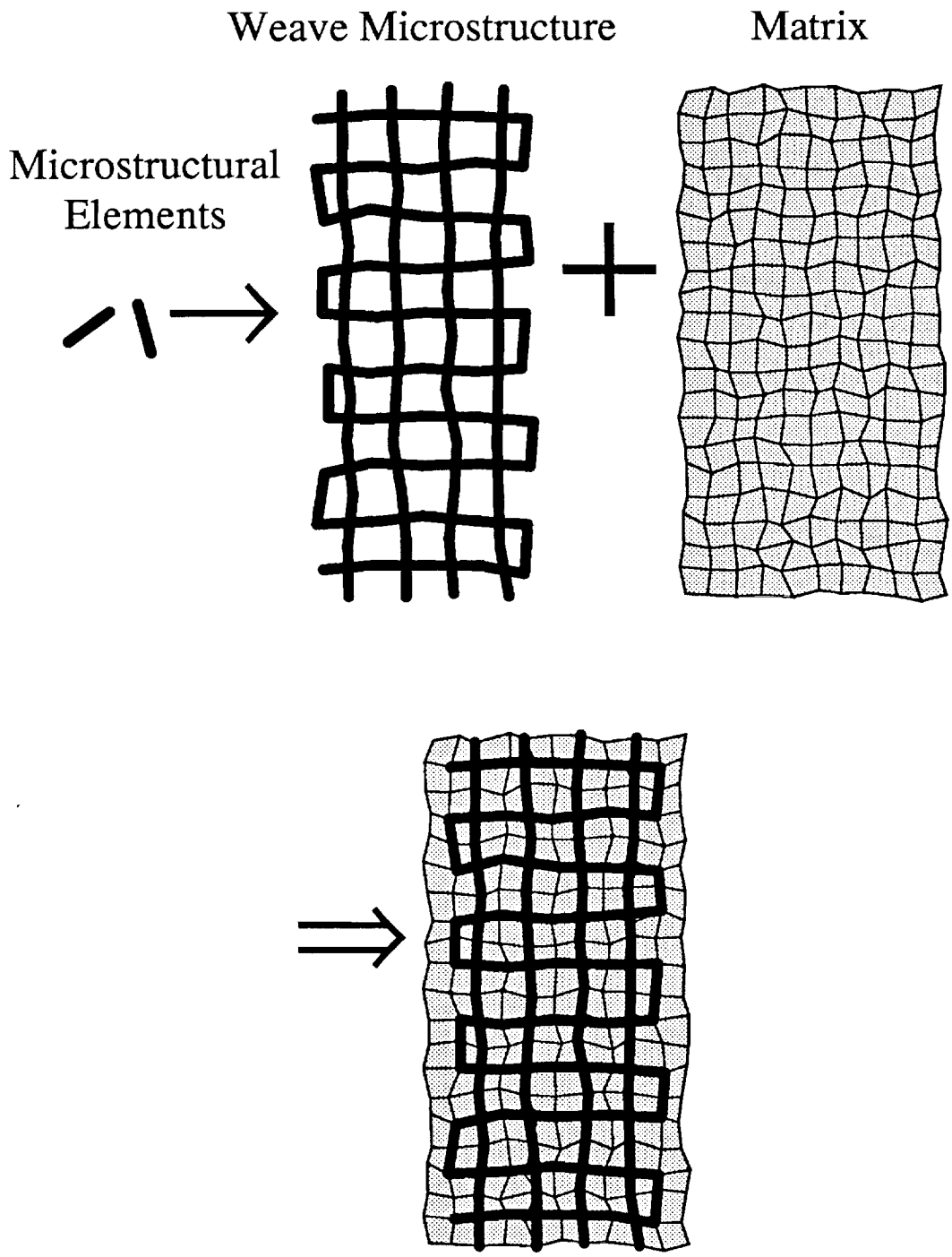

Figure 5: Illustration of Perturbed Geometry in Micro-element Model
Effects of inhomogeneity due to tow waviness can be modelled by perturbing the geometry of the model as in the above illustration. The size of the perturbation can be varied and arbitrary spatial correlations may be introduced. This is one of two ways statistical variations can be introduced; distibutions of parameters, such as strength, can also be imposed on the microelements taken individually.

Results from two simulations appear in Figs. 6-7. The modelled geometry is a though-thickness orthogonal interlock weave, represented in two dimensions. The two models are identical in all respects save that the one in Fig. 7 has been geometrically perturbed to simulate the inevitable effects of processing variations on the weave architecture. The elastic stiffness of the tows is ten times that of the matrix. The matrix is fully elastic in Figs. 6-7 and the stuffers fail at a critical strain of 1%. In this particular simulation, the warp weavers are assumed not to fail. The warp weavers are connected to the stuffers where they cross and the weave architecture is embedded in four-noded matrix elements.

The model in Fig. 6 shows the load-displacement curve for the ideal geometry. The cartoons A-E illustrate the damage development in the tows at increasing values of strain. In cartoon B, the outer stuffers fail over most of their length, quickly followed by general failure of the interior stuffers. Since all stuffers have nearly the same load at failure and the matrix stresses are fairly homogeneous for this ideal geometry, all the stuffers fail at once, giving rise to a large load drop in the force-displacement diagram.

The model in Fig. 7 shows the results for a perturbed geometry (the scales are the same as in Fig. 6). The load displacement diagram shows the same qualitative behavior as the experimental curves in Fig. 4. Since all the of the stuffers do not fail together, stuffers fail at higher strains and thus the work of fracture is enhanced. However, the elastic stiffness for the perturbed geometry is slightly reduced and its strength is diminished.

Load-displacement curves for a slightly different model are illustrated in Fig. 8. In this case, the matrix has plastic behavior; and, for the diagram on the right of Fig. 8, the geometry is perturbed and the tow failure strengths have been uniformly distributed about an average strength. The loading behavior is very much like what is experimentally observed. *It is reasonable to conclude that the randomness and heterogeneity in the experimental specimens have a large influence on the mechanical behavior.*

FUTURE WORK

Models for other weave architectures are being built and tested and results from those two and three dimensional stochastic models will appear in a future publication. Other microstructural elements are being developed, such as a delamination element between fibers and matrix. More realistic models for effective damage production in the matrix and orthotropic elastic behavior are being incorporated.

Monte Carlo type calculations will be made and statistical variations in the fracture response of the weave architectures will be obtained.

This technique is expected to find a wide range of applicability and utility in modelling composite architectures.

ACKNOWLEDGEMENTS

This work is funded by NASA Langley Research Center under contract NAS1-18840, contract monitors C.C. Poe and C.E. Harris. We are grateful to Mike James for insightful discussions and assistance, and to Norman Fleck for critical discussions of the model and calculations.

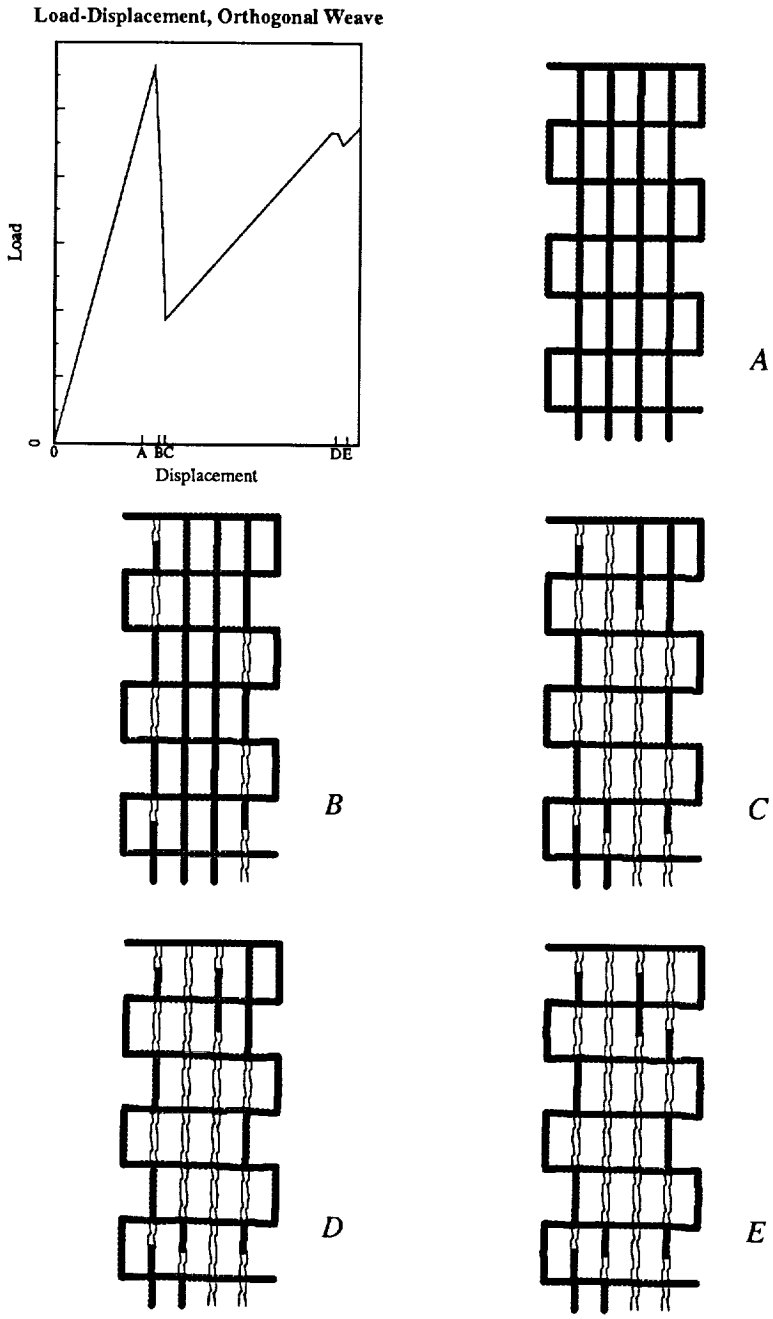

Figure 6: Ideal Orthogonal Interlock Geometry

This schematic shows the load-displacement behavior for an idealized plane of orthogonal interlock woven material. The results are obtained by a hybrid finite element technique described in the text. The tows are embedded in an elastic matrix which carries the load which is shed by a tow when it kinks (shown for illustration in outline). The orthogonal warp weavers are not allowed to fail in this particular model. The vertical tows (stuffers) have a failure strain of 0.01. The tows are 10 times stiffer than the matrix; the matrix is not illustrated.

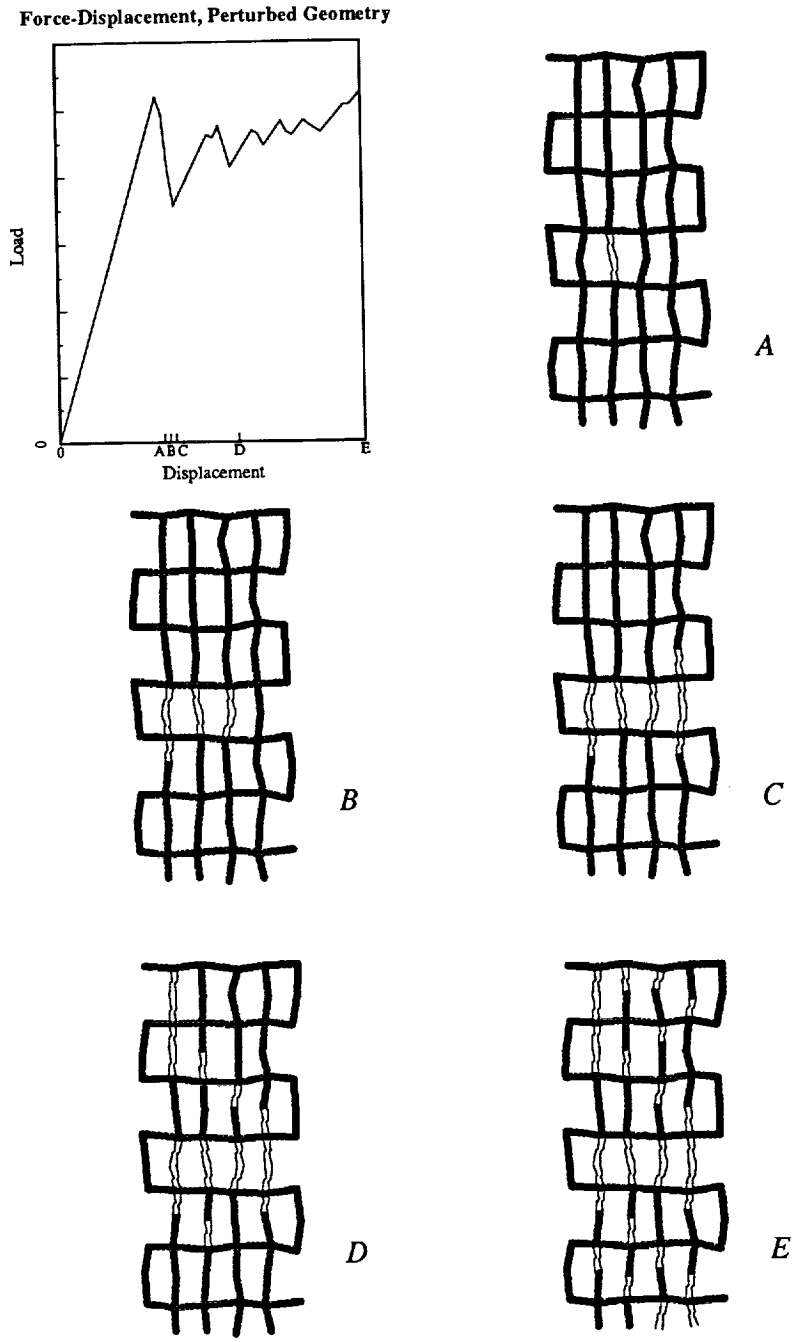

Figure 7: Perturbed Orthogonal Interlock Geometry
This shows the effect of introducing a realistic geometric distortion of the beam elements which represent the tows. The results are obtained by a hybrid finite element technique described in the text. Although the strength and stiffness of the perturbed structure are diminished, the work of fracture is distributed over a larger number of stuffers and the initial load drop is much less than for the ideal geometry.

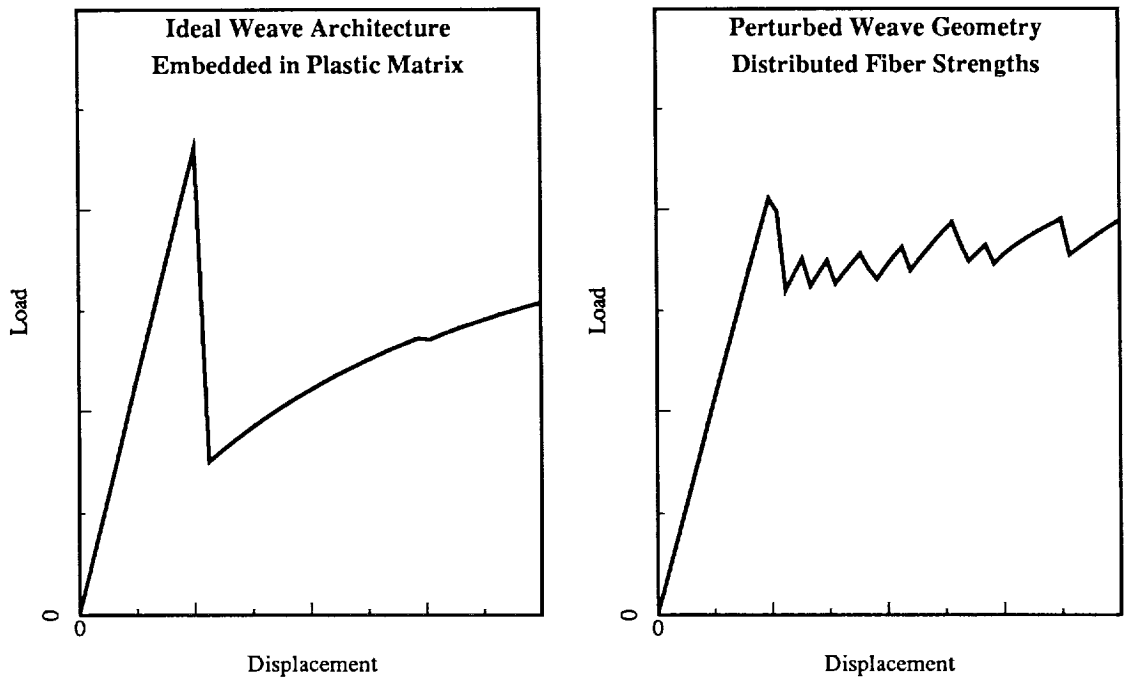

Figure 8: Results with Matrix Damage

In this model, a plastic response is associated with matrix damage and included in the simulation. For the figure on the right, the distribution of fiber kinking stresses is included as well as a geometric perturbation. The load displacement curve is qualitatively similar to the experimentally observed curves.

REFERENCES

1. Argon, A.S.: "Fracture of Composites," *Treatise of Materials Science and Technology,* Vol. 1, Academic Press, New York, 1972.
2. Fleck, N.A.; and Budiansky, B.: "Compressive Failure of Fibre Composites" submitted to J. Mat. Phys. Sols.
3. Budiansky, B.: "Micromechanics," *Computers and Structures,* Vol. 16, pp. 3-12, 1983.
4. Reifsnider, K.L.; and Mirzadeh, F.: "Compressive Strength and Mode of Failure of 8H Celion 3000/PMR15 Woven Composite Material," *J. of Comp. Tech. and Res.* vol. 10, no. 4, pp. 156-164, 1988.
5. Evans, A.G.; and Adler, W.F.: "Kinking as a Mode of Structural Degradation in Carbon Fiber Composites" *Acta Metall.* ol. 26, pp. 725-738, 1978.
6. Chaplin, C.R.: "Compressive Fracture in Unidirectional Glass-Reinforced Plastics," *J. Mater. Sci.,* vol. 12, pp. 347-352, 1977.
7. Parry, T.V.; and Wronski, A.S.: "Kinking and Compressive Failure in Uniaxially Aligned Carbon Fibre Composite Tested Under Superposed Hydrostatic Pressure," *J. Mat. Sci.* vol. 17, pp. 893-900, 1982.
8. Cox, B.N. *et al,*: "Mechanisms of Compressive Failure in 3D Composites," Submitted to *Acta Met et Mat.*
9. K.L Reifsnider, K.L.: "Life Prediction in Advanced Material Systems," pp. 85-110, Fatigue of Advanced Materials, *Proc. of the Engin. Found. Int. Conf.*, R.O. Ritchie, R.H. Dauskardt, B.N. Cox Eds, MCEP Pub., U.K. 1991.

COST MODEL RELATIONSHIPS BETWEEN TEXTILE MANUFACTURING PROCESSES AND DESIGN DETAILS FOR TRANSPORT FUSELAGE ELEMENTS[1]

Stephen L. Metschan
Boeing Commercial Airplane
Structural Designer

Kurtis S. Wilden
Boeing Commercial Airplane
Manufacturing Research and Development

Garrett C. Sharpless
Fiber Innovations
Braid/Resin Transfer Molding

Rich M. Andelman
Dow/United Technologies Composites
Cost Modeling

SUMMARY

Textile manufacturing processes offer potential cost and weight advantages over traditional composite materials and processes for transport fuselage elements. In the current study, design cost modeling relationships between textile processes and element design details were developed. Such relationships are expected to help future aircraft designers to make timely decisions on the effect of design details and overall configurations on textile fabrication costs. The fundamental advantage of a design cost model is to insure that the element design is cost effective for the intended process. Trade studies on the effects of processing parameters also help to optimize the manufacturing steps for a particular structural element.

Two methods of analyzing design detail/process cost relationships developed for the design cost model were pursued in the current study. The first makes use of existing databases and alternative cost modeling methods (e.g. detailed estimating). The second compares design cost model predictions with data collected during the fabrication of seven foot circumferential frames for ATCAS crown test panels. The process used in this case involves 2D dry braiding and resin transfer molding of curved "J" cross section frame members having design details characteristic of the baseline ATCAS crown design.

INTRODUCTION

A good design represents the best compromise between various reinforcing, competing, and relational variables that interact with the critical requirements. While this concept and related

[1] This work was funded by Contract NAS1-18889, under the direction of J. G. Davis and W. T. Freeman of NASA Langley Research Center.

equations that can describe these interactions are understandable, the sheer number results in confusion for the designer. Added to the problem is that the various relationships understood by the different disciplines involved may not always be communicated accurately, usefully or in a time effective manner to influence the design decisions. While the design build team approach improves the design process, personalities, inexperience, and obsolete information can make an optimized design difficult to achieve. In addition, there is currently no real mechanism to understand the various design trades in a timely manner other than by a pass or fail estimation by the design build team members [1]. The fundamental purpose of a design cost model is to allow the various disciplines to communicate their knowledge of how cost interacts with the design details in a timely non-ambiguous fashion such that the best compromise can be reached in the design.

To construct a good cost model it is important to understand and quantify how design and process variables interact with the critical requirements. The first step is to understand the key design features and cost drivers of a particular design/process. The second step involves the formulation of the cost interactions with the design and processing details such that a cost model can be developed. The final step is to calibrate the model based on actual results of real design/process cost interactions.

KEY DESIGN FEATURES

The identification of the key design features helps to define a structural element or assembly to the cost of manufacturing. This paper focuses on transport fuselage frame elements. The design features for fuselage frames include curvature, cross section, length, gage, and material, shown in figure 1. These features in turn are not at the sole discretion of the fuselage frame designer.

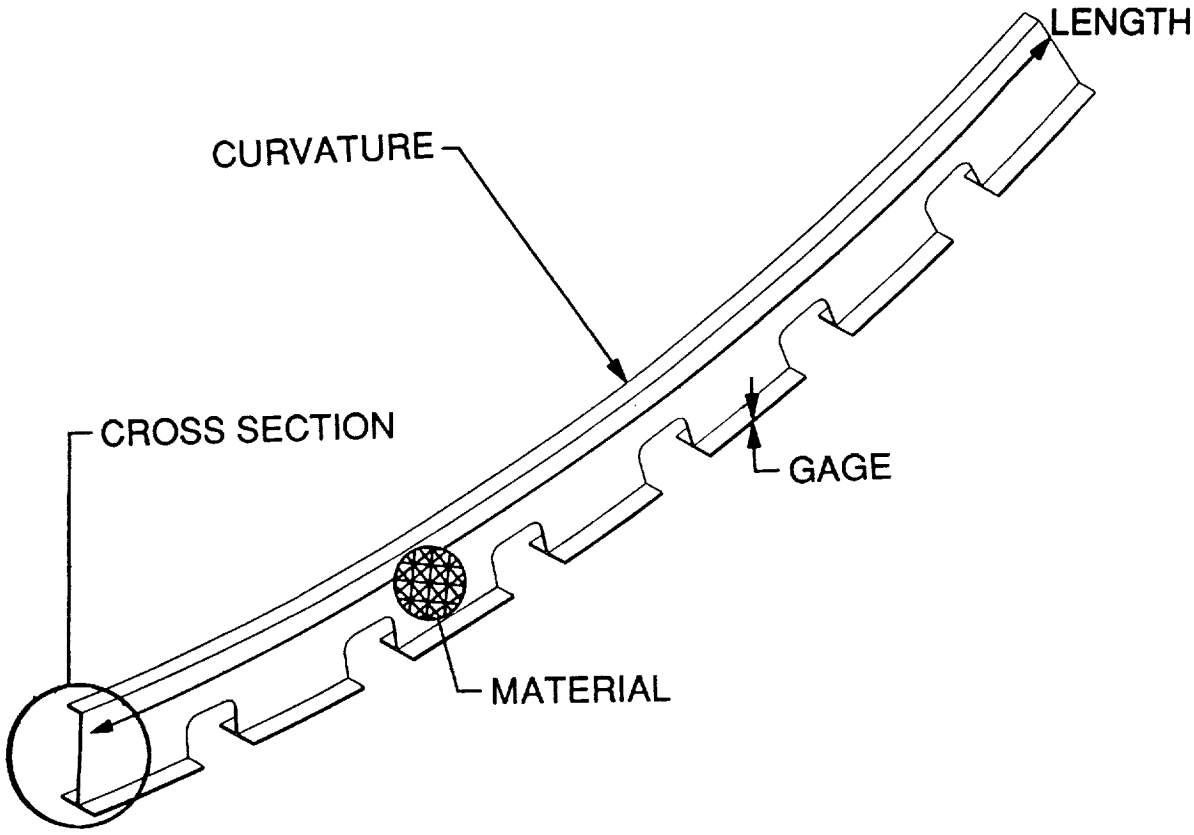

Figure 1. Typical Fuselage Frame

Frame curvature variation is largely a function of the optimum balance between aerodynamic design and required passenger capacity. Frame cross section is influenced by the loads and skin design. Frame length is dictated by manufacturing breaks and cutout locations. Frame gage is a function of loads and manufacturing capability. Frame material selection is driven by design application and manufacturing capabilities.

KEY COST DRIVERS

The key cost drivers for fuselage frames include the key design features identified in figure 1. Superimposed on these design features are criteria not normally considered at the design level. Production quantity, production rate, and part commonality can have a strong influence on overall cost. Additional factors to consider include the cost interactions with the manufacturing processes and design features. While individual effects of these variables are reasonably easy to quantify at the process step level, the overall effect on the cost of a complete assemble can be very elusive.

UNDERSTANDING THE DESIGN ENVIRONMENT

Fundamental to a good cost model is understanding the design environment and the various process and cost interactions with the design details. The first step is to begin to quantify an actual design by the design features. Shown in figure 2 is a typical widebody subsonic transport. Figure 3 represents a skin/stringer/frame layout of a typical widebody commercial transport aircraft. The diagram is produced by essentially splitting the fuselage tube at the lower centerline and unrolling it into a flat pattern.

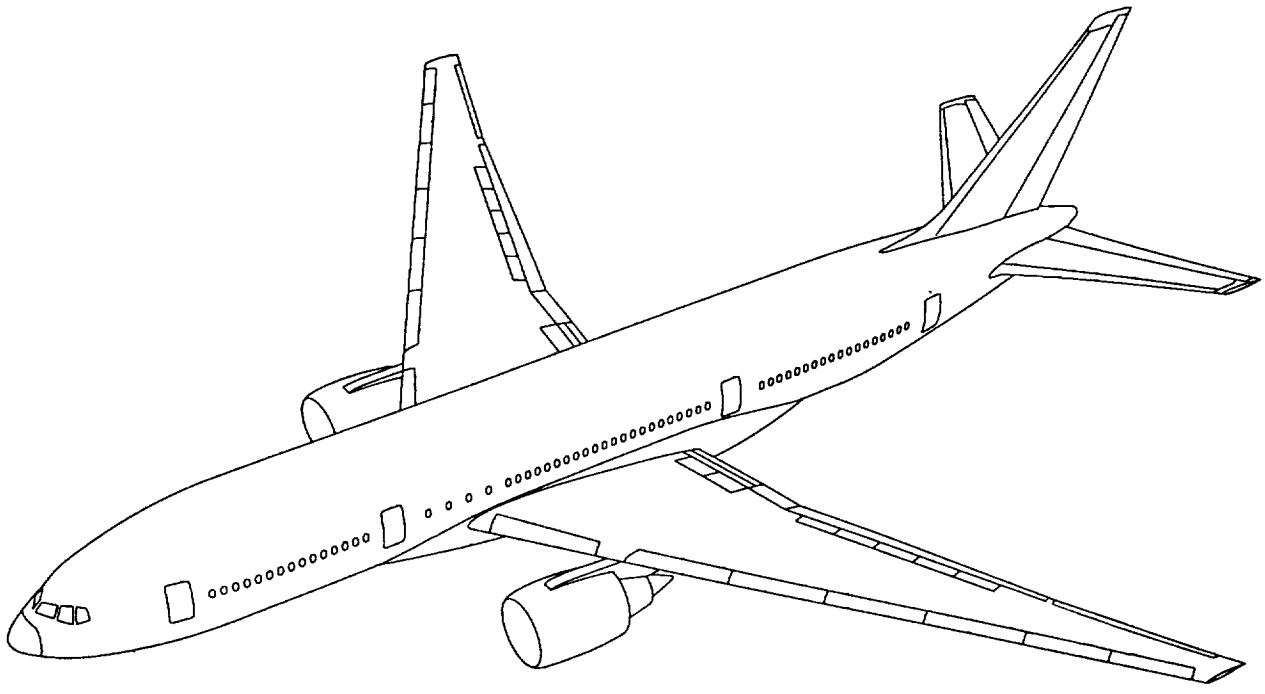

Figure 2. Typical Widebody Commercial Transport

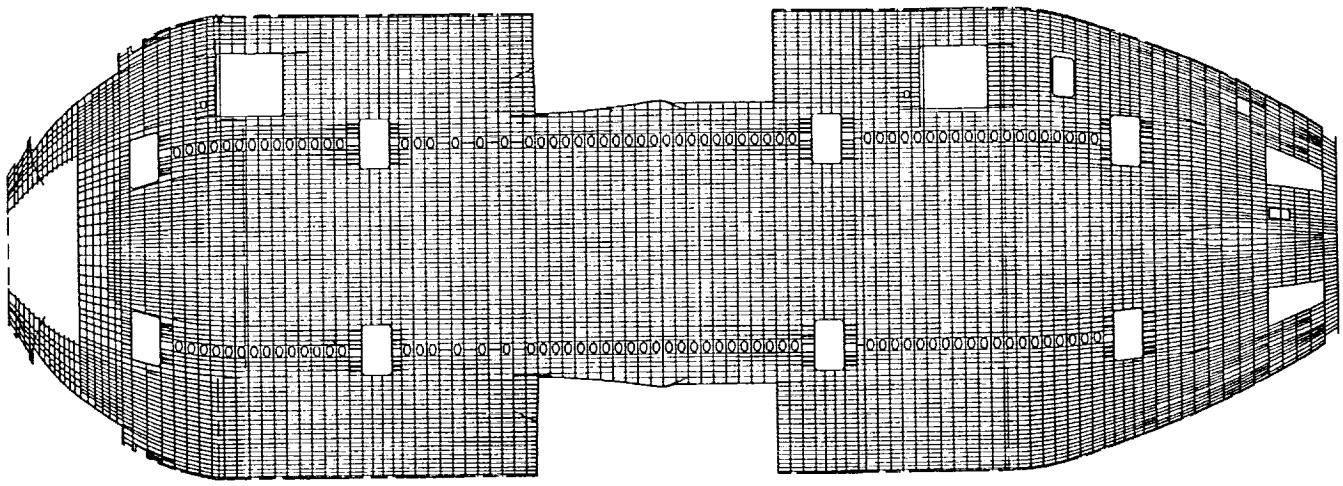

Figure 3. Skin/Stringer/Frame Layout

First, all the stringers were removed from figure 3 since the current modeling effort is to focus on just the fuselage frame elements. Secondly, all the fuselage frames aft of the rear pressure bulkhead and in the cockpit area, shown in figure 4, were removed. The frames aft of the rear pressure bulkhead are in a non-pressurized area of the airplane and have fundamentally different design drivers. The frames in the cockpit area, while in the pressurized portion of the aircraft, might be better fabricated using a different method due to the highly complex shape interactions between skin, stringer and frame.

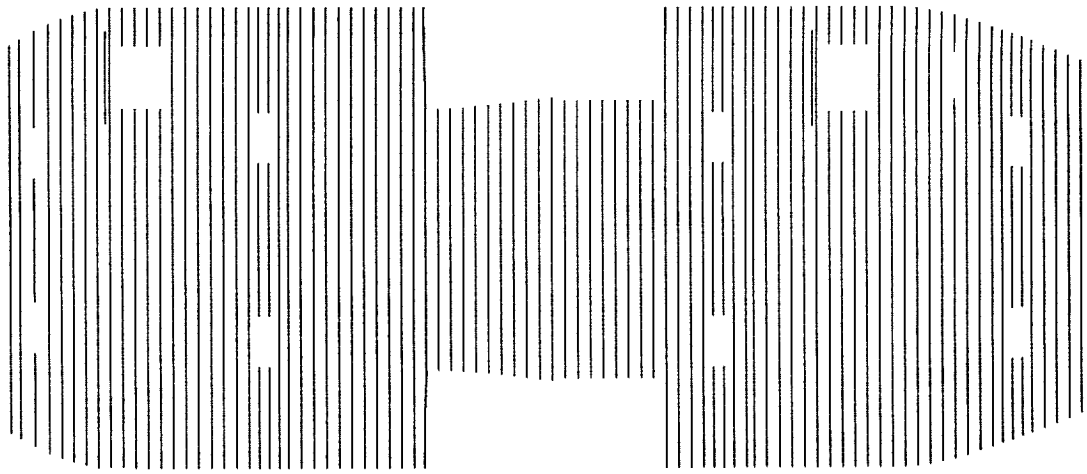

Figure 4. Fuselage Frame Members

Further simplification to figure 4 was achieved by removing all fuselage frames around the door areas, see figure 5. The main and auxiliary frame sill design is strongly influenced by the door design and fundamentally different load patterns and damage criteria. It is reasonable to assume that this structure would have different optimal design and fabrication methods. In addition, all major fuselage frame bulkheads, which again have fundamentally different requirements from most fuselage frame members, were removed. What is left are the frames which will be considered in the cost model for relationships between textile manufacturing processes and design details.

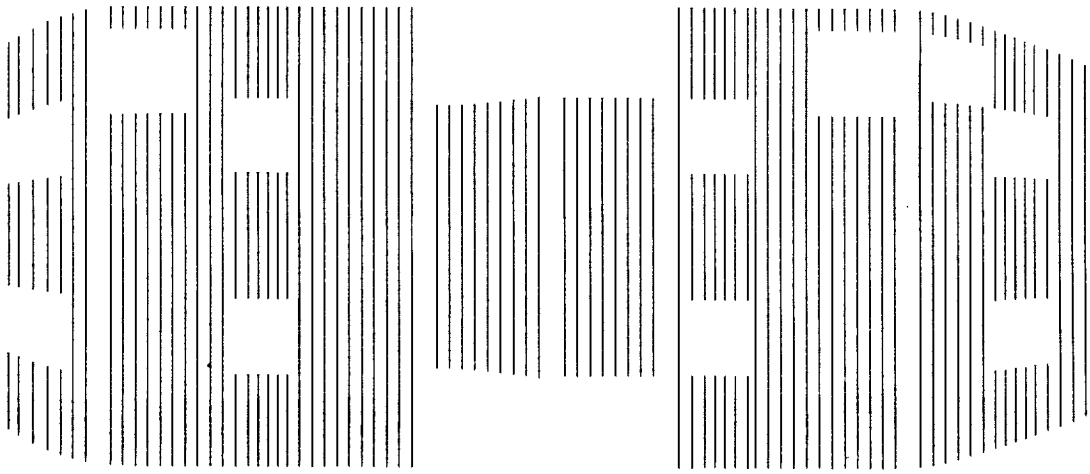

Figure 5. Fuselage Frames in Study

The fuselage frames in this study were then grouped by two key design features: curvature and length. The frame length was dictated by manufacturing breaks and cutout locations. The manufacturing breaks used were assumed to be the same as the ATCAS quadrant approach shown in figure 6 [2].

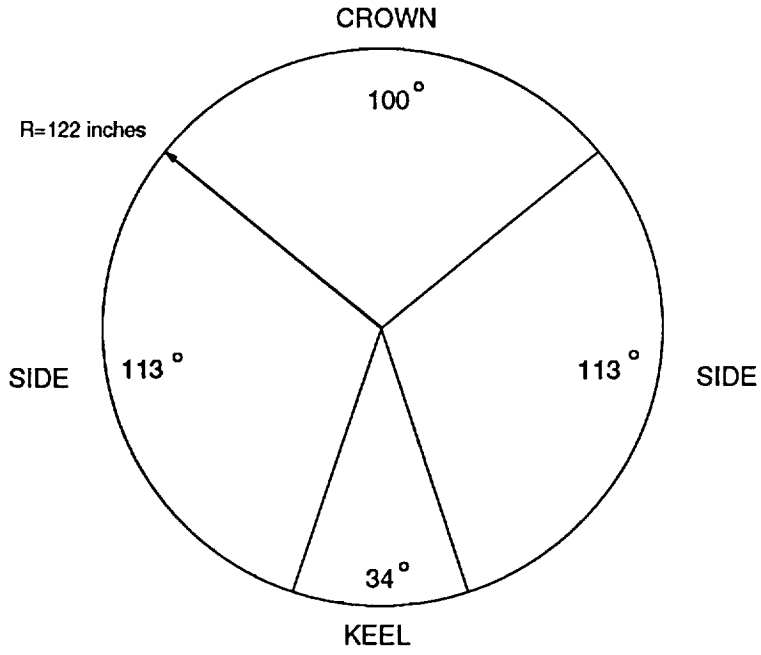

Figure 6. ATCAS Fuselage Manufacturing Breaks

Frame curvature was defined by either constant curvature frames or non constant curvature frames. The group of frames by length and curvature are shown in figure 7. This results in eight different frame design groups. Frame design family one would include all frames with similar frame lengths and constant curvature. Frame design family two would include all frames with similar lengths and variable curvature.

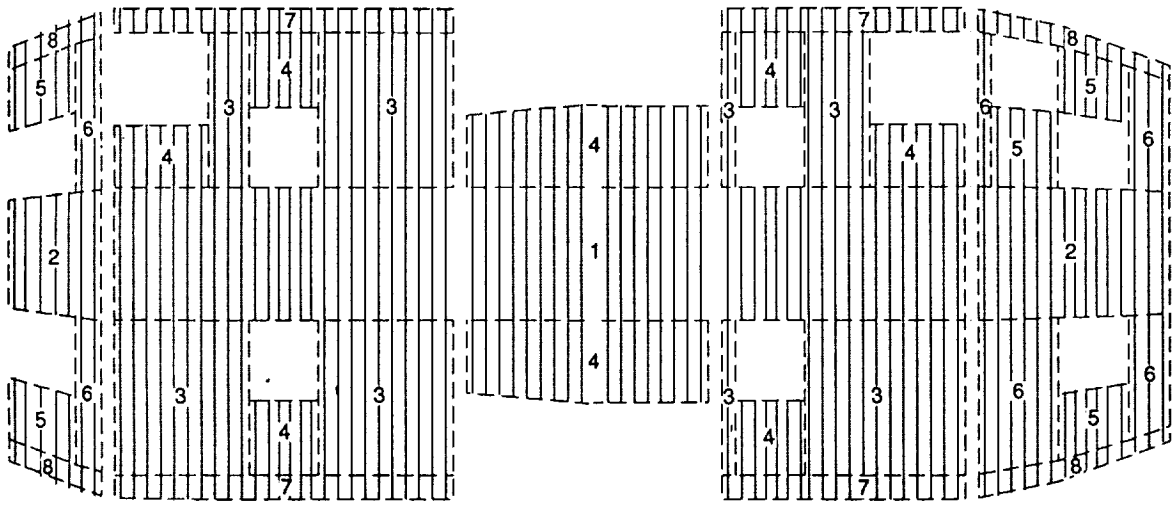

Figure 7. Frame Design Groups by Curvature and Length

Fuselage frame families were then further subdivided by another key design feature of gage. To determine gage variations within frame family detailed loads were analyzed for load patterns. Depending on the application, composite materials should save weight on the order of 10 to 40 percent. The ability to tailor the frame gage to varying loads will be important in maintaining this margin. Unfortunately, this introduces additional variation into the frame design. There were two methods used to understand load patterns. The first method, shown in figure 8, represents load variation around the fuselage at a typical frame station.

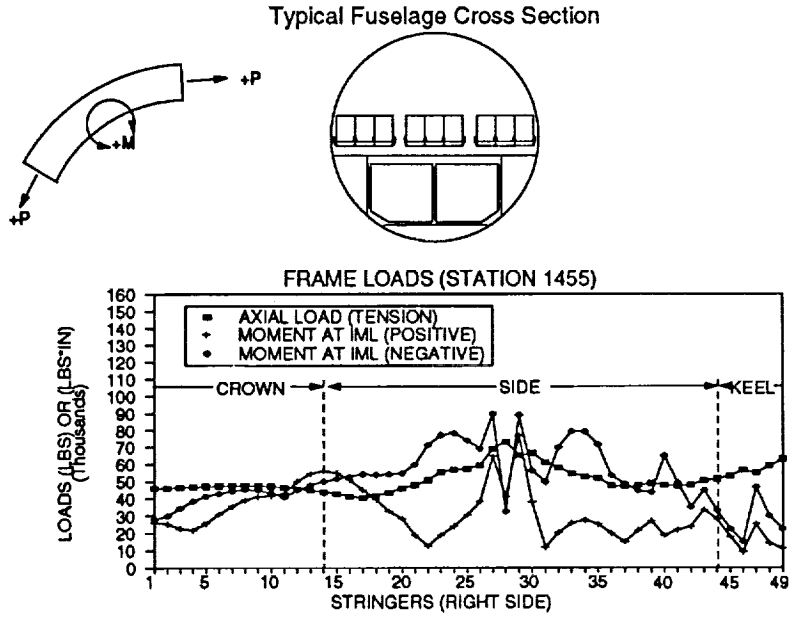

Figure 8. Frame Fuselage Loads at Station 1455

The other method used to understand load patterns was load variation in the fuselage frames along the length of the fuselage, shown in figure 9. The axial frame loads show little variation after frame station 1580. Since the positive and negative bending moments remained consistent, this would indicate a frame group categorized by curvature, length and gage.

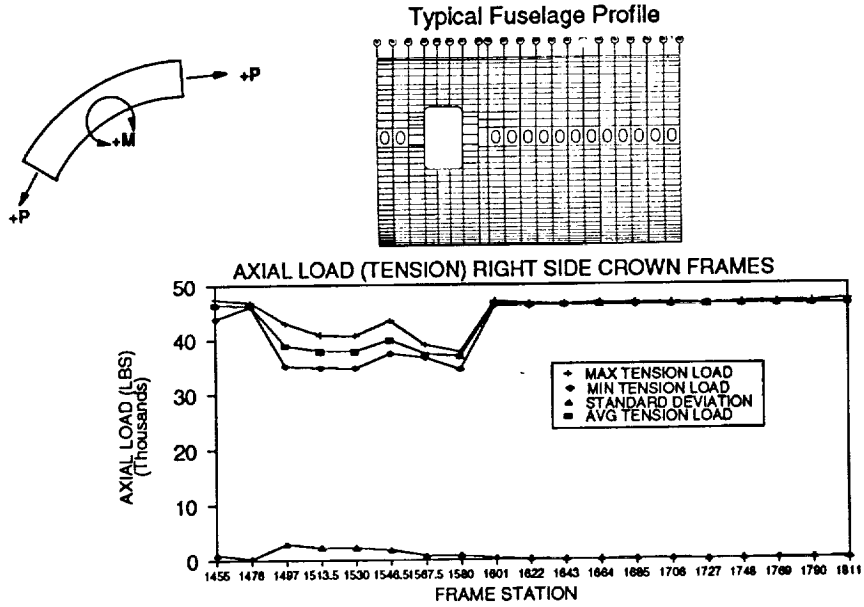

Figure 9. Frame Fuselage Loads Variation by Station

Applying this methodology to all the fuselage frames in the study resulted in the frame design families shown in figure 10 and figure 11. In a typical widebody commercial transport 80% the size of a 747, 19 frame design families were identified. There are 319 frames per airplane with an average length and area of 155 inches and 1.0 in^2 respectively. Using the ACT cost estimating ground rules of 5 airplane/month over 5 years this results in 3350 lbs of graphite/epoxy per airplane or 210,000 lbs/year.

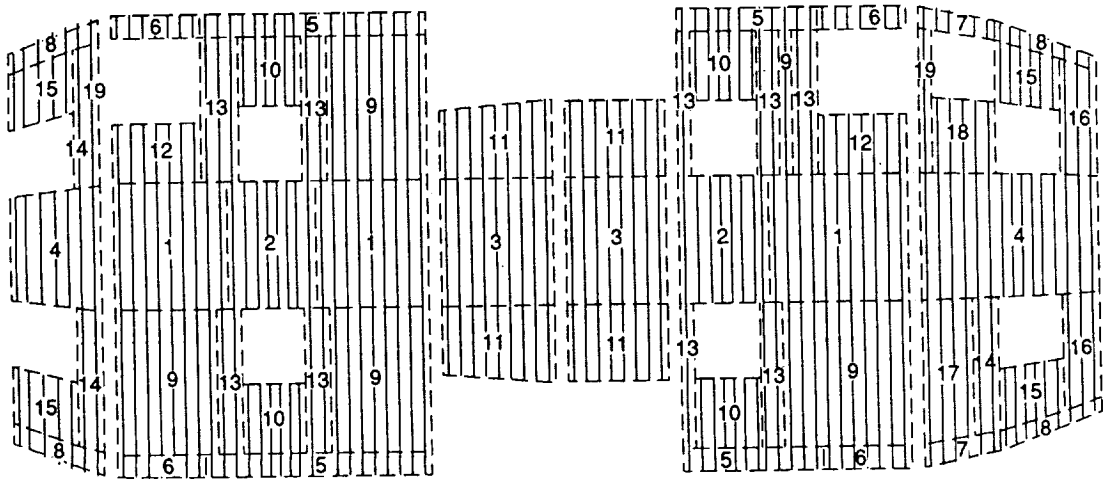

Figure 10. Frame Design Groups by Length, Curvature, and Gage

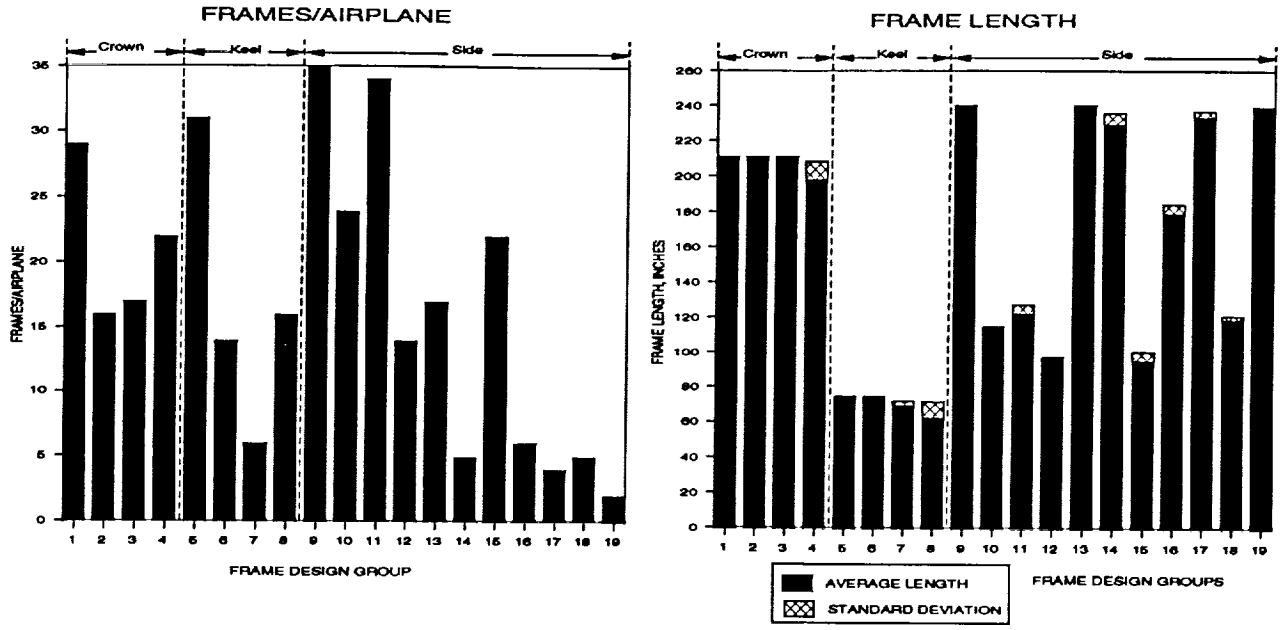

Figure 11. Frame Design Families

Superimposed on the frame design families categorized by curvature, length, and gage is the key design feature of cross section. The cross section design is a strong function of the skin design as shown in figure 12. In the stiffened design the mousehole requires the outer flange to be trimmed unlike the sandwich design. If damage were to occur or progress into the skin area under the mousehole the frame would fail due to an applied moment. The additional flange above the mousehole replaces reinforcement that was provided by the undamaged skin.

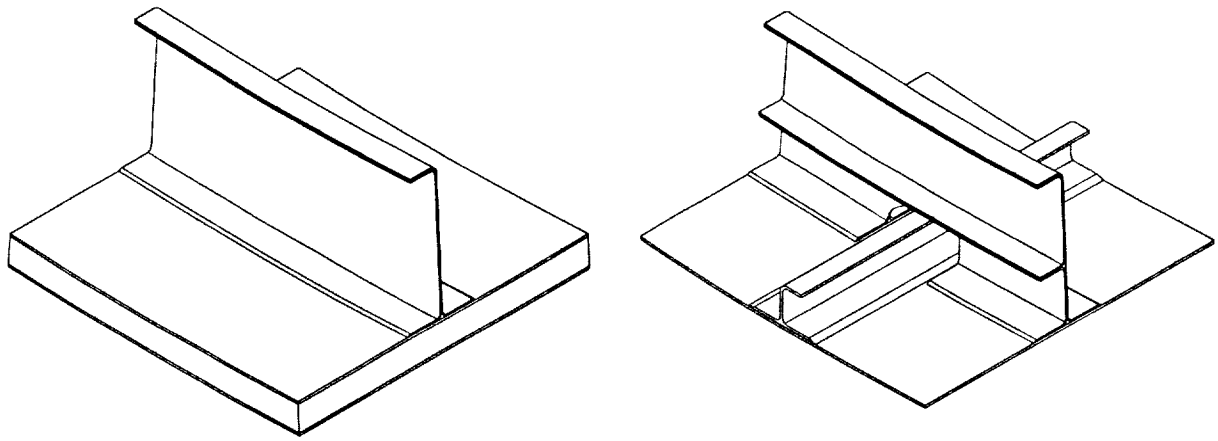

"J" Frame Sandwich Design **"F" Frame Skin/Stringer Design**

Figure 12. Fuselage Frame Cross Section Designs

The final key design feature is material. In this study the tri-axial 2D braided AS4[2]/1895[3] material was assumed as the baseline material. Other materials and preforming techniques can be evaluated but would require an analysis model to weigh the relative cost and weight trades [3].

UNDERSTANDING THE PROCESS ENVIRONMENT

The cost of producing a part is an interaction between the design detail and the intended process. Understanding the processes sensitivities and advantages is essential to evaluating the effects of design features on cost. The braid/resin transfer molding process which was modeled for the current study is shown in figure 13. Each step in the process was modeled with an equation which described cost as a function of the key design features and processing parameters.

The general operating philosophy of this factory layout is that frame design families have many design features that are common. Smaller frames are cut from longer segments (i.e., batched) to help equalize handle requirements. This allows the material handling system to be designed to handle similar size frame blanks. Assembly line techniques comprise an important way of reducing cost. While low commercial aircraft production rates and less part commonality do not encourage production techniques commonly found in the automotive industry, flexibility in the process and grouping common processing steps can significantly improve costs. In this factory layout, the part type specific portion of the process comes in braiding the correct preform to the correctly matched braiding and cure tools. After these steps are accomplished the differences between one frame and the next is transparent to the process.

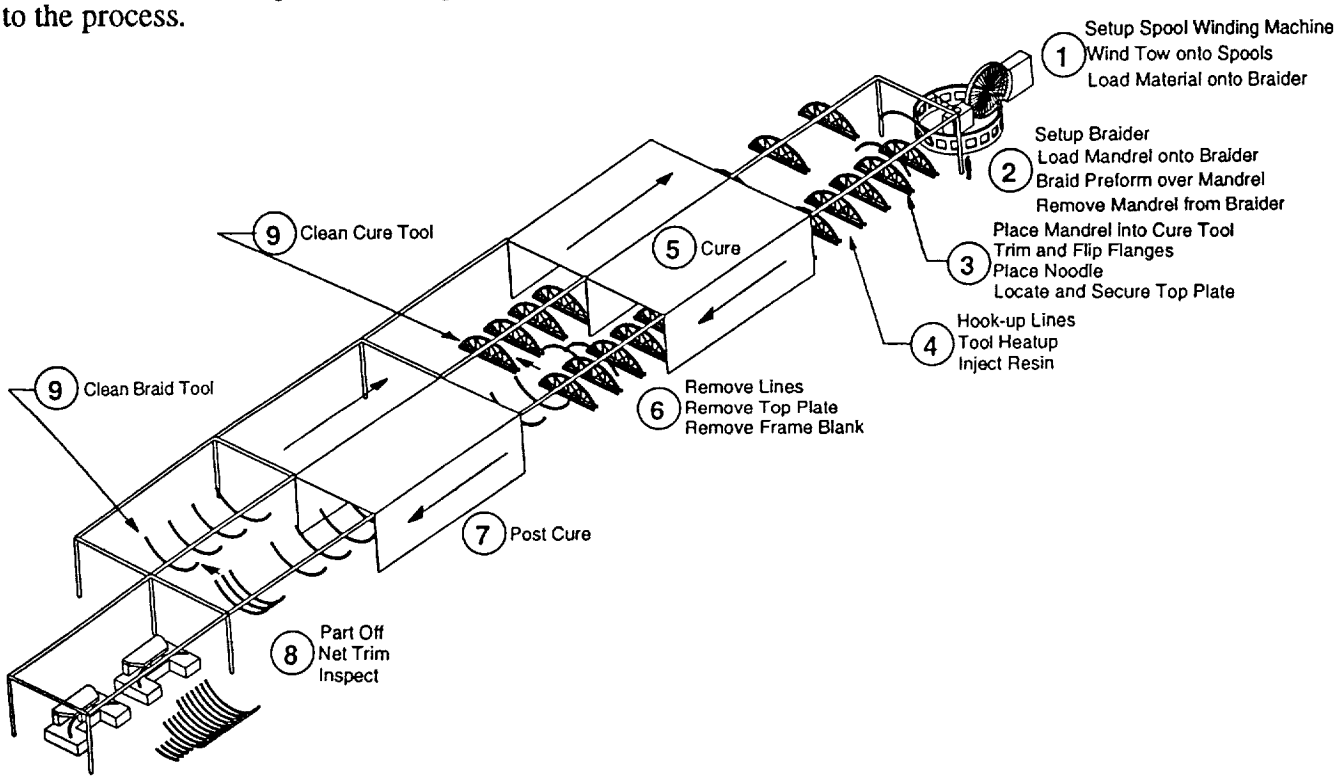

Figure 13. Braid/RTM Fuselage Frame Factory Flow

[2] AS4 is a graphite fiber system produced by Hercules, Inc.

[3] 1895 is a epoxy resin system produced by Shell.

Another area of importance to the cost of braid/resin transfer molding processes is the interaction between tooling approaches and the design environment. It should be noted that while 19 frame design families were identified, there can and will be very minor differences between frames within a family which may require a different set of tools. Simply fabricating a different set of tools for every slightly different frame design could render the resin transfer molding process uncompetitive. The key to cost effective tool design is the integration of the tool design to the part design and process flow.

In the process flow, the braiding mandrel follows the part through most of the fabrication cycle. The cure tool, on the other hand, bypasses the post cure cycle and would have an inherently higher utilization rate. It would follow that more braiding mandrels would be required to support the production rate. Therefore, the gage variations could be tailored into the braiding mandrel shown in figure 14. This allows the cure tool to be fabricated as a datum tool. This cure tool could be baselined and fabricated early on in a production program. The braiding mandrel could then be fabricated once the frame design was finalized. Additionally, tooling design should incorporate shim areas such that slight variations between frame designs can be incorporated allowing for the tooling cost to be amortized over a greater number of parts.

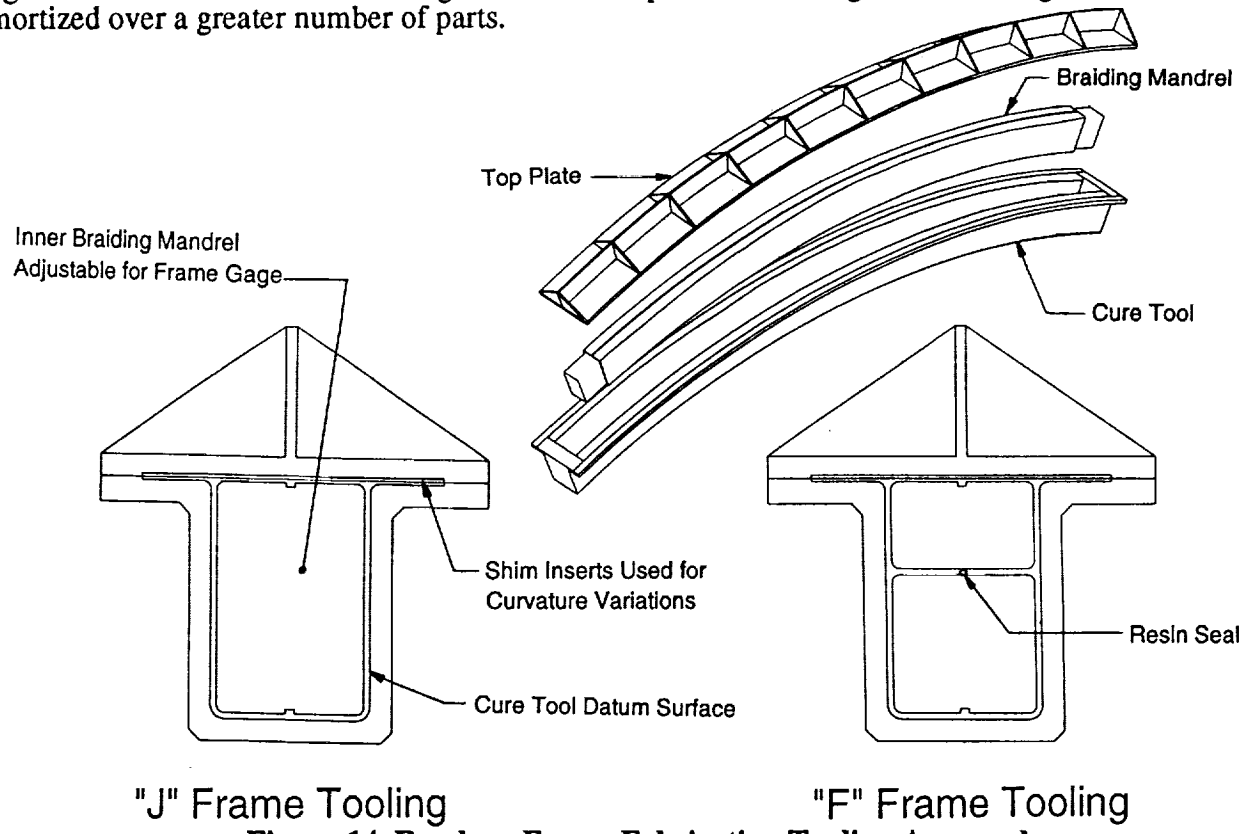

Figure 14. Fuselage Frame Fabrication Tooling Approach

CALIBRATION OF THE COST MODEL

Once the manufacturing environment and the relationships between design details and cost were understood, the model was calibrated. Two types of data were available to calibrate the model. The first was the detailed estimates done at Boeing for the ATCAS keel and crown design studies. Roughly thirty percent of the Boeing cost estimate is based on labor standards which apply directly to current fabrication methods used at Boeing. The remaining cost data was developed from Manufacturing Research and Development input and extrapolation of existing processes and equipment.

The second source of cost information was actual time studies performed on braided and resin transfer molding fabrication of seven foot "J" frames used on the ATCAS test panels. The comparisons of actual fabrication touch labor and Boeing estimated standard labor, averaged over 300 shipsets, is shown in figure 15. While only the Boeing estimate had learning and variance factors applied, the Fiber Innovations actuals give a good reference point for comparison. With only eight frame fabrication runs available at the time of model calibration, a Boeing estimator judged that it was too early to develop labor standards from the Fiber Innovations actuals. As more actuals are collected the Fiber Innovations curve will be modified in order to apply the Boeing methodology of variance and learning curves over 300 shipsets. This should allow a one to one comparison.

The calibration curve is broken into the nine basic processing steps. Areas where improvements between the process used successfully in an R&D environment and full scale production environment are noted as A through G. The first area involves loading the material onto the braiding equipment. Currently, there are 216 spools on the braiding equipment. Only one third pounds of fiber are loaded per spool. Due to the number of different parts being fabricated and fiber types being used at Fiber Innovations, it would be impractical to load more material per spool. In a production environment where production rate would require dedicated braiding equipment and consistent fiber types, these variations could be eliminated by loading more material onto each spool. This allows for amortization of material load times over more parts, thus lowering the final cost. Loading 2.63 pounds of fiber per spool would allow the braider, in a production environment, to produce frames at a normal operating speed for 70 hours between cleaning and reloading of the braiding equipment.

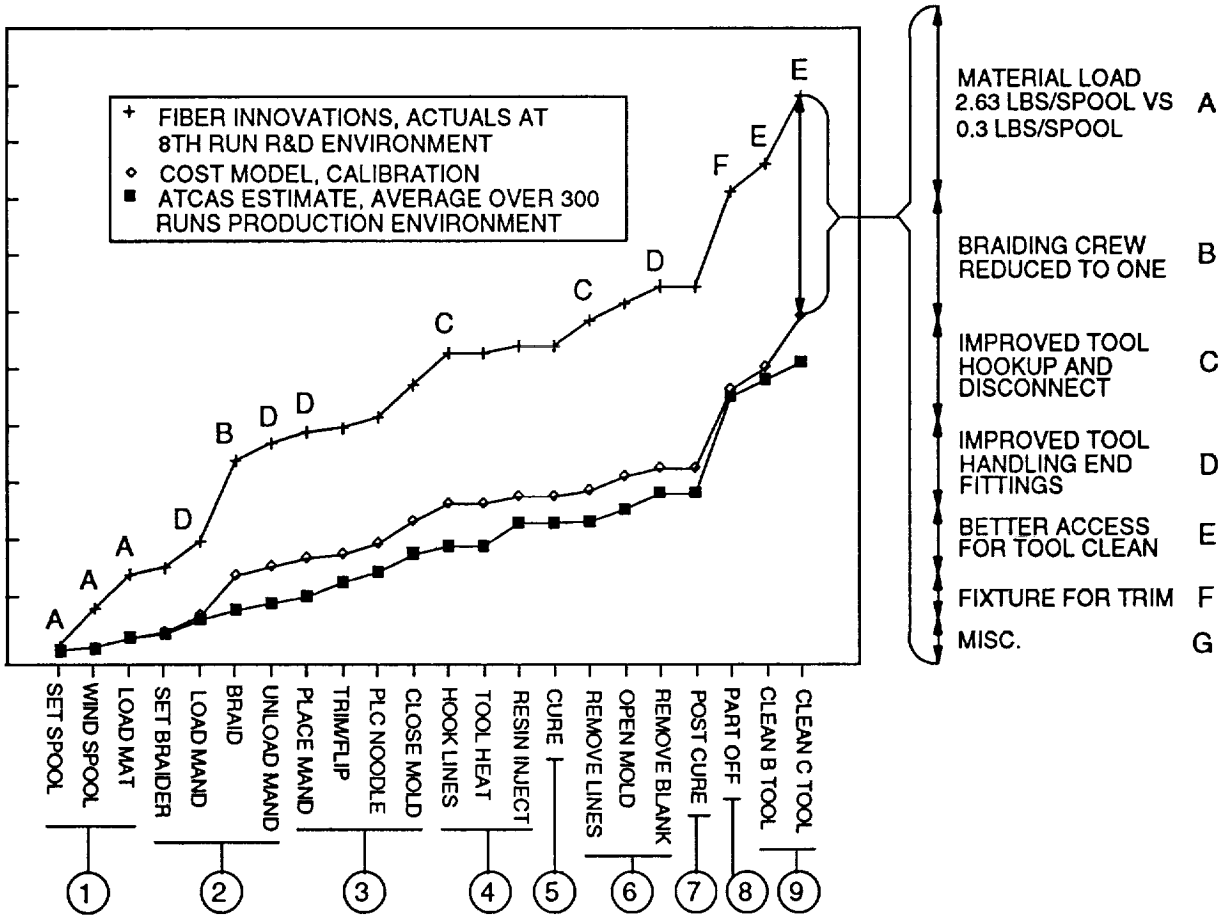

Figure 15. Calibration of Cost Model

The second area of improvement is the number of operators required for the braiding equipment. Two operators are currently used at Fiber Innovations with the second person preforming quality control. The ACT cost estimating ground rules require quality control to be accounted as an overhead function. In addition, projected future improvements in braiding equipment could self monitor the braiding process. Therefore it was judged that one operator would be sufficient for the production scenario.

Capital and equipment improvements not justifiable for R&D environments were assumed in place for future frame production. These include improved connectors for hook-up and disconnect of heater, thermocouple and injection lines. Other improvements include tool handling using overhead equipment, optimized factory layout, and improved fixtures. Tool clean in resin transfer molding can be time consuming but improvements in tool design and cleaning methods, such as resin knock outs, can improve labor costs.

RESULTS

Once the calibration of the cost model was completed the fabrication cost of the various fuselage frame design families could be predicted. There were large cost differences between the various design families largely due to tooling cost differences, shown in figure 16.

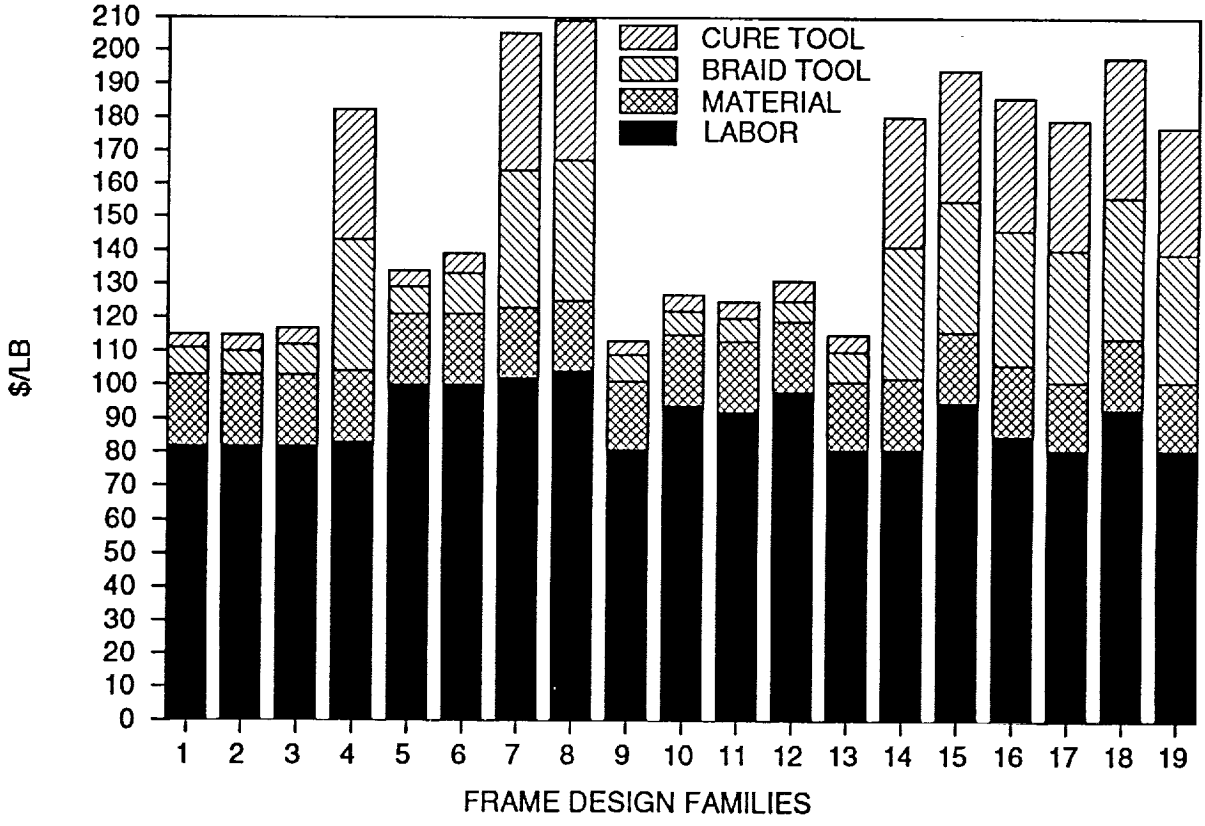

Figure 16. Fuselage Frame Family Fabrication Cost

While the cost breakdown for every family can be identified, the reasons for the differences can be elusive. One of the fundamental reasons for the cost difference between frame design families is tooling. Most of the constant curvature frames did not require any more tooling than was required to support rate. The non-constant curvature frames required a different closed mold tool for every frame. In addition, the quantity of frames in any one design family was not always sufficient to fully utilize the tooling. Frame length can also be seen to have a slight effect on labor costs due to the amortization of setup cost over smaller frames. While this type of information is important it does not allow the designer to find the optimum point between design details and cost. The primary advantage of a cost model is to allow the designer to incrementally vary design details and gain an understanding of how this affects cost.

As shown in figure 17, one strong relationship between cost and frame design details predicted by the model was frame length. Using an average of 17 frames per design family found in the study, frame cost as a function of frame length is plotted. Significant improvements in frame cost were seen for increasing lengths up to about 100 inches. These cost improvements were largely due to amortization of operations in the process which are required regardless of how short the frame is. Superimposed are processing improvements which interact with frame length to allow for the batching of additional frames per tool, amortizing the setup cost over more frames.

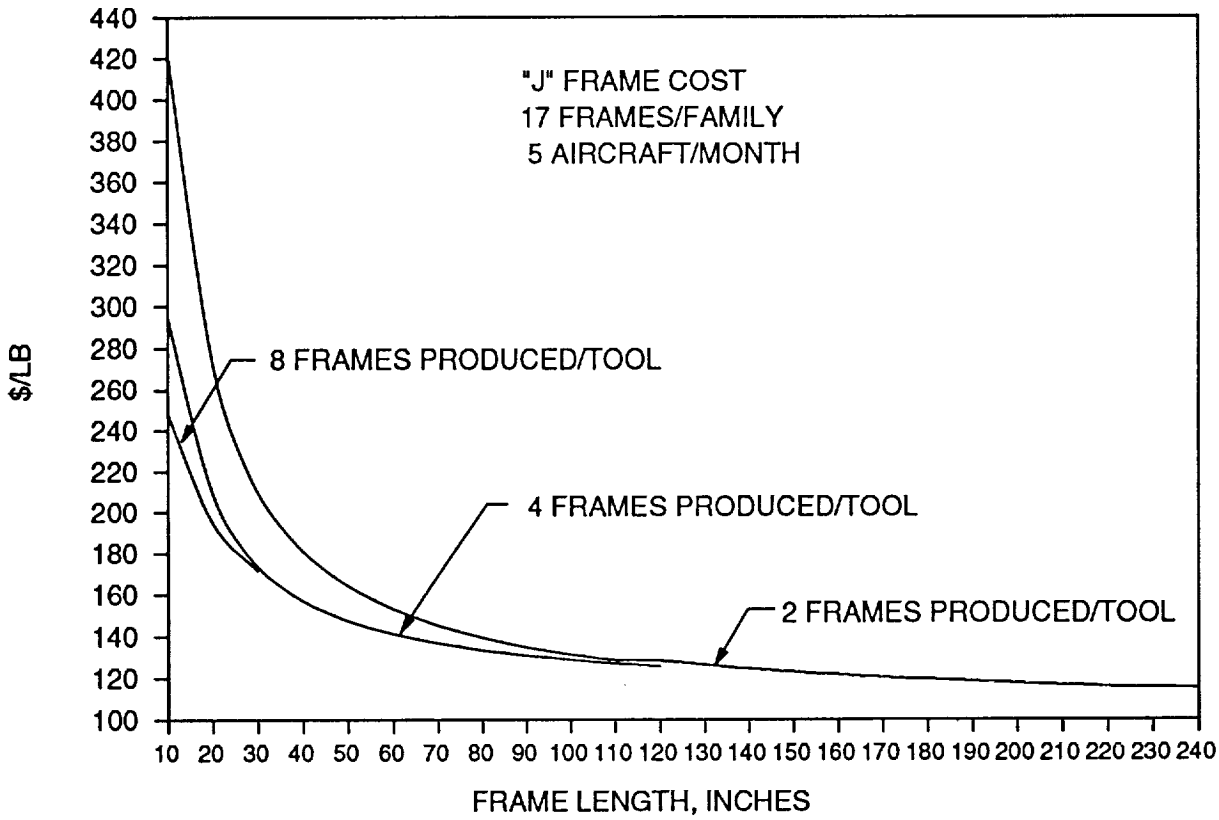

Figure 17. Cost Model Predictions of Frame Cost as a Function of Length

Another strong relationship predicted by the cost model was that of frame commonality. For example, a frame commonality of four would represent an average of four common frames in every frame design family. In figure 18, frame cost versus frame commonality is plotted. As frame commonality increases, frame costs come down and level out at about six frames per family. The leveling out of frame cost is a result of the rate tooling requirement driving the frame cost. Frame commonalities greater than six will not result in any significant advantage in the existing manufacturing environment.

One design detail which can strongly affect frame commonality is frame tailoring to save weight. The cost model would give the designer non ambiguous thresholds for the impact of weight savings versus cost through its impact on commonality. In addition, suppose the optimum cost/weight commonality for fuselage frames is three frames per family. Improvements in unattended cure cycle time would have little impact on frame cost due to the under-utilization of tooling at this frame production rate. If the frame commonality of the design is nine, then improvements in the cure cycle time could improve the frame cost by lowering rate tooling requirements.

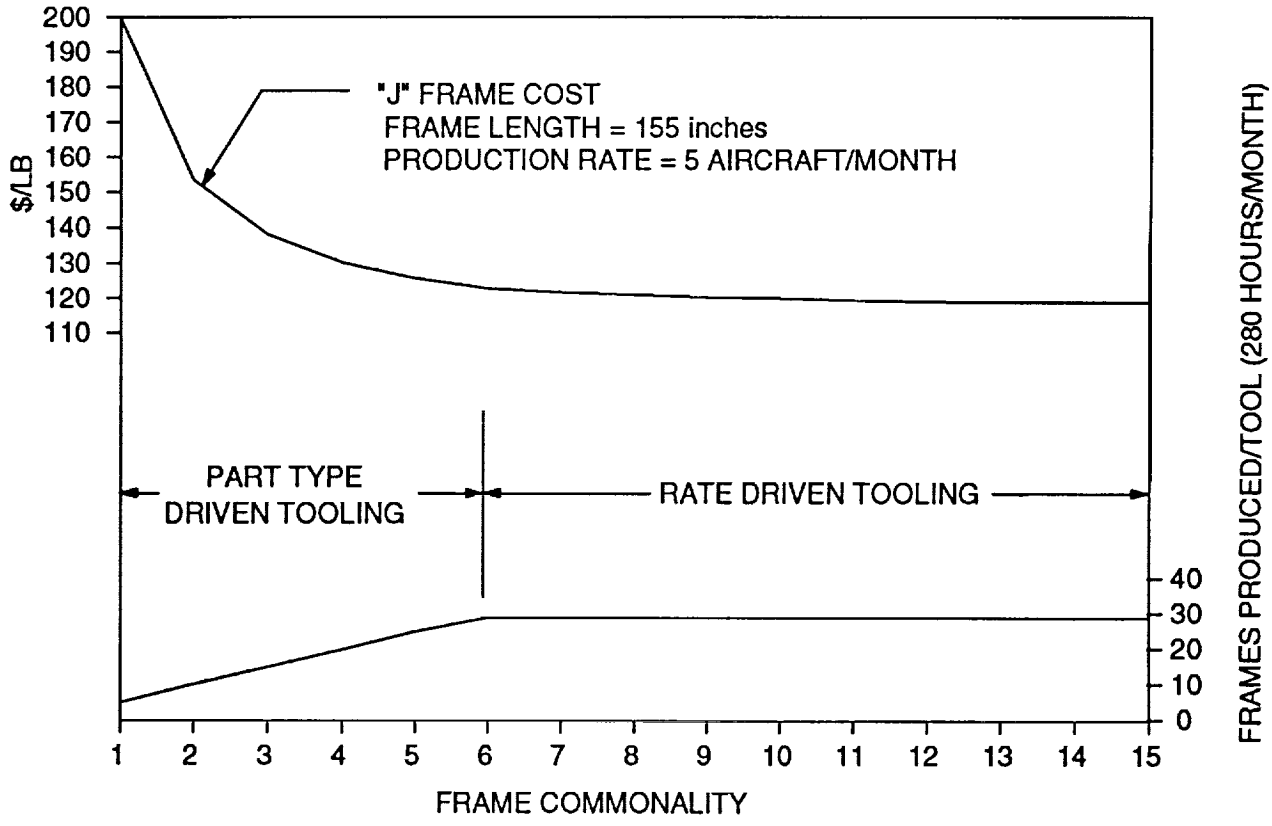

Figure 18. Cost Model Predictions of Frame Cost as a Function of Commonality

Since frame commonality was seen as such a strong driver it follows that aircraft production rate should also be important. The current ground rules used in the ACT program call for a production rate

of 5 aircraft/month over 5 years. Actual production rates can vary between 1 and 21 aircraft/month depending on the aircraft model. Figure 19 shows frame costs versus aircraft production rate. This was also predicted by the model to be strong cost driver, though certainly not at the discretion of the fuselage frame designer.

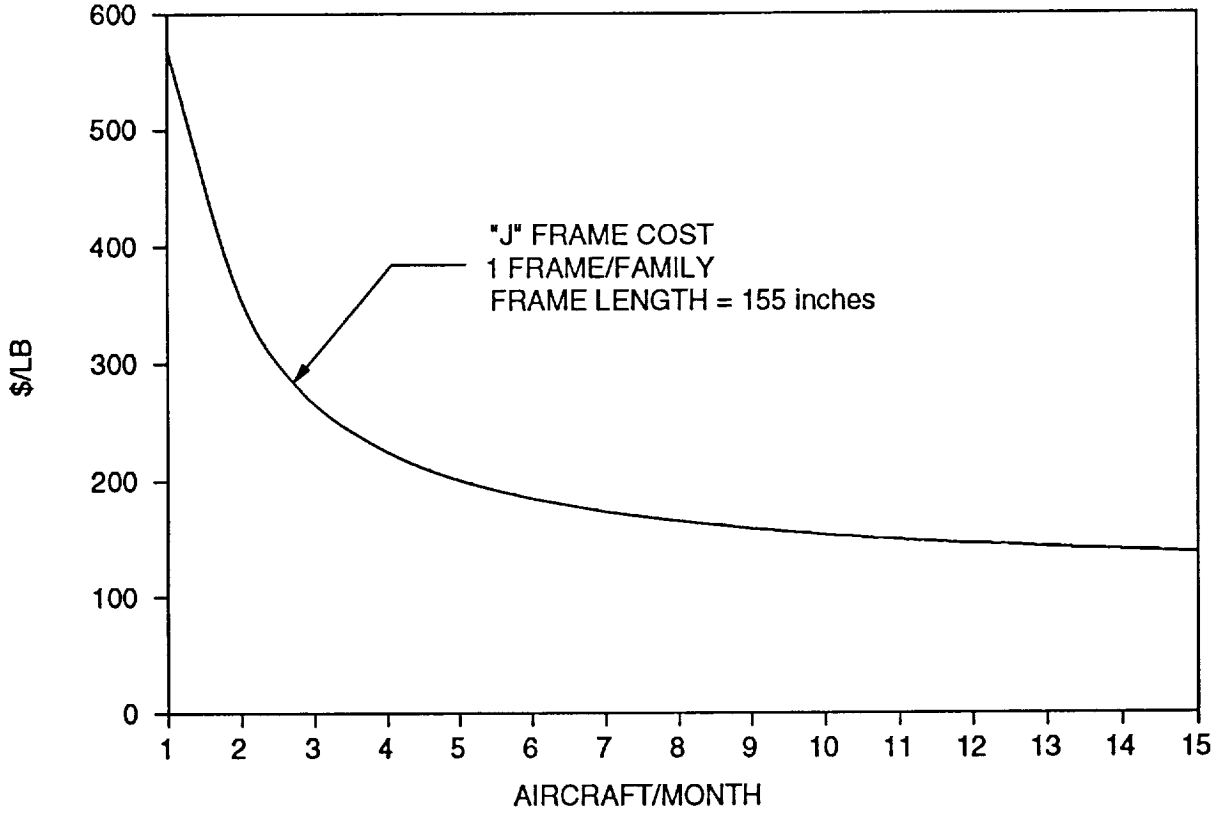

Figure 19. Cost Model Predictions of Frame Cost as a Function of Production Rate

The importance of the aircraft production rate with design details only becomes important to the designer through its interaction with the design detail of frame commonality. The graph, shown in figure 20, represents constant frame cost lines as a function of frame commonality and aircraft production rate. For a high production rate aircraft, lower frame commonality would not impact the frame cost as much as a lower rate production aircraft. The cost model would help the designer understand how best to design the fuselage frame detail to allow for the most cost effective application in the baseline production environment. It could also suggest another process be utilized for certain production environments if tied to alternative process models.

The braided/resin transfer molding fabrication process, when applied to fuselage frames, is most cost effective in high production quantities. Whether the higher frame fabrication rate is due to higher aircraft production rates or increased frame commonality does not matter. This is due to the tooling requirements being driven by rate rather than part number variations. Conveying this information to the designer early on could head off production and cost problems which are difficult and expensive to

solve after design release.

In an environment of high production rates braid/resin transfer molding fabrication is cost competitive with other composite fabrication techniques. But more importantly, the cost model prediction, based on actual fabrication labor and tooling costs associated with frames fabricated for the ATCAS test panels, is cost competitive with aluminum fuselage frame fabrication costs. This is in addition to any weight savings through the use of advanced composite materials.

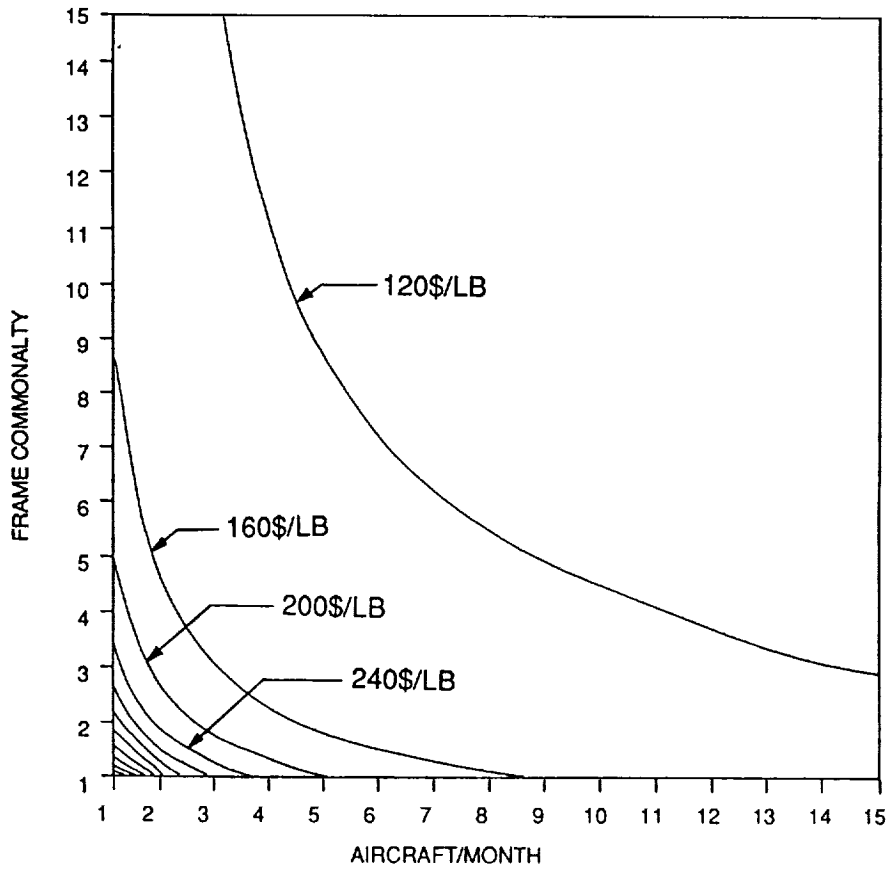

Figure 20. Cost Model Predictions of Frame Cost as a Function of Commonality and Production Rate

CONCLUSION

Important characteristics of a good cost model are to first identify the key features of the design detail. The second step is to develop all cost relationships between the design details and process steps. The third step is to calibrate the model to actual fabrication costs and detailed production estimated costs.

The most important requirement of a good cost model is that it is a flexible communications tool to allow the various disciplines to convey the relationships between design details and cost. No cost

model will be perfect the first time around nor will all possible improvements be known, so flexibility is key. Non-ambiguous and timely communication is the primary problem with the current design optimization process; any worthwhile cost model must address this issue. The last important feature is an open programing architecture such that all the logic from which the cost is derived can be queried and explained. This is very important in preventing any model from becoming a black box to future users, a key failing of past models.

Strong cost drivers predicted by the cost model of braid/resin transfer molding of fuselage frames were frame length, frame commonality, and production rate. When a design environment and production environment are correctly matched, changes in design detail have little impact on cost. When they are not matched significant cost can result. The current study confirms that braid/resin transfer molding of fuselage frames can not only be cost effective versus other advanced composite fabrication methods, but can be on par with detail fabrication costs of metal fuselage frames.

References

1. Ilcewicz, L. B., T. H. Walker, K. S. Wilden, G. D. Swanson, G. Truslove, and C. L. Pfahl: "Application of a Design-Build-Team Approach to Low Cost and Weight Composite Fuselage Structure," NASA Contractor's Report 4418, 1991.

2. Walker, T. H., P. J. Smith, G. Truslove, K. S. Wilden, K. S. Wilden, S. L. Metschan, C. L. Pfahl: "Cost Studies for Commercial Fuselage Crown Design," In Proceedings of the Ninth DoD/NASA/FAA Conference on Fibrous Composites in Structural Design, Lake Tahoe, NV, FAA Publication, 1991.

3. Fedro, M. J., C. Gunther, F. K. Ko: "Mechanical and Analytical Screening of Braided Composites for Transport Fuselage Applications," NASA Conference Publication 3104, 1990.

omit

Session IV

DESIGN AND MANUFACTURING OF LOW COST COMPOSITES

Session Co-Chairmen: Paul Pirrung and Richard Holzwarth
Wright Laboratory

Papers from this session appear in Volume II, NASA CP-3179

omit

Session V

RTM/STITCHED TECHNOLOGY

Session Chairman: Norman J. Johnston
NASA Langley Research Center

[redacted]

DEVELOPMENT OF RTM AND POWDER PREPREG RESINS FOR SUBSONIC AIRCRAFT PRIMARY STRUCTURES

Edmund P. Woo, and Michael R. Groleau
The Dow Chemical Company
Midland, Michigan

James L. Bertram, Paul M. Puckett, and Shawn J. Maynard
The Dow Chemical Company
Freeport, Texas

SUMMARY

In task 1.3 of NASA Contract NAS-1-18841, Dow developed a thermoset resin which could be used to produce composites via the RTM process. The composites formed are useful at 200°F service temperatures after moisture saturation, and are tough systems that are suitable for subsonic aircraft primary structure. At NASA's request, Dow also developed a modified version of the RTM resin system which was suitable for use in producing powder prepreg. In the course of developing the RTM and powder versions of these resins, over 50 different new materials were produced and evaluated.

INTRODUCTION

Historically, design engineers have selected metals for use in primary aircraft structures. Metals, which are isotropic, are well characterized and valued for their excellent strength, stiffness and ductility. The introduction of lighter anisotropic polymer-based composites into primary aircraft structures places certain demands on this class of materials. Many critical portions of an aircraft are subject to compressive forces, demanding that the composite possess excellent compressive strength and maintain good compressive properties following an impact. The ductility of metals, by contrast, insures that they suffer little damage from low energy impact and maintain most of their initial properties.

The substitution of polymer based composites for metal has proven to be problematic, especially in the area of damage tolerance. As composite technology has evolved over the years, state-of-the art prepreg materials (e.g. Toray T800/3900-2, Hercules IM-7/8551-7, Fiberite IM-7/977-2) have been developed which can provide very tough, damage tolerant composite products [1]. These impact resistant prepreg-based composites typically possess a resin-rich interlaminar region which has been toughened by the addition of relatively large elastomeric or thermoplastic particles. This type of composite micro-architecture is not easily transferable to applications where RTM is used to form the composite. Firstly, it is difficult to control the thickness of the interlaminar region in a dry preform into which a liquid is injected. Secondly, the use of large elastomeric or thermoplastic particles in an RTM formulation is unworkable, primarily because the preform acts as a filter, trapping particles as the resin flows through the fiber bundles. Furthermore, elastomeric or thermoplastic particles increase the resin viscosity to a level that prohibits saturation of the fibers during RTM.

Another approach to generating impact resistance in composites is the use of a three dimensional (3-D) preform [2]. On impact of a typical 2-D preform, one of the primary causes of failure is the development of interlaminar cracks and delamination. The use of through-the-thickness stitching (Z-axis) in a 3-D woven preform drastically reduces the possibility that failure can occur via delamination, since the plane of failure is constrained by the presence of reinforcement. Indeed, it has been demonstrated that composites made from brittle thermoset systems, that would typically have compression after impact values of 20-25 ksi, can exhibit CAI values of 30-35 ksi by stitching the preform through the thickness [3].

The use of these "tough" 3-D reinforced preform structures is compatible with resin impregnation via RTM. However, the use of a 3-D preform produces an unexpected side effect. The 3-D structure of the preform produces a triaxial stress on the polymer in the resin-rich interstitial pockets of the preform. The stress is generated by a combination of resin cure shrinkage and dissimilar thermal expansion coefficients between the polymer and fiber. Most of the relatively brittle polymers used in RTM relieve this stress by microcracking. However, there has been no reduction observed in static mechanical properties tested to date, which can be directly related to the presence of microcracks. Although the presence of microcracks does not typically result in a reduction in static mechanical properties, they do lead to increased moisture absorption and an increased probability of inter- and intra-laminar crack formation. These problems would most likely occur in an environment where thermal cycling of the composite is

anticipated. Therefore, an RTM resin that has a minimum tendency to microcrack when used with damage tolerant 3-D preforms would be desirable.

An alternative approach to forming tough, three-dimensionally reinforced composites is the use of powder prepreg. Following impregnation of fiber tows with a powder, these materials can be woven or braided into a 3-D structure. The consolidation of this type of 3-D preform with heat and pressure should provide a high quality composite via a process that could be economically competitive with RTM. However, as with RTM, it is the 3-D braiding, and not the processing method, which improves the toughness of the composite.

DEVELOPMENT OF RTM RESINS

Task 1.3 called for the development of a tough, one-part resin suitable for RTM that can be processed at temperatures of less than 300°F (149°C). TACTIX*695 epoxy resin [4], a resin originally developed for prepreg and adhesive applications, met the thermal and mechanical performance requirements of this task, but did not have the necessary processability. TACTIX*695 is the original member of the CET (Crosslinkable Epoxy Thermoplastic) resin family. The resins described as CET materials are designed to cure with linear advancement of the epoxy, generating a thermoplastic-like structure, which then crosslinks in the last stages of reaction to form the final thermoset polymer. The crosslinking agent that is normally used in TACTIX*695 formulations is diaminodiphenylsulfone (DDS). It is the addition of amines to TACTIX*695, which contains both epoxy and phenolic components, that limits the RTM processability of this material. Because amines and phenolics act as catalysts for each other in the reaction with epoxy resins, the rate of reaction is increased, and the time available to mold the resin is significantly reduced.

Producing a formulation that was RTM processable began with the development of a non-amine curing agent substitute for DDS that increased the available pot-life and molding time. A key to the development was the identification of a catalyst package which would allow the resin and curing agent to be heated to temperatures of 200-250°F (93-121°C) for several

---

* Trademark of The Dow Chemical Company

hours before significant reaction and viscosity build began. This elevated temperature stability is essential to molding flexibility.

The absorption of moisture into a polymer plasticizes the matrix, causing a reduction in modulus and glass transition temperature [5]. Thus, the service temperature of a composite will be dependent on the initial polymer Tg and the amount of absorbed moisture. Our development efforts were guided by the concept that moisture absorption of the final polymer should be minimized.

Experimental resins XU-71992.00 and XU-71992.01 were identified as formulations that possessed the thermal, mechanical, and processing characteristics required for an RTM resin system. Experimental resin XU-71991.00, a modified, high molecular weight version of XU-71992.01, was developed for use in powder-prepregging applications. The data in Table 1 compares the unreinforced thermal and mechanical properties of TACTIX*695 with experimental resins XU-71992.00, XU-71992.01 and XU-71991.00. This data shows that the experimental formulations provide increased toughness, equivalent modulus and moisture absorption, with slightly lower Tg's, as compared to TACTIX*695.

The retention of flexural strength and modulus in unreinforced parts made from resins XU-71992.00, XU-71992.01 and XU-71991.00, tested at elevated temperatures following equilibrium moisture absorption obtained by 14 days water boil, is seen in Figures 1, 2 and 3 respectively. Note that the materials maintain greater than 80% of their initial modulus values at 200°F (93°C). In Figure 4, a comparison of the modulus retention of TACTIX*695 and the three experimental resins is shown. TACTIX*695 and all three experimental resins have equivalent moisture absorption values of 1.4-1.6%. The useful service temperature of each polymer, as defined by the break point in the modulus retention curve, can be correlated to the dry polymer glass transition temperature. The service temperature for each of the polymers (200-225°F / 93-107°C) is approximately 40-50°C below the Tg.

PROCESSING

Figures 5 and 6 show DSC traces of XU-71992.01 and XU-71991.00, respectively. The cure energy profiles of the two RTM resins XU-71992.00 and XU-71992.01 are very similar,

liberating only 140-180 joules/gram. The resin for powder prepreg applications, XU-71991.00, which is a thermally advanced resin, liberates only 112 joules/gram of energy. In contrast, typical epoxy systems have a cure energy of approximately 300-400 joules/gram. Care must be taken to control the cure of epoxies because of the large amount of potential energy inherent in their chemistry. Problems normally associated with the release of this energy include generation of thermal stresses in a part during cure, and occasionally an uncontrolled adiabatic exotherm during the curing of thick composite parts. With the substantially reduced amount of energy liberated during the cure of CET resins, the problems associated with energetic cures are significantly reduced.

Figure 7 compares the viscosity of experimental resins XU-71992.00, XU-71992.01 and XU-71991.00 as a function of temperature. The RTM resins, XU-71992.00 and XU-71992.01, reach a pumpable viscosity at about 200°F (93°C) and a viscosity suitable for molding (500cps) at temperatures above 250°F (121°C). Temperatures of 200 -250°F are easily achievable in standard processing equipment and provide an excellent process window for these resins. Because it was developed for powder prepreg applications, experimental resin XU-71991.00 has a much higher molecular weight and therefore a much higher viscosity at 200-250°F.

Figures 8 and 9 show the viscosity increase with time at three isothermal temperatures (200, 250, 300°F) for XU-71992.00 and XU-71992.01, respectively. A comparison of Figures 8 and 9 shows these two RTM materials are very similar in terms of their processability, with the XU-71992.01 being slightly more viscous. This higher viscosity means that the material must be processed at slightly higher temperatures. Even at 275°F (135°C) the XU-71992.01 gives approximately two hours of molding life, while the XU-71992.00 has over three hours of molding life at 250°F.

Figure 10 shows the increase in viscosity with time at 300°F for XU-71991.00. The viscosity (at 300°F) is quite low (~1000 cps) for a thermally advanced epoxy resin, and the catalyst system apparently retains some latency. The latency of this resin is further seen in Figure 11. A dynamic viscosity profile obtained by heating experimental resin XU-71991.00 at a ramp rate of 2°C/min shows a minimum viscosity of ~300 cps at 350°F (177°C) for several minutes before the viscosity begins to rise.

The relationship between cure temperature and resin properties is shown in Table 2. Here, clear-castings of XU-71992.01were cured at temperatures ranging from 248°F (120°C) to 392°F (200°C), and dynamic mechanical spectroscopy (DMS) was used to evaluate their T_g, shear modulus below T_g, and shear modulus above T_g. These three parameters are closely linked to the structure of the crosslinked network, which typically dominates the properties of the resin. As can be seen, the effect of cure temperature on the properties of the neat resin is insignificant. This should provide a substantial amount of flexibility in the design of cure schedules for different parts and processes.

COMPOSITE PROPERTIES

Composite panels made with experimental resins XU-71992.00, XU-71992.01 and an unadvanced version of XU-71991.00 were produced via resin infusion molding. In this process, which is used by Dow for evaluating laboratory-scale quantities of resin, a plaque of degassed resin is placed into the bottom of a mold and a dry preform made of Celion G30-500, 3K, 8 Harness Satin fabric is placed on top. The mold is closed, and a vacuum, heat and pressure schedule is applied. In this process, the resin flows into the preform through the thickness direction. The typical consolidation pressure of 200 psi, combined with the vacuum on the mold cavity, allows for the formation of high quality, void-free panels. While resin infiltration was performed at temperatures ranging from 266°F (130°C) to 293°F (145°C), the cure schedule for these systems was 1 hour at 302°F (150°C), 1 hour at 347°F (175°C), and 2 hours at 392°F (200°C).

The data in Table 3 compares the composite performance of experimental resins XU-71992.00, XU-71992.01 and XU-71991.00. As would be expected, based upon their formulation, the materials have very similar properties. The short beam shear, compressive strength, and open hole compressive (OHC) strength values are very good and are comparable to values reported for standard prepreg systems (e.g. Fiberite 934). The 38-39 ksi compression strength after impact (CAI) values measured for these materials are outstanding. Such high CAI strengths are normally seen only in thermoplastic-modified prepreg-based materials, or in composites that are woven, braided or stitched through the third dimension (Z-axis reinforcement). The experimental CET resins provide sufficient matrix toughness to produce

composites with high impact resistance, without the aid of second phase toughening agents or Z-axis reinforcement.

Further, preliminary field trials using XU-71992.00 indicate a high resistance to microcracking in 3-D woven preforms. A study of the resistance of CET resins to microcracking is currently in progress.

CONCLUSIONS

Two new RTM systems (experimental resins XU-71992.00 and XU-71992.01) have been developed for use in composites that have a 200°F/wet service temperature requirement. These materials are easily processed at temperatures of approximately 250°F (121°C) and provide a molding time of about 2 hours. The composites absorb very little moisture and have very good impact resistance.

A resin similar to these two has been produced by reaction advancement, forming a solid resin with a low melting point. This advanced epoxy system (experimental resin XU-71991.00) is useful in making prepreg via a powder process. While the composite properties of the powdered version of this resin have not been characterized, properties of the unadvanced resin have proven to be similar to those of the RTM resins.

NOTICE

The information in this paper is presented in good faith, but no warranty is given, nor is freedom from any patent to be inferred.

REFERENCES

1 a. C. B. Bucknall, Chapter 4, "Approaches to Toughness Enhancement," Advanced Composites, ed. Ivana K. Partridge, Elsevier Applied Science, NY,1989, pp. 145-161.

b. G. Almen, P. Mackenzie, V. Malhotra, and R. Maskell, "977: Characterization of a Family of New Toughened Epoxy Resins," 35th International SAMPE Symposium, April 2-5, 1990, pp. 419-431.

c. Dodd H. Grande, Larry B. Ilcewicz, William B. Avery, Willard D. Bascom, "Effects of Intra- and Inter-laminar Resin Content on the Mechanical Properties of Toughened Composite Materials," First NASA Advance Composites Technology Conference, Seattle, WA, Oct. 29 - Nov. 1, 1990, 455-475, NASA Conference Publication 3104.

d. F. W. Lee, Maureen A. Boyle, and Pierre Lefebvre, "High Service Temperature, Damage Tolerant Prepreg Systems Based on Cyanate Chemistry," 35th International SAMPE Symposium, April 2-5, 1990, pp. 162-174.

e. H. G. Recker, V. Alstadt, W. Eberle, T. Folda, D. Gerth, W. Heckmann, P. Ittemann, H. Tesch, T. Weber , "Toughened Thermosets for Damage Tolerant Carbon Fiber Reinforced Composites," SAMPE Journal, Vol. 26 (2), March/April 1990, pp. 73-78.

f. Brian P. Rice and Ran Y. Kim, "Fracture Characterization of Toughened Bismaleimide/Graphite Composites," 35th International SAMPE Symposium, April 2-5, 1990, pp. 455-467.

g. H. G. Recker, V. Altstadt, M. Stangle, "Rigidite 5276 - A Highly Damage Tolerant Epoxy System for Primary Aircraft Structure Applications," 37th International SAMPE Symposium, March 9-12, 1992, pp. 493-505.

2 a. Conference Proceedings: 3-D Composite Materials, ed. H. Benson Dexter, Eugene T. Camponeschi, Leighton Peebles, NASA Conference Publication 2420, Annapolis, MD, November 5-7, 1985.

b. Joan G. Funk and Jerry W. Deaton." The Interlaminar Fracture Toughness of Woven Graphite/Epoxy Composites," NASA Technical Paper 2950, November 1989.

c. David S. Brookstein, "Interlocked Fiber Architecture: Braided and Woven," 35th International SAMPE Symposium, April 2-5, 1990, pp. 746-756.

d. D. Brosius and S. Clarke, "Textile Preforming Techniques for Low Cost Structural Composites" Advanced Composite Materials: New Developments and Applications Conference Proceedings, Detroit MI, Sept 30 - Oct. 3, 1991, pp. 1-10.

3 a. M. B. Dow, D. L. Smith, S. J. Lubowinski, "An Evaluation of Stitching Concepts for Damage Tolerant Composites," Fiber-Tex Conference, Greenville, SC, Sept. 13-15, 1988, NASA Conference Publication 3038, June 1989.

b. Raymond J. Palmer, Marvin B. Dow, Donald L. Smith, "Development of Stitching Reinforcement for Transport Wing Panels," First NASA Advanced Composites Technology Conference, Seattle, WA, Oct. 29 - Nov. 1, 1990, 621-646, NASA Conference Publication 3104.

4 a. James L. Bertram, Louis L. Walker, Jody R. Burman, James A. Clarke, US Pat. 4,494,291, June 16, 1988.

b. James L. Bertram, Louis L. Walker, Van I. Stuart, US Pat. 4,725,652, Feb. 16, 1988.

c. James L. Bertram, Louis L. Walker, John W. Muskopf, US Pat. 4,925,901, May 7, 1990.

d. James L. Bertram, Louis L. Walker, Van I. Stuart, US Pat. 4,946,817, Aug. 7, 1990.

5 a. H. M. Clancy and D. E. Lufti, "Moisture in Composites - A Reminder, "18th International SAMPE Technical Conference, Oct. 7-9, 1986, 135-141.

b. Diffusion in and Through Polymers, Wolf R. Vieth, Hanser Publishers/Oxford University Press, NY, 1991.

TABLE 1. CET Resins: A Comparison of Clear Cast Properties#.

Mechanical Test	Measurement	TACTIX*695	XU-71992.00	XU-71992.01	XU-71991.00
Fracture Toughness	K_{1c} (psi $\sqrt{in}$)	650	835	835	711
	G_{1c} (J/m^2)	140	245	245	192
	G_{1c} (in lbs/in^2)	0.8	1.4	1.4	1.1
Density	Polymer (g/cc)	1.48	1.37	1.27	1.27
Tensile	Strength (ksi)	13	13	13	13
	Modulus (ksi)	445	440	425	410
	Elongation (%)	8.5	5.0	5.5	5
Flexural	Strength (ksi)	19	21	18.5	21
	Modulus (ksi)	455	495	450	450
	Strain (%)	>5	>5	>5	>5
Moisture Absorption	Weight %	1.6	1.4	1.6	1.4
Thermal	Tg (Tan δ,°C)	165	155	156	164
	Tg (DSC °C)	160	140	146	156

Cure Schedule: 4 hrs @ 150°C: Post Cure Schedule: 2 hrs @ 200°C
Trademark of The Dow Chemical Company
[a]Compact tension geometry
[b]After two weeks in boiling water
#Typical properties, not to be construed as specifications

TABLE 2. A Comparison of DMS Properties for Unreinforced Panels of Experimental Resin XU-71992.01 Cured Isothermally

Initial cure T (°C)	G' @ 25°C (GPa)	Tg from T at G" = max (°C)	Tg from T at tan δ = max (°C)	G' @ 200°C (dyn/cm^2)
120	1.167	151	160	4.35e7
135	1.202	152	159	4.90e7
150	1.174	150	159	4.67e7
165	1.214	---	---	---
200	1.176	150	159	4.63e7

All clear-castings cured to 95% conversion at the temperatures shown above, followed by a post-cure for 2 hr. @ 200°C.

TABLE 3. A Comparison of Composite Mechanical Properties# of Experimental CET Resins With G30-500 8HS

Mechanical Test	Measurement	XU-71992.00	XU-71992.01	XU-71991.00
0° Flex	77°F-Dry Strength (ksi) Modulus (ms)	152 8.0	138 8.8	137 8.3
Short Beam Shear	77°F-Dry Strength (ksi)	10	10	10
0° Compression	77°F-Dry Strength (ksi)	113	108	109
Open-hole Compression (OHC)	77°F-Dry Strength (ksi) 180°F-Wet Strength (ksi)	38 34	39 33	38 34
Compression After Impact (CAI)	77°F-Dry Strength (ksi)	39	39	38

The cure schedule on all composite panels is 1 hr @ 150°C, 1 hr @ 175°C; followed by a post cure schedule of 2 hrs @ 200°C.

All tests were conducted according to SACMA recommended test methods.

#Typical properties, not to be construed as specifications

FIGURE 1. Effects of Moisture Absorption and Elevated Temperature on Unreinforced Flexural Properties of Experimental Resin XU-71992.00

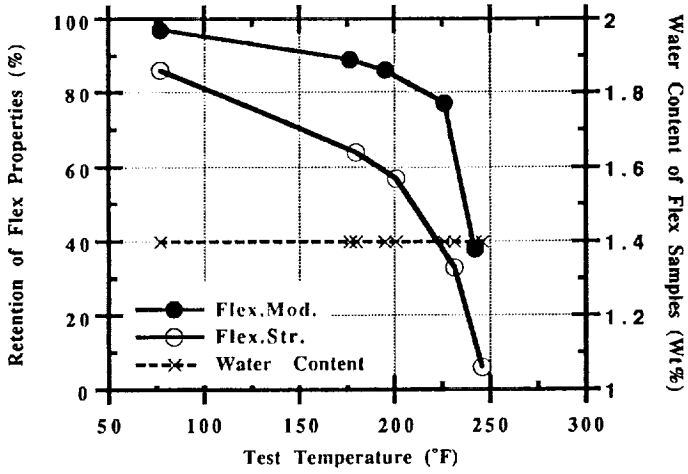

Cure Schedule: 4 hrs @ 150°C: Post Cured 2 hrs @ 200°C

Equilibrium Moisture Absorption Obtained by 14 Days Water Boil

FIGURE 2. Effects of Moisture Absorption and Elevated Temperature on Unreinforced Flexural Properties of Experimental Resin XU-71992.01

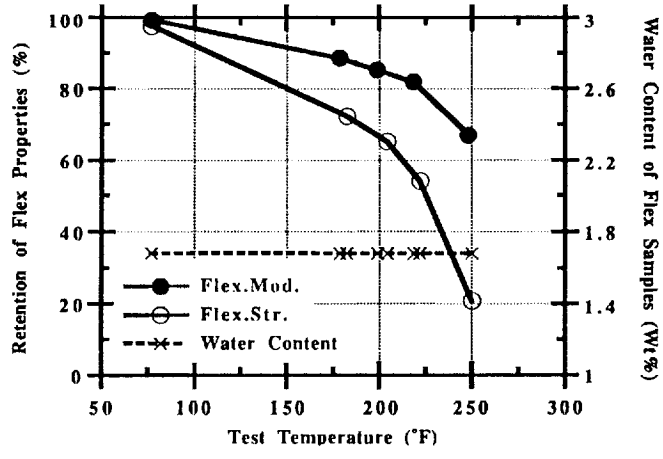

Cure Schedule: 4 hrs @ 150°C: Post Cured 2 hrs @ 200°C

Equilibrium Moisture Absorption Obtained by 14 Days Water Boil

FIGURE 3. Effects of Moisture Absorption and Elevated Temperature on Unreinforced Flexural Properties of Experimental Resin XU-71991.00

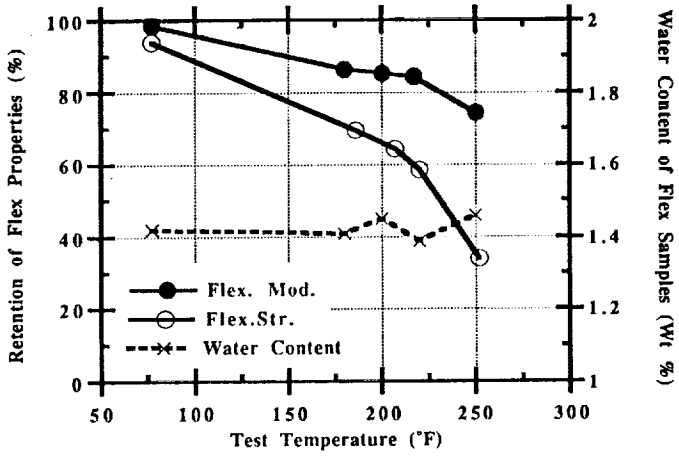

Cure Schedule: 4 hrs @ 150°C: Post Cured 2 hrs @ 200°C

Equilibrium Moisture Absorption Obtained by 14 Days Water Boil

FIGURE 4. A Comparison of Flexural Modulus Retention of Unreinforced Panels Made With CET Resins

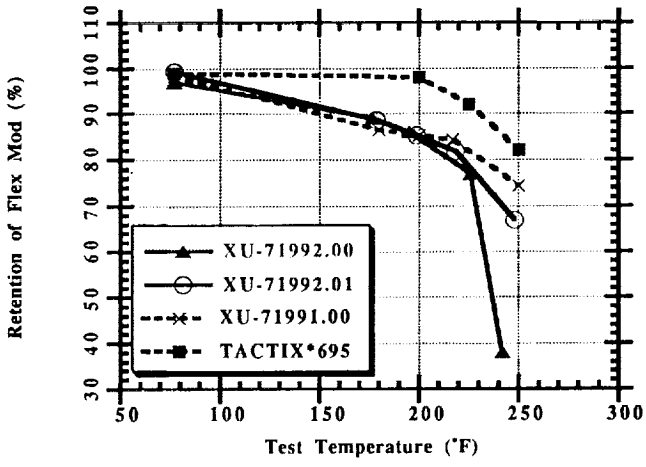

Cure Schedule: 4 hrs @ 150°C: Post Cured 2 hrs @ 200°C

Equilibrium Moisture Absorption Obtained by 14 Days Water Boil

*Trademark of The Dow Chemical Company

FIGURE 5. DSC of XU-71992.01 (Uncured)

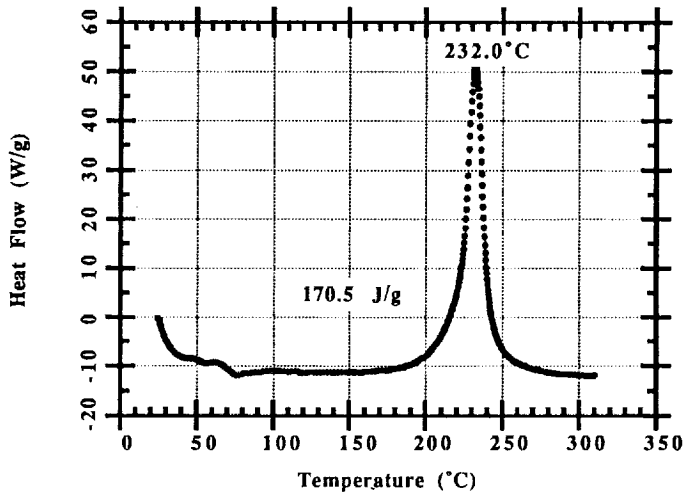

Ramp 10°C/min

FIGURE 6. DSC of XU-71991.00 (Uncured)

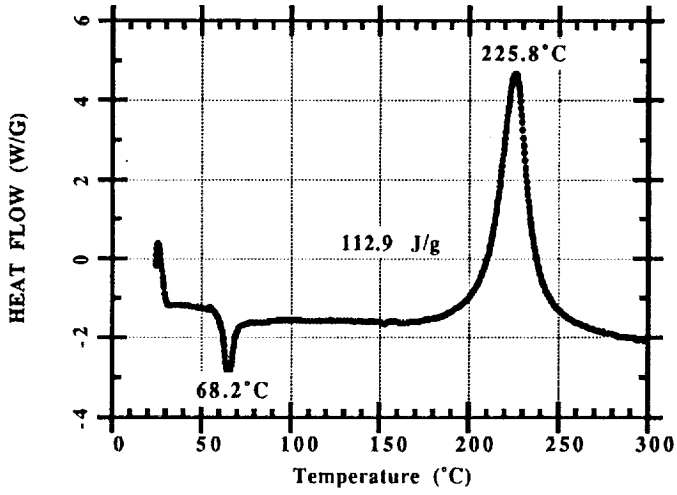

Ramp 10°C/min

FIGURE 7. Effect of Temperature on the Viscosity of Experimental CET Resins

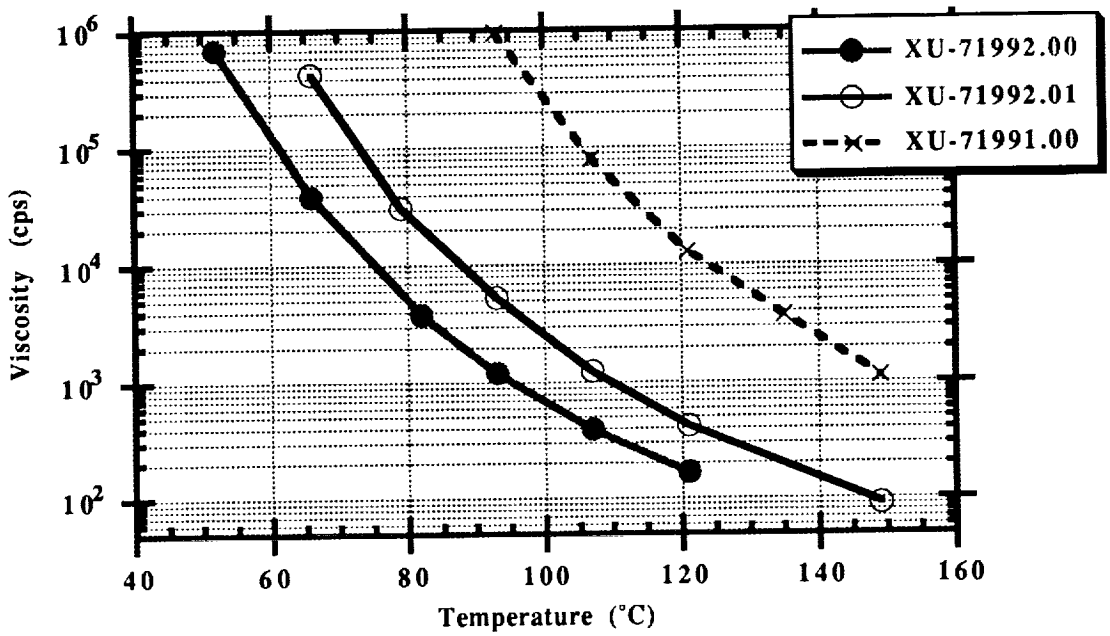

FIGURE 8. Isothermal Viscosity Profiles of Experimental Resin XU-71992.00

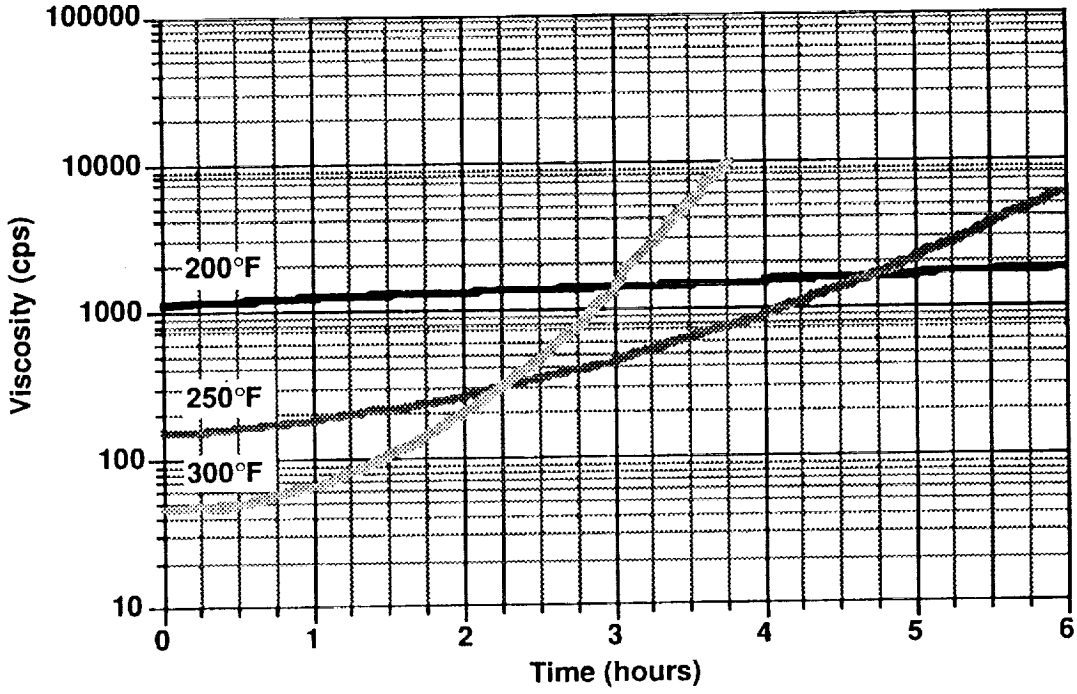

FIGURE 9. Isothermal Viscosity Profiles of Experimental Resin XU-71992.01

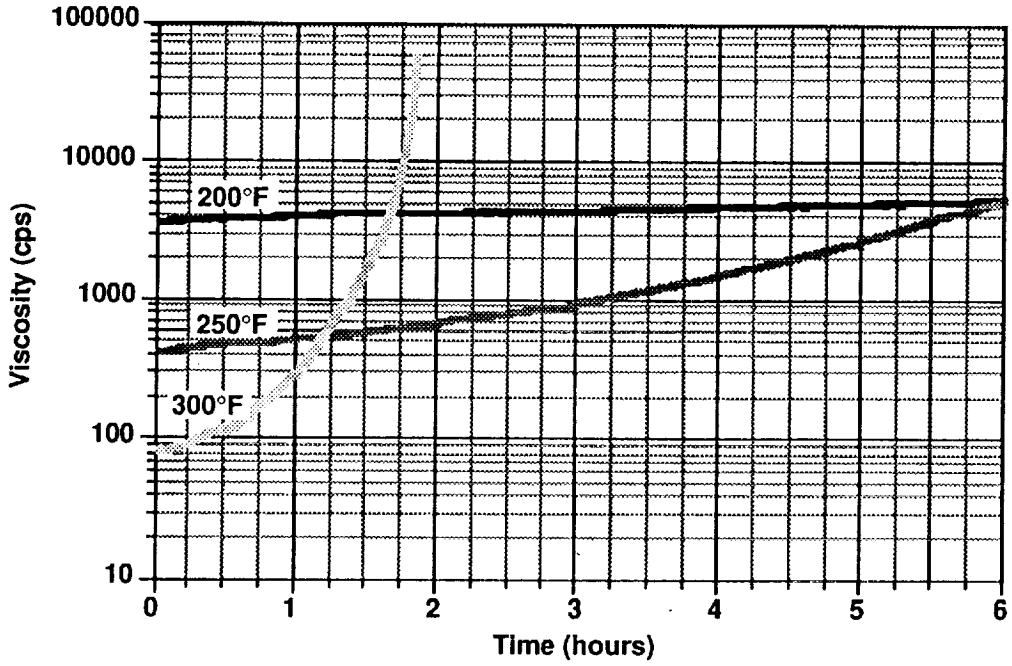

FIGURE 10. Isothermal Viscosity Profile of XU-71991.00 at 300°F (150°C)

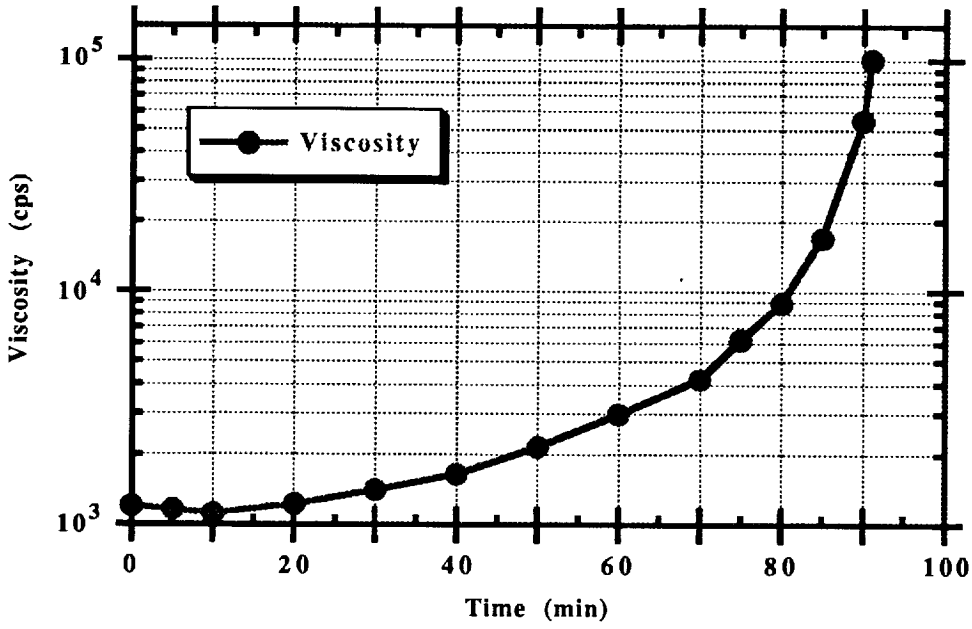

FIGURE 11. Dynamic Viscosity Profile of Experimental Resins XU-71991.00

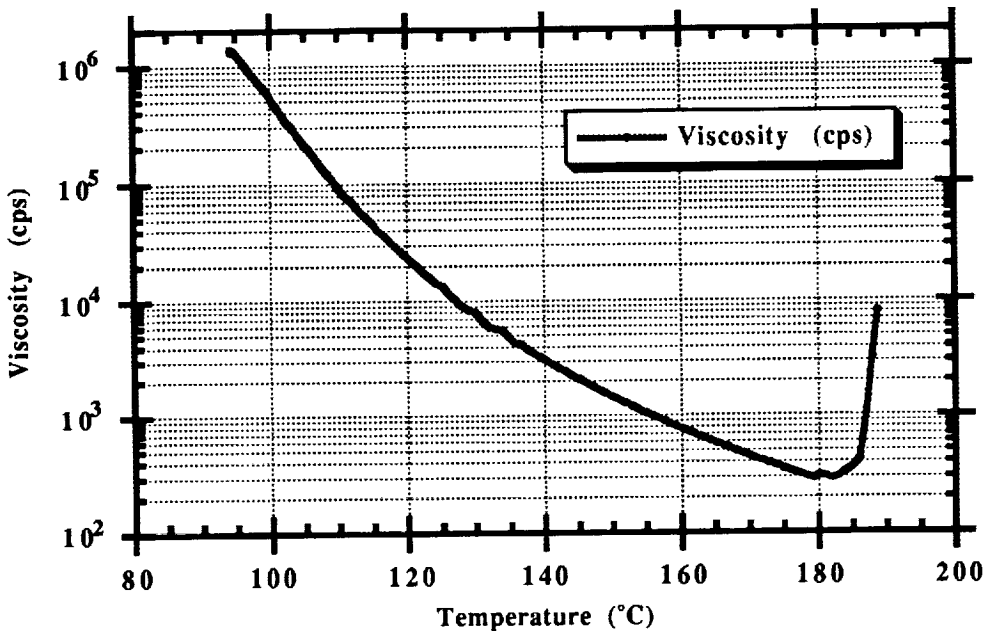

Heating Rate 2°C/min
Parallel Plate - 50 mm: 0.5 mm Gap

ANALYTICAL MODELING AND SENSOR MONITORING FOR OPTIMAL PROCESSING OF ADVANCED TEXTILE STRUCTURAL COMPOSITES BY RESIN TRANSFER MOLDING*

Alfred C. Loos, John D. MacRae, and Vincent H. Hammond
Department of Engineering Science and Mechanics
Virginia Polytechnic Institute and State University
Blacksburg, VA 24061

David E. Kranbuehl and Sean M. Hart
Chemistry Department
College of William and Mary
Williamsburg, VA 23185

Gregory H. Hasko
Lockheed Engineering and Sciences Co.
NASA Langley Research Center
Hampton, VA 23665

Alan M. Markus
Douglas Aircraft Company
Long Beach, CA 90846

ABSTRACT

A two-dimensional model of the resin transfer molding (RTM) process was developed which can be used to simulate the infiltration of resin into an anisotropic fibrous preform. Frequency dependent electromagnetic sensing (FDEMS) has been developed for in situ monitoring of the RTM process. Flow visualization tests were performed to obtain data which can be used to verify the sensor measurements and the model predictions. Results of the tests showed that FDEMS can accurately detect the position of the resin flow-front during mold filling, and that the model predicted flow-front patterns agreed well with the measured flow-front patterns.

* **This work was made possible through the support of the National Aeronautics and Space Administration-Langley Research Center grant no. NAG1-343 with Virginia Tech and grant no. NAG1-237 with the College of William and Mary.**

INTRODUCTION

Resin transfer molding (RTM) is seen as a cost-effective method of fabricating primary aircraft structures. It also enables the use of a variety of automated textile processes for making the dry fiber preforms, several of which offer through-the-thickness reinforcement. RTM has been used for decades in various industries for less critical structures having low fiber volumes and readily processed resins. The challenge in adapting RTM to primary aircraft structures lies in ensuring successful injection and cure for high fiber volumes, limited resin processing windows and geometrically complex shapes.

A joint research program between NASA Langley Research Center, Virginia Polytechnic Institute and State University, The College of William and Mary, and Douglas Aircraft Company is underway to develop a science-based understanding of the RTM process in order to minimize costly trial-and-error steps during process development of a structure, and to ensure quality during production. This involves characterizing the processing behavior of the fibers and resins, developing mathematical models of the RTM process, and monitoring significant process variables in real time. The ultimate goals of this program are to develop a comprehensive three-dimensional RTM model for complex shape fiber architectures and to incorporate the model into an intelligent process control system which uses frequency dependent electromagnetic sensing (FDEMS) for sensing the process variables in real-time.

The first result of this collaborative research program was the development of a mathematical model of the resin film infusion process [1,2]. The model can be used to simulate one-dimensional, through-the-thickness infiltration of resin into a fabric preform and cure of the resin saturated preform. Compaction and permeability characteristics of the fabric preform along with the kinetic and viscosity characteristics of the thermosetting resin are incorporated into the model to predict, as a function of applied temperature and pressure boundary conditions, the following parameters: a) initial resin mass; b) resin front position and time required for preform infiltration; c) preform temperature distribution; d) resin viscosity and degree of cure; and e) final part thickness and fiber volume fraction. Basic features of the RTM computer model are shown in Fig. 1.

Verification of the one-dimensional resin film infusion model has been accomplished for two types of textile preforms, Hercules 3501-6 resin, and several thermal cycles. Frequency dependent electromagnetic sensors (FDEMS) were used for in situ measurements of the infiltration time, resin viscosity, and resin degree of cure. The physical arrangement of the FDEMS sensors and measuring system is shown in Fig. 2. The results of the one-dimensional model verification and utilization studies were reported at the first and second NASA Advanced Technology Conferences [3,4].

Recent research has focused on extending the model to two-dimensional anisotropic geometries. Specific applications include in-plane injection of liquid resin into a flat preform (Fig. 3) and resin infiltration of a complex shape preform by the resin film infusion process (Fig. 4).

The purpose of this paper is to discuss experimental and analytical techniques that are being used in the development of the two-dimensional RTM flow model. Specifically, a series of flow visualization experiments were performed to verify the flow-front and infiltration-time predictions of the RTM process simulation model, to verify the permeability versus compaction measurements obtained from preform characterization experiments, and to demonstrate the ability of FDEMS sensing to detect the position of the flow-front.

RESIN INFILTRATION MODEL

The two-dimensional resin flow model was developed to determine the position of the resin flow-front and the pressure distribution inside the preform. In development of the flow model the following assumptions are made: 1) the textile preform is a porous medium; 2) the preform permeability is heterogeneous and anisotropic; and 3) the resin is incompressible, and capillary and inertia effects are neglected (low Reynolds number flow).

For flow through porous media, the momentum equation can be replaced by Darcy's Law which relates the flow rate to the pressure gradient. Darcy's Law for an anisotropic porous medium can be written as

$$\begin{Bmatrix} q_x \\ q_y \end{Bmatrix} = -\frac{1}{\mu}\begin{bmatrix} S_{xx} & S_{xy} \\ S_{xy} & S_{yy} \end{bmatrix}\begin{Bmatrix} \frac{\partial P}{\partial x} \\ \frac{\partial P}{\partial y} \end{Bmatrix} \tag{1}$$

where q_x and q_y are the flow rates per unit area (superficial velocities) in the x- and y-coordinate directions, S_{xx}, S_{xy}, and S_{yy} are the components of the permeability tensor for the textile preform, μ is the viscosity of the resin, and $\frac{\partial P}{\partial x}$ and $\frac{\partial P}{\partial y}$ are the pressure gradients.

The continuity equation of two-dimensional, incompressible flow is written as

$$\frac{\partial q_x}{\partial x} + \frac{\partial q_y}{\partial y} = 0 \tag{2}$$

The combination of Darcy's Law and the continuity equation yields the governing equation for resin infiltration into a textile preform:

$$\frac{\partial}{\partial x}\left[\frac{-S_{xx}}{\mu}\frac{\partial P}{\partial x} + \frac{-S_{xy}}{\mu}\frac{\partial P}{\partial y}\right] + \frac{\partial}{\partial y}\left[\frac{-S_{xy}}{\mu}\frac{\partial P}{\partial x} + \frac{-S_{yy}}{\mu}\frac{\partial P}{\partial y}\right] = 0 \tag{3}$$

Solution of Eq. (3) gives the pressure distribution $P(x, y)$ within the region of the textile preform where the resin has infiltrated. Once the pressure distribution is determined, the resin velocity at any point inside the preform can be calculated from Darcy's Law.

Solution of the governing equations requires specification of the boundary conditions. At any instant of time, the pressure or flow rate must be specified at each resin inlet port (gate).

If the wetting force due to the resin advancing through the dry fiber preform is neglected, the pressure at the flow front is

$$P = 0 \tag{4}$$

The final boundary condition requires that there be no flow across the surfaces of the mold wall which for an anisotropic material can be expressed as

$$q_n = -\frac{1}{\mu}\left(S_{nn}\frac{\partial P}{\partial n} + S_{nt}\frac{\partial P}{\partial t}\right) = 0 \tag{5}$$

where n and t represent the directions normal and tangent to the mold wall, respectively.

The flow area (area of the pores) is less than the cross-sectional area of a porous material. The relationship between the superficial velocities (q_x and q_y) and the interstitial resin velocities (v_x and v_y) is given as

$$\begin{aligned} q_x &= v_x(1 - \nu_f) = v_x\phi \\ q_y &= v_y(1 - \nu_f) = v_y\phi \end{aligned} \tag{6}$$

where ν_f is the fiber volume fraction and ϕ is the porosity of the fabric preform. The interstitial resin velocity is calculated at the front and is used to determine the advancement of the flow-front during infiltration.

Numerical Solution Procedure

Many methods of modeling free boundary movement have been explored over the past decade [5]. The modeling of the RTM process presents several challenges. A method must be chosen that will allow for the variation in permeability of the media into which resin is being injected. Perhaps as important is that the method chosen must be computationally efficient. Due to the complexity of the part geometry and manufacturing conditions, a typical model of the RTM process can be quite large. For these reasons the finite element/control volume technique was chosen for use in this investigation.

The finite element/control volume approach has several advantages. The use of finite elements allows for the inclusion of variation in material properties throughout the domain with little difficulty. Also, the control volume approach allows for the use of a fixed mesh which eliminates the need to do computationally expensive remeshing to track the flow front movement.

The Finite Element model used is based on a 2-D model developed by Reddy [6]. At present, the model uses a fixed mesh of isoparametric quadrilateral elements. Each element has constant properties. Also, for convenience, the local Cartesian coordinate system of each element is aligned with the global coordinate system. This allows for the global stiffness matrix to be formulated without any transformations. PATRAN is used as a pre and post

processor for the simulation model. The boundary conditions and the material properties are input into the processing model via PATRAN. PATRAN also is used to plot the results after the simulation is completed.

The governing equations describing fluid flow through a porous medium are coupled to a technique which is used to determine the flow front position within the preform. The control volume approach consists of constructing a region around each node in a fixed finite element mesh. These regions, called control volumes, can then be either empty, full, or partially full depending on whether the resin flow front has reached that point in the computational domain. The resin flow front is then tracked from one time step to the next by locating all the positions where the nodal control volumes are partially filled. A nodal fill factor is used to keep track of the state of each node. A fill factor of 0 represents an empty nodal control volume (no resin); whereas, a fill factor of 1.0 means that the nodal control volume is filled. A detailed explanation of the control volume technique and flow front advancement is given in Ref. 7.

Preform Characterization

The preform permeability must be specified in order to obtain a numerical solution of the resin infiltration model. Textile preforms are deformable and anisotropic porous materials. Hence, the permeability depends not only on direction but on the amount of deformation or compression of the preform.

Presently, analytical models that can be used to calculate the permeabilities of advanced architecture preforms do not exist. Thus, the compaction characteristics and the permeabilities in the principal material directions must be measured for each textile preform.

Compaction characteristics of preforms are quantified by mounting a sample between rigid plates, applying a compaction load, and measuring the resulting thickness. Data are commonly reported by constructing plots of fiber volume fraction (ν_f) or porosity (ϕ) versus applied pressure. The fiber volume fraction and porosity can be calculated using the following expression

$$\nu_f = 1 - \phi = \frac{\xi}{d\rho_s} \tag{7}$$

where ξ is the preform areal weight, d is the preform thickness and ρ_s represents the preform density.

Permeability is also a nonlinear function of preform compaction pressure. For the two-dimensional resin infiltration model, the three components of the permeability tensor (S_{xx}, S_{xy}, S_{yy}) must be determined. If the preform is orthotropic, permeability versus compaction pressure measurements are performed in each of the two principal material directions to obtain S_{xx} and S_{yy}. The cross term permeability, S_{xy}, can be calculated using the principal permeabilities in a second order tensor transformation.

Two techniques are commonly used to measure preform permeability. The first method, denoted the steady-state technique, measures the permeability of a fluid saturated preform under constant flow rate conditions. In the second method, denoted the advancing front technique, the permeability is determined by measuring the velocity of the advancing resin front into the dry preform [8]. The steady-state technique was used in the present investigation to measure the permeability. A schematic diagram of the test fixture used to measure in-plane permeability is shown in Fig. 5. To measure the permeability of the preform the following procedure is followed. The sample is placed inside the test chamber and compressed to the specified thickness. A fluid with a known viscosity is allowed to pass through the preform at a constant flow rate and the pressure drop across the preform is measured. The permeability is calculated using the one-dimensional form of Darcy's Law.

EXPERIMENTAL

The three major components used in the flow visualization experiments are shown in Fig. 6. These include the visualization fixture, the video camera and high resolution tape recorder, and the air pressurized resin pot.

The fixture consisted of a square aluminum frame with a 1.5 inch thick poly (methyl methacrylate) top plate. The dimensions of the test cavity are $2ft \times 2ft$. A total of nine FDEMS sensors were mounted in the aluminum bottom plate of the mold. The locations of the sensors in the bottom plate are shown in Fig. 7. The FDEMS sensors were installed into aluminum mounting plugs and the mounting plugs were inserted into cavities that were machined into the bottom plate, as shown in Fig. 8. A $1/4in.$ diameter by $3/8in.$ deep hole was drilled into the center of each cavity which allows resin at the flow-front to enter the cavity and wet-out the sensor. The output leads from the sensors were connected to a multiplexer as shown in Fig. 2.

Fluid was transferred from the pressure pot to the visualization fixture using $1/4in.$ inner diameter plastic hoses. Pressure was monitored during the experiment using gages installed at the exit of the resin pot and at the visualization fixture resin inlet ports. Resin injection pressure was controlled by an air pressure regulator mounted on the resin pot.

At the beginning of each experiment, the video camera was mounted above the visualization fixture. The flow patterns from the experiments were recorded using the high resolution video tape recorder. The video tape was used to determine the infiltration times and to provide a means of correlating the measured flow patterns with the predictions of the resin infiltration model. A total of fourteen images were captured from each taped sequence and stored in 32 bit form on a computer disk for later retrieval.

The textile preform used in the visualization experiments was a style 162, plain weave, E-glass fabric. Eleven layers of the fabric were stacked into the fixture and compressed to the cavity thickness of 0.15 in. The fluid used in the experiments was corn oil. A small amount

of red dye was added to the oil. The viscosity of the oil and dye mixture was measured to be 40 cp.

RESULTS

Preform Characterization

Compaction characteristics of the E-glass fabric are shown in Fig. 9. Note that the fiber volume fraction is calculated from the preform thickness measurements using Eq. (7). The fiber volume fraction of the eleven ply stack of E-glass fabric compressed to fit into the 0.15 in. thick cavity was calculated to be 43%. Based on the fabric compaction data, a pressure of 10.3 psi is required to compress the E-glass preform to a 43% fiber volume fraction.

The permeabilities of the E-glass fabric were measured in the warp and fill directions using the fixture shown in Fig. 5. Data from the permeability experiments are plotted on Fig. 10. The solid and dashed lines are power law regression fits to the warp and fill direction data, respectively. Results of the measurements show that the permeabilities in the warp and fill directions are nearly the same. Hence, a center port injection experiment should result in circular flow-front patterns.

Single Side Port Injection

A schematic diagram of the single side port injection experiment along with pertinent preform and fluid data are shown in Fig. 11. Resin enters the cavity through a single side port and flows along the $1/8in.$ channel around the perimeter of the fabric. Resin then begins to infiltrate through the edges of the preform, saturates the preform, and exits through the center port.

The finite element mesh for the resin infiltration model consisted of 2707 quad elements and a total of 2816 nodes. Since the coordinate axes coincide with principal material directions of the fabric the elements are orthotropic. The measured E-glass fabric warp and fill direction permeabilities at 43% fiber volume fraction were input for each element.

One difficulty in modeling the side port injection experiment was that at the beginning of the test, the resin pressure at the fixture inlet port drops below the specified injection pressure. The pressure at inlet port remains low until the channel is completely filled with resin. As resin begins to infiltrate the fabric, the inlet port pressure increases to the specified injection pressure. Thus, the inlet port pressure was monitored as a function of time during the experiment and the data input into the model as boundary conditions.

The influence of the channel was considered in the model by adjusting the permeability of the elements representing the channel until the model predicted inlet port and channel pressures matched the measured values. This technique gave a reasonably good representation of the resin channel in the simulation.

Comparisons between the model predicted and recorded flow-fronts are shown in Figs. 12-14. The time that the image was captured on the video tape is denoted on each figure. The dark shaded area is the resin saturated region of preform, the whitish area is the dry preform and the solid line represents the model predicted flow-front. The images of the model predicted flow-fronts were taken at times corresponding to the images stored to disk from the video tape. Each model predicted flow pattern was overlaid on top of the appropriate video image taken from the experiments.

As can be seen from the figures the model matched the experimental results at the three different infiltration times very well. Note that measured flow front is somewhat wavy during infiltration. This may be due to the waviness of the plastic top plate.

A grid showing the positions of the FDEMS sensors, which are located underneath the glass fabric, has been overlaid on Figs. 12 and 14. The grid was helpful in comparing the FDEMS sensor response to the flow-front position. The sensor locations and measured wet-out times are denoted on each figure. The sensors are numbered in the order that they are scanned by the computer measuring system. As can be seen from the figures, the FDEMS sensors can detect the location of the resin flow-front to within 5s of the measured infiltration time. The accuracy of the FDEMS measurements can be improved by increasing the scanning rate of the data acquisition system.

Center Port Injection

A schematic diagram of the center port injection experiment along with the preform and fluid data are shown in Fig. 15. Resin enters the cavity through a port in the center of the plastic top plate, infiltrates the preform, and exits through the vents in the sides of the mold.

The same finite element mesh that was generated for the single side port resin infiltration model was used for the center port model. On the first attempt at modeling the center port injection experiment, the measured E-glass fabric warp and fill direction permeabilities at 43% fiber volume fraction were input for each element. The resulting model predicted flow-fronts were considerably slower than the recorded flow-fronts. After an examination of the data and the flow fixture, we concluded that when the resin entered the mold under pressure the plastic top plate was deflecting. This caused an increase in the cavity depth, a decrease in the fiber volume fraction and a corresponding increase in the fabric permeabilities. Considering both the deflection and the nonuniform thickness of the plastic top plate, it was estimated that the depth of the cavity at the center of the fixture was about 12% greater

than the designed cavity depth of 0.15 in. This resulted in a decrease in the fabric fiber volume fraction to 38%. When the model was rerun using the E-glass fabric warp and fill direction permeabilities at 38% fiber volume fraction, the predicted flow-fronts agreed well with the recorded flow-fronts.

Comparisons between the model predicted and recorded flow-fronts are shown in Figs. 16-18. Again, the time that the image was captured on video tape is denoted on each figure. As can been seen from the figures, the model predicted flow-fronts with the adjusted fabric permeabilities agreed well with the recorded flow-fronts at the three infiltration times. Note that the flow patterns are circular due to the nearly equal permeabilities in the fabric warp and fill directions.

Grids showing the positions of the FDEMS sensors have been overlaid on Figs. 17 and 18. The locations and wet-out times of the sensors at the flow-front are denoted on each figure. As was shown in the side port experiments, the FDEMS sensors can accurately detect the location of the resin flow-front.

SUMMARY AND CONCLUSIONS

A two-dimensional RTM process simulation model was developed which can be used to describe the infiltration of resin into a dry textile preform, and cure of the resin saturated preform. The model can be utilized in the development of optimal cure cycles and in mold design by specifying the location of resin injection parts which result in complete wet-out of a complex shape preform. Frequency dependent electromagnetic sensors (FDEMS) have been developed for in situ monitoring of the RTM process. FDEMS sensing can be used to detect the position of the resin front inside the mold during infiltration and to measure the resin properties during cure.

A series of flow visualization experiments were performed to obtain data which can be used to verify the sensor and the model. The results of these tests showed that FDEMS can accurately detect the location of the flow-front in the mold during infiltration, and that the model predicted flow-front patterns agreed well with the recorded flow-front patterns.

In-plane fabric permeabilities were measured using the steady-state technique. When the warp and fill direction permeabilities at the measured fiber volume fraction of the E-glass preform were input into the RTM simulation model, agreement between the model predicted and measured flow patterns was good. However, in the center port injection experiment, the permeabilities were adjusted due to excessive deflection of the plastic top plate. The center port injection experiments will be repeated using auxiliary supports to minimize the deflection of the top plate.

In future studies, the visualization experiments will be repeated using different fabric preforms and epoxy resin as the infiltrating fluid. Once the two-dimensional model has been

verified, the model will be extended to simulate resin transfer molding of three-dimensional complex shape preforms.

REFERENCES

1. Loos, Alfred C.; and Weideman, Mark H.: RTM Process Modeling for Advanced Fiber Architectures. Advanced Composite Materials: New Developments and Applications Conference Proceedings, ASM International, 1991, pp. 209-216.

2. Weideman, Mark H.; Loos, Alfred C.; Dexter, H. Benson; and Hasko, Gregory H.: An Infiltration/Cure Model for Manufacture of Fabric Composites by the Resin Infusion Process. Virginia Tech Center for Composite Materials and Structures, Report no. CCMS-92-05, Virginia Tech, February, 1992.

3. Loos, Alfred C.; Weideman, Mark H.; Long, Edward R., Jr.; Kranbuehl, David E.; Kinsley, Philip J.; and Hart, Sean M.: Infiltration/Cure Modeling of Resin Transfer Molded Composite Materials Using Advanced Fiber Architectures. First NASA Advanced Composite Technology Conference, Seattle, WA, Oct. 29 - Nov. 1, 1990, NASA Conference Publication 3104, pp. 425-441.

4. Hasko, Gregory H.; Dexter, H. Benson; and Weideman, Mark H.: Resin Transfer Molding of Textile Preforms for Aircraft Structural Applications. Proceedings of the 9th DOD/NASA/FAA Conference on Fibrous Composites in Structural Design, Lake Tahoe, CA, Nov. 4-7, 1991 (in print).

5. Wang, H. P.; and Lee, H. S.: Numerical Techniques for Free and Moving Boundary Problems. Fundamentals of Computer Modeling for Polymer Processing, C. L. Tucker, ed., Hanover Publishers, New York, 1989, pp. 369-401.

6. Reddy, J. N.: An Introduction to the Finite Element Method. McGraw-Hill, Inc., 1984.

7. Fracchia, Carlos, A.; Castro, Jose; and Tucker, Charles L.: A Finite Element/Control Volume Simulation of Resin Transfer Mold Filling. Proceedings of the American Society for Composites, Fourth Technical Conference, Oct. 1989, pp. 157-166.

8. Foley, Michael, F.; and Gutowski; Timothy G.: The Effect of Process Variables on Permeability in the Flexible Resin Transfer Molding (FRTM) Process. 23rd International SAMPE Technical Conference, Oct. 1991, pp. 326-340.

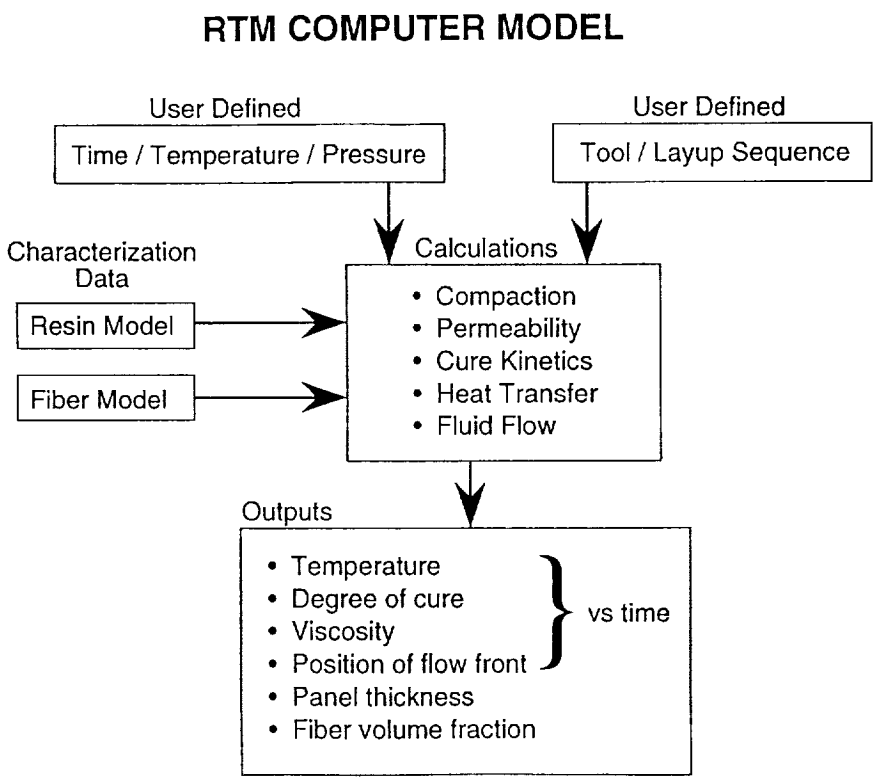

Figure 1. Schematic diagram of the RTM computer model.

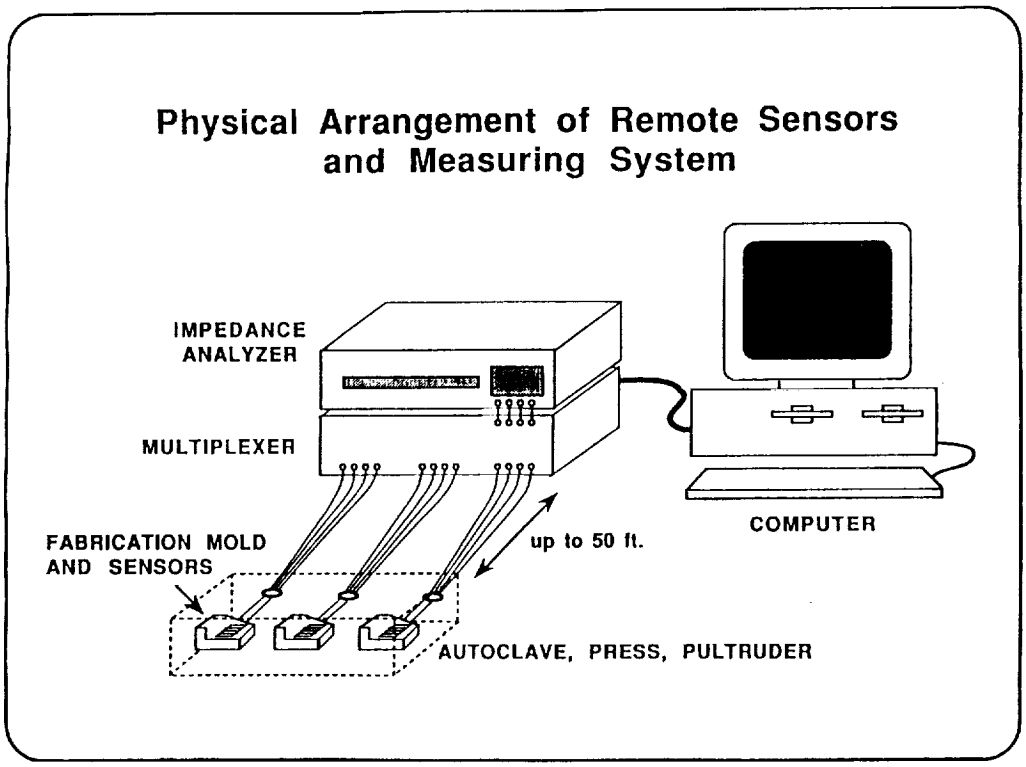

Figure 2. Physical arrangement of the FDEMS sensors and measuring system.

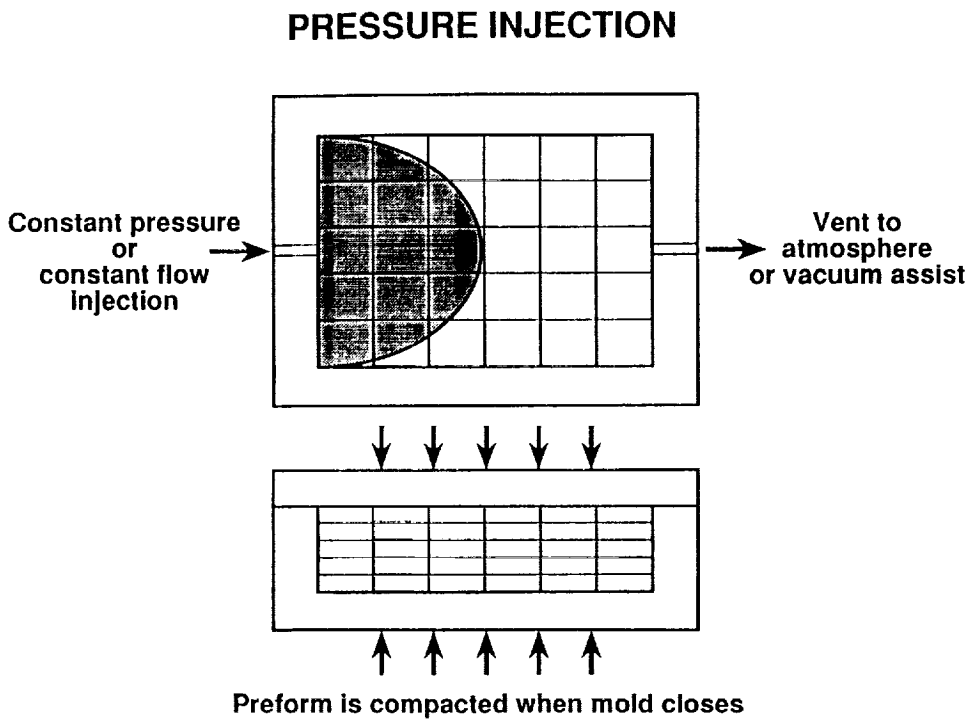

Figure 3. Pressure injection of liquid resin into a flat preform.

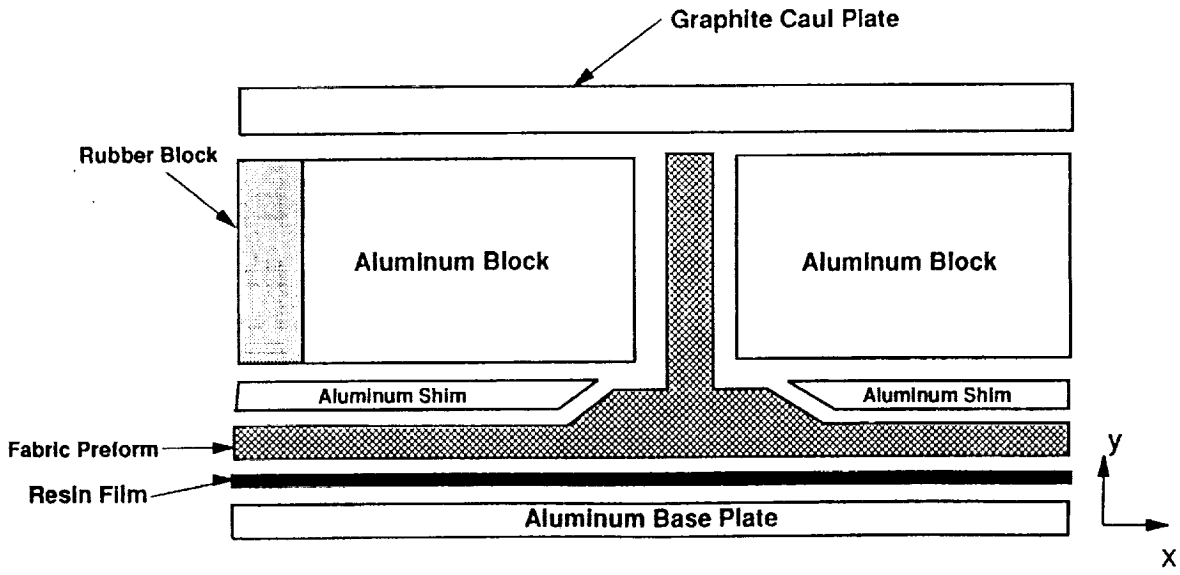

Figure 4. Resin infiltration of a complex shape preform by the resin film infusion process.

C-5

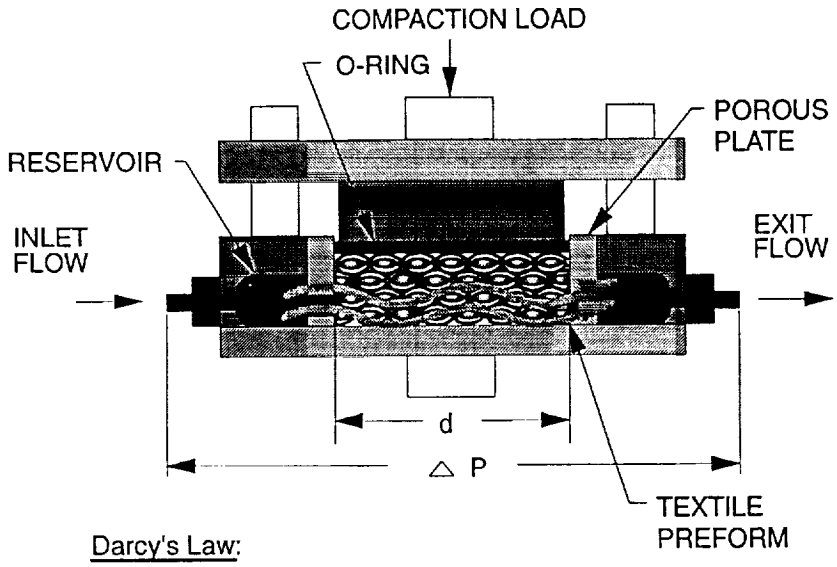

Darcy's Law:

$$Q = A \frac{K}{\mu} \frac{\triangle P}{d}$$

WHERE:
- Q = VOLUMETRIC FLOW RATE
- K = PERMEABILITY CONSTANT
- μ = VISCOSITY OF FLUID
- $\triangle$ P/d = PRESSURE GRADIENT
- A = AREA NORMAL TO FLOW

Figure 5. Permeability test fixture.

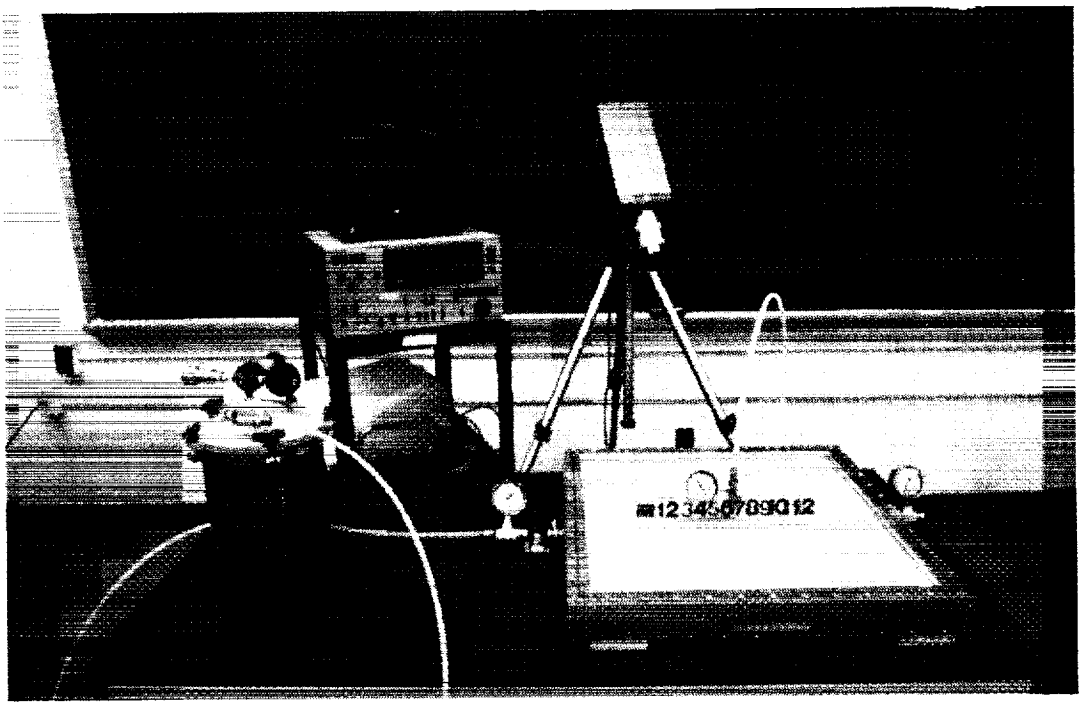

Figure 6. Equipment used in the flow visualization experiments.

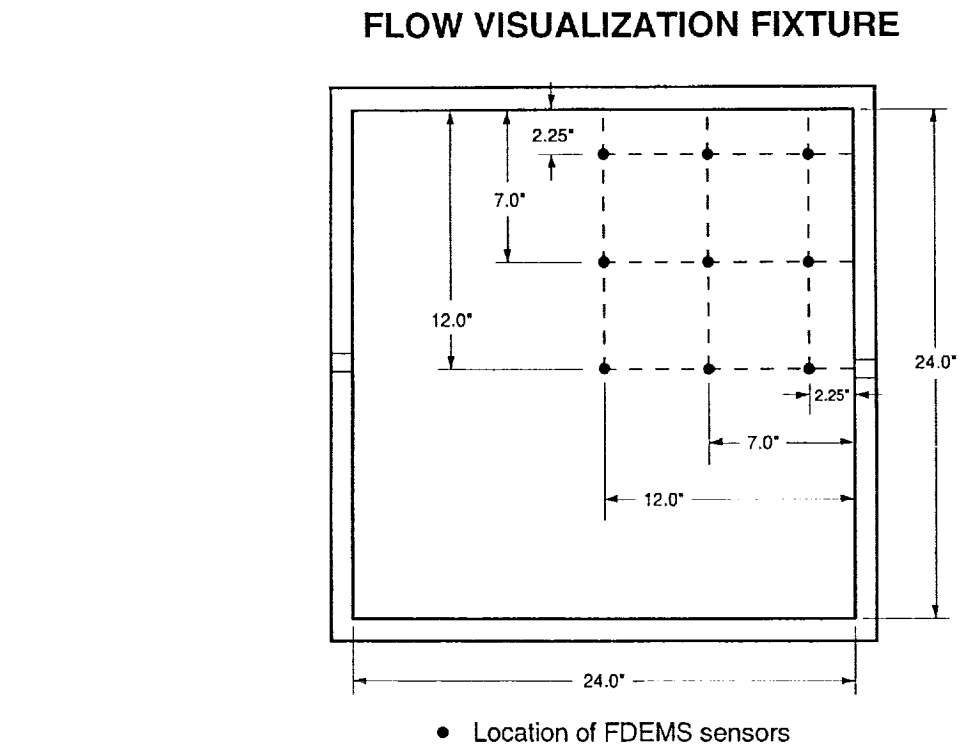

Figure 7. Location of the FDEMS sensor array in the visualization fixture.

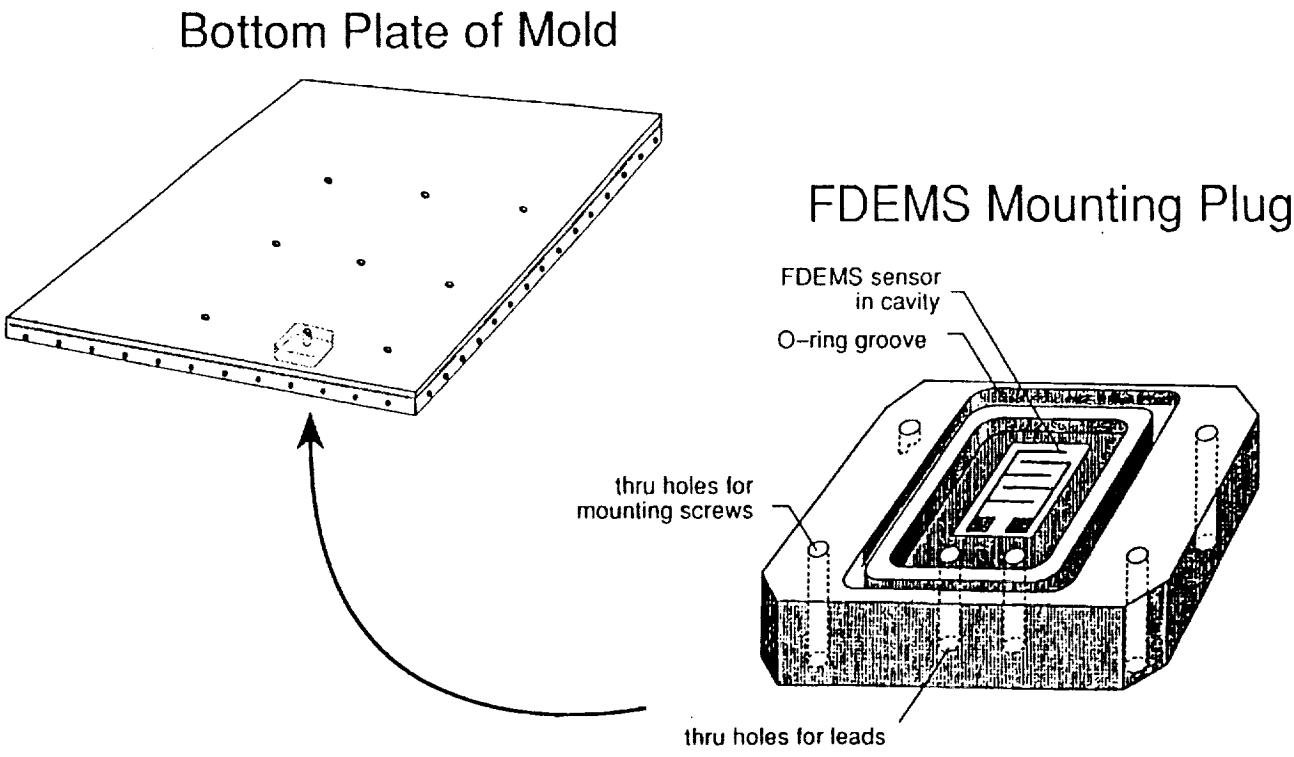

Figure 8. Installation of FDEMS mounting plugs into the bottom plate of the mold.

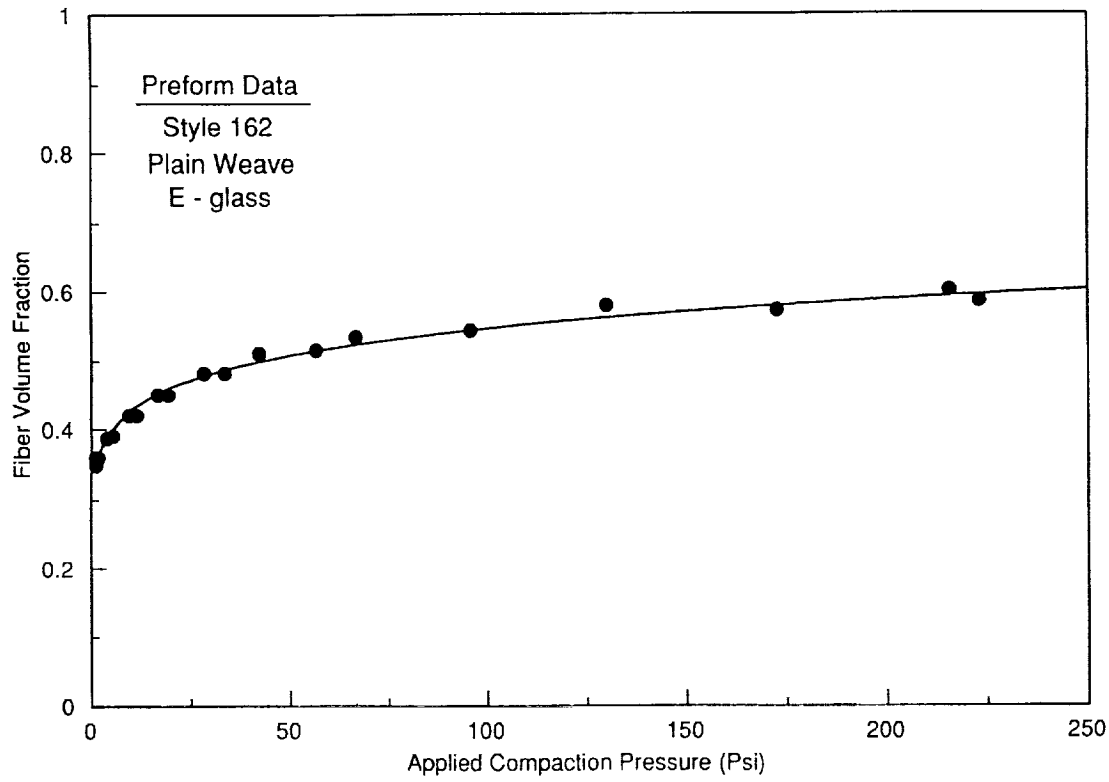

Figure 9. Compaction characteristics of style 162, plain weave, E-glass fabric.

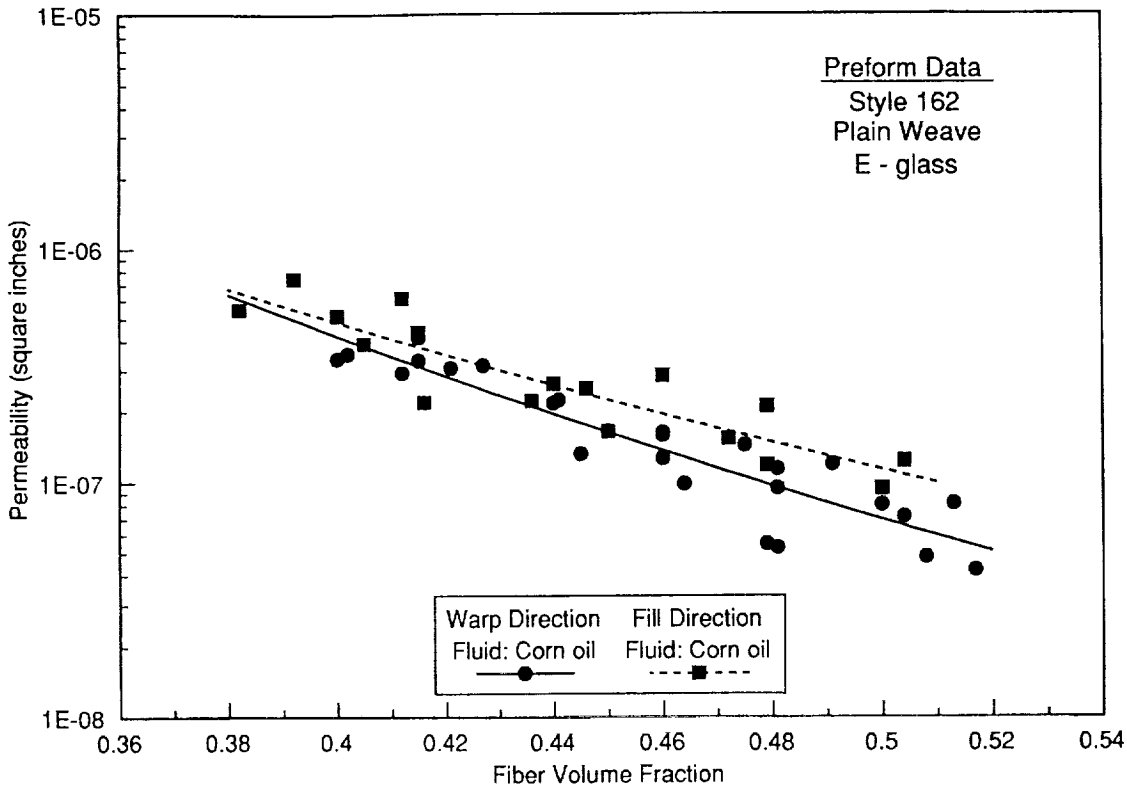

Figure 10. Permeability of style 162, plain weave, E-glass fabric.

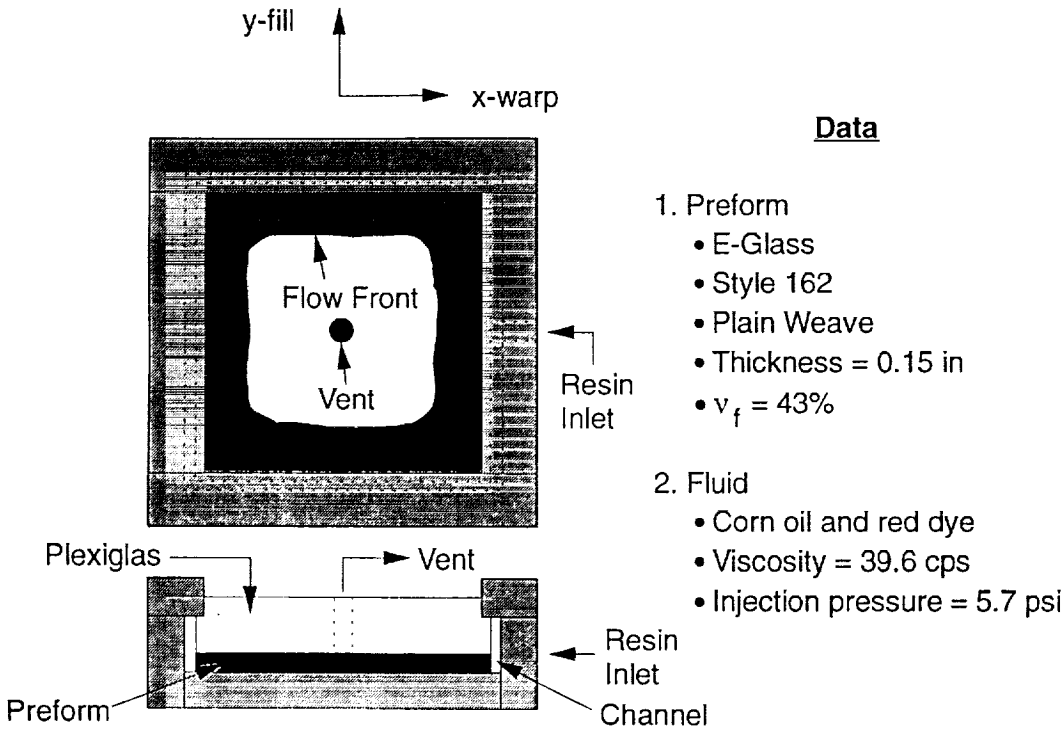

Figure 11. Single side port injection experiment.

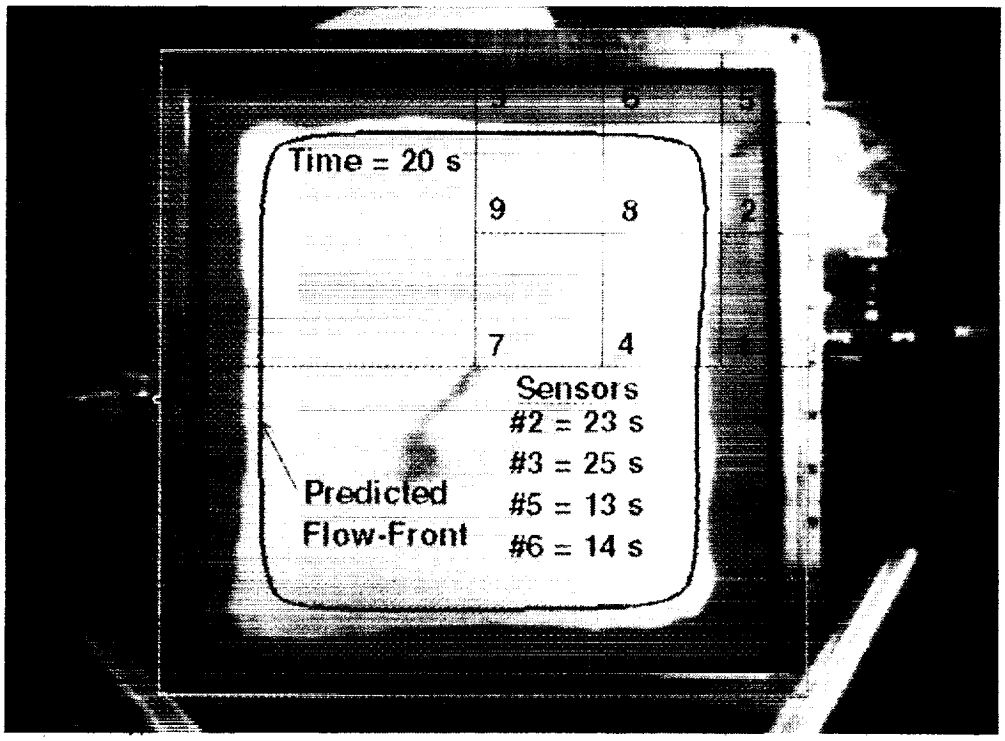

Figure 12. Comparison between the model predicted and recorded flow-front at an infiltration time of 20s.

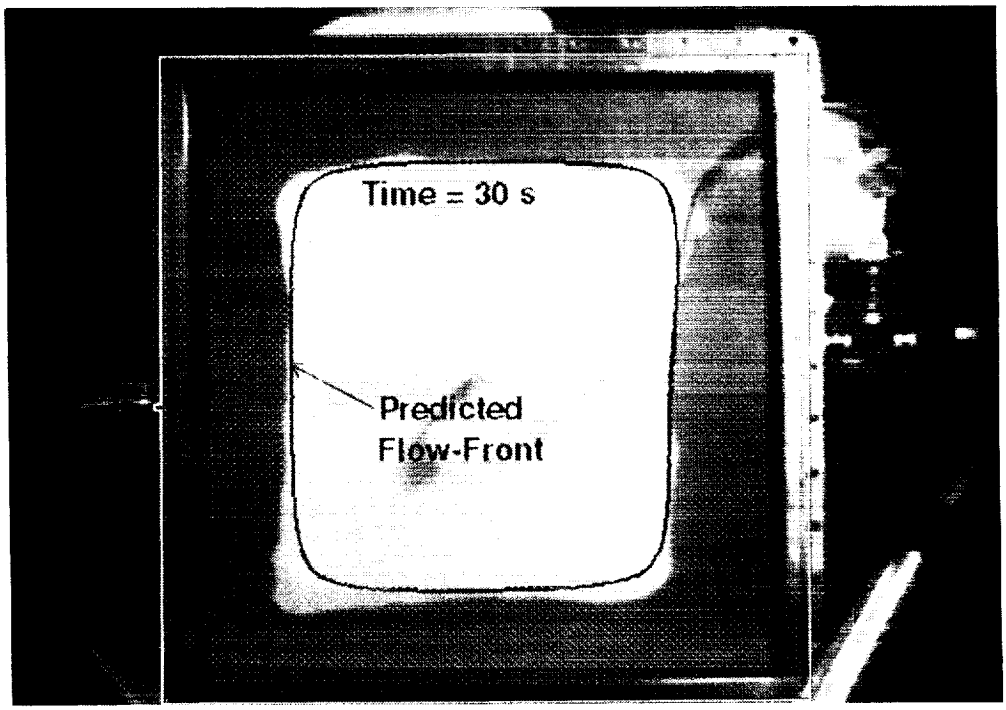

Figure 13. Comparison between the model predicted and recorded flow-front at an infiltration time of 30s.

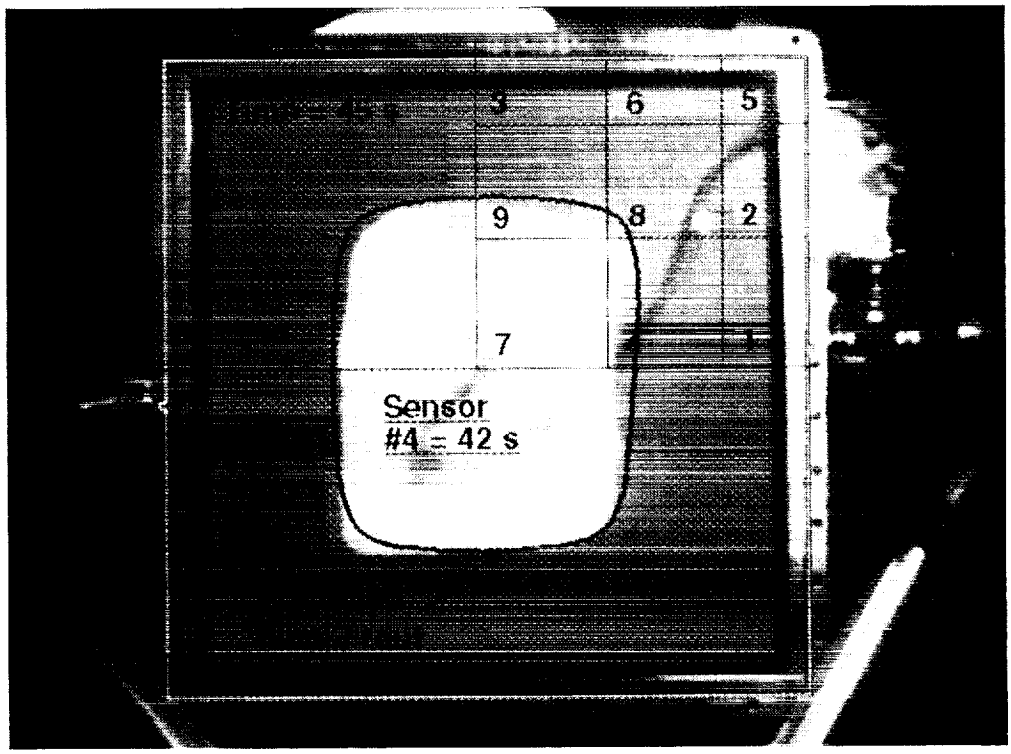

Figure 14. Comparison between the model predicted and recorded flow-front at an infiltration time of 45s.

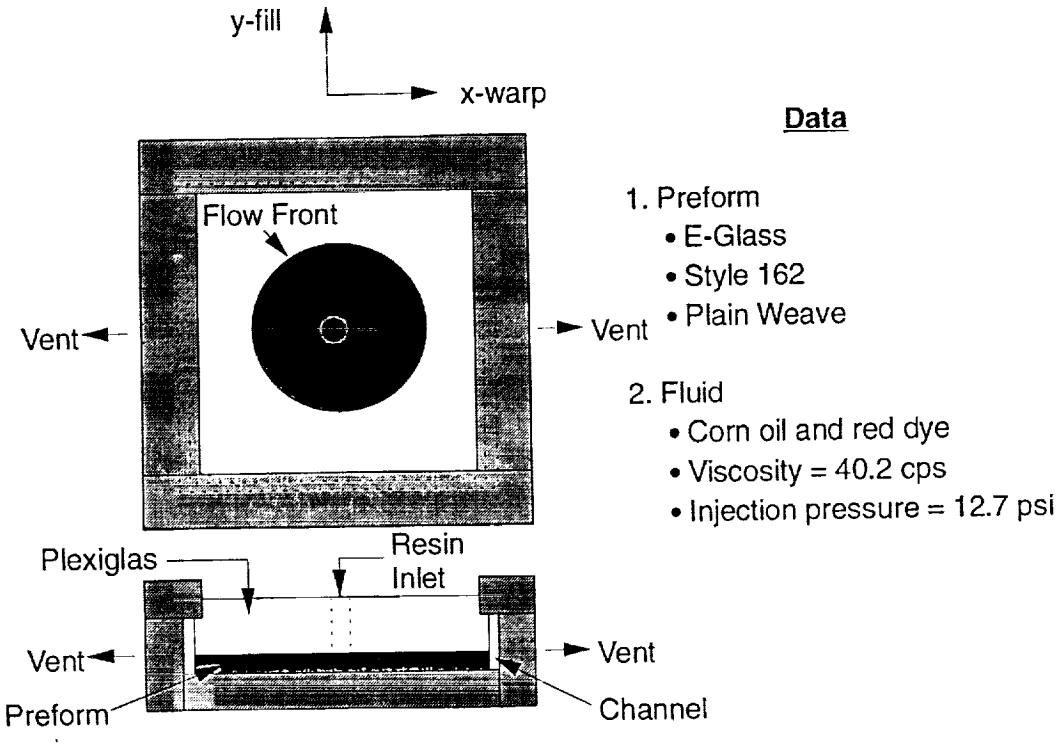

Figure 15. Center port injection experiment.

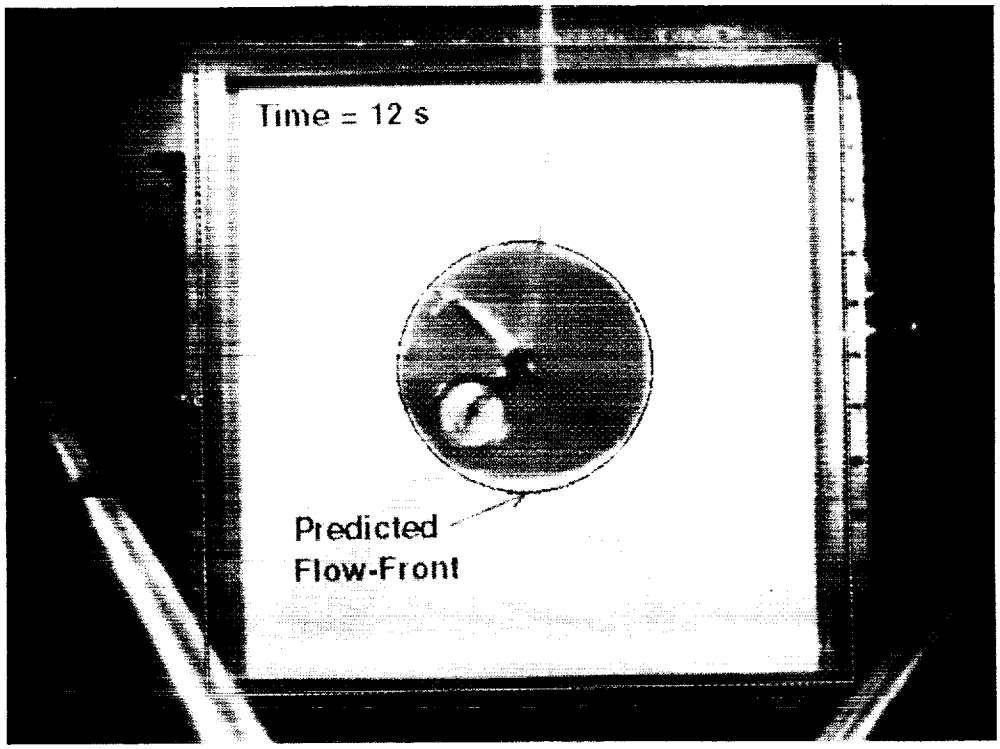

Figure 16. Comparison between the model predicted and recorded flow-front at an infiltration time of 12s.

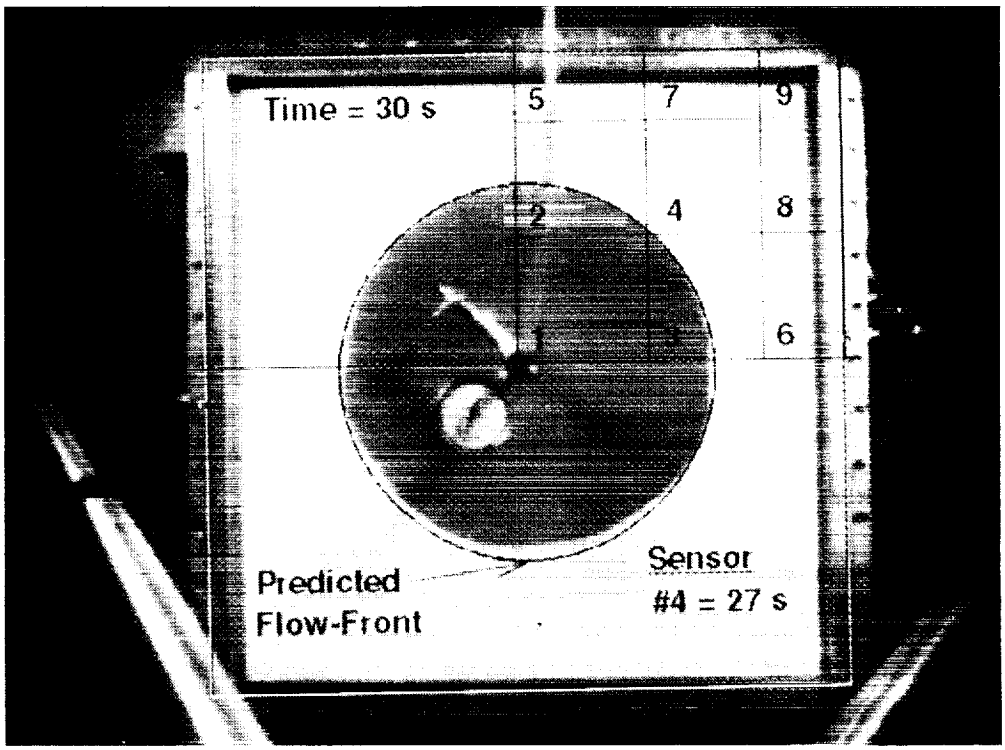

Figure 17. Comparison between the model predicted and recorded flow-front at an infiltration time of 30s.

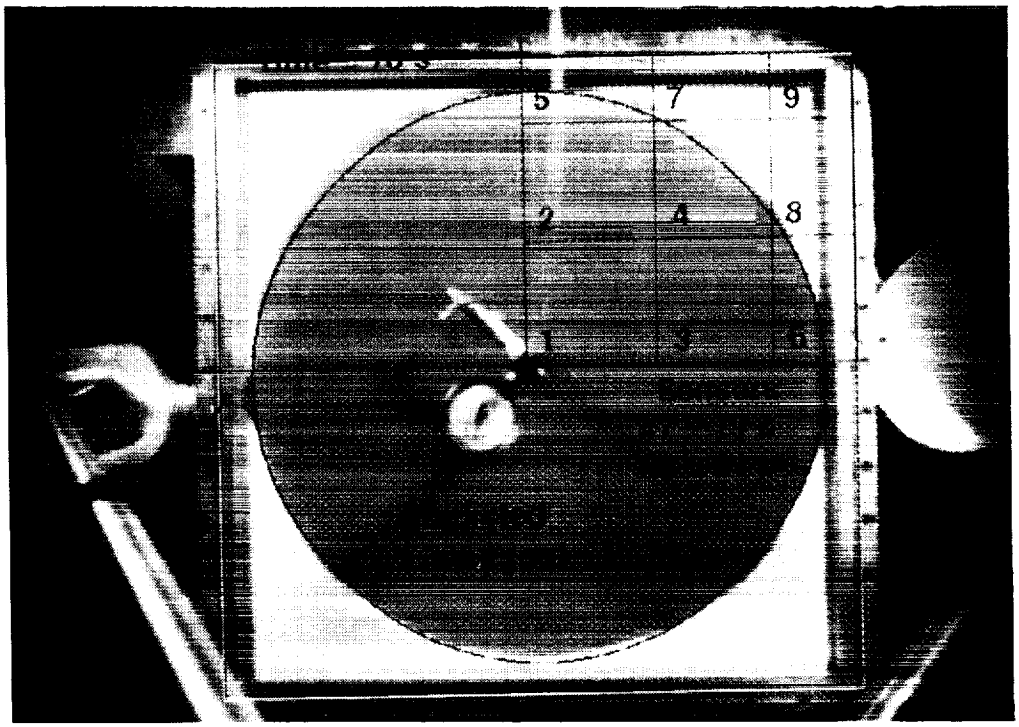

Figure 18. Comparison between the model predicted and recorded flow-front at an infiltration time of 78s.

A Designed Experiment in Stitched/RTM Composites

Larry C. Dickinson

Lockheed Engineering and Sciences Company
NASA Langley Research Center
Hampton, VA

ABSTRACT

The damage tolerance of composite laminates can be significantly improved by the addition of through-the-thickness fibrous reinforcement such as stitching. However, there are numerous stitching parameters which can be independently varied, and their separate and combined effects on mechanical properties need to be determined. A statistically designed experiment (a 2^{5-1} fractional factorial, also known as a Taguchi L16 test matrix) used to evaluate five important parameters is described. The effects and interactions of stitch thread material, stitch thread strength, stitch row spacing and stitch pitch are examined for both thick (48 ply) and thin (16 ply) carbon/epoxy (AS4/E905L) composites. Tension, compression and compression after impact tests are described. Preliminary results of completed tension testing are discussed. Larger threads decreased tensile strength. Panel thickness was found not to be an important stitching parameter for tensile properties. Tensile modulus was unaffected by stitching.

INTRODUCTION

Advanced polymeric composite materials offer significant potential for weight savings and performance advantages over traditional aircraft materials. Compared to metallic materials, composites offer tailorability of properties along with very high specific strengths and stiffnesses. However, conventional laminated composite structures are presently expensive to manufacture and are less damage tolerant than desired. A major goal of the NASA Advanced Composite Technology (ACT) program is to develop these materials for use in primary structure of commercial aircraft. To meet this goal, the problems of high cost and low damage tolerance must be overcome.

One of the innovative manufacturing concepts being explored under the ACT program is the resin transfer molding (RTM) of dry fabric lamina which have been stitched together. References [1] through [5] discuss the advantages of using modified sewing technology to place fibrous reinforcement through the thickness of a laminated composite preform. The approach offers great potential for lowering manufacturing cost and improving damage tolerance. Aircraft part fabrication using both single needle and multiple needle stitching machines in conjunction with resin transfer molding offers economies in materials handling, automation and reduced part count. In addition, the transverse (thickness direction) reinforcement has been shown to significantly improve the damage tolerance of otherwise brittle composites.

Previous research (references [2]-[5]) has shown that strong threads (e.g., 1000 denier Kevlar®) stitched at a high density (on the order of 30 to 60 stitches per square inch) can significantly improve the compression after impact properties and interlaminar fracture toughness of laminated composites. In fact, sufficient transverse reinforcement can effectively eliminate interlaminar failure modes. However, this improvement in out-of-plane performance comes with a degradation of the in-plane mechanical behavior (e.g., lower tensile and compressive properties) [2]-[5].

Experimental research such as that discussed in references [2]-[5] form the basis for the current state-of-the-art in composite stitching technology. Adequate analytical tools able to accurately predict the mechanical behavior of these 3-D reinforced composites do not exist. Work is being done under the ACT program to develop such tools. Although the data base on stitched composites is growing, it is heavily slanted towards thick laminates. Current stitching work by the aerospace industry has focused on transport point designs, e.g., a thick wing layup. General empirical material design guidelines do not exist for selecting stitching patterns, thread material, thread strength, etc.

With these ideas in mind an experimental study was undertaken to determine the relative significance of important stitching variables. The research examines the trade-offs involved in improvement of damage tolerance combined with the loss of in-plane mechanical performance. The interaction of important variables such as panel thickness and the amount of stitching are also addressed. Experimental design techniques were used to lay out a test matrix with five important stitching variables. This research is well underway, but this study is not yet complete. Results available to date are presented in this paper. The results gained from the completion of the test matrix will be used to build regression models with the overall objective of providing stitching guidelines for aircraft material design.

MATERIALS

Constituent Materials

The materials manufactured for this study were flat panels of stitched carbon/epoxy. The in-plane lamina were AS4 3k uniweave fabric produced by Textile Technologies Inc. A uniweave fabric is a loosely woven fabric where roughly 98% of the fiber (3k carbon warp tows, 18 tows per inch,150 g/m^2 of graphite) lies in one direction. The 2% fill fiber is a fine

denier E-glass yarn (Owens/Corning ECD 450 1/0 1.0Z 620-1, 9 yarns per inch) which serves only to hold the carbon together as a fabric. All fibers were purchased with an epoxy compatible sizing.

Two types of stitching thread were selected, Kevlar® 29 and S2 glass, with two threads of each type. The four stitching threads are listed in table I along with the other constituent materials. The threads were selected such that one Kevlar® and one glass would have a breaking load of about 60 lbs. The other two threads were chosen to have breaking loads of about 10 lbs. A fifth thread, a 200 denier two-end-twisted Kevlar®, was used as a needle thread in all panels. Stitching details will be discussed in detail in the next section

The matrix resin was British Petroleum's E905L two part epoxy. E905L was developed as an aerospace grade RTM resin and is one of the RTM resins being evaluated under the ACT program.

Preform Details and Stitching Variables

The preform details are shown in figure 1. The uniweave fabric layers were stacked in a quasi-isotropic layup, $[+45/0/-45/90]_{ns}$. These preforms were then stitched by Ketema, Textile Products Division. The stitching was done in parallel rows in the 0° direction using a modified lock stitch. It has been shown that stitching in only one direction provides adequate damage tolerance [3]. The modified lock stitch shown in figure 1 may be referred to as a "modified lock stitch up." In this case, the needle and needle thread punctures through the fabric stack and pulls the bobbin thread and stitching knot back up through the preform. The bobbin thread is thus the "stitching" thread since it acts as the through the thickness reinforcement. The knot and the smaller needle thread lie on the top surface. Actual photos of panel surfaces showing the

stitch threads are displayed in figure 2.

In the future, economies of production may warrant using the larger thread as a needle thread, thus creating a "modified lock stitch down." The bobbin has a limited thread supply while the needle thread supply is much larger. Hence, if the larger thread is used with the larger supply, the bobbin would not need to be refilled as often. In the case of the modified lock stitch down, the needle thread acts as the through the thickness fiber. The needle thread follows a path down through the preform and the stitching knot and bobbin thread lie on the bottom surface. This resulting structure is a mirror image of the modified lock stitch up. The effect on mechanical properties of such variations in the stitching process remain to be explored.

The important stitching variables selected for consideration in this work are shown in figure 1. These parameters are stitch pitch (stitches per inch in each row), stitch row spacing, stitch thread material, and stitch thread strength or size (diameter) and panel thickness (no. of plies). Panel thickness, while not exactly a stitching variable, may play a significant role in the material behavior. Reference [6] suggests that the loop on the surface formed by the heavy stitching thread has a detrimental effect on mechanical performance due to the crimping of the in-plane load carrying fibers. This fact suggests that there could be a strong interaction between thickness and stitching. Given the same amount of stitching, a thinner composite may suffer a greater loss than a thick composite since the loops of large stitching thread on the surface could crimp a higher percentage of in-plane fibers.

Resin Transfer Molding

The dry stitched preforms were resin transfer molded (RTM) by Boeing Aerospace. A schematic of the RTM process is shown in figure 3. The two part liquid resin (E905L) was mixed and pumped into the picture frame mold containing the preform. The entire

mold assembly was placed in a hot press. The mold was closed to a preset thickness controlled by a shim or caul plate (see figure 3). To avoid as much variation as possible, the same shim was used to make all panels of the same thickness. Based on fabric areal density, a panel thickness was calculated to result in a nominal in-plane fiber volume fraction (i.e., volume fraction of the carbon fiber only) of 0.60. All panels were manufactured to within ± 0.005 in. of their targeted thickness.

DESIGN OF THE EXPERIMENT

There are a large number of potentially important variables associated with stitched composites. In addition, many interactions among the variables may be as much or more important than individual variables themselves. A large number of variables and their interactions can be studied with a relatively small number of tests with the proper use of experimental design techniques. This cannot be done with the traditional "change one factor at a time" approach. For these reasons, experimental design techniques were employed for this research. Discussion of such techniques may be found in many textbooks including reference [7].

Two key elements of the experimental design techniques used in this work are a balanced orthogonal test matrix and factor transformation. A balanced orthogonal test matrix enables the different variables (factors) and their interactions to be evaluated simultaneously and independently of each other. In effect, the test matrix (i.e., different combinations of levels of the assorted factors) is laid out in such a way that the responses of the variables and variable interactions do not overlap at all or overlap in a known manner.

Factor transformation is another key element of experimental design. It would be difficult to statistically analyze a discrete variable such as stitch thread material which is measured in increments of "Kevlar®" and "glass." To enable variables measured in

different units to be compared equally, the factor's values are transformed into a common domain. In a two level experiment (variables evaluated at two levels, a high and a low value), the values are transformed into a -1 and +1. Thus Kevlar® and glass become -1 and +1, respectively, and can be evaluated equally along with the other variables, all having transformed ranges from -1 to +1. A well designed experiment using transformed factors in a balanced and orthogonal test matrix will enable tools such as multiple regression to be used to develop a predictive capability based on both important variables *and* their interactions.

A 2^{5-1} fractional factorial experiment was selected to study the five variables described in the previous section. The 2 refers to a two level experiment where each variable was evaluated at two different levels. In all, 32 different combinations of five factors at two levels are possible. A 2^{5-1} is a resolution V design (reference [7]), allowing all five variables and their two-way interactions to be evaluated independently with only 16 different combinations (tests or runs). This experimental design is equivalent to a Taguchi L16 test matrix [7].

A stitched composite panel was made for each of the 16 different combinations of stitching variables. Two unstitched panels were also manufactured for comparative purposes. The test matrix is shown in table II. Panel thickness was evaluated at 16 plies (thin, 0.09 in.) and 48 plies (thick, 0.27 in.). These thicknesses approach practical applications in an aircraft fuselage (thin) skin and a wing (thick) skin. The values of stitch thread material, stitch thread strength, stitch row spacing and stitch pitch were selected based on the findings of references [2]-[5]. Heavy Kevlar®, glass and carbon threads were found to be equally effective in improving damage tolerance in [2] and [3]. Kevlar® and glass threads were selected over carbon stitching thread based on cost, availability and ease of stitching. The thread strengths (breaking loads) of 10 and 60 lbs were selected to give an adequate range which might apply to both thick and thin panels. The high and low values of row spacing and pitch were chosen to be 4 and 8. These values resulted in stitching densities (stitches per square inch) ranging from 16 to 64, a range similar to those studied in [2]-[5].

Efforts were made to reduce process variations to only those described above for the five variables. These efforts included using the same manufacturers, equipment and operators (where possible) to make all panels. To insure resin consistency, all panels were made from the same batch of E905L resin. To keep thickness constant, the same shim was used to make all panels of the same thickness.

MECHANICAL TESTING

Tension, compression and compression after impact (CAI) testing was planned to evaluate the effects of the stitching process. The test specimen configurations are shown in figure 4. To date only the tension testing has been completed for the full test matrix. Hence, the remainder of this paper will focus on some of the preliminary results from the tensile testing.

Three tensile specimens were cut and tested from each panel. The testing was performed in the 0° direction, parallel to the rows of stitching. The specimens were instrumented with 350 ohm back-to-back strain gages as shown in figure 4. Data were gathered with a 16 bit resolution A/D micro-computer-based data acquisition system. The tension tests were performed at a constant stroke of 0.05 in./min in a 50 kip electro-hydraulic test machine equipped with hydraulic grips. The specimens were un-tabbed, but each end had a coarse grit paper and lexan film between the knurled grips and specimen.

RESULTS AND DISCUSSION

Tensile properties for both the stitched and unstitched panels are listed in table III. The values listed are the averages of three tests. The coefficients of variation for the strength and ultimate strain were typically less than 5% and were 10% or less in all cases.

The modulus had much less variation with coefficients of variation being 3% or less.

Figure 5 compares the strengths and moduli for the thick and thin unstitched materials. The error bars in the graphs represent the entire range of the three repeat tests. While there was no difference between the moduli of the thick (48 ply) and the thin (16 ply) materials, figure 5 shows a slight difference in strength. The average strength of the thin panels was 100 ksi while the average strength of the thick panels was 95.9 ksi. The respective data ranges overlapped slightly and the difference in strength was not large enough to be considered significant. It should be noted that the thin unstitched specimens were inadvertently cut in the 90° direction. Several short (5.75 in.) tension specimens were cut in the proper direction from scrap material and then tested. As expected for a quasi-isotropic layup, the strengths, moduli and failure strain results for these additional tests suggested that there was no significant difference between 0° and 90° properties.

The tensile strengths for the stitched materials are shown in figure 6. The strength is shown as a fraction of the unstitched material strength, i.e., a ratio of thick stitched strength over thick unstitched strength or thin stitched strength over thin unstitched strength. This fraction of unstitched strength has been plotted in the form of a marginal means plot. Each data point in the plot (X) represents the average of the strengths of all panels made at the value of the corresponding variable on the abscissa. For example, the first X , shown above the thread strength of 10, is the average of the strengths of all panels stitched with a thread breaking load of 10 lbs. There were 16 stitched panels with 8 panels manufactured at the high value of each variable and 8 panels at the low value. Therefore each X represents 24 tension tests (8 panels, 3 tension coupons each). This type analysis allows the variables to be independently considered and compared with each other. The slope of the line connecting the X's for the high and low values of each variable is a measure of the significance of that variable. A steep slope indicates that variable has a large effect on tensile strength. The variables have been listed on the abscissa in the order of decreasing significance (decreasing absolute value of slope).

As shown in figure 6, increasing the thread breaking load from 10 to 60 lbs

decreases the tensile strength. This decrease in tensile strength may be attributed to the larger diameter of the larger threads. A larger diameter thread will cause more crimping and curvature of the in-plane carbon fiber, and hence, a larger reduction of unstitched strength. The effect of the stitch thread diameter may also be seen in the effect of the thread type. The glass threads reduced the tensile strength more than the Kevlar® threads. Of the two larger threads, the glass thread had a significantly larger diameter than the Kevlar® (see table I).

The effects of changing the stitching density (penetrations per unit area) can also be seen in figure 6. Increasing the number of stitching rows per inch decreased the tensile strength. Similar results were reported in [2]-[5] where increased stitching lowered the in-plane properties. The increase in tensile strength gained by increasing the pitch from 4 to 8 cannot be explained at this time. A similar finding can be seen in the data of [2]; however, thickness was not kept constant in reference [2] and a strong trend is not identifiable . In the current work, an analysis of variation has yet to be completed. More analysis is underway to establish the level of noise or random variation, and thus gain a better measure of the significance of the effects of changing theses variables.

Even without considering the level of noise, the effect thickness (number of plies) on tensile strength is negligible. As discussed earlier, reference [6] reported that the unavoidable surface loop associated with stitching reduced compression strength. However no tensile testing was performed in [6]. Thickness may play a more significant role in the subsequent compression and CAI testing yet to be completed.

The effects on strength caused by changing the variables as discussed above are plainly evident in figure 6. However, these same variables had no significant effect on modulus (see table III). Over the ranges of the parameters studied, stitching did not cause meaningful changes in tensile modulus.

CONCLUDING REMARKS

A research project investigating the effects of five stitching variables on the mechanical properties of stitched carbon/epoxy composites has been outlined. The effects of panel thickness, stitching thread material, stitch thread strength, stitch row spacing and stitch pitch on tension, compression and compression after impact properties were included. The tension testing has been completed and preliminary analysis has revealed that tensile modulus remained unaffected by stitching. Larger stitching threads were found to have a detrimental effect on the tensile strength. The loss of tensile strength due to stitching was found to be the same in both the thick (48 plies) and thin (16 plies) panels. In fact, the data suggested that an interaction between thickness and stitching did not occur. However, these findings apply only over the specific parameter ranges covered in this study, and are true only for tension properties. Since fiber waviness or crimp plays a more significant role in compression than in tension, the effects of the variables on the compressive and CAI properties may be expected to be different.

The described compression and CAI testing is in progress. Some testing 90° to the stitched direction is also planned. Experimental design analysis techniques will continue to be employed. The future work will include a detailed look at the random variation within the experiment. Once the unimportant variables are eliminated (e.g., thickness in the case of tension), regression models will be developed to describe the behavior of these materials. These models, along with knowledge gained from the experiment, will be used to generate general stitching guidelines for the design of stitched composite materials.

ACKNOWLEDGEMENTS

This paper describes work performed under Work Order E020 of Contract NAS1-19000 and its release has the concurrence of the Technical Monitor, H. Benson Dexter.

REFERENCES

1. Chen, V.; Hawley, A.; Klotzsche, M.; Markus, A.; and Palmer, R.: Composites Technology for Transport Primary Structure. First NASA Advanced Composites Technology Conference, NASA CP 3104, January 1991.

2. Palmer, R. J.; Dow, M. B.; and Smith, D. L.: Development of Stitching Reinforcement for Transport Wing panels. First NASA Advanced Composites Technology Conference, Part 1, NASA CP 3104, 1991.

3. Dow, M. B.; and Smith, D. L.: Damage-Tolerant Composite Materials Produced by Stitching Carbon Fabrics. SAMPE Technical Conference Series Vol. 21, 1989.

4. Dow, M. B.; and Smith, D. L.: An Evaluation of Stitching Concepts for Damage-Tolerant Composites. Fibertex 88, NASA CP 3038, 1989.

5. Pelstring, R. M.; and Madan, R. C.: Stitching to Improve Damage Tolerance of Composites. 34th International SAMPE Symposium, 1989.

6. Farley, G. L.; and Dickinson, L. C.: Mechanical Response of Composite Materials with Through-The-Thickness Reinforcement. Presented at Fiber-Tex 1991, Oct. 1991, NASA Conference Publication 3176.

7. Schmidt, S. R.; and Launsby, R. G.: *Understanding Industrial Designed Experiments*. CQG Ltd Printing, Longmont, CO, 1989.

Table I. Constituent Materials

Unlweave fabric	**AS4 3k carbon fiber**	
Matrix resin	**E905L epoxy**	
Stitching threads	**breaking load (lb)**	**cross sectional area ($in.^2$)**
• Kevlar 29 1500 denier	60	1.79
• Kevlar 29 400 denier	10	0.48
• S2 1250 449AA glass	60	2.52
• S2CG 150 493 glass	10	0.41

Table II. Test Matrix

PANEL #	# OF PLIES	THREAD TYPE	THREAD STR. (lbs)	ROW SPACING (rows/in.)	PITCH (stitches/In.)	THICKNESS (in.)
1	16	KEVLAR	10	4	8	0.09
2	16	KEVLAR	10	8	4	0.09
3	16	KEVLAR	60	4	4	0.09
4	16	KEVLAR	60	8	8	0.09
5	16	GLASS	10	4	4	0.09
6	16	GLASS	10	8	8	0.09
7	16	GLASS	60	4	8	0.09
8	16	GLASS	60	8	4	0.09
9	48	KEVLAR	10	4	4	0.27
10	48	KEVLAR	10	8	8	0.27
11	48	KEVLAR	60	4	8	0.27
12	48	KEVLAR	60	8	4	0.27
13	48	GLASS	10	4	8	0.27
14	48	GLASS	10	8	4	0.27
15	48	GLASS	60	4	4	0.27
16	48	GLASS	60	8	8	0.27
17	16	Unstitched	-	-	-	0.09
18	48	Unstitched	-	-	-	0.27

Table III. Tensile Properties of Stitched and Unstitched Quasi-isotropic Laminates

PANEL ID	STRENGTH (KSI)	Strength fraction of unstitched	ULTIMATE STRAIN (%)	Ult. strain fraction of unstitched	MODULUS (MSI)	Modulus fraction of unstitched
1	91.1	0.91	1.27	0.91	7.44	1.02
2	96.3	0.96	1.31	0.94	7.68	1.05
3	92.7	0.93	1.22	0.87	7.81	1.07
4	89.1	0.89	1.26	0.89	7.48	1.02
5	89.6	0.90	1.26	0.90	7.36	1.01
6	95.6	0.96	1.31	0.94	7.67	1.05
7	93.5	0.93	1.30	0.92	7.71	1.05
8	80.7	0.81	1.17	0.83	7.18	0.98
9	91.5	0.95	1.25	0.93	7.53	1.03
10	90.4	0.94	1.28	0.95	7.30	1.00
11	87.9	0.92	1.24	0.92	7.22	0.99
12	84.5	0.88	1.18	0.87	7.35	1.00
13	92.9	0.97	1.29	0.95	7.42	1.01
14	81.3	0.85	1.14	0.85	7.34	1.00
15	82.3	0.86	1.18	0.87	7.37	1.01
16	82.8	0.86	1.22	0.91	6.93	0.95
17	100.0	1.00	1.40	1.00	7.31	1.00
18	95.9	1.00	1.35	1.00	7.33	1.00

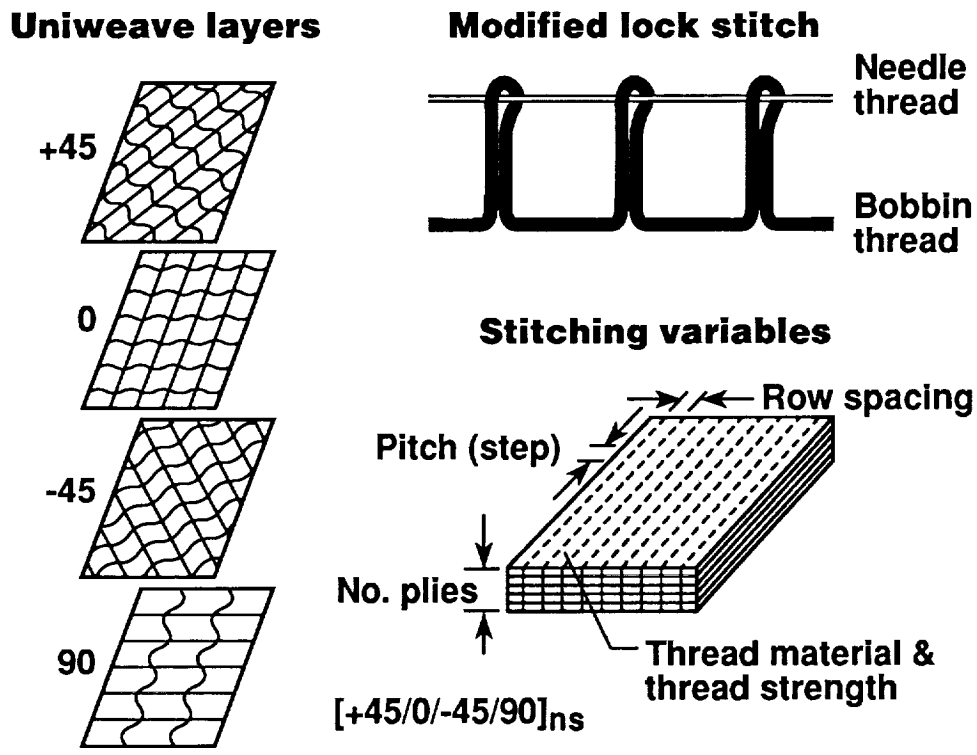

Figure 1. Preform stacking sequence and stitching parameters.

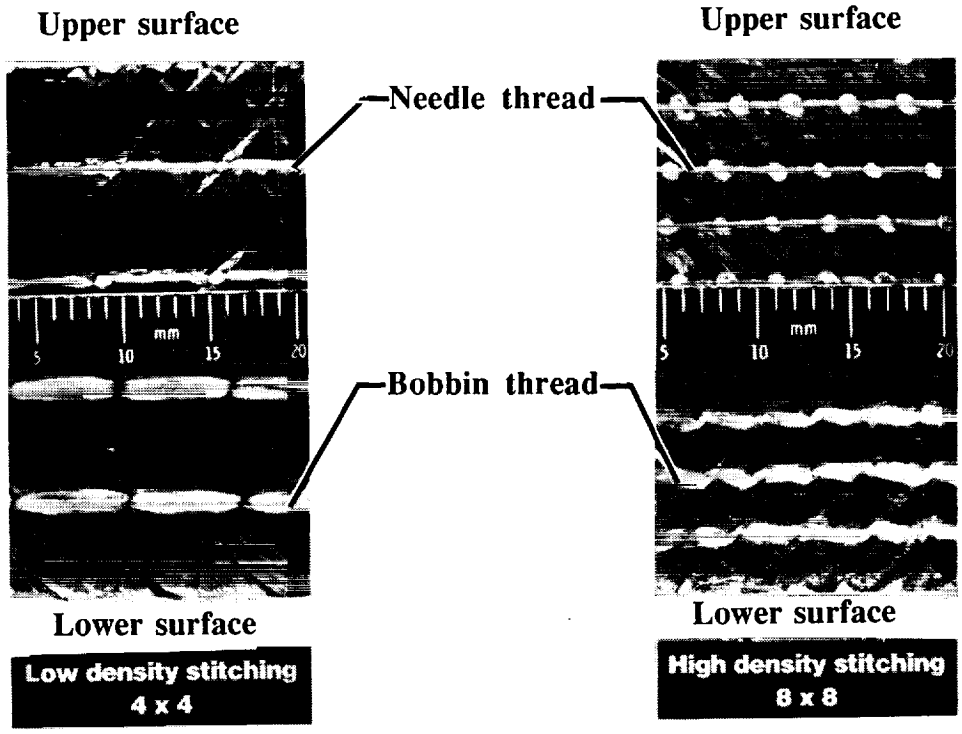

Figure 2. Surfaces of stitched panels.

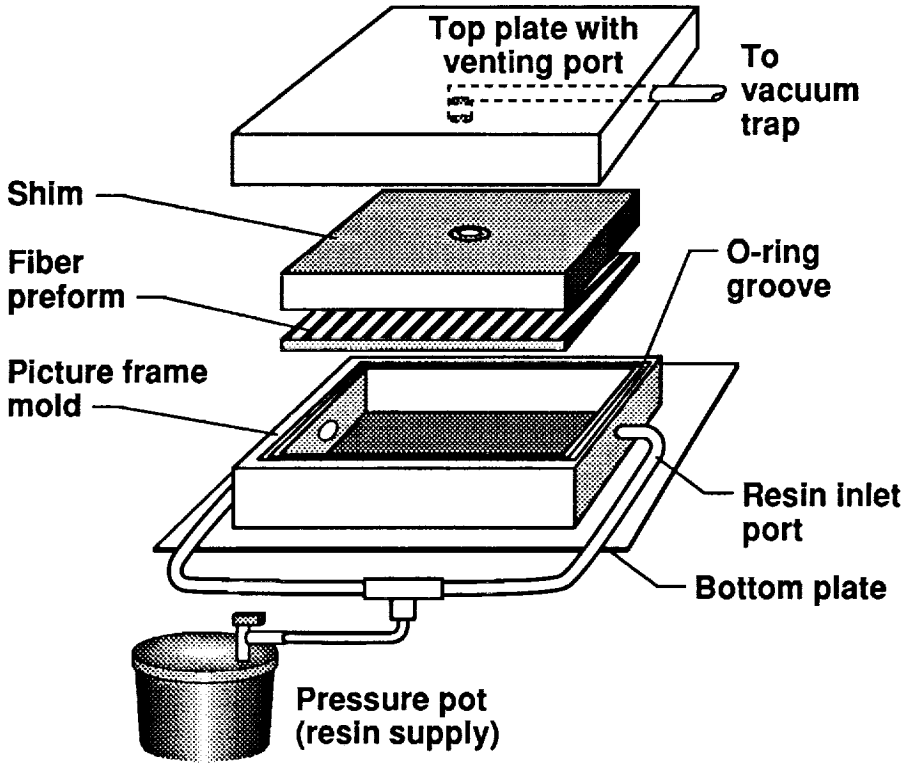

Figure 3. RTM process schematic.

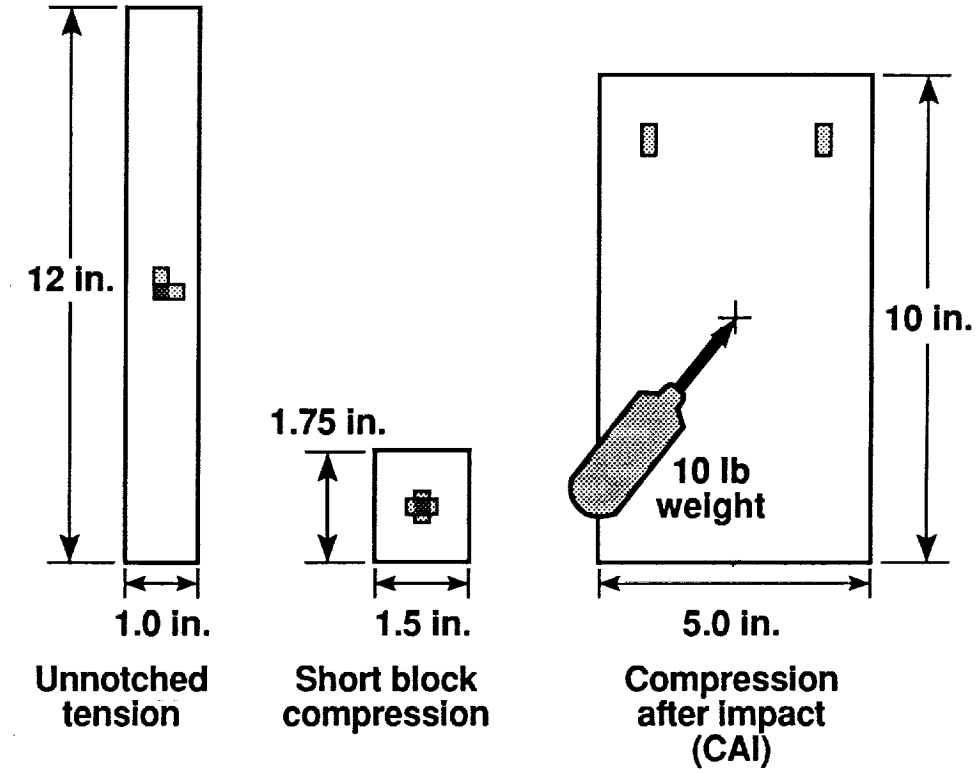

Figure 4. Test specimen configurations.

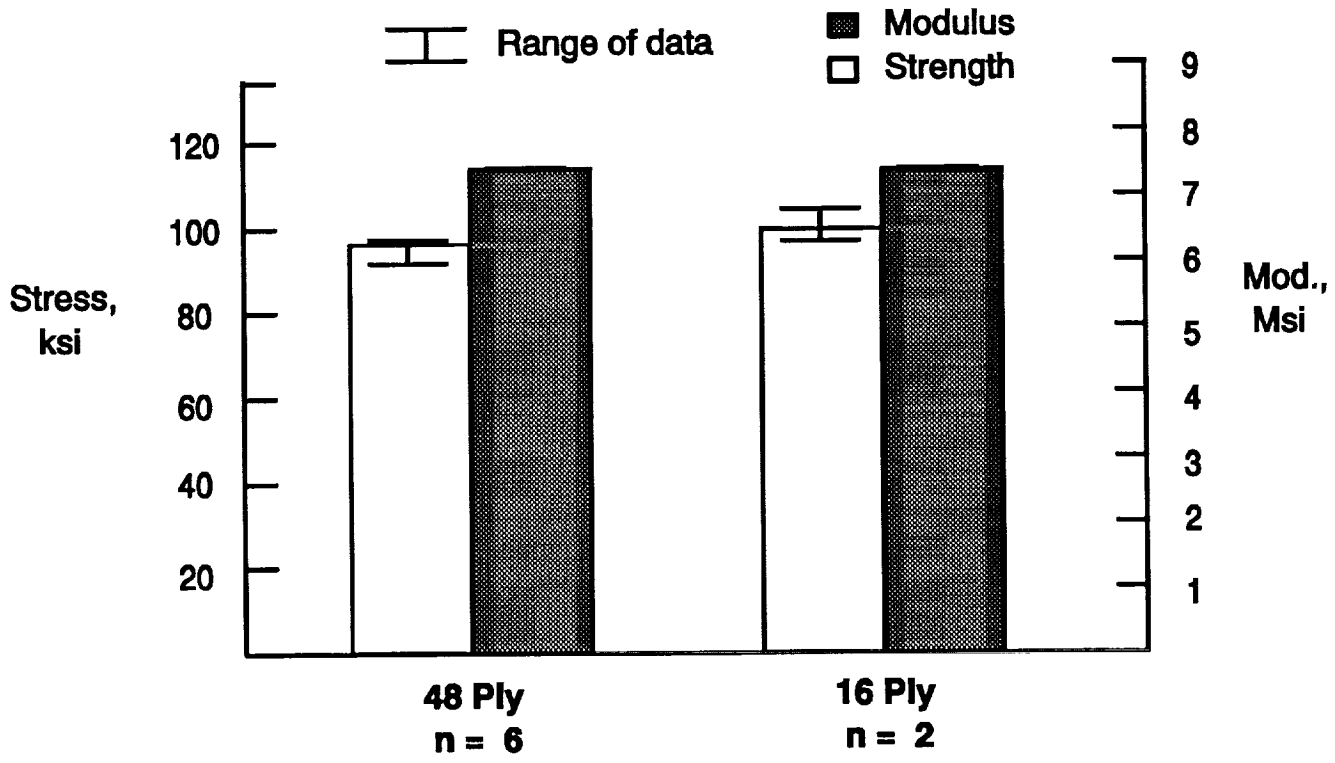

Figure 5. Unstitched tensile properties of quasi-isotropic panels.

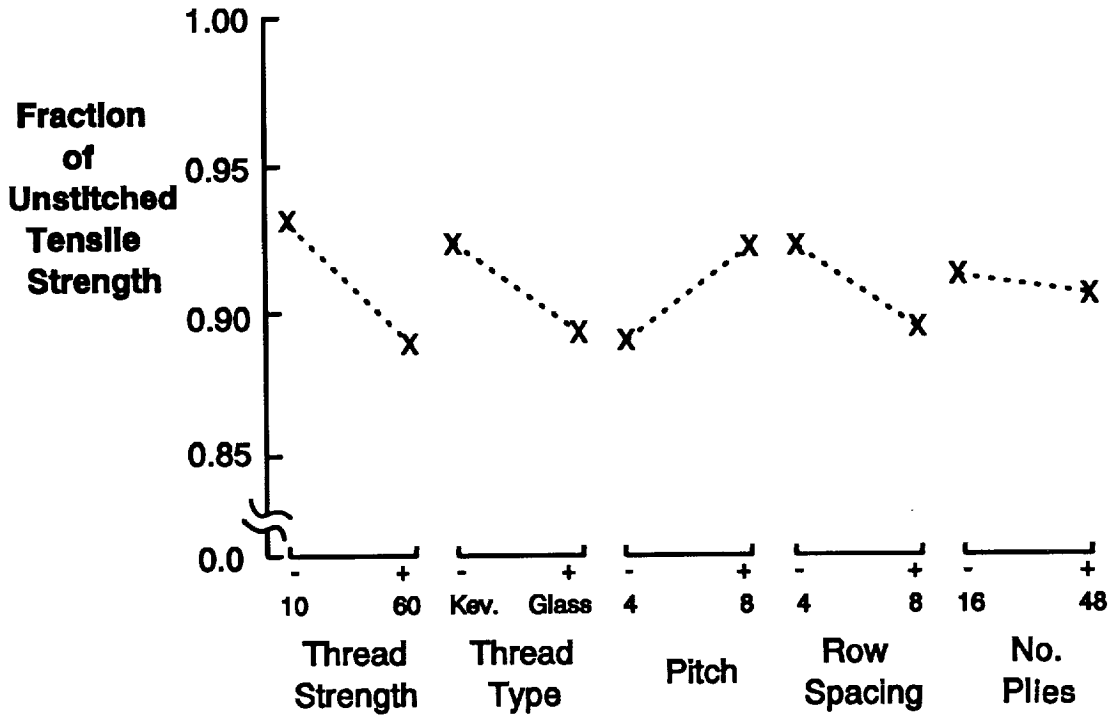

Figure 6. Tensile strengths of stitched quasi-isotropic panels.

THE EFFECTS OF AIRCRAFT FUEL AND FLUIDS ON THE STRENGTH PROPERTIES OF RESIN TRANSFER MOLDED (RTM) COMPOSITES*

Anthony Falcone
Boeing Defense & Space Group
Seattle, WA

Marvin B. Dow
NASA Langley Research Center
Hampton, VA

SUMMARY

The resin transfer molding (RTM) process offers important advantages for cost-effective composites manufacturing, and consequently has become the subject of intense research and development efforts. Several new matrix resins have been formulated specifically for RTM applications in aircraft and aerospace vehicles. For successful use on aircraft, composite materials must withstand exposure to the fluids in common use. The present study was conducted to obtain comparative screening data on several state-of-the-art RTM resins after environmental exposures were performed on RTM composite specimens. Four graphite/epoxy composites and one graphite/bismaleimide composite were tested; testing of two additional graphite epoxy composites is in progress. Zero-deg tension tests were conducted on specimens machined from eight-ply (+45-deg, -45-deg) laminates, and interlaminar shear tests were conducted on 32-ply 0-deg laminate specimens. In these tests, the various RTM resins demonstrated widely different strengths, with 3501-6 epoxy being the strongest. As expected, all of the matrix resins suffered severe strength degradation from exposure to methylene chloride (paint stripper). The 3501-6 epoxy composites exhibited about a 30% drop in tensile strength in hot, wet tests. The E905-L epoxy exhibited little loss of tensile strength (< 8%) after exposure to water. The CET-2 and 862 epoxies as well as the bismaleimide exhibited reduced strengths at elevated temperature after exposure to oils and fuel. In terms of the percentage strength reductions, all of the RTM matrix resins compared favorably with 3501-6 epoxy.

INTRODUCTION

The resin transfer molding (RTM) process offers important advantages for cost-effective composites manufacturing. Consequently, RTM is currently the subject of intense research and development efforts. One of the main advantages of RTM composite manufacturing is that the resin and reinforcement are not combined until a part is actually produced, eliminating the need for prior production of prepregged materials. Other advantages of RTM include the use of a wide variety of textile reinforcements such as woven, braided, and stitched preforms, and the ability to fabricate complex molded parts.

Several new matrix resins have been formulated specifically for RTM applications in aircraft and aerospace vehicles. For successful application in aircraft structures, composite materials must withstand exposure to fluids in use during operation and maintenance. Extensive studies have been conducted in the past with actual in-service exposure of graphite and boron/epoxy test coupons on operating aircraft (refs. 1, 2, and 3). The present study was conducted to obtain comparative screening data on several state-of-the-art RTM composites after environmental exposure.

*Work performed on Contract NAS1-18954 by Boeing Defense & Space Group.

Fluids in the operating environment can affect both the matrix resin and the fiber-matrix interface, thereby reducing composite properties. The fiber-matrix interface in RTM composites is formed during infiltration of resin into the preform and subsequent resin cure, and requires thorough wetting of the fibers by the resin. Of interest was the determination of what effect fluids would have not only on the resin matrix, but also on the resin-fiber interface in RTM composites, which could be different from the interface in composite structures produced from prepreg.

Composite tests that would give matrix-dominated failures were selected. Zero-deg tension tests were conducted on specimens machined from eight-ply (+45-deg, -45-deg) laminates, and interlaminar shear tests were conducted on 32-ply 0-deg laminate specimens. Tensile strength and modulus were measured; however, other properties could have been selected, such as tensile yield strength. There is no general agreement on which point should be selected on the stress-strain curve for property comparison and for relation to composite performance in service.

The panel preforms were produced from AS4 uniweave carbon fiber fabric. Four epoxy composites and one bismaleimide composite were tested; two additional graphite epoxy composites are in test.

EXPERIMENTAL

Zero-deg tension tests were conducted on (+45-deg, -45-deg) laminates per ASTM D3518 and D3039. Interlaminar short beam shear tests of 0-deg laminates were conducted per ASTM D2344. The tensile test specimens (Figure 1) were machined from 8-ply laminates with a nominal thickness of 1.14 mm (0.045 in); the interlaminar shear test specimens (Figure 2) were machined from 32-ply 0-deg laminates with a nominal thickness of 4.57 mm (0.180 in). Tensile test coupons were fabricated by bonding tapered E-glass/epoxy tabs (1.52 mm (0.060 in) thick) to rectangular blanks with epoxy adhesive, and then cutting specimens from these bonded blanks.

The laminates were layed up and resin transfer molded by the Douglas Aircraft Company from uniweave Hercules AS4 carbon fiber fabric. Five resins were evaluated (Table I), and panels from two additional resins are being resin transfer molded at Boeing for testing (Table I). Laminates were ultrasonically scanned to locate porosity or other defects. Some (+45-deg, -45-deg) laminates produced with E905-L epoxy had porosity in limited areas, possibly due to the location of injection and venting ports, and, where possible, specimens were cut outside of these porous areas. Fiber and void volume fractions were determined for selected panels (Table II).

The tensile and interlaminar shear test specimens were exposed to seven fluids (Table III). Some fluid exposures were conducted at an elevated temperature of 71°C (160°F), and tests were run at both ambient temperature and 82°C (180°F). The specimens exposed to JP-4 jet fuel were exposed at ambient temperature only, since special equipment and additional safety procedures would not be required. The specimens were exposed for 14 days (336 hours) to the fluids. The fluid exposures were accomplished by putting the specimens in cans filled with the fluid so that the specimens were fully immersed and, for elevated temperature exposures, the loosely capped cans were placed in an air-circulating oven at 71°C (160°F). Control specimens (unexposed) were placed in the same oven for 14 days.

The 14-day exposure period is somewhat arbitrary and was selected based on the time required for thin graphite/epoxy laminates to reach moisture saturation at 71°C (160°F). In the Boeing specification for secondary graphite epoxy structure, BMS 8-212 (ref. 4), a 14-day exposure period to moisture is used, while in the Boeing specification for toughened graphite/epoxy (ref. 5), a 6-day fluid exposure period is used. The exposure period is selected to produce a desired amount of fluid absorption in the composite test specimens. These time periods are not related to the lifetime exposures to which composite airplane

structures are subjected. The testing performed in this effort was intended to provide a relative indication of composite performance.

The ends of some of the specimens were wrapped with aluminum foil and aluminum foil tape to reduce solvent absorption by the tabs and tab adhesive; only the specimen gauge area was exposed to the solvent. The short-beam shear specimens were held within small folded wire screen sections to keep specimens from the same material grouped together.

Weight gain was measured to determine the percent of fluid absorbed by some of the short beam shear specimens (Table IV). The percent of weight gain was usually small, except for water at 71°C (160°F) and methylene chloride. Additional weight gain measurements will be obtained to confirm this data.

Five specimens were mechanically tested for each material, fluid, and condition. Both shear strength and shear modulus were measured for the tensile specimens. The modulus was measured for only two of the five specimens in each group. A biaxial extensometer (Figure 3) was used to measure displacement in both the axial and transverse directions to determine the shear modulus. All tensile specimens were tested to failure, which usually took 30 to 40 minutes per specimen due to the high elongation of the specimens. A crosshead speed of 1.27 mm (0.05 in.) per minute was used. One of the test machines is shown in Figure 4, and the environmental chamber used to heat the specimens is shown in Figure 5.

RESULTS AND DISCUSSION

The mechanical test results for all groups of specimens are summarized in bar charts for the tensile test specimens (Figures 6 through 10) and for the interlaminar shear specimens (Figures 11 through 15). In general, test results indicated that all of the composites retained adequate strength after exposure to JP-4 jet fuel, commercial hydraulic fluid, turbine oil, methyl ethyl ketone, deicing fluid, and water. Methylene chloride exposure usually caused significant deterioration of mechanical properties.

Tensile coupons immersed in methylene chloride usually retained only 50% to 60% of the room-temperature control specimens' shear strength with the exception of AS4/3501-6 epoxy, which retained 80% of its strength. Decreases in interlaminar shear strength similar to tensile strength degradation did not occur for all composites tested, however. Since methylene chloride is readily absorbed by polymeric materials, it should not be used around composite aircraft structures.

Other than methylene chloride, water at 82°C (180°F) caused the next largest drop in properties, usually a 10% to 25% decrease in shear strength. The AS4/CET-2 epoxy, however, showed no drop in shear strength under this hot/wet exposure, and the AS4/3501-6 showed its greatest drop (24%) in shear strength. Interlaminar shear strength typically showed a 10% reduction at 82°C (180°F) after 14 days exposure in 71°C (160°F) water.

The AS4/CET-2 material exhibited a 16% drop in shear strength after exposure to hydraulic fluid and testing at 82°C (180°F). A similar decline was not observed in the interlaminar shear strength, however.

It could not be determined why the AS4/5292 bismaleimide control specimens had a low room temperature shear strength. The ambient interlaminar shear strength did not show a similar trend. Exposure to JP4 jet fuel also caused an appreciable (19%) decrease in shear strength of AS4/5292.

JP4 jet fuel did not cause significant property deterioration in the RTM composites under these exposure conditions, however, more significant deterioration can occur with longer exposures (ref. 6). Work at Boeing on military airplane programs has indicated that the water that collects in fuel systems is more detrimental to composite properties than the fuel itself.

CONCLUSIONS

In these tests, the various RTM resins demonstrated widely different strengths, with 3501-6 epoxy being the strongest. As expected, all of the matrix resins suffered severe strength degradation from exposure to methylene chloride (paint stripper). The 3501-6 epoxy composites exhibited about a 30% drop in tensile strength in hot, wet tests. The E905-L epoxy exhibited little loss of tensile strength (< 8%) after exposure to water. The CET-2 and 862 epoxies as well as the bismaleimide exhibited reduced strengths at elevated temperature after exposure to oils and fuel.

In terms of the percentage of strength reductions, all of the RTM matrix resins compared favorably with 3501-6 epoxy. By inference, an adequate fiber-matrix interface is apparently forming in these RTM composites, indicating that the fibers are sufficiently wet-out with resin in the RTM process.

ACKNOWLEDGEMENTS

This work was performed under contract from the NASA Langley Research Center (Contract NAS1-18954) and their support is gratefully acknowledged. Resin transfer molded laminates were supplied by the Douglas Aircraft Company; Mr. Raymond Palmer of Douglas Aircraft and Mr. William Avery of the Boeing Defense & Space Group provided recommendations on fluid exposure testing. Boeing technicians, Mr. Oscar Davis and Mr. Allen Kelly, conducted the mechanical tests. Ms. Erica Smith, a summer intern at Boeing, measured most of the specimens and performed the initial mechanical property calculations.

REFERENCES

1. Dexter, H. B.: Long-Term Environmental Effects and Flight Service Evaluation, *Engineered Materials Handbook,* vol. 1, *Composites.* ASM International, 1987.

2. Dexter, H. B. : Long-Term Environmental Effects and Flight Service Evaluation of Composite Materials, NASA TM-89067, National Aeronautics and Space Administration, Jan. 1987.

3. Tanimoto, E. Y.: Effects of Long-Term Exposure to Fuels and Fluids on Behavior of Advanced Composite Materials, NASA CR-165763, National Aeronautics and Space Administration, Aug. 1981.

4. Boeing Material Specification 8-212: Epoxy Preimpregnated Graphite Tapes and Woven Fabrics - 350°F (177°C) Cure, The Boeing Company, Revised Nov. 1987.

5. Boeing Material Specification 8-276: Advanced Composites - 350°F (177°C) Cure Toughened-Epoxy Preimpregnated Carbon Fiber Tapes and Fabrics, The Boeing Company, Revised Nov. 1991.

6. Curliss, D. B., Carlin, D. M., and Arnett, M. S.: The Effect of Jet Fuel Absorption on Advanced Aerospace Thermoset and Thermoplastic Composites. SAMPE, v. 35, 1990.

Table I. RTM Matrix Resins Under Investigation

Carbon fiber fabric used with all resins: 3K AS4 uniweave fabric at 145 g/m^2.

Testing has been completed on:

Manufacturer	Matrix resin	Identification code
Dow Chemical Company	Tactix* CET-2 Epoxy	D
Shell Chemical Company	Epon** DPL 862 Epoxy/Curing Agent W	S
Hercules	3501-6 Epoxy	H
BP Chemicals	E905-L Epoxy	B
Ciba Geigy Corp.	Matrimid*** 5292 Bismaleimide	C

Testing is in progress on:

Manufacturer	Matrix resin	Identification code
Dow Chemical Company	Tactix* CET-3 Epoxy	T
Shell Chemical Company	RSL 1895 Epoxy/Curing Agent W	R

*Trademark of the Dow Chemical Company
**Trademark of the Shell Chemical Company
***Trademark of Ciba Geigy Corp.

Table II. Selected RTM Laminate Physical Properties*

Laminate	Density (g/cm^3)	Fiber vol. fraction (%)	Void content (%)
0-deg, 32 plies, AS4/E905-L epoxy	1.59	61	< 1
0-deg, 32 plies, AS4/5292 bismaleimide	1.58	57	< 1
0-deg, 32 plies, AS4/CET-2 epoxy	1.77	55	< 1
±45-deg, 8 plies, AS4/E905-L epoxy	1.49	52	3
±45-deg, 8 plies, AS4/CET-2 epoxy	1.75	46	1

*Calculations based on an AS4 carbon fiber density of 1.80 g/cm^3 and resin densities of 1.24 g/cm^3 for E905-L epoxy, 1.23 g/cm^3 for 5292 bismaleimide, and 1.75 g/cm^3 for CET-2 epoxy.

Table III. RTM Laminate Exposure Fluids and Temperatures

Code Number	Fluid	Exposure temp.	Test temp.
1	JP-4 jet fuel	Ambient	Ambient
2	Chevron HyJet IVA Hydraulic Fluid	71°C (160°F)	Ambient
3	MIL-L-7808 Turbine Oil	71°C (160°F)	Ambient
4	Methyl ethyl ketone	Ambient	Ambient
5	Methylene chloride	Ambient	Ambient
6	Deicing fluid	Ambient	Ambient
7	Water	71°C (160°F)	Ambient
8	Control (no fluid exposure)	71°C (160°F)	Ambient
9	JP-4 jet fuel	Ambient	82°C (180°F)
10	Chevron HyJet IVA Hydraulic Fluid	71°C (160°F)	82°C (180°F)
11	MIL-L-7808 Turbine Oil	71°C (160°F)	82°C (180°F)
12	Water	71°C (160°F)	82°C (180°F)
13	Control (no fluid exposure)	71°C (160°F)	82°C (180°F)

Table IV. Percent Weight Gain of 32-Ply Unidirectional Laminate Coupons

	Exposure fluid and temperature (table III)												
Laminate	1	2	3	4	5	6	7	8	9	10	11	12	13
AS4/5292	0.06	0	0	0	0.08	0.08	1.15	N/A	0.05	0	0	1.11	N/A
AS4/CET-2	0	1.76	0.02	1.42	**	0.06	0.16	N/A	0.03	1.67	0.05	0.12	N/A
AS4/3501-6	0.07	**	**	0	**	0.07	**	N/A	0.06	0	0.05	**	N/A
AS4/862/W	0.04	0.06	0	**	4.42	0.18	**	N/A	0.12	0.07	0.01	**	N/A

*Values for the AS4/E905-L epoxy laminates were high (6% to 8%) and were probably in error.

**Not measured.

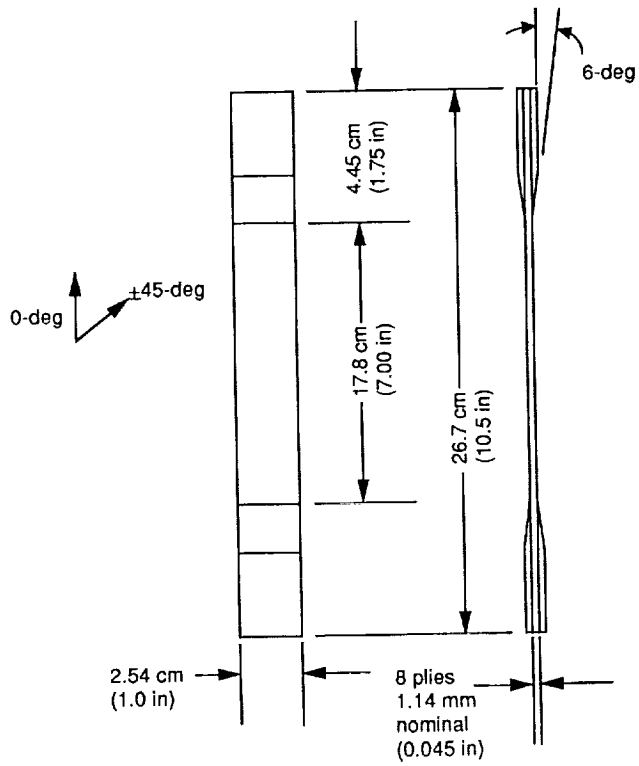

Figure 1. A ±45-deg tensile test specimen with bonded tabs, after ASTM D3518 and D3039.

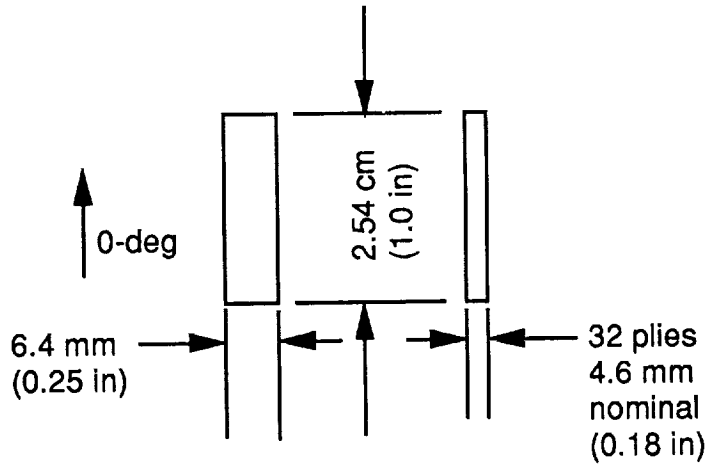

Figure 2. A 0-deg interlaminar shear test specimen, after ASTM D2344.

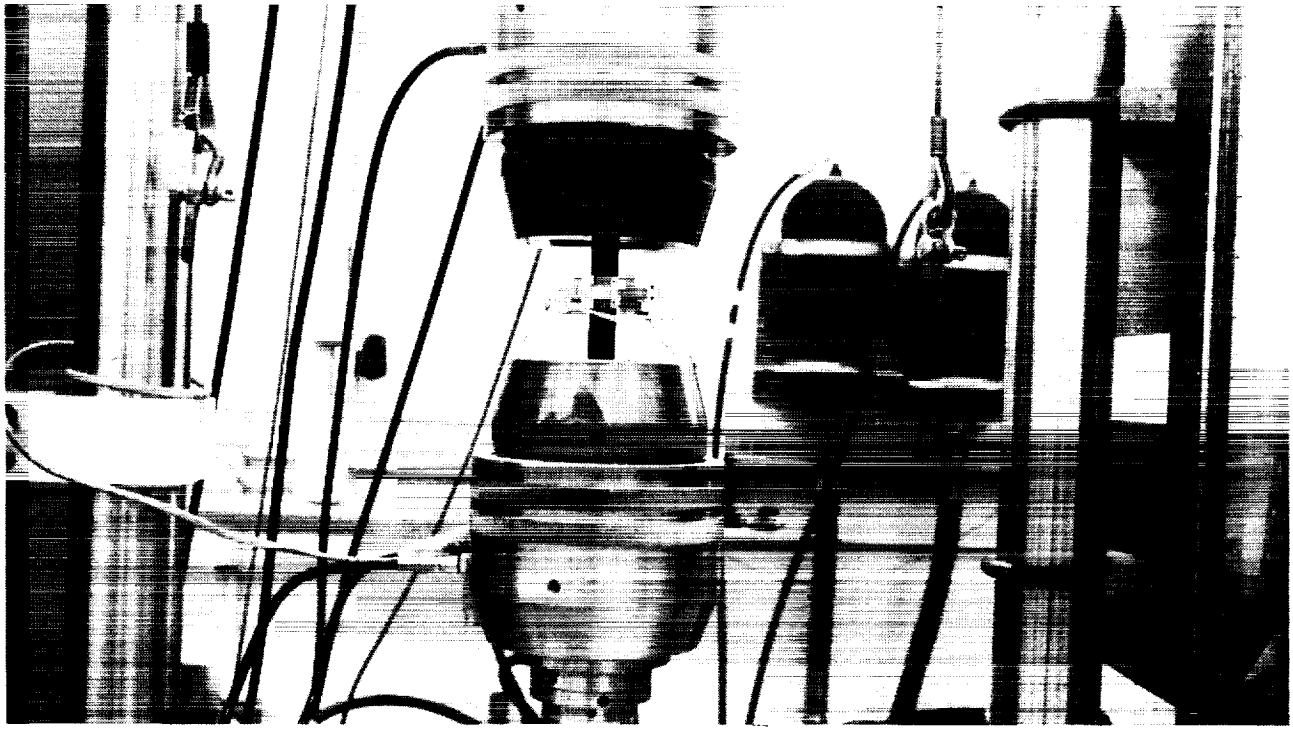

Figure 3. Biaxial extensometer on a tensile test specimen.

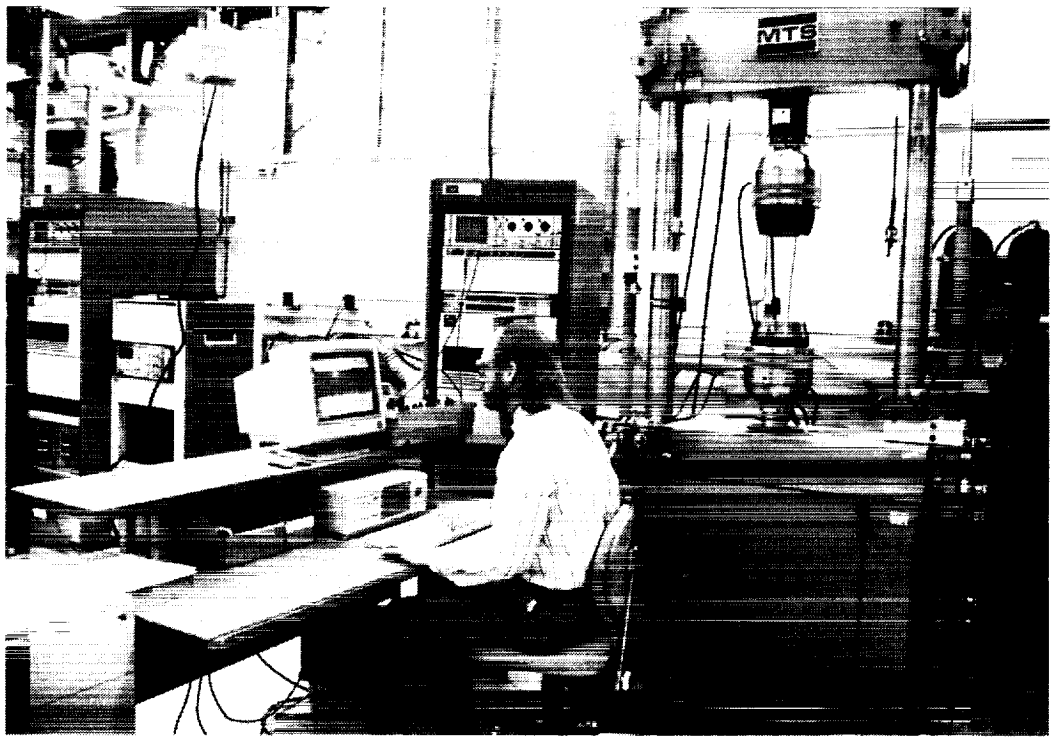

Figure 4. Mechanical test machine.

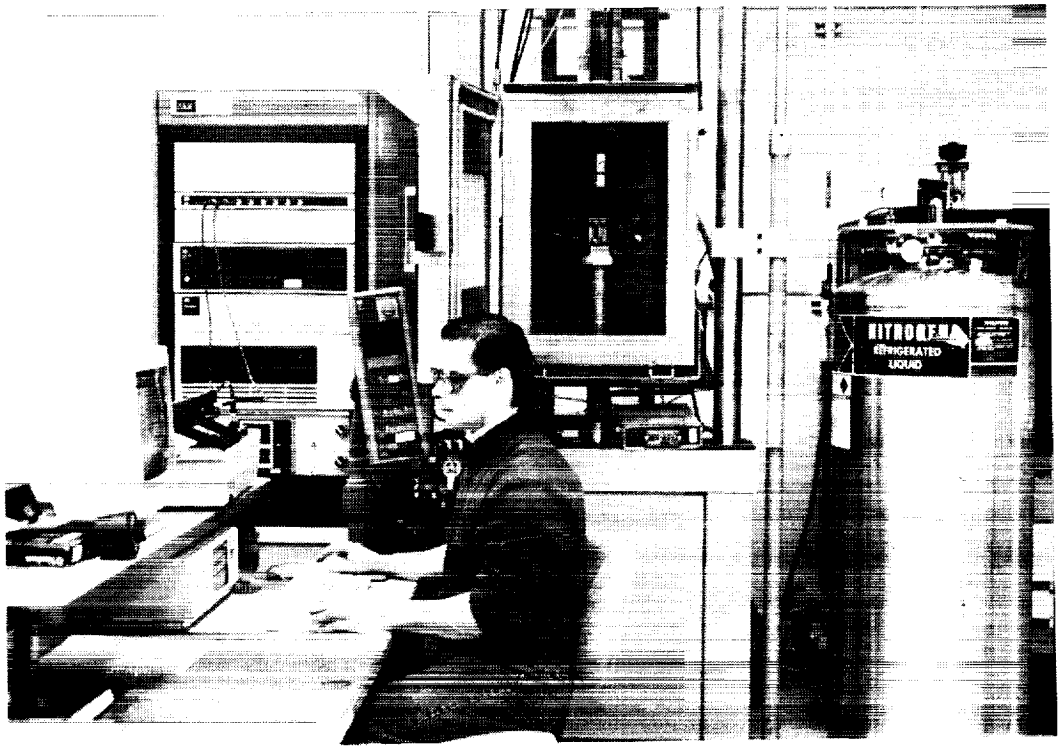

Figure 5. Mechanical test machine with environmental chamber.

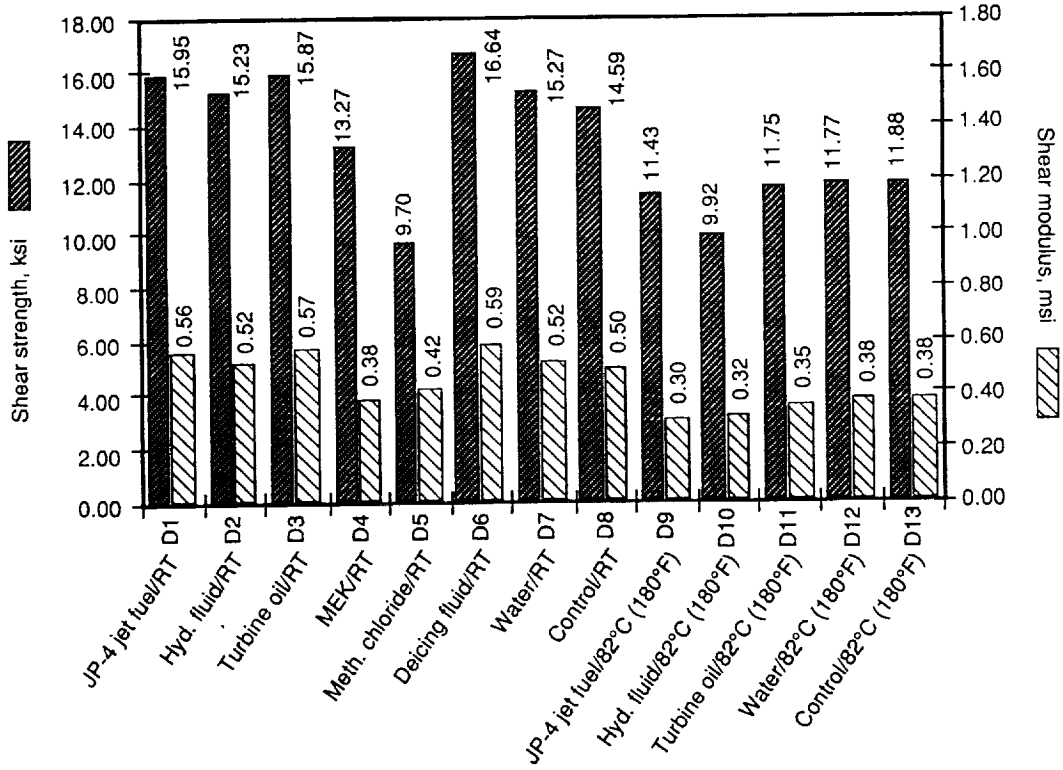

Figure 6. Average shear strength and shear modulus from ±45-deg tensile coupons of AS4/Dow Tactix CET-2 epoxy after fluid exposures.

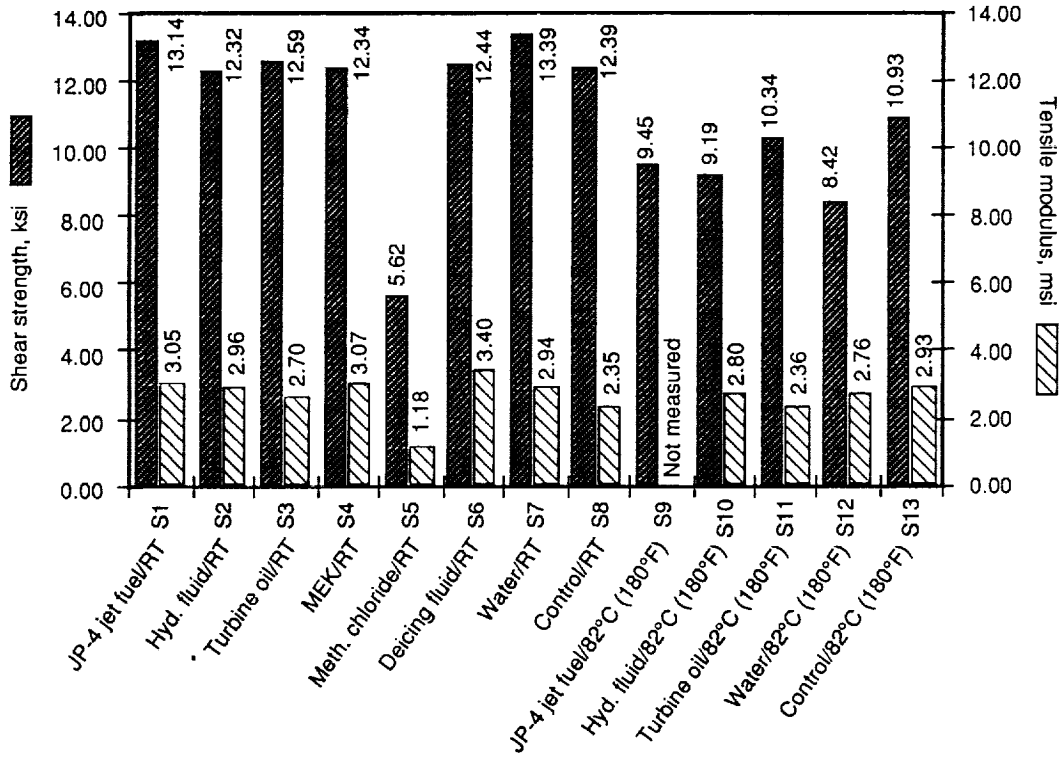

Figure 7. Average shear strength and shear modulus from ±45-deg tensile coupons of AS4/Shell Epon DPL 862/W epoxy after fluid exposures.

Note: Tensile modulus, not shear modulus (G_{12}), was measured.

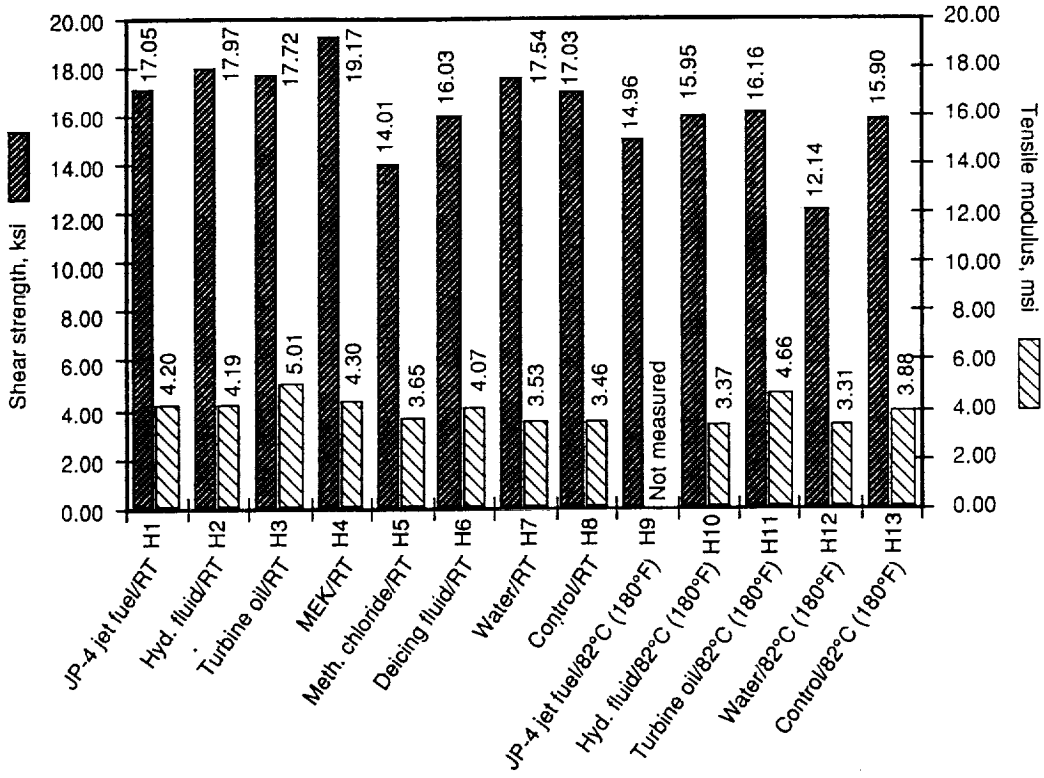

Figure 8. Average shear strength and shear modulus from ±45-deg tensile coupons of AS4/Hercules 3501-6 epoxy after fluid exposures.

Note: Tensile modulus, not shear modulus (G_{12}), was measured.

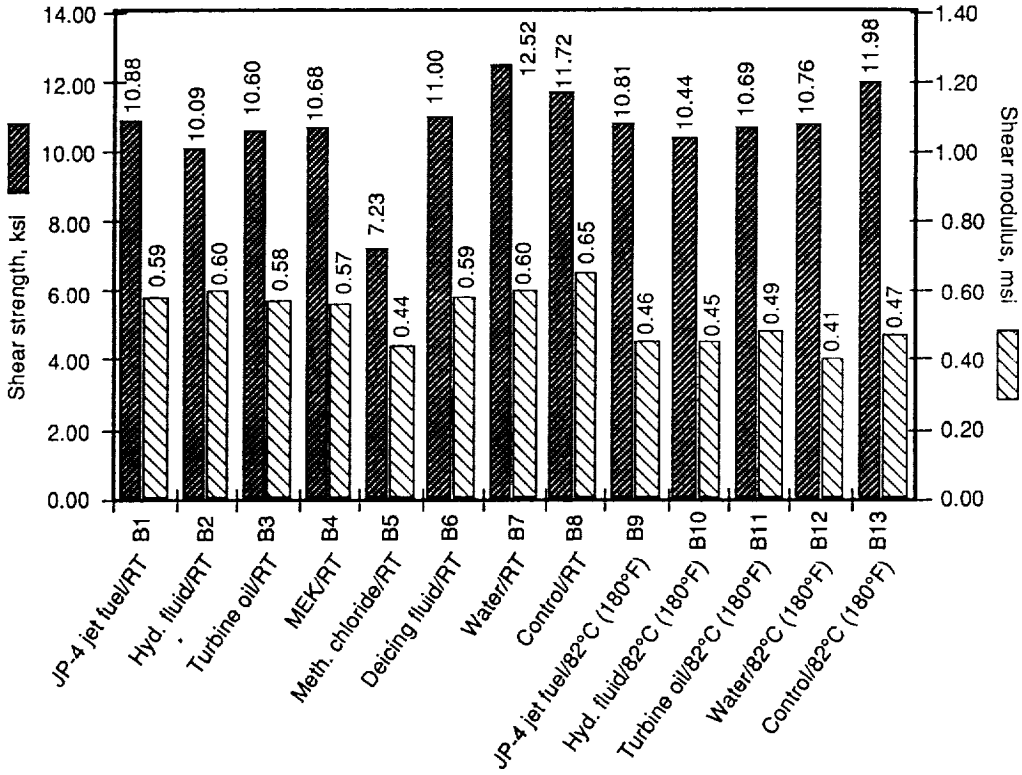

Figure 9. Average shear strength and shear modulus from ±45-deg tensile coupons of AS4/BP Chemicals E905-L epoxy after fluid exposures.

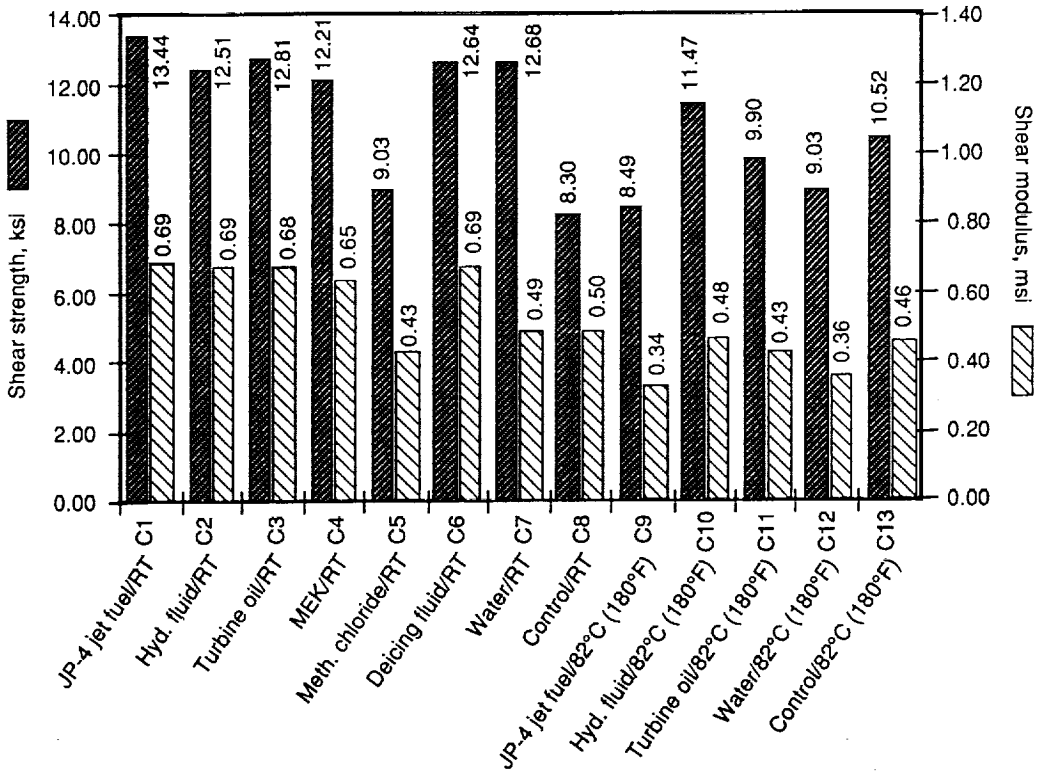

Figure 10. Average shear strength and shear modulus from ±45-deg tensile coupons of AS4/Ciba Geigy Matrimid 5292 bismaleimide after fluid exposures.

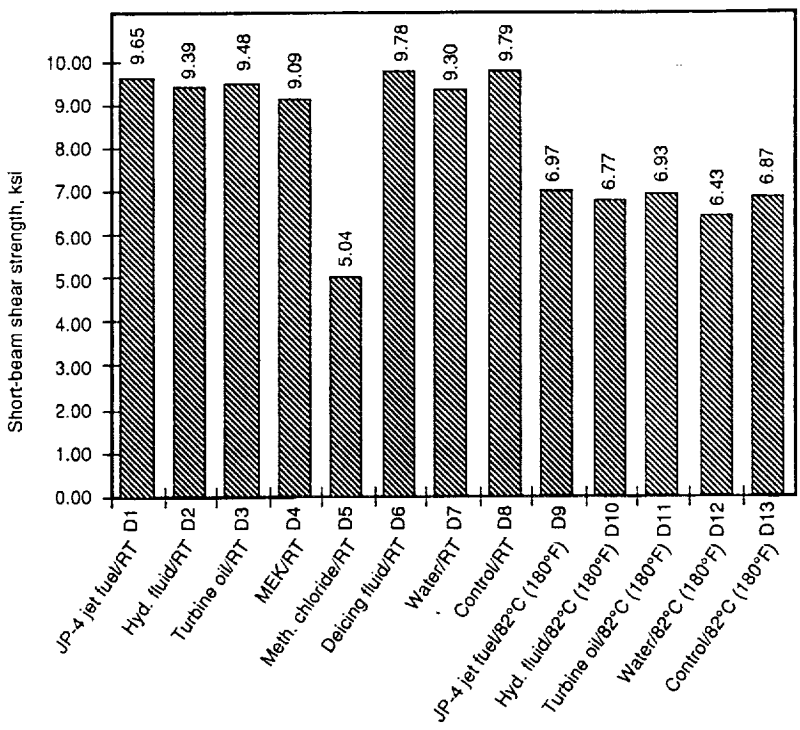

Figure 11 Average interlaminar shear strength of AS4/Dow Tactix CET-2 epoxy after fluid exposures.

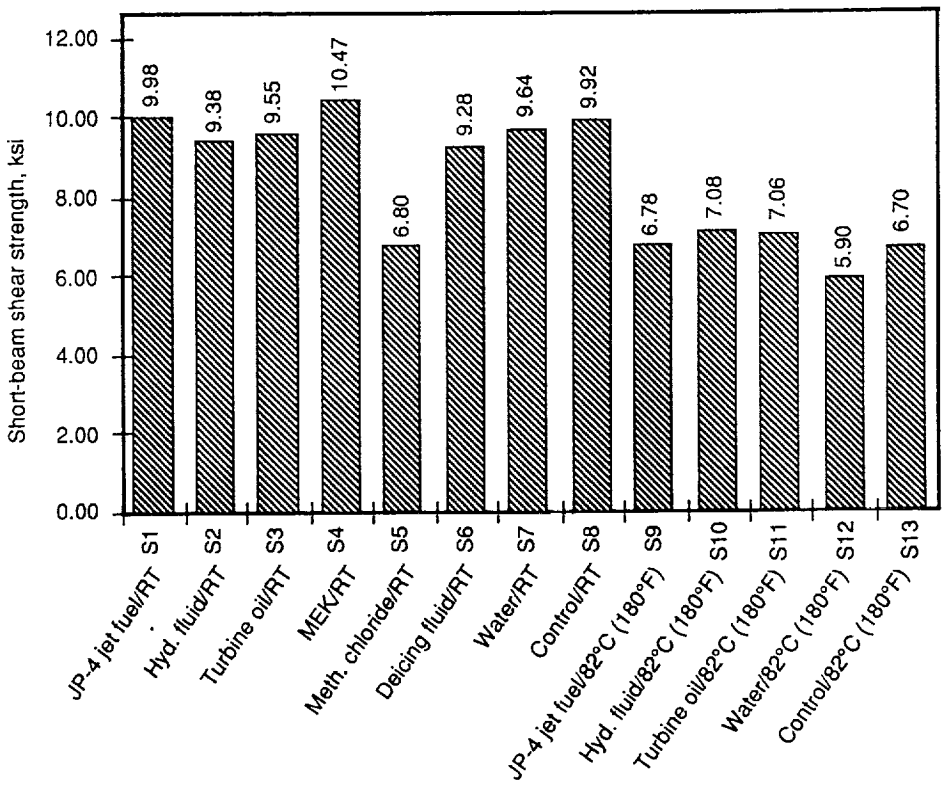

Figure 12. Average interlaminar shear strength of AS4/Shell Epon DPL 862/W epoxy after fluid exposures.

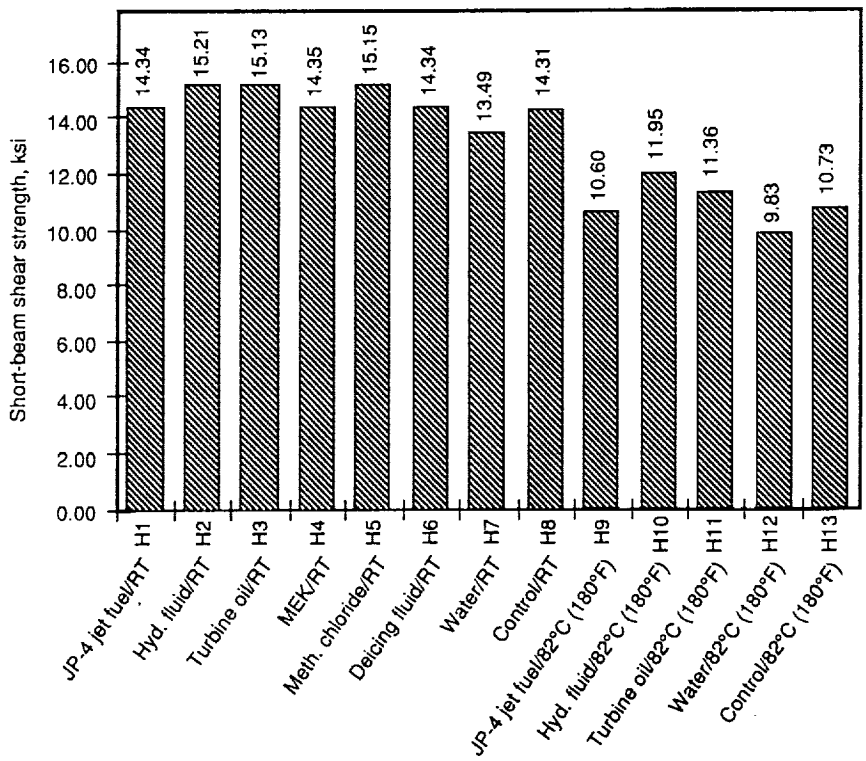

Figure 13. Average interlaminar shear strength of AS4/Hercules 3501-6 epoxy after fluid exposures.

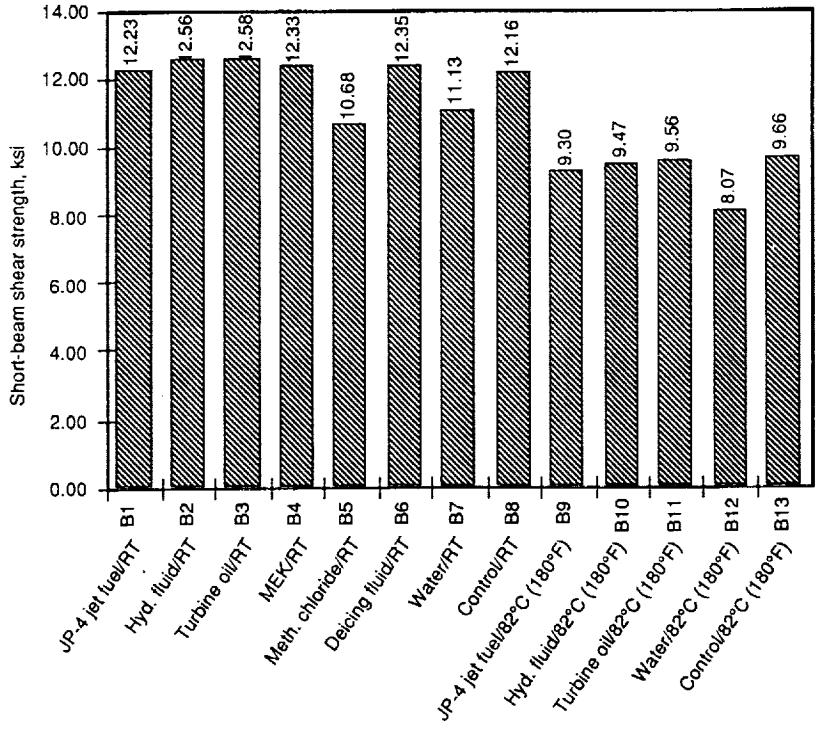

Figure 14. Average interlaminar shear strength of AS4/BP Chemicals E905-L epoxy after fluid exposures.

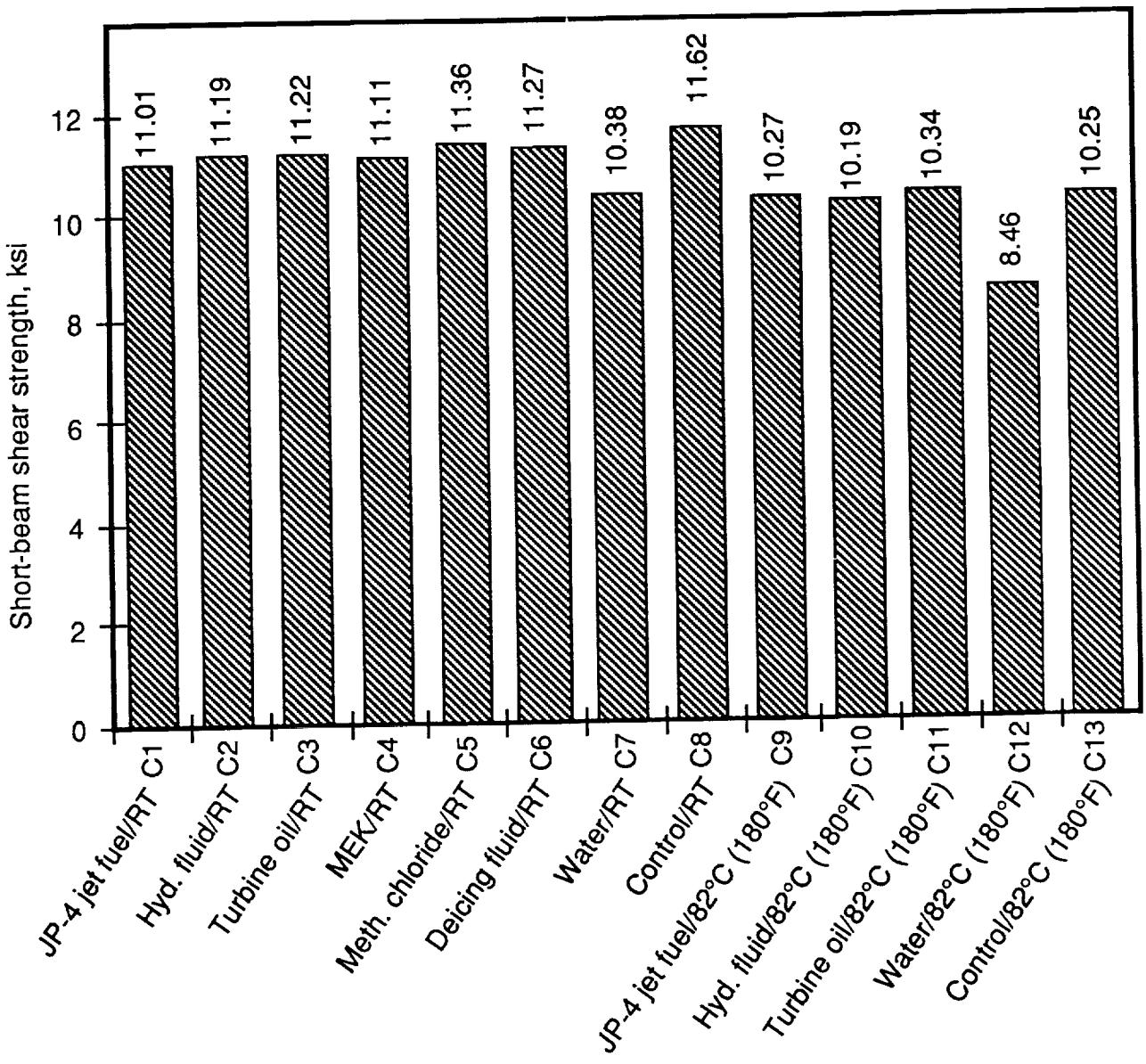

Figure 15. Average interlaminar shear strength of AS4/Ciba Geigy Matrimid 5292 bismaleimide after fluid exposures.

EFFECTS OF THERMAL AND MOISTURE CYCLING ON THE INTERNAL STRUCTURE OF STITCHED RTM LAMINATES *

Jeff Walker
Douglas Aircraft Company
Long Beach, CA

Lance Roundy
McDonnell Aircraft Company
St. Louis, MO

Jon Goering
McDonnell Aircraft Company
St. Louis, MO

SUMMARY

Conventional aerospace composites are strong and stiff in the directions parallel to the carbon fibers, but they are prone to delaminations and damage in the through-the-thickness directions. Recent research has shown that substantial improvements in damage tolerance are obtained from textile composites with Z-direction reinforcement provided by stitching, weaving, or braiding. Because of the mismatch in thermal and moisture expansion properties of the various material components, there is a potential for microcracks to develop in the resin matrix. These cracks can form to relieve the mechanical stresses that are generated during curing or in-service temperature cycles.

INTRODUCTION

The NASA Innovative Composite Advanced Primary Structure (ICAPS) program has utilized Z-axis stitching to increase damage tolerance and stabilize and compact dry fiber preforms. These preforms are then impregnated with resin using the resin transfer molding (RTM) technique or autoclave resin film infusion (RFI) (Figure 1).

* Work done on contract at McDonnell Douglas, NAS1-18580

Microscopic evaluation of panels stitched with fiberglass thread and impregnated with Hercules 3501-6 resin has shown evidence of cracks and voids at the thread/resin interface (Figure 2). Closer inspection reveals two distinct kinds of cracks forming in the resin-rich areas around the thread:

- Resin separation cavities -- These areas appear to form before the epoxy matrix has completely set-up as seen by the smooth fracture surfaces (Figure 3). These voids may be formed due to the resin shrinking away from the surface of the thread during cure.

- Matrix cracks -- These cracks appear to be traditional fracture surfaces created after the resin has hardened. They are most often found at the ends of the separation cavities and propagate into a resin-rich area either inter- or intraply.

This paper describes the work being performed under the NASA Langley Research Center (NASA LaRC) Effect of Environment on Textile Composites program which is investigating the causes, effects, and possible solutions in minimizing microcracking. The research plan designed to address microcracking takes advantage of previous MCAIR, Douglas, NASA LaRC, and DuPont data gathered over the last 10 years. Thermal expansion mismatch and matrix cracks have been observed in conventional prepreg laminates as well as Z-axis stitched parts.

WEIGHT GAIN - HOT/WET ENVIRONMENT

A possible variable in predicting resin cracking is the effect of moisture. If voids and cracks exist around the stitching thread, water could permeate into the laminate and be absorbed into the resin matrix, which could cause fracture propagation during freeze/thaw cycles. A weight gain study (Figure 4) was carried out using 0.325 inch thick wing skin stiffened panels. The control specimens were nonstitched panels with stiffeners secondarily bonded. The stitched specimens were sections from wing element panels fabricated using the resin film infusion method. In each case, the resin system used was Hercules 3501-6 with AS4 fiber.

The specimens were weighed and then placed in a 140°F oven at 95-percent relative humidity. The data show that the stitched panels pick up moisture at twice the rate of the unstitched panels. It is important to note that the 0.54-percent increase in weight is not considered excessive, but the test was only run for 50 days because of an equipment malfunction. This was not enough time for the samples to reach complete saturation, but it is clear that a surface seal coat may be required to protect Z-axis stitched parts in service environments. An unstitched laminate usually reaches moisture equilibrium with a weight increase of approximately 1-percent. This experiment will continue until a saturation level is reached in the stitched specimens.

RESEARCH PLAN DEVELOPMENT

This information collected on in service matrix cracking has been used to define a test program to identify the possible causes of microcracking in stitched laminates. The research will focus on the following key areas:

- Test specimens and fabrication
- Critical environmental parameters/cycle definition
- Resin system selection
- Exterior surface treatments
- Assessment of susceptibility to fuel leaks
- Analytical methods evaluation

The test matrix (Table I) was finalized in a meeting between NASA Langley, McDonnell Aircraft, and Douglas Aircraft. Effort will be distributed between these three principals with Douglas focusing on fabrication, MCAIR on conditioning and testing, and NASA on open hole compression testing and program guidance.

Test Specimens and Fabrication

The test matrix will focus on compression-after-impact (CAI) and open hole compression (OHC) values. These are essentially matrix-dominated properties and should help quantify the effects of microcracks in predicting property knockdowns. The specimens will be 48-ply quasi-isotropic laminates, [45,0,-45,90]6s, per NASA Reference Document 1092.

To fabricate the dry preform panels, the 145 g/m^2 uniwoven dry carbon fabric is cut, laid up, and then sent to Pathe Corporation, New Jersey, to be stitched on a multiple-needle sewing machine (Figure 5). The penetration thread is made up of four strands of 400 denier Kevlar treated with a low melt nylon to aid the stitching process. The stitch density is typical of the 0.20 inch spacing used on the NASA ICAPS program with 40 penetrations per square inch.

The stitched panels will then be impregnated using resin film infusion. This process begins with casting a neat resin plug approximately the size and thickness of the preform. The dry preform is laid on the resin with a perforated caul plate on top. The lay-up is bagged and placed in the autoclave to undergo a step cure cycle where isothermal holds are used to fully impregnate the preform with resin.

Critical Environmental Parameters

Work done under NASA contract by Roberto Cano at LaRC (Ref. 1) showed that compression strength was not substantially affected by cycling between hot/wet and cold environments (Figure 6). The data supports the conclusion that strength knockdowns occur initially during cycling but do not continue to decrease substantially over time.

Earlier studies by Dupont and Douglas indicated that microcracking could be induced in laminates by dry temperature cycling alone. To investigate a potentially more severe environment, it was agreed that specimens would be loaded in bending while temperature and moisture were simultaneously applied.

The cycle (Figure 7) requires 90 minutes to complete and simulates a worst-case environment for the aircraft. Specimens will be examined after 10, 100, and 1,000 cycles, and surface crack density will be compared to service parts to establish cycle-to-flight ratios.

Resin System Selection

Resin system selection for the program was finalized during a NASA, MCAIR and Douglas meeting in Langley, Virginia. The baseline carbon fiber will be Hercules AS4, and the following resin systems were chosen for evaluation:

- Hercules 3501-6
- Hercules 3502
- Dow Chemical CET-3
- 3M PR 500

The resin systems selected present a fairly broad cross section of properties thought to contribute to microcracking. The CET-3 and PR 500 show good improvement over 3501-6 in shrinkage, moisture resistance, and fracture toughness. The Hercules 3502 is excellent in hot/wet properties retention and has the lowest viscosity during the process cycle for good fiber wet-out.

Laminate compression properties developed at NASA Langley confirm predictions from the neat resin data (Table II). Resin modulus is a good indicator of the relative compression strength of a quasi-isotropic specimen. These properties will then be compared after being notched or impacted and subjected to moisture/temperature cycling.

Previous process experience was important to the resin selection criteria. Excellent results were achieved at both NASA and Douglas with the PR 500 (Figure 8). Cross sectional micrographs of a Kevlar-stitched, NASA-processed panel show good fiber wet-out and no evidence of postprocessing microcracks, as seen in Figure 2. A non-

stitched Douglas panel 0.50 inch thick also showed good results when using PR 500. Reports from the industry indicate the CET-3 material should have similar processing characteristics, which led to its selection.

Exterior Surface Treatments

The Kevlar panel study performed by DuPont recognized that surface finish preparation and materials could have a marked effect on the onset of microcracking. The most promising candidates were investigated further:

- Calendered Kevlar S-285
- Koroflex® flexible primer from DeSoto Corporation
- Film adhesives cocured to the panel's tool side
- Nonwoven Kevlar mat impregnated with adhesive

This program will focus on the use of Koroflex to minimize surface cracking. This solution makes the most sense from a weight and manufacturing viewpoint, and test results showed no cracking after 3,000 hot/cold cycles.

Assessment of Susceptibility to Fuel Leak

Potential microcracking in wing skin panels creates concerns of possible fuel absorption or leakage through the skins. This program will expand on the work done by C.F. Griffin of Lockheed on fuel containment under the NASA ACEE program (Reference 2).

A MCAIR chamber designed to environmentally cycle test coupons while exposing them to JP5 fuel under pressure will be used to evaluate post impact leakage (Figure 9). The specimens will be coated on the surface opposite the impact with Chemglaze® or polysulfide sealer per production process standards. The coupons will then be impacted to the threshold level of visible damage ($\sim$ 35 foot-pounds), C-scanned, and subjected to the pressurized fuel. Fluorescent dye added to the fuel will help detect the degree of penetration into the damaged laminate.

Analytical Methods Evaluation

The analytical methods task will be jointly coordinated among MCAIR, NASA LaRC and Virginia Polytechnic Institute (VPI). The objective of the analytical program is to develop models that will be used to determine stress states in and around a stitch through a composite lamina. Once developed, these models will be used to perform parametric studies with different resin systems, stitching fibers, and/or processing cycles to identify those combinations that minimize microcracking. The modeling effort focus is divided as follows:

- MCAIR - Develop three dimensional models.
- NASA LaRC - Develop two dimensional plane strain models.
- VPI - Develop two dimensional axisymmetric models.

Processing stresses that develop in the matrix pockets around the stitch are of particular interest, since they can be used to predict when microcracks will occur. Preliminary axisymmetric models of a stitch surrounded by concentric annuli of matrix and composite (Figure 10) have been used to predict order of magnitude stresses in a matrix pocket. Through-the-thickness stress distributions, predicted by the 3D models, near the stitch/matrix and matrix/composite interfaces are shown in figure 11 for a -275°F temperature change (Tg to room temperature). Since the tensile and shear strengths of the neat resin are roughly 8-10 ksi, the predicted stresses could easily have caused cracking. In addition, this simple model demonstrates that a complex three dimensional stress state exists in the matrix pocket.

Several more detailed models are being developed for this study, all of which utilize the finite element method to characterize a representative volume element (RVE) of the stitched composite. In these models, the RVE is taken as a single stitch and half of the composite between it and adjacent stitches (Figure 12). The laminates being modeled are always mid-plane symmetric, and only include 0, 90, and ±45 degree plies.

The MCAIR model utilizes three dimensional solid brick elements to explicitly model each ply of the laminate. The mesh for this model is based on the intersections of the matrix pockets in 0, 90, and ±45 degree plies. A generic mesh for a single ply, regardless of orientation, has been developed. This mesh includes all possible matrix pockets, and can be used for any ply by specifying that matrix properties be used for elements in the appropriate pocket, and that lamina properties be used for elements in all other areas. Since the same mesh is used for all plies, a laminate model is built by stacking the required number of ply models (Figure 13). Symmetry conditions are used at the mid-plane of the laminate, and anti-symmetry conditions are used along a plane through the centerline of the stitch to reduce the size of the model to one-fourth of the actual RVE.

The three dimensional model is very powerful, since it will predict three dimensional distributions of all six stress components. One drawback is the considerable amount of modeling time and substantial computing resources required, although the use of a generic ply mesh helps. The two dimensional models at NASA LaRC and VPI will be faster to run and should provide good ballpark correlation especially when using geometric parameters as variables.

The two dimensional models being developed by NASA LaRC explicitly model the matrix pocket and the cross-sectional shape of the stitch. Since they are two dimensional, much finer meshes can be used, and it is easier to make changes in the geometry. These models will be used to determine the relative effects of different stitch geometries and matrix pockets. The drawback to the NASA LaRC models are that they do not include through-the-thickness shear distributions. The two dimensional axisymmetric models being developed by VPI do include these shears, but can only account for

geometric changes in an average sense. For example, the volume of the matrix pocket can be changed, but it must still be an annulus. The VPI model is therefore most appropriate for parametric analyses that consider material property changes.

To support the analyses, photos were taken at several through-the-thickness locations to define thread/resin interfaces (Figures 14, 15, and 16). The displacement of the surrounding carbon fibers due to thread diameter is shown in Figure 17. The triangle shaped resin-rich areas are the principal sites of voids due to shrinkage which can serve as origins of microcracks.

SCHEDULE

The period of performance involves a 12 month effort. The critical path involves the timely receipt of the neat resin systems and panel stitching to be done at Pathe Corporation.

CONCLUSIONS

Douglas and industry experience with resin matrix cracking to date supports the following conclusions:

- Microcracking is not strickly a phenomenon of Z-axis stitched composites.
- Several variables affect the initation and distribution of cracks. Resin systems, stitching threads and process cycles, to name a few, have been shown to affect the microcrack frequency and appearance.

At the conclusion of the task, several key parameters involving microcracking will have been investigated and quantified. This research will focus on answers to the following questions:

- Does microcracking affect long-term strength of stitched composites? Current evidence suggests it does not.
- Can severity of cracking in service be duplicated in the laboratory? DAC and DuPont were successful in a previous program.
- Are these cracks dependent on materials or processes?
- Which neat resin properties are important in eliminating the cracks?
- Will fuel containment be a problem?
- Will surface finish eliminate the observable cracks? Materials currently used in production have eliminated surface cracks in Kevlar/honeycomb panels.
- Can finite-element modeling be used to predict strength knockdowns and identify likely crack sites?

References

1. Cano, Roberto and Furrow, Keith: **Effect of Temperature and Humidity Cycling on Strength of Textile Reinforced Carbon/Epoxy Materials,** Third Advanced Composites Technology (ACT) Industry Review, Long Beach, CA, June 8-11, 1992. **NASA CP-3178.**

2. Griffin, C.F.: **Composite Wing Fuel Containment and Damage Tolerance - Technology Development,** ACEE Composites Structures Technology Conference, August 13-16, 1984.

Bibliography

Loken, H.Y.,Dr.: **Review of Water Ingression Into Commercial Transport Aircraft Composites,** Douglas Aircraft Presentation, June 19, 1985.

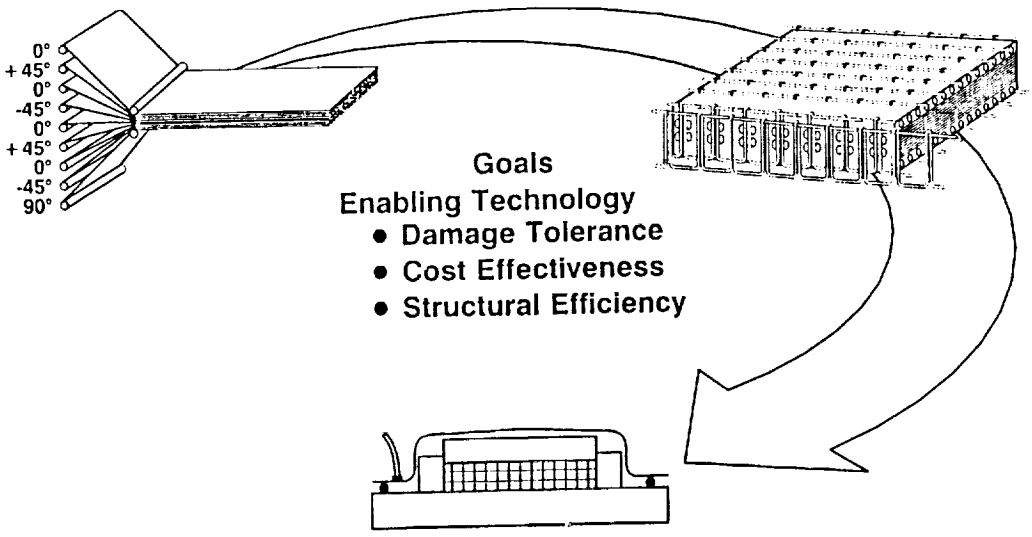

Figure 1. Process Overview

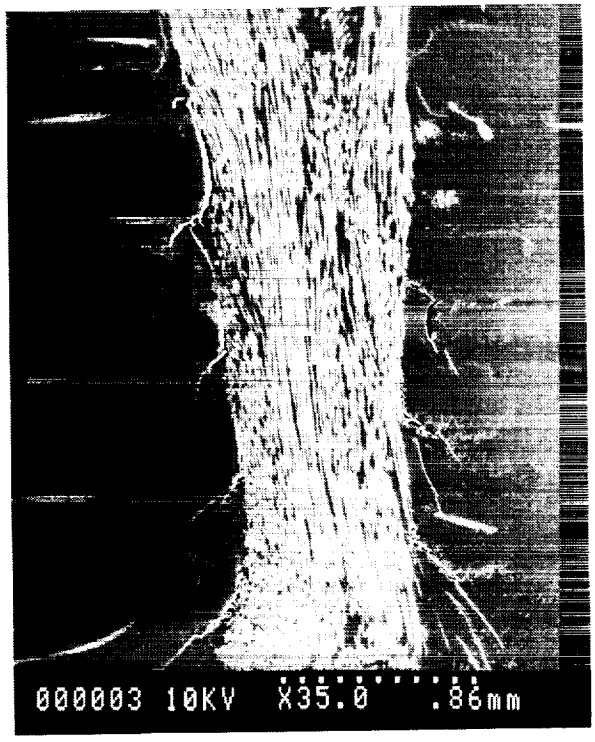

Figure 2. Glass Stitch w/3501-6 Laminate

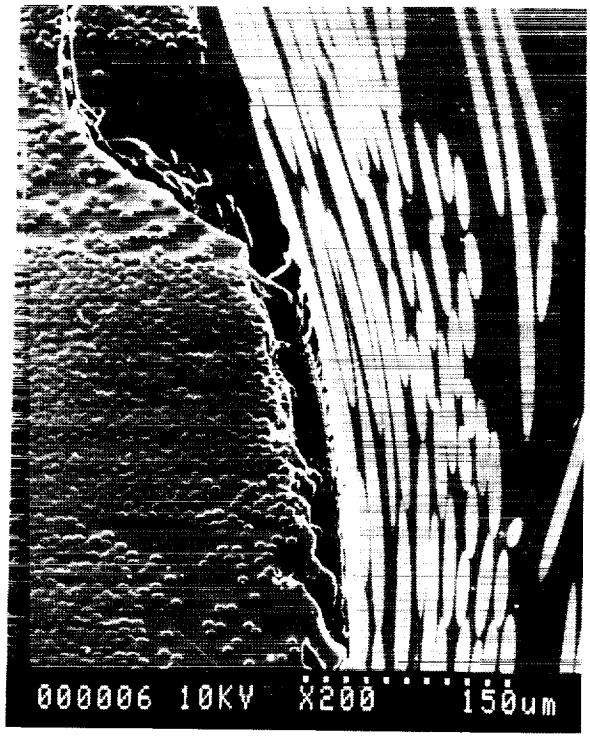

Figure 3. Resin Cavities at Thread

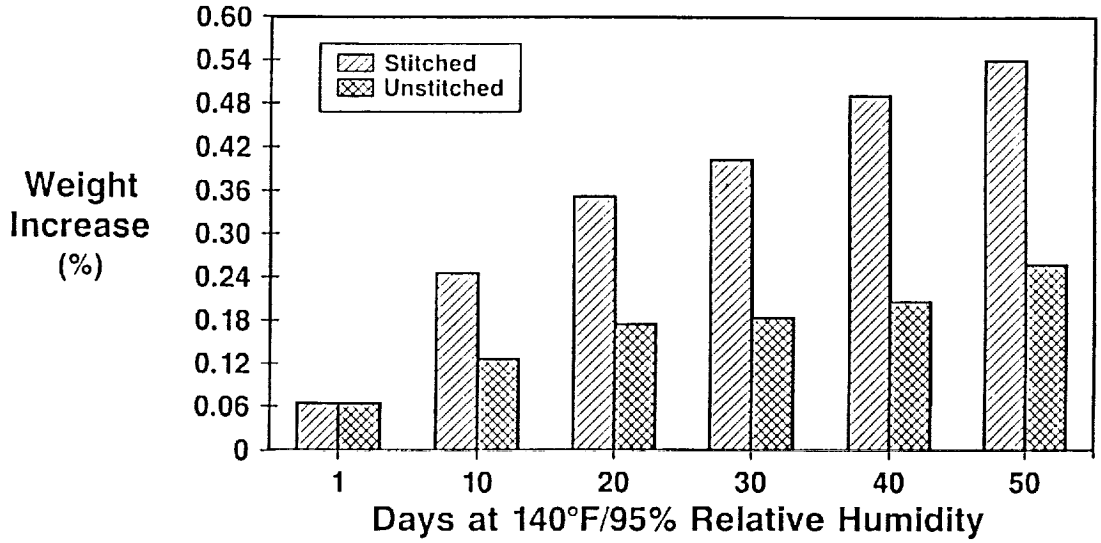

Figure 4. Weight Gain Study

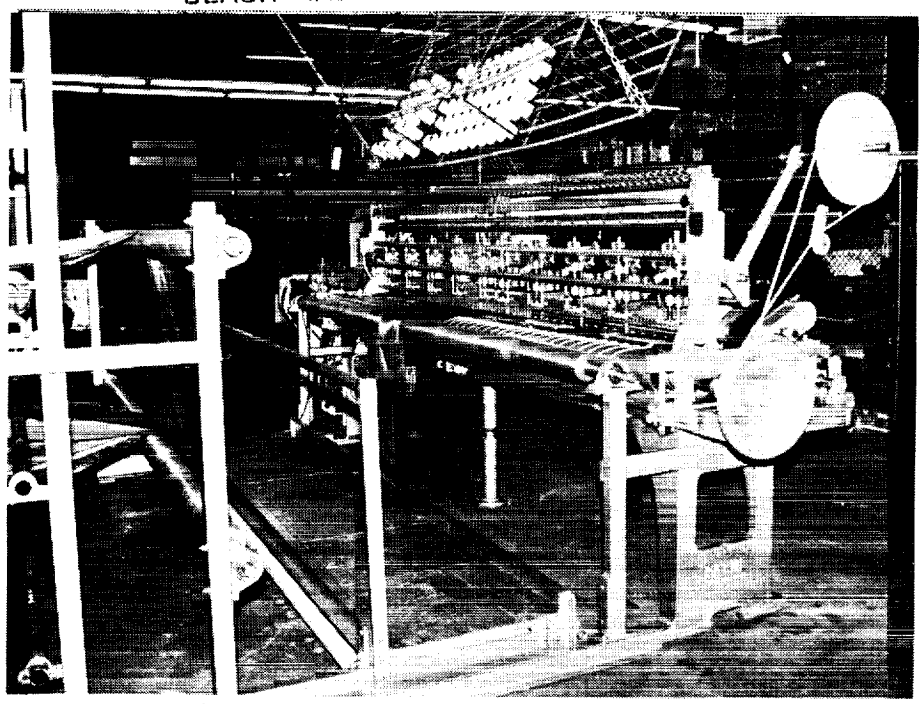

Figure 5. Pathe Multi-Needle Machine

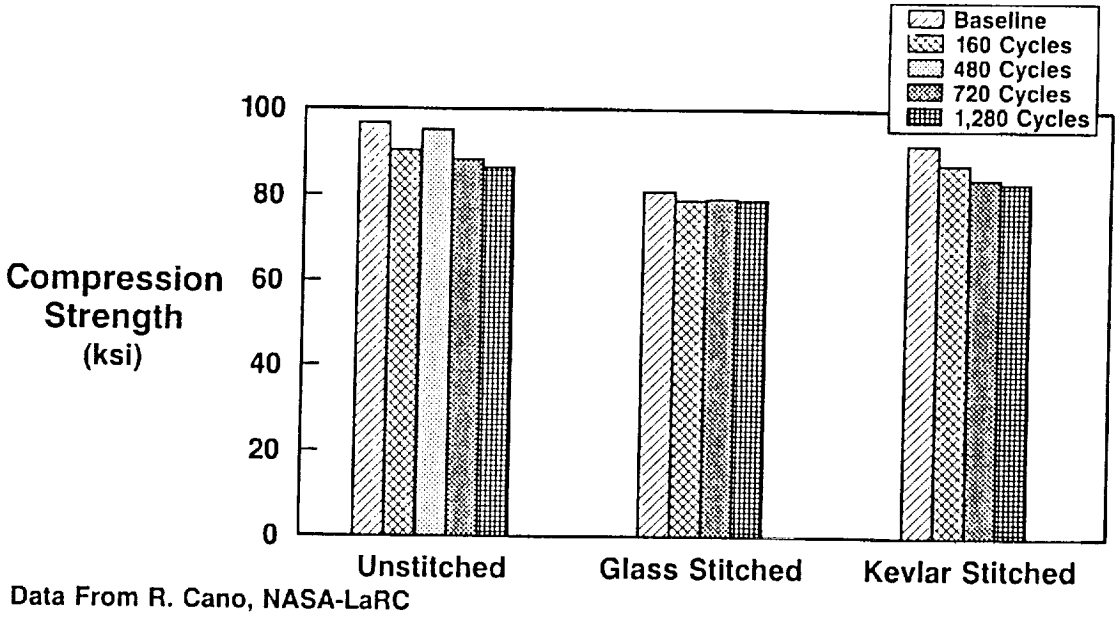

Figure 6. NASA Compression Data

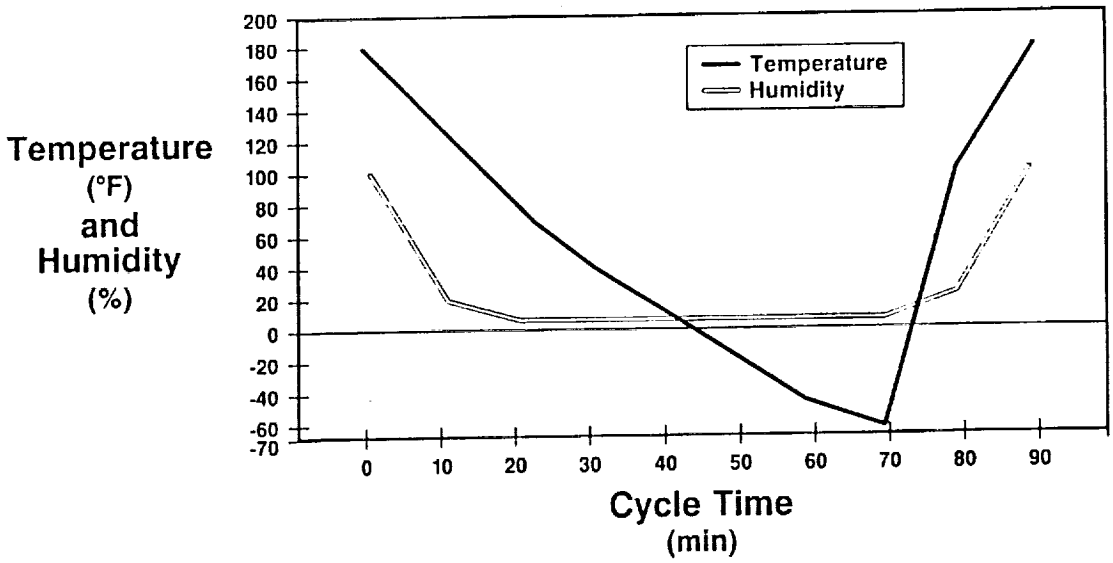

Figure 7. Enviromental Cycle

Figure 8. PR 500 w/Kevlar Stitch

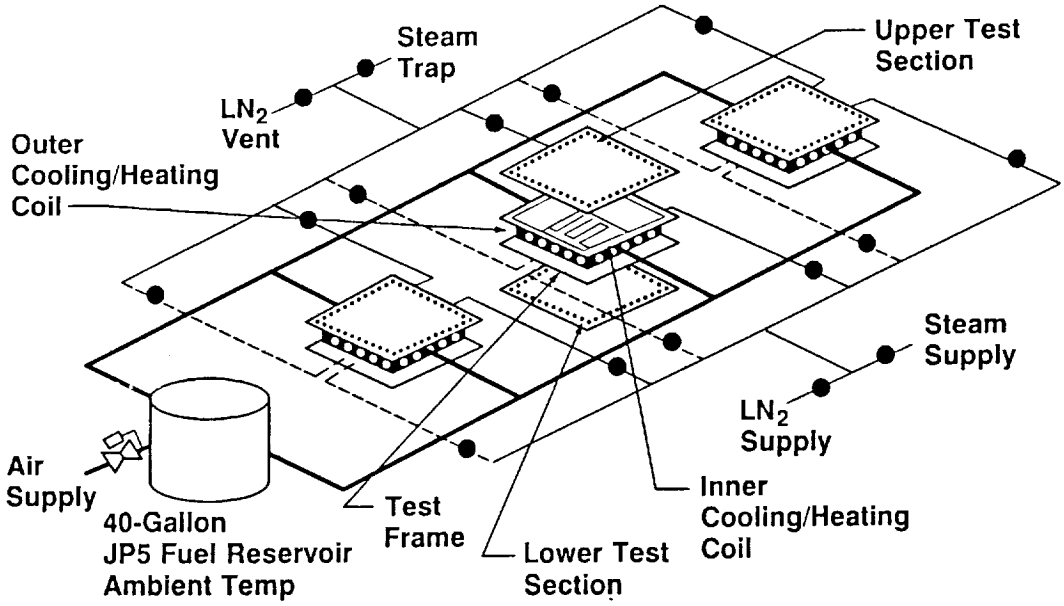

Figure 9. Fuel Leak Test Set-Up

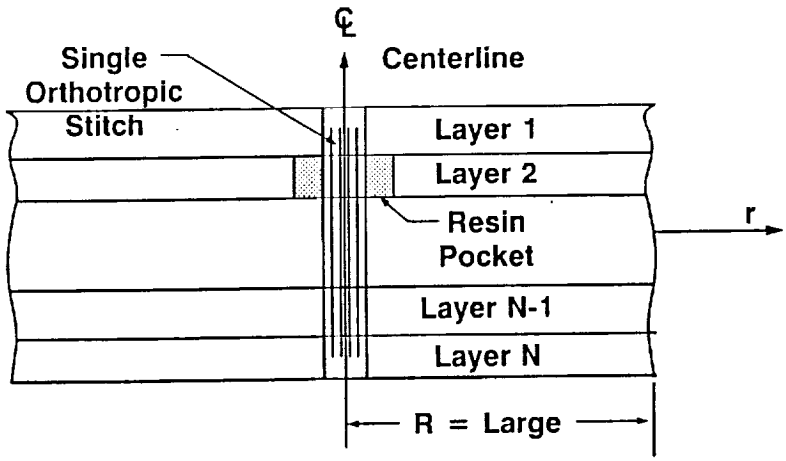

VPI modeling focuses on an analytical tool that provides short computational times and qualitative assessment of cracking

Figure 10. VPI Model, 2D

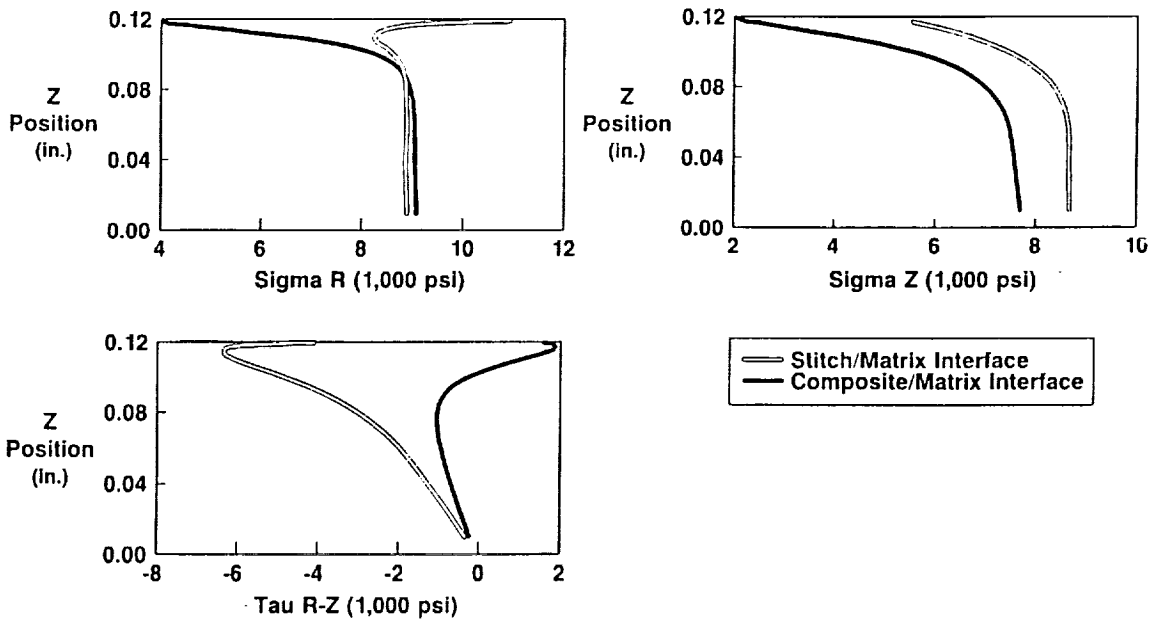

Figure 11. 3D Model Analysis Results

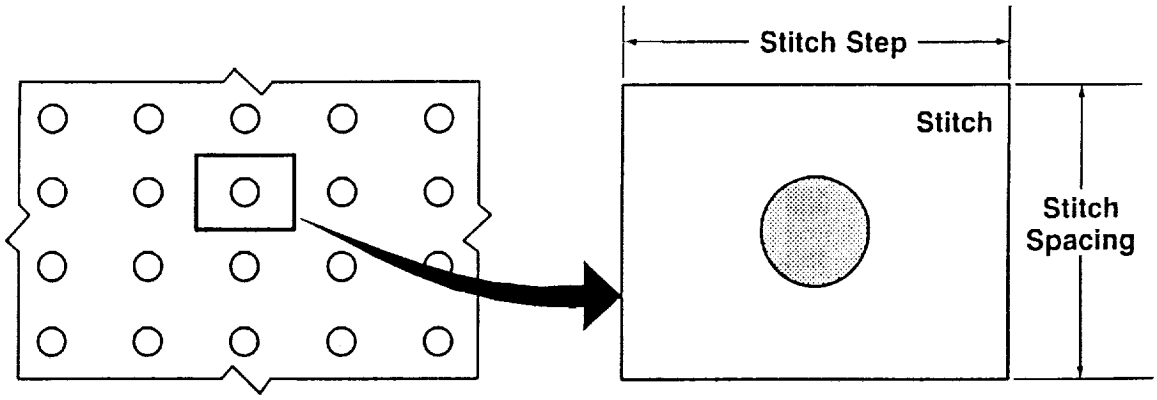

A representative volume element (RVE) for stitched laminates will be utilized by each of the investigators

Figure 12. Representative Volume Element

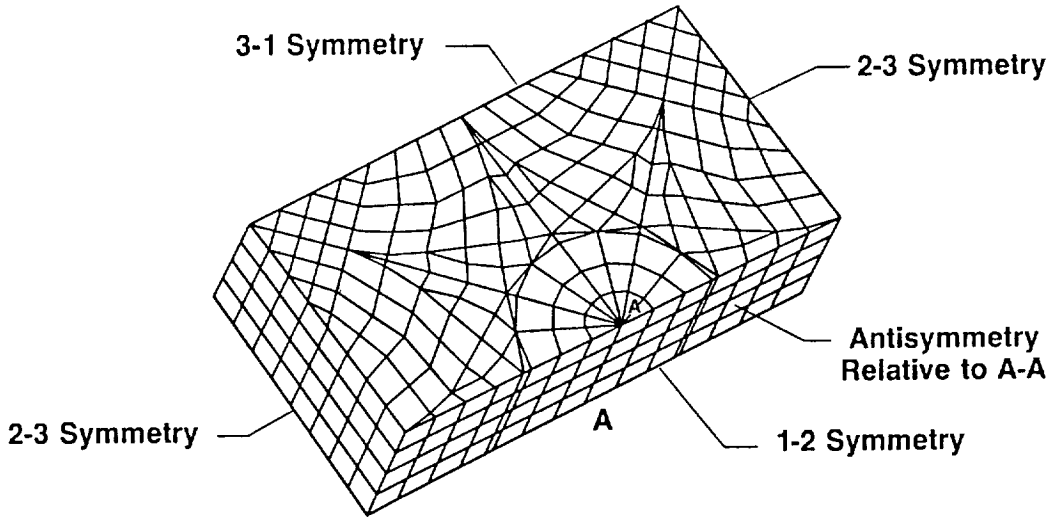

MCAIR modeling encompasses through-the-thickness effects, utilized to ensure the accuracy of the previous models

Figure 13. MCAIR 3D Model

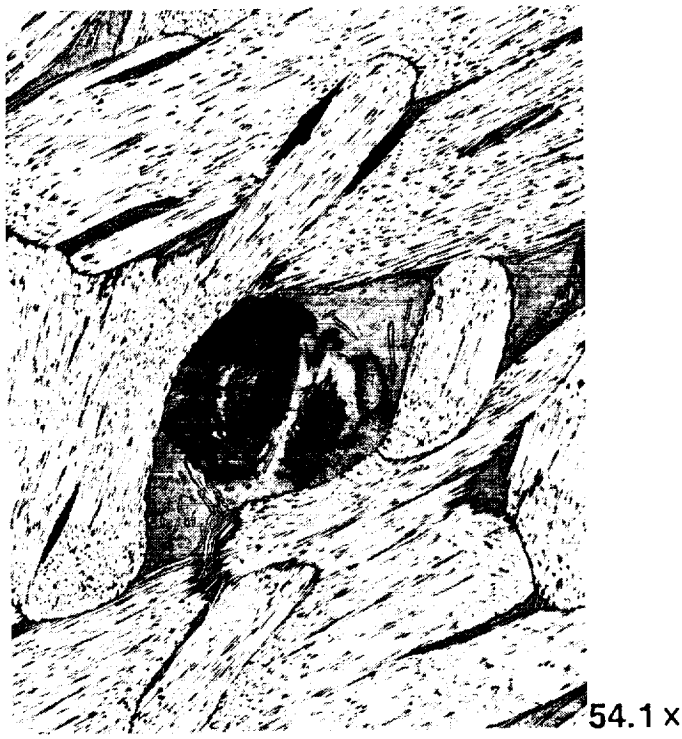

Figure 14. Ply of 48, PR 500

Figure 15. Ply 8 of 48, PR 500

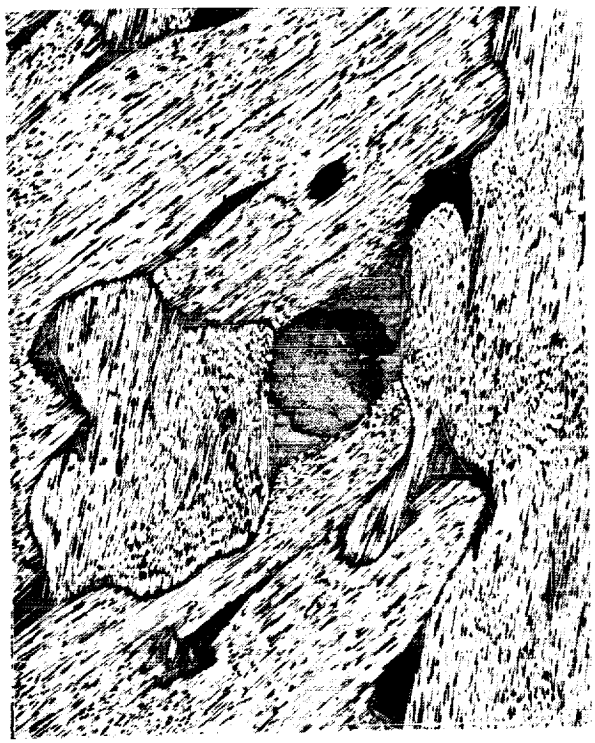

Figure 16. Ply 24 of 48, PR 500

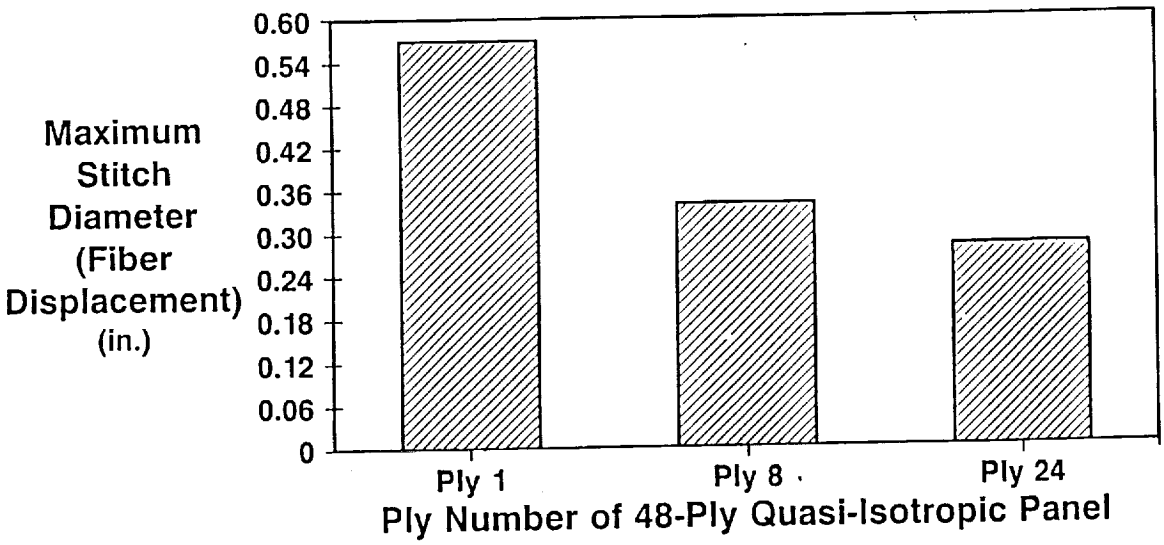

Figure 17. Fiber Displacement Around Stitch

Table I. Microcracking Test Matrix

Environment	Material	Surface Finish	Test	No. of Cycles				Total
				0	10	100	1,000	
Simultaneously Applied Thermal and Moisture Cycles (90-min Duration) Specimens Loaded in Bending	AS4/3501-6 Unweave	Unfinished	OHC CAI Microphotography	3 3 3	3 3 3	3 3 3	3 3 3	12 12 12
		Primed and Painted	Visual Inspection	3	3	3	3	12
		Sealant	Impact and Leak Proof Test	2		2		4
	AS4/3501-6 Kevlar Stitched RTM	Unfinished	OHC CAI Microphotography	3 3 3	3 3 3	3 3 3	3 3 3	12 12 12
		Primed and Painted	Visual Inspection	3	3	3	3	12
		Sealant	Impact and Leak Proof Test	2		2		4
	AS4/3502 Kevlar Stitched RTM	Unfinished	OHC CAI Microphotography	3 3 3	3 3 3	3 3 3	3 3 3	12 12 12
		Primed and Painted	Visual Inspection	3	3	3	3	12
		Sealant	Impact and Leak Proof Test	2		2		4
	AS4/CET-3 Kevlar Stitched RTM	Unfinished	OHC CAI Microphotography	3 3 3	3 3 3	3 3 3	3 3 3	12 12 12
		Primed and Painted	Visual Inspection	3	3	3	3	12
		Sealant	Impact and Leak Proof Test	2		2		4
	AS4/PR500 Kevlar Stitched RTM	Unfinished	OHC CAI Microphotography	3 3 3	3 3 3	3 3 3	3 3 3	12 12 12
		Primed and Painted	Visual Inspection	3	3	3	3	12
		Sealant	Impact and Leak Proof Test	2		2		4

Note: OHC - to Be Tested by NASA

Table II. Selected Resin Properties

Vendor-Supplied Data

Properties	Hercules 3501-6	Hercules 3502	Dow Chemical CET-3	3M PR 500
Shrinkage (%)*	~ 1.6	~ 1.6	~ 0.75	~ 0.80
Moisture (% Increase) (2 Wks at 200°F)	2.3	2.4	1.6	1.5
Fracture Toughness G1c (J/m^2)	150	120	245	653
Tensile Modulus (ksi)	643	526	425	528
Elongation (%)	1.7	0.9	5.5	1.8

* Highly Dependant on Cure Cycle

THE COMBINED EFFECT OF GLASS BUFFER STRIPS AND STITCHING ON THE DAMAGE TOLERANCE OF COMPOSITES

Susan M. Kullerd
Lockheed Engineering & Sciences Company
NASA Langley Research Center
Hampton, VA

INTRODUCTION

Recent research has demonstrated that through-the-thickness stitching provides major improvements in the damage tolerance of composite laminates loaded in compression. However, the brittle nature of polymer matrix composites makes them susceptible to damage propagation, requiring special material applications and designs to limit damage growth. Glass buffer strips, embedded within laminates, have shown the potential for improving the damage tolerance of unstitched composite laminates loaded in tension. The glass buffer strips, less stiff than the surrounding carbon fibers, arrest crack growth in composites under tensile loads. The present study investigates the damage tolerance characteristics of laminates that contain both stitching and glass buffer strips.

EVALUATION OF STITCHED CARBON/EPOXY COMPOSITES CONTAINING GLASS BUFFER STRIPS

Research reported in references 1 and 2 showed that when carbon/epoxy composite panels with buffer strips were subjected to tensile loads, the buffer strips arrested the cracks and increased the residual strengths significantly over those of laminates without buffer strips. The top left sketch in figure 1 shows a composite laminate containing fiberglass buffer strips in the 0° direction and a machined slit in the center of the panel. The laminate is made of carbon uniweave fabric with half inch strips of the carbon fibers replaced with glass fibers. Cracks initiate at the slit, propagate to the buffer strips and stop. The cracks are arrested because the modulus of resilience, or toughness, of the S-glass is greater than that of the carbon fibers. The compression properties of these buffer strip laminates were never completely characterized or documented. The lower left sketch in figure 1 shows an impacted carbon/epoxy composite panel with through-the-thickness stitching. Results reported in reference 3 showed that stitching improves the compression-after-impact strength of composites. The objective of this study was to evaluate the laminate mechanical properties of composites containing both glass buffer strips and stitching.

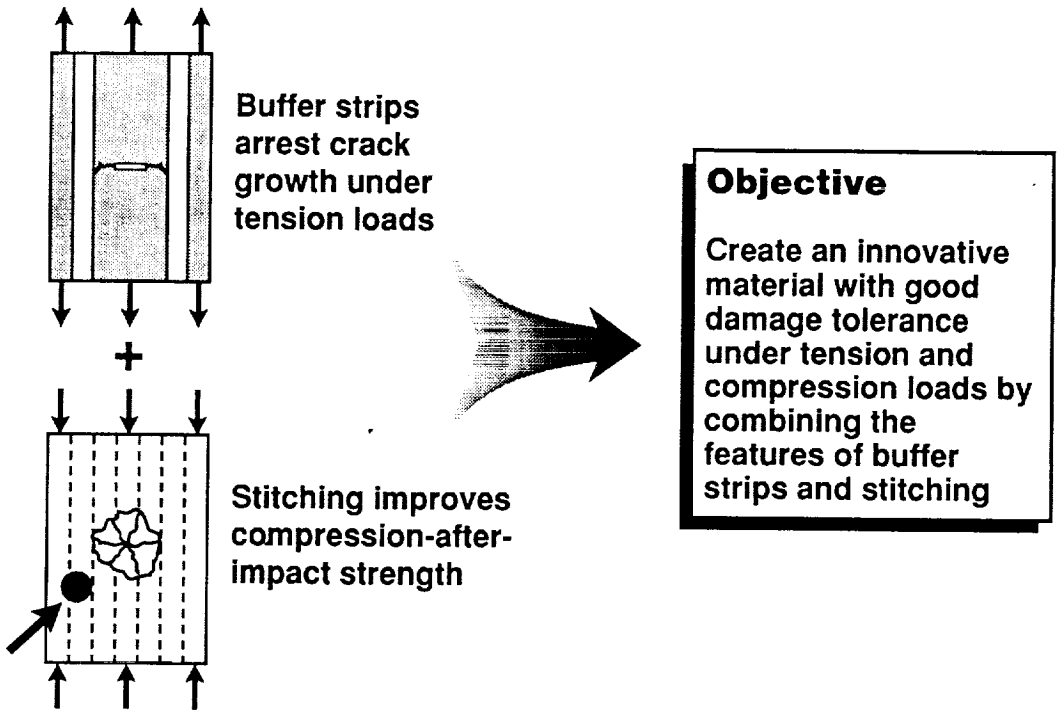

Figure 1

SPECIFIC OBJECTIVES

In order to assess the potential benefits of combining stitching and glass buffer strips to improve the damage tolerance of composites, three variables were investigated. The variables are listed in figure 2 and include buffer strip placement, buffer strip orientation, and a combination of stitching and buffer strip placement. All test panels were either 16- or 40-ply, quasi-isotropic laminates with buffer strips placed in either the 0° plies only, or in all plies (+45°, 0°, -45°, 90°). Laminates with buffer strips in the 0° plies only had the strips oriented (stacked) on top of each other, or aligned, through the thickness. Laminates with buffer strips in all plies were fabricated with the strips aligned through the thickness, as well as unaligned, or randomly placed through the thickness. Stitched and unstitched panels of each configuration were tested to determine the best combination of stitching and buffer strip placement.

Assess potenial benefits of combining stitching and glass buffer strips to improve damage tolerance and bearing strength

- Buffer strip placements
- Buffer strip orientations
- Combinations of stitching and buffer strips

Figure 2

APPROACH

Figure 3 shows the approach used to characterize the material properties of composites containing fiberglass buffer strips and through-the-thickness stitching. Because the compressive properties of buffer strip composites have not been completely characterized or documented, the first task was to complete basic mechanical property tests such as short block compression, compression-after-impact and open-hole compression, in addition to tension and open-hole tension. These tests have been completed and the results are the subject of this paper. Tests remaining to be performed include single bolt bearing and multiple-hole bolted joint tests, as well as transverse tension and compression tests, with loads 90° to the buffer strips. Additionally, the tension fracture tests performed in references 1 and 2 will be repeated to determine whether stitching degrades the crack arresting capability of buffer strips.

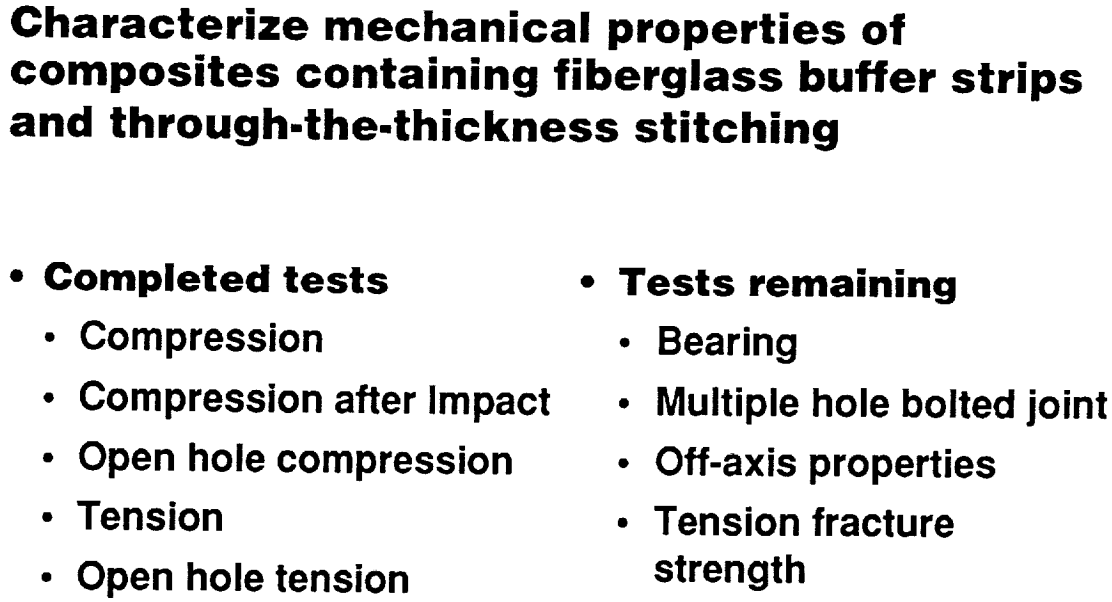

Figure 3

MATERIALS EVALUATED

The laminates used in this investigation were fabricated with a 3K AS4 uniweave fabric with integrally woven 0.5-inch wide S-2 fiberglass buffer strips as shown in figure 4(a). Results in reference 1 showed that the S-glass buffer strip material had the highest tension fracture strength. A photograph of the fabric is shown in figure 4(b). Three different buffer strip spacings were selected, as listed in figure 4(a). Fabric with buffer strips on 2 1/2-inch centers was tested in reference 2 and was chosen for the 0° buffer strip laminates in this study. The 2 1/2-inch buffer strip spacing was also used for the laminates with unaligned buffer strips in all plies. Buffer strips spaced at both 2 3/4-inches and 3 7/8-inches were used to make the quasi-isotropic laminate with aligned buffer strips in all plies shown in figure 4(a). The 2 3/4-inch buffer strip fabric was used for the 0° and 90° plies; the buffer strips form the two sides of a right triangle. The 3 7/8-inch buffer strip fabric was used for the +45° and -45° plies; the buffer strips form the hypotenuse of this right triangle, resulting in a uniform pattern of intersecting buffer strips. The buffer strip uniweave fabric layers for all configurations were stacked in a quasi-isotropic orientation $[+45°/0°/-45°/90°]_{ns}$ and then stitched with S-2 glass (1250 yd/lb) thread. Both stitched and unstitched preforms were then resin transfer molded using BP E905L resin. Stitching and processing parameters will be discussed subsequently.

- 3K AS4 uniweave carbon fabric
- Integrally woven 1/2" wide S-2 glass strips
- Glass buffer strip spacing
  - 2 1/2 in. centers
  - 2 3/4 in. centers
  - 3 7/8 in. centers
- Fabric layers stacked in $[+45/0/-45/90]_{ns}$ orientation
- Stitched and unstitched preforms
- Stitching thread S-2 glass 1250 yd/lb
- Resin transfer molded using BP E905L resin

Aligned buffer strips

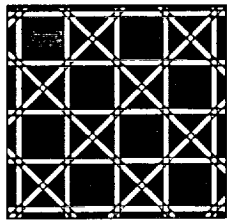

(a)

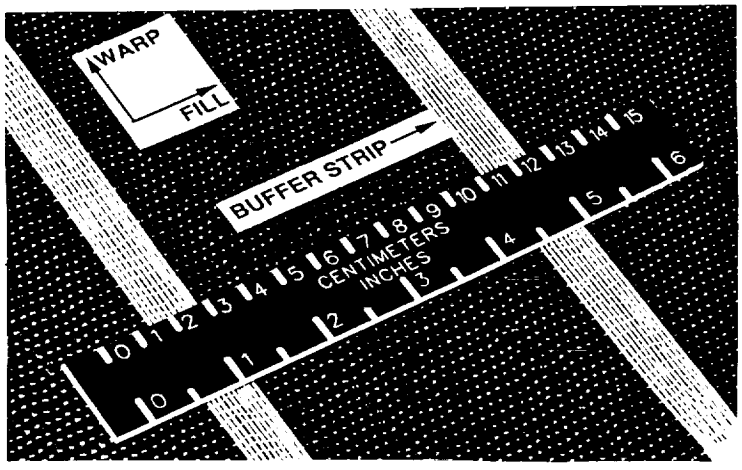

(b)

Figure 4

BUFFER STRIP CONFIGURATIONS

Figure 5 shows the three buffer strip configurations described earlier. All test panels were quasi-isotropic laminates. A series of unstitched, 16-ply laminates of each configuration were tested in tension to establish baseline properties and for comparison to results reported in reference 2. Additionally, both stitched and unstitched 40-ply laminates of each configuration were tested to evaluate tension and compression properties, as well as open-hole properties of these materials. Laminates with 0° buffer plies contained 5% glass by volume and were 2% heavier than uniweave. The laminates with aligned buffer strips in all plies added 15% glass by volume and had a weight penalty of 5.5%, whereas the laminates with unaligned buffer strips in all plies contained 20% glass by volume and were 7% heavier than plain uniweave.

Quasi-isotropic laminates

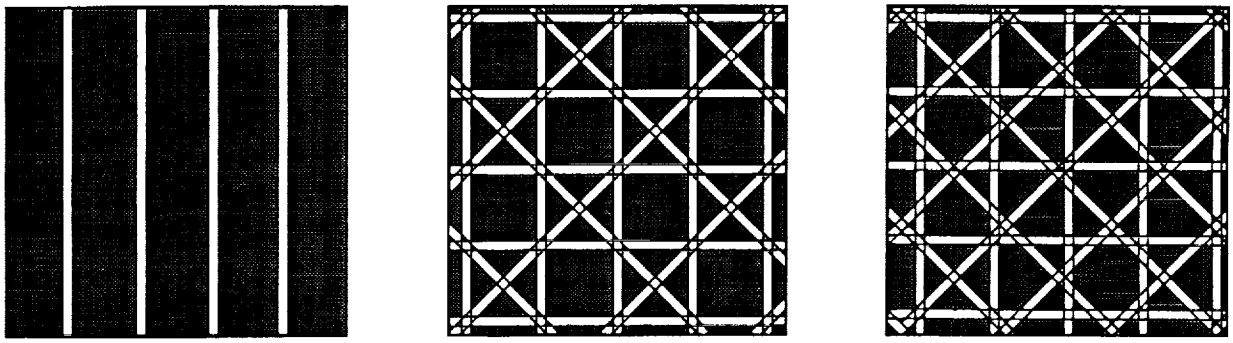

0° buffer plies
Stitched and Unstitched
5% glass by volume
(2% heavier than uniweave)

All buffer plies aligned
Stitched and Unstitched
15% glass by volume
(5.5% heavier)

All buffer plies unaligned
Stitched and Unstitched
20% glass by volume
(7% heavier)

Figure 5

FABRICATION OF STITCHED BUFFER STRIP TEST PANELS

The fabrication process for the buffer strip laminates is shown in figure 6. Single plies of the dry, plain uniweave and buffer strip uniweave fabrics were cut and stacked in $[+45°/0°/-45°/90°]_{2S}$ orientations to form 16-ply quasi-isotropic laminates and in $[+45°/0°/-45°/90°]_{5S}$ orientations to form 40-ply quasi-isotropic laminates. All three configurations shown in figure 5 were assembled in this manner. The 40-ply stacks were then stitched with a modified lock stitch using S-2 glass (1250 yd/lb) as the needle thread and 200 denier Kevlar 29 as the bobbin thread. The stitch row spacing was 3/16-inch and the stitch density was eight penetrations per inch. Both stitched and unstitched preforms were then resin transfer molded using a pressure injection process with BP E905L resin. The mold cavity depth was the same for all laminates of each thickness, resulting in 60% in-plane fibers for the 16-ply laminates and 56% in-plane fibers for the 40-ply laminates.

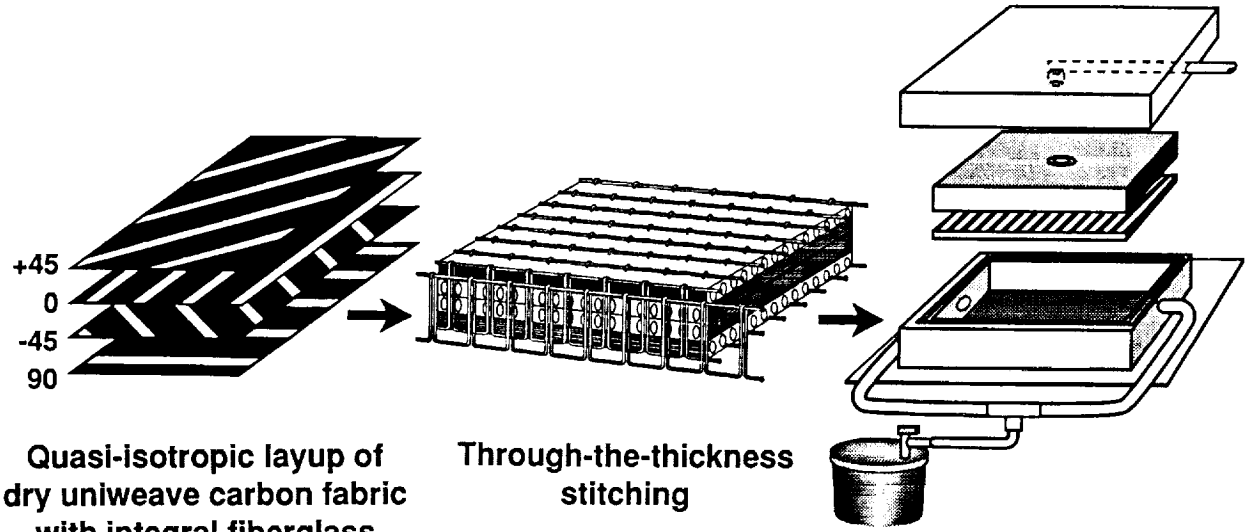

Figure 6

C-SCAN OF CARBON/EPOXY COMPOSITE CONTAINING ALIGNED FIBERGLASS BUFFER STRIPS

Figure 7 shows an ultrasonic C-scan of a typical composite panel with aligned glass buffer strips. The white region near the center of the panel is a resin-poor (dry) area where resin did not fully saturate the preform during resin transfer molding. Such areas were seen in most of the buffer strip panels. The uniform cross-hatch pattern in the C-scan indicates good alignment of the glass buffer strips through the thickness of the laminate. In general, the C-scans were an excellent tool in assessing the overall quality of the buffer strip laminates.

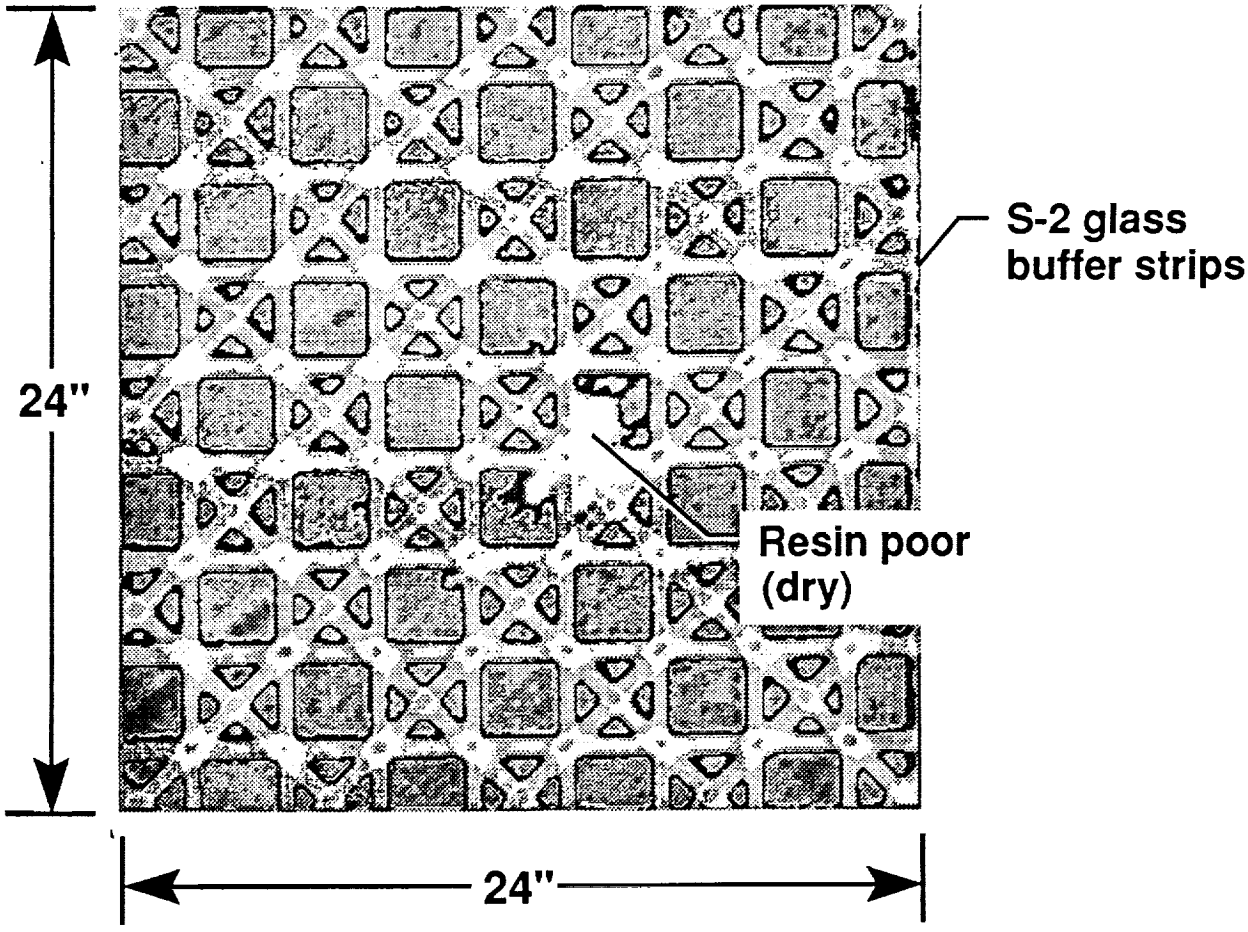

Figure 7

PHOTOMICROGRAPH OF CARBON/EPOXY COMPOSITE CONTAINING GLASS BUFFER STRIPS

Figure 8 shows a photomicrograph of a typical 40-ply, quasi-isotropic composite laminate containing aligned glass buffer strips in all plies. The carbon fibers appear white in the figure; the fiberglass fibers appear dark gray. The overall laminate thickness is 0.244 inch, which corresponds to a ply thickness of 0.006 inch. Fiber volume fraction was determined by acid digestion and was measured at 56%. Microcracks can be seen in the lower (outer) three plies of the laminate. Microcracks were also seen around stitches in the stitched buffer strip laminates. The microcracking is caused by residual thermal stresses that occur during cool-down of the laminate after the resin is cured.

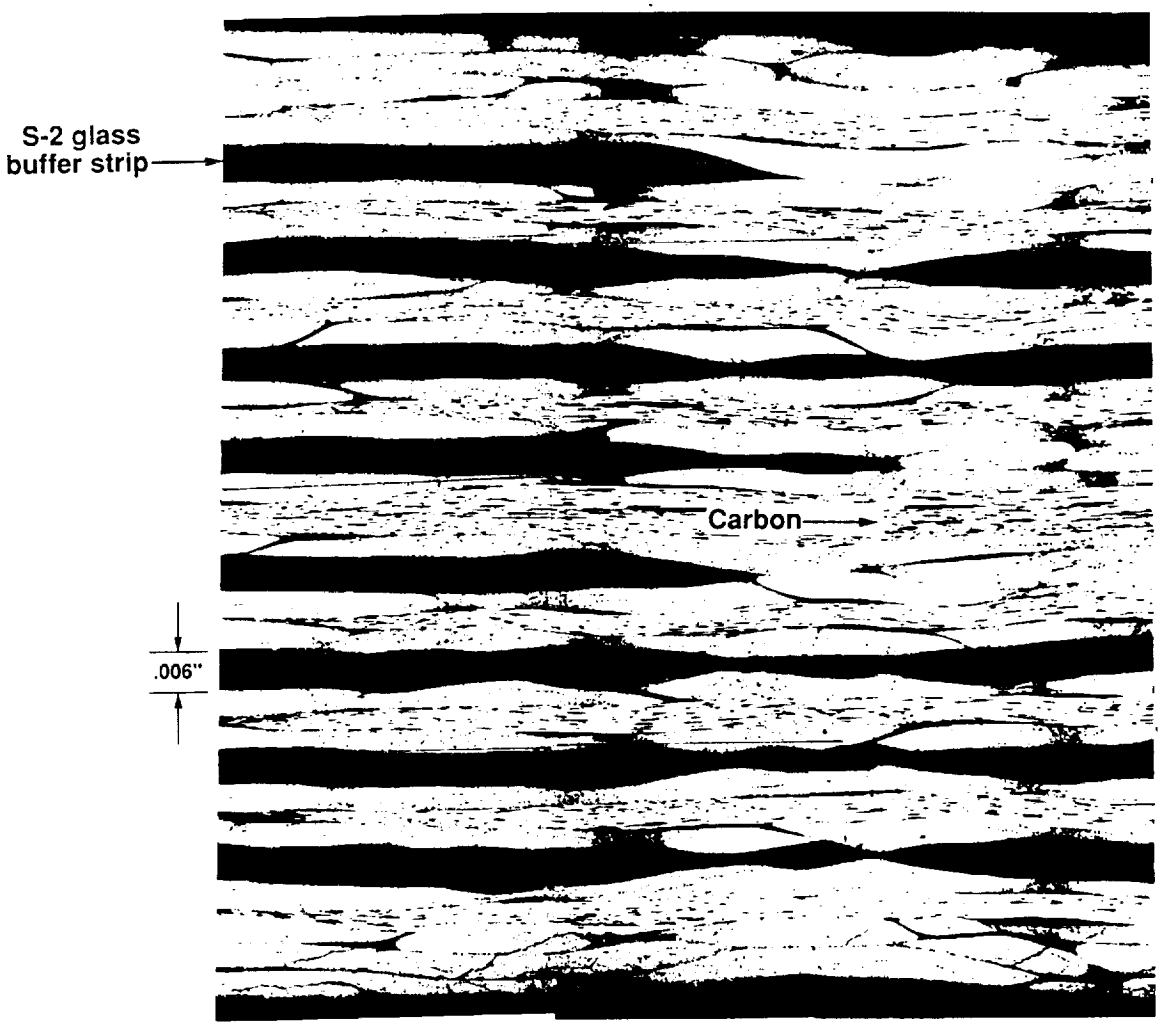

Figure 8

TEST SPECIMENS

Test specimen geometries are shown in figure 9. All specimens were untabbed. The 1.75-inch by 1.5-inch short block compression specimen is a NASA Langley configuration suitable for tests of angle ply laminates. A 10-inch by 1-inch specimen was used for the tension tests. The open-hole tension and open-hole compression specimens had 0.25-inch holes were 10 inches long and 1.5 inches and 3 inches wide, respectively. The compression-after-impact (CAI) specimen was 6 inches by 4 inches as recommended in reference 4. The CAI specimens were drop-weight impacted at 1500 inch-pounds/inch impact energy with a ten pound weight and 0.5-inch spherical impactor.

The short block compression, open-hole compression and CAI specimens were end-clamped to prevent brooming and were tested to failure at 0.05 inch/minute in a 120-kip hydraulic test machine. The open-hole compression and CAI fixtures also had knife-edge side supports to inhibit specimen buckling. The tension and open-hole tension specimens were end-gripped in a 50-kip hydraulic test machine and also loaded to failure at 0.05 inch/minute. Load, strain and displacement were recorded continuously for all tests using an IBM PC-based data acquisition system.

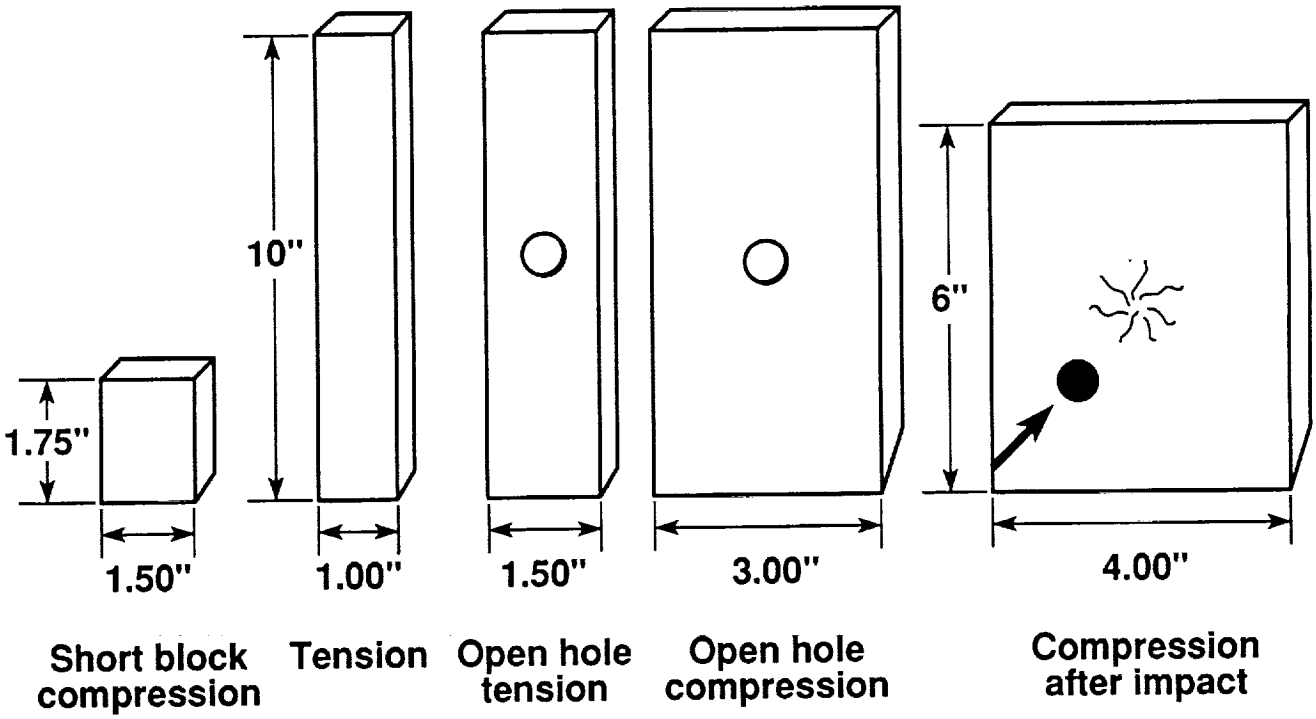

Figure 9

TENSION PROPERTIES OF UNSTITCHED COMPOSITES CONTAINING GLASS BUFFER STRIPS

Strength and stiffness data for 16-ply, quasi-isotropic, unstitched composites containing glass buffer strips are shown in figure 10. The data shown on the left are results reported in reference 2 for T300/S-1014 uniweave buffer strip fabric that was resin transfer molded with 5208 resin. The results shown on the right are for AS4/S-2 buffer strip uniweave fabric laminates that were resin transfer molded with BP E905L resin for this investigation. Each bar on the right represents the average of ten replicates, and the nominal fiber volume fraction was 60%. The AS4/S-2 laminates are considerably stronger and somewhat stiffer than the T300/S-1014 laminates. One reason for these differences is that the AS4/S-2 uniweave fabric was woven with fewer glass fill yarns and thus the carbon warp fibers had less crimp than the T300/S-1014 uniweave fabric. Also, reference 1 did not report the fiber volume fraction of the T300/S-1014 laminates. A lower fiber volume fraction might also explain the lower strengths and stiffnesses for the T300/S-1014 laminates.

The AS4/S-2 laminates with no buffer strips (plain uniweave) had a tension strength of 98 ksi. Adding buffer strips in the 0° plies (5% glass by volume) resulted in a 15% reduction in strength and 13% reduction in modulus. Adding buffer strips in all plies (20% glass by volume) resulted in a 26% reduction in strength and a 17% reduction in modulus.

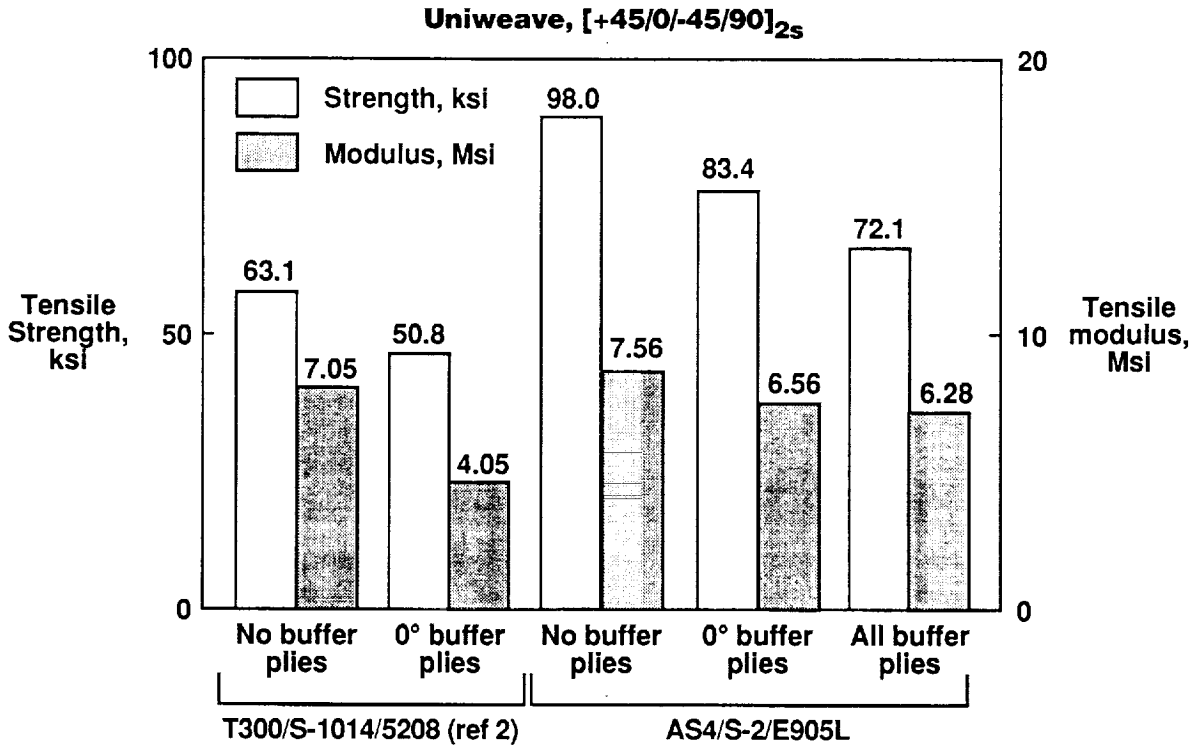

Figure 10

TENSION AND OPEN-HOLE TENSION STRENGTH OF CARBON/EPOXY COMPOSITES CONTAINING GLASS BUFFER STRIPS AND STITCHING

Tension strength and stiffness data for 40-ply quasi-isotropic composites containing glass buffer strips and stitching are shown in figures 11(a) and 11(b). Each bar represents the average of three replicates with the range of data shown. Figure 11(a) shows the tension and open-hole tension strengths compared to a 50 ksi reference value for AS4/3501-6 tape. Except for the stitched laminate with buffer strips in the 0° plies, open-hole tension strengths for all laminates fell below the 50 ksi reference value. The results show that laminates with buffer strips have lower open-hole tension strengths than the reference value, and that the open-hole strengths are relatively unaffected by stitching. The results show no strength benefit from careful buffer strip placement, or from having buffer strips in all plies. This is not in agreement with reference 2 which showed higher strengths for laminates with buffer strips in all plies. The results also show a high degree of variability in the strengths. There are several possible explanations for the variability and discrepancy with reference 2. First, the specimens were cut randomly from the panels with no regard to the amount or location of buffer strips within the specimen. Additionally, the hole location with respect to the buffer strip location was random and not consistent from specimen to specimen. Moreover, the hole size and specimen width may not have been large enough to adequately characterize the open-hole properties of the buffer strip material. These issues will be investigated in future work.

Figure 11(b) shows the tension modulus of composites containing glass buffer strips. The results show that adding more glass by means of buffer strips and/or stitching does not affect the stiffness properties of glass buffer strip/carbon fiber composites, as might be expected due to the lower stiffness of the glass fibers. These results agree with those published in references 1 and 2 for laminates without stitching.

(Figures 11a and 11b are shown on the next page.)

(a)

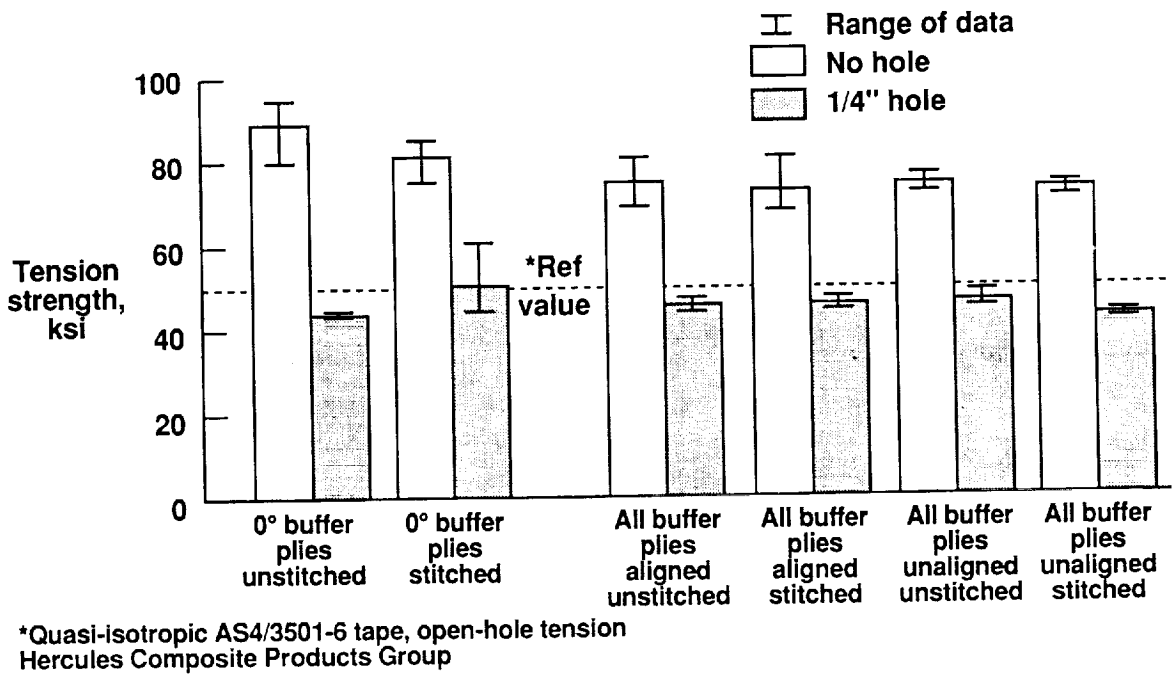

*Quasi-isotropic AS4/3501-6 tape, open-hole tension
Hercules Composite Products Group

(b)

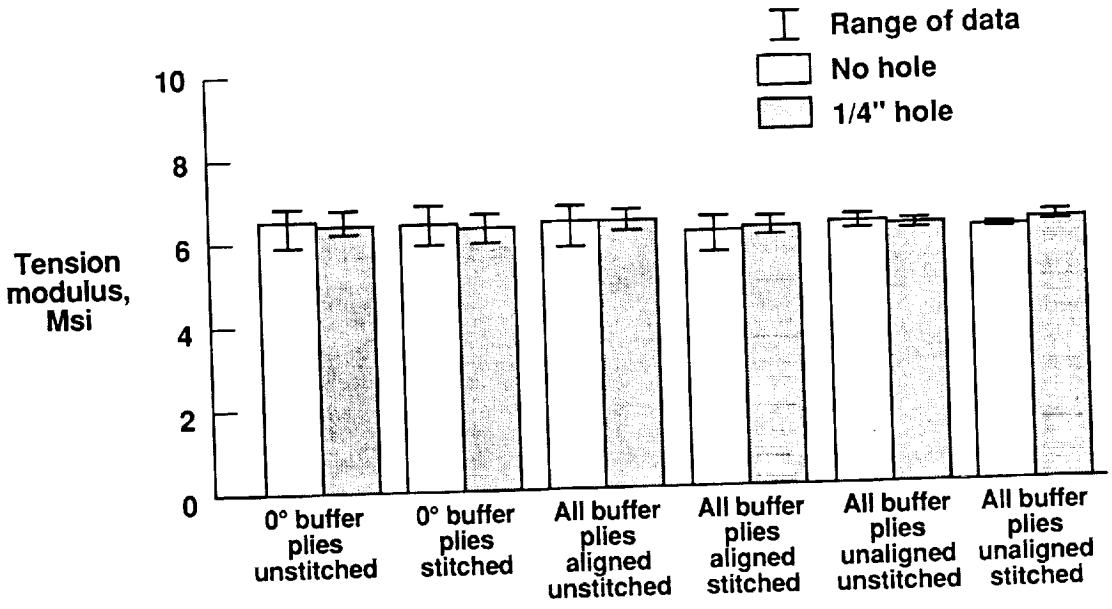

Figure 11

COMPRESSION AND OPEN-HOLE COMPRESSION STRENGTH OF CARBON/EPOXY COMPOSITES CONTAINING GLASS BUFFER STRIPS AND STITCHING

Compression strength and stiffness data for 40-ply quasi-isotropic composites containing glass buffer strips and stitching are shown in figures 12(a) and 12(b). Each bar represents the average of three replicates with the range of data shown. Figure 12(a) shows the compression and open-hole compression strengths compared to a 42 ksi reference value (Boeing Material Specification, BMS-8-276). The highest compression strength was 89 ksi for the unstitched laminates with 0° buffer plies. Open-hole compression strengths for all laminates exceeded the 42 ksi reference value. The results show that buffer strip laminates have acceptable open-hole compression strength and that the open-hole strengths are unaffected by stitching. The open-hole compression results show no strength benefit from careful buffer strip placement, or from having buffer strips in all plies. The results show the same high degree of variability as seen in the tension data. Specimen geometry, notch location and buffer strip location are, again, factors contributing to the scatter in the data and will be investigated in future work.

Figure 12(b) shows the compression modulus of composites containing glass buffer strips. As with the tension results, adding more glass by means of buffer strips and/or stitching does not degrade the compressive stiffness properties of composites.

(Figures 12a and 12b are shown on the next page.)

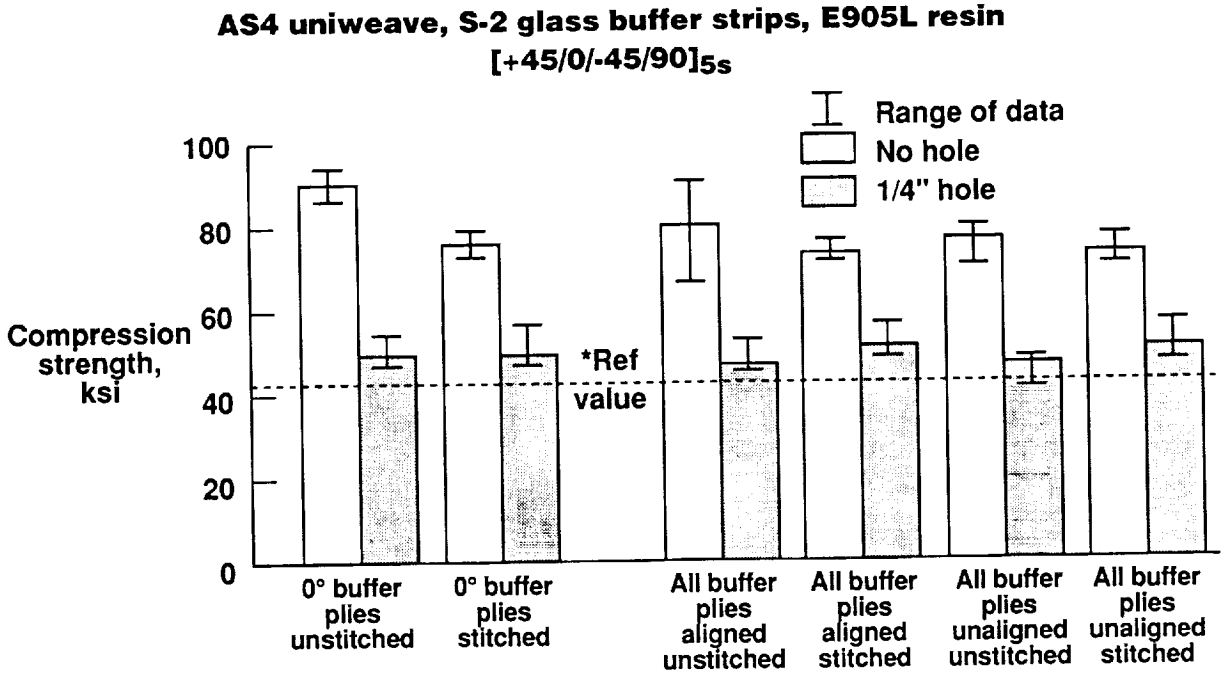

* Boeing material specification, BMS-8-276

(a)

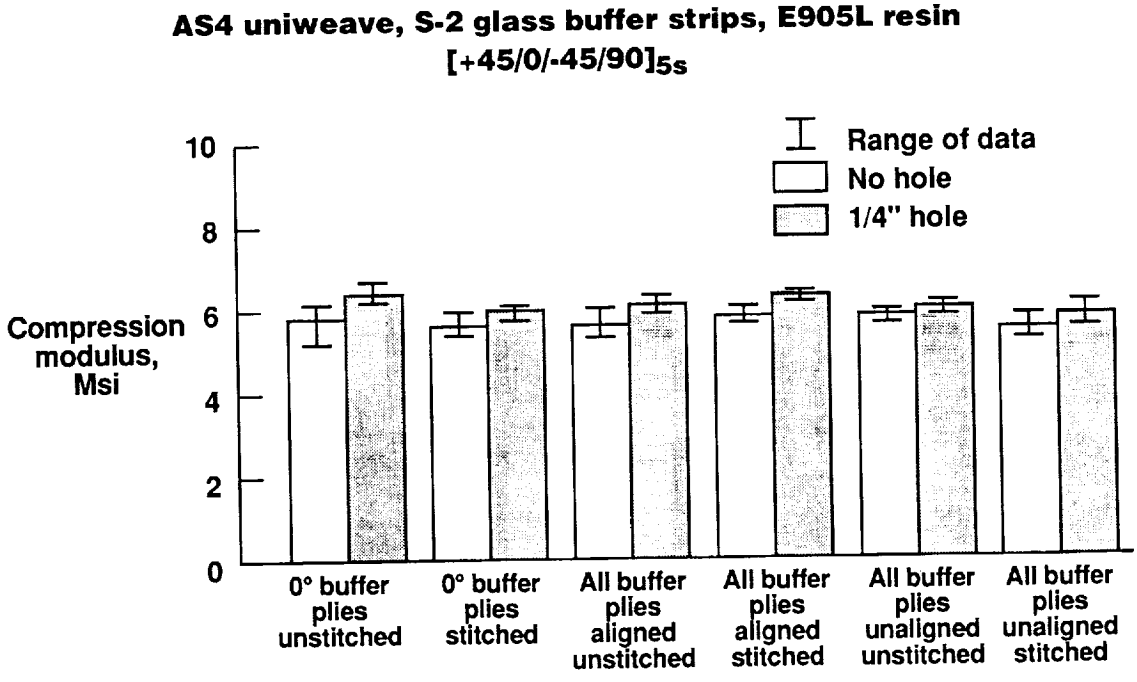

(b)

Figure 12

COMPRESSION AND COMPRESSION AFTER IMPACT STRENGTH OF CARBON/EPOXY COMPOSITES CONTAINING GLASS BUFFER STRIPS AND STITCHING

Compression and compression-after-impact (CAI) strengths for 40-ply quasi-isotropic composites containing glass buffer strips and stitching are shown in figure 13. Each bar represents the average of three replicates with the range of data shown. Specimen dimensions are 6 inches by 4 inches and were drop weight impacted at an energy level of 1500 inch-pounds/inch, as recommended by reference 4. The CAI strengths are compared to a 40 ksi target value for acceptable damage tolerance reported in Boeing Material Specification BMS-8-276. All of the unstitched laminates had a CAI strength of about 20 ksi, which is typical for tape or woven composites without stitching. All of the stitched laminates met the 40 ksi target value and demonstrated acceptable damage tolerance. The compression strengths show the same degree of variability as seen in the tension specimens, but the CAI results show very little scatter, for both the stitched and unstitched laminates. Additionally, the results show no strength benefit from careful buffer strip alignment or from having buffer strips in all plies, as was the case for the open-hole tension and open-hole compression specimens, described earlier.

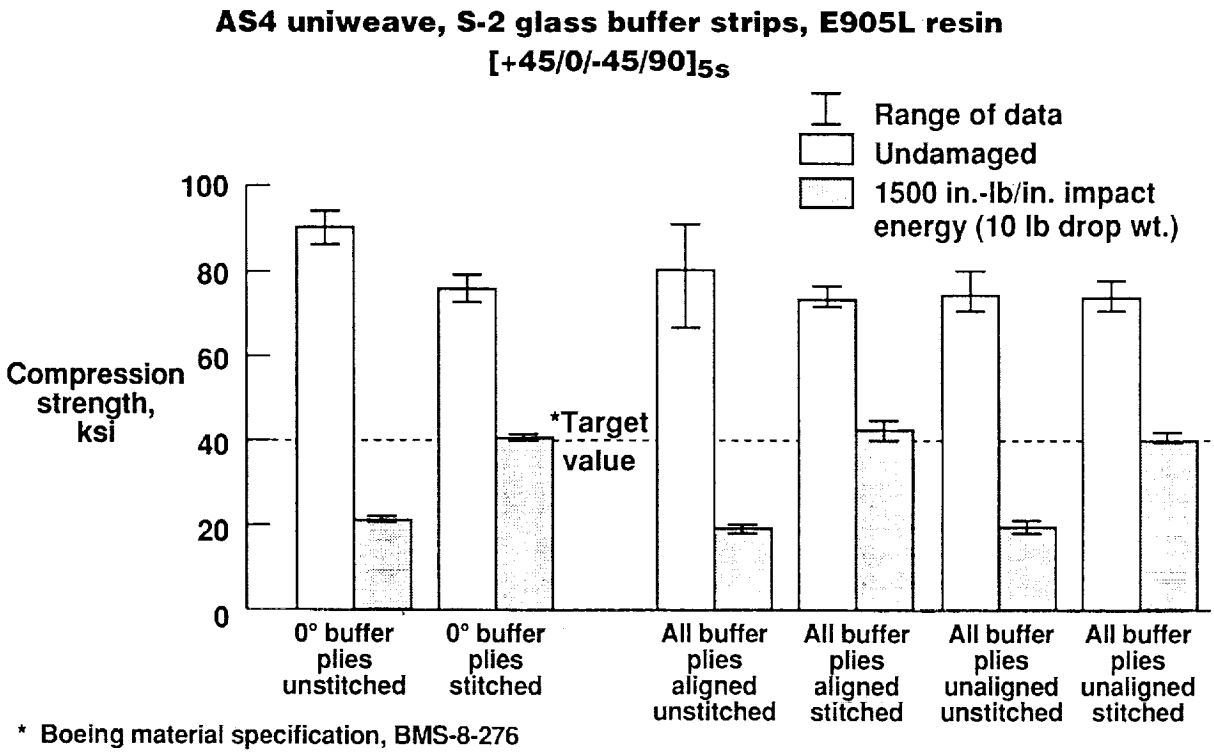

Figure 13

INTERIM FINDINGS

When this study was started, there was concern that buffer strips would degrade the compression after impact strength of composites; however, as outlined in Figure 14, the results show that composites containing glass buffer strips and stitching have good compression damage tolerance. Additionally, buffer strip laminates have acceptable open-hole compression strengths, and the open-hole strengths are unaffected by stitching. The results also show that composites with buffer strips have marginal open-hole tension strengths, and the open-hole strengths are unaffected by stitching. Finally, the results show no strength benefit from careful buffer strip alignment and no performance benefit from having buffer strips in all plies.

- **Buffer strip laminates with stitching have good damage tolerance.**
- **Buffer strip laminates have acceptable open-hole compression strength. Strengths are unaffected by stitching.**
- **Laminates with buffer strips have marginal open-hole tension strengths. Strengths are unaffected by stitching.**
- **Data reveals no strength benefits from careful buffer strip alignment and no performance benefit from having buffer strips in all plies.**

Figure 14

FUTURE WORK

Figure 15 outlines the tasks remaining in the evaluation of stitched composites containing glass buffer strips. The first task is to assess the tension fracture strength of laminates containing buffer strips and stitching and will involve performing tension tests with center slits to determine if stitching degrades the crack arresting capability of buffer strips. Secondly, tests will be performed to determine the effect of hole and buffer strip location on laminate tension properties. Holes will be placed at various locations to determine if there is an effect on laminate properties. Third, tests will be performed to assess the bearing strength and bolted joint strength of stitched composites containing glass buffer strips. Finally, tests will be performed on laminates containing 0° buffer strips, with the loads applied transversely to the strips to evaluate the effect of off-axis loads on laminate strength.

- **Assess tension fracture strength of laminates with buffer strips and stitching**
- **Determine effect of hole and buffer strip location on laminate tension properties**
- **Assess bearing strength and multiple hole bolted joint strength of stitched composites containing glass buffer strips**
- **Assess effect of off-axis loads on strength of laminates with 0° buffer strips**

Figure 15

ACKNOWLEDGMENT

This paper describes work performed at NASA Langley Research Center under Work Order E020 of Contract NAS1-19000 and its release has the concurrence of the Technical Monitor, H. Benson Dexter.

REFERENCES

1. Poe, C. C., and Kennedy, J. M., "An Assessment of Buffer Strips for Improving Damage Tolerance of Composite Laminates", Journal of Com-posite Materials Supplement, vol. 14, 1980, pp. 57-70.

2. Kennedy, J. M., "Damage Tolerance of Woven Graphite/Epoxy Buffer Strip Panels", Journal of Composite Materials, vol. 25, Sept. 1991, pp.1218-1241.

3. Palmer, R. J., Dow, M. B., and Smith, D. L., "Development of Stitching Reinforcement for Transport Wing Panels", NASA CP 3104, Part 2, Oct. 29-Nov. 1, 1990, pp. 621-646.

4. SACMA Recommended Test Method for Compression-After-Impact Properties of Oriented Fiber-Resin Composites, SRM-2-88.

PROGRESS IN MANUFACTURING LARGE PRIMARY AIRCRAFT STRUCTURES USING THE STITCHING / RTM PROCESS

Alan Markus, Patrick Thrash, and Kim Rohwer
Douglas Aircraft Company

INTRODUCTION

The Douglas Aircraft/NASA Act contract has been focused over the past three years at developing a materials, manufacturing, and cost base for stitched/Resin Transfer Molded (RTM) composites. The goal of the program is to develop RTM and stitching technology to provide enabling technology for application of these materials in primary aircraft structure with a high degree of confidence. Presented in this paper will be the progress to date in the area of manufacturing and associated cost values of stitched/RTM composites.

Figure 1 below describes the stitched/RTM approach being developed at Douglas.

STITCHING CONCEPT

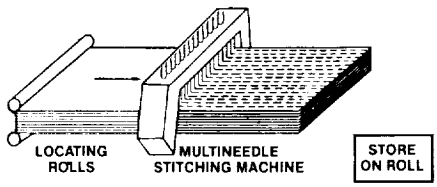

MULTI-NEEDLE STITCHING IS USED TO PROVIDE DAMAGE TOLERANCE TO WING SKINS

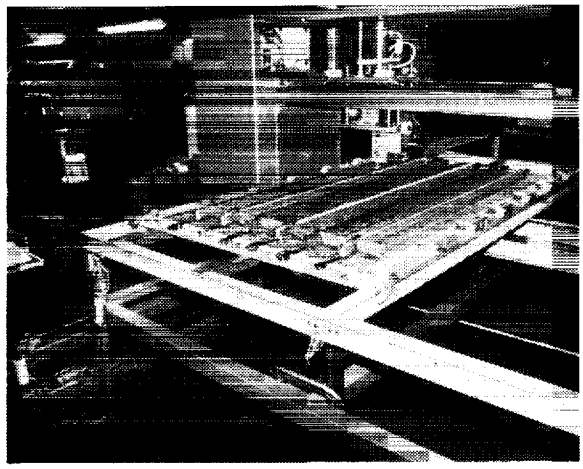

COMPUTER CONTROLLED SINGLE NEEDLE STITCHING IS USED TO PERFORM STITCHING ASSEMBLY OPERATIOINS

RTM FABRICATION METHODS

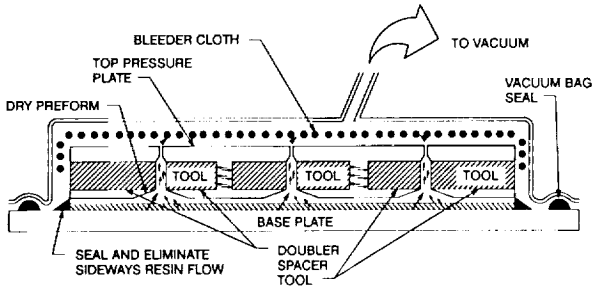

RESIN FILM INFUSION IS USED FOR WING COVER PANEL FABRICATION

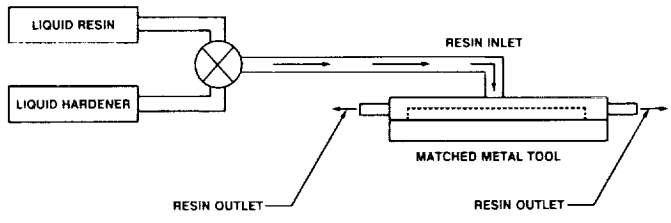

PRESSURE IMPREGNATION IS USED FOR FUSELAGE SHELL FABRICATION

Figure 1

Douglas Wing Structures

Over the course of the first two years of development, Douglas concentrated its efforts in two areas: 1.) wing development using resin film infusion with stitched preform and, 2.) fuselage development using pressure injection RTM with stitched preforms. Figures 2 through 5 cover the development in stitching, tooling, and processing for both the wing and fuselage over that two year period.

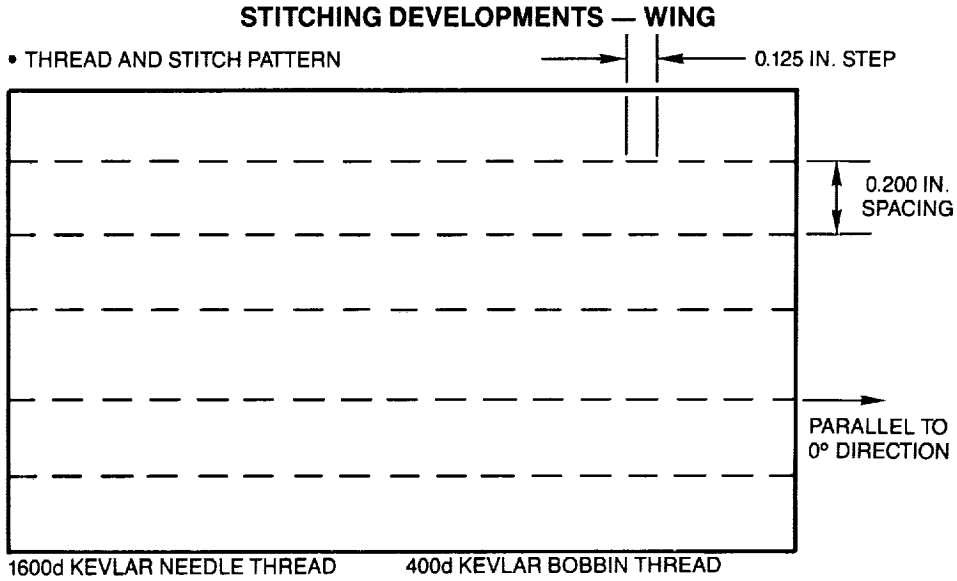

In the development period, stitching patterns and thread selections were based upon many tests and the capabilities of existing stitching machines. Figure 2 shows the stitching thread and pattern now used in wing preforms.

Figure 2

PREVIOUS DEVELOPMENTS

Douglas Wing Structure

DAC established the requirements necessary to make high quality carbon fiber preforms. Dimensional requirements for the preform were established for fabrication tool fit-up. To meet these requirements, specialized tooling was created for stitching the wing skin, stiffeners, and attaching the stiffeners to the skin (Figure 3).

- PREFORM QUALITY REQUIREMENTS

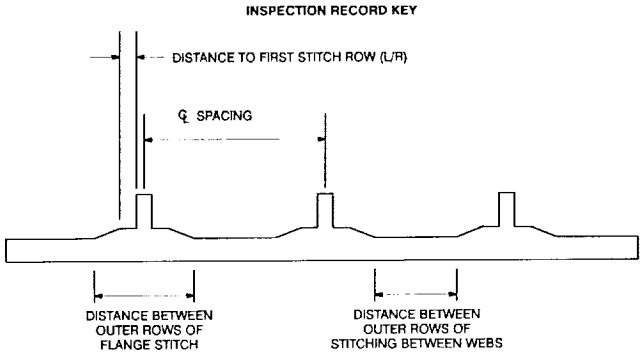

PROGRAM QUALITY REQUIREMENTS

ITEM 1
S/N ___ DATE _____
RIGHT STIFFENER WAS 8 ROWS OF STITCHING
STITCHING SPACE – 0.1875 IN
STITCHING STEP AVERAGE – 7/IN
P THRASH

CHARACTERISTIC	VALUE	LEFT WEB	CENTER WEB	RIGHT WEB	LEFT	RIGHT
℄ - ℄ SPACING BETWEEN STIFFENERS	7.0	–	–	–		
DISTANCE TO 1st STITCH ROW	0.37/ 0.44	L R	L R	L R	–	–
DISTANCE BETWEEN OUTER ROWS OF FLANGE STITCH	2.68/ 2.81				–	–
DISTANCE BETWEEN OUTER ROWS OF STITCHING BETWEEN WEBS	4.19/ 4.32	–	–	–		

STITCHING DEVELOPMENTS — WING

- SEWING MACHINE DEVELOPMENT/ TOOLING REQUIREMENTS

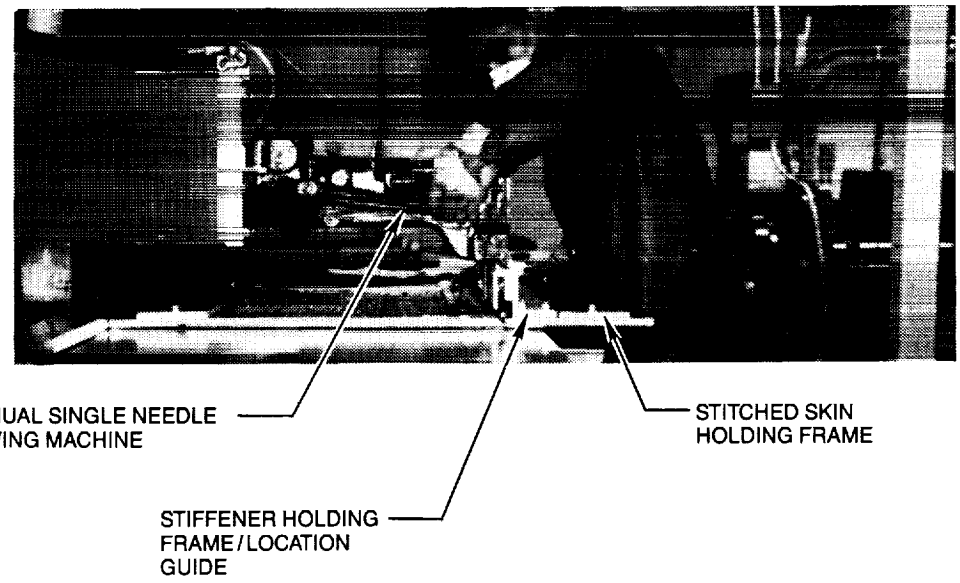

Figure 3

PREVIOUS DEVELOPMENTS

Douglas Wing Structures

Tooling for wing panels was designed to achieve a major cost savings benefit by RTM of a preform in which the rib clips and stiffeners are stitched to the skin. This tooling, Figure 4, utilizes a graphite/epoxy upper tooling plate to hold the matched metal aluminum details in place during the RTM autoclave cure process. To help insure the thermal compatibility of the upper tool with the lower tool, a graphite/epoxy lower plate was also used.

FABRICATION DEVELOPMENTS — WING

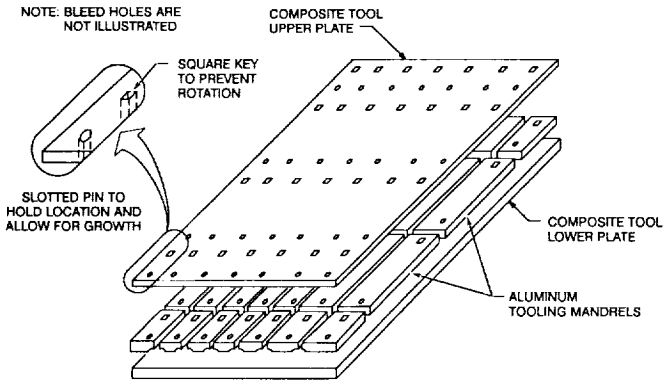

Figure 4

PROCESSING DEVELOPMENTS

Douglas Wing Structures

In developing a single step resin infiltration and curing cycle, the subcontractor team of Virginia Polytechnic Institute and William and Mary College played a critical role. Findings from their work established that preform thermal equilibrium and application of initial pressure are essential to a single step cure cycle. Figure 5 below, shows an extended cure cycle based upon their work versus the earlier standard created to achieve thermal equilibrium.

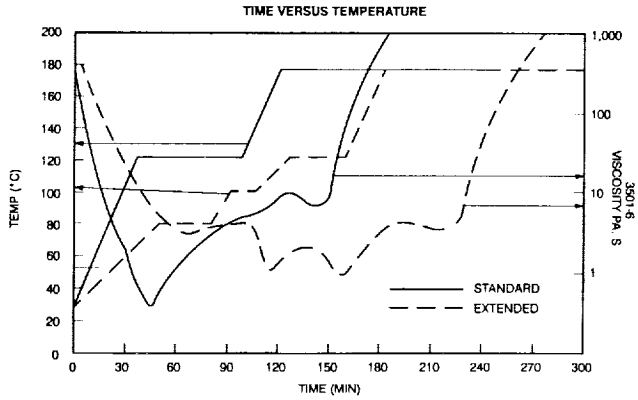

MULTIDWELL CURE CYCLE DEVELOPED TO ALLOW PREFORM THERMAL EQUILIBRIUM DURING INFILTRATION

Figure 5

Douglas Fuselage Structures

As in the case of the wing, many test results were used to establish both stitch parameters and material selections for the fuselage. Below are the stitching parameters with preform quality requirements developed for the fuselage. In this concept, the fuselage skin preform is lightly stitched with nylon thread to facilitate handling whereas the longerons are stitched with heavy Kevlar thread in a dense pattern. The longeron flanges are stitched to the skin to complete the preform.

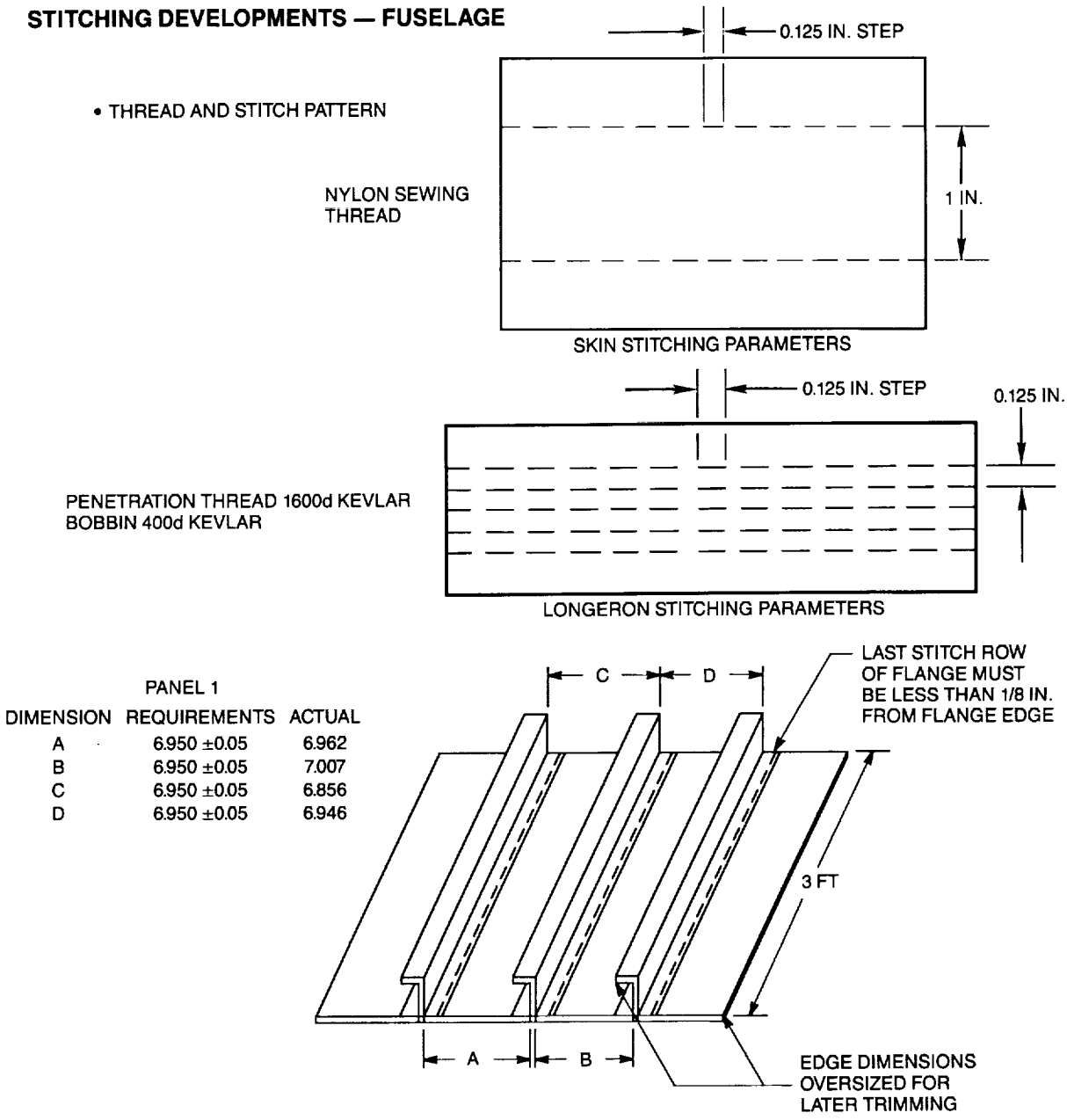

Figure 6

Douglas Fuselage Structures

To achieve the desired fiber loading in fuselage panels, the matched metal tool must be closed to stops. This requires approximately 48 psi compaction pressure. Preform fit to the final (net) size is critical to avoid edge path travel of the resin and excessive tolerance ($< \mp 0.01$) mismatches which cause non-uniform resin flow paths.

Edge path travel was a frequent problem in the tooling development. To avoid unwanted edge travel, a tooled edge or O-ring was devised and can be used to apply greater compaction along the edge of the part, thus forcing resin to stay within the preform. Figure 7 below, illustrates the tolerance range for uniform non-impeded resin flow and the tooling approach for eliminating edge path flow effects. In the curve below, the vertical line between 0.67 and 0.79 represents the area of normal or acceptable resin flow. Areas to either side of these lines represent areas of impeded resin flow.

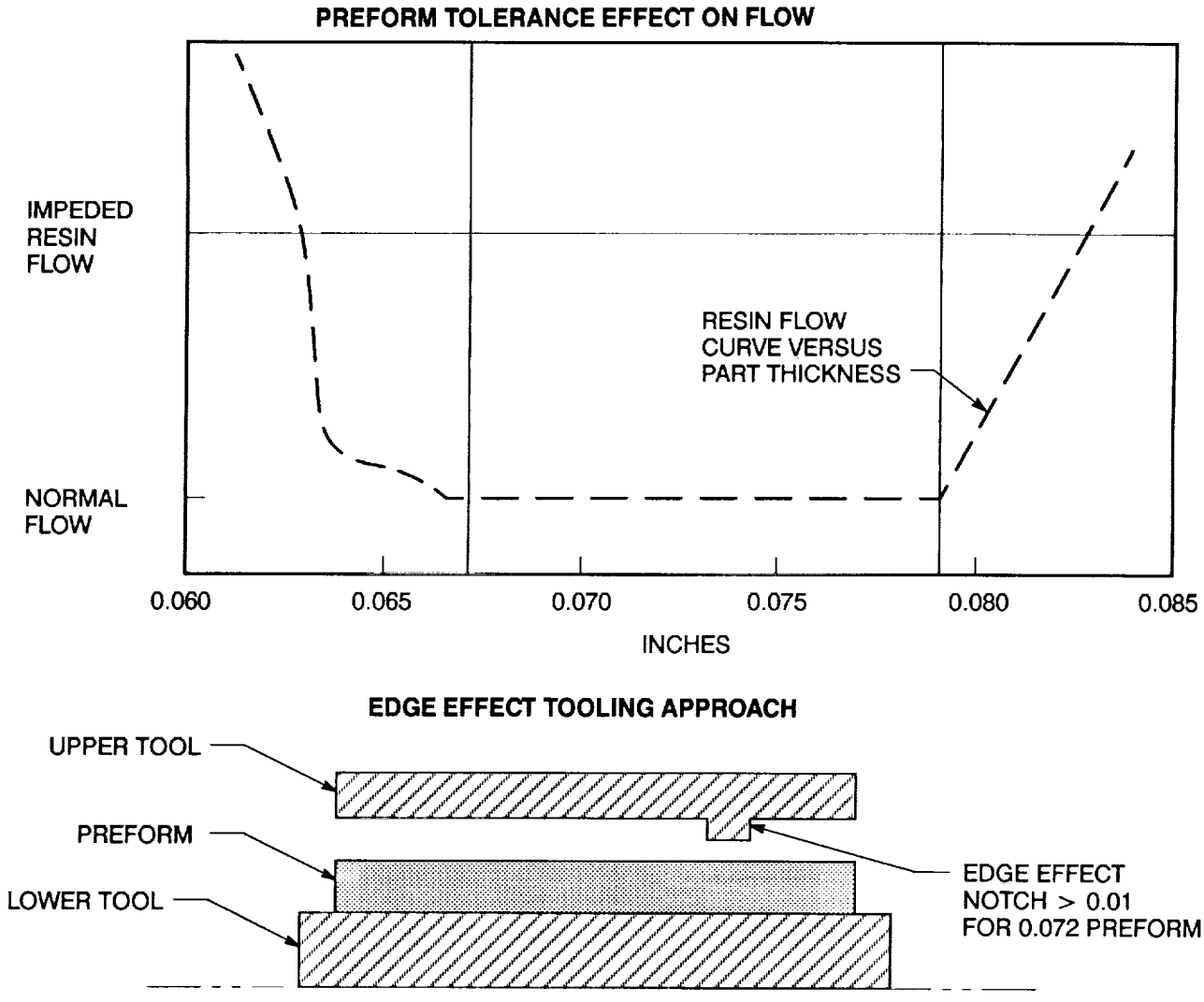

Figure 7

CURRENT STATUS

Douglas Wing - Stitching

Since the inception of this program, Douglas has been developing two sewing machines to stitch dry graphite wing preforms. These machines represent a first generation version of cost effective preform fabrication using a stitching process. Shown below in Figure 8 are the 128-needle sewing machine and a computer controlled single needle machine that are products of this development. Contractor for the machines is Pathe, Inc.

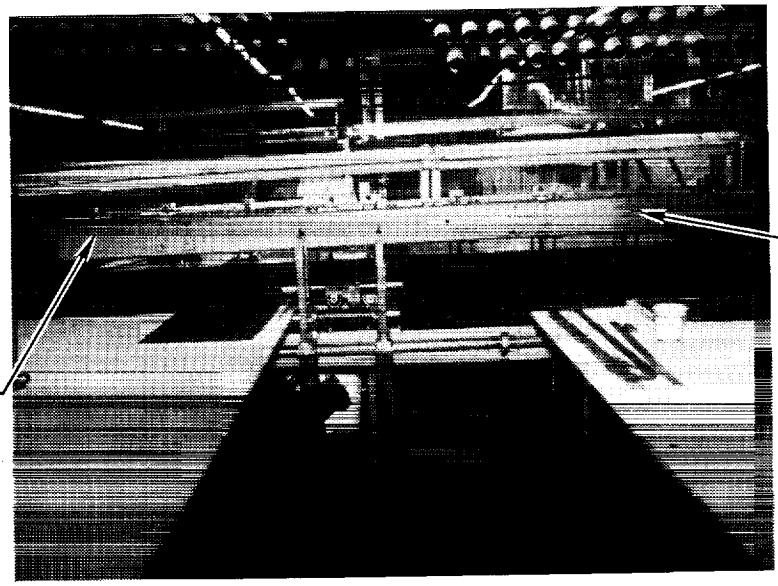

- The multi-needle machine made use of an existing 128-needle machine and was split into two machines: a right hand side to do the heavy density stitching and a left hand side to do the light density stitching.

- The single needle machine is a machine newly designed to Douglas specifications.

Figure 8

Douglas Wing - Stitching

The Douglas fabrication approach for stitching 4- by 6-foot stiffened wing skins is shown in Figures 9 through 13. As shown in Figure 11, the multi-needle (128-needle) machine is used for both light density 9-ply stack stabilization stitching and the heavy density damage tolerance stitching of the skin plank and stiffeners.

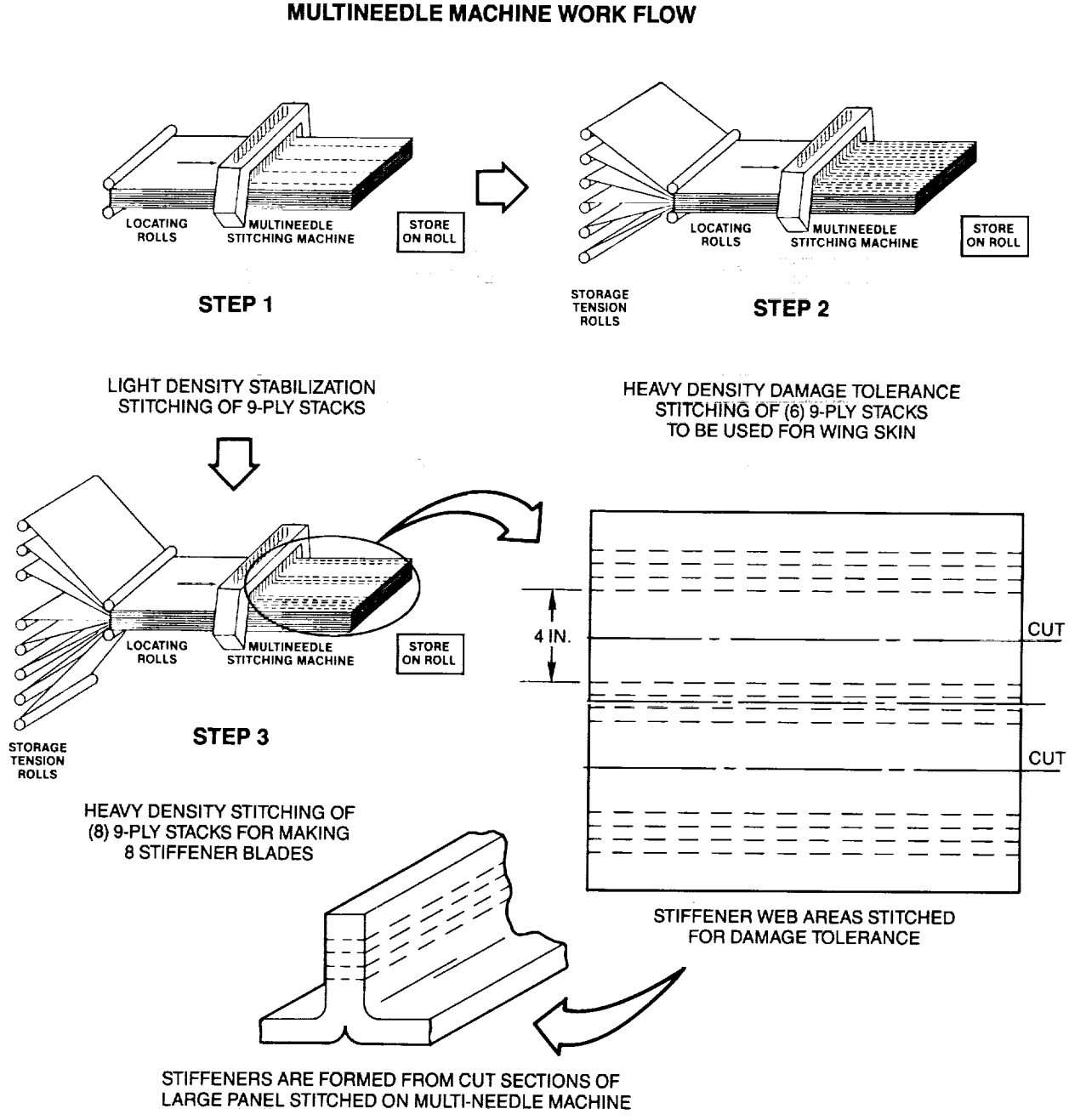

Figure 9

Douglas Wing - Stitching

The multi-needle machine (Figure 10) has been modified to perform the heavy and light density stitching. The left hand side is for heavy density stitching while the right hand side is for light density stitching. In this photo, the multi-needle machine is stitching a test specimen with 0.200-inch parallel row heavy density Kevlar stitching.

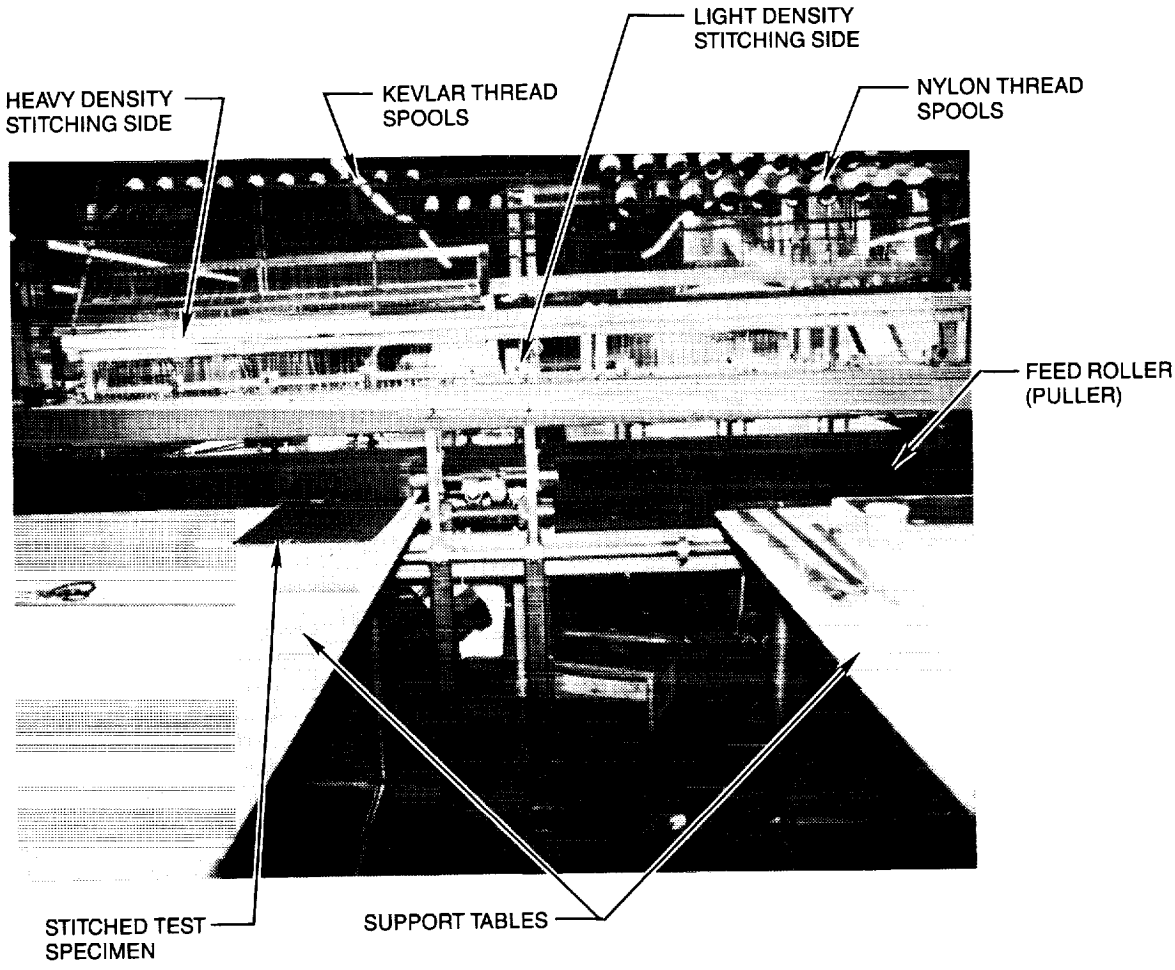

Figure 10

Douglas Wing - Stitching

Figure 11 shows the single needle computer controlled machine. This machine is used for high speed stitching of wing rib clips as well as all attachment or assembly stitching.

SINGLE NEEDLE COMPUTER CONTROLLED MACHINE

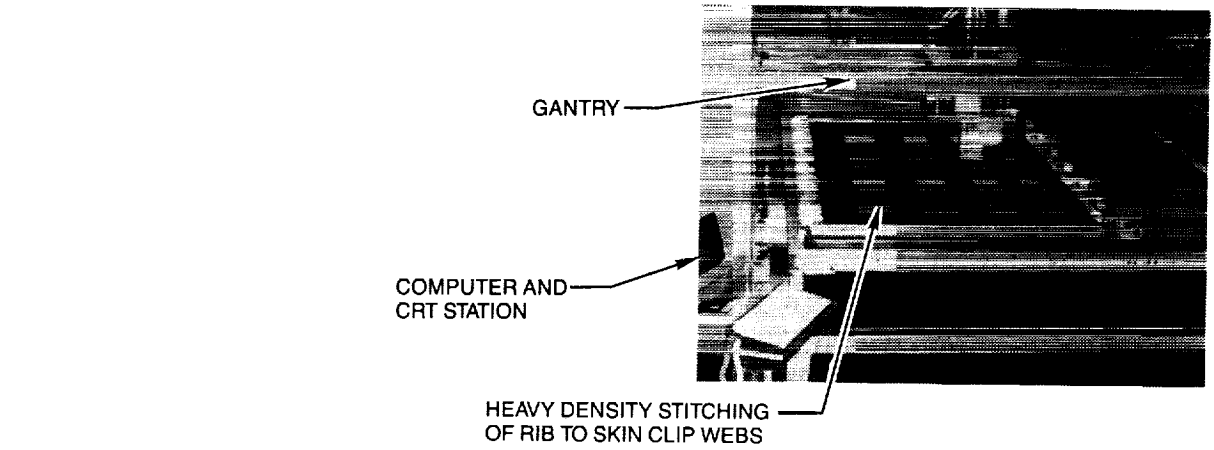

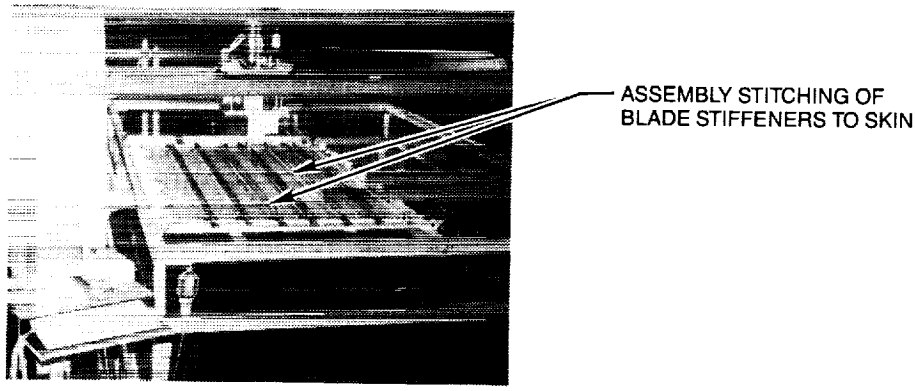

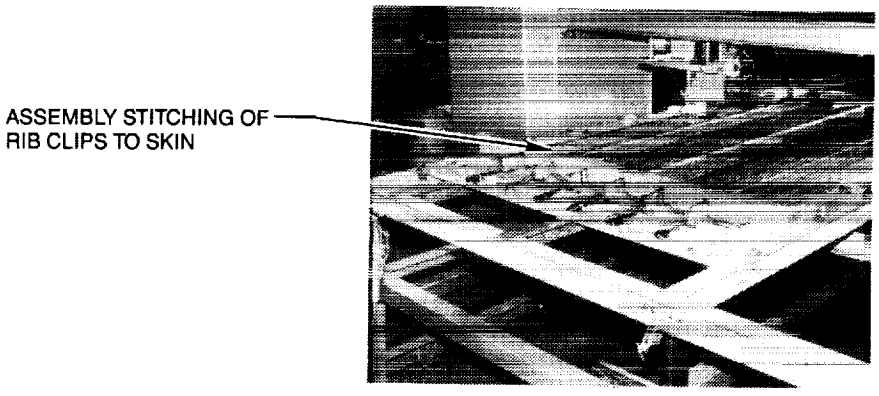

Figure 11

Douglas Wing - Stitching

Some of the steps involved in making stitched preforms for rib clips are shown in Figure 12. The computer controlled single needle machine is used to stitch patterns for the wing rib clips. Upon completion, rib clip patterns are cut from the stitched goods. Shown below is the stitched fabric from the single needle machine being cut into rib clips using a template. Also shown are the clips being placed into the rib/skin attachment location frame. Similar procedures are used to make panel stiffener preforms.

RIB-CLIP PATTERNS WITH TEMPLATE

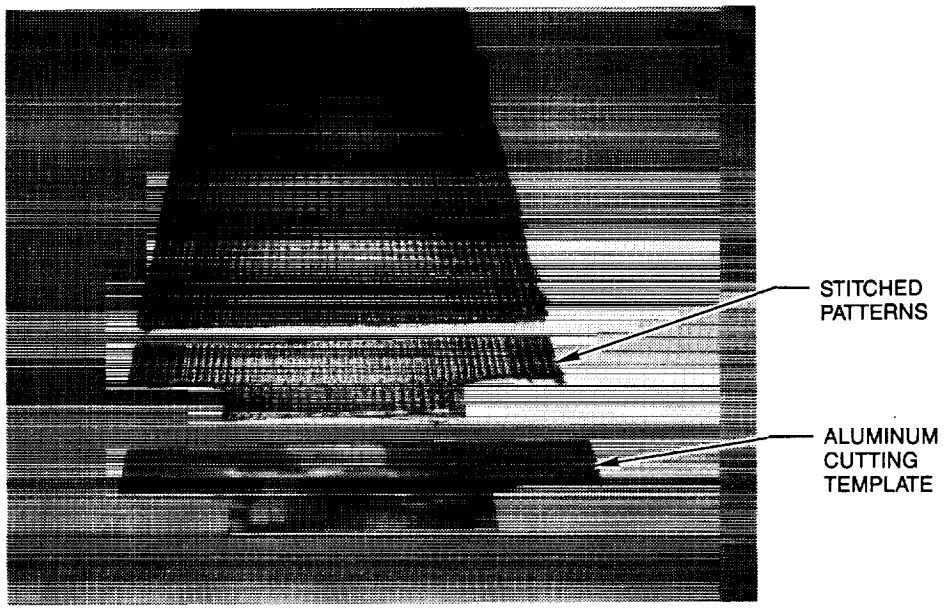

RIB/SKIN ATTACHMENT LOCATION FRAME

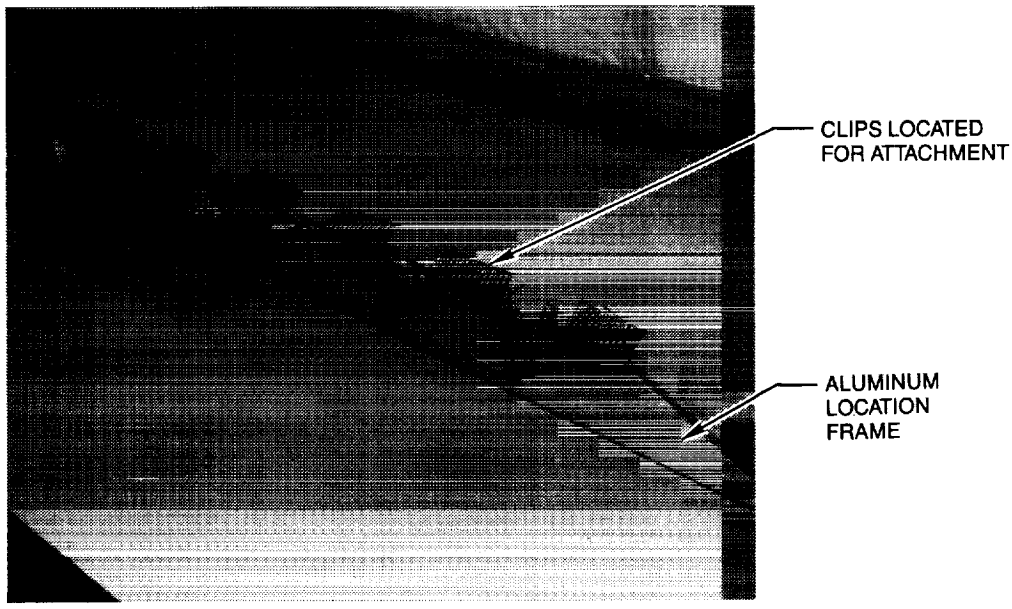

Figure 12

Douglas Wing - Stitching

Once all stiffeners and rib clip preforms have been fabricated, the computer controlled single needle machine is used to assemble the details into a stiffened wing preform. In a series of photos shown below, the single needle computer controlled machine is shown attaching stiffeners and rib clips to a 4- by 6-foot stitched wing skin.

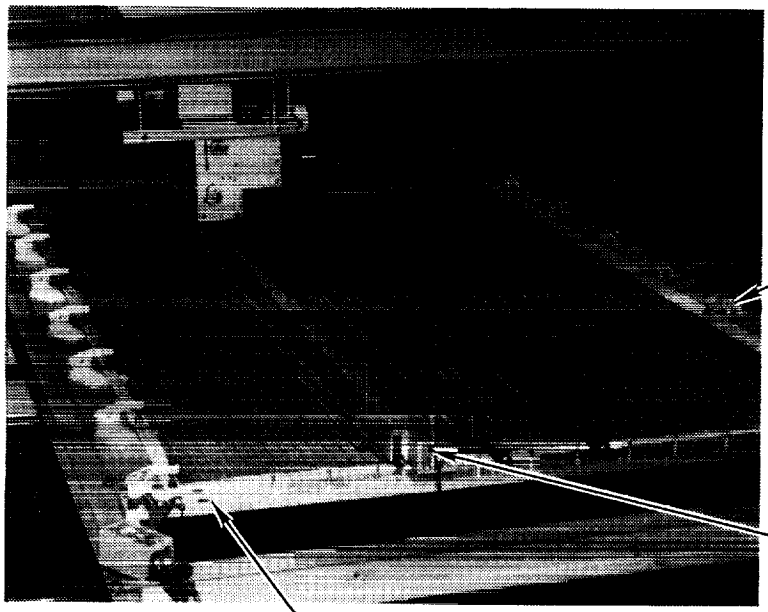

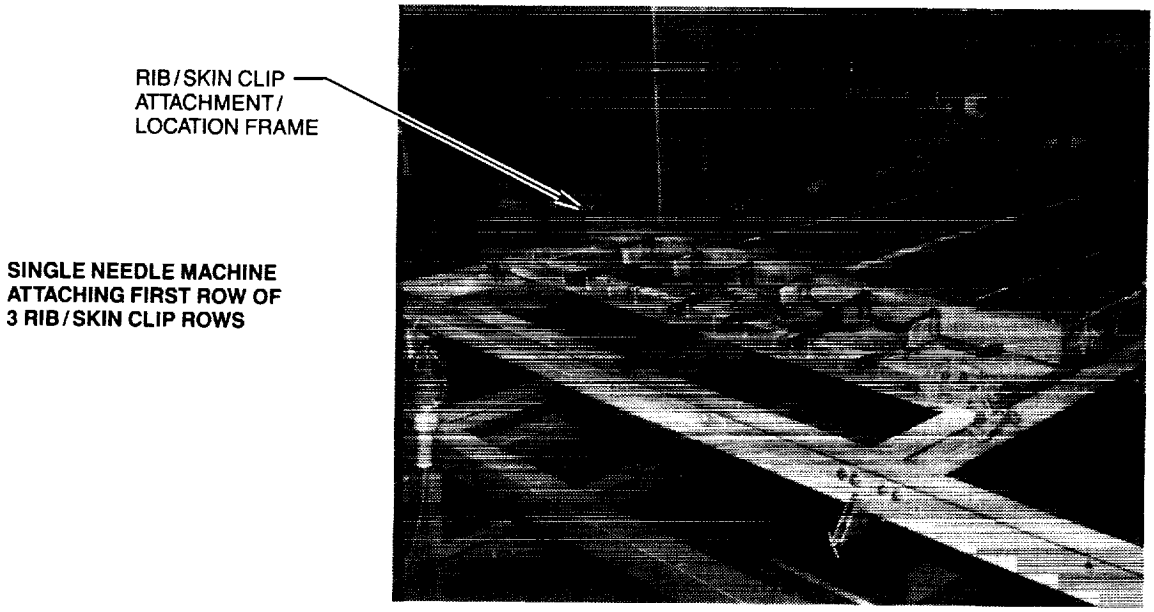

Figure 13

Douglas Wing - Stitching

The final result of this stitching process is a high quality preform (Figure 14) with the associated quality and cost aspects also shown in the figure.

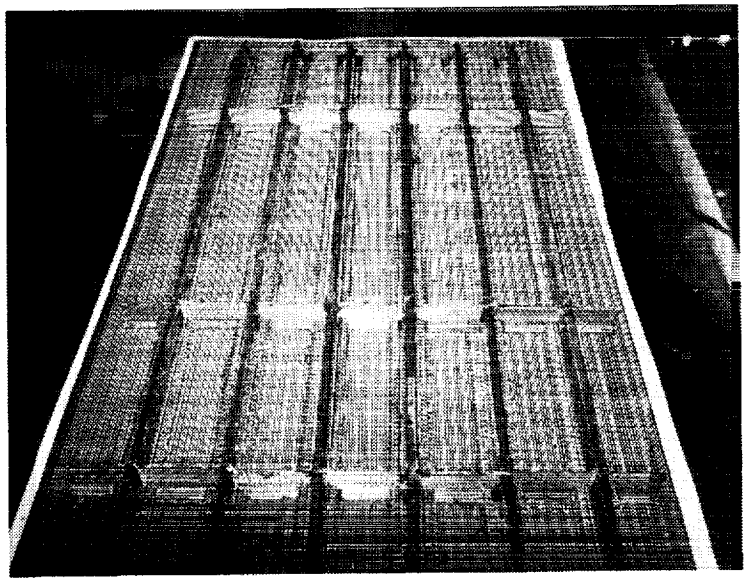

FINISHED STIFFENED WING SKIN PREFORM

QUALITY

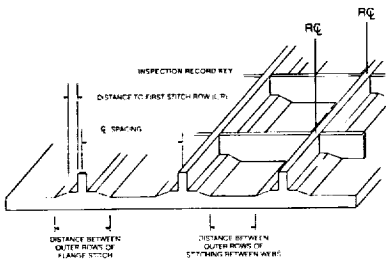

*BULK FACTOR ≤ 10% FOR ALL THICKNESS

PROGRAM QUALITY REQUIREMENTS

ITEM 1

S/N DATE

CHARACTERISTIC	VALUE	LEFT WEB	CENTER WEBS	RIGHT WEB	LEFT	RIGHT
℄ - ℄ SPACING BETWEEN STIFFENERS	7.0	–	–	–		
		L R	L R	L R		
DISTANCE TO FIRST STITCH ROW	0.37/ 0.44				–	–
DISTANCE BETWEEN OUTER ROWS OF FLANGE STITCH	2.68/ 2.81	–	–	–		
DISTANCE BETWEEN OUTER ROWS OF STITCHING BETWEEN WEBS	4.19/ 4.32	–	–	–		
RC - RC SPACING BETWEEN RIB CLIPS	30.0					

PREFORM COST BREAKDOWN

OPERATION	TIME
• LDS 9 PLY MATERIAL 52"x120" ON MULTI-NEEDLE MACHINE AT 120 RPM	2.7 HRS
• SET UP MULTI-NEEDLE MACHINE TO PERFORM HDS	4 HRS
• HDS 54 PLY SKIN 52"x88" ON MULTI-NEEDLE AT 60 RPM (5 PASSES)	1.2 HRS
• HDS 72 PLY STIFFENER WEB AREA ON MULTI-NEEDLE MACHINE AT 60 RPM (5 PASSES)	1.2 HRS
• 90° LDS STIFFENER FLANGE AREA ON SINGLE NEEDLE MACHINE AT 400 RPM *	20 HRS
• 90° LDS INTERCOSTAL FLANGE AREA ON SINGLE NEEDLE MACHINE AT 400 RPM *	5 HRS
• HDS INTERCOSTAL CLIP WEB AREA ON SINGLE NEEDLE MACHINE AT 400 RPM	2 HRS
• CUT TAPER INTO STIFFENER FLANGE AREAS (6 STIFFENERS TOTAL)	4 HRS
• LDS ZIG-ZAG PATTERN FOR ATTACHING STIFFENER FLANGE TO SKIN AT 100 RPM *	8.2 HRS
• HDS STIFFENER FLANGE TO SKIN AT 100 RPM	8.4 HRS
• HDS INTERCOSTAL CLIP FLANGE TO SKIN, TOTAL FOR 21 CLIPS	1 HR
• SET UP SINGLE NEEDLE MACHINE	1 HR
TOTAL:	58.7 HRS

NOTE: *IDENTIFIES COSTLY ITEMS TO BE DESIGN REVIEWED FOR COST PURPOSES
LDS — LIGHT DENSITY STITCHING
HDS — HEAVY DENSITY STITCHING

Figure 14

Douglas Wing - Stitching

In developing the automated sewing equipment, a tremendous learning curve has been established. As shown in Figure 15A, an improvement of 50 percent has been realized in just fabricating three wing preforms. As the curve becomes more established the overall cost of preform fabrication will be substantially reduced. Figure 15B shows that learning curves were different for the many areas of preform fabrication. The area indicated in Figure 15B represents improvement in attachment of details of assembly stitching. Reasons for this improvement are predominantly related to improved work flow and refinement in stitching parameters.

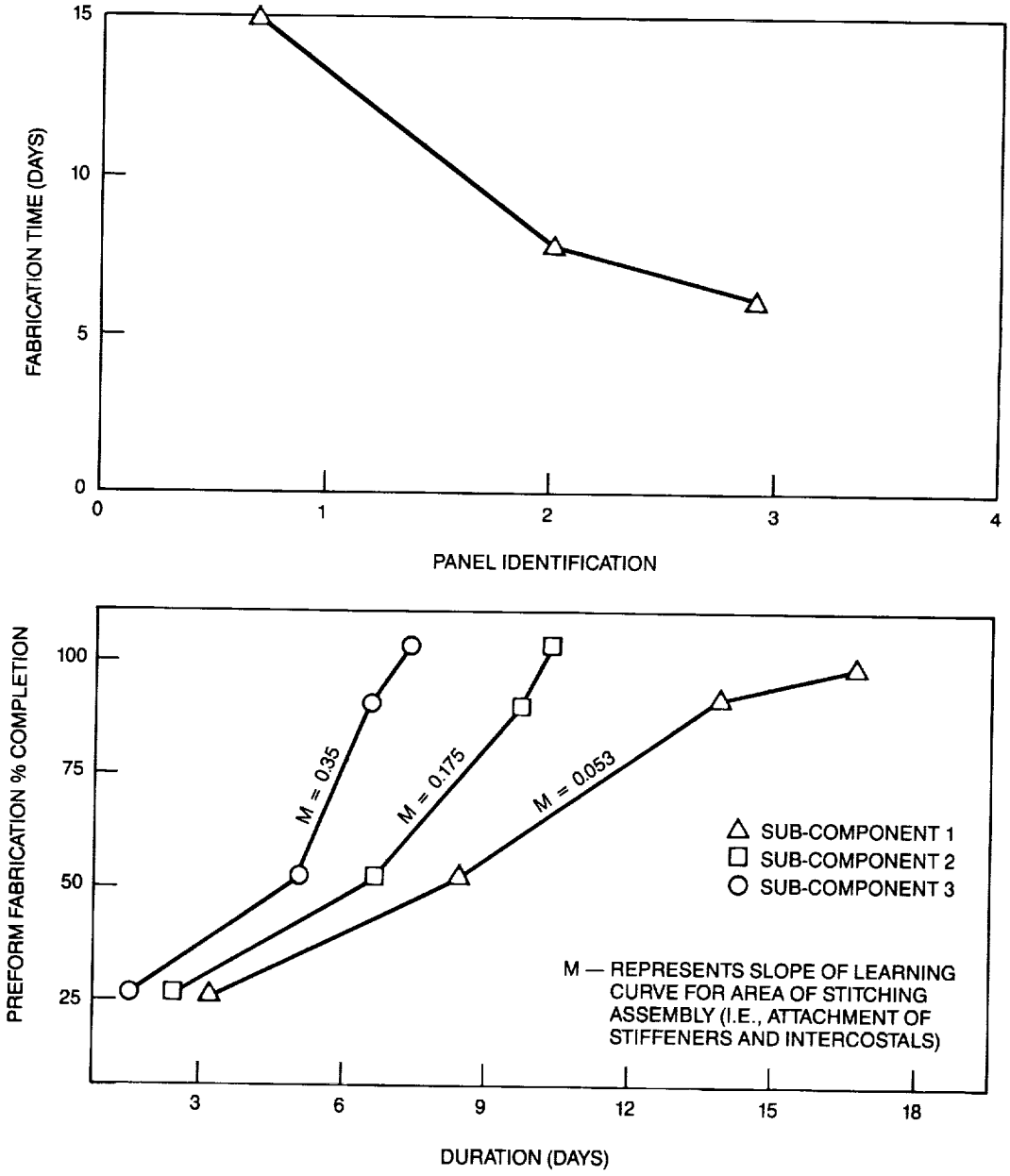

Figure 15

CURRENT PROGRESS

Douglas Wing - Fabrication

Upon completion of the preform fabrication, RTM fabrication was conducted using a resin film infusion autoclave curing process with a combination aluminum/graphite epoxy tooling approach. Figure 16 illustrates the tool layout as well as the first mandrel assembly within the preform.

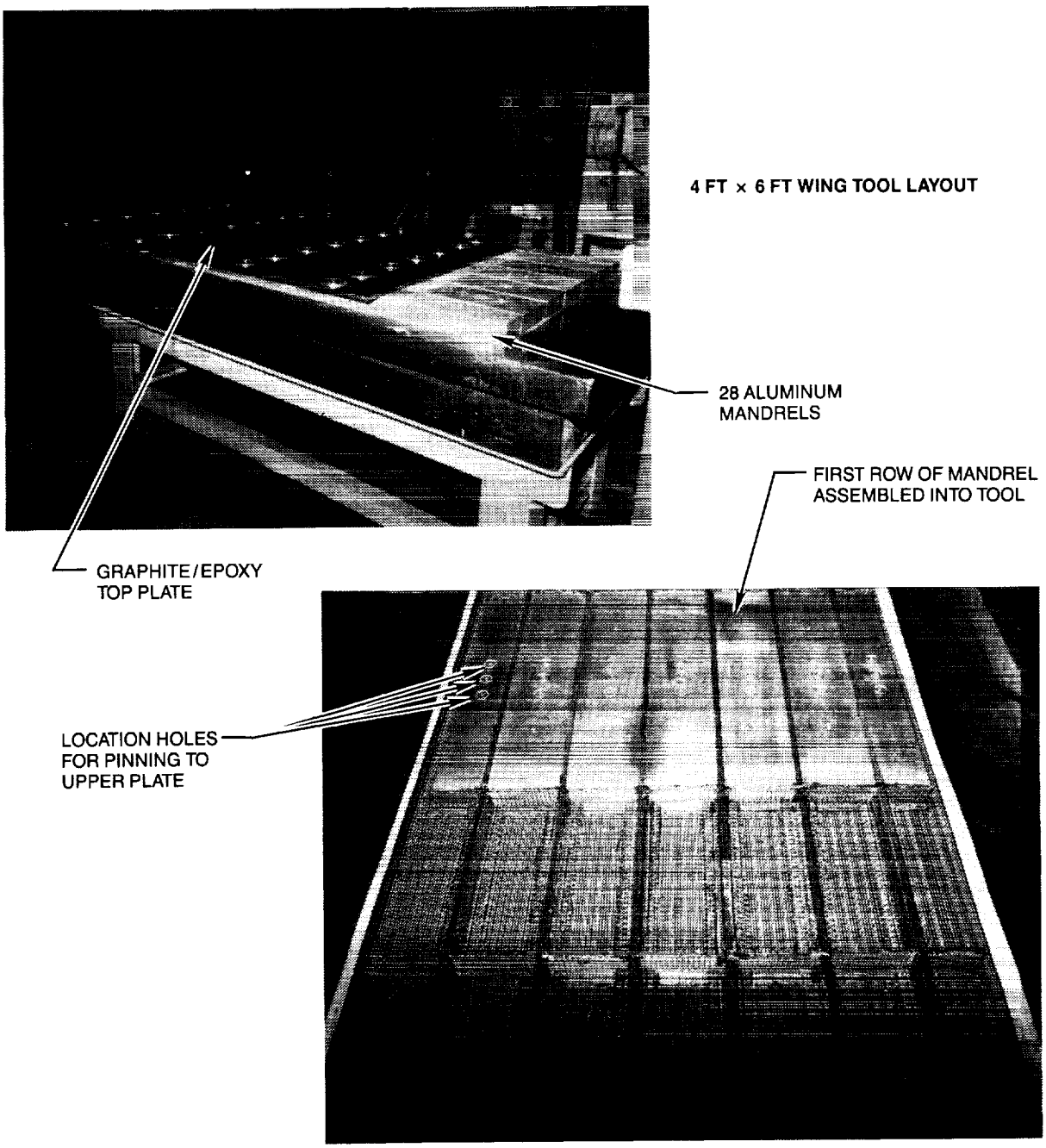

Figure 16

Douglas Wing - Fabrication

Shown below is the finished part with exploded views of the stiffener/clip intersections.

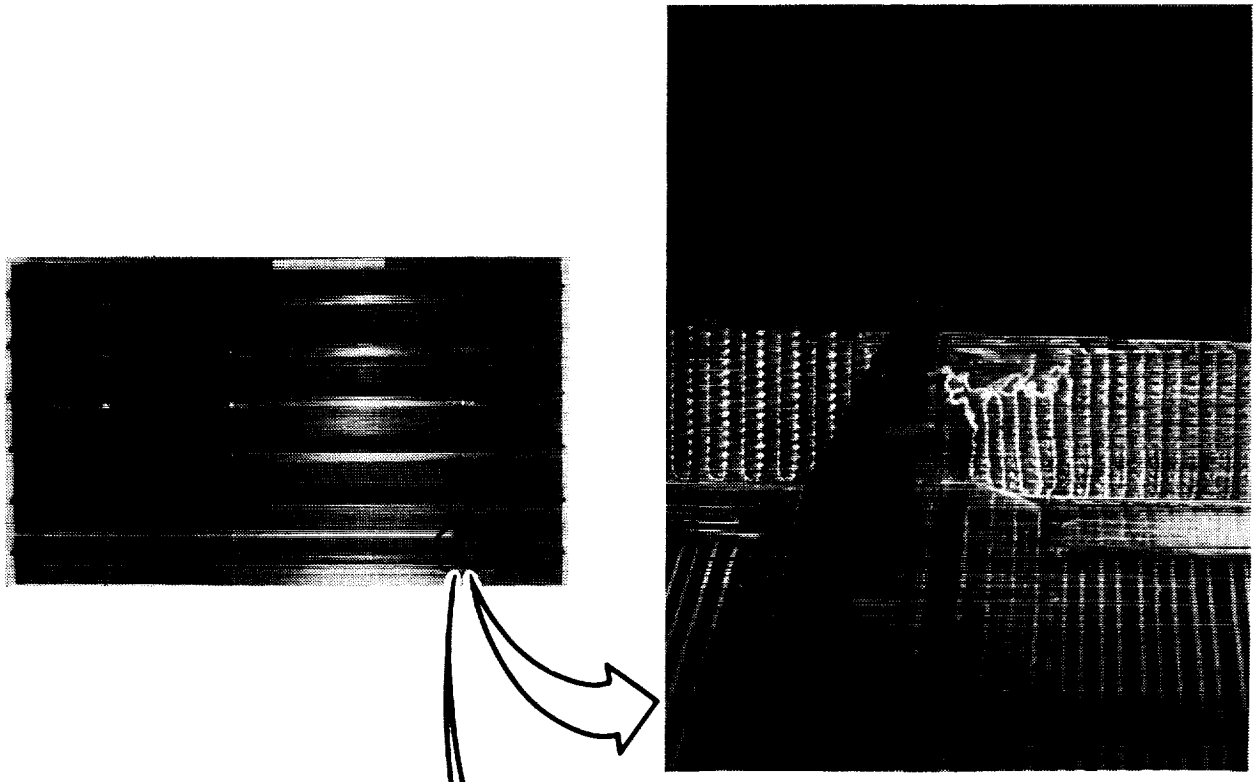

DIMENSIONAL ANALYSIS — FINISHED PART

THICKNESS	INCHES HIGH/LOW
SKIN	0.335/0.315
STIFFENER — PER STIFF.	0.465/0.451
RIB CLIP — PER ROW	0.129/0.123
RIB-CLIP ROW LOCATION/TOLERANCE	30.0/29.0

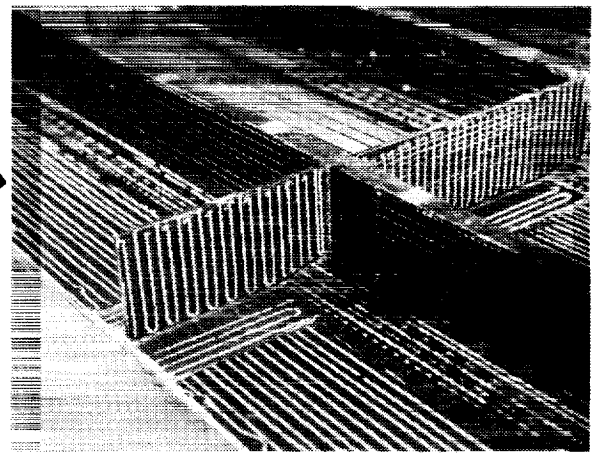

Figure 17

C-6.

CURRENT PROGRESS

Douglas Wing - Cost

Cost studies for the Douglas stitched/RTM wing process versus the automated tape layup (ATL) with hand layup reveal that the costs for the new process are approximately 50 percent less than conventional composites fabrication concepts.

RTM

Task	Hours
Preform fab	58
Trim preform	2
Tool clean/prep	16
Assemble tool	12
Bag part	4
Cure	9
Unbag	4
Trim	4
Total hours:	109

ATL/Hand Layup

Task	Skin	Stringers	Clips
ATL	14	7	
Hand layup (cut/collate/debulk)	4	40	100
Tool prep	16		
Assemble tool	12		
Bag	5		
Cure	4		
Unbag	1		
Trim part	4		
	60	47	100
Total:	207 hours		

Figure 18

Douglas Fuselage - Stitching

The Douglas fabrication plan for stitching 4- by 5-foot 126-inch radius fuselage panels is illustrated in Figure 19. In this process, the 12-ply skins are light density stitched (LDS) to provide stabilization for handling (Figure 19A). The 20-ply stiffeners are (LDS) stitched in 10-ply segments, stacked to make 20-ply stiffeners and heavy density stitched in the web area (Figure 19B). The stiffeners are then formed similarly to that of wing stiffeners (see Figure 9); then stitched to a flat skin in the specified locations. Once the stitched preform is complete, the skin can be draped to the required 126-inch radius with no skin wrinkling or buckling.

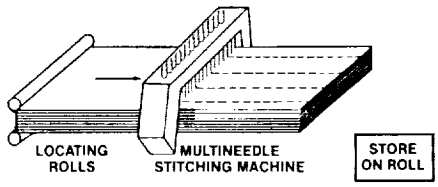

FIGURE 19a LIGHT DENSITY STABILIZATION STITCHING

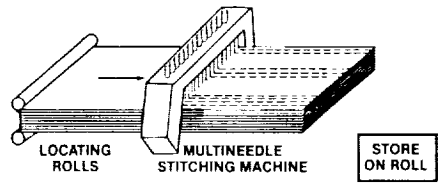

FIGURE 19b HEAVY DENSITY STITCHING OF LONGERON WEB AREAS

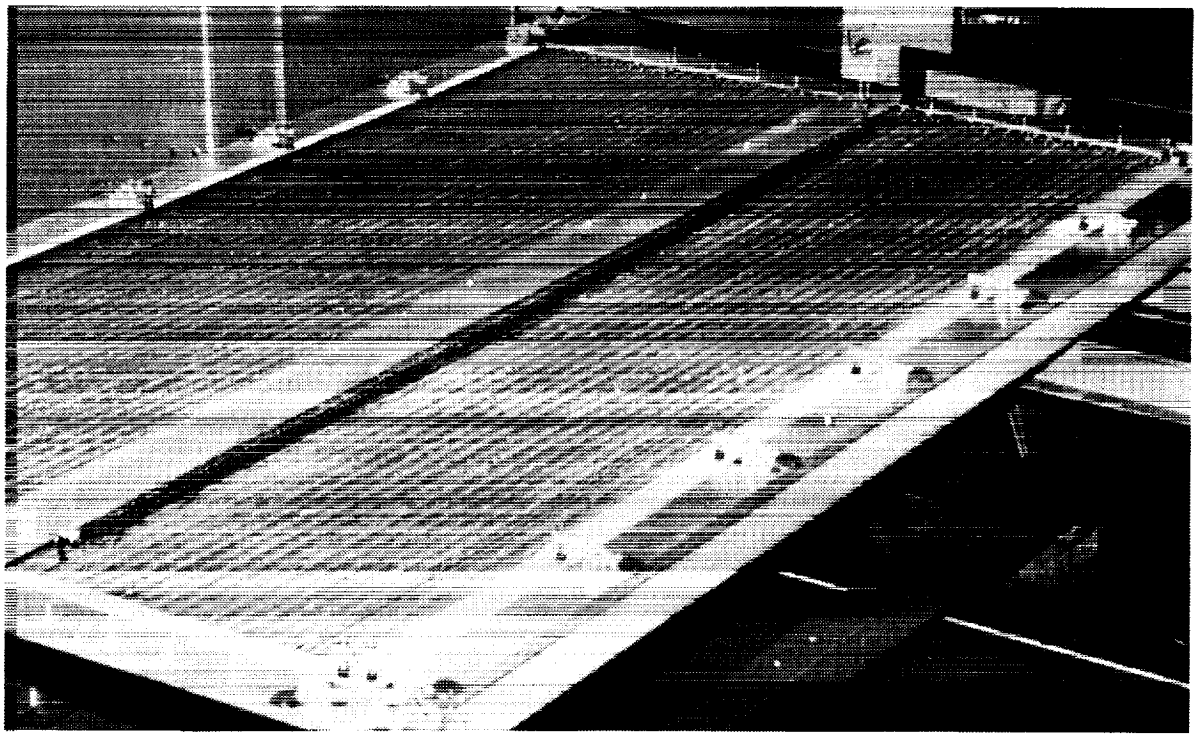

FIGURE 19c FUSELAGE ASSEMBLY STITCHING ON SINGLE NEEDLE MACHINE

Figure 19

Douglas Fuselage - Tooling

Douglas has devised two tooling methods for making fuselage panels using the pressure RTM fabrication process. In the first approach, a complete matched metal tool is assembled in pieces as shown below in Figure 20A. The second approach was to use a one piece cavity tool with mandrels, providing definition for the stiffeners, Figure 20B.

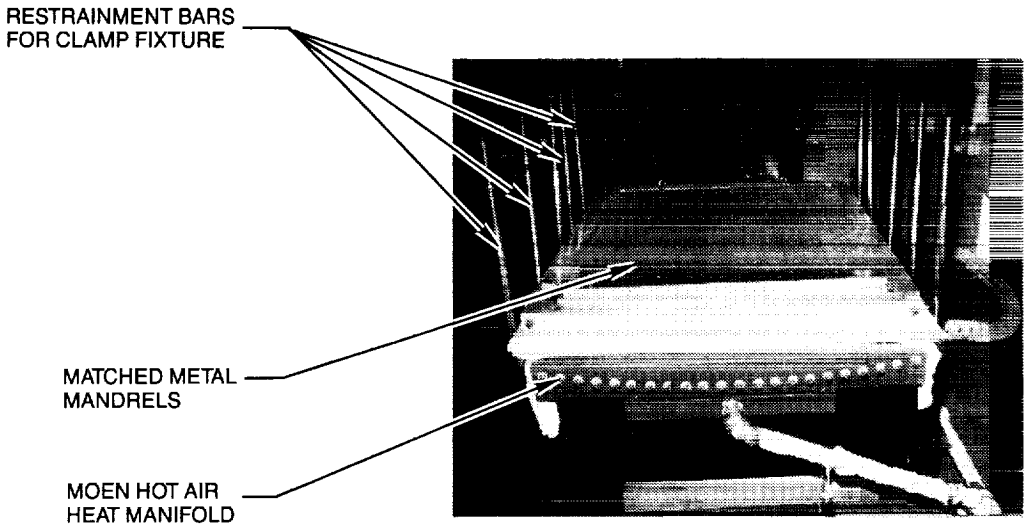

MATCHED METAL TOOL CONCEPT
SHOWN PARTIALLY ASSEMBLED

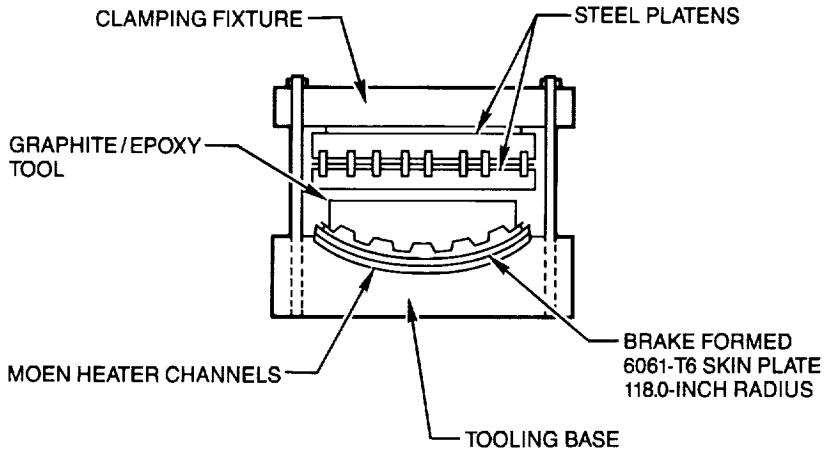

GRAPHITE TOOL CONCEPT

Figure 20

CURRENT STATUS

Douglas Fuselage - Fabrication

Prior to fabrication of the RTM fuselage panels, a series of tool proof parts were fabricated to verify process procedures and tooling tolerances. Results of the first tool proof part revealed numerous dry spots due to tooling tolerance mismatches. Shown below (Figure 21) is the first tool proof part with the associated dimensions. A skin thickness of 0.072 inches was the design target.

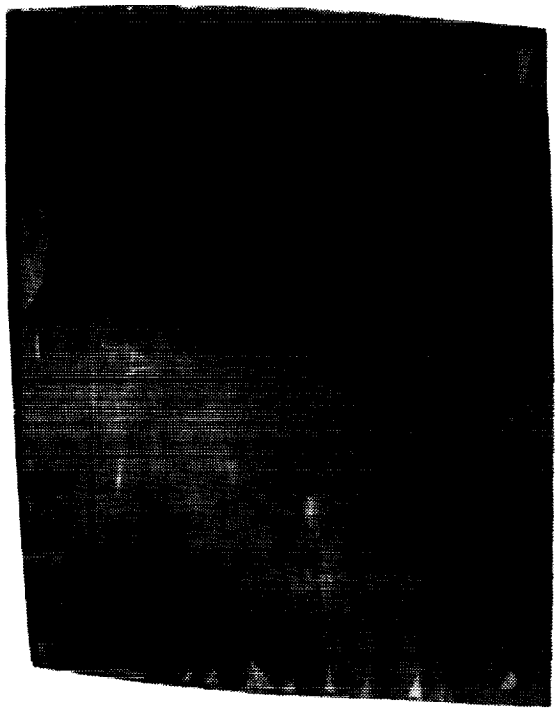

TOOL PROOF PART

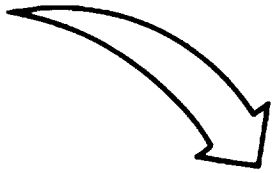

TOOL PROOF SKIN

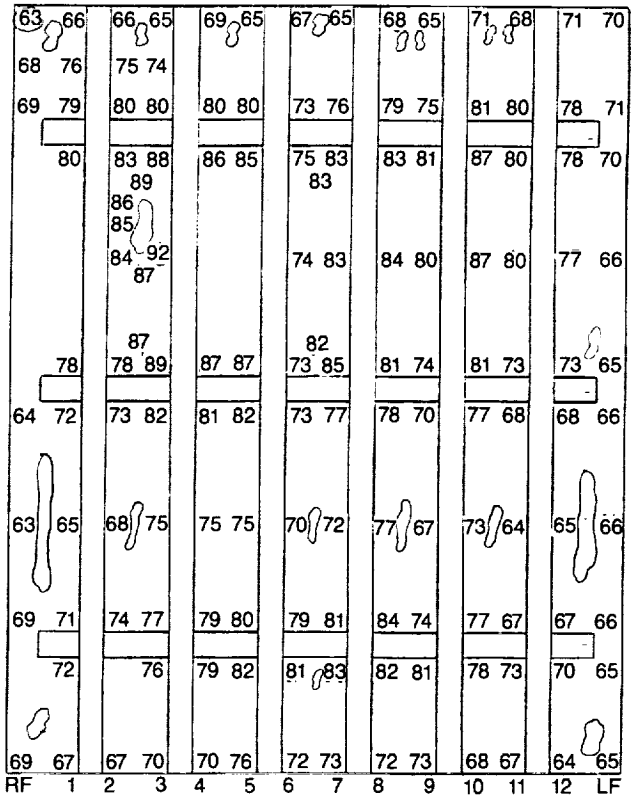

LOCATION OF DRY SPOTS WITH
PART DIMENSIONS IN 1/1,000 OF AN INCH

Figure 21

CURRENT STATUS

Douglas Fuselage - Fabrication

A closer examination of the tooling tolerance mismatches reveals interesting information on the effect of bulk factor, clamp pressure, porosity, permeability, and hydrostatic resin pressure. In tool proof part #1, the bulk factor was 8.3 percent greater than the tool design value (materials with a .0065 per ply thickness were used instead of a .006 per ply thickness material). This resulted in a decrease in porosity, thus causing resin not to flow in the areas of decreased permeability. Shown below is a graph of compaction pressure versus porosity. If one follows the porosity curve generated for this preform down to the compaction pressure necessary for design goals, the midpoint porosity for that preform tool combination is established. In this case, it is $\simeq 0.475$. Also shown on the graph are the tool design limits for porosity based upon ± 0.006 per ply tool tolerances. Combination of these curves gives a visual aid in helping determine that the desired porosity range $0.428 < \phi < 0.510$ was too close to the porosity midpoint for the tool proof part thus causing tooling tolerance mismatches to become very sensitive on flow profiles.

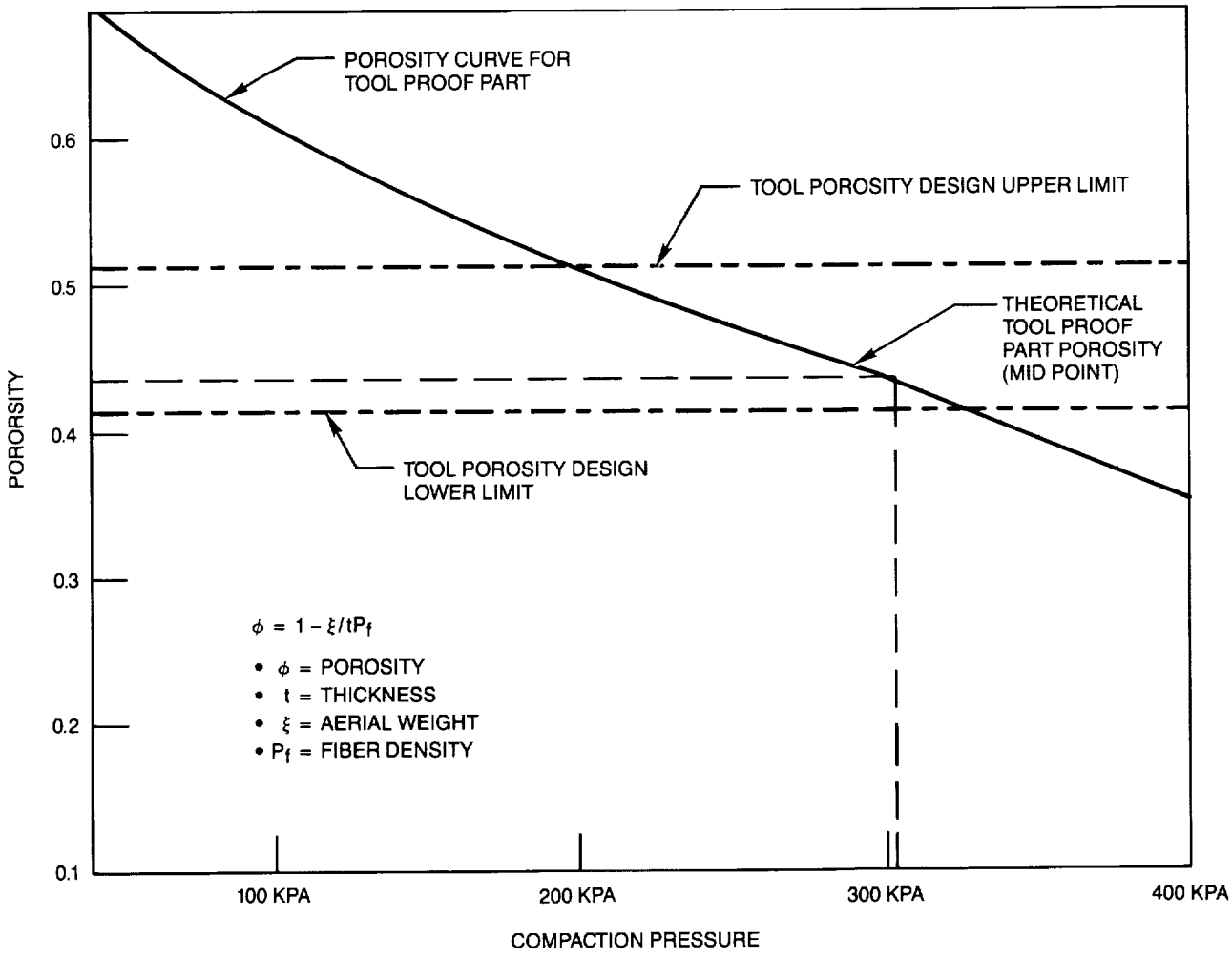

Figure 22

CURRENT STATUS

Douglas Fuselage - Fabrication

A detailed look at permeability sensitivity (P_s) is seen below.

$$P_s \alpha \frac{HydrostaticResin}{Permeability}$$

This graph indicates the tool design P_s is 12.5 (at midpoint). The upper and lower bounds at tool tolerances of $\pm$.006 inches yield a P_s boundary from 8 and 37.5. (Notice the significant change in -.006 inches versus +.006 inches. This indicates flow is three times harder at -.006 than at +.006.) This information provides a boundary in which the tool designer can expect resin to flow easily, unimpeded. Once the tooling limits are set, a designer should verify that the preform actually being used fits the design criteria. Shown here is the average $P_s = 30$ for the tool proof part (based on per ply thickness of .0065). In this case, the tool proof part P_s was at a lower extreme of the tooling tolerance limit. The actual upper and lower flow permeabilities in this part are 5.4 and 200. One can easily see this far exceeds the tool design. From this information a tool design for any part can be made accurately if the data is available.

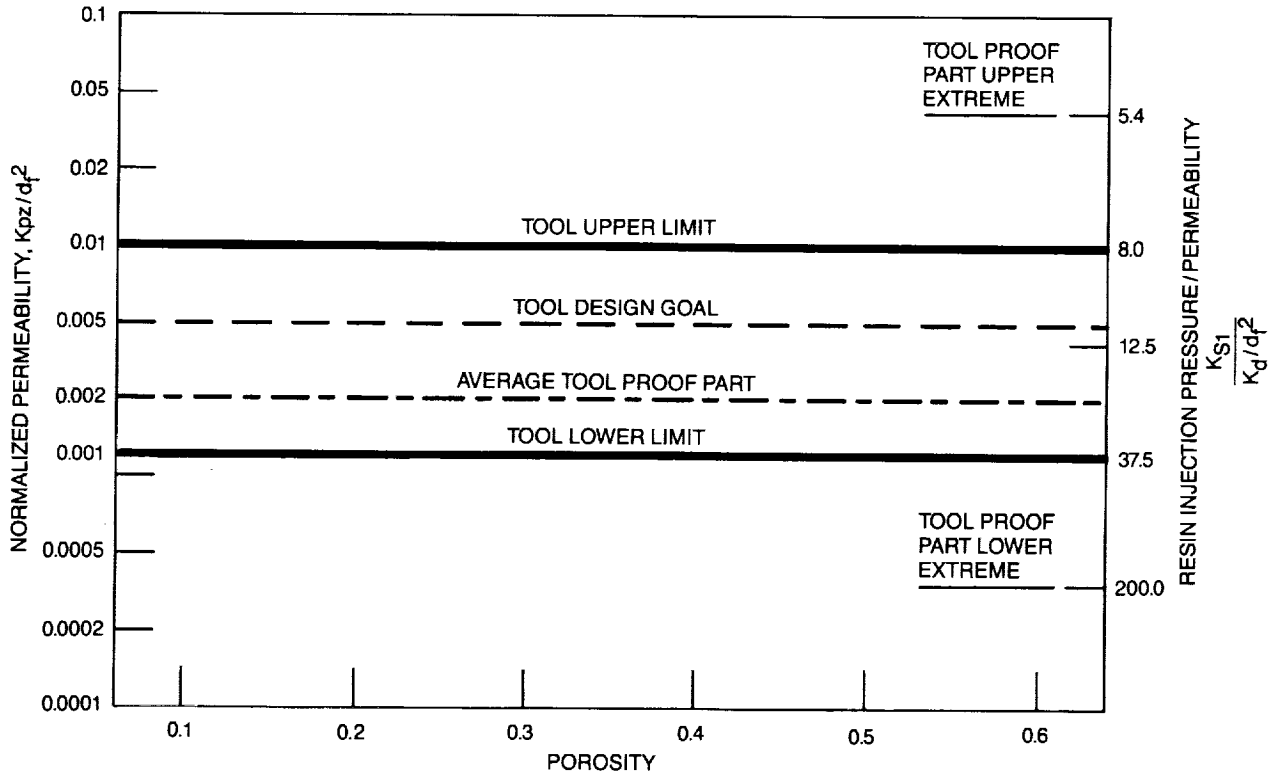

Figure 23

Douglas Fuselage - Fabrication

With the tooling tolerances brought into specification, the fabrication of three 4- by 5-foot 126-inch radius fuselage panels proceded without incident. Figures 24 and 25 are a series of photos showing the tool assembly, injection, and disassembly process.

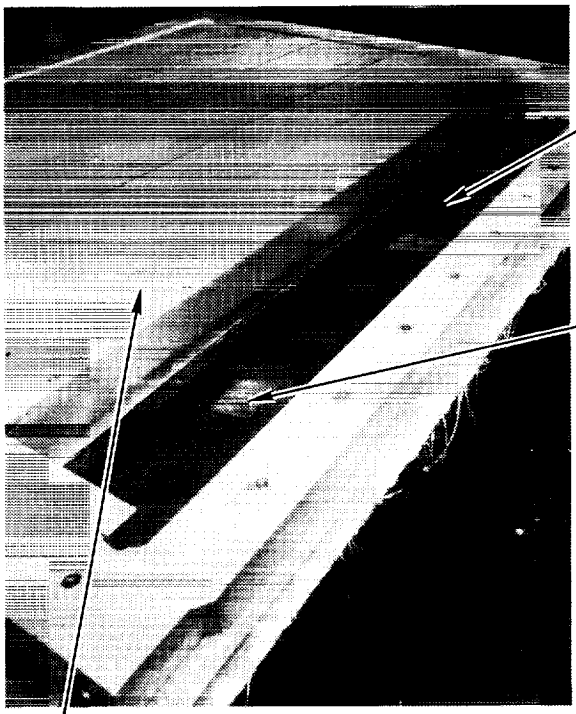

MATCHED METAL TOOL FINAL ASSEMBLY

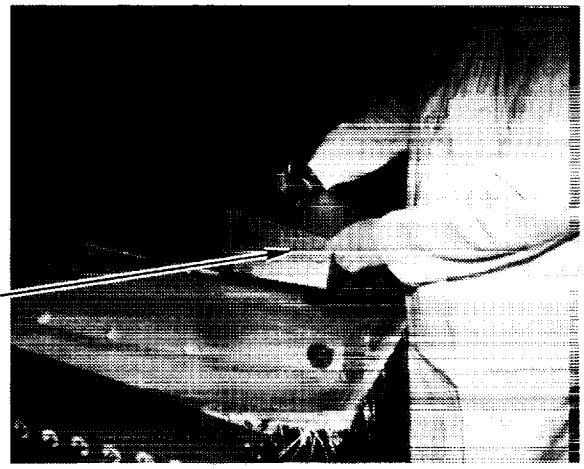

Figure 24

Douglas Fuselage - Fabrication

Shown below is the injection and tool disassembly process.

Figure 25

CURRENT PROGRESS

Illustrated below are the completed RTM fuselage panels.

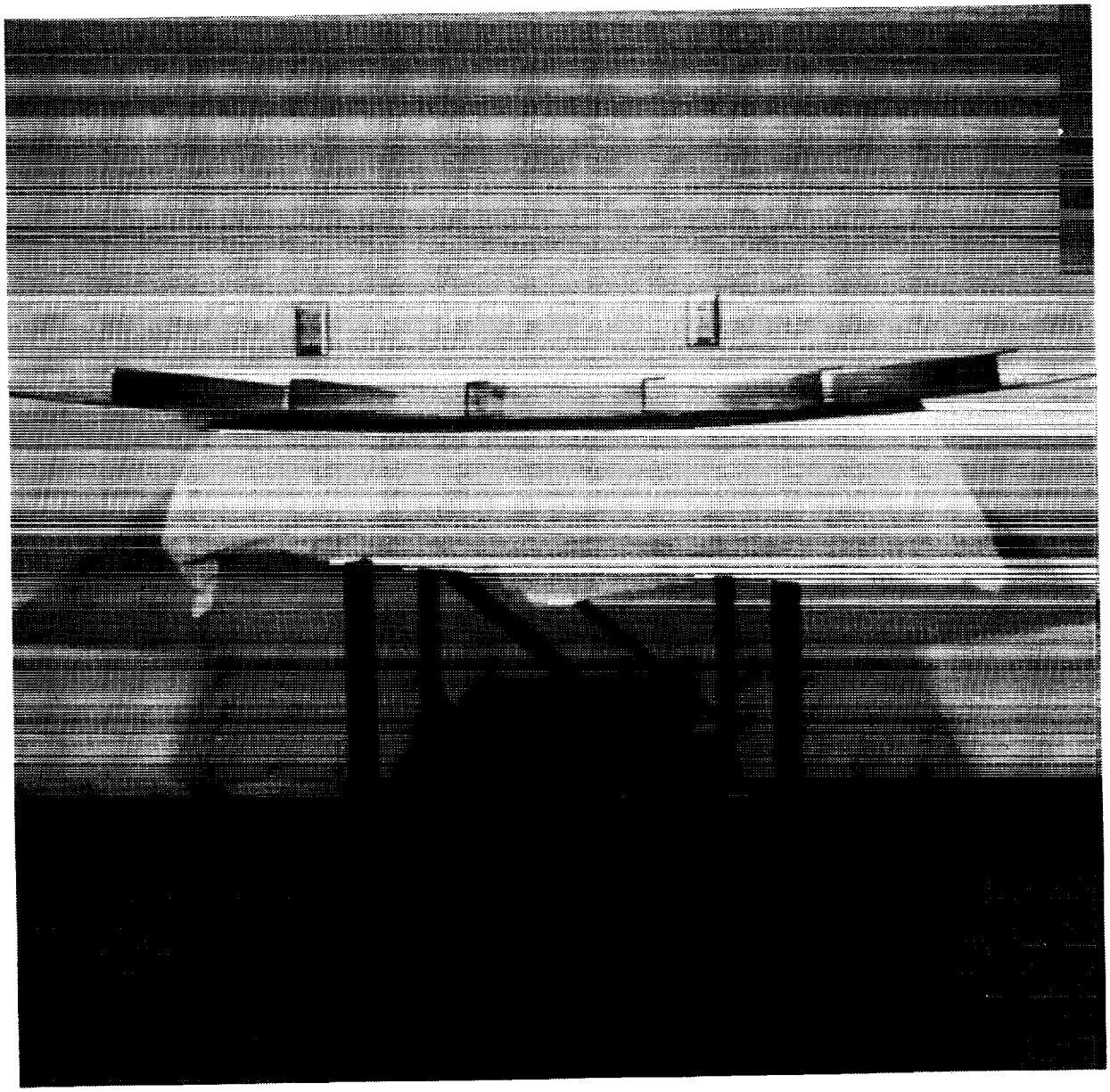

Figure 26

CURRENT STATUS

Douglas Fuselage - Cost Studies

RTM Fuselage

Task	Hours
Preform fab	8.0
Trim preform	8.0
Tool clean/prep	2.0
Assemble tool	24.0*
Resin inject/cure	12.0
Disassemble tool	8.0
Trim	8.0
Total:	88.0

*Multi-piece tooling provides excessive costs.

ATP Fuselage

Task	Hours
Fiber placement of skin	
• set-up	4.09
• machine	8.40
Stringers - hand layup	
• 4.5 hrs x 2 men x 6 parts	54.00
Shear tee doubler	
• 5 min/doubler x (3) x 1 man	.25
Panel assembly	
• 4 hrs x 2 men	8.00
Panel cure	
• 4 hrs x 2 men	8.00
• autoclave process time	8.00
Final trim	
• 4 hrs x 2 men	8.00
Total:	82.77
Process	8.00
	90.77

Note: Total is per panel. NDI and QA is not included.

Figure 27

CONCLUSIONS

RTM Wing Development

- RTM/stitching goals were achieved
- High quality preforms have been fabricated using automated stitching equipment
- Learning curve on utilizing automated sewing equipment is very short (result of mature textile technology)
- RTM fabrication process for complex stiffened wing structure works well
- A reduction of 50% in touch labor of RTM versus state-of-the-art composite fabrication process was realized during this phase of program
- Scale-up to large wing structure is possible

RTM Fuselage

- RTM/stitching goals were achieved
- High quality preforms have been fabricated using automated stitching equipment
- RTM fabrication processes for complex stiffened fuselage structure have been successfully developed
- Tool design requires a thorough understanding of process modeling, preform porosity and permeability
- Costs of RTM versus ATP are extremely competitive
- Scale-up to large fuselage structure requires extensive tooling development

TEST RESULTS FROM LARGE WING AND FUSELAGE PANELS

Ram C. Madan and Mike Voldman
Douglas Aircraft Company
McDonnell Douglas Corporation
Long Beach, CA

SUMMARY

This paper presents the first results in an assessment of the strength, stiffness, and damage tolerance of stiffened wing and fuselage subcomponents. Under this NASA-funded program, 10 large wing and fuselage panels, variously fabricated by automated tow placement and dry-stitched preform/resin transfer molding, are to be tested.

The first test of an automated tow placement six-longeron fuselage panel under shear load was completed successfully. Using NASTRAN finite-element analysis the stiffness of the panel in the linear range prior to buckling was predicted within 3.5 percent. A nonlinear analysis predicted the buckling load within 10 percent and final failure load within 6 percent. The first test of a resin transfer molding six-stringer wing panel under compression was also completed. The panel failed unexpectedly in buckling because of inadequate supporting structure. The average strain was 0.43 percent with a line load of 20.3 kips per inch of width. This strain still exceeds the design allowable strains. Also, the stringers did not debond before failure, which is in contrast to the general behavior of unstitched panels.

INTRODUCTION

While application of composites in secondary and medium primary structures has produced worthwhile weight savings, wing and fuselage primary structures offer a far greater opportunity because these structures comprise approximately 75 percent of the total structural weight of a large transport aircraft. As part of efforts to develop the composite primary structure, a comprehensive test program, ranging from coupon testing to subcomponent verification tests, was initiated to demonstrate the behavior of components utilizing automated tow placement (ATP) and resin transfer molding (RTM) techniques.

The objectives of this program were to validate experimentally a number of wing and fuselage panel designs, to provide correlation data for analytical predictions of failure loads and failure modes, and to provide scale-up data for wing boxes and fuselage sections. In the early phases of this program, several test elements were designed, fabricated, and tested (Reference 1). These included pull-off tension, single-stringer crippling, and three-stringer compression specimens. This activity was then extended to cover subcomponent primary structure. Work done under prior NASA contracts (References 2 and 3) generated the design concepts for the ATP and stitched RTM fuselage and wing panels.

The subsequent NASA Innovative Composite Advanced Primary Structure (ICAPS) program extends this work to subcomponents appropriate to the primary structure of a large transport aircraft. The relevant portion of this program is presented in this paper, together with the test results thus far.

ICAPS PANEL TEST PROGRAM

Under Phase A of the ICAPS program, 10 large panels fabricated by ATP and RTM are to be tested in shear or compression (Table I). These panels represent typical structural arrangements for major components of a fuselage and wing. The specific geometries employed were drawn from two McDonnell Douglas projects. The panels are related to the MD-100 120-inch-radius fuselage barrel and the MD-XX inner wing. The plan calls for seven of the panels to be fabricated using the RTM and dry-stitched preform technique. Uniwoven AS4 fabric is used with 1895 Shell resin for the fuselage and 3501-6 resin for wing subcomponents. The use of these materials, in combination with the stitching technique, is intended to result in an effective and low-cost structure. The other three panels were fabricated by Hercules from the toughened IM7/8551-7 composite system using the ATP method. One of the RTM wing compression panels has an 18- by 15-inch elliptic hole to accommodate a glass/epoxy access door. Similarly, one of the RTM fuselage shear panels incorporates two reinforced fuselage windows.

Each of the panels described in Table I is to be damaged before the test, three of the panels suffering penetration damage. After each test, results will be correlated with predictions.

PANEL TESTS

ATP Fuselage Subcomponent Tests

The fuselage subcomponent specimen is shown in Figure 1. The J-stiffened curved six-longeron panel (56 inches long and 48 inches wide with a 126-inch radius) was constructed by Hercules using the ATP technique. Three composite Z-section frames were attached to the panel by shear clips. Three panels were fabricated and the first of these was subjected to a shear test carried out at Douglas.

Prior to the shear test, the panel had been impacted with 20 foot-pounds of energy on the skin side at midlength of the third longeron between the upper and middle frames. A 1-inch steel impactor was employed in this test. The panel was supported along the outer longitudinal sides by wooden supports during the impact, as shown in Figure 2. The affected area was marked and is shown in Figure 3.

For the shear test, the panel was attached to the fixture by means of a steel hat-section frame around the four sides to provide flexibility so as to discourage premature failure at the corners (Figure 3). The Douglas shear fixture is shown in Figures 4 and 5. The panel was connected to the hat-frame with angle section attachments, and the hat-frame was fastened to the shear fixture picture frame.

When the panel was in place in the fixture, it was instrumented with strain gage rosettes, as shown in Figure 6. The rosette leads were connected to the data acquisition system. A hydraulic actuator was employed to pull down the right lower corner of the picture frame (Figure 3) so as to load the panel in shear. A calibrated extensometer was used to record vertical displacement. The data from all the channels were recorded and stored on a disk for plotting and further investigation. The load was applied at 0.05 inch per minute.

Test Results and Discussions

When the load exceeded 30,000 pounds, the panel began to buckle. As the load was increased beyond buckling, the diagonal tension field formed in every bay of the panel. These wrinkles were

clearly observable from the skin side of the panel. When the load exceeded 70,000 pounds, a cracking sound was heard. This could be attributed to either some local longeron debonding or a few separate tows of fiber breaking. Overall, the structure stayed intact until it failed catastrophically at 100,000 pounds.

Figures 7 through 11 show close-up pictures of the damage in different parts of the panel. Almost all the damage occurred across the main tension diagonal where a big wrinkle was formed, as shown in Figure 7. The impacted area happened to be away from the main diagonal and did not influence the onset of damage, nor was this area damaged as the panel failed. The damage shown in the upper right corner of Figure 8 and upper left corner of Figure 9 can be attributed to the high intensity of compressive stress in that region. The failure propagated along the main diagonal and subsequently caused the longerons to debond and break. Figure 8 shows the skin wrinkled, broken, and delaminated under the longerons and the skin longeron broken in the area where it separated from the skin. Figure 9 shows the skin delaminated in the corner and broken along the crest of the wrinkle. Figures 10 and 11 show the stringers broken and debonded from the skin. Typical damage on the shear tees and frames is shown in Figures 12 and 13.

A NASTRAN model of the panel is shown in Figure 14, while the material and lay-up of each element are shown in Table II. The load deflection curve is shown in Figure 15 and some typical results from back-to-back strain rosettes data are presented in Figure 16. Shear strains were calculated using the right angle rosette formula and were plotted on the same graphs. A good correlation was found between the test results and the predictions of the analytical model of the tested panel.

The model was analyzed in the linear and nonlinear postbuckled state using NASTRAN Solution 5 for linear static and eigenvalue analysis and Solution 66 for large displacement type nonlinear stress analysis. The load deflection curves obtained by both the test and the analyses are compared in Figure 15. As shown, the stiffness of the panel in the linear range was predicted within 3.5 percent. The initial onset of buckling predicted by linear buckling analysis (Solution 5 NASTRAN) was within 20 percent of the value measured in the test. This degree of accuracy was expected in applying FEA linear buckling analysis to the stiffened plates. A better result was obtained by using the nonlinear analysis (Solution 66), which predicted the buckling load within 10 percent. Solution 66 was also used to predict the final failure load, which was predicted within 6 percent of the value measured in the test.

Future Plans

Two additional ATP panels, as shown in Items 5 and 6 of Table I, will be tested in compression. As indicated in Table I, Item 5 will be loaded in compression until the panel begins to buckle. The panel will be unloaded, supported as shown in Figure 2, and impacted at the crest point of the buckled shape with 20-foot pounds of impact energy using a 1-inch-diameter steel impactor. The panel will be A-scanned to assess the damage area and will then be tested to failure. The test results will be compared with predictions made with the finite-element analysis models. The third ATP panel will be saw-cut as shown in Item 6 of Table I and will be loaded in compression to 70 percent of design limit load. If no failure occurs at this load, the panel will be unloaded and the saw-cut increased by 0.5 inch at each end. The panel will again be loaded to 70 percent of design limit load. This process will be repeated until the panel fails. All the data will be recorded and damage tolerance characteristics will be evaluated. The test results will be compared with predictions made with NASTRAN finite-element analysis.

RTM Fuselage Subcomponent Tests

Four curved RTM fuselage panels using stitched preforms were fabricated at Douglas. They are shown as Items 7 through 10 in Table I. As noted in the table, the first three panels will be tested similarly to the ATP panels in shear and compression. The fourth panel has two cutouts representing two fuselage windows, as shown in Figure 17, which will be tested in shear after impacting it with 20 foot-pounds of impact energy. The test results will be compared with analytical predictions.

RTM Wing Subcomponent Tests

Three RTM wing panels have been fabricated using stitched preforms to verify the composite damage tolerance requirements of FAR 25.571. One of the panels, with invisible impact damage, was tested in compression, while the other two will be tested in the future. The six-stringer wing panel configuration is shown in Figure 18.

The panel was simply supported at rib locations (31 inches apart) and impacted at midbay with 100 foot-pounds of energy from the skin side using a 1-inch-diameter steel impactor. The inflicted damage was invisible. A C-scan showing the extent of impact damage is presented in Figure 19. The damage was small, particularly when compared with the damage one would expect for a conventional toughened resin panel, where far-side delamination would be normal. The panel was instrumented with 20 strain gages, as shown in Figure 18. Figure 20 shows the panel in the MTS machine with lateral support. The panel was potted at the top and bottom edges using Hysol 934 potting material with a 1-inch-deep rectangular aluminum frame all around. Before formally applying the load, all the strain gage channels were checked by loading the panel to 30 percent of design limit load.

Test Results and Discussions

A six-stringer RTM panel was tested in the Hercules MTS 1.5 million-pound machine at Magna, Utah. The panel was loaded at the rate of 0.05 inch per minute. The data were recorded at load intervals of 50 kips when the panel was loaded from 0 to 500 kips and at intervals of 10 kips thereafter. As shown in Figures 21 and 22, a lateral restraint fixture was attached to the panel on the stringer side to stabilize it during compression loading. Linear variable-displacement transformers (LVDT), shown in Figure 23, were attached to the panel from the skin side to measure out-of-plane displacement. Two LVDTs were used to measure the vertical shortening of the panel. Another LVDT measured the expansion in width in order to determine the Poisson's effect. The load and strain data were recorded on a disk with a data acquisition system.

The plots showing displacement data from LVDTs are shown in Figure 24. Axial and transverse displacement data were found to be in agreement with Poisson's ratio. The strain gage data from two sets of back-to-back axial direction strain gages on the skin and stringer blade near the impact location are shown in Figure 25. These results indicate that the panel failed at 791.1 kips load with average strain of 0.43 percent and line load of 20.28 kips per inch. The predicted failure strain of 0.53 percent was obtained by using the parametric residual stress prediction model discussed in Reference 5. The preliminary posttest analysis indicates that the panel failed prematurely because of the insufficient stiffness of the lateral support. However, a few favorable results attributable to the stitching concept have been attained. First, the failure strain definitely exceeded the design strain allowable set by the bolted repair requirements. Second, a favorable comparison can be made with the state-of-the-art toughened epoxy composite systems (1808I/IM6) described in Reference 4:

- The stringers did not debond from the skin
- The cost of material and fabrication is lower

A summary comparison between the six-stringer RTM panel and the five-stringer prepreg panel is given in Table II. Although, as previously mentioned, the strain achieved exceeded the design level, it is considered probable that the failure strain would be even higher had the panel not failed prematurely. Photographs of the panel after the failure are shown in Figures 26 and 27.

Future Plans

Two additional wing panels (Table I, Items 2 and 3) are to be tested in compression. Panel 2 has the same dimension as Panel 1, but it has a 3-inch-wide, 1/8-inch saw-cut in one of the midstringers through the skin, flange, and blade. This panel test will satisfy the discrete source damage requirement for damage tolerance of composite aircraft structure. The panel will be loaded in compression to 70 percent of design limit load. If the panel survives this load, it will be unloaded and the saw-cut will be widened by 1 inch by increasing the cut 1/2 inch toward each adjacent bay. The panel will be loaded, and this process of increasing saw-cut size will be repeated until the panel fails at 70 percent or at a smaller load. The test results will be compared with analytical predictions.

The third RTM wing panel has an 18- by 15-inch elliptic opening to represent an access door. The opening will be covered with a glass/epoxy access door panel. The access door panel will be impacted with 100 foot-pounds of impact energy in a test conducted at the Hercules facility. A finite-element analysis will be conducted and the predictions compared with the test results.

CONCLUSIONS

ATP Fuselage Shear Panel

Results of the test indicated that the behavior of the panel closely agreed with the analytical predictions. Predictions were about 3.5 percent high for panel stiffness prior to buckling, in the proper vicinity for the onset of buckling, and 6 percent low for failure. Postbuckling failure load of the panel was about three times the buckling load.

RTM Wing Compression Panel

Under 100 foot-pounds of impact energy, the damage was not visible and appeared small in the C-scan. The panel was proven to be damage tolerant, particularly when compared with the damage one would expect for a conventional toughened resin panel, where far-side delamination would be normal.

The failure strain of the panel exceeded the design ultimate strain set by bolted repair requirements. Several favorable results were attained when comparison is made with the five-stringer panel fabricated with a state-of-the-art toughened resin system:

- Stringers did not debond from the skin.
- Higher failure strain (0.43 compared to 0.41). It is probable that the difference would be greater had the panel not failed prematurely.
- Lower cost of matreial and fabrication.

REFERENCES

1. Deaton, J. W.; Kullerd, S. M.; Madan, R. C.; and Chen, V. C: "Test and Analysis Results for Composite Transport Fuselage and Wing Structures," NASA Advanced Composites Technology Conference, Lake Tahoe, Nevada; November 4-7, 1991.
2. Sumida, P. T.; Madan, R. C.; and Hawley, A. V.: "Test Results for Composite Specimens and Elements Containing Joints and Cutouts," NASA CR-178246, August 1988.
3. Madan, R. C.: "Composite Transport Wing Technology Development," NASA CR-178409, February 1988.
4. Madan, R. C.; and Shuart, M. J.: "Impact Damage and Residual Strength Analysis of Composite Panels with Bonded Stiffeners," Ninth ASTM Symposium on Composite Materials, Testing and Design; Sparks, Nevada; April 27-29, 1988.
5. May 1992 Technical Progress Report, "Innovative Composite Aircraft Primary Structures," NASA CRAD - 5909 TR 8430, June 26, 1992.

Table I. Wing and Fuselage Test Panels

ITEM	TEST PANELS	DIMENSIONS L X W (IN.)	DAMAGE TYPE / SIZE	TYPE OF TEST (ULTIMATE FAILURE)	REMARKS
1.	SIX-STRINGER RTM WING PANEL	56 X 39	100 FT-LB MIDBAY IMPACT	COMPRESSION	TESTED IN MAY 1992
2.	SIX-STRINGER RTM WING PANEL	56 X 39	3-INCH-WIDE SAW CUT IN STRINGER FLANGE AND SKIN	COMPRESSION	TO BE TESTED
3.	FOUR-STRINGER RTM WING ACCESS DOOR PANEL	56 X 39 18 X 12 OPEN-ING WITH DOOR	100 FT-LB IMPACT	COMPRESSION	TO BE TESTED
4.	SIX-LONGERON ATP FUSELAGE PANEL	60 X 48	20 FT-LB MIDLONGERON	SHEAR	TESTED IN FEB 1992
5.	SIX-LONGERON ATP FUSELAGE PANEL	56 X 39	20 FT-LB MIDSTRINGER	COMPRESSION	TO BE TESTED
6.	SIX-LONGERON ATP FUSELAGE PANEL	56 X 39	2-INCH-WIDE SAW CUT IN LONGERON FLANGE AND SKIN	BUCKLING / ULT COMPRESSION	TO BE TESTED
7.	SIX-LONGERON RTM FUSELAGE PANEL	60 X 48	20 FT-LB MIDLONGERON	SHEAR	TO BE TESTED
8.	SIX-LONGERON RTM FUSELAGE PANEL	56 X 39	20 FT-LB MIDLONGERON	BUCKLING / COMPRESSION	TO BE TESTED
9.	SIX-LONGERON RTM FUSELAGE PANEL	56 X 39	2-INCH-WIDE SAW CUT IN LONGERON FLANGE AND SKIN	BUCKLING / COMPRESSION	TO BE TESTED
10.	SIX-LONGERON RTM WINDOW BELT FUSE-LAGE PANEL	60 X 48 WITH TWO WINDOWS	20 FT-LB MIDLONGERON	SHEAR	TO BE TESTED

Table II. ATP Fuselage Panel Materials

Lay-ups:		
Skin	(0, 90, 45, 0, –45, 90) s	8551-7/IM7 Tape
Longeron	(0, 45, 90, –45, 0) 2s	8551–7/IM7 Tape
Frame	(0/90, ±45) 3s	AS4/3501–6 Cloth
Shear Tee	(0.90, ±45) 3s	AS4/3501-6 Cloth

Table III. Wing Panel Test Results Comparison

	Stitched RTM	Toughened Resin* (Prepreg)
Panel	6-Stringer	5-Stringer
Damge Due to 100 ft-lb Impact	Not Visible	Far Side Delam
Line Load (kips/in.)	20.3	21.4
Strain (%)	0.43	0.41
Matl Modulus (msi)	9.85	10.05
Stress (ksi)	40.5	41.1
Failure Mode	Column Instability	Stringer Separation

*ASTM Conference (Nov 1989) by Shuart and Madan

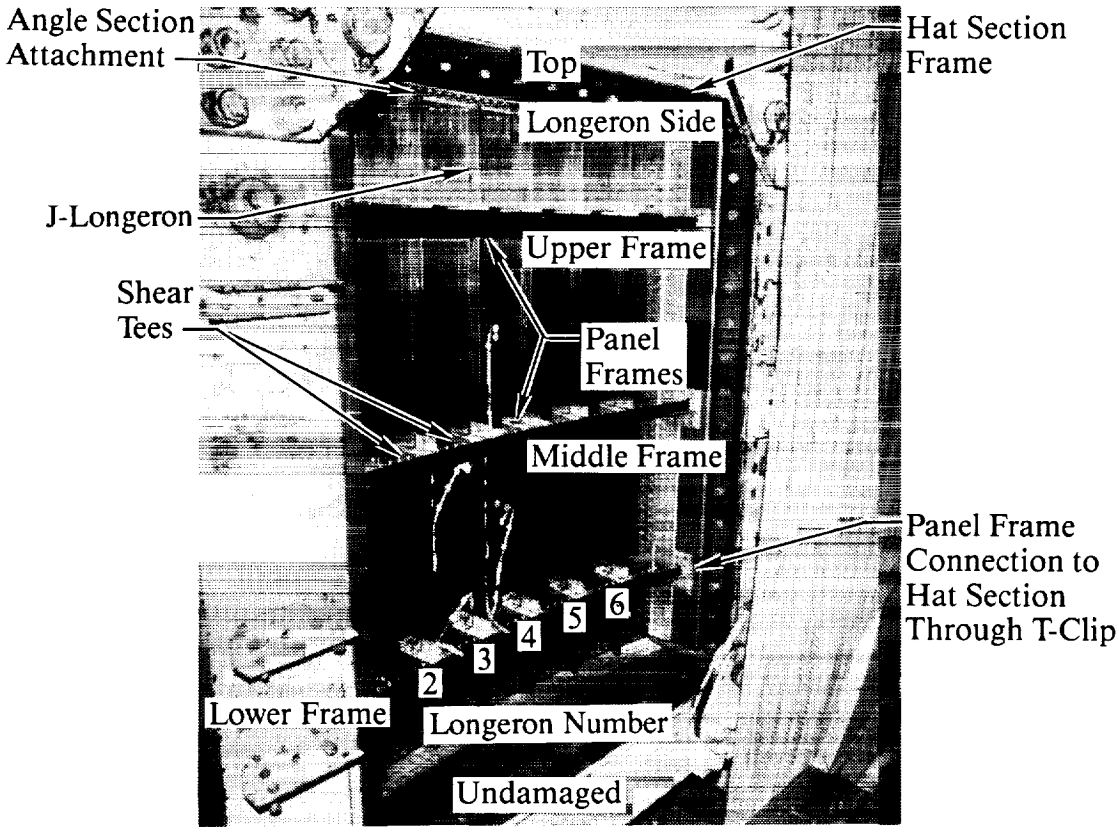

Figure 1. ATP six-Longeron fuselage panel in shear test fixture (longeron side)

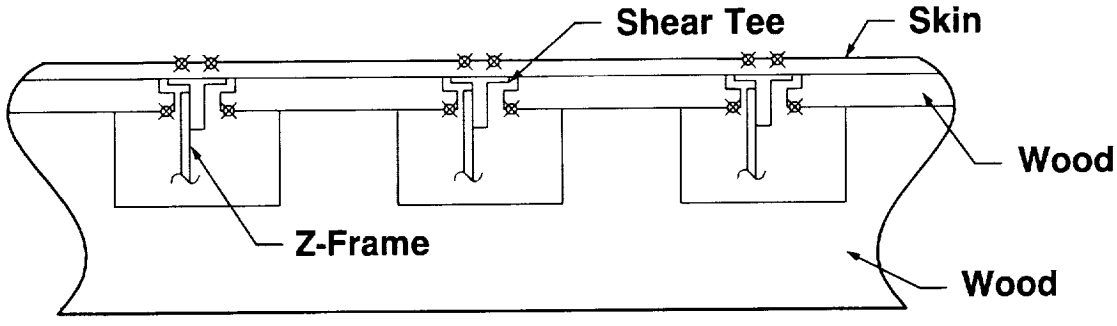

⊠ C-Clamps Support Points on Skin (Top) and Wood Sides (Bottom)

Wooden Support at Frame Ends (Two Reqd)

Figure 2. Impact support fixture

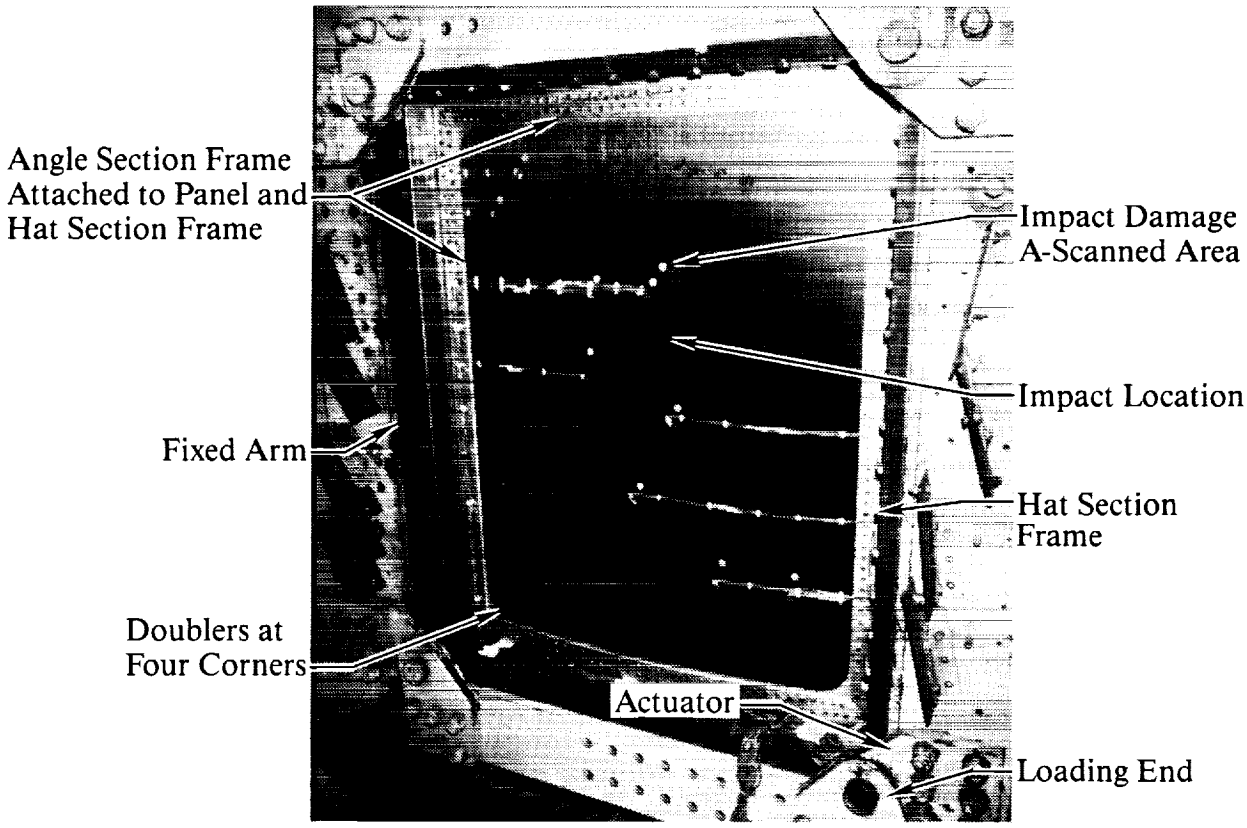

Figure 3. ATP six-longeron shear panel in test setup (skin side)

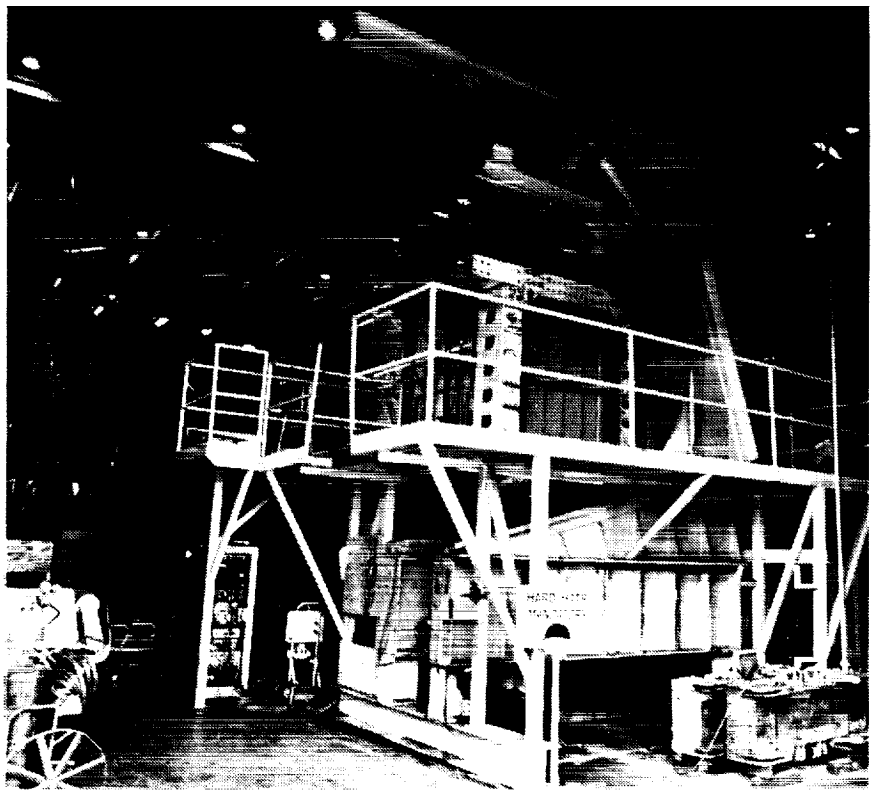

Figure 4. Shear test setup with panel (front view)

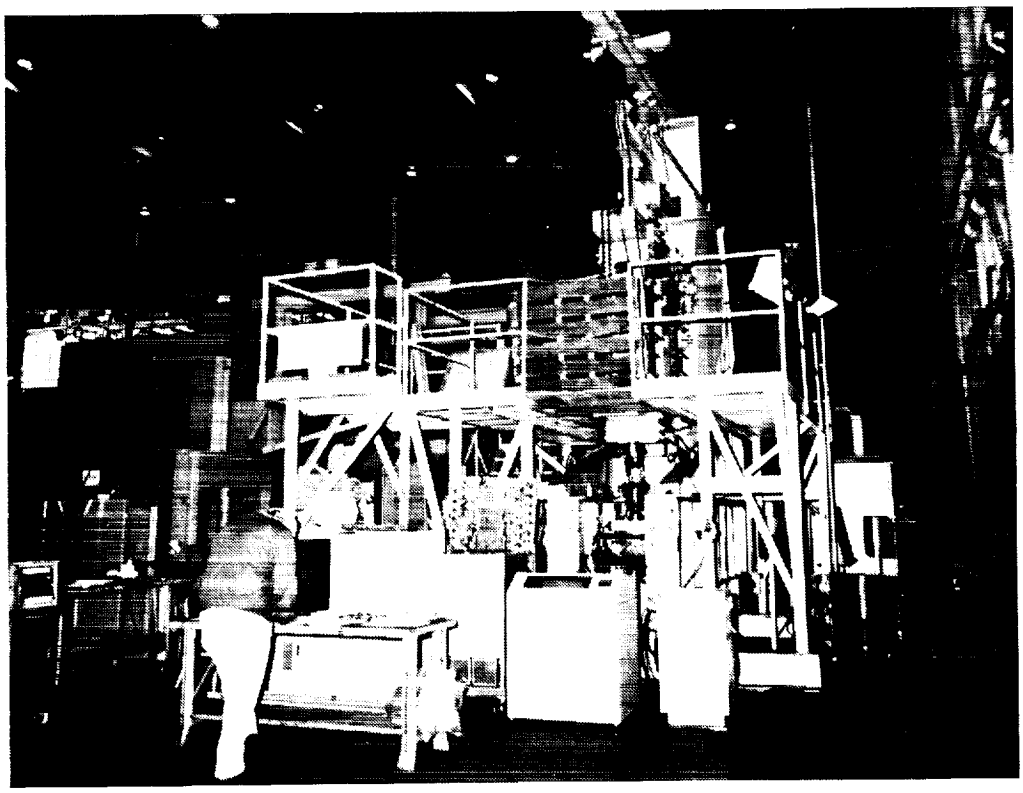

Figure 5. Shear test setup (side view)

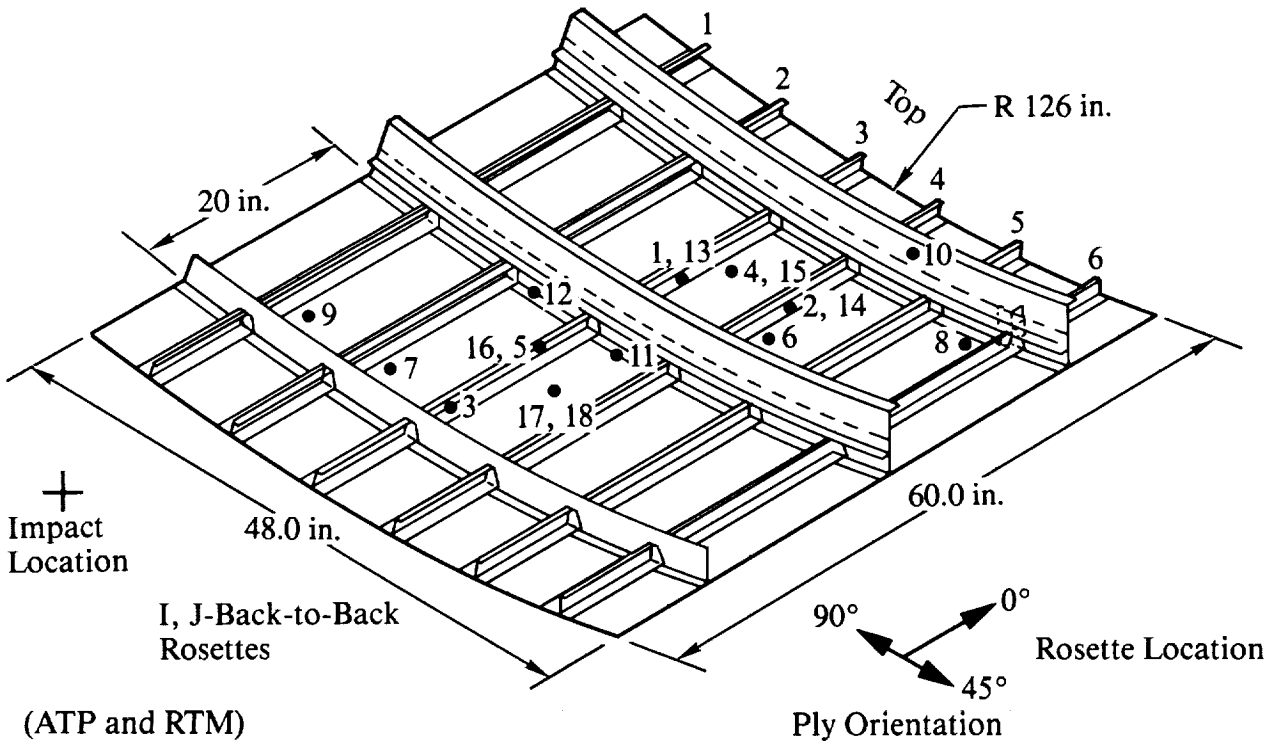

Figure 6. Six-J-stiffened fuselage shear test panel

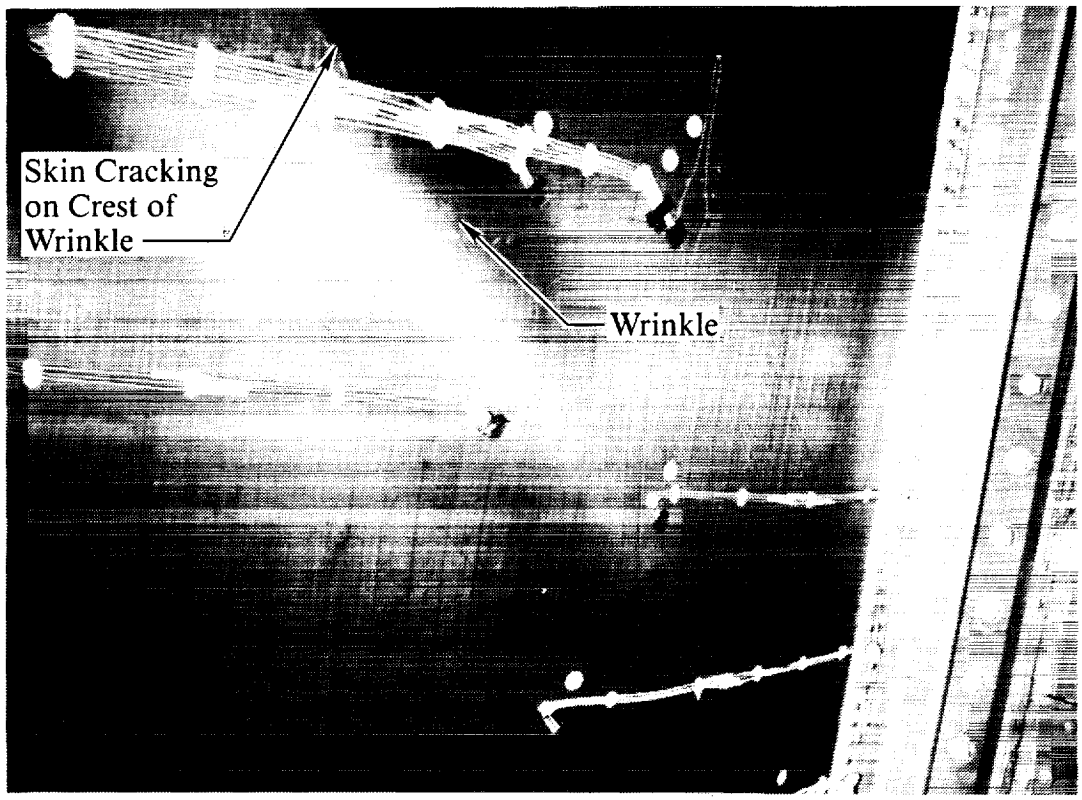

Figure 7. Buckling wrinkle in ATP fuselage shear test panel

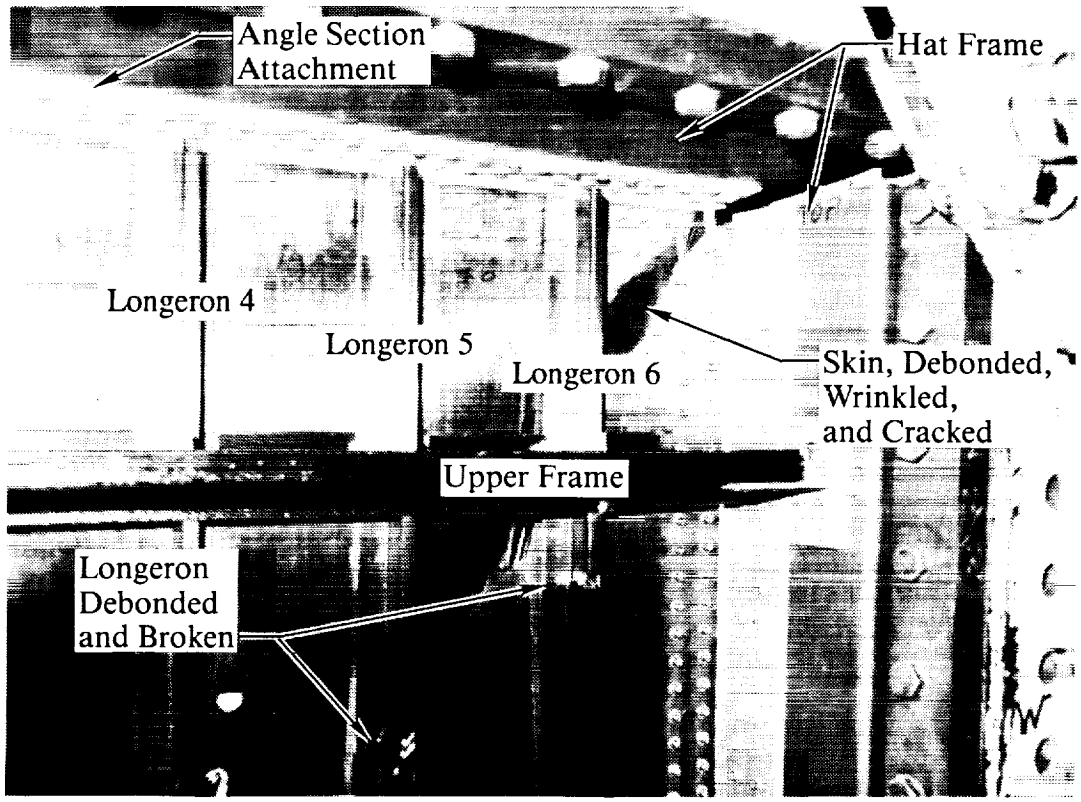

Figure 8. Damage in upper right corner of ATP shear panel

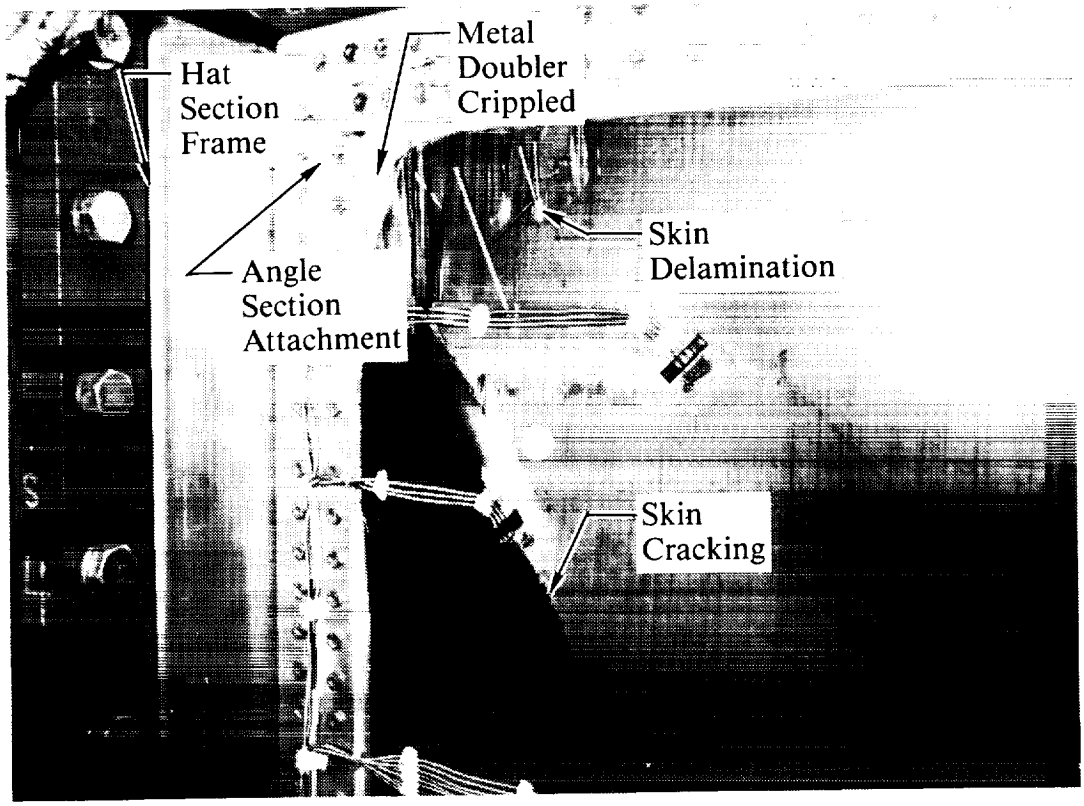

Figure 9. Damage in left top corner (skin side) in ATP shear panel (pinching effect)

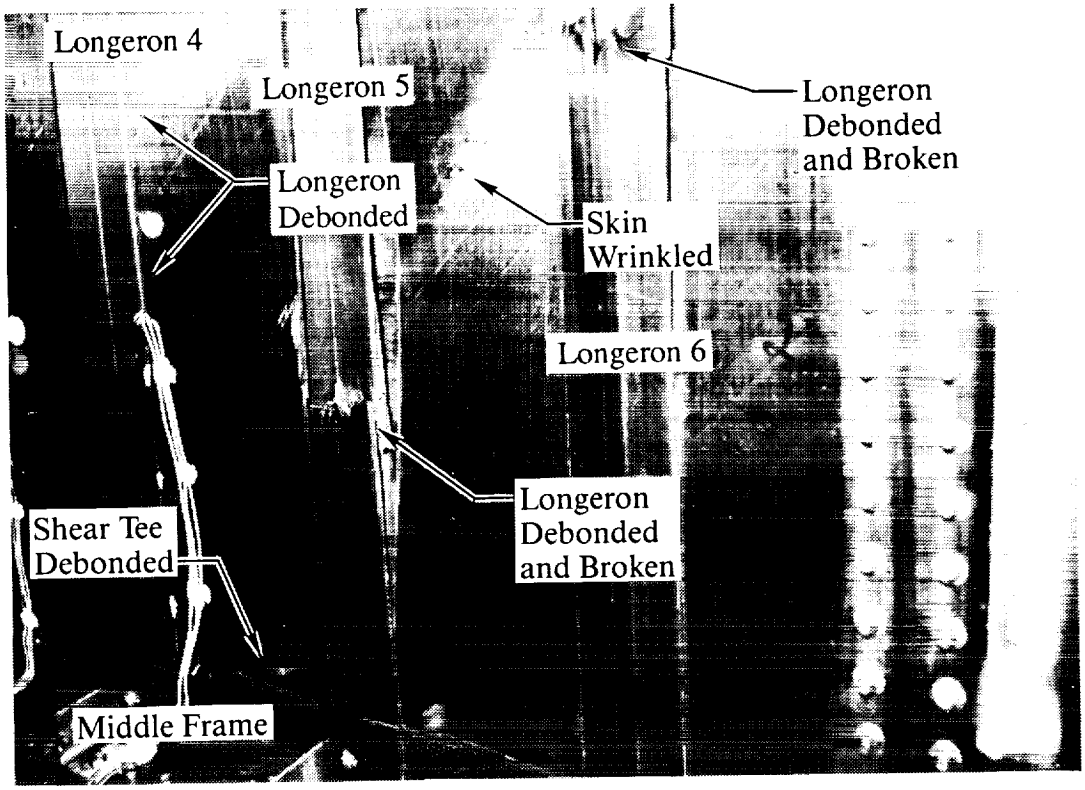

Figure 10. Damage above midframe in ATP shear panel

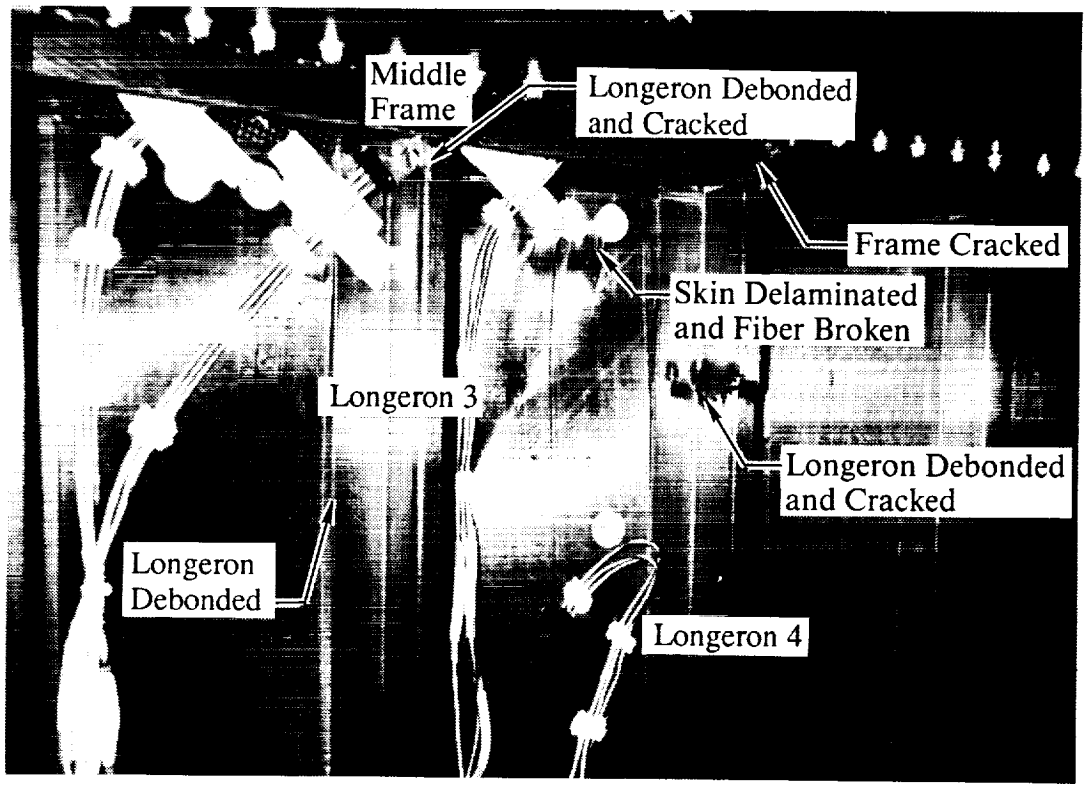

Figure 11. Damage below midframe in ATP shear test panel

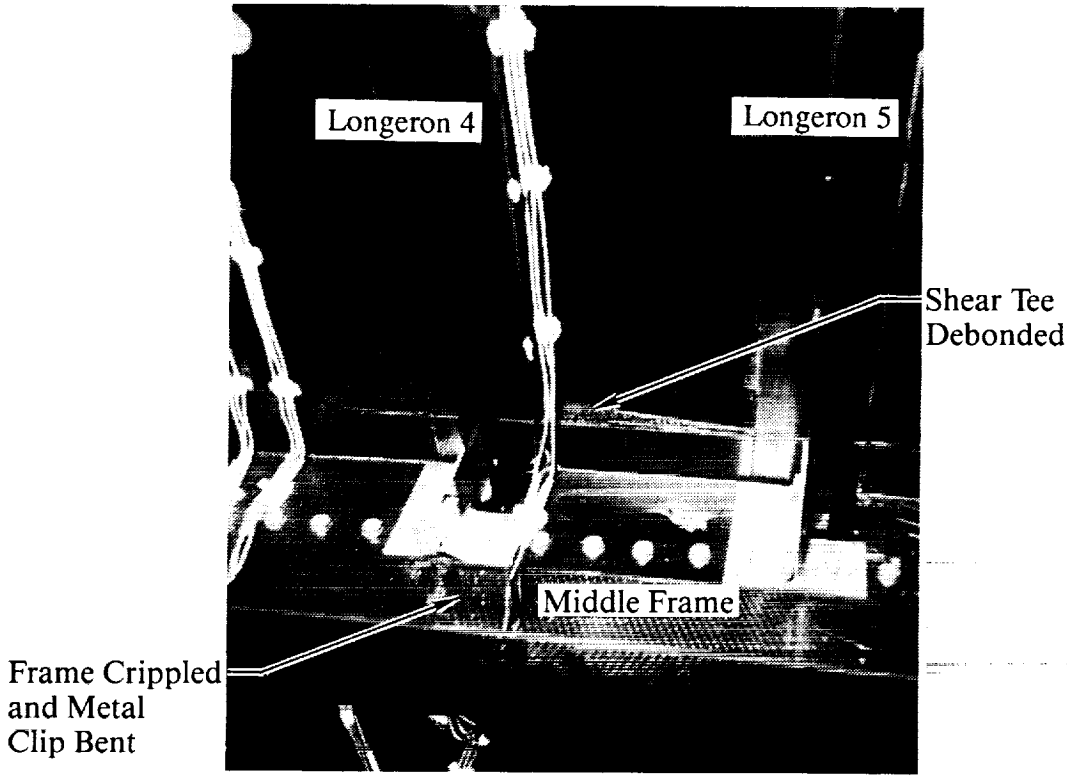

Figure 12. Damage above midframe in ATP shear panel

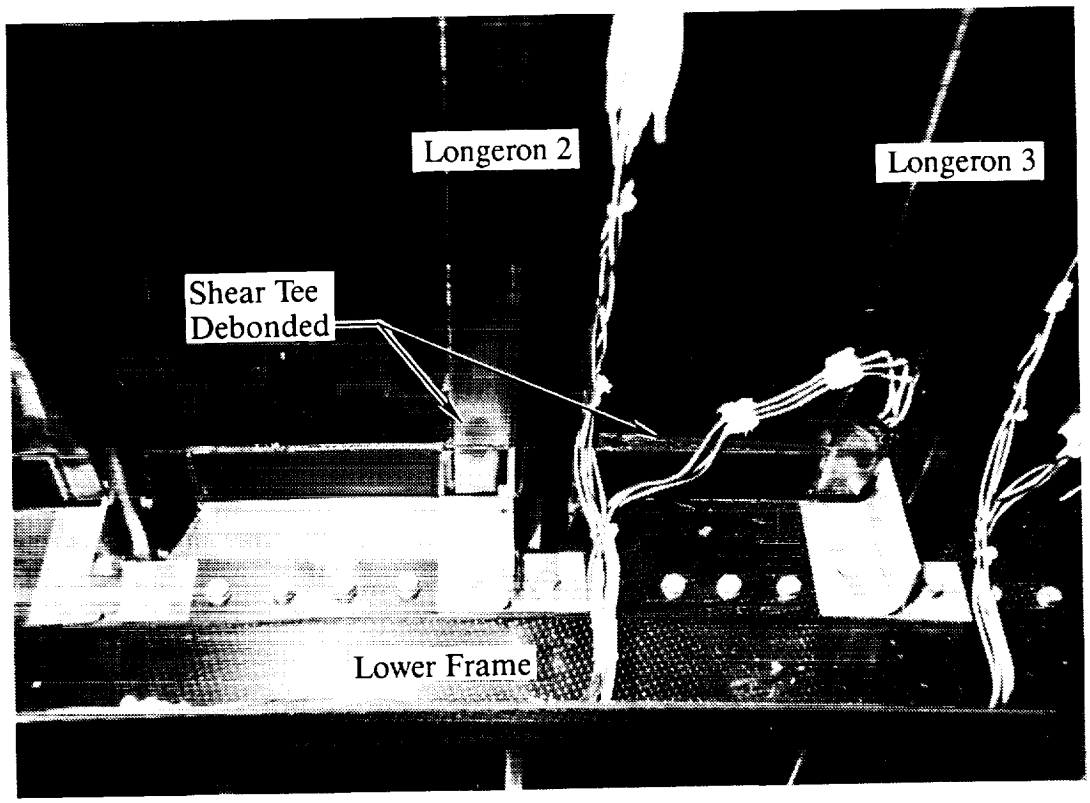

Figure 13. Damage in ATP shear panel test at midframe

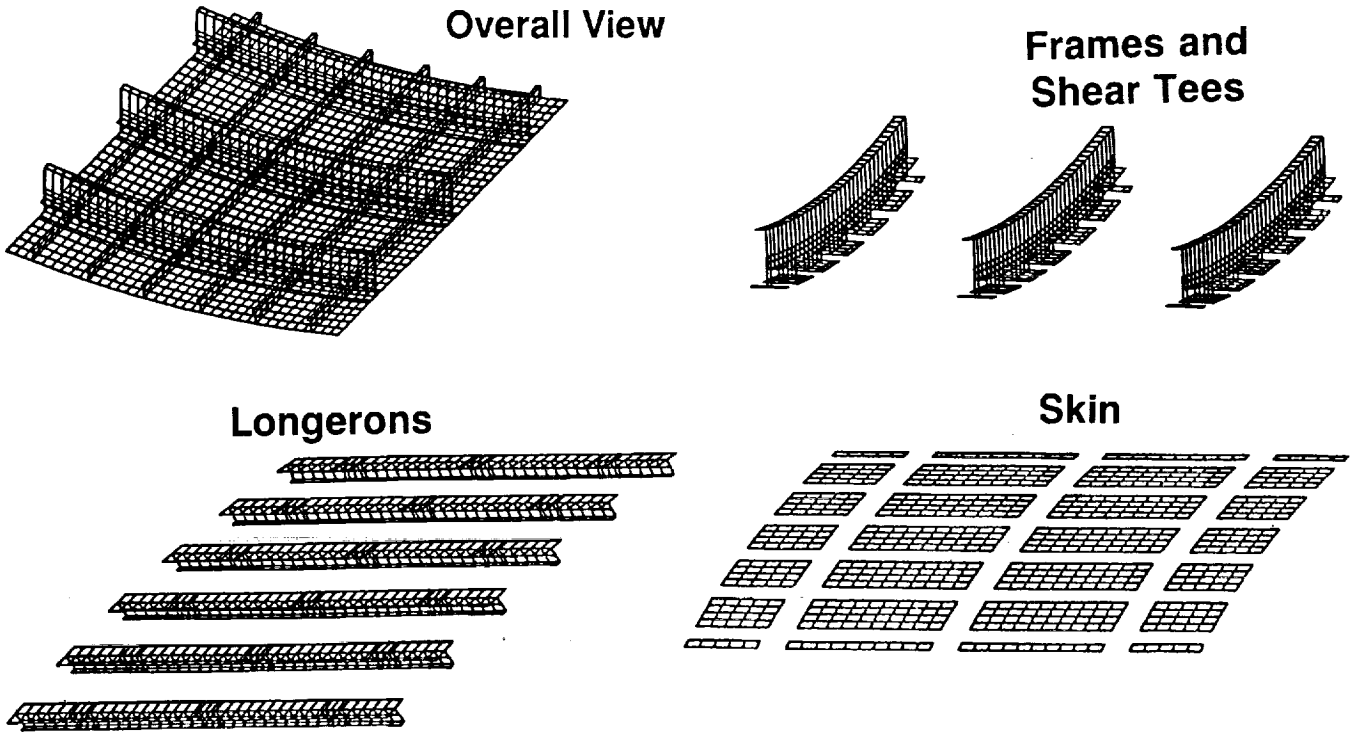

Figure 14. NASTRAN FEM model of the panel

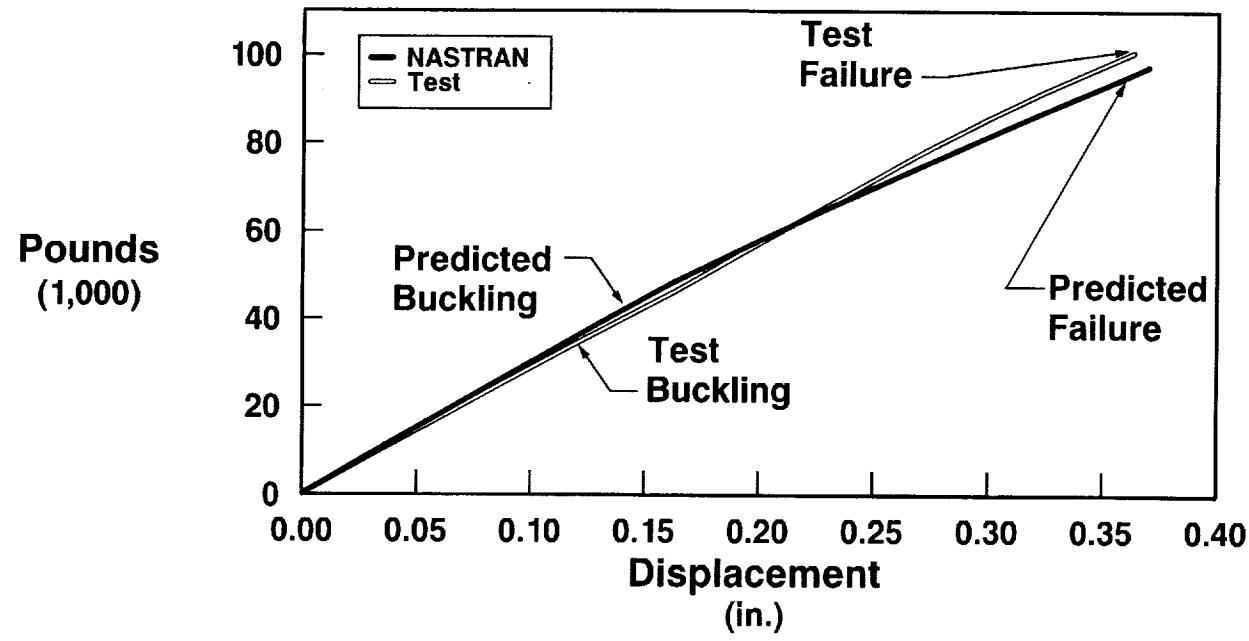

Figure 15. Panel nonlinear analysis shear postbuckling

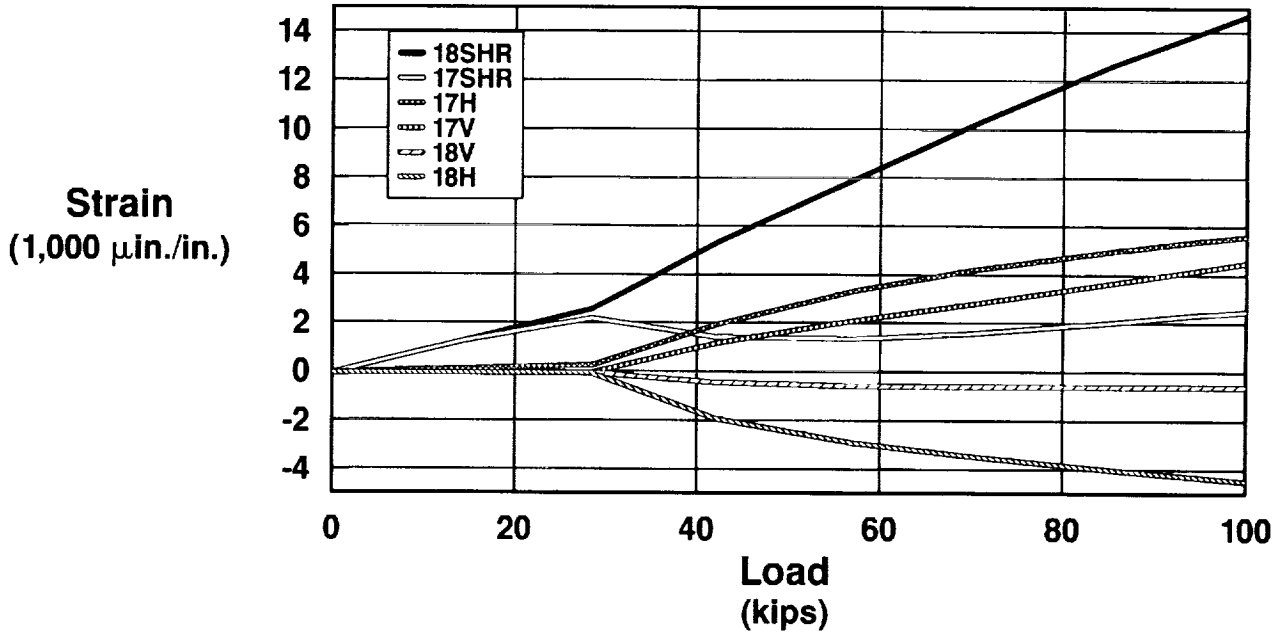

Figure 16. Six-longeron shear panel – Strain Gage 17 and 18 data

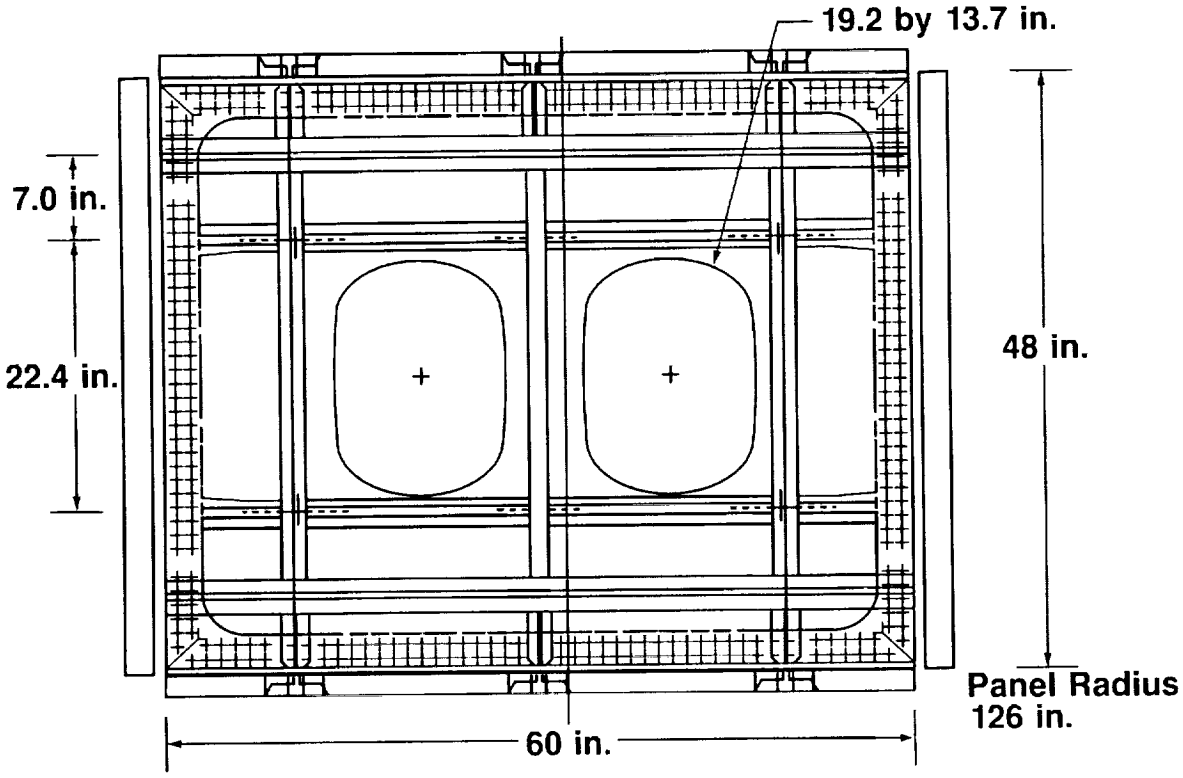

Figure 17. Window belt shear panel test

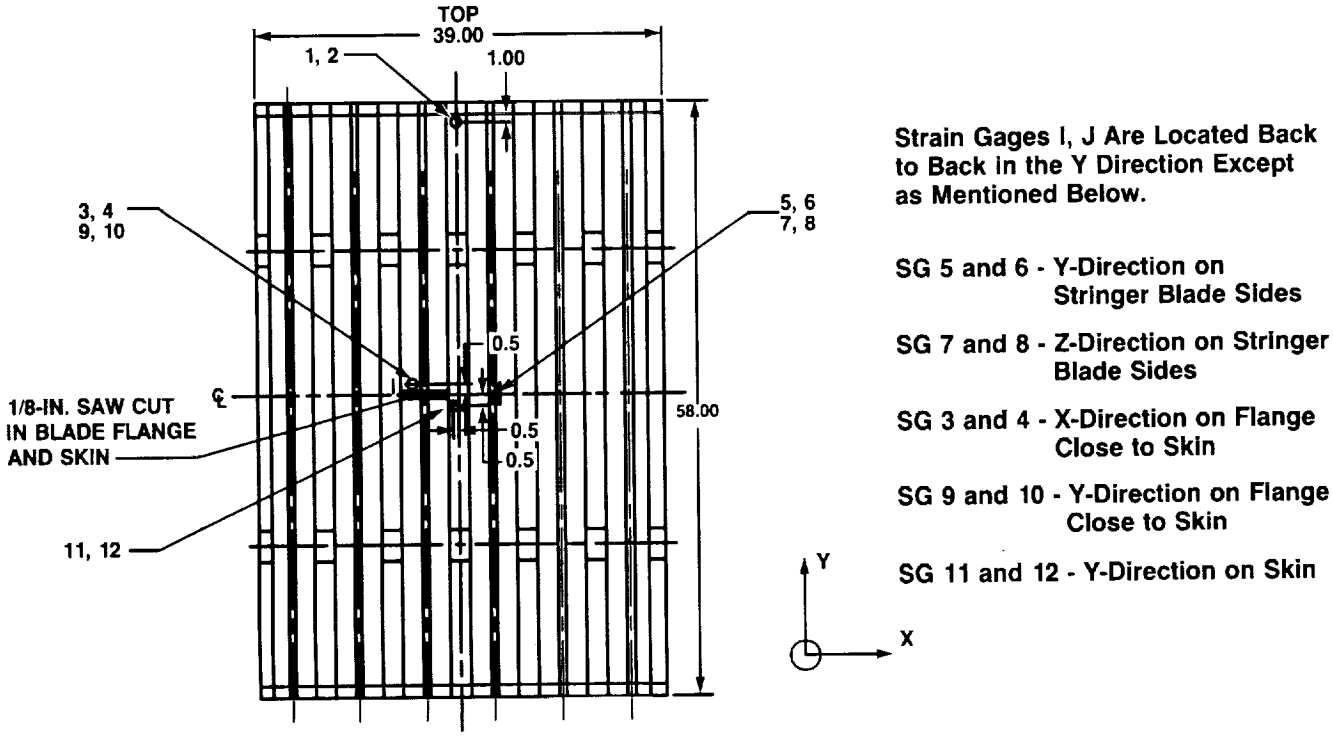

Figure 18. Strain gage locations for six-stringer RTM wing compression test panel

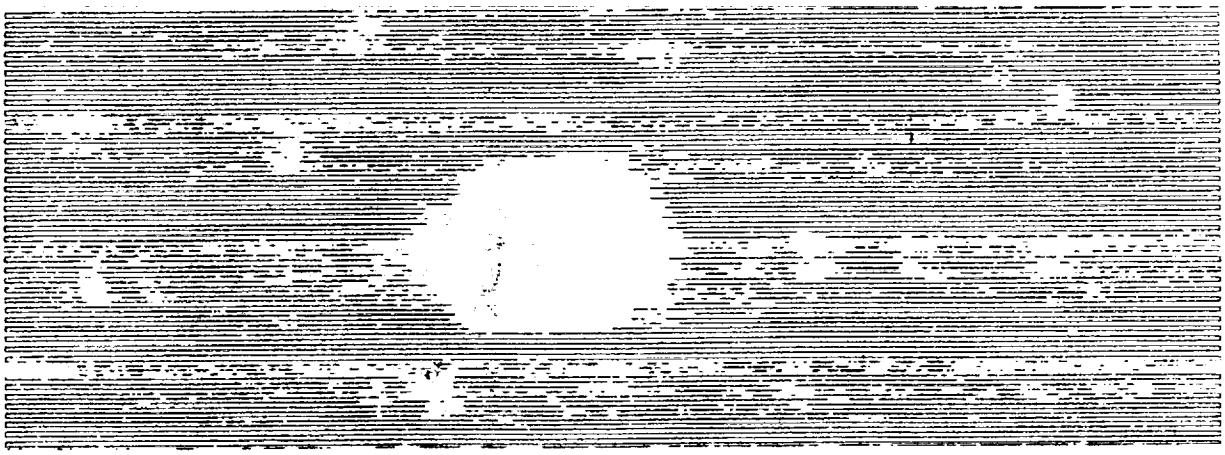

Figure 19. C-scan of midbay impact damage

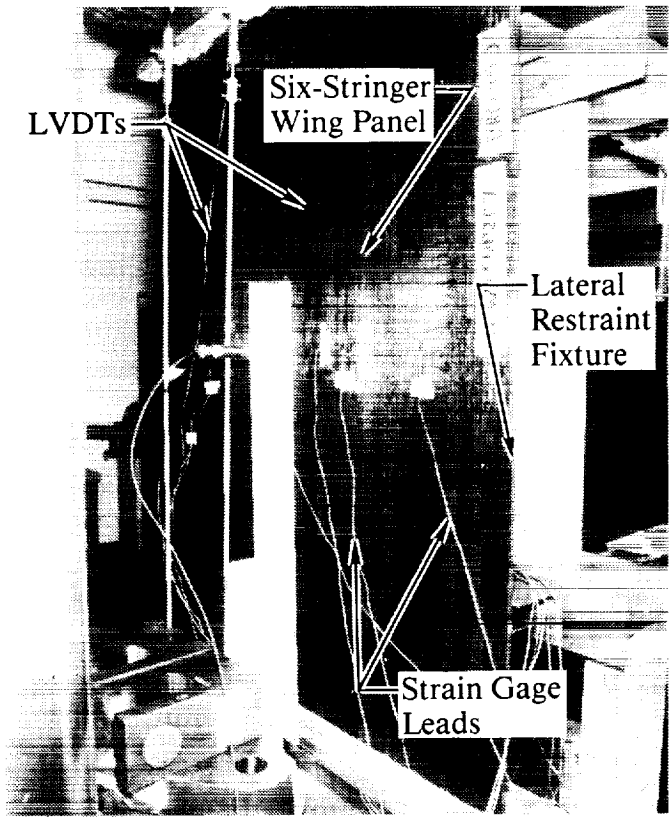

Figure 20. LVDT to measure out-of-plane deflection

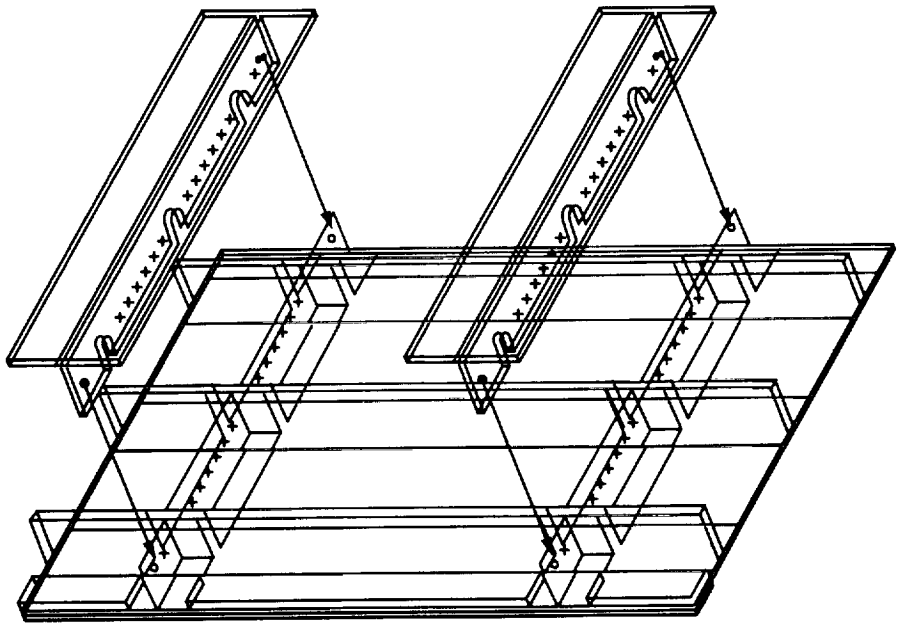

Note: Similar Fixture Can Be Used for Two-, Four-, and Six-Stringer Panels

Figure 21. 3-D view of panel with lateral supports

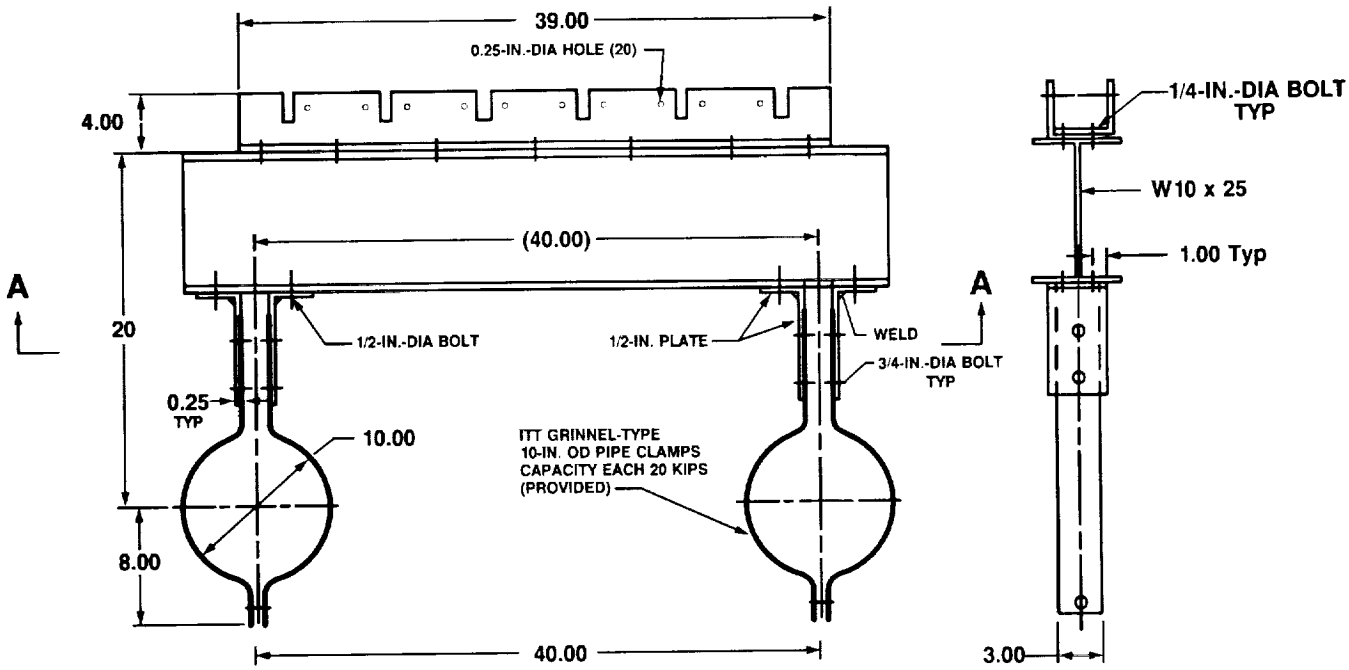

Figure 22. Lateral restraint fixture

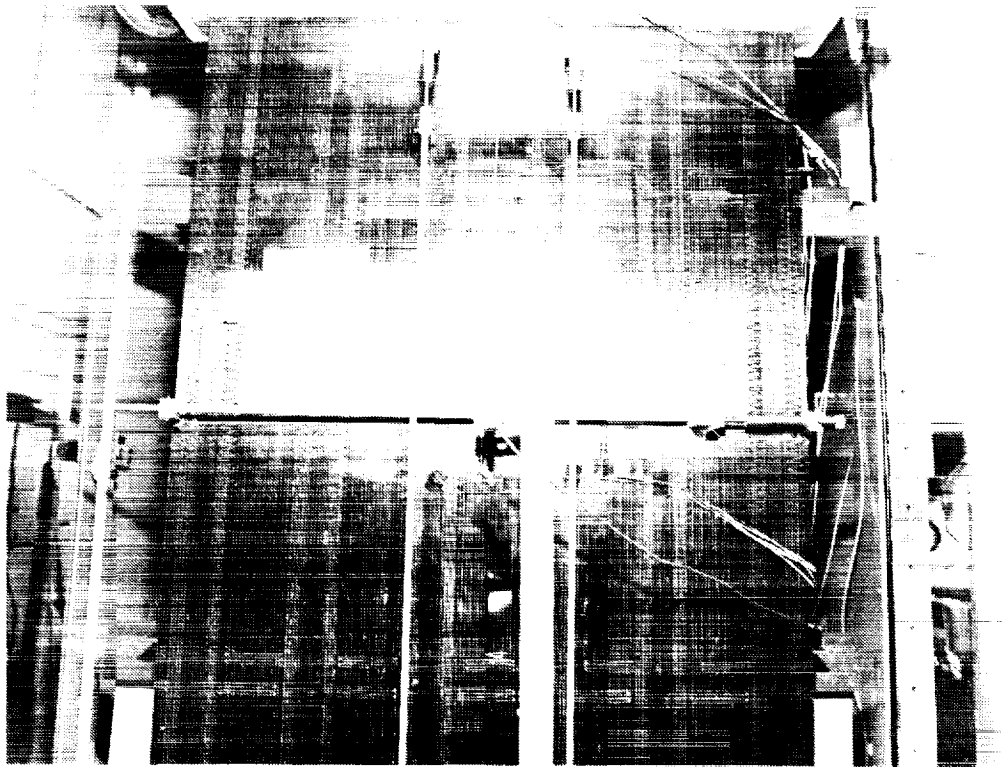

Figure 23. LVDTs on six-stringer compression test panel for displacement measurement

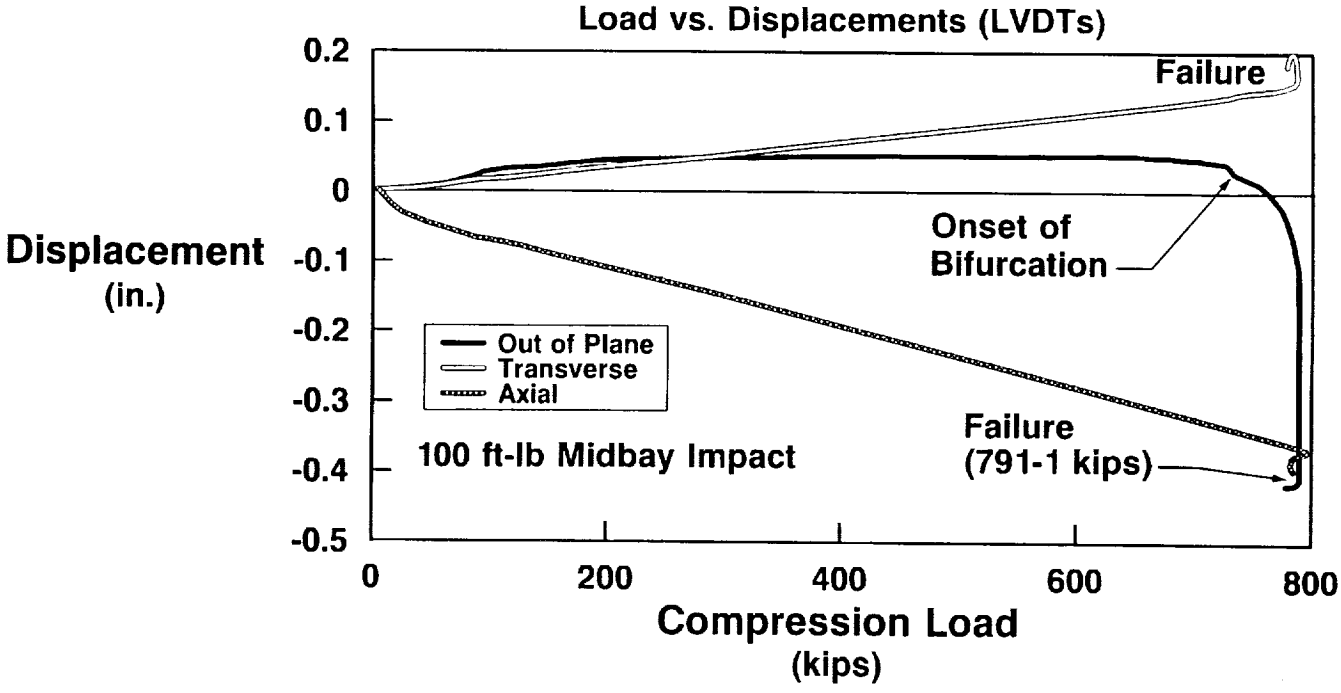

Figure 24. Six-stringer RTM wing compression panel test

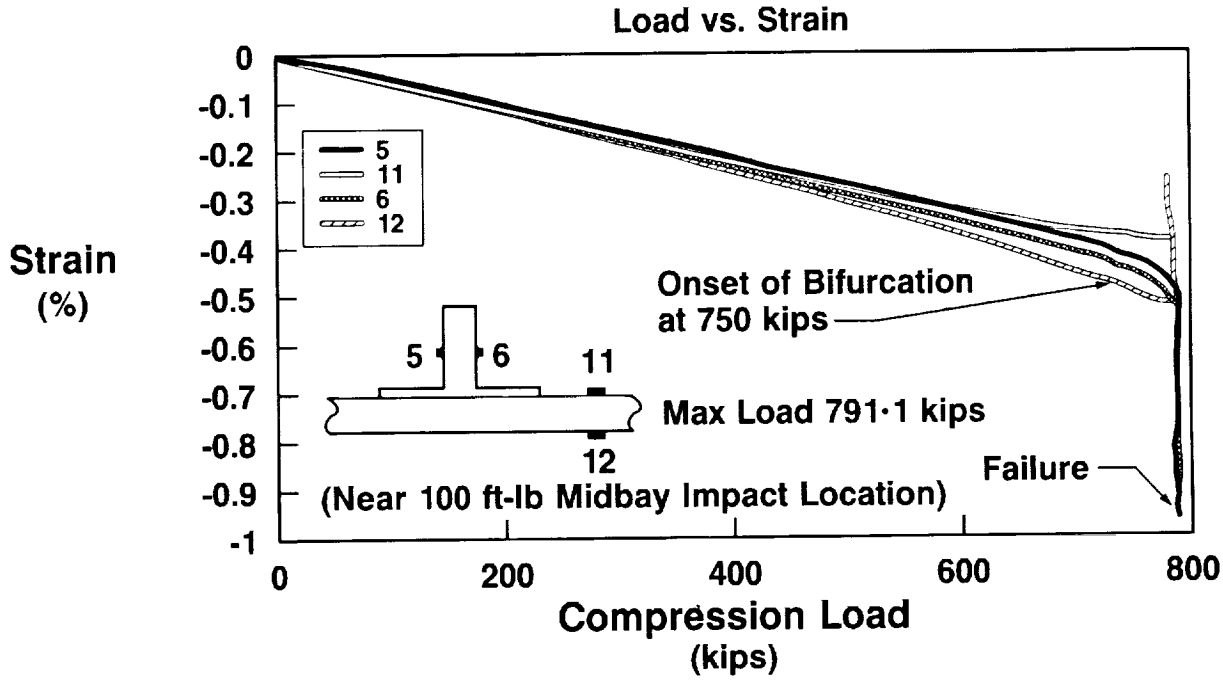

Figure 25. Six-stringer RTM wing compression panel test

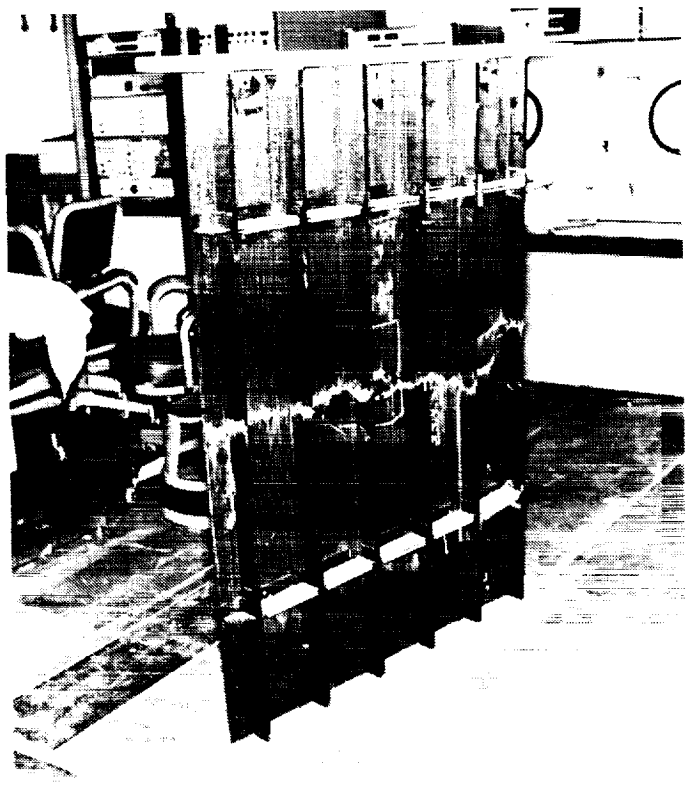

Figure 26. Six-Stringer RTM wing compression panel after the test (stringer side)

Figure 27. Six-stringer RTM wing compression panel after the test (skin side)

REPORT DOCUMENTATION PAGE

Form Approved
OMB No. 0704-0188

1. AGENCY USE ONLY *(Leave blank)*	2. REPORT DATE	3. REPORT TYPE AND DATES COVERED
	January 1993	Conference Publication

4. TITLE AND SUBTITLE
Third NASA Advanced Composites Technology Conference
Volume I, Part 1

5. FUNDING NUMBERS
510-02-13-01

6. AUTHOR(S)
John G. Davis, Jr., and Herman L. Bohon (Compilers)

7. PERFORMING ORGANIZATION NAME(S) AND ADDRESS(ES)
NASA Langley Research Center
Hampton, VA 23681-0001

8. PERFORMING ORGANIZATION REPORT NUMBER
L-17167A

9. SPONSORING/MONITORING AGENCY NAME(S) AND ADDRESS(ES)
National Aeronautics and Space Administration
Washington, DC 20546-0001
Department of Defense
Washington, DC 20301

10. SPONSORING/MONITORING AGENCY REPORT NUMBER
NASA CP-3178, Part 1

11. SUPPLEMENTARY NOTES

12a. DISTRIBUTION/AVAILABILITY STATEMENT
Review for general release November 1994
Subject Category 24

12b. DISTRIBUTION CODE

13. ABSTRACT *(Maximum 200 words)*

This document is a compilation of papers presented at the Third NASA Advanced Composites Technology (ACT) Conference held at Long Beach, California, June 8–11, 1992. The ACT Program is a major multi-year research initiative to achieve a national goal of technology readiness before the end of the decade. Conference papers recorded results of research in the ACT Program in the specific areas of automated fiber placement, resin transfer molding, textile preforms, and stitching as these processes influence design, performance, and cost of composites in aircraft structures. Papers sponsored by the Department of Defense on the Design and Manufacturing of Low Cost Composites (DMLCC) are also included in Volume II of this document.

14. SUBJECT TERMS
Thermosets; Graphite fibers; Composite design; Stitching; Preforms; Manufacturing; Processing; Analysis

15. NUMBER OF PAGES
514

16. PRICE CODE
A22

17. SECURITY CLASSIFICATION OF REPORT	18. SECURITY CLASSIFICATION OF THIS PAGE	19. SECURITY CLASSIFICATION OF ABSTRACT	20. LIMITATION OF ABSTRACT
Unclassified	Unclassified	Unclassified	